Contributors Volume 39

Numbers in parentheses indicate the pages on which the authors' contributions begin.

Vincenzo Aquilanti (71, 103), University of Perugia, Department of Chemistry, Piazza Università n.1, Perugia 06100, Italy

John Avery (71), University of Copenhagen, Department of Chemistry, Chemistry Laboratory IV, Copenhagen Ø, DK 2100, Denmark

M. C. Bacchus-Montabonnel (163), CNRS and Université Lyon I, Laboratoire de Spectrométrie Ionique et Moléculaire (UMR 5579), Villeurbanne Cedex, 69622, France

Gian Luigi Bendazzoli (189), Università di Bologna, Dipartimento di Chimica Fisica ed Inorganica, Bologna 40136, Italy

Ferenc Bogar (19), University of Szeged, Department of Theoretical Physics, Szeged 6720, Hungary

C. Bonnelle (307), CNRS and UPMC, Laboratoire de Chimie Physique, Paris 75005, France

Simonetta Cavalli (103), Università di Perugia, Dipartimento di Chimica, Perugia I-06123, Italy

Yoon Jeong Choi (325), Korea Advanced Institute of Science and Technology, Department of Chemistry, School of Molecular Science (BK21), Taejon 305-701, Korea

Jens Peder Dahl (1), Technical University of Denmark, Department of Chemistry, Lyngby DK-2800, Denmark

Dario De Fazio (103), Università di Perugia, Dipartimento di Chimica, Perugia I-06123, Italy

Ya. I. Delchev (47), Bulgarian Academy of Sciences, Institute of Nuclear Research and Nuclear Energy, Sofia 1784, Bulgaria

Ephraim Eliav (171), Tel Aviv University, School of Chemistry, Tel Aviv 69978, Israel

Stefano Evangelisti (189), Université Paul Sabatier, Laboratoire de Physique Quantique, Toulouse Cedex 4, 31062, France

G. Giorgi (307), CNRS and UPMC, Laboratoire de Chimie Physique, Paris 75005, France

V. N. Glushkov (123, 241), State University, Physics Department, Dniepropetrovsk 320625, Ukraine

Young Kyu Han (325), Korea Advanced Institute of Science and Technology, Department of Chemistry, School of Molecular Science (BK21), Taejon 305-701, Korea

I. Hubač (209, 225), Silesian University, Institute of Physics, Opava 74601, Czech Republic

Yasuyuki Ishikawa (261), University of Puerto Rico, Department of Chemistry, San Juan 00931-3346, Puerto Rico

Uzi Kaldor (171), Tel Aviv University, School of Chemistry, Tel Aviv 69978, Israel

A. Khoudir (307), CNRS and UPMC, Laboratoire de Chimie Physique, Paris 75005, France

A. I. Kuleff (295, 307), CNRS and UPMC, Laboratoire de Chimie Physique, Paris 75005, France

Janos Ladik (19), University Erlangen-Nürnberg, Laboratory of the National Foundation for Cancer Research, Erlangen D-91058, Germany

Arie Landau (171), Tel Aviv University, School of Chemistry, Tel Aviv 69978, Israel

C. Lavín (145), Universidad de Valladolid, Departamento de Química Física, Facultad de Ciencias, Valladolid 47005, Spain

Yoon Sup Lee (325), Korea Advanced Institute of Science and Technology, Department of Chemistry, School of Molecular Science (BK21), Taejon 305-701, Korea

V. M. León (357), Universidad Autónoma de Puebla, Instituto de Física, Puebla, Pue. 725570, Mexico

Wenjian Liu (325), Ruhr-Universität Bochum, Lehrstuhl für Theoretische Chemie, Bochum D-44780, Germany

P. Mach (225), Comenius University, Department of Chemical Physics, Faculty of Mathematics and Physics, Bratislava 842 15, Slovakia

I. Martín (145), Universidad de Valladolid, Departamento de Química Física, Facultad de Ciencias, Valladolid 47005, Spain

M. Martín (357), Universida Autónoma de Puebla, Facultad de Ciencias de la Computación, Puebla, Pue. 72001, Mexico

J. Maruani (47, 295, 307), CNRS and UPMC, Laboratoire de Chimie Physique, Paris 75005, France

Á. Nagy (35), University of Debrecen, Department of Theoretical Physics, Debrecen H-4010, Hungary

A. Palma (357), Universidad Autónoma de Puebla, Instituto de Física, Puebla, Pue. 725570, Mexico

R. L. Pavlov (295), Bulgarian Academy of Sciences, Institute of Nuclear Research and Nuclear Energy, Sofia 1784, Bulgaria

Harry M. Quiney (241), University of Melbourne, School of Chemistry, Parkville, Victoria 3052, Australia

L. Sandoval (357), Universida Autónoma de Puebla, Facultad de Ciencias de la Computación, Puebla, Pue. 72001, Mexico

Y. S. Tergiman (163), CNRS and Université Lyon I, Laboratoire de Spectrométrie Ionique et Moléculaire (UMR 5579), Villeurbanne Cedex 69622, France

M. Tronc (307), CNRS and UPMC, Laboratoire de Chimie Physique, Paris 75005, France

Vick Van Doren (19), University of Antwerp, Department of Physics, Antwerpen B3030, Belgium

Christoph Van Wüllen (325), Technische Universität Berlin, Berlin D-10623, Germany

A. M. Velasco (145), Universidad de Valladolid, Departamento de Química Física, Facultad de Ciencias, Valladolid 47005, Spain

Marius Jonas Vilkas (261), University of Puerto Rico, Department of Chemistry, San Juan 00931-3346, Puerto Rico

Alessandro Volpi (103), Università di Perugia, Dipartimento di Chimica, Perugia I-06123, Italy

Stephen Wilson (123, 209, 225, 241), Rutherford Appleton Laboratory, Chilton Oxfordshire OX11 0QX, United Kingdom

P. Tz. Yotov (47, 295), Bulgarian Academy of Sciences, Institute of Nuclear Research and Nuclear Energy, Sofia 1784, Bulgaria

F. E. Zakhariev (47), Tulane University, New Orleans, Louisiana 70118

Boris P. Zapol (57), University of Latvia, Department of Theoretical Physics and Institute of Chemical Physics, Riga LV-1586, Latvia

Contents Volume 39

Contributors Volume 40

Numbers in parentheses indicate the pages on which the authors' contributions begin.

Hans Ågren (191, 213), The Royal Institute of Technology, Theoretical Chemistry, Stockholm SE-10044, Sweden

Tatyana Alferova (323), Stockholm University, Department of Physics, Molecular Physics Group, Stockholm SE-113 85, Sweden

Stefan Andersson (323), Stockholm University, Department of Physics, Molecular Physics Group, Stockholm SE-113 85, Sweden

Elena S. Apostolova (143), D. I. Mendeleev Russian University of Chemical Technology, Department of Quantum Chemistry, Moscow, Russia

O. Atabek (179), Université Paris-Sud, Laboratoire de Photophysique Moléculaire, Campus d'Orsay, Orsay 91405, France

Erkki J. Brändas (225), Uppsala University, Quantum Chemistry Group, Uppsala S-75120, Sweden

P. Chaquin (161), Université Pierre et Marie Curie, Laboratoire de Chimie Théorique, Case 137, Paris Cedex 5, 75252, France

Nick J. Clarke (37), Tessella Support Services plc, Bretby Business Park, Burton Upon Trent DE15 0YZ, United Kingdom

David L. Cooper (37), University of Liverpool, Department of Chemistry, Liverpool L69 7ZD, United Kingdom

Peter Cronstrand (213), The Royal Institute of Technology, Theoretical Chemistry, Stockholm SE-10044, Sweden

I. G. Csizmadia (49), University of Toronto, Department of Chemistry, Toronto M5S1A1, Canada

L. J. Dunne (225), South Bank University, School of Applied Science, London SE1 0AA, United Kingdom

Nils Elander (323), Stockholm University, Department of Physics, Molecular Physics Group, Stockholm SE-113 85, Sweden

Bernd Engels (133), Universität Bonn, Institut für Physikalische und Theoretische Chemie, Bonn D-53115, Germany

W. Fraessdorf (345), Brock University, Department of Chemistry, St. Catherine's, Ontario L2S3A1, Canada

Y. Girard (161), Université Pierre et Marie Curie, Laboratoire de Chimie Théorique, Case 137, Paris Cedex 5, 75252, France

Mikhail V. Ivanov (361), Russian Academy of Sciences, Institute of Precambrian Geology and Geochronology, St. Petersburg 199034, Russia

I. G. Kaplan (257), Jackson State University, The Computational Center for Molecular Structure and Interactions, Department of Chemistry, Jackson, Michigan 39217

C. Kozmutza (49), Technical University of Budapest, Department of Theoretical Physics, Institute of Physics, Budapest H-1111, Hungary

Eugene S. Kryachko (79), University of Leuven, Department of Chemistry, Leuven B3001, Belgium

A. Kuleff (279), CNRS and UPMC, Laboratoire de Chimie Physique, Paris 75005, France

R. Lefebvre (179), Université Paris-Sud, Laboratoire de Photophysique Moléculaire, Campus d'Orsay, Orsay 91405, France

Jerzy Leszczynski (257), Jackson State University, The Computational Center for Molecular Structure and Interactions, Department of Chemistry, Jackson, Michigan 39217

Sergey Levin (323), Stockholm University, Department of Physics, Molecular Physics Group, Stockholm SE-113 85, Sweden

Sten Lunell (133), University of Uppsala, Department of Quantum Chemistry, Uppsala S-75120, Sweden

J. Maruani (279), CNRS and UPMC, Laboratoire de Chimie Physique, Paris 75005, France

Roy McWeeny (1), University of Pisa, Dipartimento di Chimica e Chimica Industriale, Pisa I-56100, Italy

Boris F. Minaev (191), The Royal Institute of Technology, Stockholm SE-10044, Sweden

D. C. Moule (345), Brock University, Department of Chemistry, St. Catherine's, Ontario L2S3A1, Canada

C. Muñoz-Caro (345), Universidad de Castilla-La Mancha, E. U. Informatica de Ciudad Real, Ciudad Real 13071, Spain

Minh Tho Nguyen (79), University of Leuven, Department of Chemistry, Leuven B3001, Belgium

A. Niño (345), Universidad de Castilla-La Mancha, E. U. Informatica de Ciudad Real, Ciudad Real 13071, Spain

C. Perez del Valle (179), CSIC, Instituto de Ciencia de Materiales, Cantoblanco, Madrid 28049, Spain

P. P. Raychev (279), CNRS and UPMC, Laboratoire de Chimie Physique, Paris 75005, France

Szczepan Roszak (257), Jackson State University, The Computational Center for Molecular Structure and Interactions, Department of Chemistry, Jackson, Michigan 39217

Ulf Saalmann (305), Stockholms Universitet, Atomfysik, Stockholm 10405, Sweden

Peter Schmelcher (361), Universität Heidelberg, Theoretische Chemie, Physikalisch-Chemisches Institut, Heidelberg D-69120, Germany

Vipin Srivastava (249), University of Hyderabad, School of Physics, Hyderabad 500 046, India

Phillip C. Stancil (37), University of Georgia, Department of Physics and Astronomy, Athens, Georgia 30602-2451

Brian Sutcliffe (17), University of York, Department of Chemistry, Helsington, York YO1 5DD, England

H. U. Suter (133), Universität Bonn, Institut für Physikalische und Theoretische Chemie, Bonn D-53115, Germany

O. Tapia (103), Uppsala University, Department of Chemistry, Uppsala S-75121, Sweden

E. Tfirst (49), Hungarian Academy of Sciences, Institute of Chemistry, Chemical Research Center, Budapest H-1025, Hungary

E. Yarevsky (323), Stockholm University, Department of Physics, Molecular Physics Group, Stockholm SE-113 85, Sweden

Bernard Zygelman (37), University of Nevada, Las Vegas, Department of Physics, Las Vegas, Nevada 89154-4002

Preface

Quantum mechanics has existed for more than 75 years and forms the basis for the fundamental description of microscopic phenomena and processes. Contemporary research on quantum systems covers a vast area, from investigations on nuclei, atoms, and molecules to complex chemical and biological systems. To foster the development of innovative theory and concepts, the first European Workshop on Quantum Systems in Chemistry and Physics (QSCP I) was organized in San Miniato, near Pisa, Italy (1996). The meeting was a great success and was followed by *QSCP II* in Oxford (1997), *QSCP III* in Granada (1998), and *QSCP VI* in Paris (1999). The *QSCP II* proceedings were published in *Advances in Quantum Chemistry*, Volumes 31 and 32.

The fifth European Workshop in the series was held in Uppsala, April 13–18, 2000, at Ihresalen, Teknikum, Uppsala University. The workshop was organized as follows:

Density Matrices and Density Functionals *(Chair: J. Maruani)*
Electron Correlation Treatments *(Chair: S. Wilson)*
Relativistic Formulations *(Chair: U. Kaldor)*
Valence Theory *(Chair: Y. G. Smeyers)*
Nuclear Motion *(Chair: O. Goscinski)*
Response Theory *(Chair: B. T. Sutcliffe)*
Condensed Matter *(Chair: H. Ågren)*
Chemical Reactions *(Chair: C. Minot)*
Computational Chemistry *(Chair: I. Hubač)*
Posters *(Chairs: R. Lefebvre, E. Brändas)*

It attracted 95 scientists from 25 different countries who gathered to give 49 talks and 40 posters.

Additionally, a special *leitmotiv* was made to run through the lectures and discussions, relating to the pioneering work and achievements of Per-Olov Lowdin. In 1982, Uppsala University created a fund through collected contributions from Per-Olov Löwdin's colleagues, collaborators, and students, with the purpose of inviting prominent lecturers to Uppsala at regular intervals. The aim of

the lectures was to stimulate interest in quantum chemistry through one general lecture for a broader audience and a more specialized lecture targeted at experts in the field. The Löwdin Lecturers during 1984–2000 were R. Zahradnik, A. Pullman, R. S. Berry, R. Pauncz, H. Shull, E. R. Davidson, P. Fulde, M. Quack, F. A. Gianturco, J. P. Dahl, and R. McWeeny.

During the year 2000, two Löwdin Lecturers were invited: *Professor Roy McWeeny,* Pisa, Italy, and *Professor Jens Peder Dahl,* Copenhagen, Denmark. They both agreed to deliver their lectures during *QSCP V.* Due to unforeseen circumstances, only one lecturer could attend *QSCP V.* The second lecture was therefore presented half a year later and then as the Löwdin Memorial Lecture. Both are published as introductory chapters of the two proceedings volumes as a joint tribute to a great leader and pioneer in quantum chemistry. We are very proud to present *QSCP V: New Perspectives in Quantum Systems in Chemistry and Physics,* in the series *Advances in Quantum Chemistry,* founded by Löwdin.

The workshop was sponsored by the *European Commission - COST D9,* the *French Embassy* in Stockholm, the *Swedish Natural* Science *Research Council,* the *Foundation for Strategic Research,* and *Uppsala University.* We are greatly indebted to our sponsors for their generosity. In particular, we acknowledge the help and advice offered by Gérard Rivière from the COST Chemistry Secretariat. It is a pleasure to thank the members of the scientific organizing committee, R. McWeeny, J. Maruani, Y. G. Smeyers, and S. Wilson, for their excellent support and advice, and the local organizing committee and members of the Department of Quantum Chemistry at Uppsala University for their competence and efficiency which made for the smooth running of the workshop.

E. Brändas
Chair
Organizing Committee

O. Goscinski
Chair
Löwdin Lectureship Fund

Workshop Participants

M. Agback, Department of Quantum Chemistry, Uppsala University, SE-751 20 Uppsala, Sweden

H. Ågren, Theoretical Chemistry, Royal Institute of Technology, S-10044 Stockholm, Sweden

T. Alferova, Department of Physics, Stockholm University, SE-113 85 Stockholm, Sweden

M. Andersson, Department of Quantum Chemistry, Uppsala University, SE-75120 Uppsala, Sweden

S. Andersson, Department of Physics, Stockholm University, SE-113 85, Stockholm, Sweden

V. Aquilanti, Dipartimento di Chimica, Università di Perugia, I-06123 Perugia, Italy

J. S. Avery, H.C. Ørsted Institute, University of Copenhagen, DK-2100 Copenhagen, Denmark

M.-C. Bacchus-Montabonnel, Laboratoire de Spectrometrie Ionique et Moleculaire, Université Lyon I, 69622 Villeurbanne, Cedex, France

R. J. Bartlett, Quantum Theory Project, University of Florida, Gainesville, Florida 32611

G. L. Bendazzoli, Dipartimento di Chimica Fisica ed Inorganica, Università di Bologna, I-40136 Bologna, Italy

E. J. Brändas, Department of Quantum Chemistry, Uppsala University, SE-751 20 Uppsala, Sweden

J. Caillat, Laboratoire de Chimie Physique de l'Université Pierre et Marie Curie, 75231 Paris, Cedex 05, France

N. Capron, Laboratoire de Chimie Physique de l'Université Pierre et Marie Curie, 75231 Paris, Cedex 05, France

S. Carniato, Laboratoire de Chimie Physique de l'Université Pierre et Marie Curie, 75231 Paris, Cedex 05, France

D. L. Cooper, Department of Chemistry, University of Liverpool, Liverpool L69 7ZD, United Kingdom

P. Cronstrand, Theoretical Chemistry, Royal Institute of Technology, S-10044 Stockholm, Sweden

J. P. Dahl, Department of Chemistry, Technical University of Denmark, DK-2800 Kgs. Lyngby, Denmark

Ya. Y. Delchev, Institute of Nuclear Research and Energy, Bulgarian Academy of Sciences, 1784 Sofia, Bulgaria

B. Durbeej, Department of Quantum Chemistry, Uppsala University, SE-751 20 Uppsala, Sweden

N. O. Elander, Department of Physics, Stockholm University, SE-113 85 Stockholm, Sweden

M. Engström, Theoretical Chemistry, Royal Institute of Technology, S-10044 Stockholm, Sweden

M. L. Ericsson, Department of Quantum Chemistry, Uppsala University, SE-751 20 Uppsala, Sweden

L. A. Eriksson, Department of Quantum Chemistry, Uppsala University, SE-751 20 Uppsala, Sweden

J.-S. Filhol, Ecole Normale Superieure de Lyon, 69364 Lyon, Cedex 07, France

P. Froelich, Department of Quantum Chemistry, Uppsala University, SE-751 20 Uppsala, Sweden

Y. Girard, Laboratoire de Chimie Theorique, Université Pierre et Marie Curie, 75252 Paris Cedex 05, France

A. V. Glushkov, Institute of Applied Mathematics, OHMI, Odessa-9, 65009, Ukraine

O. Goscinski, Department of Quantum Chemistry, Uppsala University, SE-751 20 Uppsala, Sweden

I. Hubač, Department of Chemical Physics, Faculty of Mathematics and Physics, Comenius University, 842 15 Bratislava, Slovakia

Y. Ishikawa, Department of Chemistry, University of Puerto Rico, San Juan, Puerto Rico 00931-3346, USA

M. Ivanov, Theoretische Chemie, Physikalisch-Chemisches Institut, Universität Heidelberg, D-69120 Heidelberg, Germany

M. Jansson, Department of Quantum Chemistry, Uppsala University, SE-751 20 Uppsala, Sweden

S. Jonsell, Department of Quantum Chemistry, Uppsala University, SE-751 20 Uppsala, Sweden

U. Kaldor, School of Chemistry, Tel Aviv University, 69978 Tel Aviv, Israel

I. G. Kaplan, Instituto de Fisica, UNAM, 01000 Mexico, D. F., Mexico

E. B. Karlsson, Department of Physics, Uppsala University, S-75121 Uppsala, Sweden

H. O. Karlsson, Department of Quantum Chemistry, Uppsala University, SE-751 20 Uppsala, Sweden

I. S. K. Kerkines, Laboratory of Physical Chemistry, Department of Chemistry, University of Athens, 157 10 Zografou, Athens, Greece

E. S. Kryachko, Department of Chemistry, University of Leuven, B-3001 Heverlee-Leuven, Belgium

A. Kuleff, Laboratoire de Chimie Physique, Université Pierre et Marie Curie, 75005 Paris Cedex, France

J. Ladik, Chair for Theoretical Chemistry, University of Erlangen-Nürnberg, D-91058 Erlangen, Germany

P. O. Lantto, University of Oulu, Department of Physical Sciences, University of Oulu, FIN-90014 Oulu, Finland

Å. Larson, Department of Physics, Stockholm University, SE-113 85 Stockholm, Sweden

B. Larsson, Department of Quantum Chemistry, Uppsala University, SE-751 20 Uppsala, Sweden

P.-E. Larsson, Department of Quantum Chemistry, Uppsala University, SE-751 20 Uppsala, Sweden

R. Lefebvre, Laboratoire de Photophysique Moleculaire, Campus d'Orsay, 91405 Orsay, France

S. B. Levin, Department of Physics, Stockholm University, SE-113 85 Stockholm, Sweden

W. Liu, Lehrstuhl für Theoretische Chemie, Ruhr-Universität Bochum, D-44780, Germany

J. Llano, Department of Quantum Chemistry, Uppsala University, SE-751 20 Uppsala, Sweden

M. J. Lundqvist, Department of Quantum Chemistry, Uppsala University, SE-751 20 Uppsala, Sweden

S. G. B. Lunell, Department of Quantum Chemistry, Uppsala University, SE-751 20 Uppsala Sweden

Y. Luo, Theoretical Chemistry, Royal Institute of Technology, S-10044 Stockholm, Sweden

P. Macak, Theoretical Chemistry, Royal Institute of Technology, S-10044 Stockholm, Sweden

S. V. Malinovskaya, NPO-Computer Centre, Odessa-9, 65009, Ukraine

A. Markovits, Laboratoire de Chimie Théorique, Université Pierre et Marie Curie, 75252 Paris Cedex 05, France

I. Martín, Departamento de Quimica Fisica, Facultad de Sciencias, Universidad de Valladolid, Valladolid, Spain

C. Martinsky, Laboratoire de Chimie Théorique, Université Pierre et Marie Curie, 75252 Paris Cedex 05, France

J. Maruani, Laboratoire de Chimie Physique, Université Pierre et Marie Curie, 75252 Paris Cedex 05, France

B. F. Minaev, Theoretical Chemistry, Royal Institute of Technology, S-10044 Stockholm, Sweden

C. Minot, Laboratoire de Chimie Théorique, Université Pierre et Marie Curie, 75252 Paris Cedex 05, France

D. C. Moule, Department of Chemistry, Brock University, St. Catharines, Ontario L2S3A1, Canada

V. Mujica, Facultad de Ciencias, Escuela de Quimica, Universidad Central de Venezuela, Caracas 1020A, Venezuela

P. K. Mukherjee, Spectroscopy Department, Indian Association for the Cultivation of Science, Calcutta 700 032, India

A. Nagy, Lajos Kossuth University, Department of Theoretical Physics, Lajos Kossuth University, H-4010 Debrecen, Hungary

J. V. Ortiz, Department of Chemistry, Kansas State University, Manhattan, Kansas 66506-3701

A. A. Palma, Instituto de Fisica, Universidad Autónomo de Puebla, Puebla, Pue. 72570, Mexico

A. Papakondylis, Laboratory of Physical Chemistry, Department of Chemistry, University of Athens, 157 10 Zografou, Athens, Greece

D. E. Parry, School of Chemistry, University of Bristol, Bristol BS8 1TS, United Kingdom

R. L. Pavlov, Institute of Nuclear Research and Energy, Bulgarian Academy of Sciences, 1784 Sofia, Bulgaria

T. B. Pedersen, Department of Physical Chemistry, University of Santiago de Compostela, E-15706 Santiago de Compostela, Spain

Å. J. Petersson, Department of Quantum Chemistry, Uppsala University, SE-751 20 Uppsala, Sweden

O. Plashkevych, Theoretical Chemistry, Royal Institute of Technology, S-10044 Stockholm, Sweden

T. Privalov, Theoretical Chemistry, Royal Institute of Technology, S-10044 Stockholm, Sweden

P. Pyykkö, Department of Chemistry, Helsinki University, FIN-00014 Helsinki, Finland

J. Raber, Department of Quantum Chemistry, Uppsala University, SE-751 20 Uppsala, Sweden

S. Rettrup, Chemical Laboratory IV, Copenhagen University, DK-2100 Copenhagen, Denmark

G. Rivière, European Commission, DG Research, B-1049 Brussels, Belgium

J. Rung, Department of Quantum Chemistry, Uppsala University, SE-751 20 Uppsala, Sweden

U. Saalmann, Atomfysik, Stockholms Universitet, S-10405 Stockholm, Sweden

P. Salek, Theoretical Chemistry, Royal Institute of Technology, S-10044 Stockholm, Sweden

N. Salhi-Benachenhou, Department of Quantum Chemistry, Uppsala University, SE-751 20 Uppsala, Sweden

B. Silvi, Laboratoire de Chimie Théorique, Université Pierre et Marie Curie, 75252 Paris Cedex 05, France

Y. G. Smeyers, Instituto de Estructura de la Materia, C.S.I.C., 28006 Madrid, Spain

V. Srivastava, School of Physics, University of Hyderabad, Hyderabad 500 046, India

B. T. Sutcliffe, Laboratoire de Chimie Physique Moléculaire, Université Libre de Bruxelles, B-1050 Bruxelles, Belgium

O. Tapia, Department of Physical Chemistry, Uppsala University, SE-751 21 Uppsala, Sweden

D. Tzeli, Laboratory of Physical Chemistry, Department of Chemistry, University of Athens, 157 10 Zografou, Athens, Greece

J. T. Vaara, Department of Chemistry, University of Helsinki, FIN-00014 Helsinki, Finland

C. Valdemoro, Instituto de Matemáticas y Física Fundamental, C.S.I.C., Madrid 28006, Spain

A. J. C. Varandas, Departamento de Quimica, Universidade de Coimbra, P-3049 Coimbra Codex, Portugal

L. Veseth, Department of Physics, University of Oslo N-0316, Oslo, Norway

M. Villa, Instituto de Estructura de la Materia, C.S.I.C., 28006 Madrid, Spain

S. Wilson, Rutherford Appleton Laboratory, Chilton, Oxon OX11 0QX, United Kingdom

P. Tz. Yotov, Institute of Nuclear Research and Energy, Bulgarian Academy of Sciences, 1784 Sofia, Bulgaria

B. P. Zapol, Department of Theoretical Physics, Institute of Chemical Physics, University of Latvia, Riga LV-1586, Latvia

Density Matrices and Phase-Space Functions*

Jens Peder Dahl

Department of Chemistry, Technical University of Denmark

DTU 207, DK-2800 Lyngby, Denmark

Abstract

The phase-space representation of the one-particle density matrix is discussed, starting with Dirac's study of the Thomas-Fermi atom. The Weyl-Wigner description is reviewed. Its basic characteristics are illustrated with the harmonic oscillator as an example. Applications to many-electron systems are described, with emphasis on the free-electron gas, Thomas-Fermi theory, and atomic Hartree-Fock theory. The introduction of local-density functions via phase space is also discussed.

Contents

*Dedicated to Professor Per-Olov Lowdin

ADVANCES IN QUANTUM CHEMISTRY, VOLUME 39

0065-3276/01 $35 00

1 Introduction

In his *Note on Exchange Phenomena in the Thomas-Fermi Atom*, Dirac [1] made the following statement:

> Each three-dimensional wave function will give rise to a certain electric density. This density is really a matrix, like all dynamical variables in the quantum theory (although one usually considers only its diagonal elements, as one can insert these directly into one's picture of the atom)

In his paper, Dirac also referred to the electric density as the electron density. For an N-electron system in the Hartree-Fock description—which was the type of system discussed by Dirac—the electron density becomes a sum of contributions from N three-dimensional wave functions. Dirac denoted the operator behind the matrix by ρ and wrote, in his equation (8),

$$(q'|\rho|q'') = \sum_r (q'|r)(r|q''), \tag{1}$$

'with the single variable q being written to denote the three Cartesian coordinates x, y, z and also a spin variable '

Having introduced the density matrix, Dirac went on to reformulate elementary Hartree-Fock theory in terms of it. He then turned to the situation where 'the electron density ρ is spread over such a large volume of phase space that we can neglect the fact that the momenta p do not commute with the coordinates q and reduce our description of the atom to a classical one.' For use in this situation he assigned a phase-space function to any dynamical variable, and also replaced the density matrix by a density function in phase space. This, then, allowed him to relate the Thomas-Fermi description of the atom to the Hartree-Fock description, and to include exchange in Thomas-Fermi theory.

Thus, Dirac was the first to appreciate the importance of the density matrix in many-electron theory, and also the first to map it into a phase-space density. His introduction of the density matrix has been fully recognized in the literature, whereas little attention has been paid to his introduction of phase-space functions, beyond their use in the Thomas-Fermi model. The reason is probably that Dirac himself introduced the form of these functions under the simplifying assumptions spelled out above, and hence did not attempt to construct a complete phase-space theory. Nevertheless, his phase-space functions are the same as the ones that occur in the modern Weyl-Wigner description.

In the present paper, we focus on the Weyl Wigner description. We shall, in particular, discuss its theoretical basis and its connection with density-matrix

theory. We shall also present some important examples of its use.
As a starting point, we visit the world of the one-particle density matrix

2 The One-Particle Density Matrix

The notion of a density matrix was first introduced by von Neumann [2, 3] who made it the principal concept of quantum statistical mechanics. Dirac's density matrix is usually referred to as the *first-order reduced density matrix*, or the *one-particle density matrix*. It was embedded in the more general framework of statistical ensembles by Husimi [4], who also introduced an alternative phase-space distribution function, now known as the Husimi function. Husimi also discussed the introduction of higher-order reduced density matrices

Through the seminal works of Löwdin [5] and McWeeny [6, 7], reduced density matrices have become one of the most fundamental concepts in modern quantum chemistry. A large number of successive authors have significantly extended their use and added to our understanding of their properties.

Let us write

$$\gamma(x,x') = N \int \Psi(x,x_2,\ldots,x_N)\Psi^*(x',x_2,\ldots,x_N)dx_2 \quad .dx_N \tag{2}$$

for the one-particle density matrix, with x replacing the symbol q above. Ψ is the total, maybe approximate, normalized wavefunction for an N-electron system. We also introduce the spinless matrix by integrating over the spin variable σ,

$$\rho(\boldsymbol{r},\boldsymbol{r}') = \int \gamma(x,x')_{\sigma'=\sigma} d\sigma. \tag{3}$$

For a determinantal wavefunction built from an orthonormal set of spin-orbitals $\psi_1,\psi_2,\ldots,\psi_N$ we have

$$\gamma(x,x') = \sum_{i=1}^{N} \nu_i \psi_i(x)\psi_i^*(x') = \langle x|\hat{\gamma}|x'\rangle, \tag{4}$$

with all $\nu_i = 1$. $\hat{\gamma}$ is the density operator

$$\hat{\gamma} = \sum_{i=1}^{N} \nu_i |\psi_i\rangle\langle\psi_i|. \tag{5}$$

With the spin-orbitals being products of normalized spin functions and normalized and mutually orthogonal spatial orbitals, φ_k, we also have

$$\rho(\boldsymbol{r},\boldsymbol{r}') = \sum_{k=1}^{n} n_k \varphi_k(\boldsymbol{r})\varphi_k^*(\boldsymbol{r}') = \langle \boldsymbol{r}|\hat{\rho}|\boldsymbol{r}'\rangle, \tag{6}$$

with $n_k = 1$ or 2. The density operator $\hat{\rho}$ has the form

$$\hat{\rho} = \sum_{k=1}^{n} n_k |\varphi_k\rangle\langle\varphi_k|. \tag{7}$$

For more general N-electron wavefunctions, we may follow Löwdin [5] and introduce *natural orbitals*, and extend the summations in (4) and (6) accordingly. These expressions will then remain valid, with the sum of the occupation numbers $\nu_\imath$ or n_k being equal to N.

Let us recall that the trace of an operator $\hat{\Omega}$, evaluated over a complete linear space with the orthonormal basis $\Phi_1, \Phi_2, \ldots, \Phi_s, \ldots$ is defined as

$$Tr(\hat{\Omega}) = \sum_{s=1}^{\infty} \langle \Phi_s | \hat{\Omega} | \Phi_s \rangle, \tag{8}$$

and that for any two operators, $\hat{\Omega}_a$ and $\hat{\Omega}_b$, we have that

$$Tr(\hat{\Omega}_a \hat{\Omega}_b) = Tr(\hat{\Omega}_b \hat{\Omega}_a). \tag{9}$$

That the wavefunction Ψ be normalized to unity may then be expressed by requiring that the trace of $\hat{\rho}$, evaluated over the complete spin-free orbital space, equal N,

$$Tr(\hat{\rho}) = N. \tag{10}$$

The expectation value of an operator $\hat{A}$ which is a symmetric sum of spin-independent one-particle operators,

$$\hat{A} = \sum_{\imath=1}^{N} \hat{a}(\imath) \tag{11}$$

is given by

$$\langle \hat{A} \rangle = Tr(\hat{a}\hat{\rho}). \tag{12}$$

Similar expressions hold when the spin must be explicitly included, with $\hat{\rho}$ replaced by $\hat{\gamma}$, and the trace being evaluated over the complete spin-orbital space. In the following, we shall mainly limit ourselves to the spin-free expressions.

We note that the formulation of quantum mechanics as a trace algebra has been extensively discussed by Löwdin [8].

While the expectation value of an operator composed of one-particle operators may be evaluated exactly by means of the first-order reduced density

matrix, the second-order density matrix is required when two-particle operators are involved. If, however, the wavefunction Ψ is well represented by a single Slater determinant, then the first-order matrix is sufficient, as discussed in detail by Löwdin [5]. For a single determinant he actually showed how to express all the higher-order matrices in terms of the one-particle matrix $\gamma(x, x')$.

The fact that the electron density is a matrix, $\rho(\boldsymbol{r}, \boldsymbol{r}')$, implies that we don't understand its full nature unless we can expose its general and qualitative dependence on both $\boldsymbol{r}$ and $\boldsymbol{r}'$ or, equivalently, on $\frac{1}{2}(\boldsymbol{r}+\boldsymbol{r}')$ and $\boldsymbol{r}-\boldsymbol{r}'$. This dependence has been studied by some authors ([9, 10] and references therein). It has, for instance, been shown that the main impact of the presence of covalent bonding in molecules is concentrated in regions where $\boldsymbol{r} - \boldsymbol{r}'$ is non-zero. Further work in this field awaits to be done.

A viable alternative is to map the description into an $(\boldsymbol{r}, \boldsymbol{p})$ phase space. We shall now consider this alternative.

3 Dirac's Phase-Space Function

Let us begin by introducing the phase-space function that Dirac assigned to a dynamical variable $\hat{a}$, provided 'the electron density ρ is spread over such a large volume of phase space that we can neglect the fact that the momenta p do not commute with the coordinates q and reduce our description of the atom to a classical one.' It reads, in our notation,

$$a(\boldsymbol{r}, \boldsymbol{p}) = \int \langle \boldsymbol{r} + \tfrac{\boldsymbol{y}}{2} | \hat{a} | \boldsymbol{r} - \tfrac{\boldsymbol{y}}{2} \rangle e^{-\imath \boldsymbol{p}\cdot\boldsymbol{y}/\hbar} d\boldsymbol{y}. \tag{13}$$

Applying the definition to the density operator $\hat{\rho}$ gives

$$\tilde{\rho}(\boldsymbol{r}, \boldsymbol{p}) = \int \langle \boldsymbol{r} + \tfrac{\boldsymbol{y}}{2} | \hat{\rho} | \boldsymbol{r} - \tfrac{\boldsymbol{y}}{2} \rangle e^{-\imath \boldsymbol{p}\cdot\boldsymbol{y}/\hbar} d\boldsymbol{y}. \tag{14}$$

Dirac referred to this quantity as the electron density per volume $(2\pi\hbar)^3$ of phase space. We have marked it by a tilde ($\tilde{}$) to distinguish it from the density matrix (6) It is expedient to also introduce the corresponding density per unit volume,

$$f(\boldsymbol{r}, \boldsymbol{p}) = \left(\frac{1}{2\pi\hbar}\right)^3 \int \langle \boldsymbol{r} + \tfrac{\boldsymbol{y}}{2} | \hat{\rho} | \boldsymbol{r} - \tfrac{\boldsymbol{y}}{2} \rangle e^{-\imath \boldsymbol{p}\cdot\boldsymbol{y}/\hbar} d\boldsymbol{y}. \tag{15}$$

By integration over phase space it gives the total number of electrons.

The expressions (13) and (15) map the operator $\hat{a}$ into $a(\boldsymbol{r}, \boldsymbol{p})$ and the density matrix $\hat{\rho}$ into $f(\boldsymbol{r}, \boldsymbol{p})$. The equivalent of the trace operation was, however, not set up by Dirac who worked with the Hartree-Fock equations directly,

without introducing expectation values. Thus, his phase-space description was a rudimentary one. The phase-space functions $a(\boldsymbol{r},\boldsymbol{p})$ and $\tilde{\rho}(\boldsymbol{r},\boldsymbol{p})$ were explicitly introduced for a quasi-classical situation, and Dirac did not suggest to use them without this limitation. But as already stressed in the Introduction, the functions are the same as those that occur in the Weyl-Wigner representation, which we shall consider in the following section.

In that representation, the equivalent of the trace operation is integration over phase space. Thus, Eqs. (10) and (12) become

$$\int f(\boldsymbol{r},\boldsymbol{p})d\boldsymbol{r}d\boldsymbol{p} = N \tag{16}$$

and

$$\langle \hat{A} \rangle = \int a(\boldsymbol{r},\boldsymbol{p})f(\boldsymbol{r},\boldsymbol{p})d\boldsymbol{r}d\boldsymbol{p}. \tag{17}$$

The first of these expressions was implicitly present in Dirac's paper, but the second was not. As we shall see in the following section, it is by no means obvious that such a simple expression should hold.

4 The Weyl-Wigner Representation

As just mentioned, the phase-space representation characterized by the expressions (13)–(17) is the Weyl-Wigner representation. Thus, $f(\boldsymbol{r},\boldsymbol{p})$ is called the Wigner function, and $a(\boldsymbol{r},\boldsymbol{p})$ is called the Weyl transform of the operator $\hat{a}$. The Wigner function was introduced by Wigner in 1932 in a paper on the *Quantum Correction for Thermodynamic Equilibrium* [11]. The Weyl transform was introduced by Weyl in 1931, on the basis of group-theoretical arguments [12]. The synthesis of Weyl's and Wigner's approaches was primarily performed by Groenewold [13] and Moyal [14], but a large number of later authors have substantially contributed to the development. For a review, see [15].

In the present section, we shall consider some formal properties of the Weyl-Wigner representation. In so doing, it suffices to consider a single spinless particle, restricted to moving in one spatial dimension q, with p the corresponding momentum. The generalisation to three dimensions and several particles is straightforward.

With the particle in the quantum state $|\psi\rangle$, the position-space wavefunction $\psi(q) = \langle q|\psi\rangle$ and the momentum-space wavefunction $\phi(q) = \langle p|\psi\rangle$ are connected by a Fourier transformation,

$$\psi(q) = \sqrt{\frac{1}{2\pi\hbar}} \int \phi(p)e^{ipq/\hbar}dp, \qquad \phi(p) = \sqrt{\frac{1}{2\pi\hbar}} \int \psi(q)e^{-ipq/\hbar}dq, \tag{18}$$

with the integrations here, and in the following, being from $-\infty$ to ∞. The connection between the two wavefunctions allows us to write the Wigner function, the analog of (15), in two equivalent forms,

$$f(q,p) = \frac{1}{2\pi\hbar}\int \psi^*(q-y/2)\psi(q+y/2)e^{-ipy/\hbar}dy \tag{19}$$

and

$$f(q,p) = \frac{1}{2\pi\hbar}\int \phi^*(p-u/2)\phi(p+u/2)e^{iqu/\hbar}du. \tag{20}$$

These expressions display the symmetric way in which $f(q,p)$ depends on q and p. Integration gives

$$\int f(q,p)dp = \psi^*(q)\psi(q) = \rho(q), \tag{21}$$

$$\int f(q,p)dq = \phi^*(p)\phi(p) = \pi(p), \tag{22}$$

and

$$\int f(q,p)dqdq = 1. \tag{23}$$

$\rho(q)$ is the position-space density, $\pi(p)$ the momentum-space density. Similar integrations, in three dimensions, applied to the expression (15) give the electron density $\rho(\boldsymbol{r})$ and the momentum density $\pi(\boldsymbol{p})$ for the N-electron system

Thus, the Wigner function has the densities in position space and momentum space as proper marginal densities. This suggests that we follow Dirac and refer to $f(q,p)$ as the density in phase space. There are, however, difficulties with such an interpretation, for although $f(q,p)$ is real-valued it is not restricted to being positive or zero. The interpretation of $f(q,p)$ as a probability density would of course also be inconsistent with the uncertainty principle. Nevertheless, we may say that $f(q,p)$ is a measure of the way the phase-space point (q,p) supports the given quantum state. This statement may be made more precise by noting that we may also write

$$f(q,p) = \frac{1}{\pi\hbar}\langle\psi|\hat{\Pi}(q,p)|\psi\rangle = \frac{1}{\pi\hbar}Tr[|\psi\rangle\langle\psi|\hat{\Pi}(q,p)], \tag{24}$$

where $\hat{\Pi}(q,p)$ is an *inversion operator* with respect to the phase-space point (q,p) [16, 17, 18, 19]. It has the form

$$\hat{\Pi}(q,p) = \frac{1}{4\pi\hbar}\int\int e^{i(qu+pv)/\hbar}e^{-i(\hat{q}u+\hat{p}v)/\hbar}dudv. \tag{25}$$

It is hermitian and unitary, i. e.,

$$\hat{\Pi}(q,p)^\dagger = \hat{\Pi}(q,p), \qquad \hat{\Pi}(q,p)^2 = 1. \tag{26}$$

Next, let us consider the setup of the correspondence between a quantum-mechanical operator $\hat{a}$ and a phase-space function $a(q,p)$. The way in which Weyl defined this correspondence was to first represent $a(q,p)$ by its Fourier representation. He then identified the Fourier component of $\hat{a}$ with respect to the operator $\exp(\imath(\hat{q}u + \hat{p}v)/\hbar)$ with the Fourier component of $a(q,p)$ with respect to $\exp(\imath(qu+pv)/\hbar)$. The result may be expressed by means of the inversion operator (25) as

$$\hat{a} = \frac{1}{\pi\hbar}\int\int a(q,p)\hat{\Pi}(q,p)dqdp. \tag{27}$$

The inverse relation is

$$a(q,p) = 2Tr[\hat{a}\hat{\Pi}(q,p)]. \tag{28}$$

By evaluating the trace with respect to the $|q\rangle$ basis, one gets

$$a(q,p) = \int \langle q + \tfrac{v}{2}|\hat{a}|q - \tfrac{v}{2}\rangle e^{-\imath pv/\hbar}dv. \tag{29}$$

This is the basis for the relation (13).

A study of Weyl's correspondence rule (27) shows that if $a(q,p)$ is a function of q or p alone, then $\hat{a}$ is the same function of the operators $\hat{q}$ and $\hat{p}$. In the more general polynomial case, one obtains the operator $\hat{a}$ from the function $a(q,p)$ by the replacement of q and p by $\hat{q}$ and $\hat{p}$, respectively, followed by a proper symmetrization of products of non-commuting operators. Thus, the operator associated with the function $q^n p^m$ is

$$\hat{a} = \frac{1}{2^n}\sum_{r=0}^{n}\binom{n}{r}q^r p^m q^{n-r} = \frac{1}{2^m}\sum_{s=0}^{m}\binom{m}{s}p^s q^n p^{m-s}. \tag{30}$$

These expressions were first set up by McCoy [20]

Having defined the Weyl correspondence, one verifies that the mapping of operators on phase-space functions preserves the algebraic structure of the operator space. This means, firstly, that the mapping is linear such that linear combinations of operators are mapped onto the corresponding linear combinations of functions. Secondly, it means that if $\hat{c} = \hat{a}\hat{b}$, then the function $c(q,p)$ must be uniquely determined by the functions $a(q,p)$ and $b(q,p)$. But it cannot be simply the product of the two functions, for this would imply that we associate the same functions with the operators $\hat{a}\hat{b}$ and $\hat{b}\hat{a}$ which cannot be

correct, because these operators are, in general, different. Instead, $c(q,p)$ is a so-called star product of $a(q,p)$ and $b(q,p)$, and we write

$$c(q,p) = a(q,p) \star b(q,p). \tag{31}$$

The multiplication is non-commutative, but it must be associative, so that the relation

$$\hat{a}(\hat{b}\hat{c}) = (\hat{a}\hat{b})\hat{c} \tag{32}$$

is conseved under the mapping.

The explicit form of the star product contained in the mapping may be written in the following way,

$$a(q,p) \star b(q,p) = \exp\left[\frac{i\hbar}{2}\left(\frac{\partial}{\partial q_1}\frac{\partial}{\partial p_2} - \frac{\partial}{\partial p_1}\frac{\partial}{\partial q_2}\right)\right] a(q,p)b(q,p). \tag{33}$$

The subscript 1 on a differential operator indicates that this operator acts only on the first function in the product $a(q,p)b(q,p)$. Similarly, the subscript 2 is used with operators that only act on the second function in the product

The image of the commutator $\hat{a}\hat{b} - \hat{b}\hat{a}$ is called the *Moyal bracket* and denoted $\{a(q,p), b(q,p)\}_M$. It follows from the above expression that it may be written,

$$\{a(q,p), b(q,p)\}_M = \frac{2}{\hbar}\sin\left[\frac{\hbar}{2}\left(\frac{\partial}{\partial q_1}\frac{\partial}{\partial p_2} - \frac{\partial}{\partial p_1}\frac{\partial}{\partial q_2}\right)\right] a(q,p)b(q,p). \tag{34}$$

Let us finally consider the equivalence between the trace operation and integration over phase space. A comparison of the expressions (19) and (29) shows that the Wigner function is the Weyl transform of the operator $\frac{1}{2\pi\hbar}|\psi\rangle\langle\psi|$. The operator $|\psi\rangle\langle\psi|$ has trace one, and according to Eq. (23), the Wigner function is normalized to 1 on phase space. For this to be true, the general relation must be

$$Tr(\hat{a}) = \frac{1}{2\pi\hbar}\int a(q,p)dqdp. \tag{35}$$

For the trace of an operator product we get,

$$Tr(\hat{a}\hat{b}) = \frac{1}{2\pi\hbar}\int a(q,p) \star b(q,p)dqdp. \tag{36}$$

One finds, however, that the star product under the integral sign may be replaced by the ordinary product, so that we also have,

$$Tr(\hat{a}\hat{b}) = \frac{1}{2\pi\hbar}\int a(q,p)b(q,p)dqdp \tag{37}$$

The reason for this simple result may be seen to be that the inversion operator $\hat{\Pi}(q,p)$ in (25), which generates the Weyl transformation, is equal to its own inverse. This is the second relation in (26). The Weyl-Wigner representation is said to be self-dual. This point has been further discussed by the author [21, 22], in an analysis of a wider class of phase-space representations.

By using the relation (37) together with the fact that the Wigner function is the Weyl transform of the operator $\frac{1}{2\pi\hbar}|\psi\rangle\langle\psi|$, we get the following important result:

$$\langle\psi|\hat{a}|\psi\rangle = Tr(\hat{a}|\psi\rangle\langle\psi|) = \int a(q,p)f(q,p)dqdp. \tag{38}$$

This relation contains the justification for the relation (17). With $a(q,p)$ being another Wigner function it also shows that

$$\int f_1(q,p)f_2(q,p)dqdp = \frac{1}{2\pi\hbar}\langle\psi_1|\psi_2\rangle\langle\psi_2|\psi_1\rangle, \tag{39}$$

where $f_1(q,p)$ and $f_2(q,p)$ are the Wigner functions corresponding to the two states $|\psi_1\rangle$ and $|\psi_2\rangle$, respectively.

5 The Harmonic Oscillator

As a simple example, let us consider the Wigner function for a one-dimensional harmonic oscillator. For simplicity, we put $\hbar = 1$ and introduce dimensionless coordinates and momenta so that the Hamiltonian becomes

$$H = \tfrac{1}{2}p^2 + \tfrac{1}{2}q^2. \tag{40}$$

The eigenstates and their energies are given by the well-known expressions

$$\psi_n(q) = \sqrt{\frac{1}{2^n n!\sqrt{\pi}}}\, H_n(q)e^{-\frac{1}{2}q^2}, \qquad E_n = n + \tfrac{1}{2}, \quad n = 0,1,2,\ldots \tag{41}$$

where $H_n(q)$ is the nth Hermite polynomial [23].

The Wigner function for the harmonic oscillator was first determined by Groenewold [13], and independently by Bartlett and Moyal [24], and Takabayasi [25], as well as later authors. Two independent derivations have also been given by the present author [18, 26]. We have,

$$f_n(q,p) = \frac{(-1)^n}{\pi}e^{-R^2}L_n^{(0)}(2R^2), \qquad R^2 = q^2 + p^2, \tag{42}$$

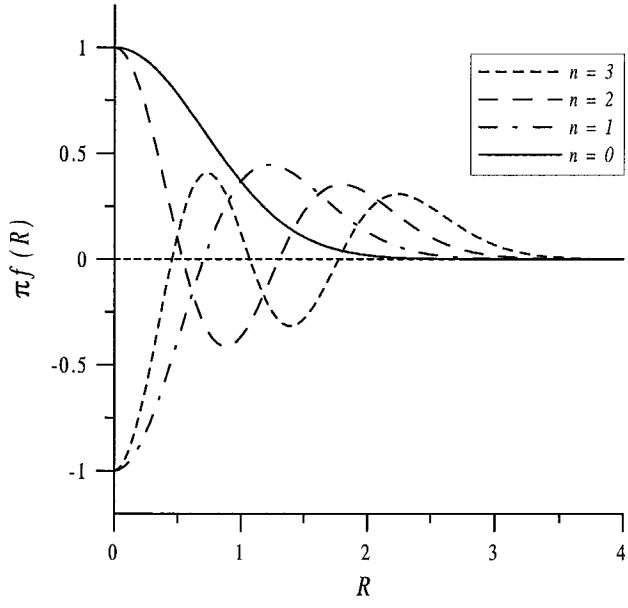

Figure 1: Wigner functions for the four lowest states of the harmonic oscillator

where $L_n^{(0)}(2R^2)$ is a Laguerre polynomial [23],

$$L_n^{(m)}(x) = \frac{(m+n)!}{m!n!}\,{}_1F_1(-n, m+1, x). \tag{43}$$

According to the expression (24), $f(q,p)$ equals $1/\pi\hbar$ times the expectation value of an operator that inverts in the phase-space point (q,p). The states of the harmonic oscillator are alternately even and odd under inversion in the origin. In accordance with this, we see that

$$f_n(0,0) = \frac{(-1)^n}{\pi}, \qquad (\hbar = 1). \tag{44}$$

The expectation value of an inversion operator can never be numerically larger than 1. Hence we have, for any Wigner function, that

$$|f(q,p)| \leq 1/\pi\hbar. \tag{45}$$

The Wigner function for the lowest four states of the harmonic oscillator are shown in Figure 1.

6 The Free-Electron Gas

Let us now return to the three-dimensional case and the relations of Section 3. We begin by looking at a hypothetical situation where the sum in Eq. (7) extends to infinity, and $n_k = 2$ for all k. This corresponds to a completely filled 'sea' of electrons, the number 2 referring to the two spin states. The general completeness relation

$$\sum_{k=1}^{\infty} |\varphi_k\rangle\langle\varphi_k| = 1 \tag{46}$$

gives then that $\hat{\rho} = 2$, and the Wigner function (15) becomes

$$f(\boldsymbol{r}, \boldsymbol{p}) = \frac{2}{(2\pi\hbar)^3}, \tag{47}$$

where we have used that

$$\langle \boldsymbol{r}' | \boldsymbol{r}'' \rangle = \delta(\boldsymbol{r}' - \boldsymbol{r}''). \tag{48}$$

This corresponds to two electrons per volume $(2\pi\hbar)^3$ of phase space. It is the value that one associates with 'saturation' of phase space. For a single electron, the generalization of the relation (45) leads to the general requirement that $|f(\boldsymbol{r}, \boldsymbol{p})| \leq 1/(\pi\hbar)^3$.

Next, let us consider a Wigner function corresponding to saturation for all values of $\boldsymbol{r}$, and for values of $\boldsymbol{p}$ for which $|\boldsymbol{k}| \leq K$, where we have put $\boldsymbol{p} = \hbar\boldsymbol{k}$. For larger values of K, the Wigner function is taken to be zero. We want to determine the density matrix corresponding to this distribution of electrons which is referred to as a free-electron gas.

To this end, we note that the expression (15) for $f(\boldsymbol{r}, \boldsymbol{p})$ may be inverted to give

$$\rho(\boldsymbol{r}, \boldsymbol{r}') = \int f\left(\tfrac{1}{2}(\boldsymbol{r} + \boldsymbol{r}'), \boldsymbol{p}\right) e^{i\boldsymbol{p}\,(\boldsymbol{r}-\boldsymbol{r}')/\hbar} d\boldsymbol{p}. \tag{49}$$

Let us define the relative position vector $\boldsymbol{s} = \boldsymbol{r} - \boldsymbol{r}'$ and then introduce spherical polar coordinates (k, θ, ϕ) for the vector $\boldsymbol{k}$ relative to the direction of $\boldsymbol{s}$. We get then,

$$\rho(\boldsymbol{r}, \boldsymbol{r}') = \frac{2}{(2\pi\hbar)^3} \int_0^{2\pi} d\phi \int_0^{\pi} \sin\theta d\theta\, \hbar^3 \int_0^{K} e^{iks\cos\theta} k^2 dk \tag{50}$$

which is readily evaluated to give

$$\rho(\boldsymbol{r}, \boldsymbol{r}') = \frac{K^3}{\pi^2} \frac{\sin(Ks) - Ks\cos(Ks)}{(Ks)^3}, \qquad \boldsymbol{s} = \boldsymbol{r} - \boldsymbol{r}'. \tag{51}$$

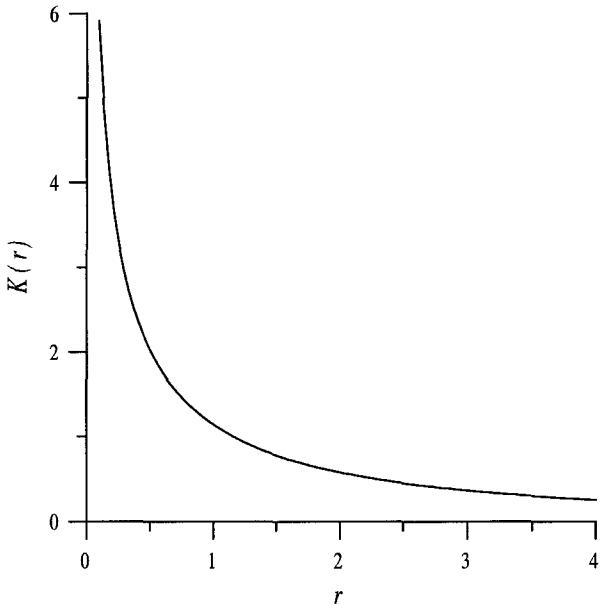

Figure 2: Thomas-Fermi boundary curve for the helium atom. Atomic units.

This is a well-known result in the theory of the free-electron gas, but it is usually derived with a Slater determinant of plane waves as a starting point (See, for instance, [27]). The present derivation is a simple alternative.

By allowing the value of K to depend upon $\boldsymbol{r}$, we make a valuable contact to Thomas-Fermi theory [28, 29]. For an atom, we assume that K merely depends upon the magnitude of $\boldsymbol{r}$. The expression (50) is then still valid, but as the expression for the Wigner function shows, we must interpret K as $K(\frac{1}{2}(\boldsymbol{r}+\boldsymbol{r}'))$. With this modification. the expression(51) also remains valid

The problem in atomic Thomas-Fermi theory is to determine the boundary curve $K = K(r)$. This is done by variational methods, and results in the following expression, in atomic units,

$$K(r) = \sqrt{\frac{2Z}{r}\phi(r/\mu)}, \qquad \mu = 0.885341 Z^{-1/3}. \tag{52}$$

It is valid for all neutral atoms. $\phi(r/\mu)$ is a universal function. An approximate analytical expression has ben given by Latter [30].

Figure 2 shows the function $K = K(r)$, with the helium atom ($Z = 2$) as an example.

7 Atoms in Phase Space

The Wigner function $f(\boldsymbol{r},\boldsymbol{p})$ for a real atom depends on three position variables and three momentum variables. For a closed-shell atom it is independent of the three Euler angles that describe the orientation of the $(\boldsymbol{r},\boldsymbol{p})$ plane. Hence, it may be reduced to a function of (r,p,u), where r and p are the magnitudes of $\boldsymbol{r}$ and $\boldsymbol{p}$, respectively, and u is the angle between $\boldsymbol{r}$ and $\boldsymbol{p}$. Integrating over the Euler angles and multiplying by r^2p^2, from the volume element, gives the function

$$\tilde{F}(r,p,u) = 8\pi^2 r^2 p^2 f(\boldsymbol{r},\boldsymbol{p}). \tag{53}$$

We have made a very detailed study of this function for the ground state of the hydrogen atom [31]. It is found to be large and non-negative in a dominant region where $\boldsymbol{r}$ and $\boldsymbol{p}$ are perpendicular to each other. Outside this region it is characterized by an oscillatory behavior, although the amplitudes of the oscillations are fairly small. Integrating $\tilde{F}(r,p,u)$ over u leads to a function that we denote $F(r,p)$. Figure 3 is a contour map of this function for the hydrogen atom. It has a large positive region and regular, albeit weak, damped oscillations when the product of r and p is large. Similar contour maps have been worked out for the ground state of a hydrogen atom in higher dimensions [32].

We have performed a related analysis for a number of closed-shell Hartree-Fock atoms [33] and presented contour maps similar to that of Figure 3, both for the various shell contributions and for the total electron distribution We have also related the form of the total distribution to the shape of the Thomas-Fermi curve. A comparison between Figure 2 and Figure 3 already indicates the satisfactory, albeit very qualitative, correlation that exists between the quantitative phase-space description and the very approximate Thomas-Fermi description. For further analysis of many-electron results, we refer to [33].

The expression (17) for the expectation value of a many-electron operator $\hat{A}$ of the type (11) is a natural starting point for the definition of a local position-space density for a given electronic state. Thus, we may define the local-density function

$$\tilde{a}(\boldsymbol{r}) = \int a(\boldsymbol{r},\boldsymbol{p}) f(\boldsymbol{r},\boldsymbol{p}) d\boldsymbol{p}, \tag{54}$$

from which the expectation value of $\hat{A}$ emerges as

$$\langle \hat{A} \rangle = \int \tilde{a}(\boldsymbol{r}) d\boldsymbol{r}. \tag{55}$$

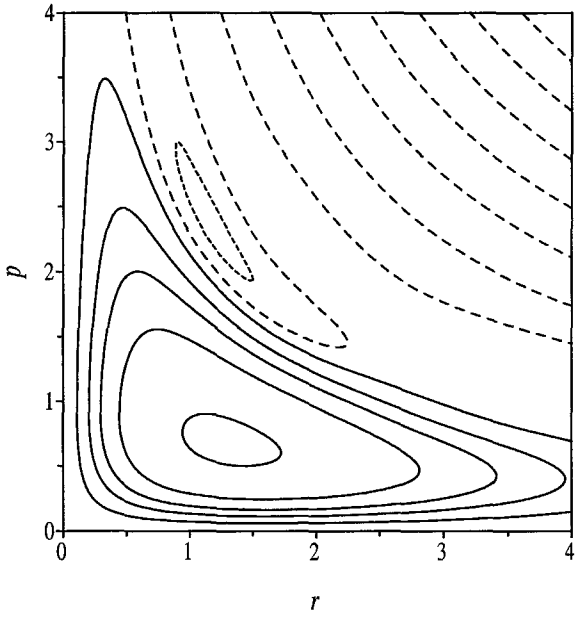

Figure 3: Contour curves for the Wigner function $F_{1s}(r,p)$ for the hydrogen atom. The contour values are the following: positive (solid curves), 0.5, 0.2, 0.1, 0.05, 0.015; dashed, 0 0; negative (dotted) -0.01. Atomic units.

Local densities have played a large role in the development that has led to modern density-functional theory, and although (54) is only one out of several possible definitions of a local density, it turns out to have a number of qualitatively superior features. This has been demonstrated for local kinetic-energy densities and local exchange-energy densities in [34, 35, 36].

8 Conclusions

We have presented a brief review of the Weyl-Wigner phase-space representation of quantum mechanics, with emphasis upon its relation to the theory and applications of the one-particle density matrix. We have stressed the fundamental importance of the generalized inversion operator (25) as the generator of the Weyl transformation. It is the fact that this generator is its own inverse, that has caused the Weyl-Wigner representation to become the canonical phase-space representation. A number of additional phase-space distributions

satisfying the marginal conditions (21) and (22) may be introduced [37], and they are sometimes used, but they are not self dual and must be used in pairs. Phase-space distributions that do not satisfy the marginal conditions are also used. Thus, the Husimi distribution mentioned in Section 2 is quite popular. It is everywhere non-negative and corresponds to convoluting the Wigner function with the Wigner function for a minimum-uncertainty state. For its use in analyzing electronic densities, see for instance [38, 39].

As a point of some historical significance, we have discussed Dirac's early introduction of quantum-mechanical phase-space functions. We have emphasized that his work on Thomas-Fermi theory may be considered a precursor of modern phase-space theory.

The examples that we have discussed in our communication have been tied to the harmonic oscillator, the free-electron gas, Thomas-Fermi theory, atomic Hartree-Fock theory, and density-functional theory. For the latter, we have discussed the introduction of local-density functions for operators of the type (11).

In closing, we emphasize that the Weyl-Wigner representation of quantum mechanics also has a natural role to play in several other branches of physics. We mention, in particular, spectroscopy, quantum optics and the discussion of the classical limit of quantum mechanics.

References

[1] P. A. M. Dirac, Proc. Cambridge Phil. Soc. **26**, 376 (1930).

[2] J. von Neumann, Gött. Nachr. **1927**, 245, 273.

[3] J. von Neumann, *Mathematische Grundlagen der Quantenmechanik* (Springer, Berlin, 1932); English translation by R. T. Beyer, *Mathematical Foundations of Quantum Mechanics* (Princeton University Press, 1955).

[4] K. Husimi, Proc Phys. Math. Soc. Japan **22**, 264 (1940).

[5] P.-O. Löwdin, Phys. Rev. **97**, 1474, 1490, 1509 (1955).

[6] R. McWeeny, Proc Roy. Soc. London, Ser. A **232**, 114 (1955).

[7] R. McWeeny, Rev. Mod. Phys. **32**, 335 (1960).

[8] P.-O. Löwdin, Int. J. Quantum Chem. **12**, Suppl. 1, 197 (1955).

[9] T. Asthalter and W. Weyrich, Ber. Bunsenges. Phys. Chem **96**, 1747 (1992).

[10] H. Schmider and V. H. Smith, Jr. Theoret. Chim. Acta **86**, 115 (1993).

[11] E. Wigner, Phys. Rev. **40**, 749 (1931).

[12] H. Weyl, *The Theory of Groups and Quantum Mechanics* (Methuen, London, 1931).

[13] H. J. Groenewold, Physica **12**, 405 (1946).

[14] J. E. Moyal, Proc. Cambridge Phil. Soc. **45**, 99 (1949).

[15] M. Hillery, R.F. O'Connell, M. O. Scully, and E. P. Wigner, Physics Reports **106**, 121 (1984).

[16] A. Grossmann, Commun. Math. Phys. **48**, 191 (1976).

[17] A. Royer, Phys. Rev. A **15**, 449 (1977).

[18] J. P. Dahl, Phys. Scripta **25**, 499 (1982).

[19] J. P. Dahl, Physica **114A**, 439 (1982).

[20] N. H. McCoy, Proc. Natl. Acad. Sci. U.S.A. **18**, 674 (1932).

[21] J. P. Dahl, in *Classical and Quantum Systems*, p.420 (Eds. H. D. Doebner, W. Scherer and F. Schroeck, Jr., World Scientific, Singapore, 1993).

[22] J. P. Dahl, in *Conceptual Trends in Quantum Chemistry*, p. 199 (Eds. E. S. Kryachko and J. L. Calais, Kluwer, The Netherlands, 1994).

[23] M. Abramowitz and I. A. Stegun, *Handbook of Matematical Functions* (Dover, 1965).

[24] M. S. Bartlett and J. E. Moyal, Proc. Cambridge Philos. Soc. **45**, 545 (1949).

[25] T. Takabayasi, Prog. Theor. Phys. (Japan) **11**, 341 (1954).

[26] J. P. Dahl, in *Energy Storage and Redistribution in Molecules*, p. 557 (Ed J. Hinze, Plenum, New York, 1983).

[27] P. Gombas, *Pseudopotentiale* (Springer, Wien, 1967).

[28] L. H. Thomas, Proc. Cambridge Phil. Soc. **23**, 542 (1926).

[29] E. Fermi, Z. Physik **48**, 73 (1928).

[30] R. Latter, Phys. Rev. **99**, 510 (1955).

[31] J. P. Dahl and M. Springborg, Mol. Phys. **47**, 1001 (1982).

[32] J. P. Dahl, in *Dimensional Scaling in Chemical Physics*, p. 165 (Eds. D. R. Herschbach, J. Avery and O. Goscinski, Kluwer, Dortrecht, 1993).

[33] M. Springborg and J. P. Dahl, Phys. Rev. A **36**, 1050 (1987).

[34] M. Springborg and J. P. Dahl, in *Local Density Approximations in Quantum Chemistry and Solid-State Physics*, p. 381 (Eds. J. P. Dahl and J. Avery, Plenum, New York, 1984).

[35] J. P. Dahl and B. Amstrup, J. Mol. Struct. (Theochem) **261**, 345 (1992).

[36] M. Springborg and J. P. Dahl, J. Chem. Phys. **110**, 9360 (1999).

[37] L. Cohen, J. Math. Phys. **7**,781 (1966).

[38] J. E. Harriman and M. E. Casida, Int. J. Quantum Chem. **45**, 263 (1993).

[39] H. Schmider, J. Chem. Phys. **105**, 3627 (1996).

Correlation Corrected Hartree-Fock and Density Functional Computations on Periodic Polymers

by

Janos Ladik[a†], Ferenc Bogar[ab] &

Vick Van Doren[c],

[a] *Chair for Theoretical Chemistry and Laboratory of the National Foundation for Cancer Research, University Erlangen- Nürnberg, Egerlandstr. 3, D-91058 Erlangen, Germany.*

[b] *Institute for Theoretical Physics, University of Szeged, Tisza L. k-rl. 84-86, H-6720 Szeged, Hungary.*

[c] *Department of Physics, University of Antwerp (RUCA), Groenenbergenlaan 171, B3030 Antwerpen, Belgium*

Abstract

Ab initio Hartree-Fock (HF) band structures and crystal orbitals were calculated for polyethylene, for polytetrafluoroethylene, for polyparaphenylene and for the nucleotide base stacks. The HF results were corrected for correlation using the inverse Dyson equation in its diagonal approximation. The self energy was computed in the Moeller Plesset 2 (MP2) level taking into account also relaxation. The quasi particle energies, giving the correlation corrected band structures were iterated until selfconsistency.The band structures of the same periodic polymers were also computed using the density functional theory (DFT) in the form applied in Mintmire's program for periodic polymers.The resulting physically most interesting features (widths and positions of the valence-and conduction bands, respectively, ionization, potentials and electron affinities, the value of the fundamental gap) of the resulting band structures using the mentioned three different methods will be

ADVANCES IN QUANTUM CHEMISTRY VOLUME 39

0065-3276/01 $35 00

compared. Whenever experimental data are available they will be used for comparison.

Contents

† Corresponding author

1 Introduction

As it is well known, 1D, 3D and 3D polymers have a continuously increasing importance in material science as structural elements (plastics) and as biopolymers (DNA, RNA, proteins, polysacharides etc.) they play a key role in life processes. Recently they have become important in non-linear optics, in the construction of protheses, new kind more effective batteries with larger stronger capacities (which is very important in the development of electric cars) and as light emitting diodes. Further already polymer based lasers exist and it seems so that further miniaturization of chips will be possible only if one turns to polymers. This latter fact will make in the near future polymers very important in computer technology, too.

Therefore, the band structure of periodic polymers it is important to understand the different physical and chemical properties of these systems. To obtain a good quality band structure (with a fundamental gap not too far from the experimental value) one has to perform either a Hartree-Fock (HF) [1] crystal orbital (CO) calculation with a good quality basis set and correct this band structure for correlation using the electronic polaron model [3] in its *ab initio* form (for details see next section). The correlation corrected so-called quasi particle band structures can be used then for the calculation of ionization

potentials, of exciton spectra applying the intermediate exciton model, for the determination of transport, mechanical, nonlinear optical etc. properties of the corresponding polymers.

On the other hand, the computation of the quasi particle band structure of a periodic polymer with a larger unit cell is very CPU time consuming. Therefore, at least for their ground state properties density functional theory (DFT) methods have been tried also One hopes that in the next few years DFT methods which treat successfully the excited states and virtual bands of periodic polymers will exist also.

The purpose of this paper is to compare HF+ correlation corrected band structures with those computed with the help of the DFT method in the form which is used in Mintmire's polymer program [3]. Comparative calculations were performed for polyethylene, for tetrafluoroethylene (teflon), for polyparaphenylene and for the nuelcotide base stacks.

In section 2, we shall summarize the methods used and in section 3 the results obtained for the above mentioned polymers will be compared. A short section of conclusion will be at the end of the paper.

2 Methods

The Hartree-Fock crystal orbital (CO) method is described in numerous places in detail, therefore here we only call the attention to the references given as [1]. It should be mentioned that the method is formulated in the 1D case not only for simple translation, but also for general periodic symmetry operations (like translation and rotation) [4]. In references [1] and in a recent review paper [5] the problem of balanced and accurate enough cut off of the different types of integrals occurring in the expressions are also discussed. One should mention that the method is formulated and coded for 3D crystals [6].

To correct the band structure for correlation one can start from the Dyson equation in its matrix form

$$\mathbf{G} = \mathbf{G_0} + \mathbf{G_0}\boldsymbol{\Sigma}\mathbf{G} \tag{1}$$

$$\mathbf{G_0} = \frac{\mathbf{1}}{\boldsymbol{\omega} - \boldsymbol{\varepsilon}^{\mathbf{HF}}} \tag{2}$$

$$\mathbf{G} = \frac{\mathbf{1}}{\boldsymbol{\omega} - \boldsymbol{\varepsilon}^{\mathbf{HF}} - \boldsymbol{\Sigma}} \tag{3}$$

Here $\mathbf{G_0}$ and $\mathbf{G}$ are the unperturbed, or perturbed Green's matrices, respectively, and the diagonal $\boldsymbol{\omega}$ and $\boldsymbol{\varepsilon}^{\mathbf{HF}}$ matrices contain as elements the quasi particle energies ω_I (the combined index I stands for the band index i and a

k-value k_i) and HF energies ε_I^{HF}, respectively. Finally the non-diagonal matrix $\mathbf{\Sigma}$ is the self-energy matrix.

It was shown that in the cases of excitation and ionization energies of molecules if one neglects the off-diagonal elements of $\mathbf{\Sigma}$ (using the CI method or many body perturbation theory (MBPT), the error is very small [7]. Therefore, one can expect that there is a similar situation also in the case of the band structures of polymers.

Multiplying equ. (1) from the left by $\mathbf{G_0^{-1}}$ and from the right by $\mathbf{G}^{-1}$ one obtains the inverse Dyson equation [8]

$$\mathbf{G_0^{-1}} = \mathbf{G}^{-1} + \mathbf{\Sigma} \tag{4}$$

and in the diagonal approximation

$$\left(\mathbf{G_0^{-1}}\right)_{I,I} = \left(\mathbf{G}^{-1}\right)_{I,I} + (\mathbf{\Sigma})_{I,I} \tag{5}$$

Since $(\mathbf{G}^{-1})_{I,I}$ at a pole is 0 $\left(\omega_I - \varepsilon_I^{HF} - [\mathbf{\Sigma}]_{I,I} = 0\right)$one obtains finally for the quasi particle energies the equation

$$\omega_I = \varepsilon_I^{HF} + [\mathbf{\Sigma}(\boldsymbol{\omega_I})]_{I,I} \tag{6}$$

($\mathbf{\Sigma}$ is generally a function of the ω_Is)

For $[\mathbf{\Sigma}(\boldsymbol{\omega_I})]_{I,I}$ one can apply in the case of polymers any size extensive method if one wishes to apply equ.(4) for the correlation correction of the band structure. This can be in the simplest case MBPT in its Moeller-Plesset (MP) form [9]. In actual polymer calculations (with very few exceptions) the MP method was applied in its second order (MP2; the MP1 energy is already contained in the HF total energy). In this case

$$\begin{aligned}
[\mathbf{\Sigma}(\boldsymbol{\omega_I})]_{I,I} &= \left[\mathbf{\Sigma}(\boldsymbol{\omega_I})^{\mathbf{MP2}}\right]_{I,I} \\
&= \lim_{\eta \to 0} \left[\sum_{\substack{J \in occ \\ A,B \in unocc.}} \frac{V_{IJAB}\left(2V^*_{IJAB} - V^*_{IJBA}\right)}{\omega_I + \varepsilon_J^{HF} - \varepsilon_A^{HF} - \varepsilon_B^{HF} + i\eta} \right. \\
&\quad \left. + \sum_{\substack{J \in unocc \\ A,B \in occ.}} \frac{V_{IJAB}\left(2V^*_{IJAB} - V^*_{IJBA}\right)}{\omega_I + \varepsilon_J^{HF} - \varepsilon_A^{HF} - \varepsilon_B^{HF} - i\eta} \right]
\end{aligned} \tag{7}$$

as can be shown [10] on the basis of the electronic polaron model [3] if one takes into accountalso relaxation [11]. In equ. (5) the matrix elements V_{IJAB} are defined as

$$V_{IJAB} = \left\langle \phi_I(\mathbf{r_1})\,\phi_J(\mathbf{r_2}) \left| \frac{1}{r_{12}} \right| \phi_A(\mathbf{r_1})\,\phi_B(\mathbf{r_2}) \right\rangle \tag{8}$$

where in the 1D case $\phi_I(\mathbf{r_1})$ etc. are HF crystal orbitals which are linear combinations of Bloch orbitals,

$$\phi_I(\mathbf{r_1}) = \frac{1}{\sqrt{2N+1}} \sum_{t=-N}^{N} e^{ik_i t} \sum_{s=1}^{m} c_{i,s}(k_i)\, \chi_s^t \tag{9}$$

Here $2N+1$ is the number of unit cells, m the number of Gaussians in the unit cell, a the elementary translation, the $c_{i,s}$ the LCAO coefficients and χ_s^t stands for the s-th basis function in the cell characterized by t.a.

The non-linear system of equations (4) - (5) can be solved with a vectorized program quite quickly in a few iteration steps [13]. This is, however, true only in the case of insulators or semiconductors with a non-negligible gap. In this case among the different solutions of (4) there is always a main value with a pole strength

$$P_I = \left[1 - \left(\frac{\partial \left[\mathbf{\Sigma}(\boldsymbol{\omega})_{\mathbf{I,I}}\right]}{\partial \omega}\right)_{\omega=\omega_I}\right]^{-1} \tag{10}$$

[8]. Not this is the case, however, for metals with partially filled bands, where there are many P_I values of the order 0.1 - 0.3. In this case one has to write into equ. (5) instead of ω_I, ε_I^{HF} and determine in this way (without) iterations) the ω_I values from equ. (4).

One should mention that if in the course of the calculation of $\left[\mathbf{\Sigma}(\boldsymbol{\omega_I})_{\mathbf{I,I}}\right]$ poles occurs one has to apply the principal value theorem and takes for ω_I-s the real part of the result.

One should try of course to use instead of MBPT some other methods, like the coupled cluster approach (which was introduced to shell-physics using a diagrammatic technique first by Cizek [13]). We have programmed this method in the $\hat{T}_2 + \frac{1}{2}\hat{T}_2\hat{T}_2$ ($\hat{T}_2$ contains all double excitations) approximation and have performed a band structure calculation for alternating trans polyacetylene. In this way we have obtained 110% of the MP2 total energy per unit cell and the decreased in a small amount as compared to the quasi particle gap obtained with the MP2 method. On the other hand the calculation required very large CPU times even for this system with small unit cell and with optimally localized Wannier functions [14] (in the quasi particle band structure calculations it is advantageous to perform the four index transformations from AO-s to CO-s for non-metallic systems in two steps. First the AO-s are transformed to Wannier functions and afterwards from the Wannier functions CO-s are computed [15]).

Turning now to the density functional method applied in Mitmire's program [3] written for 1D periodic polymers with a general symmetry operation. The program uses the LDA approximation with a separate exchange and correlation

functional. For the exchange functional [16], [17] either the Gaspar-Kohn-Sham (GKS) [16] or the Kohn-Sham [17] functionals were used. For the correlation functional the Perdew-Zunger (PD) analytic fit [18] to the numerical electron gas correlation results of Ceperley, and Alder [19] was applied. These exchange and correlation functionals as well the change density were expressed as linear combinations of auxiliary Gaussian basis sets [3]. Both these basis functions as well the nuclear cantered Gaussians used for the CO-s were optimized for LDA calculations by, Godbout et al. [30]. Their results can be easily expressed in Huzinaga's notation [31] (see [3]). The program automatically cuts off the different types of integrals by given cut off radii [3]. The rest of the Coulomb integrals after the cut off is calculated by a multipole expansion [32].

3 Results and their Discussion

3.1 Polyethylene and polyetrafluoroethylene

There is an HF + MP2 calculation for polyethylene (PE) [23]. A 6-31 G**- and Clementi's double ζ basis [24] was applied and a geometry optimization was performed both at the HF and MP2 level. In the first PE calculation no relaxation was applied for the self energy and no iterations were performed. This is equivalent to Suhai's original formalism [10] which takes the differences of the N (ground state), N+1 (one additional electron in the conduction band) and N-1 systems (one hole in the valence band) and calculates the total energy differences with the help of the pair correlation functions [10]. In the second case the inverse Dyson equation with the self energy (7) was solved iteratively [32].

The gap value obtained in the first case was 10.3 eV, while in the second case it is 11.6 eV [35] (due to the poorer basis). In this case the lower edge of the conduction band lies at 3.4 cV while $\varepsilon_{v,\max}(QP)$ is at -8.3 eV. The latter value agrees quite well with the experimental ionization potentials (7.6 - 8.8 eV) [36]. From the large gap, high lying $\varepsilon_{v,\min}(QP)$ and low lying $\varepsilon_{v,\max}(QP)$ it is clear that there is no hope of doping PE and making it in this way better conducting though the widths of the valence and conduction bands, respectively, is quite large (6.5 and 5.1 eV, respectively). The gap values (10.3 and 11.6 eV, respectively) in both calculations are substantially larger than the estimated experimental value of 8.8 eV [36]. Most probably if one would use much more many neighbors's interactions (in the second calculation the number of neighbors explicitly taken into account was five), use a high level basis set and would use for the Coulomb integrals for the part remaining after the cut off the multipole expansion [32], one would get down the theoretical gap close to the experimental one. One should mention that no total energy

per. unit cell calculation was performed for PE at the correlation corrected level.

For PE also a density functional calculation was performed [27] using both the GKS [16] and KS [17] exchange potentials and the form of the LDA method described above. The geometry was minimized for different dihedral angles. The minimum of the total energy per unit cell was found in the planar zig-zag conformation in good agreement with experiment. A second with about 0.4 kcal/mol higher lying minimum was found at a dihedral angle of 55-60° and a rotational barrier of 3.6 - 3.7 kcal/mol of 130°. This latter result agrees also well with the values obtained by *ab initio* HF calculations [28] of PE.

Band structure calculations of PE resulted in a gap of 8.0 eV which is quite close to the above mentioned experimental value of 8.8 eV [36]. This result is somewhat surprising because LPA calculations usually provide gaps in the case of semiconductors by 3 to 5 smaller than the experimental ones. On the other hand the one-electron energies lie by 3 -5 eV higher than the experimental values. Thus the ionization potential is 7.6 - 9.8 eV [39], while our KS result lies at -6.4 eV. It is also unusual that the two highest filled valence bands are crossing σ- and π- bands, while the cnduction band is a σ band.

The HF+MP2 band structure of polytetrafluororethylene (teflon, PTFE) with the same basis set and after geometry optimization is similar to that of PE [25]. Due to the four negative F-atoms, the whole band structure is, however, strongly shifted downwards. In this way the lower limit of the conduction band, $\varepsilon_{c,\mathrm{mm}}$ (QP) = -5.5 eV. Therefore one can expect that with the help of appropriate electron donor- doping electrons could be injected into the conduction band which would increase the conductivity of this very good insulator.

The density functional calculation [30] of teflon has given a minimum at the dihedral angle of 164° (slightly deformed planar zig-zag conformation). Two other local minima have been found for the helical conformations in the gauche form at the dihedral angles of 60° and angles of 60° and 90°, respectively. The position of the absolute minimum is in good agreement with the result of X–ray investigation of the PTFE crystal below 393 K [31].

The LDT band structure of PTFE shows nine valence bands which are separated into two groups. The two bands of the lower group are formed mainly by the symmetric combination of the $3s$ orbitals of F, while the seven bands of the higher lying group of valence bands are due to the $3p$ orbitals of F and sp^3 hydrid orbitals of C. The band gap is 5.5 and 5.8 eV, respectively, for the GKS and KS = PZ exchange functionals, respectively. They are substantially smaller, than the -10.3 eV and 11.6 eV values, respectively, obtained for PE and the experimental value of 8.8 eV of PE.

3.2 Polyparaphenylene

A HF + MP2 calculation has been performed for polyparaphenylene (PPP) [33] with Clementi's double ζ [24] supplemented by polarization functions with second neighbors' interactions and 7 k points in the MP level. The geometry used was taken from the middle part of a terphenyl molecule which was determined by X-ray diffraction [32] (for details see [32]), the torsion angles of subsequent rings of 33.7^o come also from X-ray measurements [34].

For the ionization potential (using Koopman's theorem for the QP band structure) +7.10 eV and for the electron affinity -3.31 eV was obtained. Their difference gives a gap of 4.79 eV (in the DZ case it is 5.51 eV). The ionization potential estimated from experiment is 5.6 - 5.7 eV [35] (by 1.4 eV larger than our value). The experimental u.v. spectrum of PPP gives a spectroscopic value of 3.7 eV [36]. It should be emphasized, however, that the gap value determined on the basis of the u.v. visible spectra is usually smaller than the real gap because of the occurrence of exciton bands. Further the still not good enough basis, the limited number of neighbors without the treatment of long range Coulomb interactions and by stopping the MP expansion at the second order certainly contributes also to this discrepancy.

For PPP also an LDA calculation was performed [37] again in the way as described in point 3. The minimum of the total energy per unit cell has been obtained at the torsional angle of 34.8^o (exp. value $33.7\ ^o$ [34]. The internal coordinates were optimized also and they are in good agreement with recent X-ray results on PPP crystals [38].

The band structure at 34.8^o torsion angle is similar to the one obtained in a planar conformation [37]. The value of the direct gap (which is the smallest one) at this torsional angle is 3.54 eV, while the experimental value provided by optical measurements is in the solid phase 3.8 eV [39] and 3.4 eV in the gas phase [35]. Since we have performed the calculation for a single chain the smaller gas phase value should be used for comparison. As mentioned before the optical gap is usually smaller than the solid state physical gap, because of the presence of exciton bands. Therefore, our theoretical gap value is by 1.5 - 3.0 eV smaller, than the gap which can be postulated on the basis of experiments. This is not surprising, because (as mentioned also before) the LDA gives usually too small gaps and band dispersions.

The valence and conduction band widths obtained at the torsion angle of 34.8^o are 3.58 and 3.86 eV, respectively. These values are also considerably smaller than the HF + MP2 values (calculated at 33.7^o torsional angle) of 4.13 -and 5.33 eV, respectively [32]. The gas phase UPS valence band width [40] is on the other hand only 3.9 eV [40] in rather good agreement with our 3.6 eV result. Finally the theoretical ionization potential is 4.93 eV, while the HF +

MP2 calculation resulted in 7.10eV [32]. The experimental UPS [41] and XPS [41] results are 5.65 and 6.50 eV [41], respectively. If one takes the UPS result, which refers to the gas phase, the agreement between experiment and LDA results is quite good. For the electron affinity this calculation has provided a value of -1.4 eV, while the HF + MP2 result is -3.2 eV [32]. (No experimental value is available).

The results obtained for PPP show again the general trend: for ground state properties the LDA approach works quite well, but this is not the case for the virtual bands and therefore for the fundamental gap.

3.3 The Nucleotide Base Stacks

The stacks of the four nucleotide bases cytosine (C), adenine (A), thymine (T) and guanine (G) were calculated in the HF and HF + MP2 level (in the latter cases using the Dyson equation in its diagonal approximation) [43]. The basis set was Clementi's double one [24], but in the case of C also better basis sets were applied. For the geometries of the stacks those of DNA B were used [44] (3.36 stacking distance, 36^o rotation around the main axis). The calculations were executed in the second neighbor's interactions approximation. One should mention here that though the sugar- phosphate chains in DNA were neglected, the band structures of the nucleotide base stacks provide a rather good approximation of that of DNA, because according to previous HF calculations [45], [46] the band structure of a homopolynucleotide is equivalent in a rather good approximation to the superposition of the band structures of the base stacks and that of the sugar-phosphate chain. There are K^+ counterions around DNA and the phosphate groups are negatively charged, the deoxyribose molecules have positive charges and the bases again negative ones. Therefore these alternating charges mostly screen out each others effect [47]. Further an early HF calculation has shown that if a C stack is surrounded by water clusters in a way as in DNA B, the effect of the water environment has little influence on the band structure of the C stack [48]. Taking into account all these facts one can say that the band structures of the free nucleotide base stacks correspond in a good approximation to those of the stacks in DNA B

Table 1 shows the quasi particle band structures obtained for the four stacks calculated in the above described way.

Table 1
The Quasi Particle Band Structure of the Four Nucleotide Base Stacks†

		C	A	T	G
Conduction band	max.	1.92	2.43	1.42	2.98
	min.	1.62	2.24	1.13	1.89
	width	0.30	0.19	0.29	1.09
Valence band	max.	-7.04	-7.26	-7.96	-6.58
	min.	-7.20	-7.34	-8.55	-7.10
	width	0.16	0.08	0.59	0.52
Gap‡		8.66	9.50	9.09	8.47
		(11.55)	(11.84)	(11.79)	(10.41)

† in eV-s

‡HF gap values are given in parenthesis

From the Table one can see that the QP gaps are 3 - 3 eV-s smaller than the HF ones, but they are still too large (the experimental values can be estimated on the basis of the exciton spectra of the stacks to be 5.0 - 6.0 eV [49]).To test the quality of the calculations we have investigated (1) the dependence of the band structure of the number of neighbors explicitly taken into account, (2) the dependence on the number of k-points used and last but not least (3) the dependence of the results on the quality of the basis set. These tests we have performed in the case of the simplest C stack.

The investigations have shown (1) that the QP band structures hardly change going from the second to the third neighbor's interactions [43]. This obviously is due to the rather large stacking distance of 3.36 . (The third neighbor is already 10.1 away from the first molecule). (3) The number of k-points taken into account also practically does not change the band structure if one goes from 7 k points to 9 [43].

We have supplemented the double ζ basis of the C stack by a set of d functions on each non-H atom. This had a small effect on the QP band structure, (for instance the gap changed from 8.66 to 8.17 eV), but the overall effect was not significant.

On the other hand if we introduced 3 sets of p- functions on the positions of the non-H atoms of a "phantom" molecule (a C molecule placed ad mid stacking distance of 1.68 and 18^o rotation without nuclear charges and electrons) the effect in the HF case was not very large, but the QP band structure changed strongly [43], [50]. The QP valence band was shifted upwards by $\sim$0.5 eV as compared to the double ζ QP calculation and the QP conduction band comes down by $\sim$1.5 eV. This resulted in a gap of 6.60 eV instead of 8.66 eV [43], [50]. This value is already not far from the estimated theoretical value of 5.5 eV. One can take the ratio of the double ζ QP gap of 8.66 in the case of the C stack and the phantom molecule gap of 6.60 eV, $\frac{6\,60}{8\,66} = 0.76$ to scale the

gap values of the other base stacks. One obtains in this way for A 7.33 eV, for T 6.91 eV and for G 6.44 eV. These approximate values are not far from the estimated experimental gap values of 5 - 6 eV.

One should point out that by stopping the MP perturbation series at the second order and still not having a very good basis set one cannot expect a better agreement between experiment and theory.

From the double ζ HF band structures one can have an approximate ionization potential if one uses Koopman's theorem [51]. The agreement witli the experimental values [52]-[56] is surprisingly good. (C: 8.7 eV (theor.), 8.9 eV (exp.); A: 8.4 eV (theor.), 8.4 eV (exp.); T: 9.3 eV (theor.), 9.1 eV (exp.) and G: 7.7 eV (theor.), 8.3 eV (exp.) On the other hand the QP ionization potentials (taking the upper edge at the valence band) are systematically by 1 - 3 eV smaller than the experimental ones. This can be understood, if we take into account that for the QP band structures in the MP2 approximation there is no proof for the validity of Koopman's like theorem (as in the HF case there is one). To obtain the right ionization potentials one had to calculate the difference of the exact total energies of the N and N-1 systems which is of course not the case in our calculations.

For the nucleotide base stacks + for a stack of uracil (U) molecules in the same conformation also LDA calculations have been performed [57] in the same way as described before. In the calculations the helix operation, which is included in Mintmire's code, has been used to be able to take only one base as unit cell. Total energy per unit cell calculations have been performed either changing the stacking distance d keeping the rotation angle constant at 36^o or reversely by d 3.36 the rotation angle was changed.

In the first series of computations for the A, C and U stack we have found the minimum at d 3.36 in agreement with experiment, but both in the cases of the T and G stacks, respectively, the minimum was at d = 3.30 .

In the second series of calculations keeping d constant at 3.36 we have found in the case of the A stack the deepest minimum at 330^o and a second one lying only by 0.03 eV higher at 30^o. Since a screw angle of 330^o in a right handed helix is equivalent to 30^o in a left handed one, the small difference of the energy of the two minima (most probably due to the accumulation of numerical errors) shows an energetic equivalence of the right- and left handed periodic helices. The case of the T stack is similar with energetically equivalent minima at 36^o and 330^o. The G stack has also two equivalent minima at 36^o and 370^o, but the absolute minimum lies by 0.05 eV deeper at 180^o. Finally the U stack has a deeper minimum at 30^o and two shallower ones at 60^o and 300^o, respectively.

Turning to the band structures one can see [57] that 1) the upper edges of the valence bands lie between -3.7 and -4.6 eV, 2) the lower edges of the

conduction bands one can find between -0.03 and -1.3 eV, 3) the band widths of both bands are small (values between 0.6 and 0.03 eV). The valence bands lie essentially higher and the conduction bands lower, than in the cases of the QP (HF + MP3) band structures [43]. Therefore the fundamental gaps are substantially smaller (between 3.1 and 3.3 eV), than the QP ones (between 6.4 - 7.3 eV in the scaled cases [43]). The LDA gaps found for the base stacks are certainly by 3 - 3 eV smaller than the ones estimated on the basis of the experimental spectra. To improve the LDA results one could try to supplement the basis set also in this case with functions centered on the nuclei of a "phantom" molecule as was done previously in the HF + MP2 case [43]. Further one could try to use a more sophisticated form of the DFT theory developed for the treatment of excited states of atoms and molecules [58]. It is, however, unclear, whether this would work also in the case of the band structures of polymers.

4 Conclusion

If one compares the HF + MP2 results witli those obtained with the help of the DFT in the form as applied in Mintmire's program the following general features occur: 1) The DFT theory gives definitely better results for ground state properties (conformations, positions and widths of the filled bands etc.) than the HF ones. In some cases they are even better than the HF + MP2 QP band structure results. 3) On the other hand the fundamental gap (which is in most cases too small) and the positions and widths of the unfilled bands (at least in the used form of the DFT theory) are generally in worse agreement with experiment than those obtained from QP band structures. 3) One hopes that both methods will give - after some improvements - more satisfactory results also for the unfilled part of the band structures of polymers.

Acknowledgement

The authors should like to express their gratitude to the late Professors P.E. Van Camp and E. Kapuy as well to Professors Ch. Alsenoy, W. Förner, J. Mintmire and P. Otto for fruitful discussions and for putting to our disposal their programs. We are further very thankful to Dr-s M.S. Miao, A. Peters and M.L. Zhang for executing different parts of the calculations.

References

[1] P.-O.- Löwdin, Adv. Phys. 5, 1 (1956); G. Del Re, J. Ladik and G. Biezo, Phys. Rev, 155, 997 (1967); J.-M. André, L. Govemeur and G. Leroy,

Int. J. Quant. Chem. 1, 437; 481 (1967). See Also in J. Ladik, Quantum Theory of Polymers as Solids, Plenum Press, New York, 1988, Chapt. 1.

[2] Y. Toyozawa, Progr. Theor. Physics (Kyoto) 13, 433 (1954); J.T. Devreese, A.B. Kunz, J. Mintmire, T. C. Collins, Solid State Comm. 11, 679, 1993.

[3] See for instance: J. Mintmire in J. Labanowski and J. Andzelm (Eds.), Density Functional Methods in Chemistry, Springer, New York, 1991, p. 135.

[4] A. Blumen and C. Merkel, Phys. Status Solidi B 83, 435 (1977); J. Ladik in Excited States in Quantum Chemistry, C.A. Nicolaides and D. Beck eds., D. Reidel, Dordrecht, 1979, p. 495.

[5] J. Ladik, Physics Reports, Elsevier (North Holland), Amsterdam, 313, 1999, p. 171 and references therein.

[6] C. Pisani, R. Dovesi and C. Roetti, Ab Initio Hartree Fock Treatment of Crystalline Systems, Techn. Notes in Chemistry, Springer, New York, 1988, Vol. 48.

[7] L.S. Cederbaum and W. Domcke, Adv. Chem. Phys. 36, 308, (1977).

[8] C.M. Liegener, J. Phys. C 18, 6011 (1985).

[9] C.M. Moeller and M.S. Plesset, Phys. Rev. 46, 618 (1934).

[10] S. Suhai, Phys. Rev. B 37, 3506 (1983).

[11] A. Szabo and N.S. Ostlund, Modern Quantum Chemistry, McGraw-Hill, New York, 1982, p. 398

[12] I. Palmer and J. Ladik, J. Comput. Chem. 15, 819 (1994)

[13] J. Čížek, J. Chem. Phys. 45, 4256 (1966); J. Čížek, Adv. Quantum Chem. 3, 35 (1969); J. Paldus and J. Čížek, Adv. Quantum Chem. 9, 105 (1975)

[14] W. Förner, R. Knab, J. Čížek and J. Ladik, J. Chem. Phys. 106, 10248 (1997)

[15] See: J. Ladik, Quantum Theory of Polymers as Solids, Plenum, New York, 1988

[16] R. Gáspár, Acta. Phys. Acad. Sci. Hung. 3, 363 (1954)

[17] W. Kohn and L.J. Sham, Phys. Rev. A 140, 1133 (1965)

[18] J.P. Perdew and A. Zunger, Phys. Rev. B 23, 5948 (1981)

[19] D.M. Ceperley and B.J. Alder, Phys. Rev. Lett. 45, 566 (1980)

[20] N. Godbout, D.R. Salahub, J. Andzelm and E. Wimmer, Can. J. Chem. 70, 560 (1992)

[21] S. Huzinaga (ed), Gaussian Basis Sets for Molecular Calculations, Elsevier, Amsterdam (1984)

[22] J. Delhalle, L. Piella, J.-L. Bredas and J.M. Andre, Phys. Rev. B 22, 6254 (1980)

[23] S. Suhai, J. Polym. Sci. Polym. Phys. ed. 21, 1341 (1983); J. Chem. Phys. 84, 5071 (1986)

[24] L. Gianolo and E. Clementi, Gazz. Chim. Ital. 110, 179 (1980)

[25] M. Oppel, P. Otto and J. Ladik (unpublished)

[26] K.J. Less and E.G. Wilson, J. Phys. C 6, 3110 (1973)

[27] M.S. Miao, P.E. Van Camp, V.E. Van Doren, J. Ladik and J.W. Mintmire, Phys. Rev. B 54, 10430 (1996)

[28] A. Karpfen and A. Beyer, J. Comp. Chem. 5, 11 (1984)

[29] K..Seki, N. Ueno, U.O. Karlsson, R. Engel hardt and E.E. Koch, Chem. Phys. 105, 247 (1986)

[30] M.S. Miao, P.E. Van Camp, V.E. Van Doren, J. Ladik and J.W. Mintmire, Int, J. Quantum Chem. 64, 243 (1997)

[31] M. Kimming, G. Strobl and B. Stühn, Macromolecules 27, 2481 (1984)

[32] H.M. Rietveld, E.N. Maslen, P. Vogl and G. Leising, Phys. Rev. B 51, 9668 (1995)

[33] F. Bogar, W. Förner, E. Kapuy and J. Ladik, Theochem 391 193 (1997)

[34] J.L. Badour, Y. Delugeard and P. Rivet, Acta. Cryst. B 34, 625 (1978)

[35] L.W. Shacklette, H. Eckhardt, R.R. Chance, G.G. Miller, D.M. Ivory and R. Baughman, J. Chem. Phys. 73, 4098 (1980)

[36] G. Leising, K. Picher and F. Selzer, in Electronic Properties of Conjugated Polymers, ed. H. Kuzmany and S. Roth, Vol. III, p. 100, Springer, Heidelberg (1989)

[37] M.S. Miao, P.E. Van Camp, V.E. Van Doren, J. Ladik and J.W. Mintmire, J. Chem. Phys. 109, 9623 (1998)

[38] K.N. Baker, A.V. Fratini, T. Resch, H.C. Knachel, W.W. Adams, E.P Socci and B.L. Farmer, Polymer 34, 1571 (1993)

[39] G. Froyer, Y. Pelous and G. Olliver, Springer Series Solid State Sci. 76, 303 (1987)

[40] S. Narioka, H. Ishii, K. Edamatsu, K. Kamiya, S. Hasegawa, T. Ohta, N. Ueno and K. Seki, Phys. Rev. B 52, 2362 (1995)

[41] K. Seki, U.O. Karlsson, R. Engelhardt, E.E. Koch and W. Schmidt, Chem. Phys. 91, 459 (1984)

[42] J. Riga, J.J. Pireaux, J.P. Boutique, R. Caudano, J.J. Verbist and Y. Gobillon, Synth. Met. 4, 99 (1981)

[43] F. Bogar and J. Ladik, Chem. Phys. 237, 273 (1998)

[44] S. Arnott, S.D. Dover and A.J. Wonacott, Acta. Cryst. B 28, 2198 (1969); R. Fieldman, in Atlas of Macromolecular Structure on Microfiche (AMSOM), Document 13.2.1.1.1, National Institute of Health, Bethesda, Washington (1986)

[45] J. Ladik and S. Suhai, Int. J. Quant. Chem. QBS 7, 189 (1980)

[46] P. Otto, E. Clementi, and J. Ladik, J. Chem. Phys. 78, 4547 (1983)

[47] Y.J. Ye, unpublished result

[48] P. Otto, J. Ladik, G. Corongiu, S. Suhai and W. Förner, J. Chem. Phys. 77, 8026 (1982)

[49] J. Ladik, A. Sujianto and P.Otto, J. Mol. Struct. (Theochem) 228, 271 (1991)

[50] F. Bogar and J. Ladik, J. Mol. Struct. (Theochem) 501-501, 445 (2000)

[51] T. Koopmans, Physica 1, 104 (1933)

[52] A. Sygula and A. Buda, J. Mol. Struct. (Theochem) 92, 267 (1983)

[53] V. Norinder, J. Mol. Struct. (Theochem) 151, 259 (1983)

[54] I.R. Gould, N.A. Burton, R.J. Hall and I.H. Hillier, J. Mol. Struct. (Theochem) 331, 147 (1995)

[55] M.J. Nowak, L. Lapinski, J.S. Kwiatkowski and J. Leszcynski, J. Phys. Chem. 100, 3527 (1996)

[56] A. Sygula, J. Mol. Struct. (Theochem) 92, 355 (1983)

[57] M.I. Zhang, M. Miao, V. Van Doren, J. Ladik and J.W. Mintmire, J. Chem. Phys. 111, 8696 (1999)

[58] See, for instance, T. Grabo and E.K.U. Gross, Int. J. Quantum Chem. 64, 95 (1997)

Effective potential of a single excited state along the adiabatic path

Á. Nagy
Department of Theoretical Physics
University of Debrecen
H–4010 Debrecen, Hungary

Table of contents

Abstract

A recently proposed theory for a single excited state based on Kato's theorem and the concept of adiabatic connection is reviewed. A method constructing the effective potential along the adiabatic path is presented.

ADVANCES IN QUANTUM CHEMISTRY VOLUME 39

0065-3276/01 $35 00

1 Introduction

The density functional theory (1) was first generalized for excited states by Theophilou (2) and later by Gross, Oliveira and Kohn (3). Several calculations were done with this method (4). Görling (5) also presented a density fuctional formalism for excited states based on density functional perturbation theory (6). Alternatively, time-dependent density functional theory (7,8) is also used to obtain excitation energies. The work formalism proposed by Sahni and coworkers (9) is applied in excited-state density functional calculations (10), too. Görling (11) also presented a generalized density fuctional formalism based on generalized adiabatic connection. The local scaling theory of Kryachko and Ludena (12) was also generalized for excited states.

There exists a non-variational theory (13) for a single excited state. It is based on Kato's theorem (14,15) and the concept of adiabatic connection and is valid for Coulomb external potential (i.e. free atoms, molecules and solids). A variational density functional theory was also obtained for an individual excited state (16).

In this contribution a method constructing the effective potential of a single excited state along the adiabatic path is presented.

2 Theory for a single excited state

According to the Hohenberg-Kohn theorem of the density functional theory the ground state electron density determines in principle all molecular properties. Bright Wilson (17) argued that for a Coulomb system it can be very easily seen: Kato's theorem (14,15) states that

$$Z_\beta = -\frac{1}{2n(r)} \left.\frac{\partial n(r)}{\partial r}\right|_{r=R_\beta} , \tag{1}$$

where the partial derivatives are taken at the nuclei β. So the cusps of the density tell us where the nuclei are (R_β) and what the atomic numbers Z_β are. Moreover, the integral of the density gives us the number of electrons:

$$N = \int n(\mathbf{r}) d\mathbf{r} . \tag{2}$$

Thus from the density the Hamiltonian can be readily obtained from which every property of the system can be determined. One has to emphasize, however, that this argument holds only for Coulomb systems, while the density functional theory is valid for any external potential.

Kato's theorem is valid not only for the ground state but also for the excited states. Consequently, if the density n_i of the i-th excited state is known, the Hamiltonian $\hat{H}$ is also in principle known and its eigenvalue problem

$$\hat{H}\Psi_k = E_k\Psi_k \qquad (k = 0, 1, ..., i, ...) \tag{3}$$

can be solved, where

$$\hat{H} = \hat{T} + \hat{V} + \hat{V}_{ee} \,. \tag{4}$$

$$\hat{T} = \sum_{j=1}^{N}(-\frac{1}{2}\nabla_j^2) \,, \tag{5}$$

$$\hat{V}_{ee} = \sum_{k=1}^{N-1}\sum_{j=i+1}^{N}\frac{1}{|\mathbf{r}_k - \mathbf{r}_j|} \,, \tag{6}$$

and

$$\hat{V} = \sum_{k=1}^{N}\sum_{J=1}^{M} -Z_J/|\mathbf{r}_k - \mathbf{R}_J| \,, \tag{7}$$

are the kinetic energy, the electron-electron energy and the electron-nucleon operators, respectively.

We mention by passing that there are certain special cases, where Eq. (1) do not provide the atomic number. The simplest example is the $2p$ orbital of the hydrogen atom. In this case the spherical average of the derivative of the wave function is zero and the value of the wave function is also zero at the nucleus. It means, that though Kato's theorem (1) is valid in this case, too, it does not give us the desired information, that is the atomic number. Similar cases occur in those highly excited atoms, ions or molecules, for which the spherical average of the derivative of the wave function is zero

at a nucleus, that is where we have no s-electrons. Pack and Brown (18) derived cusp relations for the wave functions of these systems, while a recent study (19) focused on the appropriate nuclear cusp conditions on the density corresponding to the excited states, particularly the non s-states. It was found that the atomic number can be easily obtained from higher-order cusp relations.

Using the concept (10,21) of adiabatic connection Kohn-Sham-like equations can be derived. It is supposed that the density is the same for both the interacting and non-interacting systems, and there exists a continuous path between them. A coupling constant path is defined by the Schrödinger equation

$$\hat{H}_i^\alpha \Psi_k^{i,\alpha} = E_k^\alpha \Psi_k^{i,\alpha} , \tag{8}$$

where

$$\hat{H}_i^\alpha = \hat{T} + \alpha \hat{V}_{ee} + \hat{V}_i^\alpha . \tag{9}$$

The subscript i denotes that the density of the given excited state is supposed to be the same for any value of the coupling constant α. $\alpha = 1$ corresponds to the fully interacting case, while $\alpha = 0$ gives the non-interacting system:

$$\hat{H}_i^0 \Psi_k^{i,0} = E_k^0 \Psi_k^{i,0} . \tag{10}$$

For $\alpha = 1$ the Hamiltonian $\hat{H}_i^\alpha$ is independent of i. For any other values of α the 'adiabatic' Hamiltonian depends on i, we have different Hamiltonian for different excited states. Thus the non-interacting Hamiltonian ($\alpha = 0$) is different for different excited states. The potential V_i^α is given by the condition that the density of the given excited state is fixed. In this paper a method to determine V_i^α self-consistently is proposed.

3 Pauli potential for an excited state

It has been shown (22) that the ground-state electron density n_0 satisfies the differential equation

$$\left[-\frac{1}{2}\nabla^2 + v(\mathbf{r}) + w(\mathbf{r}) \right] n_0^{1/2}(\mathbf{r}) = \mu n_0^{1/2}(\mathbf{r}) , \tag{11}$$

where $v(\mathbf{r})$ is the external potential and $w(\mathbf{r})$ is a local effective potential. μ is the chemical potential (23) (equal to the negative of the ionization energy (24)). Eq. (11) can also be written as

$$\left[-\frac{1}{2}\nabla^2 + v_p + v_{KS}\right] n_0^{1/2}(\mathbf{r}) = \epsilon_M n_0^{1/2}(\mathbf{r}) \,, \tag{12}$$

where v_{KS} is the Kohn-Sham potential, while v_p is the so-called Pauli potential. It has been proved (23,25) that the highest occupied orbital energy of the ground-state density functional theory is

$$\epsilon_M = \mu \,. \tag{13}$$

Similar equations can be derived in the excited-state theory. In the following section the conterpart of Eq. (11)

$$\left[-\frac{1}{2}\nabla^2 + v(\mathbf{r}) + w_i(\mathbf{r})\right] n_i^{1/2}(\mathbf{r}) = \mu_i n_i^{1/2}(\mathbf{r}) \,, \tag{14}$$

is derived for the excited state i. The one-electron equations of the non-interacting system have the form

$$\left[-\frac{1}{2}\nabla^2 + v_i^0(\mathbf{r})\right] \phi_j^i = \varepsilon_j^i \phi_j^i. \tag{15}$$

The density n_i of the excited state is

$$n_i = \sum_{j=1}^{M} \lambda_j^i |\phi_j^i|^2 \,, \tag{16}$$

where the occupation numbers λ_j^i can be 0 or 1. M corresponds to the highest occupied orbital. Writing ϕ_M^i as

$$\phi_M^i = \chi_M^i n_i^{1/2} \tag{17}$$

and substituting it into Eq. (15) one arrives at

$$\left[-\frac{1}{2}\nabla^2 + v_p^i + v_i^0\right] n_i^{1/2}(\mathbf{r}) = \epsilon_M^i n_i^{1/2}(\mathbf{r}) \,, \tag{18}$$

where the Pauli potential of the excited state i has the form

$$v_p^i = -\frac{1}{2\chi_M^i}\nabla^2\chi_M^i - \frac{\nabla\chi_M^i}{\chi_M^i}\,\frac{\nabla n_i^{1/2}}{n_i^{1/2}} \,. \tag{19}$$

A comparison of Eqs. (15) and (18) leads to

$$w_i = v_p^i + v_i^0 - v \tag{20}$$

4 Construction of the potential V_i^α

Now, the method of Levy, Perdew and Sahni (22) is generalized for excited states. Let us write the Hamiltonian $\hat{H}_i^\alpha$ in Eq. (9) in the form

$$\hat{H}_i^\alpha = \hat{H}_{i,N}^\alpha + \hat{H}_{i,N-1}^\alpha + \alpha \sum_{j=1}^{N-1} \frac{1}{|\mathbf{r}_j - \mathbf{r}_N|} , \tag{21}$$

where

$$\hat{H}_{i,N}^\alpha = \hat{T}_N + V_i^\alpha(\mathbf{r}_N) \tag{22}$$

and

$$\hat{H}_{i,N-1}^\alpha = \sum_{j=1}^{N-1} \left(\hat{T}_j + V_i^\alpha(\mathbf{r}_j)\right) + \frac{1}{2}\alpha \sum_{l=1}^{N-1}\sum_{j=1}^{N-1} \frac{1}{|\mathbf{r}_j - \mathbf{r}_l|} . \tag{23}$$

Eqs. (21)-(23) specify a partition of the Hamiltonian in which $\hat{H}_{i,N}^\alpha$ is the Hamiltonian acting only on the electron N. The wave function $\Psi_k^{i,\alpha}$ has a subscipt k denoting that it is the kth eigenfunction of the Hamiltonian $\hat{H}_{i,N}^\alpha$. (We consider the ith excited state of the Hamiltonian $\hat{H}$ of the real system with the density n_i. The corresponding eigenstate of the Hamiltonian $\hat{H}_{i,N}^\alpha$ is the kth. k can be different from i.) The wave function $\Psi_k^{i,\alpha}$ can be written as

$$\Psi_k^{i,\alpha} = N^{-1/2} n_i^{1/2}(\mathbf{r}_N)\Phi_{N-1,k}^{i,\alpha} , \tag{24}$$

where $\Phi_{N-1,k}^{i,\alpha}$ is an antisymmetric wave function defined by this equation. From the definition (24) and Eq. (2) follows that

$$\langle \Phi_{N-1,k}^{i,\alpha} | \Phi_{N-1,k}^{i,\alpha} \rangle = 1 . \tag{25}$$

Subtract $E_{k,N-1}^{i,\alpha}\Psi_k^{i,\alpha}$ from both sides of Eq. (8), multiply by $\Phi_{N-1,k}^{i,\alpha *}$ and integrate:

$$\langle \Phi_{N-1,k}^{i,\alpha} | \hat{H}_i^\alpha - E_{k,N-1}^{i,\alpha} | \Psi_k^{i,\alpha} \rangle = \mu_i \langle \Phi_{N-1,k}^{i,\alpha} | \Psi_k^{i,\alpha} \rangle . \tag{26}$$

As $E_{k,N-1}^{i,\alpha}$ is the total energy of that $N-1$ electron system (the one obtained after removing the HOMO electron from the N-electron excited state)

$$\mu_i = E_k^{i,\alpha} - E_{k,N-1}^{i,\alpha} . \tag{27}$$

It is well-known that μ_i is determined by the long-range asymptotic decay of the electron density (26,22,27,28). μ_i is the same for any value of α, as the density is kept fixed along the adiabatic path. After simple manipulation Eqs. (24) - (27) lead to

$$\left[-\frac{1}{2}\nabla^2 + v_i^\alpha(\mathbf{r}) + w_i^\alpha(\mathbf{r})\right] n_i^{1/2}(\mathbf{r}) = \mu_i n_i^{1/2}(\mathbf{r}) \,, \tag{28}$$

where

$$w_i^\alpha(\mathbf{r}_N) = \langle \Phi_{N-1,k}^{i,\alpha} | \hat{H}_{i,N-1}^\alpha - E_{k,N-1}^{i,\alpha} | \Phi_{N-1,k}^{i,\alpha} \rangle +$$
$$\frac{1}{2}\int |\nabla_N \Phi_{N-1,k}^{i,\alpha}|^2 dx_1 ... dx_{N-1} d\sigma_N + \int \frac{\varrho_{N-1,k}^{i,\alpha}(\mathbf{r}, \mathbf{r}_N)}{|\mathbf{r} - \mathbf{r}_N|} d\mathbf{r} \,. \tag{29}$$

x denotes both the space and spin coordinates, while σ denotes a spin coordinate.

$$\varrho_{N-1,k}^{i,\alpha}(\mathbf{r}, \mathbf{r}_N) = \int |\Phi_{N-1,k}^{i,\alpha}|^2 dx_2 ... dx_{N-1} d\sigma d\sigma_N \tag{30}$$

If $\alpha = 1$ Eq. (28) gives Eq. (14), while $\alpha = 0$ corresponds to Eq. (18) with

$$v_p^i = w_i^{\alpha=0} - v_J^i - v_{xc}^i \,, \tag{31}$$

where v_J^i and v_{xc}^i are the Coulomb and exchange-correlation potentials, respectively. As the density is fixed along the adiabatic path Eqs. (14) and (28) dictate that

$$w_i^\alpha + v_i^\alpha = w_i + v = v_p^i + v_i^0 \tag{32}$$

Eq. (32) makes it possible to construct the potential

$$v_i^\alpha = w_i + v - w_i^\alpha \,. \tag{33}$$

Eqs. (29) and (33) leads to

$$\begin{aligned} v_i^\alpha \;=\; & v - \langle \Phi_{N-1,k}^{i,\alpha} | \hat{H}_{i,N-1}^\alpha - E_{k,N-1}^{i,\alpha} | \Phi_{N-1,k}^{i,\alpha} \rangle \\ & + \langle \Phi_{N-1}^i | \hat{H}_{N-1} - E_{N-1}^i | \Phi_{N-1}^i \rangle \\ & - \frac{1}{2}\int |\nabla_N \Phi_{N-1,k}^{i,\alpha}|^2 dx_1 ... dx_{N-1} d\sigma_N \\ & + \frac{1}{2}\int |\nabla_N \Phi_{N-1}^i|^2 dx_1 ... dx_{N-1} d\sigma_N \\ & - \int \frac{\varrho_{N-1}^i(\mathbf{r}, \mathbf{r}_N) - \varrho_{N-1,k}^{i,\alpha}(\mathbf{r}, \mathbf{r}_N)}{|\mathbf{r} - \mathbf{r}_N|} d\mathbf{r} \,. \end{aligned} \tag{34}$$

From expression (34) the potential v_i^α can be in principle constructed. As we know the density of the given excited state n_i, using Kato's theorem we now the Hamiltonian $\hat{H}$. That means that we also know the Hamiltonian $\hat{H}_{N-1}$, the wave function Φ_{N-1}^i and ϱ_i. With an initial trial v_i^α the Schrödinger equation (8) can be solved and with the wave function $\Phi_{N-1,k}^{i,\alpha}$ and eigenvalue $E_{k,N-1}^{i,\alpha}$ the potential (34) can be calculated. Then the Schrödinger equation (8) is solved again with this potential and so on. The procedure goes on until self-consistency is reached.

5 Discussion

Expression (34) makes it possible to determine the local 'external' potential self-consistently for any value α. The construction is not necessarily unique, it might happen that there are more than one potentials for given n_i, $\hat{H}$, $\hat{H}_{N-1}$, Φ_{N-1}^i and ϱ_i. The substitution of the potential (34) into the Schrödinger equation (8) results in an eigenvalue problem that might have several solutions.

For $\alpha = 0$ it has recently been shown (29) that for a given electron configuration, that is for given occupation numbers, the potential v_i^0 can be uniquely obtained. This statement can be straighforwardly generalized for any value α. Of course, we have to bear in mind that we do not have one-electron Kohn-Sham-like equations if $\alpha \neq 0$. Even in these cases can one, however, define the electron configuration with the occupation numbers defined by the eigenvalues of the one-electron density matrix. It is a possible way to make distinction between the solutions of the eigenvalue problem.

The derivation presented is valid both for non-degenerate and degenerate states. For degenerate case we select one wave function of the interacting Hamiltonian (4) and obtain the potential (34). Starting out from another wave function corresponding to the same degenerate excited-state energy another potential can be gained from Eq. (34), because the densities calculated from the different degenerate wave funtions are generally different.

There is, however, another way of treating degeneracy, which has already been proposed (30). This approach is based on using density matrices instead of the density. Consider the solutions of the degenerate excited state of the

Schrödinger equation

$$\hat{H}|\Psi_\gamma^i\rangle = E^i|\Psi_\gamma^i\rangle \qquad (\gamma = 1, 2, \ldots, g_i) \,, \tag{35}$$

where g_i is the degeneracy. Instead of treating one wave function Ψ_γ^i the density matrix defined in subspace S^i

$$\hat{D}^i = \sum_{\gamma=1}^{g_i} w_\gamma |\Psi_\gamma^i\rangle\langle\Psi_\gamma^i| \,, \tag{36}$$

is introduced, where the weighting factors w_γ^i should satisfy the conditions

$$1 = \sum_{\gamma=1}^{g_i} w_\gamma^i \tag{37}$$

and

$$w_\gamma^i \geq 0 \,. \tag{38}$$

In principle, any set of weighting factors w_γ^i satisfying conditions (37) and (38) can be used. The subspace density is defined as

$$n^i = \sum_{\gamma=1}^{g_i} w_\gamma^i \int |\Psi_\gamma^i|^2 ds_1 d\mathbf{x_2} ... d\mathbf{x_N} \,, \tag{39}$$

The superscript i in n^i and the subspace density matrix D^i denotes that they are constructed from wave functions that belong to the subspace S^i. One is free to select the values of the weighting factors w_γ^i, they only should satisfy the conditions (37) and (38). If the weighting factors w_γ^i are all equal, the density has the property of transforming according to the totally symmetric irreducible representation. So, for instance, for atoms the density will be spherically symmetric. But it is possible to select other values for the weighting factors w_γ^i. This approach has the advantage that with equal weighting factors the density has the symmetry of the external potential.

In this subspace approach we have a single (subspace) density and a single effective potential that can be easily derived from (26) after making the same manipulation, multiplying with $\Phi_{N-1,k\gamma}^{i,\alpha *}(x_1', ..., x_{N-1}')$ and summing for the

whole subspace. The only difference is in the fact that the new expression (34) contains the subspace density matrix instead of the wave functions:

$$w_i^\alpha(\mathbf{r}_N) = \int dx_1...dx_{N-1}\,(\hat{H}^\alpha_{i,N-1} - E^{i,\alpha}_{N-1,k})D^{i,\alpha}_{N-1,k}\Big|_{x'=x} +$$
$$\frac{1}{2}\int dx_1...dx_{N-1}d\sigma_N\nabla_{r'_N}\nabla_{r_N}\,D^{i,\alpha}_{N-1,k}\Big|_{x'=x} + \int \frac{\varrho^{i,\alpha}_{N-1,k}(\mathbf{r},\mathbf{r}_N)}{|\mathbf{r}-\mathbf{r}_N|}d\mathbf{r}\,, \qquad (40)$$

where

$$\varrho^{i,\alpha}_{N-1,k}(\mathbf{r},\mathbf{r}_N) = \int |D^{i,\alpha}_{N-1,k}\Big|_{x'=x}\,dx_2...dx_{N-1}d\sigma d\sigma_N\,. \qquad (41)$$

The final expression (34) has then the form:

$$\begin{aligned} v_i^\alpha \;=\; & v - \int dx_1...dx_{N-1}\,(\hat{H}^{i,\alpha}_{k,N-1} - E^{i,\alpha}_{N-1,k})D^{i,\alpha}_{N-1,k}\Big|_{x'=x} \\ & + \int dx_1...dx_{N-1}\,(\hat{H}_{N-1} - E^i_{N-1})D^i_{N-1}\Big|_{x'=x} \\ & -\frac{1}{2}\int dx_1...dx_{N-1}d\sigma_N\nabla_{r'_N}\nabla_{r_N}\,D^{i,\alpha}_{N-1,k}\Big|_{x'=x} \\ & +\frac{1}{2}\int dx_1...dx_{N-1}d\sigma_N\nabla_{r'_N}\nabla_{r_N}\,D^i_{N-1}\Big|_{x'=x} \\ & -\int \frac{[\varrho^i_{N-1}(\mathbf{r},\mathbf{r}_N) - \varrho^{i,\alpha}_{N-1,k}(\mathbf{r},\mathbf{r}_N)|}{|\mathbf{r}-\mathbf{r}_N|}d\mathbf{r}\,. \end{aligned} \qquad (42)$$

It was emphasized at the beginning that the present theory is valid for external Coulomb potential. It does not mean, however, that the Kohn-Sham potential is a bare Coulomb potential as was stated in a recent paper of Moiseyev (31). Only the true external potential should be a Coulomb potential. Proceeding along the adiabatic path the 'external' potential v_i^α includes not only the bare nuclear Coulomb potential v but there are other terms arising from the interaction of electrons. This can be clearly seen from Eq. (34). The first term v is the external Coulomb potential, while all the other terms are coming from the electron-electron interaction. $\alpha = 0$ gives the Kohn-Sham potential. The Kohn-Sham potential as was constructed above contains classical repulsion and exchange-correlation potentials besides the external Coulomb potential v. Kato's theorem can be derived from an arbitrary eigenfunction of an interacting Hamiltonian. (Not only in case of a bare Coulomb field.) A recent paper of March et al. (32) presents

cusps conditions for the electron-electron interaction energy density that also supports the arguments above.

Acknowledgements

The grant 'Széchenyi' from the Hungarian Ministry of Education is gratefully acknowledged. This work was supported by the grants OTKA No. T 029469 and T 025369.

References

(1) Hohenberg, P. Kohn, W. Phys. Rev. B **1964** *136*, 864.
(2) Theophilou, A.K., J. Phys. C **12**, 5419 (1978).
(3) Gross, E.K.U., Oliveira, L.N., Kohn, W, Phys. Rev. A **37**, 2805, 2809, 2821 (1988).
(4) Nagy, Á., Phys. Rev. A **42**, 4388 (1990); J. Phys. **B 24**, 4691 (1991); Int. J. Quantum. Chem. **56**, 225 (1995); J. Phys. B **29**, 389 (1996); Int. J. Quantum. Chem. S. **29**, 297 (199); Adv. Quantum. Chem. **29**, 159 (1997) Phys. Rev. A **49**, 3074 (1994). Nagy Á., Andrejkovics, I., Phys. B **27**, 233 (1994).
(5) Görling, A., Phys. Rev. A **54**, 3912 (1996).
(6) Görling, A., Levy, M., Phys. Rev. A **47**, 13105 (1993); Phys. Rev. A **47**, 196 (1994); Int. J. Quantum. Chem. S. **29**, 93 (1995).
(7) Gross, E. U. K., Dobson, J. F. , Petersilka, M., in *Density Functional Theory, (Topics in Current Chemistry)* (ed.) Nalewajski, R., Springer-Verlag, Heidelberg, vol. 181. p 81 (1996).
(8) Casida, M. F., in *Recent advances in the density functional methods, (Recent Advances in Computational Chemistry)*, (ed.) Chong, D. P., World Scientific, Singapore vol.1 p.155 (1996).
(9) Harbola, M. K. , Sahni, V., Phys. Rev. Lett. **62**, 489 (1989); see also Sahni, V., in *Density Functional Theory (Topics in Current Chemistry)*, (ed.) Nalewajski, R., Springer-Verlag, Berlin vol.182. p.1 (1996).
(10) Sen, K. D., Chem. Phys. Lett. **168**, 510 (1992) ; Singh, R., Deb, B. M., Proc. Indian Acad. Sci. **106**, 1321 (1994); J. Mol. Struc. Theochem **361**, 33 (1996); J. Chem. Phys. **104**, 5892 (1996); Roy, A. K., Singh, R. , Deb, B. M., J. Phys. B **30**, 4763 (1997).

(11) Görling, A., Phys. Rev. A **59**, 3359 (1999).
(12) Koga, T., J. Chem. Phys. **95**, 4306 (1991); Kryachko, E. S., Ludena, E. V. , Koga, T., J. Math. Chem. **11**, 325 (1992).
(13) Nagy, Á., Int. J. Quantum. Chem. **70**, 681 (1998); Nagy, Á., in *Electron Correlations and Materials Properties*, (eds.) A. Gonis, N. Kioussis , M. Ciftan ,Kluwer, New York, p. 451 (1999).
(14) Kato, T., Commun. Pure Appl. Math. **10**, 151 (1957).
(15) Steiner, E. J., Chem. Phys. **39**, 2365 (1963); March, N. H., *Self-consistent fields in atoms,* Pergamon, Oxford (1975).
(16) Levy, M , Nagy, Á., Phys. Rev. Lett. **83**, 4361 (1999).
(17) Handy, N. C., in *Quantum Mechanical Simulation Methods for Studying Biological Systems*, (eds.) Bicout D. , Field, M., Springer–Verlag, Heidelberg p.1 (1996).
(18) Pack, R. T. , Brown, W. B., J. Chem. Phys. **45**, 556 (1966).
(19) Nagy, Á , Sen, K. D., J. Phys. B. **33**, 1745 (2000).
(20) Gunnarsson, O. , Lundqvist, B.I., Phys. Rev. B **13**, 4274 (1976).
(21) Harris J. , Jones, JR. O., Phys. F **4**, 1170 (1984); Harris, J., Phys. Rev. A **29**,1648 (1984).
(22) Levy, M., Perdew, J. P. , Sahni, V., Phys. Rev. A **30**, 2745 (1984).
(23) Parr, R. G., Donelly A., Levy, M. , Palke, W. E., J. Chem. Phys. **68**, 3801 (1978).
(24) Perdew, J. P., Parr, R. G., Levy, M. , Balduz, Jr, J. L. Phys. Rev. Lett. **49**, 1691 (1982).
(25) Almbladh, C. O. , Pedroza, A. P., Phys. Rev. A **29**, 2322 (1984).
(26) Perdew, J. P., Parr, R. G., Levy M. , Balduz, Jr, J. L. Phys. Rev. Lett. **49**, 1691 (1982).
(27) Almbladh, C. O. , von Barth, U., Phys. Rev. **B 31**, 3231 (1985); von Barth, U., in *Many-body phenomena at surfaces* (eds.) Langreth, D. C. , Suhl, Academic, New York, (1984).
(28) Katriel, J. , Davidson, E. R., Proc. Natl. Acad. Sci. USA **77**,4403 (1980).
(29) Nagy, Á, submitted to *Progress in Theoretical Chemistry and Physics* ed. by Maruani, J. , Wilson, S., Kluwer, London, (2000).
(30) Nagy, Á, Phys. Rev. A **57** 1672 (1998).
(31) Moiseyev, N., Chem. Phys. Lett. **321** 469 (2000).
(32) March, N. H., Howard, I. A., Holas, A., Senet, P. , Van Doren, V. E., Phys. Rev. A (submitted).

Gradient corrections to the kinetic-energy density functional stemming from a regular two-component relativistic Hamiltonian

P. Tz. YOTOV[a], F. E. ZAKHARIEV[b], Ya. I. DELCHEV[a] and J. MARUANI[c]

[a] *Institute of Nuclear Research and Nuclear Energy, BAS, 72 Tsarigradsko Chaussee, 1784 Sofia, Bulgaria*

[b] *Tulane University, New Orleans, LA 70118, USA*

[c] *Laboratoire de Chimie Physique, CNRS and UPMC, 11 rue Pierre et Marie Curie, 75005 Paris, France*

Abstract

Gradient corrections to the kinetic-energy density (KED) functional are derived, using the regular, two-component relativistic Hamiltonian of van Lenthe, Baerends and Snijders. The KED functional obtained depends on the external field potential and remains valid in the case of large momenta of electrons.

1. Introduction

The first approach in which the charge density ρ of a many-electron system was used to describe the properties of the system was the Thomas-Fermi model [1, 2]. This approach basically consisted in considering atomic electrons as independent fermions. The model was further developed to include terms accounting for exchange interactions (Dirac, 1930) [3] as well as a correction stemming from the inhomogenity of the system (von Weizsäcker 1935) [4]

ADVANCES IN QUANTUM CHEMISTRY VOLUME 39

0065-3276/01 $35 00

An exact theoretical foundation for dealing with systems of interacting fermions in terms of the fermion distribution in the system has been provided by the theorem of Hohenberg and Kohn [5]. These authors have established that all the properties of a many-electron system in a non-degenerate ground state are fully determined by its charge density They have also proven the existence and uniqueness of the energy functional of the charge density:

$$E[\rho] = T[\rho] + \int \rho(\vec{r}) V(\vec{r})\, d\vec{r} + \int\int \frac{\rho(\vec{r})\rho(\vec{r}')}{|\vec{r} - \vec{r}'|}\, d\vec{r}\, d\vec{r}' + E_{xc}[\rho], \qquad (1)$$

and formulated the variational principle for the ground-state charge density ρ. In Eq (1), $T[\rho]$ is the kinetic-energy density functional, the next two terms represent the electron-external field and electron-electron Coulomb interactions, and $E_{xc}[\rho]$ is the exchange-correlation functional. The external field potential $V(\vec{r})$ determines the properties of the system. However, the explicit form of the above functional is not known. Several useful approximations have been proposed, the Thomas-Fermi model and its extensions being one of them

Another topic in the investigation of many-electron systems is the inclusion of relativistic effects These effects are important in the study of heavy atoms and electron systems in strong fields. A fully relativistic treatment requires solving the Breit-Dirac equation, the result being a four-component wavefunction. However, solving this equation is not necessary when there is no process of creation or annihilation of particles with negative energy. In this case, it is convenient to use a two-component approach, reached by reducing the Dirac Hamiltonian through the Foldy-Wouthuysen transformation or the Pauli elimination of small components. Many authors [6, 7, 8, 9] have pointed out the disadvantages of the resulting two-component Hamiltonians, connected with: (i) the use of an expansion of the square-root operator outside its range of convergence; (ii) the operation of the resulting Hamiltonian on the Hilbert space, (iii) some peculiarities of the Hamiltonian close to the origin of the Coulomb potential. Therefore, in this paper we use the transformation method proposed by van Lenthe, Baerends and Snijders (LBS) [10] - which avoids the problems mentioned above - to derive the kinetic-energy density functional in the framework of the two-component formalism

In the next part we give a brief overview of the LBS two-component approximation. In the third part we carry out the gradient expansions of the density matrix and of the kinetic-energy density. In the conclusion we discuss the resulting expression and compare it with the standard non-relativistic one.

2. Regular two-component relativistic Hamiltonian

The Dirac Hamiltonian works on a four-component wavefunction Ψ,

$$\Psi = \begin{pmatrix} \phi \\ \chi \end{pmatrix}, \quad \phi = \begin{pmatrix} \psi_1 \\ \psi_2 \end{pmatrix}, \quad \chi = \begin{pmatrix} \psi_3 \\ \psi_4 \end{pmatrix}, \tag{2}$$

where ϕ represents the large components and χ the small components Keeping in mind the form of the Pauli matrices $\vec{\sigma}$, the Dirac equation becomes:

$$\begin{aligned} V(\vec{r})\phi + c\vec{\sigma}.\vec{p}\chi &= E\phi \\ c\vec{\sigma}.\vec{p}\phi + (V - 2mc^2)\chi &= E\chi \end{aligned} \tag{3}$$

where $V(\vec{r})$ is the Coulomb field potential.

Eliminating the small component yields

$$\chi = (2mc^2 + E - V)^{-1} mc\,\vec{\sigma}.\vec{p}\,\phi = (1/2mc)[1 + (E-V)/2mc^2]^{-1}\,\vec{\sigma}.\vec{p}\,\phi = \hat{X}\phi, \tag{4}$$

$$\hat{H}^{esc}\phi = V\phi + mc\,\vec{\sigma}.\vec{p}\;\hat{X}\phi = V\phi + (1/2)\,\vec{\sigma}.\vec{p}\,[1 + (E-V)/2mc^2]^{-1}\,\vec{\sigma}.\vec{p}\,\phi = E\phi. \tag{5}$$

The Hamiltonian $\hat{H}^{esc}$ is energy dependent and the large component ϕ is not normalized, whereas Φ is. In standard approaches one defines a normalization operator $\hat{O}$ which satisfies the relation.

$$\int_0^\infty \Phi^+\Phi\,dr = \int_0^\infty \Phi^+\hat{O}^+\hat{O}\,\Phi\,dr = \int_0^\infty \psi^+\psi\,dr = \int_0^\infty (\phi^+\phi + \chi^+\chi)dr = 1. \tag{6}$$

One possible choice for $\hat{O}$ is

$$\hat{O} = \sqrt{1 + \hat{X}^+\hat{X}}\,. \tag{7}$$

By eliminating the small component one obtains:

$$\int_0^\infty (\phi^+\phi + \chi^+\chi)\,dr = \int_0^\infty \phi^+(1 + \hat{X}^+\hat{X})\phi\,dr. \tag{8}$$

The operator $\hat{O}$ works on the Hamiltonian as well, i.e.:

$$\hat{H} = \hat{O}\hat{H}^{esc}\hat{O}^{-1} = \sqrt{1+\hat{X}^{+}\hat{X}}\left(V + c\vec{\sigma}.\vec{p}\hat{X}\right)\frac{1}{\sqrt{1+\hat{X}^{+}\hat{X}}}. \tag{9}$$

The standard quantum mechanical approach proceeds with an expansion in powers of $(E\text{-}V)/2mc^2$ of the factor $[1+(E\text{-}V)/2mc^2]^{-1}$, in both $\hat{H}$ and $\hat{O}$. This leads to the well-known Pauli Hamiltonian:

$$\hat{H}^{Pauli} = V + \frac{\vec{p}^2}{2m} - \frac{\vec{p}^4}{8mc^2} + \frac{\nabla^2 V}{8mc^2} + \frac{\vec{\sigma}.(\nabla V \times \vec{p})}{4mc^2}. \tag{10}$$

As recalled in the Introduction, the Hamiltonian obtained in this manner presents many problems. The expansion of the square root in Eq. (9) in terms of $(E\text{-}V)/2mc^2$ is justified if $\vec{p}^2 << 4mc^2$ but, in the Coloumb field, there are regions where electron momenta are large and, therefore, the expansion cannot be performed. The Darwin term $\Delta V/8mc^2$ behaves as a δ function close to the field sources (near the nuclei). In the case of a self-consistent procedure to solve the eigenvalue equation $\hat{H}^{Pauli}\Phi = E\Phi$, the spin-orbit operator $[1/4mc^2]\vec{\sigma}.(\nabla V \times \vec{p})$ behaves as an attractive $-1/r^3$ potential, which leads to arbitrarily large negative energies close to the nuclei instead of a discrete eigenvalue spectrum. The mass-velocity term $\vec{p}^4 / 8mc^2$ is a fourth-order differential operator, which may produce non square-integrable functions working on the Hilbert space. By including this term, we get a fourth-order differential equation which does not lead to quantization of the energy under usual boundary conditions.

To overcome these problems, one can expand $\hat{H}$ and $\hat{O}$ in powers of $E/(2mc^2\text{-}V)$ [10], which yields the result:

$$\hat{H}^{esc} = V + \vec{\sigma}\,\vec{p}\,\frac{c^2}{2mc^2 - V}\left(1 + \frac{E}{2mc^2 - V}\right)^{-1}\vec{\sigma}.\vec{p} = \tag{11}$$

$$= V + \vec{\sigma}.\vec{p}\,\frac{c^2}{2mc^2 - V}\,\vec{\sigma}.\vec{p} - \vec{\sigma}.\vec{p}\,\frac{c^2}{2mc^2 - V}\left(\frac{E}{2mc^2 - V}\right)\vec{\sigma}.\vec{p} + \ldots$$

Acting on the above expansion of the Hamiltonian $\hat{H}^{esc}$ with the normalization operator $\hat{O}$, one obtains the zeroth-order Hamiltonian $\hat{H}^{0}$ [10]:

$$\hat{H}^0 = V + \vec{\sigma}.\vec{p}\,\frac{c^2}{2mc^2 - V}\,\vec{\sigma}.\vec{p}\,. \tag{12}$$

The approximate Hamiltonian $\hat{H}^0$ incorporates the relativistic effects included at the Pauli-Hamiltonian level, but it does not suffer from singularities for $r \to 0$. Therefore it may be used variationally [10], since it possesses an energy spectrum limited from below.

3. Derivation of gradient corrections to the kinetic-energy density functional

We shall derive gradient corrections to the Thomas-Fermi density functional for a system of non-interacting relativistic fermions in a strong external field, using the regular two-component relativistic Hamiltonian $\hat{H}^0$. Most of the methods used for obtaining gradient corrections are based on a semi-classical expansion of the density matrix.

The density matrix for a system described by the Hamiltonian $\hat{H}^0$ has the form.

$$\rho(\vec{r},\vec{r}') = \sum_i^{\infty} \Phi_i(\vec{r})\Phi_i^+(\vec{r}')\hat{\rho}\,(\hat{H}^0), \tag{13}$$

where Φ_i represents the renormalized large components and $\hat{\rho}\,(\hat{H}^0)$ is the density operator of the system Following the original idea of Thomas and Fermi we consider that non-interacting particles fill all energy levels up to the Fermi level and that the density operator is the Heaviside step-function $\theta\,(\varepsilon_F - \hat{H}^0)$, every level being filled by two electrons with opposite spins. We do not consider spin-orbit interactions, using the simplified spin-independent Hamiltonian:

$$\hat{H}^0 = V + \vec{p}\,\frac{c^2}{2mc^2 - V}\,\vec{p}\,, \tag{14}$$

accounting for the effects arising from the relativistic motion.

The density matrix of the considered system is·

$$\rho(\vec{r},\vec{r}') = \sum_i^{\infty} \Phi_i(\vec{r})\Phi_i^+(\vec{r}')\theta(\varepsilon_F - \varepsilon_i) = \sum_i^{\infty} \begin{pmatrix} \phi_{1i} \\ \phi_{2i} \end{pmatrix} \begin{pmatrix} \phi_{1i}^+ & \phi_{2i}^+ \end{pmatrix} \theta(\varepsilon_F - \varepsilon_i), \tag{15}$$

$$\rho(\vec{r},\vec{r}') = \sum_{i}^{\infty}\left(\phi_{1i}(\vec{r})\phi_{1i}^{+}(\vec{r}')+\phi_{2i}(\vec{r})\phi_{2i}^{+}(\vec{r}')\right)\theta(\varepsilon_F-\varepsilon_i) =$$

$$= 2\sum_{i}^{\infty}\left(\phi_i(\vec{r})\phi_i^{+}(\vec{r}')\right)\theta(\varepsilon_F-\varepsilon_i) = 2\left\langle\vec{r}\left|\theta(\varepsilon_F-\hat{H}^0)\right|\vec{r}'\right\rangle. \tag{16}$$

The expansion of the density matrix in powers of $\hbar$ is done using the Wigner transformation [11] The Wigner transform of an operator $\hat{A}$ can be written as follows:

$$A_W(\vec{p},\vec{R}) = \int_V d\vec{s}\exp\left(\frac{\imath}{\hbar}\vec{p}.\vec{s}\right)\left\langle\vec{R}-\frac{\vec{s}}{2}\left|\hat{A}\right|\hat{R}+\frac{\vec{s}}{2}\right\rangle, \tag{17}$$

where $\vec{R} = \dfrac{\vec{r}+\vec{r}'}{2}$ and $\vec{s} = \vec{r}'-\vec{r}$. The transform of the operator product $\hat{C} = \hat{A}\hat{B}$ is obtained using the composition rule for the Wigner transforms of multipliers:

$$C_W(\vec{p},\vec{R}) = A_W(\vec{p},\vec{R})\exp\left[\frac{\imath\hbar}{2}\left(\frac{\overleftarrow{\partial}}{\partial\vec{R}}\frac{\vec{\partial}}{\partial\vec{p}}-\frac{\overleftarrow{\partial}}{\partial\vec{p}}.\frac{\vec{\partial}}{\partial\vec{R}}\right)\right]B_W(\vec{p},\vec{R}) \tag{18}$$

The procedure for finding a semi-classical expansion of ρ consists of taking the Laplace transform of the density operator:

$$\hat{\rho}(E) = \theta(\varepsilon_F-\hat{H}^0), \tag{19}$$

$$\theta(\varepsilon_F-\hat{H}^0) = \frac{1}{2\pi\imath}\int_{c-\imath\infty}^{c+\imath\infty}\frac{d\beta}{\beta}\exp\left[\beta(\varepsilon_F-\hat{H}^0)\right] =$$

$$= \frac{1}{2\pi\imath}\int_{c-\imath\infty}^{c+\imath\infty}\frac{d\beta}{\beta}\exp(\beta\varepsilon_F)\exp(\beta\hat{H}^0), \tag{20}$$

and setting up a differential equation for the Laplace transform·

$$\hat{Z}(\beta) = \exp(-\beta\hat{H}^0), \tag{21}$$

or, more precisely, for the Wigner transform of $\hat{Z}(\beta)$. To do so we first differentiate $\hat{Z}(\beta)$ with respect to β and we obtain·

$$\frac{\partial \hat{Z}(\beta)}{\partial \beta} = -\hat{H}^0 \exp(-\beta \hat{H}^0) = -\hat{H}^0 \hat{Z}(\beta), \tag{22}$$

then take the Wigner transform of this equation:

$$\frac{\partial \hat{Z}_W(\beta)}{\partial \beta} = -\hat{H}_W^0 \exp\left[\frac{i\hbar}{2}\left(\frac{\overleftarrow{\partial}}{\partial \vec{R}}\frac{\vec{\partial}}{\partial \vec{p}} - \frac{\overleftarrow{\partial}}{\partial \vec{p}}\cdot\frac{\vec{\partial}}{\partial \vec{R}}\right)\right]\hat{Z}_W(\beta), \tag{23}$$

where $\hat{Z}_W(\beta)$ is the Wigner transform of $\hat{Z}(\beta)$. To solve Eq (23) we seek a solution of the form:

$$\hat{Z}_W(\beta) = \exp[-\beta(F\vec{p}^{\,2}+V)](1+\hbar W_1(\vec{p},\vec{R})+\hbar^2 W_2(\vec{p},\vec{R})+\ldots . \tag{24}$$

Substituting this form for $\hat{Z}_W$ into Eq. (23) and equating equal powers of $\hbar$ we obtain relations for the W's and, subsequently, an expression for $\hat{Z}_W$. Applying the inverse Laplace transformation we obtain the Wigner transform of the density matrix

$$\rho_W = \vartheta(E-\hat{H}) + \frac{\hbar^2}{4}\nabla^2 F\delta(\hat{H}-E) - \frac{\hbar^2}{8}\left[(\vec{p}.\nabla F)^2 - F\nabla^2\hat{H}\right]\delta'(\hat{H}-E) +$$
$$+\frac{\hbar^2}{36}\left[F(\nabla\hat{H})^2 + F^2(\vec{p}.\nabla)^2\hat{H} - 2F(\vec{p}.\nabla F)(\vec{p}.\nabla\hat{H})\right]\delta''(\hat{H}-E), \tag{25}$$

where

$$F = \frac{c^2}{2mc^2 - V} \tag{26}$$

and

$$\hat{H} = F\vec{p}^{\,2} + V. \tag{27}$$

The density distribution is given by the diagonal part of the density matrix and is derived using the inverse Wigner transformation [12].

$$\rho(\vec{r}) = \rho(\vec{r},\vec{r}) = \int_{V_p} \rho_W(\vec{p},\vec{R})\frac{d\vec{p}}{(2\pi\hbar)^3}. \tag{28}$$

For the Wigner transform of the kinetic energy density we take [12].

$$\tau_W(\vec{p},\vec{R}) = \frac{1}{4}\nabla^2_{\vec{R}}\rho_W(\vec{p},\vec{R}) + \frac{\vec{p}^2}{\hbar^2}\rho_W(\vec{p},\vec{R}). \tag{29}$$

The kinetic energy density itself is obtained through the inverse transformation of τ_W:

$$\tau(\vec{r}) = \frac{1}{4}\nabla^2\rho(\vec{r}) - \int_{V_p}\frac{\vec{p}^2}{\hbar^2}\rho_W(\vec{p},\vec{R})\frac{d\vec{p}}{(2\pi\hbar)^3}. \tag{30}$$

Inserting the density distribution from Eq. (28) into Eq (30) yields the expression for the kinetic-energy density functional:

$$\tau(\rho) = \frac{3}{10}(3\pi^2)^{\frac{2}{3}}\rho^{\frac{5}{3}} + \frac{1}{72}\frac{(\nabla\rho)^2}{\rho} + \frac{1}{6}\nabla^2\rho + \frac{1}{12}\frac{\nabla^2 F}{F}\rho - \frac{1}{24}\frac{(\nabla F)^2}{F^2}\rho + \frac{1}{12}\frac{\nabla F.\nabla\rho}{F}. \tag{31}$$

This expression depends on V through F given in Eq. (26). It can be seen that it does not suffer from the drawbacks listed above, and that it reduces to the usual gradient-corrected non-relativistic expression when V is small.

4. Conclusion

We have derived an expression for the kinetic-energy density functional $\tau(\rho)$ which is seen to depend on the external field potential $V(\vec{r})$. This expression is truly relativistic since we have used the two-component, zeroth-order relativistic Hamiltonian of van Lenthe, Baerends and Snijders, which is correct even for large electron momenta (while the Pauli Hamiltonian is not). In this paper, spin-orbit interactions were omitted since we have used the scalar part of the relativistic Hamiltonian. When V is small ($F \to 1/2m$), that is, when the Hamiltonian gets non-relativistic, our expression turns into the well-known, Thomas-Fermi kinetic-energy density functional including the von Weizsäcker gradient correction.

Acknowledgments

This work was partly supported by a twinning convention between the Universities Pierre et Marie Curie (Paris) and Saint Kliment Ohridski (Sofia) and the European COST-D9/010 contract.

References

1. Thomas L H. *Proc. Cambridge Phil. Soc.* **23** (1926) 542.
2 Fermi E. *Z. Phys.* **48** (1928) 73
3. Dirac P. A. M. *Proc. Cambridge Phil. Soc.* **26** (1930) 376
4. von Weizsäcker C. F. *Z. Phys.* **96** (1935) 431.
5. Hohenberg P. and Kohn W. *Phys. Rev. B* **136** (1964) 864
6 Farazdel A. and Smith V. H. *Int. J. Quantum Chem.* **29** (1986) 311.
7. Ketley I. J. and Moss R. E. *Mol. Phys.* **48** (1983) 1131; *ibid.* **49** (1983) 1289.
8. Moss R. E. *Mol. Phys.* **53** (1984) 269.
9. Kutzelnigg W. *Z. Phys. D* **15** (1990) 27
10. van Lenthe E., Baerends E. J. and Snijders J. G. *J. Chem. Phys.* **99** (1993) 4597
11. Wigner E. *Phys. Rev.* **40** (1932) 749
12. Grammaticos B. and Voros A. *Ann. Phys.* **123** (1979) 359.

AN ATTEMPT TO REALISE THE CONSTRAINED SEARCH APPROACH IN THE DENSITY FUNCTIONAL THEORY

Boris P. Zapol
Dept. of Theoretical Physics and Inst of Chemical Physics, Univ of Latvia
19 Rainis Blvd., Riga LV-1586, Latvia
Email: bzapol@kfi.lu.lv

ABSTRACT

The problem of reconstruction of wave functions from a given electron density is considered. A reformulation of the problem is proposed which is based on the Fourier transform. Arising mathematical problems are studied, namely, the properties of reduced spatial densities and their Fourier images are obtained, which follow from known properties of the wave functions. The proposed approach may provide a practical implementation of the Constrained Search Approach to the DFT.

TABLE OF CONTENTS

ADVANCES IN QUANTUM CHEMISTRY, VOLUME 39

0065-3276/01 $35 00

1. INTRODUCTION

1.1. The Constrained Search Approach in the Density Functional Theory

The Density Functional Theory [1-5] is an important tool for large-scale *ab initio* quantum-chemical studies of complex systems, and it has incontestable successes in theoretical investigations of the structure of matter. However, at present its application is necessarily connected with the use of some approximated form of the energy density functional $E[\rho(\mathbf{r})]$ because the exact form remains unknown. The additional problem is that the used methods of obtaining these approximated forms provide neither an evaluation of the error introduced nor a systematic way of improving the approximation. Hence, a search for an exact form of the functional not only presents a theoretical challenge, but also remains an actual and important practical problem of the Density Functional Theory. Its solution would supply grounds both for variational derivation of precise equations of the method and for construction of controllable approximations.

A way to obtain the exact density functional is presented by the Constrained Search Approach [6-9]. In general, the energy functional of density for an N-electron system in an external field $v(\mathrm{r})$ can be presented as [10]

$$E[\rho]=F[\rho]+\int \rho(\mathbf{r})v(\mathbf{r})d\mathbf{r}, \qquad (1)$$

where $F[\rho]$ is a universal functional of density. For the class of pure-state N-representable densities, that is, such functions $\rho(\mathbf{r})$ that can be obtained from an antisymmetric, normalised N-electron wave function (WF) $\Psi(q_1,...,q_N)$ as a result of the reduction

$$\rho(\mathbf{r})= N \int \Psi(\mathbf{r}\,\sigma_1, q_2,...,q_N)\, \Psi^*(\mathbf{r}\,\sigma_1, q_2,...,q_N)d\sigma_1 dq_2 ,..., dq_N \qquad (2)$$

(here $q_i=\mathbf{r}_i\sigma_i$ is the set of spatial and spin coordinates of the ith electron, and integration over spins stands for summation) the "constrained search" functional $F[\rho]$ was proposed by Levy [6] (and developed by Levy [7] and Lieb [8]) in the form

$$F_{\mathrm{LL}}[\rho]=\inf_{\Psi[\rho]}\langle\Psi|\mathbf{T}+\mathbf{W}|\Psi\rangle\,, \tag{3}$$

with $\mathbf{T}$ and $\mathbf{W}$ being the many-electron kinetic and electron interaction energy operators. The notation $\Psi[\rho]$ indicates that the infimum should be taken over all the wave functions related to the given ρ by Eq. (2). For a more general case of ensemble N-representable densities, that is, such functions $\rho(\mathbf{r})$ that correspond to a certain ensemble state of the N-electron system described by its density matrix (DM)

$$\boldsymbol{D}^N(q_1,...,q_N|\,q'_1,...,q'_N)=\sum_a w_a\Psi_a(q_1,...,q_N)\;\Psi^*_a(q'_1,...,q'_N), \tag{4}$$

with partial wave functions, Ψ_a, and nonnegative weights, w_a, normalised by conditions $\|\Psi_a\|=1$ and $\sum_a w_a=1$, the "constrained search" definition of the functional reads as [8,9]

$$F_{\mathrm{LV}}[\rho]=\inf_{\boldsymbol{D}[\rho]}\;\mathrm{tr}\,\langle D(\mathbf{T}+\mathbf{W})\,\rangle\,, \tag{5}$$

where $\boldsymbol{D}[\rho]$ denotes all DMs connected with the given $\rho(\mathbf{r})$ by the equality

$$\rho(\mathbf{r})=N\int\;\boldsymbol{D}^N\,(\mathbf{r}\,\sigma_1,\,q_2,...,q_N\,|\,\mathbf{r}\,\sigma_1,\,q_2,...,q_N)\,d\sigma_1 dq_2\,,...,\,dq_N\,. \tag{6}$$

The domains of both functionals, that is, the classes of pure-state and ensemble N-representable densities, actually coincide [1] and present [11,12] the set of all nonnegative functions $\rho(\mathbf{r})$ normalised to N as follows:

$$\int\rho(\mathbf{r})\,d\mathbf{r}=N. \tag{7}$$

1.2. The Reconstruction Problem

As follows from Eqs. (3) and (5), a practical implementation of the Constrained Search Approach requires for a systematic way of finding *all* either WFs (for the functional $F_{\mathrm{LL}}[\rho]$) or DMs (for the functional $F_{\mathrm{LV}}[\rho]$) that reduce to the given spatial density $\rho(\mathbf{r})$. Let us call such a procedure the *reconstruction* of WFs (or DMs) from the spatial density.

The reconstruction is an operation inverse to the reduction given by Eq. (2) or (6) in the following sense.

Let a class of WFs (or DMs) be chosen, which we consider *admissible* for the variational procedure. These have to meet general requirements The WF, for example, is to belong to L^2 and to be continuous and antisymmetrical. The DM

must be Hermitian, antisymmetrical (within left and right argument set), and positive definite. However, practically we can further restrict the class requiring for other desired properties. For example, these may be properties that follow from WF being a solution of the Shrödinger equation for a certain class of potentials; say, for a bounded state it may be the requirement that WF belongs to the class of fast converging functions, that is decreases exponentially at the infinity. Also, finiteness of average kinetic energy often is required from the state.

To perform the reconstruction, we have to find such a subset of the class of admissible WFs (or DMs) that contains all and only such elements that reduce to the given density $\rho(\mathbf{r})$. Equation (2) (or, resp., (6)) determines a mapping from the mentioned subset onto the set of images, which contains the only element $\rho(\mathbf{r})$. The mapping is surjective by definition. We use the symbol $\rightarrow$ for the mappings induced by the reduction:

$$\Psi \rightarrow \rho \; ; \; \boldsymbol{D}^N \rightarrow \rho. \qquad (8)$$

Here Ψ and $\boldsymbol{D}^N$ indicate the relevant sets, and $\rightarrow$ symbolises that the mapping is (normally) many-to-one. The problem of inverting the mappings given by Eq. (8) will be termed the Reconstruction Problem. It is closely related to but does not coincide with the *N*-representability problem.

The latter requires for the following two questions be answered:

1) is the given function $\rho(\mathbf{r})$ an *N*-representable density?

2) what is the class of *N*-representable densities?

For the positive answer, it is sufficient to present at least one example of WF (or DM), which reduces to the given density (in case of the first question) or to a common representative of the class (in case of the second question). In the second case, it is necessary to prove also that the elements falling out of the class under consideration cannot be obtained as a result of the reduction, that is, the set of originals of the mapping $\Psi \rightarrow \rho$ is empty for such ρ. The Reconstruction Problem poses a more general task: to actually find *all* originals of the mapping $\Psi \rightarrow \rho$ for every given ρ. Resolving this task automatically resolves also the *N*-representability problem because the density being or not being *N*-representable depends on whether the found set of originals turns out to be or, respectively, not to be non-empty. Naturally, the Reconstruction Problem is expected to be more complicated than the *N*-representability problem.

Similar reconstruction problems may be also considered for the mapping from Ψ to the 1st and 2nd order reduced density matrices (1-RDM and 2-RDM), for the two-particle density (the diagonal element of the 2-RDM), as well as for 1- and 2-particle spin-density matrices and spin-densities. The practical meaning of such studies is related to the fact that every of these values may be used as the fundamental variable in a variational theory (for a more thorough discussion, see [4, 5]). Reconstruction of *k*-particle RDM (*k*-RDM) with $k = 3$ and 4 from 1- and

2-RDM, as well as 2-RDM from 1-RDM also appears to be necessary for iterative solution of the Contracted Schrödinger Equation [15-17].

The N-representability Problem has drawn much attention (see [2, 4, 17, 18] and references therein). Number of works and results concerning the Reconstruction Problem is much scarcer. Its complete solution may be presented as an expansion of Ψ in terms of N-electron determinants, constructed on the so-called equidensity orbitals [12-14]. This method has yielded some useful evaluations for the density functional [1], but it is not applied widely in practice of quantum chemical computations due to difficulties with handling the equidensity orbitals. Reconstruction of k-RDM (k = 2 to 4) is considered by Valdemoro *et al* (see [15-17] and references therein). Reconstruction of WFs and DMs using the Radon Transform is discussed in [19-21].

In the present paper, an independent approach to the Reconstruction Problem is proposed, based on employment of the Fourier Transform (FT). We reformulate the problem in such a manner that the mapping to be inverted is replaced by a series of mappings, each of them being simpler for inversion. A general scheme of this approach is outlined in Section 2.

1.3. Electron density, its Fourier Transform, and related values

Implementation of this scheme requires for some mathematical problems to be investigated previously. Specifically, the class of FTs of eligible N-particle spatial densities is to be determined. To find the properties of FTs belonging to this class, one has first to know properties of their pre-images, that is N-particle spatial densities themselves. We consider, for generality, (reduced) k-particle spatial densities (k-RSDs) for all k = 1, ..., N, including here the case $k = N$ corresponding to non-reduced N-particle spatial density. Properties of k-RSD and their Fourier images that follow from those of the many-electron wave function such as the finiteness of its values, its norm, and its average kinetic energy, as well as its taking complex values, normalisation and antisymmetry are studied in Section 3.

Analytical properties of $\rho(\mathbf{r})$, the one-electron density in position space (corresponds to our 1-RSD), were studied by Lieb [22] These results are expressed in terms of $\rho^{1/2}(\mathbf{r})$. As we are specifically interested in studying properties of the FT of proper densities rather than their square roots, and for all k not only k =1, we cannot use these results directly. However, we shall follow the method of Ref. [22] in our study.

The available literature on properties of FTs of k-RSDs is rather scarce, excluding 1-RSD, which is $\rho(\mathbf{r})$. Its FT is merely the X-ray form-factor [23,24].

FTs of k-RSDs were formally introduced by Thakkar *et al* [25] who named them the k-electron form-factors, but they were not investigated in this work.

The one-electron momentum density $\gamma(\mathbf{p})$ which results after reducing the square module of FT of wave function attracted more attention of researchers because of its close connection with the Compton profile, a quantity rather accurately measured in experiments. The momentum distribution and the Compton profile for X-ray scattering were found by Coulson and March [26] using the Thomas-Fermi method. Ways to extract $\gamma(\mathbf{p})$ from $\rho(\mathbf{r})$ were proposed using Thomas-Fermi method [27], Density Functional Theory in its general form [27] and in the linear [27] and non-linear [28] approximation. Simultaneous analysis of $\gamma(\mathbf{p})$ and $\rho(\mathbf{r})$ using maximization of the sum of information entropies in $\mathbf{p}$ and $\mathbf{r}$ spaces was performed by Gadre *et al.* [29]. A relationship between the atomic electron densities in momentum and position spaces was studied through a non-linear deformation of momentum densities by Kryachko and Koga [30], and in the context of a finite-basis-set model problem by Harriman [31].

The problem (which is in some sense a mirror one to that studied in the present paper) of investigation of $B(\mathbf{r})$, the FT of one-electron momentum density, was considered by Weyrich *et al.* [32] and by Thakkar *et al* [25].

These results, however, only indirectly relate to the problems of our interest. The only relevant result found in the literature concerns the normalisation of FT of k-RSD [25].

2. REFORMULATION OF THE RECONSTRUCTION PROBLEM

2.1 Reduced electron densities and their Fourier images

We present here main definitions and relationships for further references. Consider a time-independent N-electron wave function, $\Psi\ (q_1,...,q_N)$, where $q_k=\mathbf{r}_k\sigma_k$ are spatial and spin coordinates of the kth electron. The state is not required to be stationary. Define (cf. Ref. [33]) the N-electron spatial density as a result of reduction (summation) of squared module of the wave function over spins:

$$P^N(\mathbf{r}_1,..., \mathbf{r}_N) = N\,! \sum_{\sigma} \int |\, \Psi(\mathbf{r}_1\sigma_1, \mathbf{r}_2\sigma_2, .., \mathbf{r}_N\sigma_N)\,|^2, \qquad (9)$$

(here $\sigma = \{\sigma_1, ..., \sigma_N\}$) and reduced k-particle spatial density as a result of its further reduction over $N - k$ spatial coordinates:

$$P^k(\mathbf{r}_1,..., \mathbf{r}_k) = [(N-k)\,!]^{-1} \int P^N(\mathbf{r}_1,..., \mathbf{r}_N)\, d\mathbf{r}_{k+1}...d\mathbf{r}_N\,. \qquad (10)$$

We restrict here ourselves to studying only pure states because the case of ensemble states involves some technical complications but does not differ in principle.

Eqs. (9) and (10) define, in particular, the following two mappings:

$$\Psi \rightarrow P^N \rightarrow P^1, \tag{11}$$

both of them being many-to-one.

Consider also the FT of P^k (for a certain k, $1 \le k \le N$),

$$F^k(\mathbf{k}_1,\ldots,\mathbf{k}_k) = (2\pi)^{-3k/2} \int P^k(\mathbf{r}_1,\ldots,\mathbf{r}_k) \exp[-i(\mathbf{k}_1\mathbf{r}_1+\ldots+\mathbf{k}_k\mathbf{r}_k)\, d\mathbf{r}_1\ldots d\mathbf{r}_k, \tag{12}$$

and the inverse FT of its image F^k,

$$P^k(\mathbf{r}_1,\ldots,\mathbf{r}_k) = (2\pi)^{-3k/2} \int F^k(\mathbf{k}_1,\ldots,\mathbf{k}_k) \exp[i(\mathbf{k}_1\mathbf{r}_1+\ldots+\mathbf{k}_k\mathbf{r}_k)\, d\mathbf{k}_1\ldots d\mathbf{k}_k. \tag{13}$$

2.2. An alternative approach to the reconstruction

Let us observe that, as it follows from Eqs. (12) and (10),

$$F^k(\mathbf{k}) = (2\pi)^{3(N-1)/2}\,[(N-1)!]^{-1}\, F^N(\mathbf{k},\mathbf{0},\ldots,\mathbf{0}). \tag{14}$$

This means that, unlike the densities of orders 1 and N that are related by Eq. (10) containing integration, their FTs are related in a simpler manner, namely, F^1 is merely a restriction of F^N to a 3-dimensional plane. This relationship between FTs of 1-particle and N-particle spatial densities is the key equation of the advanced approach. Its defines the (many-to-one) mapping

$$F^N \rightarrow F^1 \tag{15}$$

in such a form that the reconstruction of all F^N related to the given F^1 by Eq. (14) appears to be simpler than that for P^N and P^1 related by an integral as in Eq. (10).

Now, instead of the chain of mappings given by Eq. (11), we can consider another chain connecting the same initial and final items:

$$\Psi \rightarrow P^N \leftrightarrow F^N \rightarrow F^1 \leftrightarrow P^1, \tag{16}$$

where the four consecutive mappings are given by Eqs. (9), (12), (14), and (13), respectively. We used here two-sided arrows to stress that the respective mappings are bijective. Each of the intermediate relationships (12), (13), and (14) is simpler for studying the corresponding direct and inverse mappings than the complete mapping $P^N \rightarrow P^1$ defined by Eq. (10).

Inversion of the mapping $\Psi \rightarrow P^N$ consists in splitting of the P^N in 2^N admissible terms (cf. Eq. (9)), each of them being a squared spin component of Ψ. (In the present work, we do not require Ψ to describe a state with definite total spin; otherwise, the number of independent spin components naturally reduces.) Inversion of the mappings $P^N \leftrightarrow F^N$ and $F^1 \leftrightarrow P^1$ is inversion of the FT, which is

well-studied [34]. Therefore, the efforts should be directed to inversion of the mapping $F^N \rightarrow F^1$. Respectively, the Reconstruction Problem may be reformulated as follows:

To find all such $F^N(\mathbf{k}_1,\ldots,\mathbf{k}_N)$ that the restriction of each of them onto the 3-plane $(\mathbf{k},\mathbf{0},\ldots,\mathbf{0})$ in R^{3N} is the given $F^1(\mathbf{k})$.

It is simple to derive from Eqs. (12) and (10) a more general relationship than Eq. (14):

$$F^k(\mathbf{k}_1,\ldots,\mathbf{k}_k) = (2\pi)^{3(l-k)/2}\,[(N-l)!]\,[(N-k)!]^{-1}\,F^l(\mathbf{k}_1,\ldots,\mathbf{k}_k,\mathbf{0},\ldots,\mathbf{0}),$$
$$1 \le k < l \le N, \qquad (17)$$

which may be used, if necessary, for other cases of reconstruction or studies on N-representability. For example, the practically important problem of determination of the class of N-representable two-particle densities $P^2(\mathbf{r}_1, \mathbf{r}_2)$ [18] reduces to the following problem:

To find the class of such $F^2(\mathbf{k}_1, \mathbf{k}_2)$ that each of them can be presented as the restriction onto the 6-plane $(\mathbf{k}_1, \mathbf{k}_2,\mathbf{0},\ldots,\mathbf{0})$ in R^{3N} of at least one function $F^N(\mathbf{k}_1,\ldots,\mathbf{k}_N)$ belonging to the class of Fourier images of eligible N-densities.

Answers to such questions require for investigation into properties of F^1, F^2, and F^N. Some of these properties are considered in the following Section. For the sake of both brevity and generality, we study properties of P^k, $k = 1, \ldots, N$, and we use them to derive properties of F^k, $k = 1, \ldots, N$.

3. PROPERTIES OF ELECTRON DENSITIES AND THEIR FOURIER IMAGES

3.0. Technical remarks

For the sake of brevity, we shall employ the following notations for integrals in the direct space (cf. [22]):

$$\int = \sum_{\sigma} \int d\mathbf{r}_1 \ldots d\mathbf{r}_N; \qquad (18)$$

$$\int' = \int d\mathbf{r}_1 \ldots d\mathbf{r}_k; \qquad (19)$$

$$\int^+ = \sum_{\sigma} \int d\mathbf{r}_{k+1} \ldots d\mathbf{r}_N. \qquad (20)$$

It is obvious that $\int = \int' \int^+$; that $\sum_{\sigma} \int'$ converts to $\int$ at $k = N$; and that $\int^+$ converts to $\int$ at $k = 0$. Now, using Eqs. (9) and (10), P^k may be presented in the short form

$$P^k = N!\,[(N-k)!]^{-1} \int^+ |\Psi|^2. \qquad (21)$$

In this Section, we derive some properties of k-RSDs and their FTs. The original properties of the wave function inducing the mentioned properties are shown in the titles of sub-sections. The methods we use to investigate the properties of k-RSD follow in general lines the classical work by Lieb [22] where those of $\rho^{1/2}$ were studied We will make use of Cauchy and Bunjakowsky-Schwarz inequalities, that in our case give

$$|\int^{+} f_1 \, f_2|^2 \leq \int^{+} |f_1|^2 \bullet \int^{+} |f_2|^2 \text{ for any } f_1, f_2 \in L^2. \tag{22}$$

3.1. Finiteness of wave function norm.

The normalisation integral must converge:

$$\int |\Psi|^2 < \infty, \tag{23}$$

that is $\Psi \in L^2(\mathbf{R}^{3N})$. In terms of RSD this may be rewritten as

$$\int' P^k < \infty. \tag{24}$$

As P^k is by definition non-negative, this means that

$$P^k \in L^1(\mathbf{R}^3 k); \text{ and} \tag{25}$$

$$(P^k)^{1/2} \in L^2(\mathbf{R}^3 k). \tag{26}$$

As the integration in Eq. (24) may be considered as taking of the FT at all $\mathbf{k}_k$ zero, this may be written as

$$F^k(\mathbf{0}, \ldots, \mathbf{0}) < \infty. \tag{27}$$

This requirement is necessary and sufficient for F^k to correspond to a normalisable pre-image.

3.2. Normalisation.

For the wave function normalised by

$$\int |\Psi|^2 = 1, \tag{28}$$

k-RSD defined by Eq. (10) obeys the normalisation condition

$$\int' P^k = N! \, [(N-k)!]^{-1}. \tag{29}$$

In analogy with the left part of Eq. (27), the same may be written as

$$F^k(\mathbf{0}, \ldots, \mathbf{0}) = (2\pi)^{-3k/2} \, N! \, [(N-k)!]^{-1}. \tag{30}$$

Eqs. (29) and (30) present the normalisation conditions for k-RSD and its FT, respectively. In particular,

$$\int' P^1 = N; \qquad F^1(\mathbf{0}) = (2\pi)^{-3/2} \, N; \tag{31}$$

$$\int' P^N = N!; \qquad F^N(\mathbf{0}, \ldots, \mathbf{0}) = (2\pi)^{-3N/2} \, N!. \tag{32}$$

The normalisation condition similar to that given by Eq. (30) was found in Ref [25] for k-RSD normalised otherwise than in the present work.

3 3. Finiteness of kinetic energy.

To provide finite values of the total energy, admissible WFs are required [22] to yield finite average kinetic energy T in the state Ψ,

$$T[\Psi] = -\tfrac{1}{2} \sum_{i=1}^{N} \int \Psi^* \nabla_i^2 \Psi = \tfrac{1}{2} N \int |\nabla_1 \Psi|^2 < \infty , \qquad (33)$$

that is $\nabla_i \Psi \in L^2(\mathbf{R}^{3N})$.

It follows from Eq. (21) that

$$|\nabla_1 P^k| = N! [(N-k)!]^{-1} \left| \int^+ \{(\nabla_1 \Psi^*)\Psi + \Psi^* \nabla_1 \Psi\} \right|$$
$$\le 2N! [(N-k)!]^{-1} \int^+ |\nabla_1 \Psi| |\Psi| . \qquad (34)$$

The inequality sign appears due to bringing the module sign into the integrand. Now, using Eqs. (33) and (34) and applying the inequality (22), we have

$$\int' |\nabla_1 P^k| \le 2N! [(N-k)!]^{-1} \int |\nabla_1 \Psi| |\Psi|$$
$$\le 2N! [(N-k)!]^{-1} [\int |\nabla_1 \Psi|^2 \cdot \int |\Psi|^2]^{1/2}$$
$$= 4(N-1)! [(N-k)!]^{-1} T^{1/2} . \qquad (35)$$

Together with Eq. (33) this means that $\int' |\nabla_1 P^k| < \infty$, and hence

$$\nabla_1 P^k \in L^1(\mathbf{R}^{3k}). \qquad (36)$$

It is possible also to extend some results of Ref. [22] to the square root of k-RSD. It follows from Eqs. (34), (21) and (22) that

$$|\nabla_1 P^k|^2 \le \{2N! [(N-k)!]^{-1} \int^+ |\nabla_1 \Psi| |\Psi|\}^2$$
$$\le 4N! [(N-k)!]^{-1} P^k \int^+ |\nabla_1 \Psi|^2, \qquad (37)$$

that gives

$$|\nabla_1 (P^k)^{1/2}|^2 = |\nabla_1 P^k|^2 / (4P^k) \le N! [(N-k)!]^{-1} \int^+ |\nabla_1 \Psi|^2, \qquad (38)$$

and

$$\int' |\nabla_1 (P^k)^{1/2}|^2 \le 2(N-1)! [(N-k)!]^{-1} T . \qquad (39)$$

Hence, accounting for Eq. (33),

$$\nabla_1 (P^k)^{1/2} \in L^2(\mathbf{R}^{3k}),$$

that together with Eq. (26) means (cf. Ref. [22])

$$(P^k)^{1/2} \in H^1(\mathbf{R}^{3k}). \qquad (40)$$

3.4. Finiteness of wave function values.

Finiteness of wave function,

$$|\Psi(\mathbf{r}_1\sigma_1, \mathbf{r}_2\sigma_2, ..., \mathbf{r}_N\sigma_N)| < \infty , \qquad (41)$$

has been stated for potentials that have no points where they diverge faster than r^{-2} (r being the distance from this point in the physical 3D space), e.g., in Ref [34]. Eq. (41), in accordance with the definition of P^k, implies finiteness of P^k,

$$P^k(\mathbf{r}_1,..., \mathbf{r}_k) | < \infty , \tag{42}$$

and thus finiteness of the integral

$$\int F^k (\mathbf{k}_1,..., \mathbf{k}_k)\, d\mathbf{k}_1...d\mathbf{k}_k = (2\pi)^{3k/2} P^k(\mathbf{0} ,..., \mathbf{0}) < \infty, \tag{43}$$

that is, $F^k \in L^1 (\mathrm{R}^{3k})$.

3.5. Wave function being complex valued.

The wave function takes complex values. Hence, $P^k \geq 0$ for all values of arguments by definition. A necessary and sufficient condition on a function F^k for it being the Fourier image of a non-negative original P^k is [34] that F^k is a positive definite function. Such a function has the following properties It is finite and continuous; it is hermitian:

$$F^{k*}(\mathbf{k}_1, ... , \mathbf{k}_k) = F^k (-\mathbf{k}_1, . \ , - \mathbf{k}_k); \tag{44}$$

and the integral

$$\int\int F^k (\mathbf{k}_1 - \mathbf{q}_1, ... , \mathbf{k}_k - \mathbf{q}_k)\, g (\mathbf{k}_1, ... , \mathbf{k}_k)\ g^*(\mathbf{q}_1, ... , \mathbf{q}_k)\, d\mathbf{k}_1...d\mathbf{k}_k\, d\mathbf{q}_1...d\mathbf{q}_k \geq 0 \tag{45}$$

for any $g (\mathbf{k}_1, ... , \mathbf{k}_k)$ which is continuous and absolutely integrable in all the space. The latter implies also [34]

$$| F^k (\mathbf{k}_1,..., \mathbf{k}_k)| \leq F^k(\mathbf{0} ,..., \mathbf{0}), \tag{46}$$

which, together with Eq. (30), gives

$$| F^k(\mathbf{k}_1,..., \mathbf{k}_k)| \leq (2\pi)^{-3k/2} N\, !\, [(N - k)\, !]^{-1}. \tag{47}$$

3.6. Permutational antisymmetry of wave function.

The permutational antisymmetry of the wave function implies the permutational symmetry of k-RSD. It can be demonstrated as follows:

$$\mathbf{P}\, P^k = N\, !\, [(N - k)\, !]^{-1} \int {}^+\mathbf{P}\, |\, \Psi\, |^{\,2} = P^k, \tag{48}$$

and hence

$$\mathbf{S}\, P^k = P^k. \tag{49}$$

We used here Eq. (21) and antisymmetry of Ψ under any transposition of position-spin coordinates. $\mathbf{P}$ is a permutation in a set of k position-spin coordinates, P^k being naturally indifferent to permutation of spin coordinates, and $\mathbf{S} = (k!)^{-1} \Sigma\, \mathbf{P}$

(summation made over all permutations **P** of k particles) is the symmetriser for k electrons.

Further, the permutational symmetry of k-RSD implies, through Eq. (12), that for its FT:

$$\mathbf{P}\, F^k(\boldsymbol{k}) = F^k(\mathbf{P}^{-1}\boldsymbol{k}) =$$
$$(2\pi)^{-3k/2}\int P^k(\boldsymbol{r}) \exp\{-i(\mathbf{P}^{-1}\boldsymbol{k})\bullet\boldsymbol{r}\}\, d\boldsymbol{r} =$$
$$(2\pi)^{-3k/2}\int P^k(\mathbf{P}\boldsymbol{r}) \exp\{-i(\boldsymbol{k}\bullet(\mathbf{P}\boldsymbol{r})\}\, d\boldsymbol{r} = F^k(\boldsymbol{k}). \qquad (50)$$

Here $\boldsymbol{k} = \{\mathbf{k}_1,..., \mathbf{k}_k\}$, $\boldsymbol{r} = \{\mathbf{r}_1,..., \mathbf{r}_k\}$, and $\boldsymbol{k}\bullet\boldsymbol{r} = \sum_{i=1}^{k} \mathbf{k}_i\, \mathbf{r}_i$. **P** is used in the last equation to denote permutations in the set $\boldsymbol{k}$ or $\boldsymbol{r}$. At the third stage of the derivation, the invariance of $P^k(\boldsymbol{r})$ under **P** was used.

4. CONCLUSIONS

A general scheme of a new approach in the Density Functional Theory is proposed, based on reconstruction of wave functions from a given electron density using Fourier transform. The idea consists in replacing a short chain of mappings, which are difficult to invert, by a longer chain consisting of mappings that are simpler to invert. A relevant mathematical technique is developed, namely, the properties of reduced spatial densities and their Fourier images are obtained, that follow from finiteness of the wave function, of its norm and average kinetic energy, as well as from normalisation and antisymmetry of the wave function and its being complex-valued. The practical implementation of the proposed approach remains a problem.

5. ACKNOWLEDGEMENTS

The author is thankful to T. Cirulis and M. Belov for valuable discussions. The author acknowledges support of this work by the Latvian Council of Science under project Nr. 96.0620.

REFERENCES

[1] R. M. Dreizler and E. C. U. Gross, "Density Functional Theory" (Springer-Verlag, Berlin 1990).
[2] R. Erdahl and V. H. Smith, Eds., "Density Matrices and Density Functionals" (Reidel, Dordrecht 1987).
[3] R. G. Parr and W. Yang, "Density-Functional Theory of Atoms and Molecules" (Oxford University Press, New York 1994).
[4] E. S. Kryachko and E. V. Ludeña, "Energy Density Functional Theory of Many-Electron Systems" (Kluwer, Dordrecht 1994).
[5] J. Keller and J. L. Gázques, Eds., "Density Functional Theory" (Springer-Verlag, Berlin 1983).
[6] M. Levy, Proc. Natl. Acad. Sci. USA **76**, 6062 (1979).
[7] M. Levy, Phys. Rev. **A26**, 1200 (1982).
[8] M. Lieb, in "Physics as Natural Philosophy· Essays in Honor of Laszlo Tisza on his 75th Birthday", 111 (Eds. A. Shimony and H. Feshbach, MIT Publisher, Cambridge 1982).
[9] S. M. Valone, J. Chem. Phys. **73**, 4653 (1980).
[10] P. Hohenberg and W. Kohn, Phys. Rev. **B136**, 864 (1964).
[11] T. I. Gilbert, Phys. Rev. **B12**, 2111 (1975).
[12] J. E. Harriman, Phys. Rev. **A24**, 680 (1981).
[13] W. Macke, Ann. Phys. Leipzig **17**, 1 (1955).
[14] G. Zumbach and K. Maschke, Phys. Rev. **A28**, 544 (1983), Erratum: *ibid.* 29, 1585 (1984).
[15] C Valdemoro, Phys. Rev. **A45**, 4462 (1992).
[16] C. Valdemoro, L.M. Tel, and E. Pérez-Romero, in "Advan Quantum. Chem.", vol. **28**, 33 (Ed. P.-O. Löwdin, 1997).
[17] C. Valdemoro, L.M. Tel, and E. Pérez-Romero, Phys. Rev. **A61** (2000, in press).
[18] S.Kh. Samvelyan, Int. J. Quantum Chem. **65**, 127 (1997).
[19] B. P. Zapol, Int. J. Quantum Chem. **56**, 535 (1995).
[20] B. P. Zapol, Latv. J. Phys. Tech. Sci. N. 5, 30 (1996).
[21] B. P. Zapol, Latv. J. Phys. Tech. Sci. N. 6, 46 (1996).
[22] E.H. Lieb, Int. J. Quant. Chem. **24**, 243 (1983).
[23] R.A. Bonham and M. Fink, "High Energy Electron Scattering" (Van Nostrand, Princeton 1974).
[24] R. Benesch and V.H. Smith, Jr., in "Wave Mechanics - The First Fifty Years" (Eds. W C. Price, S.S. Chissick and T. Ravensdale (Butterworths, London 1973)

[25] A.J. Thakkar, A.M. Simas and V.H. Smith, Chem. Physics **63**, 175 (1981).
[26] C.A. Coulson and N.H. March, Proc. Phys. Soc. London Ser. A **63**, 367 (1950).
[27] S.R. Gadre, R. K. Pathak, Phys. Rev. A **24**, 2906 (1981).
[28] S.R. Gadre and S.J. Chakravorty, J. Chem. Phys **86**, 2224 (1987).
[29] S.R. Gadre, R. D. Bendale and S.P. Gejji, Chem. Phys. Lett **117**, 138 (1985).
[30] E.S. Kryachko, T. Koga, J. Chem. Phys **91**, 1108 (1989).
[31] J.E. Harriman, Z. Naturforsch **47a**, 203 (1992).
[32] W. Weyrich, P. Pattison, and B. G Williams, Chem. Physics **41**, 271 (1979)
[33] M.M. Mestechkin, "Density Matrix Method in the Theory of Molecules" (Naukova Dumka, Kiev 1977, in Russian).
[34] S. Bochner, "Lectures on Fourier Integrals" (Princeton Univ. Press, Princeton 1959).
[35] L.D. Landau, E.M. Lifshitz, "Quantum Mechanics" (Pergamon, Oxford 1977).

Sturmian expansions for quantum mechanical many-body problems, and hyperspherical harmonics

by Vincenzo Aquilanti, Department of Chemistry,
University of Perugia
and John Avery, H.C. Ørsted Institute,
University of Copenhagen

May 3, 2000

Abstract

Generalized Sturmian basis sets make it possible to solve the many-particle Schrödinger equation directly, without the use of the SCF approximation. The functions in such a basis set are solutions to the many-particle Schrödinger equation with a weighted "basis potential", $\beta_\nu V_0(\mathbf{x})$, the weighting factor β_ν being chosen in such a way as to make all the functions in the set correspond to the same energy. For a many-electron system, it is shown that when $V_0(\mathbf{x})$ is chosen to be the nuclear attraction potential, rapidly convergent solutions can be obtained directly from a secular equation from which the kinetic energy term has vanished The close relationship between generalized Sturmian basis functions and hyperspherical harmonics is discussed, as well as the relationship between all the matrix elements of the theory, such as the Shibuya-Wulfman integrals, the generalized Wigner coefficients of angular momentum theory, and the Hahn polynomials of modern numerical analysis.

Contents

ADVANCES IN QUANTUM CHEMISTRY VOLUME 39

0065-3276/01 $35 00

1 Introduction

Early in the history of quantum theory it was thought that hydrogenlike atomic orbitals could be used as building blocks for constructing the wave functions of more complicated systems. However, it was quickly realized that unless the continuum is included, hydrogenlike wave functions do not form complete sets. To correct this defect, Shull and Lowdin [1] introduced a type of radial basis set which consisted of Laguerre polynomials multiplied by polynomials, the exponential factor being the same for the entire set. Shull and Löwdin were able to show that such basis sets are complete; and they considered such sets to be the natural type of basis for treating problems in atomic and molecular quantum theory Later, Rotenberg [2,3] gave the name "Sturmian" to the Shull-Löwdin basis sets to emphasize their connection with Sturm-Liouville theory. There is a large and rapidly-growing literature in which one-electron basis sets of this type are used In 1968, Goscinski [4] completed a study of Sturmian basis sets in which he regarded such sets as solutions to the Schrödinger equation with a zeroth-order weighted potential, the weighting factor being chosen in such a way as to make all the members of the set correspond to the same energy. This way of regarding Sturmian basis sets made generalization of the concept very easy, and a number of authors pioneered the use of many-particle Sturmian basis sets For example, Gazeau and Maquet [5,6] introduced two-electron Sturmians, while Bang, Vaagen and coworkers [7,8] studied the applications of many-particle Sturmians in nuclear physics. Herschbach, Avery and Antonsen [9-11] discussed the properties of many-electron Sturmians, taking the "basis potential" to be the potential of a d-dimensional hydrogenlike atom. More recently, Aquilanti, Avery and Sauer [12-17] showed that if $V_0(\mathbf{x})$ is taken to be the actual nuclear attraction potential of a many-electron system, the generalized Sturmians based on this potential can be used to obtain a rapidly convergent correlated solution to the many-electron Schrödinger equation without the use of the self-consistent-field approximation. We begin by illustrating these developments, offering later a momentum-space perspective which will show the connection with hyperspherical harmonics and generalized angular momentum theory. For a geometrical view in a similar spirit of the quantum

dynamics of aggregates evolving towards fragmentation, see the recent paper of Fano and coworkers, reference [18].

2 Potential-weighted orthonormality relations

Suppose that for some potential, $V_0(\mathbf{x})$, we are able to find solutions to the N-particle Schrödinger equation,

$$\left[-\sum_{j=1}^{N}\frac{1}{2}\nabla_j^2+\beta_\nu V_0(\mathbf{x})-E\right]\phi_\nu(\mathbf{x})=0 \tag{1}$$

where β_ν is a weighting factor chosen in such a way that all the solutions correspond to the same energy, E. In equation (1) $\mathbf{x}=\{\mathbf{x}_1,\mathbf{x}_2,..\,\mathbf{x}_N\}$ is a $d=3N$ dimensional vector composed of the mass-weighted Cartesiaan coordinates of the N particles in the system. Then two members of the set of solutions will satisfy respectively the equations,

$$\left[\sum_{j=1}^{N}\frac{1}{2}\nabla_j^2+E\right]\phi_\nu(\mathbf{x})=\beta_\nu V_0(\mathbf{x})\phi_\nu(\mathbf{x}) \tag{2}$$

and

$$\left[\sum_{j=1}^{N}\frac{1}{2}\nabla_j^2+E\right]\phi_{\nu'}(\mathbf{x})=\beta_{\nu'} V_0(\mathbf{x})\phi_{\nu'}(\mathbf{x}) \tag{3}$$

We now multiply (2) on the left by $\phi^*_{\nu'}(\mathbf{x})$ and integrate over all the coordinates

$$\int dx\phi^*_{\nu'}(\mathbf{x})\left[\sum_{j=1}^{N}\frac{1}{2}\nabla_j^2+E\right]\phi_\nu(\mathbf{x})=\beta_\nu\int dx\phi^*_{\nu'}(\mathbf{x})V_0(\mathbf{x})\phi_\nu(\mathbf{x}) \tag{4}$$

where $dx=dx_1dy_1dz_1....dz_N$. Similarly, interchanging ν and ν',

$$\int dx\phi^*_{\nu}(\mathbf{x})\left[\sum_{j=1}^{N}\frac{1}{2}\nabla_j^2+E\right]\phi_{\nu'}(\mathbf{x})=\beta_{\nu'}\int dx\phi^*_{\nu}(\mathbf{x})V_0(\mathbf{x})\phi_{\nu'}(\mathbf{x}) \tag{5}$$

If we take the complex conjugate of (5) and subtract it from (4), making use of the Hermiticity of the operator $\frac{1}{2}\nabla_j^2+E$, we obtain:

$$(\beta_\nu-\beta^*_{\nu'})\int dx\phi^*_{\nu'}(\mathbf{x})V_0(\mathbf{x})\phi_\nu(\mathbf{x})=0 \tag{6}$$

Thus if $\beta_\nu\neq\beta_{\nu'}$, we must have

$$\int dx\phi^*_{\nu'}(\mathbf{x})V_0(\mathbf{x})\phi_\nu(\mathbf{x})=0 \tag{7}$$

Since we are dealing with a system with many degrees of freedom, ν stands for a set of quantum numbers. Orthogonality with respect to quantum numbers on which β_ν does not depend (the "minor" quantum numbers) cannot be established through equation (7). Orthogonality with respect to the minor quantum numbers must be established - for example - through spin orthogonality or symmetry properties. It is convenient to normalize our generalized Sturmian basis set in such a way that

$$\int dx|\phi_\nu(\mathbf{x})|^2 V_0(\mathbf{x}) = \frac{2E}{\beta_\nu} \tag{8}$$

Then, assuming that we have established orthonormality with respect to the minor quantum numbers, (7) and (8) can be combined to yield

$$\int dx\phi^*_{\nu'}(\mathbf{x})V_0(\mathbf{x})\phi_\nu(\mathbf{x}) = \delta_{\nu',\nu}\frac{2E}{\beta_\nu} \tag{9}$$

Let us now introduce the Fourier-transformed functions defined by

$$\begin{aligned} \phi^t_\nu(\mathbf{p}) &= \frac{1}{(2\pi)^{d/2}}\int dx e^{-i\mathbf{p}\,\mathbf{x}}\phi_\nu(\mathbf{x}) \\ \phi_\nu(\mathbf{x}) &= \frac{1}{(2\pi)^{d/2}}\int dp e^{i\mathbf{p}\cdot\mathbf{x}}\phi^t_\nu(\mathbf{p}) \end{aligned} \tag{10}$$

where $d = 3N$ and where $e^{i\mathbf{p}\,\mathbf{x}}$ is a d-dimensional plane wave. Then it can be shown [14] that the Fourier-transformed generalized Sturmians obey the weighted orthonormality relation:

$$\int dp \left(\frac{p^2+p_0^2}{2p_0^2}\right)\phi^{t*}_{\nu'}(\mathbf{p})\phi^t_\nu(\mathbf{p}) = \delta_{\nu',\nu} \tag{11}$$

as a consequence of (9), where p_0 is a parameter related to the energy by

$$E = -\frac{p_0^2}{2} \tag{12}$$

3 Generalized Sturmian expansion of a plane wave

Equation (11) can be used to expand a d-dimensional plane wave in terms of a set of generalized Sturmian basis functions [17,19]. Assuming completeness of the basis set, we can write:

$$e^{i\mathbf{p}\,\mathbf{x}} = \left(\frac{p^2+p_0^2}{2p_0^2}\right)\sum_\nu \phi^{t*}_\nu(\mathbf{p})a_\nu \tag{13}$$

then the coefficients a_ν in the expansion can be determined by multiplying both sides of (13) by $\phi^t_{\nu'}(\mathbf{p})$ and integrating over dp. This gives:

$$\begin{aligned} \int dp \phi^t_{\nu'}(\mathbf{p}) e^{i\mathbf{p}\cdot\mathbf{x}} &= \sum_\nu a_\nu \int dp \left(\frac{p^2+p_0^2}{2p_0^2}\right) \phi^{t*}_\nu(\mathbf{p}) \phi^t_{\nu'}(\mathbf{p}) \\ &= \sum_\nu a_\nu \delta_{\nu',\nu} = a_{\nu'} \end{aligned} \tag{14}$$

Comparing (14) and (10), we can see that

$$a_\nu = (2\pi)^{d/2} \phi_\nu(\mathbf{x}) \tag{15}$$

so that finally we obtain the expansion:

$$e^{i\mathbf{p}\cdot\mathbf{x}} = (2\pi)^{d/2} \left(\frac{p^2+p_0^2}{2p_0^2}\right) \sum_\nu \phi^{t*}_\nu(\mathbf{p}) \phi_\nu(\mathbf{x}) \tag{16}$$

Equation (16) is the d-dimensional generalization of an expansion first obtained in 3 dimensions by Shibuya and Wulfman [20]. The reader is also referred to an excellent article by Weniger [21], who discusses the Shibuya-Wulfman expansion of a plane wave, and similar expansions.

4 d-dimensional Coulomb Sturmians

If we let $V_0(\mathbf{x})$ be the d-dimensional hydrogenlike potential

$$V_0(\mathbf{x}) = -\frac{Z}{r} \tag{17}$$

where r is the hyperradius, defined by

$$r^2 = \mathbf{x}_1 \cdot \mathbf{x}_1 + \mathbf{x}_2 \cdot \mathbf{x}_2 + ... + \mathbf{x}_N \cdot \mathbf{x}_N = r_1^2 + r_2^2 + \ .. + r_N^2 \tag{18}$$

then solutions to equation (1) can be written in the form.

$$\phi_\nu(\mathbf{x}) = R_{n,\lambda}(r) Y_{\lambda,\mu}(\hat{\mathbf{x}}) \tag{19}$$

where $Y_{\lambda,\mu}(\hat{\mathbf{x}})$ is a hyperspherical harmonic and

$$R_{n,\lambda}(r) = \mathcal{N}_{n,\lambda} (2p_0 r)^\lambda e^{-p_0 r} F(\lambda + 1 - n | 2\lambda + d - 1 | 2p_0 r) \tag{20}$$

Here

$$F(a|b|x) \equiv 1 + \frac{a}{b}x + \frac{a(a+1)}{b(b+1)}\frac{x^2}{2!} + ... \tag{21}$$

is a confluent hypergeometric function, while

$$\mathcal{N}_{n,\lambda} = \frac{(2p_0)^{d/2}}{(2\lambda+d-2)!}\left(\frac{(\lambda+n+d-3)!}{(n-1-\lambda)!(2n+d-3)}\right)^{1/2} \tag{22}$$

is a normalizing constant. If the constants β_ν in equation (1) are chosen to be

$$\beta_\nu = \frac{p_0(2n+d-3)}{2Z} \tag{23}$$

then all the functions in the set $\phi_\nu(\mathbf{x})$ all correspond to the same energy, and they form the type of generalized Sturmian basis set studied by Herschbach, Avery and Antonsen [9-11]. The first few hyperradial functions $R_{n,\lambda}(r)$ are shown in Table 1. Such a basis set might be used, for example, to treat the motion of nuclei on a many-dimensional potential surface The hyperspherical harmonics $Y_{\lambda,\mu}(\hat{\mathbf{x}})$ which appear in equation (19) are eigenfunctions of the grand angular momentum operator

$$\Lambda^2 \equiv -\sum_{i>j}^{d}\left(x_i\frac{\partial}{\partial x_j} - x_j\frac{\partial}{\partial x_i}\right)^2 \tag{24}$$

where $x_1, x_2, \ldots x_d$ are the Cartesian coordinaates of a d-dimensional space:

$$\left[\Lambda^2 - \lambda(\lambda+d-2)\right] Y_{\lambda,\mu}(\hat{\mathbf{x}}) = 0 \tag{25}$$

Hyperspherical harmonics are d-dimensional analogues of the familiar spherical harmonics, and they can be constructed in such a way as to obey the orthonormality relations

$$\int d\Omega\; Y^*_{\lambda',\mu'}(\hat{\mathbf{x}}) Y_{\lambda,\mu}(\hat{\mathbf{x}}) = \delta_{\lambda',\lambda}\delta_{\mu',\mu} \tag{26}$$

When the normalizing constant is that shown in equation (22) the overall orthonormality of the d-dimensional Sturmian basis set is given by

$$\int dx \phi^*_{\nu'}(\mathbf{x})\left(\frac{-Z}{r}\right)\phi_\nu(\mathbf{x}) = -\delta_{\nu',\nu}\frac{p_0^2}{\beta_\nu} \tag{27}$$

in agreement with equation (9). The completeness property of this generalized Sturmian basis set follows from the completeness of the set of functions $r^n e^{-p_0 r}$ (with constant p_0) and from the completeness of the set of hyperspherical harmonics. Any well-behaved single-valued function of the same variables which falls to zero at very large values of r can be expanded in terms of this basis set. In equation (26), μ represents a set of minor indices. These may be organized in a variety of ways as a matter of convenience. Aquilanti and coworkers, as well as a number of Russian authors, have discussed methods for constructing orthonormal sets of hyperspherical harmonics by means of *the method of trees* [32-40]. This method of constructing orthonormal sets of hyperspherical harmonics is also discussed in reference [17].

5 The generalized Sturmian secular equation

The momentum-space Schrödinger equation of a many-particle system has the form [9,17].

$$(p_0^2 + p^2)\psi^t(\mathbf{p}) = -\frac{2}{(2\pi)^{d/2}} \int dp' V^t(\mathbf{p} - \mathbf{p}')\psi^t(\mathbf{p}') \tag{28}$$

According to the Fourier convolution theorem,

$$\int dp' V^t(\mathbf{p} - \mathbf{p}')\psi^t(\mathbf{p}') = \int dx e^{-i\mathbf{p}\,\mathbf{x}} V(\mathbf{x})\psi(\mathbf{x}) \tag{29}$$

so that (28) can be rewritten in the form:

$$(p_0^2 + p^2)\psi^t(\mathbf{p}) = -\frac{2}{(2\pi)^{d/2}} \int dx e^{-i\mathbf{p}\cdot\mathbf{x}} V(\mathbf{x})\psi(\mathbf{x}) \tag{30}$$

If we replace the d-dimensional plane wave $e^{-i\mathbf{p}\,\mathbf{x}}$ by the complex conjugate of the expansion (16), equation (30) becomes

$$\psi^t(\mathbf{p}) = \frac{1}{p_0^2} \sum_\nu \phi_\nu^t(\mathbf{p}) \int dx' \phi_\nu^*(\mathbf{x}')V(\mathbf{x}')\psi(\mathbf{x}') \tag{31}$$

and taking the Fourier transform of both sides, we obtain

$$\psi(\mathbf{x}) = \frac{1}{p_0^2} \sum_\nu \phi_\nu(\mathbf{x}) \int dx' \phi_\nu^*(\mathbf{x}')V(\mathbf{x}')\psi(\mathbf{x}') \tag{32}$$

Equation (32) can be iterated, starting with a trial solution; or alternatively we can obtain a secular equation by expanding the wave function in terms of our generalized Sturmian basis. If we write:

$$\psi(\mathbf{x}) = \sum_\nu \phi_\nu(\mathbf{x}) B_\nu \tag{33}$$

then $\psi(\mathbf{x})$ will be a solution to (32) if

$$\sum_\nu \left[V_{\nu',\nu} - 2E\delta_{\nu',\nu}\right] B_\nu = 0 \tag{34}$$

where

$$V_{\nu',\nu} \equiv \int dx \phi_{\nu'}^*(\mathbf{x})V(\mathbf{x})\phi_\nu(\mathbf{x}) \tag{35}$$

It is interesting to notice that the kinetic energy has vanished from the generalized Sturmian secular equation.

The hyperangular integrals needed for evaluation of the matrix elements $V_{\nu',\nu}$ may be evaluated by means of the following very powerful angular integration theorem [17,44]: Let $d\Omega$ be the element of generalized solid angle, related to the d-dimensional volume element by

$$dx_1 dx_2 ... dx_d = r^{d-1} dr \; d\Omega \tag{36}$$

where r is the hyperradius; and let $F(\mathbf{x})$ be any function which can be expanded as a series in terms of polynomials involving the Cartesian coordinates $x_1, x_2, .. , x_d$ Then

$$\int d\Omega \; F(\mathbf{x}) = \frac{(d-2)!! 2\pi^{d/2}}{\Gamma\left(\frac{d}{2}\right)} \sum_{n=0}^{\infty} \frac{r^{2n}}{(2n)!!(d+2n-2)!!} \left[\Delta^n F(\mathbf{x})\right]_{\mathbf{x}=0} \tag{37}$$

where Δ is the generalized Laplacian operator, defined by

$$\Delta \equiv \sum_{j=1}^{d} \frac{\partial^2}{\partial x_j^2} \tag{38}$$

6 An alternative generalized Sturmian basis set

An alternative type of generalized Sturmian basis set, appropriate for treating N-electron atoms, may be obtained by letting

$$V_0(\mathbf{x}) = -\sum_{j=1}^{N} \frac{Z}{r_j} \tag{39}$$

be the attractive potential of the nucleus. We can build up a set of N-electron Sturmian basis functions for this system from one-electron orbitals of the form·

$$\chi_{n,l,m,m_s}(\mathbf{x}_j) = R_{nl}(r_j) Y_{lm}(\theta_j, \phi_j) \begin{cases} \alpha(j) \\ \beta(j) \end{cases} \tag{40}$$

where

$$\begin{aligned} R_{nl}(r_j) &= \mathcal{N}_{nl} (2k_\mu r_j)^l e^{-k_\mu r_j} F(l+1-n|2l+2|2k_\mu r_j) \\ \mathcal{N}_{nl} &= \frac{2k_\mu^{3/2}}{(2l+1)!} \sqrt{\frac{(n+l)!}{n(n-l-1)!}} \end{aligned} \tag{41}$$

and where $F(a|b|z)$ is a confluent hypergeometric function. These are just the familiar hydrogenlike atomic orbitals (which also can be expressed in terms

of Laguerre polynomials), except that the parameters k_μ will be determined later by means of subsidiary conditions. The one-electron hydrogenlike orbitals satisfy

$$\begin{aligned}\left[-\frac{1}{2}\nabla_j^2+\frac{1}{2}k_\mu^2-\frac{nk_\mu}{r_j}\right]\chi_\mu(\mathbf{x}_j) &= 0\\ \int d^3x_j|\chi_\mu(\mathbf{x}_j)|^2\frac{1}{r_j} &= \frac{k_\mu}{n}\\ \int d^3x_j|\chi_\mu(\mathbf{x}_j)|^2 &= 1\end{aligned} \tag{42}$$

where we have let μ stand for the set of indices $\{n,l,m,m_s\}$. If we introduce subsidiary conditions which require that

$$k_\mu^2+k_{\mu'}^2+k_{\mu''}^2+\ldots=p_0^2 \tag{43}$$

and

$$nk_\mu=n'k_{\mu'}=n''k_{\mu''}=\ldots=Z\beta_\nu \tag{44}$$

then the antisymmetrized product function

$$\begin{aligned}\phi_\nu(\mathbf{x}) &= |\chi_\mu\chi_{\mu'}\chi_{\mu''}\ldots|\\ &\equiv \frac{1}{\sqrt{N!}}\begin{vmatrix}\chi_\mu(\mathbf{x}_1) & \chi_{\mu'}(\mathbf{x}_1) & \chi_{\mu''}(\mathbf{x}_1) & \ldots\\ \chi_\mu(\mathbf{x}_2) & \chi_{\mu'}(\mathbf{x}_2) & \chi_{\mu''}(\mathbf{x}_2) & \ldots\\ \vdots & \vdots & \vdots & \\ \chi_\mu(\mathbf{x}_N) & \chi_{\mu'}(\mathbf{x}_N) & \chi_{\mu''}(\mathbf{x}_N) & \ldots\end{vmatrix}\end{aligned} \tag{45}$$

will be a solution to

$$\left[-\sum_{j=1}^{N}\frac{1}{2}\nabla_j^2+\frac{p_0^2}{2}+\beta_\nu V_0(\mathbf{x})\right]\phi_\nu(\mathbf{x})=0 \tag{46}$$

since from (42), (43) and (44),

$$\begin{aligned}&\left[\sum_{j=1}^{N}\frac{1}{2}\nabla_j^2\right]\chi_\mu(\mathbf{x}_1)\chi_{\mu'}(\mathbf{x}_2)\ldots\\ =&\left[\frac{1}{2}k_\mu^2-\frac{nk_\mu}{r_1}+\frac{1}{2}k_{\mu'}^2-\frac{nk_{\mu'}}{r_2}+\ldots\right]\chi_\mu(\mathbf{x}_1)\chi_{\mu'}(\mathbf{x}_2)\\ =&\left[\frac{p_0^2}{2}+\beta_\nu V_0(\mathbf{x})\right]\chi_\mu(\mathbf{x}_1)\chi_{\mu'}(\mathbf{x}_2)\ldots\end{aligned} \tag{47}$$

The determinantal function shown in (45) is a superposition of products, all of which satisfy (46), and therefore $\phi_\nu(\mathbf{x})$ satisfies (46), provided that the

subsidiary conditions (43) and (44) are fulfilled. We can see that the normalization condition (8) is automatically fulfilled by the generalized Sturmian basis functions in our illustrative example, since from (42),

$$\begin{aligned}\int dx|\phi_\nu(\mathbf{x})|^2 V_0(\mathbf{x}) &= -\sum_{\mu\subset\nu} Z\int d^3x_j|\chi_\mu(\mathbf{x}_j)|^2\frac{1}{r_j}\\ &= -\sum_{\mu\subset\nu} Z\frac{k_\mu}{n} = -\frac{1}{\beta_\nu}\sum_{\mu\subset\nu} k_\mu^2 = -\frac{p_0^2}{\beta_\nu}\end{aligned} \tag{48}$$

In the case of atoms, the total potential is given by

$$V(\mathbf{x}) = V_0(\mathbf{x}) + V'(\mathbf{x}) \tag{49}$$

where $V_0(\mathbf{x})$ is the nuclear attraction potential shown in equation (39) while

$$V'(\mathbf{x}) = \sum_{i>j}^{N}\sum_{j=1}^{N}\frac{1}{r_{ij}} \tag{50}$$

is the interelectron repulsion potential. If we let

$$T^0_{\nu',\nu} \equiv -\frac{1}{p_0}\int dx\ \phi^*_{\nu'}(\mathbf{x})V_0(\mathbf{x})\phi_\nu(\mathbf{x}) \tag{51}$$

$$T'_{\nu',\nu} \equiv -\frac{1}{p_0}\int dx\phi^*_{\nu'}(\mathbf{x})V'(\mathbf{x})\phi_\nu(\mathbf{x}) \tag{52}$$

and

$$\mathcal{R}_\nu \equiv \left(\frac{1}{n^2}+\frac{1}{n'^2}+\frac{1}{n''^2}+...\right)^{1/2} \tag{53}$$

then from the potential-weighted orthonormality relation (9) and the subsidiary conditions (43) and (44) it follows that

$$T^0_{\nu',\nu} = \delta_{\nu',\nu}Z\mathcal{R}_\nu \tag{54}$$

The generalized Sturmian secular equation for the atom can then be rewritten in the form:

$$\sum_\nu \left[T'_{\nu',\nu} + \delta_{\nu',\nu}Z\mathcal{R}_\nu - \delta_{\nu',\nu}p_0\right]B_\nu = 0 \tag{55}$$

It turns out that $T'_{\nu',\nu}$, as defined by equation (52), is a pure number, independent of p_0. In a crude approximation, we can represent the ground states of the atoms and ions in the 2-electron isoelectronic series by a single configuration:

$$\phi_\nu(\mathbf{x}) = |\chi_{1s}\chi_{\bar{1}s}| \tag{56}$$

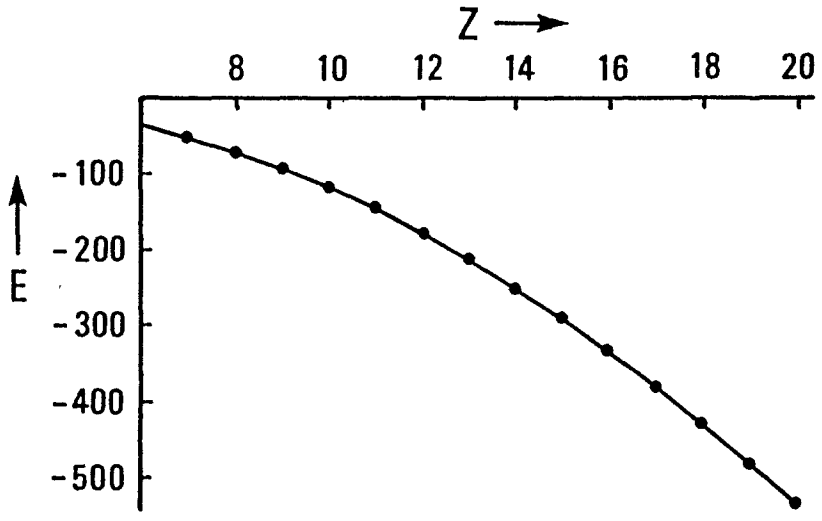

Figure 1: This figure shows the electronic energy in Hartrees as a function of nuclear charge for the 6-electron isoelectronic series: C, N^{+}, O^{2+}, F^{3+}, Ne^{4+},..etc. The dots show Clementi's Hartree-Fock values [24], while the smooth curve was generated from equation (42).

Similarly, the ground states of the 3-electron isoelectronic series can be approximated by the single configuration:

$$\phi_\nu(\mathbf{x}) = |\chi_{1s}\chi_{\bar{1}s}\chi_{2s}| \tag{57}$$

and so on In the crude one-configuration approximation, the generalized Sturmian secular equation, (34), reduces to the requirement that

$$p_0 \approx ZR_\nu + T'_{\nu,\nu} \tag{58}$$

For the first few isoelectronic series, this becomes:

$$\begin{aligned}
p_0 &\approx Z\sqrt{\frac{2}{1}} - 0.441942 \qquad N = 2 \\
p_0 &\approx Z\sqrt{\frac{2}{1} + \frac{1}{4}} - 0.681870 \qquad N = 3 \\
p_0 &\approx Z\sqrt{\frac{2}{1} + \frac{2}{4}} - 0.993588 \qquad N = 4 \\
p_0 &\approx Z\sqrt{\frac{2}{1} + \frac{3}{4}} - 1.40773 \qquad N = 5 \\
p_0 &\approx Z\sqrt{\frac{2}{1} + \frac{4}{4}} - 1.88329 \qquad N = 6 \\
p_0 &\approx Z\sqrt{\frac{2}{1} + \frac{5}{4}} - 2.41491 \qquad N = 7
\end{aligned} \tag{59}$$

The energies calculated from (59) agree reasonably well with Clementi's Hartree-Fock calculations [15,24], as illustrated in Figure 1. Higher accuracy can, of course, be obtained by using more configurations in the basis; and with the addition of only a few configurations, correlated solutions can be obtained which are a considerable improvement over Hartree-Fock solutions. Excited states can also be obtained with good accuracy from a multiconfigurational generalized Sturmian basis set. Table 2 shows calculated values for triplet excited states of the 2-electron isoelectronic series compared with experimental values taken from Moore's tables [43]. The calculations were made with a basis consisting of fifteen generalized Sturmian configurations of the form $\phi_\nu(\mathbf{x}) = |\chi_{1,0,0}\chi_{n,l,0}|$. For the lower excited states, a slightly larger basis set was used, involving functions of the form $\phi_\nu(\mathbf{x}) = |\chi_{n',0,0}\chi_{n,l,0}|$ Accuracy of the calculations is greatest for highly excited states with large Z, but in this region of the tables, experimental values are lacking. Unlike the basis set $R_{n,\lambda}(r)Y_{\lambda,\mu}(\hat{\mathbf{x}})$, the generalized Sturmian basis set which results when $V_0(\mathbf{x})$ is chosen to be the attractive potential of the nuclei in the system is believed to

lack the formal completeness property; i.e. it is believed that not every well-behaved function of the same variables obeying the same boundary conditions can be expanded in terms of this basis. However, one should remember that if this extremely stringent condition were applied to the conventional many-electron basis sets actually used in configuration interaction calculations, all of them would be disqualified!

7 The many-center one-electron problem, and the many-center many-electron problem

In 1965, Shibuya and Wulfman [20] introduced a generalization of Fock's momentum-space treatment of hydrogenlike atoms [22]. Following this approach, one can show [17] that if

$$v(\mathbf{x}_j) = -\sum_a \frac{Z_a}{|\mathbf{x}_j - \mathbf{X}_a|} \tag{60}$$

then the one-electron equation

$$\left[-\frac{1}{2}\nabla_j^2 + \frac{k_\mu^2}{2} + b_\mu k_\mu v(\mathbf{x}_j)\right] \varphi_\mu(\mathbf{x}_j) = 0 \tag{61}$$

can be solved by expanding $\varphi_\mu(\mathbf{x}_j)$ in terms of a set of one-electron Sturmian basis functions.

$$\varphi_\mu(\mathbf{x}_j) = \sum_\tau \xi_\tau(\mathbf{x}_j) C_{\tau,\mu} \tag{62}$$

or, in momentum space,

$$\varphi_\mu^t(\mathbf{p}_j) = \sum_\tau \xi_\tau^t(\mathbf{p}_j) C_{\tau,\mu} \tag{63}$$

where τ stands for the set of indices, $\{a, n, l, m\}$, and where

$$\begin{aligned} \xi_\tau(\mathbf{x}_j) &= \sqrt{\frac{Z_a}{nk_\mu}} \chi_{nlm}(\mathbf{x}_j - \mathbf{X}_a) \\ \xi_\tau^t(\mathbf{p}_j) &= \sqrt{\frac{Z_a}{nk_\mu}} e^{-i\mathbf{p}_j \cdot \mathbf{X}_a} \chi_{nlm}^t(\mathbf{p}_j) \end{aligned} \tag{64}$$

The functions χ_{nlm} have the form shown in equations (40) and (41), all of the functions in the expansions (62) and (63) being understood to belong to the same value of k_μ. Solutions to equation (61) can be found by solving the secular equation [17]

$$\sum_\tau \left[K_{\tau',\tau}^2 - b_\mu^{-1} K_{\tau',\tau}\right] C_{\tau,\mu} = 0 \tag{65}$$

where

$$K_{\tau',\tau} = \int d^3p_j \left(\frac{k_\mu^2 + p_j^2}{2k_\mu^2}\right) \xi_{\tau'}^{t*}(\mathbf{p}_j)\xi_\tau^t(\mathbf{p}_j) \tag{66}$$

If the basis set were infinite, the matrix K^2 could be found by squaring K. However, when the basis set is truncated, it is preferable, if possible, to evaluate K^2 by means of the relation [17]

$$K^2_{\tau',\tau} = -\int d^3x_j \xi^*_{\tau'}(\mathbf{x}_j) v(\mathbf{x}_j) \xi(\mathbf{x}_j) \tag{67}$$

through which K^2 can be related to nuclear attraction integrals. The matrix K can be rewritten with the help of (64):

$$K_{\tau',\tau} = \sqrt{\frac{Z_{a'}Z_a}{n'n}} S^{nlm}_{n'l'm'}(\mathbf{X}_{a'} - \mathbf{X}_a) \tag{68}$$

where

$$S^{nlm}_{n'l'm'}(\mathbf{R}) \equiv \int d^3p_j \left(\frac{p_j^2 + k_\mu^2}{2k_\mu^2}\right) e^{i\mathbf{p}\,\mathbf{R}} \chi^{t*}_{n'l'm'}(\mathbf{p}_j)\chi^t_{nlm}(\mathbf{p}_j) \tag{69}$$

The integrals shown in (69) were introduced by Shibuya and Wulfman in their pioneering paper on momentum-space quantum theory [20]. The one-electron hydrogenlike Sturmians can be shown to obey weighted orthonormality relations analogous to (9) and (11):

$$\frac{n}{k_\mu} \int d^3x_j \chi^*_{n'l'm'}(\mathbf{x}_j) \frac{1}{r_j} \chi_{nlm}(\mathbf{x}_j) = \delta_{n',n}\delta_{l',l}\delta_{m',m} \tag{70}$$

$$\int d^3p_j \left(\frac{p_j^2 + k_\mu^2}{2k_\mu^2}\right) \chi^{t*}_{n'l'm'}(\mathbf{p}_j)\chi^t_{nlm}(\mathbf{p}_j) = \delta_{n',n}\delta_{l',l}\delta_{m',m} \tag{71}$$

From (71), it follows that

$$e^{i\mathbf{p}_j\,\mathbf{x}_j} = (2\pi)^{3/2} \left(\frac{p_j^2 + k_\mu^2}{2k_\mu}\right) \sum_{nlm} \chi^{t*}_{nlm}(\mathbf{p}_j)\chi_{nlm}(\mathbf{x}_j) \tag{72}$$

a relationship which is analogous to (16) Then since

$$\begin{aligned} \chi^t_{nlm}(\mathbf{p}_j) &= \frac{1}{(2\pi)^{3/2}} \int d^3x_j e^{-i\mathbf{p}_j\,\mathbf{x}_j} \chi_{nlm}(\mathbf{x}_j) \\ \chi_{nlm}(\mathbf{x}_j) &= \frac{1}{(2\pi)^{3/2}} \int d^3p_j e^{i\mathbf{p}_j\cdot\mathbf{x}_j} \chi^t_{nlm}(\mathbf{p}_j) \end{aligned} \tag{73}$$

it follows that

$$\chi_{nlm}(\mathbf{x}_j + \mathbf{R}) = \frac{1}{(2\pi)^{3/2}} \int d^3p_j e^{i\mathbf{p}_j\,(\mathbf{x}_j + \mathbf{R})} \chi^t_{nlm}(\mathbf{p}_j) \tag{74}$$

Introducing the expression (72) into (74), we obtain:

$$\chi_{nlm}(\mathbf{x}_j + \mathbf{R}) = \sum_{n'l'm'} \chi_{n'l'm'}(\mathbf{x}_j) S^{nlm}_{n'l'm'}(\mathbf{R}) \tag{75}$$

where the integrals $S^{nlm}_{n'l'm'}(\mathbf{R})$ are those shown in (69). The Shibuya-Wulfman integrals form a representation of the translation group in a 3-dimensional space, since from (75) it follows that

$$S^{nlm}_{n'l'm'}(\mathbf{R}+\mathbf{R}') = \sum_{n''l''m''} S^{n''l''m''}_{n'l'm'}(\mathbf{R}) S^{nlm}_{n''l''m''}(\mathbf{R}') \tag{76}$$

The Shibuya-Wulfman integrals can also be interpreted as nuclear attraction integrals, since from (70) and (75),

$$\begin{aligned} & \frac{n}{k_\mu} \int d^3x_j \chi^*_{n'l'm'}(\mathbf{x}_j) \frac{1}{r_j} \chi_{nlm}(\mathbf{x}_j + \mathbf{R}) \\ = & \sum_{n''l''m''} S^{nlm}_{n''l''m''}(\mathbf{R}) \frac{n}{k_\mu} \int d^3x_j \chi^*_{n'l'm'}(\mathbf{x}_j) \frac{1}{r_j} \chi_{n''l''m''}(\mathbf{x}_j) \\ = & S^{nlm}_{n'l'm'}(\mathbf{R}) \end{aligned} \tag{77}$$

Having solved equation (61) by means of the secular equation, (65), we then construct the many-electron Sturmian basis function:

$$\phi_\nu(\mathbf{x}) = \mathcal{N}_\nu |\varphi_\mu \varphi_{\mu'} \varphi_{\mu''} ...| \tag{78}$$

This will be a solution to the N-electron equation

$$\left[-\sum_{j=1}^{N} \frac{1}{2} \nabla_j^2 + \frac{p_0^2}{2} + \beta_\nu V_0(\mathbf{x}) \right] \phi_\nu(\mathbf{x}) = 0 \tag{79}$$

where

$$V_0(\mathbf{x}) = \sum_{j=1}^{N} v(\mathbf{x}_j) \tag{80}$$

provided that the subsidiary conditions

$$k_\mu^2 + k_{\mu'}^2 + k_{\mu''}^2 + \quad . = p_0^2 \tag{81}$$

and

$$b_\mu k_\mu = b_{\mu'} k_{\mu'} = b_{\mu''} k_{\mu''} = ... = \beta_\nu \tag{82}$$

are fulfilled. To see this, we notice that from (61),

$$\begin{aligned} & \left[\sum_{j=1}^{N} \frac{1}{2} \nabla_j^2 \right] \varphi_\mu(\mathbf{x}_1) \varphi_{\mu'}(\mathbf{x}_2) ... \\ = & \left[\frac{1}{2} k_\mu^2 + b_\mu k_\mu v(\mathbf{x}_1) + \frac{1}{2} k_{\mu'}^2 + b_{\mu'} k_{\mu'} v(\mathbf{x}_2) + ... \right] \varphi_\mu(\mathbf{x}_1) \varphi_{\mu'}(\mathbf{x}_2) .. \\ = & \left[\frac{1}{2} p_0^2 + \beta_\nu V_0(\mathbf{x}) \right] \varphi_\mu(\mathbf{x}_1) \varphi_{\mu'}(\mathbf{x}_2) \ . \end{aligned} \tag{83}$$

Since $\phi_\nu(\mathbf{x})$ is built up from products of the form $\varphi_\mu(\mathbf{x}_1)\varphi_{\mu'}(\mathbf{x}_2)$ .., and since each of these satisfies (83), the configuration (78) satisfies (79). The normalization factor $\mathcal{N}_\nu$ is necessary in the definition of the many-electron many-center Sturmian basis set because the functions are not automatically normalized, as they were in the atomic case, and $\mathcal{N}_\nu$ must be chosen so that (9) and (11) will be fulfilled The full potential of a molecule contains not only the nuclear attraction term, $V_0(\mathbf{x})$, but also an interelectron repulsion term.

$$V'(\mathbf{x}) = \sum_{i>j}^{N}\sum_{j=1}^{N}\frac{1}{r_{ij}} \tag{84}$$

Correspondingly, we can let

$$T_{\nu',\nu} = -\frac{1}{p_0}\int dx\phi^*_{\nu'}(\mathbf{x})V(\mathbf{x})\phi_\nu(\mathbf{x}) = T^0_{\nu',\nu} + T'_{\nu',\nu} \tag{85}$$

where

$$T^0_{\nu',\nu} = -\frac{1}{p_0}\int dx\phi^*_{\nu'}(\mathbf{x})V_0(\mathbf{x})\phi_\nu(\mathbf{x}) = \frac{p_0}{\beta_\nu}\delta_{\nu',\nu} \tag{86}$$

In our representation, the nuclear attraction term is already diagonal because of the potential-weighted orthonormality relation, (9). From the subsidiary conditions, (81) and (82), it follows that

$$\frac{p_0^2}{\beta_\nu^2} = \frac{k_\mu^2}{b_\mu^2 k_\mu^2} + \frac{k_{\mu'}^2}{b_{\mu'}^2 k_{\mu'}^2} + ... \tag{87}$$

so that

$$T^0_{\nu',\nu} = \delta_{\nu',\nu}\left(\frac{1}{b_\mu^2} + \frac{1}{b_{\mu'}^2} + \frac{1}{b_{\mu''}^2} + ..\right)^{1/2} \tag{88}$$

Thus the generalized Sturmian secular equation for a molecule becomes

$$\sum_\nu\left[T'_{\nu',\nu} + \delta_{\nu',\nu}\left(\frac{1}{b_\mu^2} + \frac{1}{b_{\mu'}^2} + ...\right)^{1/2} - p_0\delta_{\nu',\nu}\right]B_\nu = 0 \tag{89}$$

where the constants b_μ are obtained from the secular equations (48), while $T'_{\nu',\nu}$ is the interelectron repulsion matrix·

$$T'_{\nu',\nu} = -\frac{1}{p_0}\int dx\phi^*_{\nu'}(\mathbf{x})\sum_{i>j}^{N}\sum_{j=1}^{N}\frac{1}{r_{ij}}\phi_\nu(\mathbf{x}) \tag{90}$$

The evaluation of this term is the heavy computational step in molecular calculations using the generalized Sturmian formalism; but much progress in the evaluation of many-center two-electron integrals involving Slater-type orbitals has recently been made by Fernández Rico and his co-workers in Madrid [25,26] and by Steinborn, Weniger and co-workers in Germany [27,28]

8 Representation in terms of hyperspherical harmonics

In his famous momentum-space treatment of hydrogenlike atoms, Fock [22] introduced a projection which maps 3-dimensional momentum space onto the surface of a 4-dimensional hypersphere:

$$\begin{aligned} u_1 &= \frac{2k_\mu p_1}{k_\mu^2 + p^2} = \sin\chi \sin\theta \cos\phi \\ u_2 &= \frac{2k_\mu p_2}{k_\mu^2 + p^2} = \sin\chi \sin\theta \sin\phi \\ u_3 &= \frac{2k_\mu p_3}{k_\mu^2 + p^2} = \sin\chi \cos\theta \\ u_4 &= \frac{k_\mu^2 - p^2}{k_\mu^2 + p^2} = \cos\chi \end{aligned} \tag{91}$$

(where we have dropped the electron index, j). He was then able to show that the Fourier-transformed hydrogenlike orbitals can be written in the form

$$\chi^t_{nlm}(\mathbf{p}) = M(p) Y_{n-1,l,m}(\hat{\mathbf{u}}) \tag{92}$$

where

$$M(p) \equiv \frac{4k_\mu^{5/2}}{(k_\mu^2 + p^2)^2} \tag{93}$$

is a universal factor which is independent of the quantum numbers, and where $Y_{\lambda,l,m}(\hat{\mathbf{u}})$ is a 4-dimensional hyperspherical harmonic:

$$Y_{\lambda,l,m}(\hat{\mathbf{u}}) = \mathcal{N}_{\lambda,l} C^{1+l}_{\lambda-l}(u_4) \sin^l\chi Y_{lm}(\theta_p, \chi_p) \tag{94}$$

In equation (94), $\mathcal{N}_{\lambda,l}$ is a normalizing constant

$$\mathcal{N}_{\lambda,l} = (-1)^\lambda i^l (2l)!! \sqrt{\frac{2(\lambda+1)(\lambda-l)!}{\pi(\lambda+l+1)!}} \tag{95}$$

while $C^\alpha_\lambda(u_4)$ is a Gegenbauer polynomial:

$$C^\alpha_\lambda(u_4) = \sum_{t=0}^{[\lambda/2]} \frac{(-1)^t \Gamma(\lambda+\alpha-t)}{t!(\lambda-2t)!\Gamma(\alpha)} (2u_4)^t \tag{96}$$

The first few 4-dimensional hyperspherical harmonics of this type are shown in Table 3. Fock was able to explain in this way the puzzling n^2-fold degeneracy

of hydrogenlike atoms, since $(\lambda+1)^2 = n^2$ linearly independent 4-dimensional hyperspherical harmonics belong to a given value of the principal quantum number, λ. The generalized solid angle of the 4-dimensional hypersphere onto which momentum-space is projected by Fock's mapping is related to the volume element of momentum space by [9,17]

$$d\Omega = d^3p \left(\frac{2k_\mu}{k_\mu^2 + p^2}\right)^3 \tag{97}$$

From (92), (93) and (97) it follows that the Shibuya-Wulfman integrals defined in equation (69) can be rewritten in the form:

$$S^{nlm}_{n'l'm'}(\mathbf{R}) = \int d\Omega e^{i\mathbf{p}\,\mathbf{R}} Y^*_{n'-1,l',m'}(\hat{\mathbf{u}}) Y_{n-1,l,m}(\hat{\mathbf{u}}) \tag{98}$$

If we replace $\mathbf{x}_j$ by $\mathbf{R}$ in equation (72), and if we make use of (92), we can write:

$$e^{i\mathbf{p}\,\mathbf{R}} = (2\pi)^{3/2} \left(\frac{2k_\mu^{1/2}}{k_\mu^2 + p^2}\right) \sum_{nlm} Y^*_{n-1,l,m}(\hat{\mathbf{u}}) \chi_{nlm}(\mathbf{R}) \tag{99}$$

Thus the Shibuya-Wulfman integrals can also be expressed in the form:

$$\begin{aligned} S^{nlm}_{n'l'm'}(\mathbf{R}) &= \left(\frac{2\pi}{k_\mu}\right)^{3/2} \sum_{n''l''m''} \chi_{n''l''m''}(\mathbf{R}) \\ &\quad \times \int d\Omega (1+u_4) Y^*_{n''-1,l'',m''}(\hat{\mathbf{u}}) Y_{n'-1,l',m'}(\hat{\mathbf{u}}) Y_{n-1,l,m}(\hat{\mathbf{u}}) \end{aligned} \tag{100}$$

where we have made use of the relationship

$$\frac{2k_\mu^2}{k_\mu^2 + p^2} = 1 + u_4 \tag{101}$$

which can be derived from equation (91). From equation (100), it is clear that the Shibuya-Wulfman integrals can be expressed in terms of the generalized Wigner coefficients of the 4-dimensional hyperspherical harmonics [29,30]. These, in turn, are closely related to the Hahn polynomials [31] A few Shibuya-Wulfman integrals are shown in Table 4. It can be seen from this table, that if we let

$$\mathbf{s} \equiv k_\mu \mathbf{R} \tag{102}$$

then the Shibuya-Wulfman integrals always consist of an exponential factor, e^{-s}, multiplied by a polynomial in s_1, s_2, and s_3. Thus the integrals define a special type of polynomial, related to Legendre polynomials and Hahn polynomials by equation (100).

9 Alternative hyperspherical harmonics; the method of trees

Interestingly, Fock's treatment of hydrogenlike atoms [22] leads one to the conclusion that

$$\chi_n^t(\mathbf{p}) = M(p)Y_{n-1}(\hat{\mathbf{u}}) \tag{103}$$

will be a solution to the momentum-space Schrödinger equation of the atom provided only that $Y_\lambda(\hat{\mathbf{u}})$ is a 4-dimensional hyperspherical harmonic. The minor quantum numbers need not be organized according to a scheme where one of them is an eigenvalue of L^2 and the other of L_z. Any alternative way that we have of constructing an orthonormal set of hyperspherical harmonics will lead us to a set of orthonormal solutions. General methods for constructing orthonormal sets of hyperspherical harmonics have been developed by a number of authors in Russia and Italy [32-40]. For the case of 4-dimensional hyperspherical harmonics, the indices may be organized either according to the chain of subgroups $SO(4) \supset SO(3) \supset SO(2)$, or according to the chain $SO(4) \supset SO(2) \times SO(2)$, as symbolized by the "trees" shown in Figure 2.

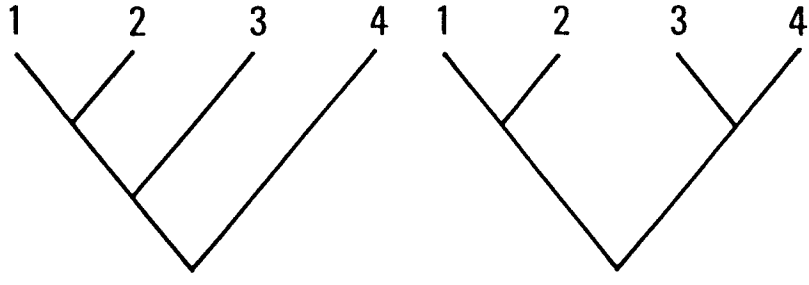

Figure 2:

If we organize the indices according to the "standard tree", (Figure 2a), we are led to hyperspherical harmonics of the form shown in equations (94-96). Alternatively, we can define the hyperangles according to the relationship:

$$\begin{aligned} u_1 &= \frac{2k_\mu p_1}{k_\mu^2 + p^2} = \sin\Theta \sin\phi \\ u_2 &= \frac{2k_\mu p_2}{k_\mu^2 + p^2} = \sin\Theta \cos\phi \\ u_3 &= \frac{2k_\mu p_3}{k_\mu^2 + p^2} = \cos\Theta \sin\Phi \end{aligned}$$

$$u_4 = \frac{k_\mu^2 - p^2}{k_\mu^2 + p^2} = \cos\Theta\cos\Phi \tag{104}$$

as symbolized by the second tree, (Figure 2b); and we can construct an orthonormal set of hyperspherical harmonics by coupling an irreducible representation of the group of rotations in the 1,2-space, $e^{im\phi}$, with an irreducible representation of rotations in the 3,4-space, $e^{i\mu\Phi}$. This leads to a set of 4-dimensional hyperspherical harmonics of the form:

$$\mathcal{Y}_{n-1,\mu,m}(\hat{\mathbf{u}}) = (-1)^{n-1} i^m \left(\frac{n}{2\pi^2}\right)^{1/2} D^{(n-1)/2}_{(\mu+m)/2,(\mu-m)/2}(-\Phi-\phi, 2\Theta, \phi-\Phi) \tag{105}$$

The first few harmonics of this alternative type are shown in Table 5. We can now ask - to what coordinate-space hydrogenlike Sturmians do the hyperspherical harmonics correspond? The answer is that they correspond, through the relationships

$$U^t_{n\mu m}(\mathbf{p}) = M(p)\mathcal{Y}_{n-1,\mu,m}(\hat{\mathbf{u}}) \tag{106}$$

and (73), to the set of solutions to the hydrogenlike atom where the separation has been made in the paraboloidal coordinates:

$$\begin{aligned} \lambda_1 &= r + z \\ \lambda_2 &= r - z \\ \phi &= \tan^{-1}\left(\frac{y}{x}\right) \end{aligned} \tag{107}$$

The set of paraboloidal coordinate-space hydrogenlike Sturmians which are related to $U^t_{n\mu m}(\mathbf{p})$ through an inverse Fourier transform are

$$\begin{aligned} U_{n\mu m}(\mathbf{x}) &= \mathcal{N}_{n\mu m}(k_\mu\sqrt{\lambda_1\lambda_2})^m e^{-(\lambda_1+\lambda_2)/2} \\ &\quad \times L^m_{(n+\mu-m-1)/2}(k_\mu\lambda_1) L^m_{(n-\mu-m-1)/2}(k_\mu\lambda_2) e^{im\phi} \end{aligned} \tag{108}$$

where $\mathcal{N}_{n\mu m}$ is a normalizing constant,

$$\mathcal{N}_{n\mu m} = \sqrt{\frac{k_\mu^3[(\mu+n-m-1)/2]![(n-\mu-m-1)/2]!}{\pi n\{[(\mu+n+m-1)/2]![(n-\mu+m-1)/2]!\}^3}} \tag{109}$$

and where L^m_n is an associated Laguerre polynomial. We can call this basis the "Stark basis", since it is the set of Sturmians which is most appropriate for treating the Stark effect in atoms. It is also the basis which is most appropriate for the treatment of diatomic molecules. It is possible to derive (from an equation analogous to (106) an explicit expression for the Shibuya-Wulfman integrals in the Stark basis; and this expression is given in reference [42]. The

possibilities for alternative hyperspherical harmonics and alternative hydrogenlike Sturmians are very rich, since in addition to the two alternative trees of Figure 2, we have the possibility of permuting the indices associated with the "branches" of the trees. Thus, for example, we might construct a set of harmonics quantized according to eigenvalues of the quantum analogue of the Runge-Lenz vector. In all there are 15 alternative hydrogenlike basis sets at our disposal, and we can choose the set most appropriate to the problem at hand [40].

10 Final remarks and conclusions

In this paper we have emphasized the close relationships between Sturmian basis sets and hyperspherical harmonics. The connection with generalized angular momentum theory provides further insight as well as powerful and flexible mathematical tools for the computation of matrix elements [45]. From this perspective, recent advances in the theory of orthogonal polynomials of a discrete variable are of great interest [46]. Specifically, we remarked above that the generalized Wigner coefficients which enter expressions for the Shibuya-Wulfman coefficients are closely related to Hahn polynomials [31]. The Hahn polynomials are defined by the relation:

$$Q_n(x,\alpha,\beta,N) = {}_3F_2(-n,-x,n+\alpha+\beta+1;\alpha+1,-N;1) \tag{110}$$

where ${}_3F_2$ is a generalized hypergeometric function. From (110), it can be seen that n is the degree of the polynomial. x is a discrete index, and N is chosen to be a positive integer such that

$$0 \leq n, x \leq N \tag{111}$$

Both α and β are restricted to be greater than -1. When these conditions are fulfilled, the Hahn polynomials enjoy the discrete orthonormality relations:

$$\sum_{n=0}^{N} Q_n(x,\alpha,\beta,N)Q_n(x',\alpha,\beta,N)\pi_n = \frac{\delta_{x',x}}{w(x)} \tag{112}$$

and

$$\sum_{x=0}^{N} Q_n(x,\alpha,\beta,N)Q_{n'}(x,\alpha,\beta,N)w(x) = \frac{\delta_{n',n}}{\pi_n} \tag{113}$$

where

$$w(x) \equiv \frac{(\alpha+x)!(\beta+N-x)!(\alpha+\beta+1)!N!}{x!\alpha!\beta!(N-x)!(N+\alpha+\beta+1)!} \tag{114}$$

and

$$\pi_n \equiv \frac{N!(N+\alpha+\beta+1)!\beta!(n+\alpha)!(n+\alpha+\beta)!(2n+\alpha+\beta+1)}{(N-n)!(N+\alpha+\beta+n+1)!\alpha!(\alpha+\beta)!(n+\beta)!n!(\alpha+\beta+1)} \quad (115)$$

If we introduce the notation [31]

$$Q_{n,x}^{\alpha,\beta,N} \equiv \sqrt{w(x)\pi_n} Q_n(x,\alpha,\beta,N) \quad (116)$$

then the "Hahn coefficients" $Q_{n,x}^{\alpha,\beta,N}$ obey

$$\sum_{n=0}^{N} Q_{n,x}^{\alpha,\beta,N} Q_{n,x'}^{\alpha,\beta,N} = \delta_{x',x} \quad (117)$$

and

$$\sum_{x=0}^{N} Q_{n,x}^{\alpha,\beta,N} Q_{n',x}^{\alpha,\beta,N} = \delta_{n',n} \quad (118)$$

We can write in terms of these coefficients the unitary transformation matrix

$$< nlm|n\mu m >= \int d\Omega Y^*_{n-1,l,m}(\hat{\mathbf{u}}) \mathcal{Y}_{n-1,\mu,m}(\hat{\mathbf{u}}) \quad (119)$$

which links the spherical polar hydrogenlike Sturmians with the Stark basis This applies also to the basis transformations of d-dimensional extensions needed in many-particle problems. The same can be done for the Shibuya-Wulfman integrals which, as we have seen above, may prove to be extremely important to future developments in quantum theory. These integrals define a set of polynomials, which are linked to Hahn polynomials and Laguerre polynomials Because of their great practical importance, the polynomials associated with Shibuya-Wulfman integrals present a challenge to the community of mathematicians, a community which now is making very rapid progress in the general theory of polynomials· It would be highly desirable to develop efficient methods for generating the polynomials associated with Shibuya-Wulfman integrals; and we offer this problem as a challenge to the mathematical community.

Acknowledgements

Work in Perugia is supported by the Italian CNR and MURST, and by the European Union COST program.

Table 1
***d*-dimensional hydrogenlike Sturmians**

n	λ	$R_{n,\lambda}(r) \qquad t \equiv k_\mu r$
1	0	$\dfrac{(2k_\mu)^{d/2}}{\sqrt{(d-1)!}} e^{-t}$
2	0	$\dfrac{(2k_\mu)^{d/2}}{(d-2)!}\sqrt{\dfrac{(d-1)!}{d+1}}\left[1-\dfrac{2t}{d-1}\right]e^{-t}$
2	1	$\dfrac{(2k_\mu)^{d/2}}{\sqrt{(d+1)!}}(2t)e^{-t}$
3	0	$\dfrac{(2k_\mu)^{d/2}}{(d-2)!}\sqrt{\dfrac{d!}{d+3}}\left[1-\dfrac{4t}{d-1}+\dfrac{4t^2}{d(d-1)}\right]e^{-t}$
3	1	$\dfrac{(2k_\mu)^{d/2}}{d!}\sqrt{\dfrac{(d+1)!}{d+3}}(2t)\left[1-\dfrac{2t}{d+1}\right]e^{-t}$
3	2	$\dfrac{(2k_\mu)^{d/2}}{\sqrt{(d+3)!}}(2t)^2 e^{-t}$

Table 2
Triplet excited states of the 2-electron isoelectronic series

Calculated values are shown uppermost. Experimental values, where available (taken from Moore's tables [43]), are shown below for comparison. The multiconfigurational calculation made use of 15 generalized Sturmian basis functions of the form $|\chi_{1,0,0}\chi_{n,l,0}|$ for the levels $7s\ ^3S - 12s\ ^3S$, while for lower levels a slightly larger basis set was used, with 36 configurations, some of which involved doubly excited states.

	He	Li^+	Be^{2+}	B^{3+}	C^{4+}	N^{5+}
$2s\ ^3S$	−2.17359	−5.10790	−9.29368	−14.7300	−21.4166	−29.3533
expt	−2.17503	−5.11079	−9 29825	−14.7372	−21.4290	−29.3736
$3s\ ^3S$	−2.06815	−4.75035	−8.54419	−13.4496	−19.4663	−26 5943
expt.	−2.06850	−4.75214				
$4s\ ^3S$	−2.03627	−4.63601	−8 29825	−13.0232	−18.8109	−25.6613
expt.	−2.03632	−4.63722				
$5s\ ^3S$	−2.02250	−4 58537	−8 18801	−12.8307	−18.5136	−25.2367
expt.	−2.02243	−4.58618				
$6s\ ^3S$	−2 01529	−4.55856	−8.12931	−12.7278	−18.3541	−25.0084
expt	−2.01519	−4.55913				
$7s\ ^3S$	−2.01097	−4 54251	−8.09421	−12.6662	−18.2586	−24.8715
expt.	−2.01094	−4.54309				
$8s\ ^3S$	−2 00832	−4.53237	−8.07182	−12.6267	−18.1973	−24.7835
expt.	−2.00824					
$9s\ ^3S$	−2.00653	−4.52547	−8.05657	−12.5999	−18.1554	−24.7234
expt.	−2.00641					
$10s\ ^3S$	−2.00526	−4.52057	−8.04573	−12.5807	−18.1256	−24.6805
expt.	−2.00512					
$11s\ ^3S$	−2.00432	−4.51695	−8.03773	−12.5666	−18.1036	−24.6489
expt.	−2.00418					
$12s\ ^3S$	−2 00348	−4.51421	−8.03166	−12.5559	−18.0870	−24.6250
expt	−2.00346					

Table 2 continued

	He	Li^{+}	Be^{2+}	B^{3+}	C^{4+}	N^{5+}
$2p\ ^3P$	−2.12931	−5.02020	−9.16547	−14.5625	−21.2103	−29 1086
expt.	−2.13297	−5.02774	−9.17591	−14.5762	−21.2290	−29.1349
$3p\ ^3P$	−2.05705	−4.72777	−8.51022	−13.4044	−19.4101	−26.5272
expt.	−2 05789	−4.73054				
$4p\ ^3P$	−2.03191	−4.62702	−8 28440	−13.0045	−18.7874	−25.6331
expt.	−2.03213	−4.62850				
$5p\ ^3P$	−2.02034	−4.58092	−8.18106	−12.8212	−18.5015	−25.2220
expt.	−2.02036	−4.58182				
$6p\ ^3P$	−2.01407	−4.55604	−8.12535	−12.7223	−18.3471	−24.9998
expt.	−2.01401	−4 55665				
$7p\ ^3P$	−2.01023	−4.54098	−8.09178	−12.6628	−18.2542	−24.8661
expt.	−2.01022					
$8p\ ^3P$	−2.00783	−4 53135	−8.07022	−12.6245	−18.1943	−24 7797
expt.	−2.00776					
$9p\ ^3P$	−2.00619	−4 52476	−8.05546	−12.5983	−18.1533	−24.7207
expt	−2.00608					
$10p\ ^3P$	−2.00501	−4.52005	−8.04492	−12.5796	−18 1241	−24 6786
expt.	−2 00488					
$11p\ ^3P$	−2 00412	−4 51657	−8.03712	−12.5658	−18 1025	−24.6475
expt	−2.00400					
$12p\ ^3P$	−2.00321	−4.51392	−8.03120	−12.5553	−18.0861	−24.6055
expt.	−2 00332					

Table 2 continued

	He	Li^{+}	Be^{2+}	B^{3+}	C^{4+}	N^{5+}
$3d\ ^3D$	−2 05551	−4.72178	−8.49901	−13 3875	−19.3872	−26.4982
expt.	−2.05544	−4.72260			−19.3967	
$4d\ ^3D$	−2.03122	−4.62460	−8.28009	−12.9981	−18.7787	−25 6220
expt	−2.03109	−4.62524				
$5d\ ^3D$	−2.01998	−4.57971	−8.17901	−12.8182	−18.4974	−25.2168
expt.	−2.01983	−4.58016				
$6d\ ^3D$	−2.01386	−4.55535	−8.12423	−12.7207	−18.3449	−24.9970
expt.	−2 01371	−4.55569				
$7d\ ^3D$	−2.01007	−4.54066	−8.09102	−12.6617	−18.2528	−24.8644
expt	−2.01002	−4 54093				
$8d\ ^3D$	−2 00772	−4.53102	−8.06972	−12.6238	−18.1935	−24.7787
expt.	−2 00763					
$9d\ ^3D$	−2.00611	−4.52453	−8 05512	−12.5978	−18 1528	−24 7200
expt.	−2.00599					
$10d\ ^3D$	−2.00495	−4.51988	−8.04467	−12.5793	−18.1237	−24.6781
expt.	−2.00482					
$11d\ ^3D$	−2.00411	−4 51644	−8.03694	−12.5655	−18.1022	−24.6472
expt	−2.00395					
$12d\ ^3D$	−2.00364	−4.51382	−8.03105	−12.5551	−18.0859	−24.6236
expt.	−2.00329					
$13d\ ^3D$	−2.00280	−4.51180	−8.02649	−12.5469	−18.0732	−24.6053
expt	−2.00277					

Table 2 continued

	He	Li^+	Be^{2+}	B^{3+}	C^{4+}	N^{5+}
$4f\ ^3F$	−2.03125	−4.62493	−8.28101	−12.9996	−18.7806	−25.6242
expt.	−2.03106	−4.62509				
$5f\ ^3F$	−2.01999	−4.57992	−8.17968	−12.8194	−18.4991	−25 2188
expt.	−2.01981	−4.58008				
$6f\ ^3F$	−2.01373	−4.55549	−8.12470	−12.7216	−18 3462	−24.9986
expt.	−2.01370	−4 55565				
$7f\ ^3F$	−2.01010	−4.54075	−8.09157	−12.6626	−18.2541	−24.8659
expt.	−2.01002	−4.54090				
$8f\ ^3F$	−2 00775	−4.53120	−8.06997	−12.6243	−18 1942	−24.7798
expt.	−2.00763	−4.53134				
$9f\ ^3F$	−2.00613	−4 52458	−8.05529	−12.5982	−18.1534	−24.7209
expt.	−2.00600					
$10f\ ^3F$	−2.00497	−4.51992	−8 04480	−12.5795	−18.1242	−24.6788
expt.	−2.00481					
$11f\ ^3F$	−2.00410	−4.51647	−8 03703	−12.5657	−18.1026	−24.6477
$12f\ ^3F$	−2.00349	−4.51384	−8.03113	−12.5552	−18.0862	−24.6241
$13f\ ^3F$	−2.00275	−4.51180	−8 02653	−12.5471	−18 0735	−24 6057
$14f\ ^3F$	−2.00179	−4.51029	−8.02290	−12.5406	−18 0633	−24 5911

Table 3
4-dimensional hyperspherical harmonics

λ	l	m	$\sqrt{2}\pi\ Y_{\lambda,l,m}(\mathbf{u})$
0	0	0	1
1	1	1	$\imath\sqrt{2}(u_1 + iu_2)$
1	1	0	$-\imath 2u_3$
1	1	-1	$-i\sqrt{2}(u_1 - \imath u_2)$
1	0	0	$-2u_4$
2	2	2	$-\sqrt{3}(u_1 + \imath u_2)^2$
2	2	1	$2\sqrt{3}u_3(u_1 + iu_2)$
2	2	0	$-\sqrt{2}(2u_3^2 - u_1^2 - u_2^2)$
2	2	-1	$-2\sqrt{3}u_3(u_1 - \imath u_2)$
2	2	-2	$-\sqrt{3}(u_1 - \imath u_2)^2$
2	1	1	$-\imath 2\sqrt{3}\ u_4(u_1 + \imath u_2)$
2	1	0	$2\imath\sqrt{6}\ u_4 u_3$
2	1	-1	$2\imath\sqrt{3}\ u_4(u_1 - \imath u_2)$
2	0	0	$4u_4^2 - 1$

Table 4: Shibuya-Wulfman integrals, $S^{\alpha}_{\alpha'}$

α'	$\alpha = 1s$	$\alpha = 2s$
$1s$	$(1+s)e^{-s}$	$-2s^2e^{-s}/3$
$2s$	$-2s^2e^{-s}/3$	$(3+3s-2s^2+s^3)e^{-s}/3$
$2p_j$	$2s_j(1+s)e^{-s}/3$	$s_j(1+s-s^2)e^{-s}/3$

α'	$\alpha = 2p_1$
$2p_1$	$(3+3s+s^2-s_1^2-ss_1^2)e^{-s}/3$
$2p_2$	$s_1s_2(1+s)e^{-s}/3$
$2p_3$	$s_1s_3(1+s)e^{-s}/3$

Table 5
Alternative hyperspherical harmonics.

λ	μ	m	$\sqrt{2}\pi\ \mathcal{Y}_{n_1,n_2,m}(\mathbf{u})$
0	0	0	1
1	0	1	$-\imath\sqrt{2}(u_2+iu_1)$
1	0	-1	$-\imath\sqrt{2}(u_2-\imath u_1)$
1	1	0	$-\sqrt{2}(u_4+\imath u_3)$
1	-1	0	$-\sqrt{2}(u_4-iu_3)$
2	0	2	$-\sqrt{3}(u_2+\imath u_1)^2$
2	0	-2	$-\sqrt{3}(u_2-\imath u_1)^2$
2	2	0	$\sqrt{3}(u_4+iu_3)^2$
2	-2	0	$\sqrt{3}(u_4-\imath u_3)^2$
2	0	0	$\sqrt{3}(u_4^2+u_3^2-u_2^2-u_1^2)$
2	1	1	$\imath\sqrt{6}(u_4+\imath u_3)(u_2+\imath u_1)$
2	1	-1	$\imath\sqrt{6}(u_4+\imath u_3)(u_2-\imath u_1)$
2	-1	1	$\imath\sqrt{6}(u_4-\imath u_3)(u_2+\imath u_1)$
2	-1	-1	$\imath\sqrt{6}(u_4-\imath u_3)(u_2-\imath u_1)$

References

1 H. Shull and P.-O. Löwdin, J. Chem. Phys. **30**, 617 (1959).
2. M. Rotenberg, Ann. Phys. (New York), **19**, 262 (1962).
3. M. Rotenberg, Adv. At. Mol. Phys. **6**, 233 (1970).
4 O. Goscinski, *Preliminary Research Report No 217, Quantum Chemistry Group, Uppsala University*, (1968).
5. J.P Gazeau and A Maquet, Phys. Rev. A, **20**, 727 (1979)
6 J.P. Gazeau and A. Maquet, J. Chem. Phys **73**, 5147 (1980).
7 J.M. Bang and J.S. Vaagen, Z. Phys A, **297**, 223 (1980)
8. J.M. Bang, F.G. Gareev, W.T. Pinkston and J.S Vaagen, Phys Rep **125**, 253-399 (1985).
9. J Avery, **Hyperspherical Harmonics; Applications in Quantum Theory**, Kluwer Academic Publishers, Dordrecht, (1989).
10. J. Avery and D.R. Herschbach, Int J. Quantum Chem **42**, 87 (1992)
11. J Avery and F. Antonsen, Theor. Chim. Acta **85**, 33 (1993).
12. V. Aquilanti and J. Avery, Chem. Phys. Letters, **267**, 1 (1997).
13 J Avery, J. Math. Chem. **21**, 285 (1997)
14. J. Avery, Adv. Quantum Chem **31**, 201 (1999).
15. J Avery, Theochem, **458**, 1 (1999).
16. J Avery and S. Sauer, Progress in Theoretical Chemistry, Kluwer Academic Publishers, Dordrecht, (in press).
17. J. Avery **Hyperspherical Harmonics and Generalized Sturmians**, Kluwer Academic Publishers, Dordrecht, (1999).
18. U. Fano, D. Green, J.L. Bohn and T.A. Heim, J. Phys. B . At. Mol Opt. Phys. **32**, R1 (1999).
19. V Aquilanti, S. Cavalli and C. Coletti, Chem. Phys. **214**, 1 (1997).
20 T. Shibuya and C.E Wulfman, Proc. Roy Soc A, **286**, 376 (1965)
21. E.J. Weniger, J. Math. Phys. **26**, 276 (1985).
22 V. Fock, Z. Phys. **98**, 145 (1935).
23 J. Avery and C. Coletti, in **Quantum Systems in Chemistry and Physics**, A. Hernández-Leguna, J. Maruanu, R. McWeeny and S Wilson editors, Kluwer Academic Publishers, Dordrecht, Vol 1, (2000).
24. E. Clementi, J Chem. Phys. **38**, 996 (1963).
25. J. Fernándex Rico, G. Ramírez, R. López and J I. Fernández Alonzo, Collect. Czech Chem. **53**, 2250 (1987).
26. J. Fernández Rico, R. López, I. Ema and G. Ramírez, (preprints).
27. E J. Weniger and E.O Steinborn, J Chem. Phys. **78**, 6121 (1983)
28. E.J. Weniger, J. Grotendorst and E O. Steinborn, Phys Rev. A, **33**, 3688 (1986).
29. L.C Biedenharn and J.D. Louck, **Angular Momentum in Quantum Physics**, Addison Wesley, Reading Mass., (1981).

30. L C. Biedenharn and J.D. Louck, **The Racah-Wigner Algebra in Quantum Theory**, Addison Wesley, Reading Mass., (1981)
31. V. Aquilanti, S. Cavalli and D. De Fazio, J. Phys. Chem. **99**, 15694 (1995).
32. M.S. Kil'dyushov, Sov. J. Nucl. Phys., **15**, 113 (1972).
33. M.S. Kil'dyushov and G.I. Kuznetsov, Sov. J. Nucl. Phys., **17**, 1330 (1973).
34. N.P Klepkov, Sov. J. Nucl. Phys. **19**, 462 (1974).
35. G.I. Kuznetsov and Ya. Smorodinskii, Sov. J. Nucl. Phys. **25**, 447 (1976).
36. A.F. Nikiforov, S.K. Suslov and V.B. Uvarov, **Classical Orthogonal Polynomials of a Discrete Variable**, Springer Verlag, Berlin, (1991).
37. Yu.F Smirnov and K.V. Shitikova, Sov. J. Part. Nucl **8**, 344, (1976).
38. N.K. Vilenkin, **Special Functions and the Theory of Group Representations**, American Mathematical Society, Providence, R.I., (1968).
39. V. Aquilanti, S. Cavalli, C. Coletti, D. De Fazio and G Grossi, in **New Methods in Quantum Theory**, C.A Tsipis, V.S. Popov, D.R. Herschbach and J.S Avery, editors, Kluwer Academic Publishers, Dordrecht, p 233, (1996)
40. V. Aquilanti, S. Cavalli and G Grossi, J. Chem Phys. **85**, 1362, (1986).
41. V. Aquilanti, S. Cavalli and C. Coletti, Phys. Rev. Letters **80**, 3209 (1998).
42. V. Aquilanti, S Cavalli, C. Coletti and G. Grossi, Chem. Phys. **209**, 405, (1996)
43. C E Moore, **Atomic Energy Levels, Circular of the National Bureau of Standards 467**, Superintendent of Documents, U.S. Government Printing Office, Washington, D.C., (1949).
44. J. Avery, J. Math. Chem. **24**, 169, (1998).
45. V. Aquilanti, C. Cavalli, C. Coletti, D. Di Dominico and G. Grossi, in **Quantum Systems in Chemistry and Physics**, A. Hernández-Leguna, J. Maruanu, R. McWeeny and S. Wilson editors, Kluwer Academic Publishers, Dordrecht, Vol. 1, p. 291 (2000).
46. V. Aquilanti and G Capecci, Theor. Chem. Acta (2000), (in press).

The A+BC reaction by the hyperquantization algorithm: the symmetric hyperspherical parametrization for J > 0

by
Vincenzo Aquilanti, Simonetta Cavalli, Dario De Fazio
and Alessandro Volpi
Dipartimento di Chimica, Università di Perugia,
I-06123 Perugia, Italy

Abstract

The methodology of the hyperspherical coordinate approach to triatomic reactions is presented, special emphasis being given to the extension of the hyperquantization algorithm in the symmetric parametrization to the general case of nonzero total angular momentum. The discrete analogs of hyperspherical harmonics, *i.e.* functions orthonormal on a lattice of points covering the interaction region, are used as basis sets to compute the adiabatic hyperspherical states parametrically dependent on the hyperradius which serve as effective potentials for reactive scattering. The relevant aspects of the method are that no integrals have to be calculated and the Hamiltonian matrix is sparse and can be evaluated analytically, using angular momentum coupling theory. A survey of numerical results and extensions is given.

ADVANCES IN QUANTUM CHEMISTRY, VOLUME 39

0065-3276/01 $35.00

Contents

1 Introduction

The hyperspherical coordinate approach (see [1] for an account) has successfully contributed to the understanding of many of the most interesting features of the three-body quantum mechanical problem and in particular of reactive scattering [2-7]. A three-atom system possesses nine degrees of freedom, but the three which describe over-all translations can be eliminated because of center-of-mass conservation. Accordingly, the complete description of the dynamics of three atoms requires the treatment of six coordinates: in the hyperspherical approach, this is accomplished by calculating in a first step for entrance and exit channels adiabatic eigenvalues and eigenvectors by solving a five-dimensional quantization problem adiabatically in the hyperradius ρ, treated as a quasi-separable variable; coupled-channel equations as a function of ρ are obtained and integrated in the final propagation step.

The hyperradius is a measure of the total inertia of the system and is a natural reaction coordinate. At small values it corresponds to the region of strong triatomic interaction while at large values it describes the asymptotic rearrangement regions corresponding to reactants and products. The other variables span a five-dimensional hypersphere: thus one has three orientational coordinates (for example the Euler angles which define appropriately a rotating body frame) and two internal "angles". Two basic hyperspherical parametrizations, which we refer to as asymmetric and symmetric, offer two alternatives for the choice of these angles. Both have been studied and used [8-11]. In particular, the symmetric hyperspherical coordinates proved to be very effective when applied to the study of triatomic reactions, and efficient algorithms are demanded to solve eigenvalue problems at fixed values of the hyperradius, for any combination of masses, the key problem for most systems being the high number of states one has to deal with in the general case. We have developed and implemented a method (*hyperquantization algorithm* [12-15]), which allows the calculation of the adiabatic (fixed hyperradius) states and wavefunctions. This step is very demanding from a computational viewpoint: systems involving more than one atom different from hydrogen and more than two open rearrangement channels are still very hard

to cope with. Also, practically all reactive scattering calculations reported so far have been carried out only on the ground potential energy surface, while our algorithm provides a framework for the treatment of couplings to the excited electronic states[13], such as those which arise when spin and electronic orbital effects are considered. In principle, the technique can be formulated for more than three bodies.

The mathematical tools of our algorithm are polynomials of a discrete variable properly weighted and normalized to be orthogonal on a lattice of points (for a recent account, see[15]). In the present application, they are generalized $3j$ symbols or Hahn coefficients [16]. Using these quantities we build up an algebraic representation of the eigenvalue equation with the very attractive computational feature of providing a natural discretization of a quantum mechanical problem (hyperquantization). Advantages are that no integrals are to be calculated, the potential is diagonal on a discrete grid and the construction of kinetic energy matrix is straightforward: salient features are the block tridiagonal structure of the Hamiltonian matrix and a number of symmetry properties. Also, the sparseness of the matrix enormously simplifies the diagonalization required to obtain the adiabatic hyperspherical channels as a function of the hyperradius.

This step is the most time consuming, but the computing time and memory requirements have been highly reduced by applying a sequential method of diagonalization and truncation of the basis[14]. For three-atom reactions there are two choices to be made for the sequence, which are related to the two ways of ordering the elements of the Hamiltonian matrix. The effectiveness of the reduction of each scheme is found to depend on the topology of the potential energy surface as the hyperradius varies, the transition between the range of applicability of the two procedures occurring astride of the appearance of the ridge line which separates the reactants' and products' asymptotic channels.

The topic of body frames and their singularities as well as those of the centrifugal potential and those due to the choice of internal angles is also relevant [17]. Sources of discontinuities of the internal wavefunction have to be taken into account in order to obtain convergent results. A proper frame is one where all singularities lie in regions where wavefunctions vanish. This can be accomplished using as a basis a prolate symmetric top set, *i.e.* keeping constant the projection Ω of the total angular momentum on the axis of least inertia. Within this choice the frame singularities lie outside the dynamically accessible region for the entrance and exit reaction channels, and also for transition states which are close to the collinear configuration of the three bodies. For systems with a bent transition state an oblate top reference Hamiltonian may be more appropriate· this choice, currently being investigated, amounts to choose a principal axis frame where the quantization axis is perpendicular to the triatomic plane.

Quantum mechanical calculations which apply the hyperquantization algorithm based on symmetric hyperspherical coordinates have been carried out on two benchmark systems, the $F+H_2$ reaction including fine structure effects [13]

and the $He+H_2^+$ reaction [18].

In the next section we define the hyperspherical symmetric coordinates under focus in this work. Asymmetric coordinates have been studied elsewhere[12, 19], and some of their advantages and disadvantages assessed[10]. In section 3 essentials of the hyperspherical approach are presented. In section 4 our algorithm (hyperquantization) is presented: the transformation from a continuum basis set into a discrete one is extended to deal with the case of any value of the total angular momentum J, as needed for calculations of observables such as cross sections and reaction rates. In Sec. 4.1 the discrete analogs of hyphersperical harmonics, *i.e.* generalized $3j$ symbols or Hahn coefficients [16], are introduced and some important properties used to develop our algorithm are reviewed. Sec. 4.2 provides the explicit construction of the Hamiltonian matrix, yielding adiabatic channels eigenvalues and eigenfunctions to be used in the propagation step along the hyperradius (Sec. 4.3). The results and some perspectives about the potentialities of this method for tackling fine structure effects and four body processes are summarized in the final Sec. 5.

2 Hyperspherical Coordinates for a three particle system

In the laboratory reference frame the motion of three particles depends on nine variables, three of which define the position of the center-of-mass while the other six describe the internal (e.g. rotational and vibrational) modes. The center-of-mass, or translational, degrees of freedom are separated out introducing two tridimensional vectors, $\boldsymbol{r}_{ij}$ and $\boldsymbol{R}_{k,ij}$ which denote the vector from atom i to j and the vector from the center of mass of the pair ij to the atom k, respectively. The choice of these Jacobi vectors is not unique: explicitly, for the reaction of an atom A with a molecule BC a suitable set for describing the reactants' channel A+BC, corresponds to the vectors $\boldsymbol{r}_{\mathrm{BC}}$ and $\boldsymbol{R}_{\mathrm{A,BC}}$. Alternatively, two other sets of vectors, $\boldsymbol{r}_{\mathrm{AB}}$ and $\boldsymbol{R}_{\mathrm{C,AB}}$ or $\boldsymbol{r}_{\mathrm{AC}}$ and $\boldsymbol{R}_{\mathrm{B,AC}}$, are more appropriate for describing the products' channels AB+C or AC+B. Under proper mass scaling (see below) these three sets of vectors can be related to each other by a planar rotation of an angle which depends only on the masses of A, B and C atoms [20] and is an extension of the so-called skewing angle concept introduced in the thirties in chemical kinetics. In a previous paper [21], we have shown that alternative coordinate systems such as the Radau-Smith vectors [22] can be obtained from the Jacobi ones by a sequence of *kinematic rotations* (for explicit expressions of the (mass-dependent-only) rotation angles see[20]). The symmetric parametrization for an n-body system [19] features the kinematic rotation angles as variables. For three bodies, only one angle, denoted as Φ following Smith [23] is sufficient. For

each set k (or i or j) of the two Jacobi vectors the mass-scaling can be written

$$\begin{aligned} \mathsf{r}_k &= \left(\frac{\mu_{ij}}{\mu}\right)^{1/2} \boldsymbol{r}_{ij} \\ \mathsf{R}_k &= \left(\frac{\mu}{\mu_{ij}}\right)^{1/2} \boldsymbol{R}_{k,ij} \end{aligned} \tag{1}$$

where μ_{ij} is the two-body reduced mass for the ij couple. The Cartesian components of the vectors r_k and R_k along the center of mass reference frame can be viewed as the rectangular coordinates which define the position in a six dimensional space of a body of mass μ, conveniently identified with the three-body reduced mass

$$\mu = \sqrt{m_i m_j m_k/(m_i + m_j + m_k)} \tag{2}$$

where m_i, m_j and m_k are the masses of the three particles. When in this multidimensional space hyperspherical coordinate systems (*i.e* one radius and five angles) are introduced, the *hyperradius* is found to be:

$$\rho^2 = |\, \mathsf{r}_k \,|^2 + |\, \mathsf{R}_k \,|^2 \tag{3}$$

and enjoys the important property of being independent on the particular choice k, or i, or j and of being a direct measure of total inertia (see below). Being invariant under kinematic rotations, it is referred to as a variable *democratic* with respect to labeling of particles and rearrangement channels.

The five angles that define the orientation of a point on the surface of the 6-dimensional sphere can be chosen in essentially two different ways, each offering advantages whose exploitations make the hyperspherical approach extremely flexible and powerful. Each parametrization corresponds to an alternative coupling scheme of angular momenta and as a consequence to an alternative representation of the Schrödinger equation for the three particles. We have given a classification of these parametrizations [19], where - as also experienced by the vast literature on three-body problems - it is basic to separately consider the two classes, which we denote as *asymmetric* [24] and *symmetric* [23] hyperangular parametrizations. The choice of the reference frame is also important.

The parametrization of hyperangles, denoted as symmetric, was first introduced by Smith [23] and has been employed successfully by many for reaction scattering problems [3, 4, 6, 7]. When the transformation to the inertia principal axis reference frame is enforced, the spatial rotations are described in terms of three external coordinates, for example the Euler angles (α, β, γ) orienting the ellipsoid of inertia with respect to the center-of-mass reference frame, and the internal dynamics is best represented in terms of rotations - specified by the angle Φ - in the kinematic two-dimensional space of two orthogonal vectors whose lengths x_1 and x_2 are democratic (or kinematic) *invariants*, because do not depend on the particular choice of the Jacobi vectors.

The coordinate transformation from the cartesian components of the mass-scaled Jacobi vectors to the coordinates $\alpha, \beta, \gamma, x_1, x_2$ and Φ is introduced as follows[19]:

$$\begin{pmatrix} r_{k1} & R_{k1} \\ r_{k2} & R_{k2} \\ r_{k3} & R_{k3} \end{pmatrix} = D(\alpha,\beta,\gamma) \begin{pmatrix} x_1 & 0 \\ 0 & x_2 \\ 0 & 0 \end{pmatrix} \begin{pmatrix} \cos\Phi & -\sin\Phi \\ \sin\Phi & \cos\Phi \end{pmatrix} \tag{4}$$

where R is an SO(3) three x three orthogonal rotation matrix depending for example on α, β and γ.

The squares of x_1 and x_2 are the eigenvalues of the scalar product matrix between the Jacobi vectors, whose trace is the hyperradius and whose determinant is proportional to the area A of the triangle formed by the three particles. So we can write:

$$\rho^2 = x_1^2 + x_2^2 \tag{5}$$

and

$$4A^2 = x_1^2 x_2^2 \tag{6}$$

The principal moments of inertia I_1 and I_2 are directly related to the kinematic invariants

$$\begin{aligned} I_1/\mu &= x_2^2 \\ I_2/\mu &= x_1^2 \end{aligned} \tag{7}$$

where μ is the three-body reduced mass, Eq. (2).

We recall that in the case of three particles only two moments of inertia need be specified, being one of them, say I_3, the sum of the other two, with the constraint $I_1 \geq I_2$. In [25], Smith defined an angular coordinate Θ for the three-body planar problem:

$$\begin{aligned} (I_1 - I_2)/\mu &= \rho^2 \cos 2\Theta \\ 4A &= \rho^2 \sin 2\Theta \end{aligned} \tag{8}$$

For the three-body problem in the physical tridimensional space, the range for Θ is from 0 to $\pi/4$ in order to span only positive values of A.

By comparison of Eqs. (8) with (6) and (7) we easily find:

$$\begin{aligned} x_1 &= \rho \sin\Theta \\ x_2 &= \rho \cos\Theta \end{aligned} \tag{9}$$

The two *kinematic invariants*, Θ and ρ, and the angle Φ are the internal coordinates for the symmetric hyperspherical parametrization of the three body problem. The hyperradius ρ and the area-angle Θ are also indicated as the *collective* [26] coordinates, because they specify the magnitude and the position of

the inertia ellipsoid and are independent of particle permutations. The *kinematic* angle Φ is a continuous generalization of the reaction skewing angle concept and distinguishes the different shapes of all triangles with the same moments of inertia. It varies between 0 and π and is defined within a phase factor which depends only on masses and specifies the particular choice of Jacobi's vectors.

In Ref.[20] we have given the explicit relationships among the variables Θ and Φ and the internal angles of the asymmetric hyperspherical parametrization as well as the distance formulae, useful for the mapping of the potential energy surface in both parametrizations.

3 The Hyperspherical Method

In hyperspherical coordinates the kinematics of three particles is equivalent to that of the motion of one body of mass μ (Eq. (2) on the five-dimensional surface of a sphere embedded in a six-dimensional space. The kinetic energy operator takes the following form:

$$\mathsf{K} = -\frac{1}{2\mu}\left[\rho^{-5}\frac{\partial}{\partial\rho}\rho^{5}\frac{\partial}{\partial\rho} - \frac{\Lambda^2}{\rho^2}\right] \tag{10}$$

where ρ is the hyperradius and the operator Λ^2 is mathematically related to the quadratic Casimir's operator of the six-dimensional rotation group and is physically interpreted as the generalized or grand orbital angular momentum operator [25]. Its eigenvalues are $\lambda(\lambda+4)$, where λ is the grand orbital angular quantum number, and its eigenfunctions are hyperspherical harmonics [19].

The grand-orbital angular momentum operator acts on five angular variables. If one considers the motion in the center-of-mass reference frame and utilizes the asymmetric hyperspherical parametrization of the Jacobi vectors, the corresponding harmonics are known in closed form for each value of the total angular momentum[19]. The asymmetric hyperangular parametrization permits explicit harmonics for any J for any number of particles, but overemphasizes a rearrangement channel over the others. This is the reason why it struggles to accurately reproduce the whole reaction. However, implementation of our algorithm and some results have been discussed [12, 10]. In the following, we will refer to the symmetric hyperangular parametrizations, which on the contrary enjoys the property of treating "democratically" all reaction channels, but for which hyperspherical harmonics are available in a closed form only for zero total angular momentum. Therefore, for J greater than zero, which is important in practice, the total Hamiltonian will be partitioned in such a way as to separate out a part exactly solvable in proper harmonics (see below, Eqs. (13) - (16)), while the remaining part will be treated in the propagation step.

In symmetric hyperspherical coordinates, the Λ^2 operator reads [3, 4, 27, 28]:

$$\Lambda^2 = -\frac{1}{\sin 4\Theta}\frac{\partial}{\partial\Theta}\sin 4\Theta\frac{\partial}{\partial\Theta} - \frac{1}{\cos^2 2\Theta}\left(\frac{\partial^2}{\partial\Phi^2} - J_3^2 - 2i\sin 2\Theta\, J_3\,\frac{\partial}{\partial\Phi}\right) + \frac{J_1^2}{\sin^2\Theta} + \frac{J_2^2}{\cos^2\Theta} \tag{11}$$

where J_1, J_2 and J_3 are the components of the total angular momentum operators in the principal axis reference frame and depend on three variables (*e.g.* the Euler angles). In the limit of a prolate top, as for example a collinearly dominated reaction, it is most natural to identify the quantization axis z as the smallest inertia axis, in this case J_1 is chosen as the component which commutes with both J^2 and Λ^2. An alternative choice, convenient in the limit of an oblate top, considers the z axis pointing along the largest inertia axis and the component J_3 is identified as J_z. The identification of J_z with J_2 may be suited for intermediate cases. The representation of the Coriolis term, $J_3\,\partial/\partial\Phi$, which couples the external rotational modes to the internal angle Φ, depends on the choice of the quantization axis: when the latter is pointing along the largest inertia axis the operator J_3 is diagonal, otherwise it has to be given in terms of ladder operators.

The calculation of the reactive cross sections requires the solutions of the following Schrödinger equation

$$\left[-\frac{1}{2\mu}\left(\rho^{-5}\frac{\partial}{\partial\rho}\rho^5\frac{\partial}{\partial\rho} - \frac{\Lambda^2}{\rho^2}\right) + V(\rho,\Theta,\Phi)\right]\Psi = E\Psi \tag{12}$$

at selected values of the total energy E, the total angular momentum (included in Λ^2) and the parity with respect to the inversion of all coordinates. V is the potential energy surface, which depends on the internal coordinates of Sec. 2.

Within the hyperspherical coordinates approach, the usual point of view is to study the dynamics on a family of effective potentials parametrically dependent on ρ, and treating the ρ dependence in a second (the propagation) step. Therefore, the first step requires the search for solutions of the angular part of the Schrödinger equation at given values of the hyperradius. The case of total angular momentum equal to zero is simpler and has been treated extensively[12]. Very demanding is the treatment of J greater than zero. It has been found convenient to first solve a restricted eigenvalue problem:

$$\left[\frac{1}{2\mu\rho^2}\Lambda_\Omega^2(\Theta,\Phi) + V(\rho,\Theta,\Phi)\right]\psi_i = \varepsilon_i^\Omega(\rho)\psi_i \tag{13}$$

where, for reactions with a nearly collinear transition state, Λ_Ω^2 is suggested by the quantum mechanics of symmetric tops [3]:

$$\Lambda_\Omega^2 = -\frac{1}{\sin 4\Theta}\frac{\partial}{\partial\Theta}\sin 4\Theta\frac{\partial}{\partial\Theta} - \frac{1}{\cos^2 2\Theta}\frac{\partial^2}{\partial\Phi^2} + \frac{4\Omega^2}{\sin^2 2\Theta} \tag{14}$$

where in this case Ω is the projection of $\mathbf{J}$ on the smallest inertia axis. We exploit the fact that the prolate top symmetry dominates not only reactants' and products' configurations, but is approximately preserved along the whole reactive event [along a similar line, we are studying an oblate top reference Hamiltonian to describe reactions with a bent transition state].

The resulting sets of eigenvalues $\varepsilon_i^{\Omega}(\rho)$ and wavefunctions ψ_i contain information on the structure and internal modes, except the motion along the reaction radius, ρ. Since eigenfunctions of Λ_{Ω}^2 are hyperspherical harmonics:

$$Y_{\frac{\lambda}{2},\frac{\sigma}{2},\Omega}(4\Theta,2\Phi,0)=\left(\frac{\lambda+2}{4\pi}\right)^{1/2}\exp(-\imath\sigma\Phi)d^{\frac{\lambda}{4}}_{\frac{\sigma}{4}+\frac{\Omega}{2},\frac{\sigma}{4}-\frac{\Omega}{2}}(4\Theta) \tag{15}$$

[here $\sqrt{(\lambda+2)/4\pi}$ is the normalization factor], solutions of the eigenvalue equation (13) are searched through the following expansion

$$\psi_i=\rho^{-\frac{5}{2}}\sum_{\lambda\sigma}t^{\Omega}_{i\lambda\sigma}(\rho)Y_{\frac{\lambda}{2},\frac{\sigma}{2},\Omega}(4\Theta,2\Phi,0) \tag{16}$$

of the adiabatic channel eigenfunctions ψ_i. The quantum number λ takes integer even (odd) values when ψ_i is symmetrical (antisymmetrical) with respect to the spatial inversion; accordingly, the quantum number σ takes even (odd) positive and negative values from $-\lambda+2\Omega$ to $\lambda-2\Omega$. When two of the three atoms are identical (as in the example worked out in Ref [13]), cosine or sine functions of 2Φ are used to describe symmetrical or antisymmetrical behavior with respect to the exchange of the equal atoms.

Introducing the expansion (16) in Eq.(13) and integrating over the angular variables an eigenvalue problem is obtained:

$$\sum_{\lambda'\sigma'}\left\{\frac{\lambda'(\lambda'+4)+15/4}{2\mu\rho^2}\delta_{\lambda\lambda'}\delta_{\sigma\sigma'}+V^{\Omega}_{\lambda\sigma,\lambda'\sigma'}(\rho)\right\}t^{\Omega}_{i\lambda'\sigma'}(\rho)=\varepsilon_i^{\Omega}(\rho)t^{\Omega}_{i\lambda\sigma}(\rho) \tag{17}$$

where the kinetic energy matrix is diagonal and the potential energy matrix elements are:

$$V^{\Omega}_{\lambda\sigma,\lambda'\sigma'}(\rho)=\int Y^{*}_{\frac{\lambda'}{2},\frac{\sigma'}{2},\Omega}(4\Theta,2\Phi,0)V(\rho,\Theta,\Phi)Y_{\frac{\lambda}{2},\frac{\sigma}{2},\Omega}(4\Theta,2\Phi,0)\,d(\cos 4\Theta)d(2\Phi) \tag{18}$$

In the application of the formalism illustrated above a main drawback is the calculation of highly oscillating integrals in Eq.(18). In order to calculate the eigenvalues $\varepsilon_i^{\Omega}(\rho)$ and eigenvectors we have proposed the hyperquantization algorithm [12] which avoids this problem. It exploits the discrete analogs of hyperspherical harmonics in Eq.(15) (see below, Sec. 4.1) and through a unitary transformation on the eigenvectors $t^{\Omega}_{i\lambda\sigma}$ a novel representation of (17) is obtained: this is the stereodirected representation, to be seen in Sec. 4.2.

4 The hyperquantization algorithm

The algorithm is now illustrated to solve the eigenvalue problem [Eq. (13)] parametrically in ρ in the two internal hyperangles of the symmetric hyperangular parametrization. It involves "hyperquantization", being based on the discrete analogs of hyperspherical harmonics which are physically generalized vector coupling coefficients and mathematically Hahn polynomials. The technique allows us to obtain an alternative representation of Eq. (17) in which the potential energy matrix is diagonal and the couplings are transferred to the kinetic energy. Moreover, no integrals have to be computed since the potential energy matrix elements are the values of the potential energy surface on a lattice of evenly spaced points specified by the discrete values of $\cos 4\Theta$ and Φ

4.1 The discrete analogs of hyperspherical harmonics

In the previous section we have illustrated how hyperspherical harmonics can be used as expansion basis sets in the quantum mechanics of three bodies. Here we define their discrete analogs as the product of functions orthonormal on a set of grid points expressed explicitly in terms of Hahn polynomials, which can be physically interpreted as generalized $3j$ coefficients [16]. The Hahn polynomials [29] are functions of a discrete variable orthonormal on a lattice of points. They are related to the Jacobi polynomials [29] by a limiting relationship leading from a discrete to a continuum set. They enjoy many interesting properties, in particular three-term recurrence equations with respect to the discrete variable, which simplify the algebraic manipulations and the explicit calculations required for the hyperquantization algorithm.

In the following, we discuss the discretization of the hyperspherical harmonics $Y_{\lambda/2,\sigma/2,\Omega}$ in Eq.(15), which are needed as the eigenfunctions of the kinetic energy operator (14), when symmetric hyperangular coordinates are employed, the lattice consisting of equally spaced points in $\cos 4\Theta$ and Φ.

The reduced Wigner d–functions, see Eq. (15), are particular cases of Jacobi polynomials $P_n^{\alpha,\beta}(\cos\theta)$ [30] and are related to the Hahn coefficients [16] by the following relation:

$$\left(\frac{I+1}{2}\right)^{\frac{1}{2}} Q_{n,\xi}^{\Omega,\sigma/2,I} \simeq \left(\frac{\lambda+2}{4\pi}\right)^{1/2} d^{\frac{\lambda}{4}}_{\frac{\sigma}{4}+\frac{\Omega}{2},\frac{\sigma}{4}-\frac{\Omega}{2}}(4\Theta) \tag{19}$$

where $n = (\lambda - \mid \sigma \mid -2 \mid \Omega \mid)/4$ is the degree of the polynomial and

$$\cos 4\Theta = \frac{I-2\xi}{I+1} \tag{20}$$

ξ is the discrete variable and both n and ξ vary in the range $0 \leq n, \xi \leq I$. Note that $I + 1$ is the number of grid points in the discretized Θ range, and (19) becomes an equality for I tending to infinity.

The Hahn coefficients defined above in Eq. (19) (see also (26) below) constitute an orthonormal set with respect to both ξ and n :

$$\sum_{\xi=0}^{I} Q_{n,\xi}^{\Omega,\sigma/2,I} Q_{n',\xi}^{\Omega,\sigma/2,I} = \delta_{nn'} \tag{21}$$

and

$$\sum_{n=0}^{I} Q_{n,\xi}^{\Omega,\sigma/2,I} Q_{n,\xi'}^{\Omega,\sigma/2,I} = \delta_{\xi\xi'} \tag{22}$$

Together with the following recurrence relation [29]

$$C(\xi) Q_{n,\xi-1}^{\Omega,\sigma/2,I} + D(\xi) Q_{n,\xi}^{\Omega,\sigma/2,I} + C(\xi+1) Q_{n,\xi+1}^{\Omega,\sigma/2,I} = 0 \tag{23}$$

where

$$D(\xi) = n(n+\Omega+\sigma/2+1) - (\Omega+\xi+1)(I-\xi) - \xi(I+\sigma/2-\xi+1) \tag{24}$$

$$C(\xi) = [\xi(\Omega+\xi)(I-\xi+1)(I+\sigma/2-\xi+1)]^{\frac{1}{2}} \tag{25}$$

they will be exploited in the next section and are responsible for the sparseness of the Hamiltonian matrix to be diagonalized in the hyperquantization algorithm. The orthogonality (Eq. (21)) and dual orthogonality (Eq. (22)) properties are the discrete analogs of the orthogonality and completeness relations for hyperspherical harmonics.

A previous paper [16] can be consulted for the explicit relationship of Hahn coefficients with generalized angular momentum coupling coefficients; analogously to Eq. (19) we can also write:

$$(-)^{\frac{I}{2}+\tau-\frac{\lambda}{2}} \begin{pmatrix} \frac{I}{2}+\frac{\Omega}{2} & \frac{I}{2}+\frac{\sigma}{4} & \frac{\lambda}{4} \\ -\tau-\frac{\Omega}{2} & \tau-\frac{\sigma}{4} & \frac{\sigma}{4}+\frac{\Omega}{2} \end{pmatrix} \simeq \left(\frac{I+1}{2}\right)^{-\frac{1}{2}} d^{\frac{\lambda}{4}}_{\frac{\sigma}{4}+\frac{\Omega}{2},\frac{\sigma}{4}-\frac{\Omega}{2}}(4\Theta_\tau) \tag{26}$$

where $\tau = \xi - I/2$. The relationship becomes exact when the number of grid points I goes to infinity. When λ and σ are even integers the $3j$ symbol is an ordinary vector coupling coefficient, otherwise it is referred to as a "generalized" vector coupling coefficient, because multiples of $1/4$ appear besides the integers and half-integers usual in quantum mechanics. This alternative form of writing the Hahn polynomials points up the link between (hyper)angular momentum theory and discrete orthogonal polynomials[15] and serves to find out their symmetry properties. Eq. (26) is well known as the semiclassical relationship holding for large values of the mock angular momentum I[15].

In order to find the discrete counterparts of the functions $\exp(-\imath\sigma\Phi)$, we generalize the one adopted in Ref.[12] for the trigonometric counterparts, using well known properties [31]. The kinematic angle varies in the range $0 \leq 2\Phi < 2\pi$ [for reactions with two identical atoms, such as those involving a homonuclear

molecule considered so far, the exchange symmetry allows to halve the interval[12] and use (real) trigonometric functions]. We divide the range into N equally spaced points:

$$\Phi_\nu = \frac{\pi\nu}{N}; \qquad \nu = 1, \ldots, N \tag{27}$$

and define the discrete analog of the exponential functions as follows:

$$f^N_{\frac{\sigma}{2}\nu} = \frac{1}{\sqrt{N}} \exp(-i\pi\nu\sigma/2N) \tag{28}$$

The $f^N_{\frac{\sigma}{2}\nu}$ coefficients are the elements of a unitary matrix

$$\sum_{\nu=1}^{N} f^{N*}_{\frac{\sigma}{2}\nu} f^N_{\frac{\sigma'}{2}\nu} = \delta_{\sigma\sigma'} \tag{29}$$

where the asterisk denotes the conjugate coefficient and

$$\sum_{\sigma=-N+1}^{N-1} f^{N*}_{\frac{\sigma}{2}\nu} f^N_{\frac{\sigma}{2}\nu'} = \delta_{\nu\nu'}. \tag{30}$$

For states of even parity, *i.e.* symmetric when acted on by the inversion operator, N is an odd number and σ takes only even values; for states of odd parity, N is even and σ is odd.

The equations (19) [or (26)] and (28) will next be exploited using the discrete analogs of the hyperspherical harmonics in Eq.(15) to turn the quantization problem in Eq.(17) into a form suitable for numerical applications (see also [13]).

4.2 The Stereodirected Representation

The hyperquantization algorithm in the symmetric hyperangular parametrization allows the transformation of the eigenvectors $t^\Omega_{in\sigma}$ in Eq.(17) to a new basis (stereodirected representation), so to obtain new eigenvectors $t^\Omega_{i\tau\nu}$ labeled by the discrete variables τ and ν:

$$t^\Omega_{in\sigma}(\rho) = \sum_{\tau\nu} Q^{\Omega\frac{\sigma}{2}I}_{n\tau} f^N_{\frac{\sigma}{2}\nu} t^\Omega_{i\tau\nu}(\rho) \tag{31}$$

where $n = (\lambda - \sigma - 2\Omega)/4$ denotes the degree of the Hahn polynomial and ranges from zero to I. The coefficients $Q^{\frac{\sigma}{2}\Omega I}_{n\tau}$ and $f^N_{\frac{\sigma}{2}\nu}$ have been defined in Eqs.(26) and (28). As apparent *e.g.* in Eq. (26), the interpretation in terms of angular momentum theory for the lattice size parameters (I and N) and the grid labels (τ and ν) shows that the transformation (31) is actually a vector recoupling. The projection-like τ and ν are the "steric" quantum numbers for this problem [32-37]. Through the use of discrete analogs of the harmonics in Eq.(15) we will obtain a very sparse and symmetric matrix representation for the kinetic energy

while, analogously to discrete variable representations [38], the potential energy matrix is diagonal.

When the transformation in (31) is inserted into (17), multiplying the left-hand side by $f^N_{\frac{\sigma}{2}\nu} Q^{\frac{\sigma}{2}\Omega I}_{n\tau}$ and summing over n and σ, one obtains explicitly the elements of the kinetic energy matrix:

$$\begin{aligned} \mathsf{K}_{\tau\nu\tau'\nu'} &= \frac{1}{2\mu\rho^2} \sum_{n\sigma} f^{N*}_{\frac{\sigma}{2}\nu} Q^{\frac{\sigma}{2}\Omega I}_{n\tau} \left[16n(n+\sigma/2+\Omega+1) + (\sigma+2\Omega)(\sigma+2\Omega+4)\right. \\ &\quad \left. +15/4\right] Q^{\frac{\sigma}{2}\Omega I}_{n\tau'} f^N_{\frac{\sigma}{2}\nu'} \end{aligned} \tag{32}$$

The sum over n can be performed analytically by exploiting Eq.(23); the result is a tridiagonal matrix with respect to the discrete variable τ:

$$\mathsf{K}_{\tau\nu\tau'\nu'} = \frac{1}{2\mu\rho^2} \sum_{\sigma} f^{N*}_{\frac{\sigma}{2}\nu} \left[-C(\tau')\delta_{\tau,\tau'-1} + B(\tau')\delta_{\tau\tau'} - C(\tau'+1)\delta_{\tau,\tau'+1}\right] f^N_{\frac{\sigma}{2}\nu'} \tag{33}$$

where

$$B(\tau) = (\sigma+2\Omega)(\sigma+2\Omega+4) + 15/4 + 16\left[I(I/2+1) - 2\tau^2 + (I/2+\tau)\sigma/2 + \Omega\right] \tag{34}$$

are the elements along the main diagonal, and (see also Eq.(25))

$$C(\tau) = -16\left[(I/2-\tau+1)(I/2-\tau+\sigma/2+1)(I/2+\tau)(I/2+\tau+\Omega)\right]^{\frac{1}{2}} \tag{35}$$

specify the elements of the lower and upper tridiagonals.

In (33) the sum over σ is easily carried out evaluating trigonometric functions at the lattice points. The kinetic energy matrix is block tridiagonal as in [12], the presence of Ω now complicating only slightly the over-all structure.

The orthogonal transformation in (31) is seen to approximately diagonalize back the potential energy matrix whose elements $V_{n\sigma n'\sigma'}$ were defined in Eq.(18):

$$V(\rho, 4\Theta_\tau, 2\Phi_\nu) = \sum_{nn'\sigma\sigma'} f^{N*}_{\frac{\sigma}{2}\nu} Q^{\frac{\sigma}{2}\Omega I}_{n\tau} V_{n\sigma n'\sigma'}(\rho) Q^{\frac{\sigma'}{2}\Omega I}_{n'\tau'} f^N_{\frac{\sigma'}{2}\nu'} \tag{36}$$

Indeed, for large I, the sum over $n = \lambda - |\sigma| - 2|\Omega|)/4$ is

$$\sum_n \left(\frac{\lambda+2}{I+1}\right)^{\frac{1}{2}} Q^{\frac{\sigma}{2}\Omega I}_{n\tau} d^{\frac{\lambda}{4}}_{\frac{\sigma+2\Omega}{4}\,\frac{\sigma-2\Omega}{4}}(4\Theta) \simeq 1 \tag{37}$$

only when (see Eq.(20))

$$\cos 4\Theta_\tau = \frac{-2\tau}{I+1} \tag{38}$$

and zero otherwise. Identically for the sum over n'. Similarly, for large N, the sum over σ (and σ') is

$$\sum_\sigma \frac{\exp(\imath\sigma\Phi)}{\sqrt{2\pi}} f^N_{\frac{\sigma}{2}\nu} \simeq 1 \tag{39}$$

when (see Eq. (27))

$$\Phi_\nu = \frac{\pi\nu}{N} \tag{40}$$

and zero otherwise.

Therefore the elements of the potential energy matrix are the values of the potential energy surface $V(\rho, 4\Theta_\tau, 2\Phi_\nu)$ at the lattice points labeled by the discrete values of τ and ν. In conclusion, in the symmetric hyperangular parametrization and the present partition of the Hamiltonian, we have to solve the following algebraic problem

$$\sum_{\tau'\nu'} [\mathsf{K}_{\tau\nu\tau'\nu'} + V(\rho, 4\Theta_{\tau'}, 2\Phi_{\nu'})\delta_{\tau\tau'}\delta_{\nu\nu'}]\, t^{\Omega}_{i\tau'\nu'}(\rho) = \varepsilon^{\Omega}_i t^{\Omega}_{i\tau\nu}(\rho) \tag{41}$$

to obtain the potential energy curves ε^{Ω}_i as function of ρ at given values of Ω. As before, only elements $\mathsf{K}_{\tau\nu\tau'\nu'}$ with $\tau' = \tau$ and $\tau' = \tau \pm 1$ are different for zero.

4.3 The propagation step along the hyperradius

The adiabatic eigenvalues ϵ^{Ω}_i and eigenvectors $t^{\Omega}_{i\tau\nu}$ are needed for calculating the reactive cross sections, solving a propagation problem along ρ. The scattering matrix for each total angular momentum J is obtained by integrating the following set of ordinary coupled second order differential equations in the hyperradius·

$$\left(\frac{1}{2\mu}\frac{d^2}{d\rho^2} + \frac{\rho_c^2}{\rho^2}\varepsilon^{\Omega}_i + E\right) F^{\mathrm{J}}_{\Omega i}(\rho) = \sum_{i'} U_{ii'} F^{\mathrm{J}}_{\Omega i'}(\rho) + \sum_{\Omega' i'} W^{\mathrm{J}}_{\Omega i,\Omega' i'} F^{\mathrm{J}}_{\Omega' i'}(\rho) \tag{42}$$

where the matrices U and W^{J} accounts for all the channel couplings. Explicit formulas are given in the literature [3, 4] and efficiently implemented by our algorithm. The construction of the interaction matrix U is straightforward, its elements being computed by treating the adiabatic eigenstates as a diabatic basis. The matrix W^{J} contains the rotational and Coriolis couplings. These are J-dependent terms arising when considering those remaining terms of the Λ^2 operator [compare Eq. (11) and (14)], which are not considered in the solution of the restricted adiabatic eigenvalue problem, see Eq. (13).

To integrate the coupled-equations (42) (see *e.g.* [39]), the overlap between neighboring sectors obtained by discretizing the range in ρ, in our algorithm simply involves sums between eigenvectors computed at their centers ρ_n and ρ_{n+1} of adjacent sectors:

$$O_{ij} = \sum_{\tau\nu} t^{\Omega}_{i,\tau\nu}(\rho_k)\, t^{\Omega}_{j,\tau\nu}(\rho_{k+1}) \tag{43}$$

The overlap matrix O is a square matrix and has dimension dictated by the number of the adiabatic eigenstates to be taken into account to describe accurately the dynamical behavior at the collision energies considered. Typically all open channels and some of the lowest close channels have to be included.

In principle, one should include in (42) all Ω values up to J· this can become a too demanding enterprise when J increases. Experience shows [3, 40] that indeed rapid convergence truncation to low Ω is achieved for collinearly dominated reactions.

5 Conclusions and further remarks: towards four-atom reactions

The hyperquantization algorithm is a general quantum mechanical method for solving eigenvalue problems. In the theory of three-atom reactive scattering its applications are exemplified by calculating adiabatic eigenstates at fixed values of the hyperradius [13]. The algorithm is based on the hyperspherical coordinates approach, reviewed in Sec. 2, and exploits generalized vector coupling coefficients (Hahn polynomials) as the discrete analogs of hyperspherical harmonics. Applying the recurrence equation, the symmetries, the orthogonality and the dual orthogonality properties of these polynomials has allowed us to develop an algebraic formalism that is shown to provide a tool to investigate the quantum dynamics of three-particle systems. The extension of the theory to $J > 0$ in the symmetric representation has been presented.

From a computational point of view, the most attractive features are the sparseness and the high symmetry of the Hamiltonian matrix. Reactive cross sections calculated by applying the hyperquantization algorithm based on the symmetric hyperspherical coordinates on two benchmark systems, *i.e.* the $F+H_2$ and $He+H_2^+$ reactions, are shown in refs.[13, 14] and refs.[18, 40], respectively.

The $F+H_2$ system offers the opportunity to investigate the effect of the excited electronic states on the reactivity. The open-shell electronic structure of the fluorine atom leads to multiple potential energy surfaces. Since the coupling among them due to the spin-orbit interaction is localized in the asymptotic region of the reactants, we expect the long range features of the interaction potential to be relevant for the dynamics. In the remainder of the configuration space the surfaces are dynamically uncoupled and the reaction proceeds only on the lowest potential energy surface. The treatment of the dynamics including excited electronic states and spin-orbit coupling has been initiated in [13]

The three electron $He+H_2^+$ system is a prototype for an ion-molecule reaction, and has been considered as a case study to perform a dynamical test on different potential energy surfaces in order to provide a contribution to the present state of the concept of chemical accuracy. Quantum mechanical calculations of the reactive cross sections exhibit a rich resonance pattern: the results [40, 18] illustrate its dependence both on the nature of the potential energy surface and on the functional form used to fit the ab-initio data.

An extremely important feature of this methodology is that it can be easily generalized to more complex reactions than a three-atom system. For tetraatomic

systems we have contributed [41, 8] to generalize the concept of symmetric (or democratic) hyperspherical coordinates, which proved very useful when applied to the study of the A + BC reactions. We have introduced hyperspherical coordinates in the space of kinematic invariants and written the associated Hamiltonian. Also, we have derived the interatomic distance formulae for the mapping of the potential energy surface. In addition, we have provided an analysis of body frames and their singularities [17]. The extension of the hyperquantization technique to four-atom systems is therefore an objective of future work.

For the general n-body dynamics, hyperspherical and related systems of coordinates have also been analyzed [21]. Within a symmetric hyperspherical coordinates framework[19], these coordinates are conveniently broken up into external (or spatial) rotations, kinematic invariants (related to the inertia moments)[26, 42] and kinematic (internal) rotations. This is a generalization of Eq. (4), see [19]. Kinematic and rotational coordinates describe collective and concerted motions, respectively.

For a given value of the hyperradius, the space of kinematic invariants is the surface of a right spherical triangle and is described by two angular variables (with proper range), that leads to a tetrahedral (for tetraatomic systems) or an octahedral (for polyatomic systems, $n \geq 5$) tessellation of the sphere [42]. Alternative parametrizations in this space are available [26]. Their usefulness was shown for the study of constrained intramolecular motions and for the collective motions of polyatomic molecules and clusters. The ammonia umbrella inversion motion near the oblate top configurations is a relevant example, but reactive scattering continues to be our target. Progress has also to be recorded regarding the development of the Hamiltonians (see *e.g.* [8]), but much has to be done before numerical implementations be feasible for the A + BCD and AB + CD cases.

Acknowledgments

This work is supported by the Italian National Research Council (CNR), by the Ministero dell'Università e della Ricerca Scientifica e Tecnologica (MURST), by the European Union within the Human Potential Research Network "Theoretical Studies of Electronic and Dynamical Processes in Molecules and Clusters" [Contract No. HPRN-CT-1999-00005] and by the COST D9 Action.

References

[1] V. Aquilanti, G. Capecchi and S. Cavalli, in Advances in Quantum Chemistry **36**, 341 (1999).

[2] A. Kuppermann, in *Dynamics of Molecules and Chemical Reactions*, edited by R.E. Wyatt et al., (Marcel Dekker, Inc., New York, 1996), p.411.

[3] B. Lepetit, J.M. Launay and M. Le Dourneuf, Chem. Phys. **106**, 103 (1986); J.M. Launay and M. Le Dourneuf, Chem. Phys. Lett. **163**, 178 (1989); J.M. Launay and M. Le Dourneuf, Chem. Phys. Lett. **169**, 473 (1990); J.M. Launay, Theor. Chem. Acta **79**, 183 (1991); B. Lepetit and J.M. Launay, J. Chem. Phys. **95**, 5159 (1991).

[4] R.T Pack and G.A. Parker, J. Chem. Phys. **87**, 3888 (1987); R.T Pack and G.A. Parker, J. Chem. Phys. **90**, 3511 (1989); G.A. Parker and R.T Pack, J. Chem. Phys. **98**, 6883 (1992)

[5] D. Skouteris, J.F. Castillo and D.E. Manolopoulos, Comp. Phys. Comm., in press (2000).

[6] G.A. Parker, A. Laganà, S. Crocchianti and R.T Pack, J. Chem. Phys. **102**, 1238 (1995).

[7] K. Nobusada, K. Moribayashi and H. Nakamura, J. Chem. Soc. Faraday Trans. **93**, 721 (1997).

[8] V. Aquilanti and S. Cavalli, J. Chem. Soc. Faraday Trans. **93**, 801 (1997).

[9] V. Aquilanti and S. Cavalli, Few Body Systems Suppl. **6**, 573 (1992)

[10] V. Aquilanti, S. Cavalli and M. Monnerville, in *Numerical Grid Methods and Their Applications to Schrödinger Equation*, edited by C. Cerjan (Kluwer, Dordrecht, 1993), p.25.

[11] V. Aquilanti, S. Cavalli, C. Coletti, D. De Fazio and G. Grossi, in *New Methods in Quantum Theory*, edited by C.A. Tsipis et al. (Kluwer, Dordrecht, 1996), p.233.

[12] V. Aquilanti, S. Cavalli and D. De Fazio, J. Chem. Phys. **109**, 3792 (1998).

[13] V. Aquilanti, S. Cavalli, D. De Fazio, A. Volpi, A. Aguilar, X. Gimenez and J.M. Lucas, J. Chem. Phys. **109**, 3805 (1998).

[14] V. Aquilanti, S. Cavalli, D. De Fazio, A. Volpi, A. Aguilar, X. Giménez and J.M. Lucas, Phys. Chem. Chem. Phys. **1**, 1091 (1999).

[15] V. Aquilanti and G. Capecchi, Theoretical Chem. Accounts **104**, 183 (2000)

[16] V. Aquilanti, S. Cavalli and D. De Fazio, J. Phys. Chem. **99**, 15694 (1985).

[17] R.G. Littlejohn, K.A. Mitchell, V. Aquilanti and S. Cavalli, Phys. Rev A 58, 3718 (1998).

[18] V. Aquilanti, G. Capecchi, S. Cavalli, D. De Fazio, A. Aguilar, X. Gimenez, J.M. Lucas, P. Palmieri and C. Puzzarini, Chem. Phys. Lett. **318**, 619 (2000).

[19] V. Aquilanti, S. Cavalli and G. Grossi, J Chem. Phys. **85**, 1362 (1986).

[20] V. Aquilanti, S. Cavalli, G. Grossi and R.W. Anderson, J. Chem. Soc. Faraday Trans. **86**, 1681 (1990); V. Aquilanti, S. Cavalli and G. Grossi, in *Advances in Molecular Vibrations and Collision Dynamics*, edited by J.M. Bowman (JAI Press, Greenwhich CT, 1993), p.147.

[21] V. Aquilanti and S. Cavalli, J. Chem. Phys. **85**, 1355 (1986).

[22] R. Radau, Ann. Sci. Ec. Norm. Sup. **5**, 311 (1868); R. Radau, J. Math. Pures Appl. **14**, 167 (1869).

[23] F.T. Smith, J. Math. Phys. **3**, 735 (1962); R.C. Whitten and F.T. Smith, J. Math. Phys. **9**, 1103 (1968).

[24] V. Fock, Kgl. Norske Videnakab. Selkabs Forh. **31**, 138 (1958); L.M. Delves, Nucl. Phys. **20**, 275 (1960).

[25] F.T. Smith, Phys. Rev. **120**, 1058 (1980).

[26] V. Aquilanti, A. Beddoni, S. Cavalli, A. Lombardi and R.G. Littlejohn, Mol. Phys. **98**, 1736 (2000).

[27] B.R. Johnson, J. Chem. Phys. **79**, 1916 (1983).

[28] H. Klar and M. Klar, J. Phys. B **13**, 1057 (1980); V. Aquilanti, G. Grossi, A. Laganà, E. Pelikan and H. Klar, Lett. Nuovo Cimento **41**, 541 (1984).

[29] S. Karlin and J. Mc Gregor, Scripta Math. **26**,33 (1961); A. Erdelyi, *Higher Trascendental Functions*, (McGraw-Hill, New York, 1953); G. Gasper, in *Theory and Application of Special Functions*, edited by R.A. Askey (Academic Press, New York, 1975), p.111; Yu F. Smirnov, S.K. Suslov and A.M. Shirokov, J Phys. A **17**, 2157 (1984).

[30] A.R. Edmonds, *Angular Momentum in Quantum Mechanics*, (Princeton University Press, 1980).

[31] F.B. Hildebrand, *Introduction to Numerical Analysis*, (McGrow-Hill, New York, 1956), chapter 9.

[32] V. Aquilanti, S. Cavalli, G. Grossi and R.W. Anderson, J. Phys. Chem. **95**, 8184 (1991).

[33] R.W. Anderson, V. Aquilanti, S. Cavalli and G. Grossi, J. Phys. Chem. **97**, 2443 (1993).

[34] J.M. Alvariño, V. Aquilanti, S. Cavalli, S. Crocchianti, A. Laganà and T. Martínez, J. Chem. Phys. **107**, 3339 (1997).

[35] J.M. Alvariño, V. Aquilanti, S. Cavalli, S. Crocchianti, A. Laganà and T. Martínez, J. Phys. Chem. **102**, 9638 (1998)

[36] B.-Y. Tang, B.-H. Yang, L. Zhang, K.-H. Han and J.Z.H. Zhang, Chem. Phys. Lett. **327**, 381 (2000).

[37] V. Aquilanti, S. Cavalli and A. Volpi, Physics Essays, in press (2000)

[38] J.C. Light, I.P. Hamilton and J.V. Lill, J. Chem. Phys. **82**, 1400 (1985).

[39] B.R. Johnson, J. Comp. Phys. **14**, 445 (1973); D.E. Manolopoulos, J. Chem. Phys. **85**, 6425 (1986).

[40] P. Palmieri, C. Puzzarini, V. Aquilanti, G. Capecchi, S. Cavalli, D. De Fazio, A. Aguilar, X. Gimenez and J.M. Lucas, Mol. Phys. **98**, 1835 (2000)

[41] V. Aquilanti, L. Bonnet and S. Cavalli, Mol. Phys. **89**, 1 (1996).

[42] R.G. Littlejohn, K. Mitchell and V. Aquilanti, Phys.Chem.Chem.Phys. **1**, 1259 (1999).

Distributed Gaussian basis sets: Variationally optimized s-type sets

V.N. Glushkov[†¶] and **S. Wilson**[‡]

[†] *Physics Department, State University, 320625, per. Nauchniy 13, Dniepropetrovsk, Ukraine*

[¶] *Physical and Theoretical Chemistry Laboratory, University of Oxford, South Parks Road, Oxford, OX1 3TG, England*

[‡] *Rutherford Appleton Laboratory, Chilton, Oxfordshire OX11 0QX, England*

Abstract

Sequences of distributed Gaussian basis sets are determined for the H_2^+ ground state at its equlibrium geometry. For basis sets containing $2n+1$, $n = 3, 4, ..., 13$, s-type Gaussian functions the variation principle is employed to determine optimal exponents and positions. The dependence of these optimal exponents and positions on the size of the basis set is analyzed.

Contents

1 Introduction

The controlled reduction of basis set truncation errors is an essential prerequisite of a quantitative quantum chemistry and recent years have witnessed a growing interest in the systematic implementation of the algebraic

ADVANCES IN QUANTUM CHEMISTRY, VOLUME 39

0065-3276/01 $35 00

approximation[1] [2], *i.e.* finite basis set expansions, in both non-relativistic and relativistic studies. Basis set truncation is often the dominant source of error in contemporary molecular electronic structure calculations and it is therefore not surprising that the development of basis sets continues unabated. For about fifty years the algebraic approximation in the form of the Linear Combination of Atomic Orbitals (L.C.A.O.) method was regarded as the poor relation of the finite difference methods which have been employed in atomic structure calculations since the pioneering work of Hartree[3] in the 1930s. In the 1970s, it was recognized that the algebraic approximation facilitated the integration over the continuum that arises in the description of electron correlation by means of many-body theories[4]. In the 1980s, it was shown that in studies of the relativistic atomic and molecular electronic structure problem, the algebraic approximation affords a representation of not only the positive energy branch but also the negative energy branch of the relativistic spectrum[5]. This facilitates the study of not only a relativistic many-body perturbation theory but also the covering theory, quantum electrodynamics[6]. Systematic implementation of the algebraic approximation has allowed, for example, the Dirac-Hartree-Fock energies of atoms to be determined to an accuracy which matches that achieved in finite difference calculations; typically $10^{-8} - 10^{-9}$ Hartree[7].

For molecules the situation is far less satisfactory[8] and, even in non-relativistic molecular structure calculations, the basis set truncation error is often seen as the largest source of error[1]. Molecular basis sets constructed from atom-centred subsets necessitate the use of functions of higher angular quantum number, ℓ, if high precision is to be achieved especially in correlation studies. This has prompted a recent renewal of interest in the use of off-atom functions of lower symmetry. Atom-centred basis sets have been most widely used in molecular calculations but, in calculations designed to match the accuracy achieved in numerical Hartree-Fock studies of diatomic molecules, it has recently been shown that they can be usefully supplemented by off-centre sets [9]-[12]. Indeed, by including bond centred functions in a systematically constructed basis set for the ground state of the nitrogen molecule it has been possible to obtain an energy that is within a few μHartree of the numerical result. The success of these calculations suggests investigation of the construction of basis sets including off-atom basis functions in more general terms.

A promising development is the distributed basis set[13] [14] in which the exponents and the distribution of the Gaussian functions are generated according to empirical prescriptions. It should be noted that Gaussian functions are particularly well suited for such a procedure since, unlike exponential basis functions, they do not introduce a cusp. This approach is distinct from the use Gaussian lobe functions[15] and the Floating Spherical Gaussian Orbital

(F.S.G.O.) model [16]-[18] in that there is no attempt to mimic higher harmonics directly and non-linear optimization is avoided. This allows the use of large basis sets resulting in high precision. However, a central problem in the distributed basis set approach is in deciding where the basis functions centres should be placed. In previous work, both the position and the exponents for the functions comprising the distributed basis set have been determined by empirical prescriptions. The Gaussian cell model [19]-[22] , a distributed basis set in which s-type basis functions are arranged on a regular cubic lattice, has been reexamined and shown to support an accuracy approaching the 1 μHartree level for the total energy of one-electron diatomic and triatomic systems. The distribution of s-type basis functions based on a Laplace transform [23] relating elliptical functions and Gaussian functions has been shown to lead to systematic convergence for the hydrogen molecular ion. More recently, a stochastic variational approach has been applied to the nitrogen molecule [24].

The purpose of the present work is to investigate the optimal distribution and exponents for a sequence of Gaussian basis sets for the ground state of the hydrogen molecular ion at its equlibrium geometry by invoking the variation principle. The sequence of distributions and exponents thus obtained can then be used to devised empirical schemes for constructing distributed Gaussian basis sets for larger systems for which the optimization of non-linear parameters would be computationally intractable.

The Floating Spherical Gaussian Orbital (FSGO) method was pursued independently in the late 1960s and early 1970s by Frost[16][17] and by Hall and his collaborators[18]. The basis functions have the form

$$\chi_p(\zeta_p, x_p, y_p, z_p) = \exp\left\{-\zeta_p\left[(x-x_p)^2 + (y-y_p)^2 + (z-z_p)^2\right]\right\} \qquad (1)$$

and both the exponents, ζ_p, and the positions (x_p, y_p, z_p) are determined by invoking the variation principle. The total electronic energy is determined subject to the conditions

$$\frac{\partial E}{\partial \zeta_p} = 0, \quad \frac{\partial E}{\partial \mu_p} = 0, \quad \mu = x, y, z, \quad \forall p \qquad (2)$$

Details of the optimization procedures employed in the present study are given in [25] and [26].

2 Variationally optimized s-type Gaussian basis sets for H_2^+ ground state

2.1 Total electronic energy

The exact ground state electronic energy of the H_2^+ molecular ion at its equilibrium nuclear separation of 2 *bohr* is known to be $-0.602\ 634\ 214\ 494\ 9$ *Hartree* [27] . We carefully optimized a sequence of distributed basis sets of Gaussian s-type functions for this one-electron system. The results are summarized in Table 1. In this Table, the basis sets are labelled $2 \times n + 1$. All basis functions are centred on points lying on the line passing through the nuclei (the z-axis). Basis sets contain an odd number of functions, have one function centred on the bond mid-point ($z = 0$) and the remaining functions are distributed symmetrically. N denotes the total number of basis functions in a given basis set. $|\mathbf{g}|$ is the reduced length defined by

$$|\mathbf{g}| = \left[\frac{1}{M}\sum {g_i}^2\right]^{\frac{1}{2}} \tag{3}$$

where g_i denotes the gradients defined in (2) and M is the number of non-linear parameters. $|\mathbf{g}|$ provides a measure of the quality of the optimization process. Δ records the difference between successive entries in Table 1 in μHartree and δ is the difference between a given entry and the exact energy, again in μHartree. It can be seen that only 9 functions are required to support sub-milliHartree accuracy, 13 functions can support an accuracy of 100 μHartree and 19 functions yield an energy which an accuracy below the 10 μHartree level. A basis set of 25 functions is seen to be capable of supporting an accuracy at the sub-μ Hartree level.

Table 1
Total energies for the ground state of the H_2^+ molecular ion at R=2.0 bohr supported by a sequence of variationally optimized distributed Gaussian basis sets of s-type functions.

Basis set	N	E	$\|\mathbf{g}\|$	Δ	δ
$2\times3+1$	7	−0.601 403 501	9.292		1230.713
$2\times4+1$	9	−0.602 318 718	3.891	915.217	315.496
$2\times5+1$	11	−0.602 512 544	7.358	193.826	121.670
$2\times6+1$	13	−0.602 552 422	1.082	39.878	81.792
$2\times7+1$	15	−0.602 604 727	2.231	52.305	29.487
$2\times8+1$	17	−0.602 623 991	0.782	19.264	10.223
$2\times9+1$	19	−0.602 629 211	0.783	5.220	5.003
$2\times10+1$	21	−0.602 630 565	0.065	1.354	3.649
$2\times11+1$	23	−0.602 632 233	0.351	1.675	1.982
$2\times12+1$	25	−0.602 633 514	0.055	1.281	0.701
$2\times13+1$	27	−0.602 633 875	0.011	0.361	0.339
Exact†		−0.602 634 214 494 9			

† Madsen and Peek[27]

The energies reported in Table 1 should be compared with those reported by Wilson and Moncrieff [13] using an *ad hoc* distribution based on electric field variant basis sets associated with each of the nuclei, a subset located on the bond centre and another subset at off-centre positions beyond the nuclei. A near saturated set of s functions centred on each nucleus gives a total electronic energy of −0.590 950 5 Hartree. Replacing these atom-centred sets by electric field variant sets lowers the energy to −0.602 274 4 Hartree, whilst adding bond centre functions gives −0.602 577 5 Hartree. The addition of off-centre subsets gives the lowest energy recorded in the study of Wilson and Moncrieff [13] −0.602 633 861 Hartree, which lies some 0.014 μHartree above the lowest energy reported in Table 1. However, the distributed sets investigated by Wilson and Moncrieff were constructed from even-tempered subsets. No exponent optimization was undertaken. This *ad hoc* distributed basis set considered of a total of 150 basis functions (30 associated with each nucleus, 30 located at the bond centre and 30 at each of the off-centre positions beyond the nuclei.) compared with the 27 basis functions in the largest of the sets employed in the present calculations.

The difference, δ, between the energy calculated with a given basis set $2n+1$ and the exact energy is plotted as a function of n in Figure 1 on a logarithmic scale. It can be seen that δ decreases monotonically with increasing n. The

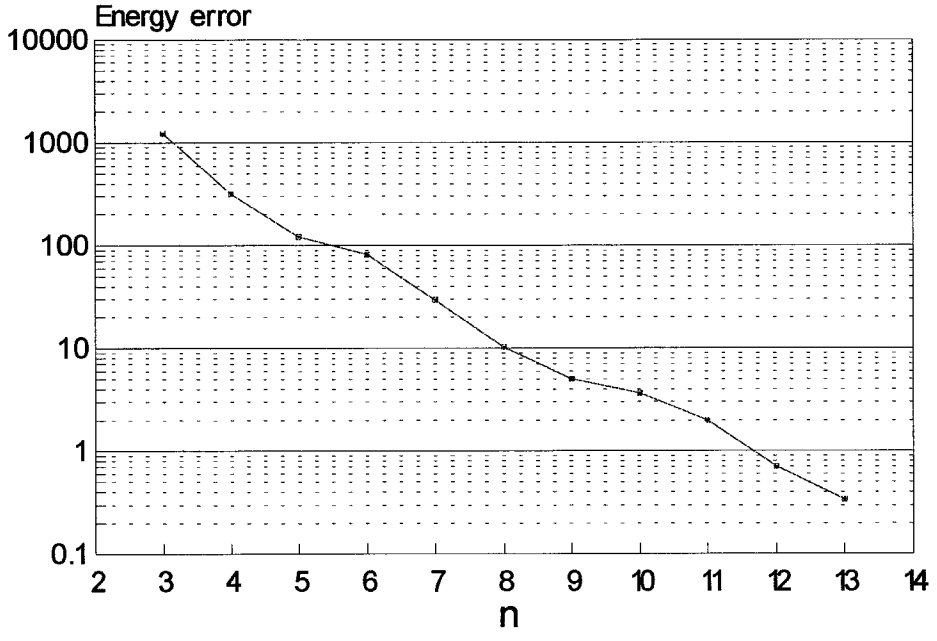

Figure 1: Error in the total energy, δ, for the basis set $[2n+1]$ plotted as a function of n.

curve is not entirely smooth and this is probably a reflection of the extent to which the optimization procedure has achieved a minimum.

2.2 Optimized distributions and exponents

The optimized distributions and exponents for the eleven basis sets of s-type Gaussian considered in this work are collected in Tables 2, 3 and 4. In Table 2, the results obtained for the smallest basis sets considered, the cases $n = 3,\ 4,\ 5$ and 6, are presented. Because of symmetry, there are for the basis set designated $2n + 1$ only $n + 1$ unique exponents. One basis functions must be centred on the bond mid-point, that is $(z = 0)$ and the remainder are distributed in pairs at $\pm z_p$. The basis function centred on the bond mid-point is given the index 1. The remaining functions are ordering according to their distance from the bond mid-point.

The results obtained for the cases $n = 7,\ 8,\ 9$ and 10, are collected in Table 3 whilst in Table 4 the optimal exponents and basis function positions are given for the largest basis sets considered, the cases $n = 11,\ 12$ and 13.

In Figure 2, the optimal positions of the s-type Gaussian functions in the smallest basis sets considered, that is $n = 3,\ 4,\ 5$ and 6, are plotted as a function of the basis function index. The function with index 1 is restricted by symmetry to be centred on the bond mid-point and $z = 1$ corresponds to the nucleus. For the $n = 3$ case, the remaining centres are roughly equidistant at $z = 0.8,\ 0.9,\ 1.0$. For the $n = 4, 5, 6$ cases, $n - 2$ functions are located close to the nucleus; obviously providing a description of the electron-nucleus cusp. The remaining 2 functions lie at about 0.2 *bohr* from the nucleus, in the direction of the other nucleus, and thus provide a description of polarization effects.

The optimal positions of the s-type Gaussian functions in the basis sets for $n = 7,\ 8,\ 9$ and 10, are plotted as a function of the basis function index in Figure 3. Here, in addition to the function at the bond mid-point, a subset describing the electron-nucleus cusp and a polarization subset, there is one function in each case which lies beyond the nucleus which could be interpreted as describing the depletion of the electron density from this region. For the sequence of basis sets considered in Figure 3, it is the number of functions associated with the description of the region near the nuclei that increases with n.

In Figure 4, the optimal positions of the s-type Gaussian functions in the largest basis sets considered, that is $n = 11,\ 12$ and 13, are plotted as a function of the basis function index. Here the single function lying beyond the nucleus observed in the cases considered in Figure 3 no longer arises. Somewhat more that half the functions in a given set are used to describe the wave

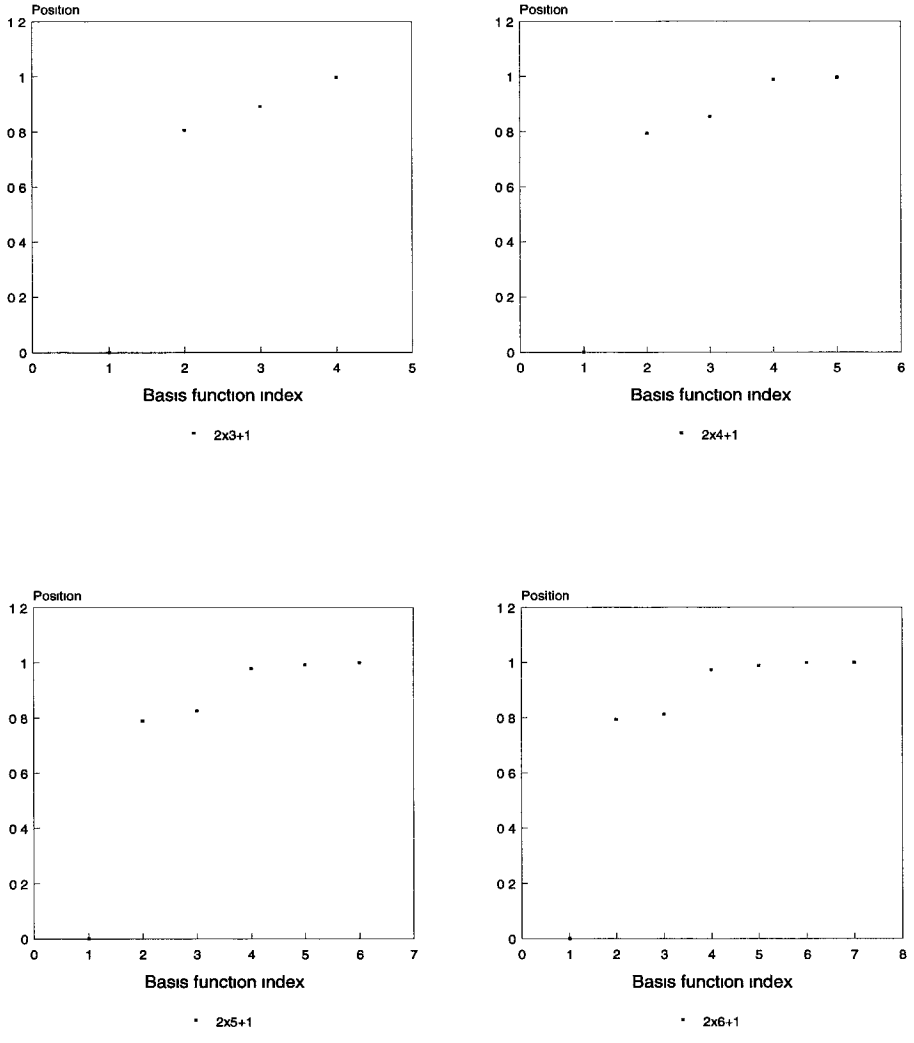

Figure 2: Optimal positions of the s-type Gaussian functions in the smallest basis sets considered, that is $n = 3,\ 4,\ 5$ and 6, plotted as a function of the basis function index.

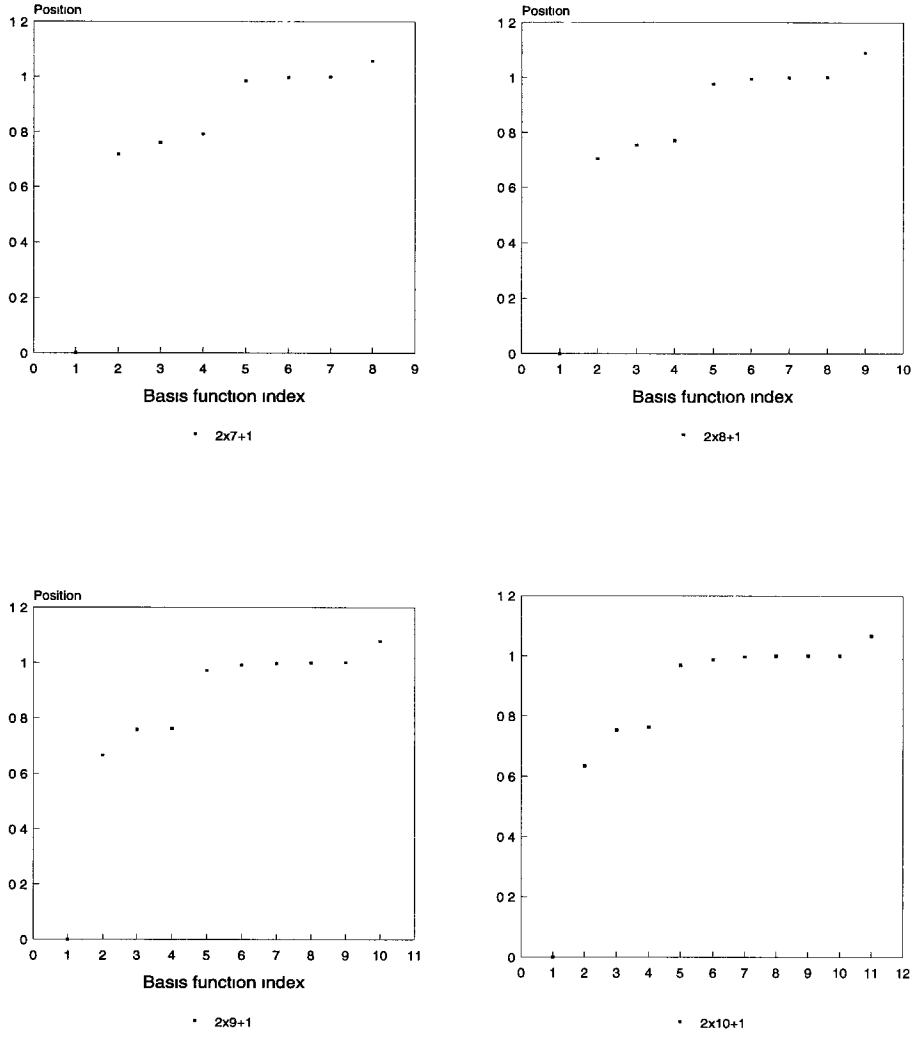

Figure 3: Optimal positions of the s-type Gaussian functions in the basis sets for $n = 7,\ 8,\ 9$ and 10, plotted as a function of the basis function index.

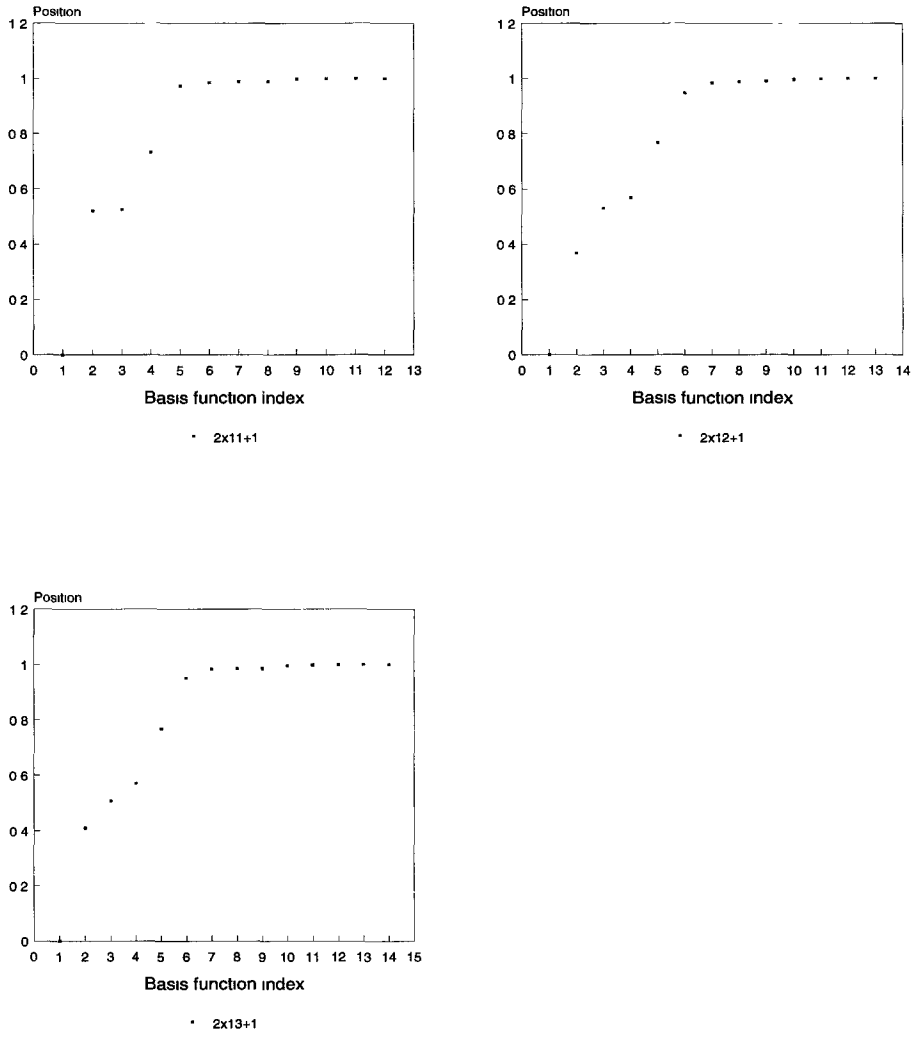

Figure 4: Optimal positions of the s-type Gaussian functions in the largest basis sets considered, that is $n = 11$, 12 and 13, plotted as a function of the basis function index.

function in the region near the nuclei and the remainder are employed to describe polarization effects.

In Figure 5, the optimal exponents of the s-type Gaussian functions in the smallest basis sets considered, that is $n = 3,\ 4,\ 5$ and 6, are plotted as a function of the basis function index defined above on a logarithmic scale. For these smallest basis sets the plots are approximately linear and are reminiscent of the even-tempered sets. The basis function centred on the bond mid-point is the most diffuse, i.e. has the smallest exponent, whilst the function closest to the nucleus is the most contracted, i.e. has the largest exponent.

Optimal exponents of the s-type Gaussian functions in the basis sets for $n = 7,\ 8,\ 9$ and 10, are plotted as a function of the basis function index in Figure 6. Here the more diffuse function lying beyond the nucleus should again be noted. An approximately linear plot is observed for the more contracted functions in the region close to the nucleus. The function centred on the bond mid-point remains the most diffuse function in the set and the function located closest to the nucleus remains the most contracted.

In Figure 7, optimal exponents of the s-type Gaussian functions in the largest basis sets considered, that is $n = 11,\ 12$ and 13, are plotted as a function of the basis function index. Again, an approximately linear plot is observed for the most contracted functions in the region close to the nucleus. Furthermore, the function centred on the bond mid-point remains the most diffuse function in the set and the function located closest to the nucleus remains the most contracted.

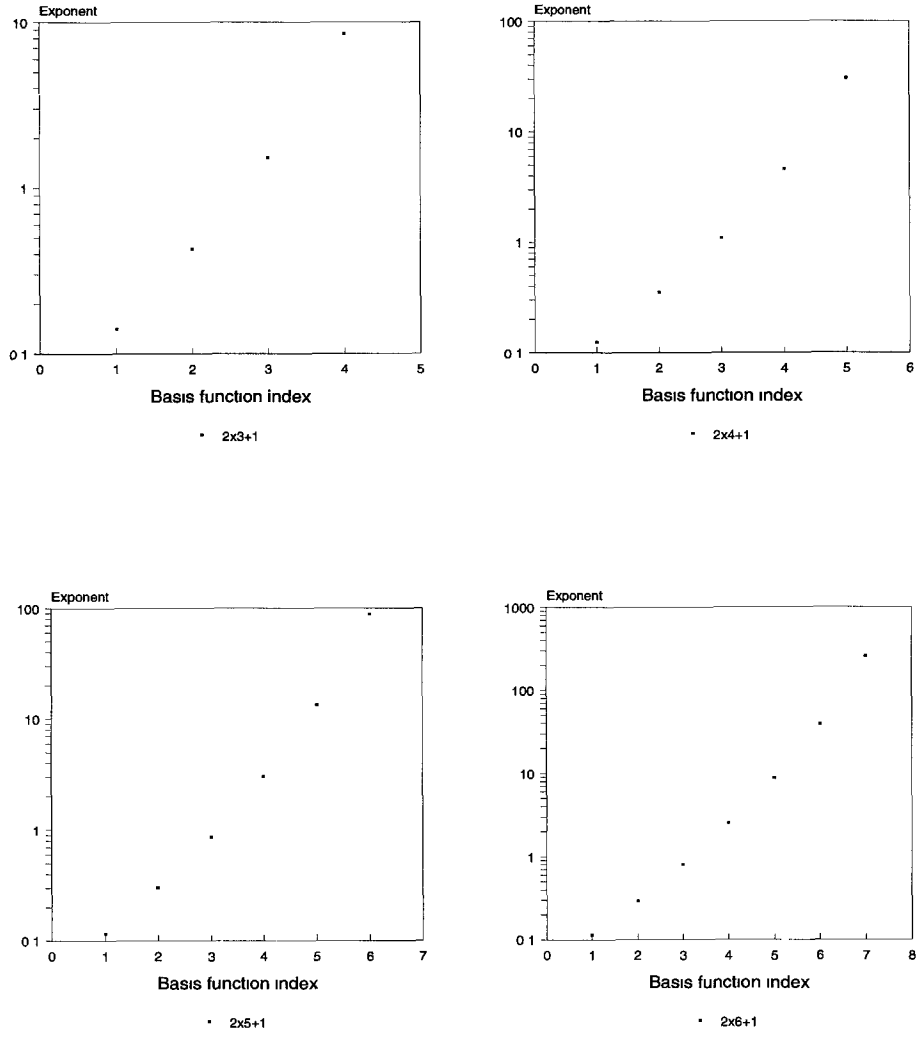

Figure 5: Optimal exponents of the s-type Gaussian functions in the smallest basis sets considered, that is $n = 3,\ 4,\ 5$ and 6, plotted as a function of the basis function index.

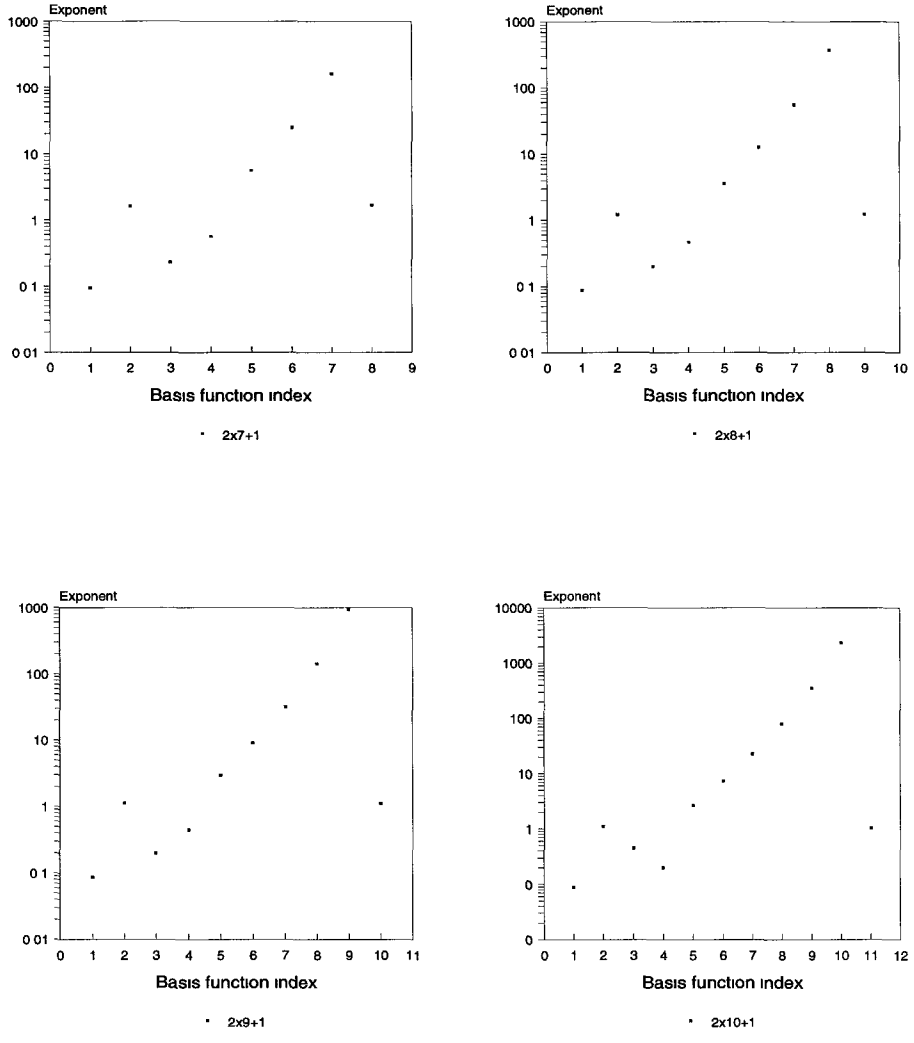

Figure 6: Optimal positions of the s-type Gaussian functions in the basis sets for $n = 7,\ 8,\ 9$ and 10 plotted as a function of the basis function index.

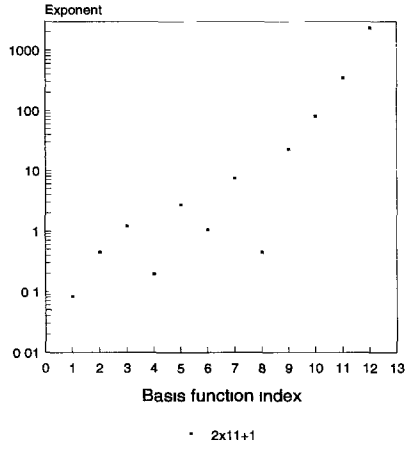

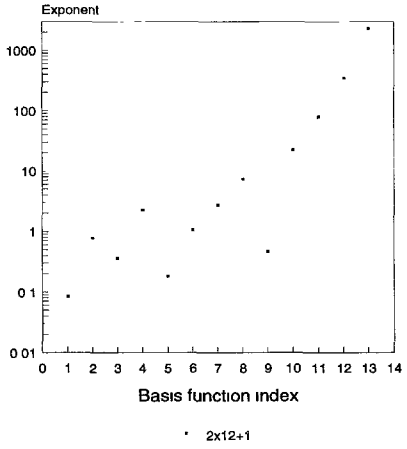

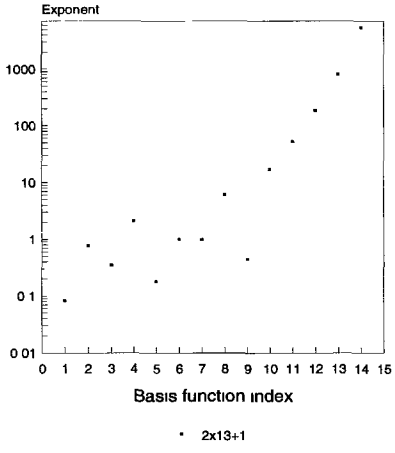

Figure 7: Optimal exponents of the s-type Gaussian functions in the largest basis sets considered, that is $n = 11$, 12 and 13, plotted as a function of the basis function index.

Table 2
A sequence of variationally optimized distributed Gaussian basis sets of s-type functions for the ground state of the H_2^+ molecular ion with $n = 3, 4, , 5$ and 6.

Basis set	N	ζ_p	z_p
$2 \times 3 + 1$	7	0.140 711 3 (0)	0
		0.430 208 1 (0)	±0.806 362 0 (0)
		0.152 571 8 (1)	±0.891 569 5 (0)
		0.852 346 3 (1)	±0.997 883 9 (0)
		ζ_p	z_p
$2 \times 4 + 1$	9	0.124 651 4 (0)	0
		0.349 759 9 (0)	±0.793 591 9 (0)
		0.108 933 8 (1)	±0.854 232 2 (0)
		0.462 539 0 (1)	±0.988 532 8 (0)
		0.305 893 5 (2)	±0.996 183 5 (0)
		ζ_p	z_p
$2 \times 5 + 1$	11	0.114 729 9 (0)	0
		0.302 791 4 (0)	±0.789 042 5 (0)
		0.864 934 8 (0)	±0.825 382 3 (0)
		0.304 500 2 (1)	±0.979 979 0 (0)
		0.133 331 9 (2)	±0.991 918 2 (0)
		0.885 739 4 (2)	±0.999 514 4 (0)
		ζ_p	z_p
$2 \times 6 + 1$	13	0.113 538 8 (0)	0
		0.293 355 9 (0)	±0.792 675 3 (0)
		0.807 967 2 (0)	±0.812 761 3 (0)
		0.253 104 0 (1)	±0.973 493 5 (0)
		0.889 358 9 (1)	±0.987 956 7 (0)
		0.388 951 8 (2)	±0.998 914 5 (0)
		0.259 236 8 (3)	±0.999 599 9 (0)

Table 3
A sequence of variationally optimized distributed Gaussian basis sets of s-type functions for the ground state of the H_2^+ molecular ion with $n = 7, 8, , 9$ and 10.

Basis set	N	ζ_p	z_p
$2 \times 7 + 1$	15	0.094 565 8 (0)	0
		0.162 880 1 (1)	±0.718 018 5 (0)
		0.229 128 5 (0)	±0.760 686 2 (0)
		0.569 375 5 (0)	±0.791 791 0 (0)
		0.561 555 2 (1)	±0.984 175 1 (0)
		0.245 177 8 (2)	±0.997 313 1 (0)
		0.163 368 1 (3)	±0.999 399 7 (0)
		0.168 742 1 (1)	±0.105 718 7 (1)
		ζ_p	z_p
$2 \times 8 + 1$	17	0.087 159 4 (0)	0
		0.121 504 7 (1)	±0.703 839 6 (0)
		0.201 304 2 (0)	±0.753 815 9 (0)
		0.467 094 3 (0)	±0.770 641 0 (0)
		0.358 854 2 (1)	±0.975 336 5 (0)
		0.126 171 6 (2)	±0.993 925 7 (0)
		0.553 799 2 (2)	±0.998 600 0 (0)
		0.369 335 8 (3)	±0.999 800 0 (0)
		0.123 937 2 (1)	±0.108 982 2 (1)

Table 3 *(continued)*

Basis set	N	ζ_p	z_p
$2 \times 9 + 1$	19	0.086 599 5 (0)	0
		0.112 034 8 (1)	±0.663 952 5 (0)
		0.196 283 3 (0)	±0.756 381 6 (0)
		0.443 881 3 (0)	±0.760 684 7 (0)
		0.296 032 8 (1)	±0.971 248 1 (0)
		0.907 266 1 (1)	±0.990 947 9 (0)
		0.320 654 3 (2)	±0.997 801 4 (0)
		0.141 014 9 (3)	±0.999 400 0 (00
		0.941 305 8 (3)	±0.100 000 0 (1)
		0.110 002 9 (1)	±0.107 740 8 (1)
$2 \times 10 + 1$	21	ζ_p	z_p
		0.088 414 0 (0)	0
		0.109 195 9 (1)	±0.631 741 7 (0)
		0.438 794 3 (0)	±0.751 322 4 (0)
		0.197 687 6 (0)	±0.763 751 4 (0)
		0.260 480 7 (1)	±0.969 377 3 (0)
		0.724 464 4 (1)	±0.987 689 6 (0)
		0.222 955 2 (2)	±0.997 040 4 (0)
		0.790 382 9 (2)	±0.998 840 3 (0)
		0.348 065 7 (3)	±0.999 844 7 (0)
		0.231 593 4 (4)	±0.999 954 5 (0)
		0.102 231 2 (1)	±0.106 641 6 (1)

Table 4
A sequence of variationally optimized distributed Gaussian basis sets of s-type functions for the ground state of the H_2^+ molecular ion with $n = 11$, 12 and 13.

Basis set	N	ζ_p	z_p
$2 \times 11 + 1$	23	0.083 083 0 (0)	0
		0.451 361 0 (0)	±0.520 361 0 (0)
		0.121 124 5 (1)	±0.524 986 2 (0)
		0.196 235 0 (0)	±0.732 211 2 (0)
		0.272 272 0 (1)	±0.972 007 3 (0)
		0.104 950 8 (1)	±0.984 024 1 (0)
		0.447 486 0 (0)	±0.988 004 9 (0)
		0.751 433 4 (1)	±0.987 481 6 (0)
		0.227 496 0 (2)	±0.997 366 6 (0)
		0.799 050 3 (2)	±0.998 771 3 (0)
		0.349 957 7 (3)	±0.999 860 2 (0)
		0.232 779 6 (4)	±0.999 953 0 (0)
		ζ_p	z_p
$2 \times 12 + 1$	21	0.083 398 1 (0)	0
		0.784 841 0(0)	±0.366 577 8 (0)
		0.358 978 0 (0)	±0.530 230 7 (0)
		0.223 742 9 (1)	±0.568 555 5 (0)
		0.182 861 0 (0)	±0.767 245 2 (0)
		0.105 959 2 (1)	±0.947 901 8 (0)
		0.269 516 7 (1)	±0.983 537 7 (0)
		0.728 696 4 (1)	±0.987 070 8 (0)
		0.464 916 0 (0)	±0.990 021 4 (0)
		0.222 145 4 (2)	±0.997 098 6 (0)
		0.783 371 7 (2)	±0.998 819 2 (0)
		0.344 075 5 (3)	±0.999 844 4 (0)
		0.229 696 2 (4)	±0.999 953 8 (0)

Table 4 *(continued)*

Basis set	N	ζ_p	z_p
$2 \times 13 + 1$	23	0.082 565 7 (0)	0
		0.761 678 0 (0)	±0.410 673 9 (0)
		0.345 619 0 (0)	±0.506 980 7 (0)
		0.211 070 6 (1)	±0.570 306 8 (0)
		0.178 753 2 (0)	±0.768 222 3 (0)
		0.100 487 6 (1)	±0.950 979 9 (0)
		0.243 218 1 (1)	±0.983 634 6 (0)
		0.614 265 8 (1)	±0.984 937 1 (0)
		0.446 132 9 (0)	±0.986 431 9 (0)
		0.170 160 4 (2)	±0.995 979 9 (0)
		0.522 443 2 (2)	±0.998 319 0 (0)
		0.184 642 3 (3)	±0.999 672 2 (0)
		0.811 832 6 (3)	±0.999 879 9 (0)
		0.542 254 8 (4)	±0.999 991 4 (0)

3 Discussion and conclusions

We have obtained a sequence of basis sets of increasing size for the hydrogen molecular ion containing only s-type Gaussian functions distributed along the axis passing through the nuclei. In each basis set both the exponents and the positions of the functions have been optimized by invoking the variation principle. A sub-μHartree level of accuracy was achieved for the total electronic energy by using only 27 basis functions.

The energy expectation values decreased monotonically with increasing size of basis set. The behaviour of the optimal exponents and positions has been analysed as a function of the basis set size. A qualitative explanation of the observed distributions of the basis functions and their exponents has been given in terms of the behaviour of the wave function in the regions close to the nuclei and in terms of polarization effects. The development of a quantitative explanation of the behaviour of the distributions and exponents as a function of basis set size requires further investigation. Progress in this direction will be reported.

ACKNOWLEDGMENTS

One of us (VNG) is grateful to the *University of Oxford College Visitors Programme* which provided support during the summer of 1999. SW acknowledges the support of EPSRC under Research Grant GR/M74627.

References

[1] S. Wilson, in *Methods in Computational Molecular Physics*, ed. G.H.F. Diercksen and S. Wilson, Reidel, Dordrecht (1983)

[2] S. Wilson, Adv. Chem. Phys. **67**, 439 (1987)

[3] D.R. Hartree, *The Calculation of Atomic Structures*, Wiley, New York (1957)

[4] S. Wilson and D.M. Silver, Phys. Rev. A**14**, 1969 (1976)

[5] H.M. Quiney, I.P. Grant and S. Wilson, Physica Scripta **36**, 460 (1987)

[6] H.M. Quiney, I.P. Grant and S. Wilson, in *Many-Body Methods in Quantum Chemistry,* Lecture Notes in Chemistry **52**, 307, edited by U. Kaldor, Springer-Verlag, Berlin (1989)

[7] S. Wilson, in *The Effects of Relativity in Atoms, Molecules and the Solid State*, edited by S. Wilson, I.P. Grant and B.L. Gyorffy, Plenum Press, New York (1991)

[8] L. Laaksonen, I.P. Grant and S. Wilson, J. Phys. B: At. Mol. Phys. **21**, 1969 (1988)

[9] D. Moncrieff and S. Wilson, J. Phys. B: At. Mol. Opt. Phys. **26**, 1605 (1993)

[10] D. Moncrieff and S. Wilson, Chem. Phys. Lett. **209**, 423 (1993)

[11] J. Kobus, D. Moncrieff and S. Wilson, J. Phys. B: At. Mol. Opt. Phys. **27**, 2867 (1994)

[12] J. Kobus, D. Moncrieff and S. Wilson, J. Phys. B: At. Mol. Opt. Phys. ***27***, 5139 (1994)

[13] S. Wilson and D. Moncrieff, Molec. Phys. **80**, 461 (1993)

[14] D. Moncrieff and S. Wilson, Molec. Phys. **82**, 523 (1994)

[15] H. Preuss, Z. Naturforsch. **11a**, 823 (1956); H. Preuss, Z. Naturforsch. **19a**, 1335 (1964); *ibid.* **20a**, 17, 21 (1965); J.L. Whitten, J. Chem. Phys. **39**, 349 (1963); F. Driessler and R. Ahlrichs, Chem. Phys. Lett. **23**, 571 (1973); V.R. Saunders, in *Methods in Computational Molecular Physics*, edited by G.H.F. Diercksen and S. Wilson, Reidel, Dordrecht

[16] A.A. Frost, J. Chem. Phys. **47**, 3707 (1967)

[17] A.A. Frost, J. Chem. Phys. **47**, 3714 (1967)

[18] B. Ford, G.G. Hall and J.C. Packer, Intern. J. Quantum Chem. **4**, 533 (1970)

[19] L.M. Haines, J.N. Murrell, B.J. Ralston and D.J. Woodnutt, J. Chem. Soc. Faraday Transactions II **70**, 1794 (1974)

[20] B.J. Ralston and S. Wilson, J. Molec. Structure THEOCHEM **341**, 115 (1995)

[21] S. Wilson, J. Molec. Structure THEOCHEM **357**, 37 (1995)

[22] S. Wilson, in *New Methods in Quantum Theory*, Ed. C.A. Tsipis, V.S. Popev, D.R. Herschbach and J.S. Avery, NATO ASI Series 3. High Technology - Vol. 8, Kluwer Academic Publishers, Dordrecht (1996)

[23] S. Wilson, J. Phys.B: At. Mol. Opt. Phys. **28**, L495 (1995)

[24] S. Wilson, Intern. J. Quantum Chem. **74**, 547 (1999)

[25] V.I. Karliichuk, V.N. Glushkov, A.I. Aprasyukhin, A.Y. Tsaune, J. Structural Chem. **24**, 914 (1983)

[26] A.Y. Tsaune, V.N. Glushkov and A.I. Aprasyukhin, Teoreticheskaya i Eksperimentalnaya Khimiya **24**, 215 (1988)

[27] M.M.Madsen and J.M. Peek, At. Data **2**, 171 (1971)

SIMILARITIES IN THE RYDBERG SPECTRA OF THE ISOVALENT RADICALS CH_3 AND SiH_3

I. Martín, A.M. Velasco and C. Lavín

Departamento de Química Física; Facultad de Ciencias; 47005 Valladolid, Spain

Abstract

In the present study of the Rydberg spectra of the methyl and silyl radicals, with the molecule-adapted Quantum Defect Orbital (QDO) method, we have sought and found important analogies between the spectral intensities of analogous transitions in these isovalent molecules. Further similarities with the spectra of their isolated central atoms and their united atom limits has not only served the purpose of assessing the quality of our calculations, but may also offer some relevant practical use.

ADVANCES IN QUANTUM CHEMISTRY, VOLUME 39

0065-3276/01 $35 00

1. Introduction

Molecular Rydberg states are attracting increasing attention, partly due to their unusual electronic structure and spectroscopic behaviour. A number of molecules in specific Rydberg states have been detected as short-lived intermediates or *transient species*, in the mechanisms of reactions that take place in terrestrial laboratories, in the atmosphere, and in different astronomical objects. The prediction of Rydberg spectra in molecules, as well as the interpretation of available observations, is constituting a challenge to the theory. Significant experimental advances have arisen in the last decade thanks to state-of-the-art laser spectroscopy techniques. Yet, there is great demand for theoretical data by the experimentalists.

The methyl radical is one of the most important free radicals in chemical reactions. In the laboratory, CH_3 has been confirmed to be a good reference to other transient species [1]. Evidence of its relevance in atmospheric and astrophysical chemistry is increasingly abundant, and its chemical and spectroscopic behaviour have been claimed to be of great importance in the modelling of the interstellar molecular clouds [2]. Similarly, over the past decade, laser spectroscopic methods have placed the silyl radical among the best characterized transient polyatomic free radicals. Only the transient H_3 [3] and CH_3 radicals have yielded spectra that are more abundant with excited electronic states and are more accesible to rotational analysis [4].

The methyl and silyl radicals have been reported as playing an important role in deposition processes that take place in plasmas as well as in etching processes [5]. In plasmas for chemical vapor deposition (CVD) the densities of neutral radicals, such as CH_3 and SiH_3, appear to be of relevance in the thin film formation. Evidence indicates that the silyl radicals govern the growth of silicon films during CVD processing of integrated circuit chips [6]. Information on the densities and temperatures of the plasmas are needed for the clarification of the thin film formation mechanisms [7]. These may partly be obtained through the knowledge of transition probability data on the participating radicals. SiH_3 may also exist in interstellar space, in view of the fact that silane has already been detected in the stellar atmosphere of a carbon-rich supergiant star IRC+10126 [8]. It appears that the SiH_3 radical should also be a candidate for astrophysical observation.

The silyl radical is an isovalent analogue of the methyl radical and, like CH_3, the SiH_3 radical has been claimed to be a benchmark for determining the ability of theoretical calculations to analysing and/or predicting experimental

observations [9]. Both the methyl and silyl radicals possess low-lying electronic states that have been shown to be predominantly Rydberg in character [9- 12].

2. Molecular Rydberg states

A very useful form in which to express a Rydberg series is:

$$\nu_n = T - R/(n - \delta_\ell)^2 \qquad (1)$$

where ν_n is the frequency in cm^{-1} of the transition, T is the convergence limit of the series, or ionization energy, R is the Rydberg constant, and n is a running integer identifying a particular member of the Rydberg series. Written in this form, n may be taken as the true principal quantum number of the excited orbital ("Rydberg orbital"). δ_ℓ is the "quantum defect", which typifies the entire series, although there are many cases in which the quantum defects of the first few members of a Rydberg series exhibit small variations before reaching a constant value.

It has long been recognized that Eq. (1), which refers to transitions in the centrally symmetric field of an atom, can only be approximate for a polyatomic molecule of arbitrary nuclear configuration [13]. For sufficiently high members of the Rydberg series the average radial electronic distance is many times greater than an average internuclear distance so that the nuclear field approximates a monopole rather well. It is, thus, to be expected that whilst Eq. (1) would predict the highest members of the Rydberg series with sufficient accuracy, and give the ionization energy with the same accuracy, the lowest members might deviate, due to the finite extent of the nuclear framework.

The number of Rydberg series which may be observed in a given molecule, and their intensity, is limited by the number and type of atoms which make up the molecule, and the molecular symmetry. Consider a molecule of AH_n type. The degeneracy of the atomic orbitals of A in spherical symmetry will be removed, at least partly, in the lowered symmetry of the molecular framework. This leads to Rydberg orbitals of the same atomic symmetry but different molecular symmetry. Ryberg orbitals are often designated as $n\ell(\Gamma_i)$, where n and ℓ are the principal and angular momentum quantum numbers of the orbital in atomic symmetry, and Γ_i is the irreducible representation of the molecular point group to which the orbital belongs.

3. Selection rules for Rydberg transitions

In the one-electron excitation picture of an A_nH molecule, the strong transitions are expected to be those arising from the non-bonding orbitals on atom A to Rydberg orbitals centred on the same atom [14]. Of these transitions, the most intense will be those which obey the atomic selection rule $\Delta\ell = \pm 1$ if they consist of one-photon transitions, in addition to the selection rules of molecular symmetry and multiplicity. The requirement $\Delta\ell = \pm 1$ has long been considered to be much less important than the latter. However, the differences between 2+1 and 3+1 resonance-enhanced multiphoton ionization spectroscopy (REMPI) spectra recently reported by Johnson and co-workers on the SiH_3 radical [10-12] are explained by the $\Delta\ell = \pm 2, 0$ for two-photon transitions and $\Delta\ell = \pm 3, \pm 1$ for three-photon transitions selection rule, as would one-photon transitions be explained by $\Delta\ell = \pm 1$. Even though the ℓ selection rules have been very seldom used, Johnson and Hudgens [12] claim that successful analyses of both methyl and silyl radical spectra require that the electronic angular momenta, ℓ, of the initial and final electronic states be considered, since the initial and final states that produce Rydberg spectra have well-defined ℓs. These authors remark that the highest occupied orbital in the ground state and in each Rydberg state is comprised mostly of an atomic orbital of the central atom, as Olbrich had predicted for both the methyl and silyl radicals, in an extensive configuration interaction calculation [9]. Johnson and Hudgens [12] expect the $\Delta\ell$ rule to govern the Rydberg spectra of many other free radicals. In the ground state of free radicals the highest occupied molecular orbital (HOMO) often consists primarily of one atomic orbital which has a well-defined ℓ. All lower MO's form a fully-occupied molecular core of $\ell = 0$. The Rydberg states of radicals are formed with this same molecular core and a Rydberg orbital of well-defined ℓ. Thus, the Rydberg spectra of these radicals should conform to the $\Delta\ell$ rule.

4. Objectives of the present work

It is the purpose of the present study to extend the available spectroscopic data on CH_3 and SiH_3 to higher Rydberg transitions . Our intensity and frequency predictions may aid in future experimental work. In order to assess the adequacy of our theoretical procedure, the Quantum Defect Orbital (QDO) method adapted to the treatment of molecular Rydberg states [15], parallel results on the isovalent methyl and silyl radicals will be jointly

examined. In addition, the correctness of our results for CH_3 and SiH_3 will be tested not only by a comparison of the results for the two radicals but also by extending the comparative analysis to the calculated transition intensities for analogous $n\ell$- $n'\ell'$ transitions (that is, those with the same Δn and the same ℓ and ℓ' values) in their respective central atoms, C and Si, and in the "united atom limits" of CH_3 and SiH_3, the flourine [16] and chlorine [17] atoms, respectively.

Similarities in the intensities of analogous electronic transitions in all the six species might be anticipated on the following grounds. First, the methyl and silyl radicals are isovalent analogs. They possess the same outer electron structure in the ground state and, thereby, their Rydberg spectra may be expected to exhibit important resemblances [10, 12] (in the absence of accidental features such as the perturbation of one or more states belonging to the same Rydberg series by a valence state of the same symmetry). Also, the electronic distribution of the Rydberg states in both the methyl atoms, respectively, in their excited states [10, 12]. In addition, over a decade ago, Herzberg suggested the existence of significant resemblances in the Rydberg spectrum of a molecule and that of its united atom limit [18]. From here our interest in seeking further analogies in the spectra of CH_3 and F and SiH_3 and Cl, respectively.

Not irrelevant to the above similarities are the ones we have recently reported [19] concerning the intensities of analogous transitions in homologous atoms, that is, atoms belonging to different rows of the periodic table but falling in the same group. These similarities are based upon the compliance of sum rules, whenever not very complex structures are involved and/or strong cancellation in the integrand of the transition integrals does not occur [20].

In other recent studies, such one involving a group of isoelectronic Rydberg radicals [21] we have also found that similarities in the spectral properties of analogous molecular systems can be established, and that those are of great usefulness. Not only for allowing the prediction of the same type of properties in other molecular species analogous to the former, but also as a good tool for assessing the reliability of our theoretical procedure.

In the method that we have presently employed to calculate absorption oscillator strengths and Einstein emission coefficients for one-photon Rydberg transitions in the methyl and silyl radicals, the studied transitions have been restricted to those that not only comply with the symmetry and multiplicity constraints but also obey the $\Delta\ell = \pm 1$ selection rule. This selection rule has obviously also been applied to our parallel calculations on the atoms.

5. Method of calculation

The QDO formalism adapted to deal with molecular Rydberg transitions has been described in detail elsewhere [3] We shall, thus, only give here a very brief summary of this method.

The QDO radial wavefunctions are the analytical solutions of a one-electron Schrödinger equation that contains a model potential of the form

$$V(r)_a = \frac{(c-\delta_a)(2\ell+c-\delta_a+1)}{2r^2} - \frac{1}{r}, \qquad (2)$$

were a represents the set of quantum numbers that define a given molecular state. Solutions of this equation are related to Kummer functions. The parameter δ_a is the quantum defect and c is an integer chosen to ensure the normalizability of the orbitals and their correct nodal pattern; the number of radial nodes is equal to $n - \ell - c - 1$.

The quantum defect, δ_a , corresponding to a given state, is related to the energy eigenvalue through the following equation (which is more specific for a given state a than Eq. (1) in Section 2),

$$E_a = T - \frac{1}{2(n_a - \delta_a)^2}, \qquad (3)$$

were T is the ionization energy. Both T and E_a are expressed here in Hartrees.

The absorption oscillator strength for a transition between two states a and b may be expressed as

$$f(a \rightarrow b) = \frac{2}{3} (E_b - E_a) Q\{a \rightarrow b\} |R_{ab}|^2 \qquad (4)$$

were $Q\{a \rightarrow b\}$, referred to as the *angular factors*, result from the angular integration, and the radial transition moment integrals are defined as

$$R_{ab} = \langle R_a(r)|r|R_b(r)\rangle . \qquad (5)$$

The detailed QDO algebraic expresions for the radial transition moments are

given in Ref. 3.

It is relevant to mention that with the quantum defect orbitals, all the radial transition integrals have closed-form analytical expressions, which offers, in our view, an important computational advantage.

The values of $Q\{a \rightarrow b\}$ for the symmetry group D_{3h}, to which the Rydberg states of both methyl and silyl radicals belong are collected in Table I. In this and the remaining tables we are employing a notation for the molecular Rydberg states that is commonly found in the literature. The $n\ell$ symbol of the atomic orbital to which the molecular Rydberg orbital can be correlated is followed by the symbol of the irreducible representation to which the Rydberg orbital belongs within the molecular symmetry group (in parenthesis), as indicated in Section 2.

The Einstein probabilities for spontaneus emission, or Einstein emission coefficients, are related to the absorption oscillator strengths through the well-known expresion,

$$A_{ba} = 6.6702 \times 10^{15}\ \tilde{\lambda}^{-2}\ (g_a / g_b)\ f_{ab}\,, \qquad (6)$$

where the wavelength for the transition, $\tilde{\lambda}$, is in Angstroms, and A_{ba} is expresed in seconds^{-1}. g_a and g_b are, respectively, the statistical weights of the initial and final states in the absorption process.

The energy data and quantum defects employed in the present calculations of intensities for vertical Rydberg transitions in the methyl and silyl radicals are discussed in the section that follows.

Table I . Values of non-zero angular factors $Q\{a \rightarrow b\}$ for D_{3h} symmetry and for $\ell = 0, 1, 2$.

$Q\{E'(p) \rightarrow A'_1(s)\} = Q\{A'_1(s) \leftrightarrow A''_2(p)\} = 1/3$
$Q\{A'_1(s) \rightarrow E'(p)\} = 2/3$
$Q\{A''_2(p) \leftrightarrow A'_1(d)\} = 4/15$
$Q\{A'_1(d) \rightarrow E'(p)\} = 2/15$
$Q\{E'(p) \rightarrow A'_1(d)\} = 1/15$
$Q\{A''_2(p) \rightarrow E''(d)\} = Q\{E'(p) \leftrightarrow E'(d)\} = 2/5$
$Q\{E''(d) \rightarrow A''_2(p)\} = Q\{E'(p) \leftrightarrow E''(d)\} = 1/5$

6. Energy values and quantum defects

The methyl radical has been reported to be planar with a D_{3h} geometry in its ground state and in all its Rydberg states, with an equilibrium bond length of 107.95 pm [9, 22- 24]. The ground state of CH_3 has the electron configuration:

$$(1a_1')^2\,(2\,a_1')^2\,(1e')^4\,(2\,a_1'')^1 \quad \tilde{X}\ ^2A_2''$$

The energy data chosen for our calculations have been the experimental values supplied by Herzberg [22, 23] and by Hudgens et al. [24]. For the ionization energy we have adopted the value of 79361.31 cm^{-1} measured by Houle and Beauchamp [25]. All these data are collected in Table II, where the same type of data for SiH_3 has also been collected. For those Rydberg states for which no experimental energy values were found in the literature we have made use of Eq.(1) with the quantum defects deduced from the spectral band assignments by Herzberg [22, 23] and those obtained by Olbrich in an extensive configuration interaction (CI) calculation [9].

The isovalent analog of the methyl radical, the silyl radical, has been reported to have a pyramidal geometry in its ground state as well as in its conventional valence states, but planar, with a D_{3h} geometry, in all its Rydberg states [9, 12, 26]. The bond lengths of SiH_3 in its $\tilde{X}\ ^2A_1$ ground state are equal to 149.6 pm, with the H-Si-H angles being about 111.8°. The Si-H bond length in the planar D_{3h} geometry is equal to 148.2 pm. Johnson and Judgens measured an ionization energy of 65610 cm^{-1} [12]. The electronic structure of the ground state of SiH_3 is the following

$$(1a_1)^2\,(2\,a_1)^2\,(3\,a_1)^2\,(1e)^4\,(4\,a_1)^2\,(2e)^4\,(5\,a_1)^1 \quad \tilde{X}\ ^2A_1 \quad ,$$

where the molecular orbital and state notations correspond to a C_{3v} symmetry, unlike that of the D_{3h} Rydberg states [12]. In both CH_3 and SiH_3 no substantial changes in bond length are expected for the different Rydberg states [12, 24]. In the present work we have always dealt with vertical electronic transitions.

For SiH_3 we have adopted the experimental energy data supplied by Johnson and co-workers [11, 12], including the ionization energy. For those Rydberg states for which no experimental energies are available, we have followed the same procedure as for CH_3 and deduced energy values from reported quantum defects within a given Rydberg series. The energy data

Table II . Rydberg excitation energies from the ground state and ionization energies for CH_3 and SiH_3. All values in cm^{-1}.

Rydberg state	CH_3	Rydberg state	SiH_3
$3s(^2A_1')$	46200	$4s(^2A_1')$	38716
$3p(^2E')$	58770	$3d(^2E')$	41257
$3p(^2A_2'')$	59925	$4p(^2E')$	48052
$3d(^2E')$	65639	$4p(^2A_2'')$	48438
$4s(^2A_1')$	65633	$3d(^2A_1')$	49787
$3d(^2E'')$	66500	$3d(^2E'')$	51602
$3d(^2A_1')$	66799	$5s(^2A_1')$	53578
$4p(^2E')$	69339	$4d(^2A_1')$	56253
$4p(^2A_2'')$	69736	$5p(^2E')$	56665
$5s(^2A_1')$	71872	$5p(^2A_2'')$	56929
$4d(^2E'')$	72227	$4d(^2E'')$	57726
$4d(^2A_1')$	72349	$6s(^2A_1')$	58819
$5p(^2A_2'')$	73634	$5d(^2A_1')$	59615
$5p(^2E')$	73452	$6p(^2A_2'')$	60341
$6s(^2A_1')$	74655	$6p(^2E')$	60498
$5d(^2E'')$	74832	$5d(^2E'')$	60705
$5d(^2A_1')$	74895	$7s(^2A_1')$	61255
$6p(^2E')$	75470	$7p(^2E')$	61986
$6p(^2A_2'')$	75567	$7p(^2A_2'')$	62060
IP	79364.31	IP	65610

adopted in the present calculations for the methyl and silyl radicals are collected in Table II.

Table III displays the quantum defects for six Rydberg series of CH_3 and SiH_3, as directly taken from the literature [9] or extracted from experimental energy data [11, 12, 22- 24]. The anomalously large quantum defects obtained by Olbrich [9] for the 3d ($^2E'$) state for both CH_3 (0.172) and SiH_3 (0.88) are explained [9] in terms of a possible Rydberg-valence mixing. As no experimental data seem to be available for the 3d ($^2E'$) state or other members of the same Rydberg series, we have not thought it safe extrapolating higher energy levels in the same series with the same quantum defects. We have assigned to the higher members of five of the six Rydberg series of both

Table III. Quantum defects corresponding to the different Rydberg series studied in the present work for the radicals CH_3 and SiH_3, their central atoms (C and Si) and their united atoms (F and Cl).

Rydberg state	C	CH_3	F	Si	SiH_3	Cl
		(n=n'=3)			(n=4,n'=3)	
ns($^2A_1'$)	1.05	1.181[c]	1.25	1.90	1.98[b]	2.09
(n+1)s($^2A_1'$)	1.04	1.173[b]	1.22	1.82	1.98	2.09
(n+2)s($^2A_1'$)		1.173			1.98	
(n+3)s($^2A_1'$)		1.173			1.98	
np($^2E'$)	0.62	0.6916[d]	0.81	1.41	1.50	1.67
(n+1)p($^2E'$)	0.60	0.6916	0.76	1.34	1.50[b]	1.57
(n+2)p($^2E'$)		0.6916			1.50	
(n+3)p($^2E'$)		0.6916			1.50	
np($^2A_2''$)	0.62	0.624[c]	0.81	1.41	1.47[a]	1.67
(n+1)p($^2A_2''$)	0.60	0.624	0.76	1.34	1.45[a]	1.57
(n+2)p($^2A_2''$)		0.624			1.44[a]	
(n+3)p($^2A_2''$)		0.624			1.44	
n'd($^2E'$)	0.01	0.172[b]	0.04	0.02	0.88[b]	0.42
n'd($^2E''$)	0.01	0.079[c]	0.04	0.02	0.22[b]	0.42
(n'+1)d($^2E''$)	0.02	0.079	0.07	0.03	0.27[a]	
(n'+2)d($^2E''$)		0.079			0.27	
n'd($^2A_1'$)	0.01	0.045[c]	0.04	0.02	0.37[a]	0.42
(n'+1)d($^2A_1'$)	0.02	0.045	0.07	0.03	0.58[a]	
(n'+2)d($^2A_1'$)		0.045			0.72[a]	

[a] Deduced from assignments in the observed spectra [11, 12].
[b] As directly reported from ab initio calculations [9].
[c] Deduced from assignments in the observed spectra [22, 23].
[d] Deduced from assignments in the observed spectra [24].

radicals a constant δ value, as done in standard procedures [10]. In this form, we have been able to predict intensities for transitions which have not been observed experimentally yet, in the hope that this information may be useful for further spectroscopic assignments in CH_3 and SiH_3 in the future.

Table III also contains the quantum defects for the central atoms of the methyl and silyl radicals, C and Si, as well as for the radicals' united atom limits, F and Cl, respectively. The atoms' quantum defects have been extracted from their tabulated energy levels and ionization energies [27]. We may regard Table III as composed of two groups of columns, one group comprising the δ values of C, CH_3 and F, and the other group the quantum defects of Si, SiH_3 and Cl. The following remarks concern first the data displayed for each of the two groups. Inspection of the quantum defects of any of the two groups reveals that in each Rydberg series (characterized by the value of the well-defined [9, 12, 24] orbital quantum number ℓ and by the irreducible representation Γ_i to which the states belong), important similarities in the magnitude of the quantum defects of the three species (isolated central atom, molecule and united atom) occur. The value of δ is seen to increase along a horizontal line (a given Rydberg state) from left (isolated central atom) to right (united atom) in both the group of the methyl radical and that of the silyl radical.

The lighter central atom (C or Si) exhibits the lowest quantum defect, the molecule an intermediate value, and the united atom (F or Cl) the highest value of the three. This feature helps to confirm the correctness of the δ values adopted for CH_3 and SiH_3. As mentioned above, the Rydberg orbitals of the two molecular species are essentially atomic orbitals centred on C or Si. Since C and Si are placed , within the radicals, in a more complex electronic environment than when they are isolated, their deviation from a hydrogenic behaviour is greater and, hence, their quantum defects are larger. However, not so large as those of the united atoms, whose more complex internal structure leads to further deviations from a hydrogenic character and to larger quantum defects.

Very similar comments can be made if one compares one of the three species (the isolated central atom, the radical, or its united atom) from the group on the left- with the equivalent species from the group on the right-hand sides of Table III. For instance, the species in the middle of each group, SiH_3 and CH_3. The two species possess the same outer electronic configuration, but SiH_3 has a more complex internal structure. From here its larger δ value in an equivalent Rydberg state.

7. Transition intensities.

The transition intensities calculated with the molecule-adapted QDO methodology [15] for one-photon vertical Rydberg transitions in the methyl and

silyl radicals are presented in Tables IV and V both in the form of absorption oscillator strengths and as Einstein emission coefficients. In Table IV we have collected the transitions that involve the ground state of CH_3, with $^2A_1$ (C_{3v}) symmetry and that of SiH_3, $^2A_2''$ (D_{3h}). Both have been generally denoted as np($\tilde{\chi}$). For the states belonging to the Rydberg series of CH_3 and SiH_3 the notation is consistent with that of the D_{3h} symmetry group, as they are all triangular planar [9, 10- 12, 22- 24].

The intensities of all the np($\tilde{\chi}$) – n's($^2A'_1$) transitions appear to be very close in magnitude for the two isovalent radicals, as happens with the intensities of the np($^2A_2''$) – n's($^2A'_1$) and np($^2E'$) – n's($^2A'_1$) transitions, which are displayed in Table IV. Very similar comments can be made as regards the intensity of each of the equivalent transitions for CH_3 and SiH_3 of the two groups that involve *ns* and *n*'p states and belong to different irreducible representations, collected in Table V.

We have not performed calculations on transitions from, or to, the nd($^2E'$) Rydberg series of SiH_3 According to Johnson and Hudgens [12] the 3d($^2E'$) state mixes with 3d($^2E''$) through a valence state of E' symmetry that lies close in energy. As a consequence, 3d($^2E'$) and 3d($^2E''$) are reported as not producing detectable REMPI spectra, and to be strongly dissociative [12]. From this anomalous behaviour may arise the large quantum defect predicted by Olbrich for the 3d($^2E'$) Rydberg state [9]. We have not dealt with other hypothetical states of either the nd($^2E'$) or nd($^2E''$) Rydberg series of SiH_3, as their stability may also be questionable. However, transitions involving the above Rydberg series in CH_3, which seem to be stable, will be mentioned later.

Up to this point we have only proved the existence of similarities in the intensities of analogous transitions for isovalent analogue radicals. We shall next refer to the oscillator strengths calculated for several multiplet transitions involving *ns*, *np* and *nd* orbitals in the respective united atom limits, F and Cl. These are displayed in Table VI. The relativistic version of the Quantum Defect Orbital (RQDO) method [28, 29] has been used in the calculations. A rather good accord between the oscillator strengths for the analogous multiplet transitions of the homologous atoms F and Cl (that is, those which are written in the same row) is observed. This feature helps establishing the reliability of these data, on physical grounds [19, 20]. No f-values are assigned to the higher n'p – n'd doublet and quadruplet transitions of Cl because the involved energy levels have been found to follow a spin-orbit coupling scheme other than LS [16], unlike the lower levels with the same orbital angular momenta and, thus,

Table IV. QDO absorption oscillator strengths and Einstein emission coefficients for $np(\tilde{\chi})$, $np(^2A''_2)$, $np(^2E')$ - $n's(^2A'_1)$ transitions for CH_3 and SiH_3.

Transition	CH_3 (n=2)		SiH_3 (n=3)	
	f_{if}	$A_{fi}(10^8 s^{-1})$	f_{if}	$A_{fi}(10^8 s^{-1})$
$np(\tilde{\chi})$ - $(n+1)s(^2A_1')$	0.1568	6.6969	0.1529	4.5861
$np(\tilde{\chi})$ - $(n+2)s(^2A_1')$	0.0170	1.4656	0.0206	1.1833
$np(\tilde{\chi})$ - $(n+3)s(^2A_1')$	0.0055	0.5686	0.0070	0.4846
$np(\tilde{\chi})$ - $(n+4)s(^2A_1')$	0.0025	0.2788	0.0032	0.2403
$(n+1)p(^2A_2'')$ - $(n+2)s(^2A_1')$	0.3106	0.2027	0.3135	0.1657
$(n+1)p(^2A_2'')$ - $(n+3)s(^2A_1')$	0.0144	0.0411	0.0189	0.0408
$(n+1)p(^2A_2'')$ - $(n+4)s(^2A_1')$	0.0041	0.0178	0.0056	0.0184
$(n+1)p(^2E')$ - $(n+2)s(^2A_1')$	0.2989	0.2818	0.3071	0.1877
$(n+1)p(^2E')$ - $(n+3)s(^2A_1')$	0.0206	0.0708	0.0214	0.0496
$(n+1)p(^2E')$ - $(n+4)s(^2A_1')$	0.0062	0.0313	0.0065	0.0227

Table V . QDO absorption oscillator strengths and Einstein emission coefficients for $ns(^2A'_1)$ - $np(^2E')$, $n'p(^2A''_2)$ transitions for CH_3 and SiH_3.

Transition	CH_3 (n=3)		SiH_3 (n=4)	
	f_{if}	$A_{fi}(10^8 s^{-1})$	f_{if}	$A_{fi}(10^8 s^{-1})$
$ns(^2A_1')$ - $np(^2E')$	0.6034	0.2120	0.6629	0.1285
$ns(^2A_1')$ - $(n+1)p(^2E')$	0.0266	0.0317	0.0254	0.0182
$ns(^2A_1')$ - $(n+2)p(^2E')$	0.0069	0.0114	0.0063	0.0065
$ns(^2A_1')$ - $(n+3)p(^2E')$	0.0029	0.0055	0.0026	0.0031
$ns(^2A_1')$ - $np(^2A_2'')$	0.2994	0.1254	0.3338	0.0702
$ns(^2A_1')$ - $(n+1)p(^2A_2'')$	0.0199	0.0245	0.0185	0.0136
$ns(^2A_1')$ - $(n+2)p(^2A_2'')$	0.0057	0.0095	0.0053	0.0058
$ns(^2A_1')$ - $(n+3)p(^2A_2'')$	0.0025	0.0048	0.0022	0.0027

no direct comparison with the corresponding transitions in F can be made.

In Table VII we have grouped the f-values for different sets of analogous transitions in the methyl radical, its isolated central atom and its united atom limit. Before comparing their magnitudes a few remarks are in order. Given that the atoms possess an infinite, higher symmetry than the molecule, the states described by a given $n\ell$ notation are symmetry-split in the radical. On the other hand, there may be several different terms and multiplets arising from a given outer $n\ell$ atomic orbital if there are, as happens in both C and F, more than one electron in the outer n shell, whilst there is only one electron in each of the $n\ell(\Gamma_1)$ Rydberg states of CH_3. The consequence of the difference in the number of analogous states in the atoms and the molecule is that a comparison in the transition intensities may only be made between the sum of the individual intensities in an $n\ell$ - $n'\ell$ "supermultiplet" in the atoms and the sum of the intensities of all the $n\ell$ - $n'\ell$ transitions that comprise all the different irreducible representations involved (if more than one) in the molecule (see the notation used in Tables VII-IX). A "supermultiplet" is [20] the group of multiplets with different L-value but the same spin multiplicity which arise from a given electron configuration in an atom.

Therefore, the oscillator strengths that are shown in Tables VII to IX are the total ones for each group of $n\ell$ - $n'\ell$ transitions in the atoms and the molecules. These f-values exhibit very similar magnitudes in C, CH_3 and F (Table VII), Si, SiH_3 and Cl (Table VIII) and the two groups of homologous atomic and molecular species in the two precedent tables. It is apparent that all the f-values for the same $n\ell$ - $n'\ell$ transitions both in Table VII and Table VIII, in each of which the two atoms and the molecule are homologous in the sense discussed above, conform generally very well. We have omitted most of the np – n'd transitions from Table VIII because of the aforementioned deviation from LS coupling of the higher n'd levels of chlorine. These data are also omitted from Table IX where those of Tables VII and VIII are jointly presented. The purpose of building up Table IX is to show that similarities between the calculated f-values of C and Si, CH_3 and SiH_3, and F and Cl, respectively, are also apparent. This feature also confirms the correctness of the present transition intensities, which rests on the physical grounds of each pair of species having the same outer electron structure.

Table VII. Oscillator strengths for analogous transitions in the methyl radical, its isolated central atom and its united atom limit.

Transition	C	Transition	CH_3	Transition	F
$2p\ ^3P\text{-}3s\ ^3P$	0.1400	$2p(^2A_2'')\text{-}3s(^2A_1')$	0.1568	$2p\ ^2P\text{-}3s^2P$	0.1519
$3s\ ^3P\text{-}3p\ ^3(S,P,D)$	1.0110	$3s(^2A_1')\text{-}3p(^2A_2'', ^2E')$	0.9028	$3s\ ^2P\text{-}3p\ ^2(S,P,D)$	0.8673
$3s\ ^1P\text{-}3p\ ^1(S,P,D)$	1.0370			$3s\ ^4P\text{-}3p\ ^4(S,P,D)$	0.8377
$3p\ ^3P\text{-}3d\ ^3(P,D)$	0.9310	$3p(^2A_2'')\text{-}3d(^2E'', ^2A_1')$	1.0045	$3p\ ^2P\text{-}3d\ ^2(P,D)$	1.1709
$3p\ ^3S\text{-}3d\ ^3P$	0.5430	$3p(^2E')\text{-}3d(^2E', ^2E'', ^2A_1')$	0.9833	$3p\ ^2S\text{-}3d\ ^2P$	1.2050
$3p\ ^3D\text{-}3d\ ^3(P,D,F)$	0.8900			$3p\ ^2D\text{-}3d\ ^2(P,D,F)$	1.2010
$3p\ ^1P\text{-}3d\ ^1(P,D)$	0.9630			$3p\ ^4P\text{-}3d\ ^4(P,D)$	1.1620
$3p\ ^1S\text{-}3d\ ^1P$	0.3990			$3p\ ^4S\text{-}3d\ ^4P$	1.1749
$3p\ ^1D\text{-}3d\ ^1(P,D,F)$	0.8687			$3p\ ^4D\text{-}3d\ ^4(P,D,F)$	1.1789
$3p\ ^3P\text{-}4s\ ^3P$	0.2887	$3p(^2A_2'')\text{-}4s(^2A_1')$	0.3107	$3p\ ^2P\text{-}4s\ ^2P$	0.2950
$3p\ ^3S\text{-}4s\ ^3P$	0.2727	$3p(^2E')\text{-}4s(^2A_1')$	0.2989	$3p\ ^2S\text{-}4s\ ^2P$	0.2858
$3p\ ^3D\text{-}4s\ ^3P$	0.2432			$3p\ ^2D\text{-}4s\ ^2P$	0.2690
$3p\ ^1P\text{-}4s\ ^1P$	0.2032			$3p\ ^4P\text{-}4s\ ^4P$	0.2582
$3p\ ^1S\text{-}4s\ ^1P$	0.3166			$3p\ ^4S\text{-}4s\ ^4P$	0.2984
$3p\ ^1D\text{-}4s\ ^1P$	0.3072			$3p\ ^4D\text{-}4s\ ^4P$	0.2776
$2p\ ^3P\text{-}3d\ ^3(P,D)$	0.1340	$2p(^2A_2'')\text{-}3d(^2E'', ^2A_1')$	0.1093	$2p\ ^2P\text{-}3d\ ^2(P,D)$	0.0415

Table VIII. Oscillator strengths for analogous transitions in the silyl radical, its isolated central atom and its united atom limit.

Transition	Si	Transition	SiH_3	Transition	Cl
$3p\ ^3P\text{-}4s\ ^3P$	0.1657	$3p(^2A_2'')\text{-}4s(^2A_1')$	0.1529	$3p\ ^2P\text{-}4s\ ^2P$	0.1603
$4s\ ^3P\text{-}4p\ ^3(S,P,D)$	0.9646	$4s(^2A_1')\text{-}4p(^2A_2'', ^2E')$	1.0015	$4s\ ^2P\text{-}4p\ ^2(S,P,D)$	0.9362
$4s\ ^1P\text{-}4p\ ^1(S,P,D)$	0.9781			$4s\ ^4P\text{-}4p\ ^4(S,P,D)$	0.9033
$4p\ ^3P\text{-}5s\ ^3P$	0.3035	$4p(^2A_2'')\text{-}5s(^2A_1')$	0.3135	$4p\ ^2P\text{-}5s\ ^2P$	0.3026
$4p\ ^3S\text{-}5s\ ^3P$	0.3098	$4p(^2E')\text{-}5s(^2A_1')$	0.3183	$4p\ ^2S\text{-}5s\ ^2P$	0.3097
$4p\ ^3D\text{-}5s\ ^3P$	0.2741			$4p\ ^2D\text{-}5s\ ^2P$	0.2862
$4p\ ^1P\text{-}5s\ ^1P$	0.2068			$4p\ ^4P\text{-}5s\ ^4P$	0.2498
$4p\ ^1S\text{-}5s\ ^1P$	0.3219			$4p\ ^4S\text{-}5s\ ^4P$	0.3139
$4p\ ^1D\text{-}5s\ ^1P$	0.3131			$4p\ ^4D\text{-}5s\ ^4P$	0.2724
$3p\ ^3P\text{-}3d\ ^3(P,D)$	0.2752	$3p(^2A_2'')\text{-}3d(^2E'', ^2A_1')$	0.2884	$3p\ ^2P\text{-}3d\ ^2(P,D)$	0.1448

Table IX. Oscillator strengths for analogous transitions in the methyl and silyl radicals, their isolated central atoms, and their united atom limits.

Transition	C	Si	Transition	CH_3	SiH_3	Transition	F	Cl
	(n=2,n'=3)	(n=n'=3)		(n=2,n'=3)	(n=n'=3)		(n=2,n'=3)	(n=n'=3)
np ^{3}P-(n+1)s ^{3}P	0 1400	0.1657	np($^2A_2''$)-(n+1)($^2A_1'$)	0 1568	0.1529	np ^{2}P-(n+1)s ^{2}P	0.1519	0 1603
(n+1)s ^{3}P-(n+1)p ^{3}(S,P,D)	1.0110	0.9646	(n+1)s($^2A_1'$)-(n+1)p($^2A_2''$, $^2E'$)	0 9028	1.0015	(n+1)s ^{2}P-(n+1)p ^{2}(S,P,D)	0.8673	0.9362
(n+1)s ^{1}P-(n+1)p ^{1}(S,P,D)	1 0370	0 9781				(n+1)s ^{4}P-(n+1)p ^{4}(S,P,D)	0.8377	0.9033
(n+1)p ^{3}P-(n+1)d ^{3}(P,D)	0.9310		(n+1)p($^2A_2''$)-(n+1)d($^2E''$, $^2A_1'$)	1.0045		(n+1)p ^{2}P-(n+1)d ^{2}(P,D)	1.1709	
(n+1)p ^{3}S-(n+1)d ^{3}P	0.5430		(n+1)p($^2E'$)-(n+1)d($^2E'$,$^2E''$,$^2A_1'$)	0.9833		(n+1)p ^{2}S-(n+1)d ^{2}P	1.2050	
(n+1)p ^{3}D-(n+1)d ^{3}(P,D,F)	0 8900					(n+1)p ^{2}D-(n+1)d ^{2}(P,D,F)	1 2010	
(n+1)p ^{1}P-(n+1)d ^{1}(P,D)	0.9630					(n+1)p ^{4}P-(n+1)d ^{4}(P,D)	1.1620	
(n+1)p ^{1}S-(n+1)d ^{1}P	0.3990					(n+1)p ^{4}S-(n+1)d ^{4}P	1.1749	
(n+1)p ^{1}D-(n+1)d ^{1}(P,D,F)	0.8687					(n+1)p ^{4}D-(n+1)d ^{4}(P,D,F)	1.1789	
(n+1)p ^{3}P-(n+2)s ^{3}P	0 2887	0.3035	(n+1)p($^2A_2''$)-(n+2)s($^2A_1'$)	0.3107	0.3135	(n+1)p ^{2}P-(n+2)s ^{2}P	0.2950	0.3026
(n+1)p ^{3}S-(n+2)s ^{3}P	0.2727	0.3098	(n+1)p($^2E'$)-(n+2)s($^{2a}{}_1'$)	0.2989	0.3183	(n+1)p ^{2}S-(n+2)s ^{2}P	0.2858	0.3097
(n+1)p ^{3}D-(n+2)s ^{3}P	0.2432	0.2741				(n+1)p ^{2}D-(n+2)s ^{2}P	0 2690	0.2862
(n+1)p ^{1}P-(n+2)s ^{1}P	0.2032	0.2068				(n+1)p ^{4}P-(n+2)s ^{4}P	0.2582	0.2498
(n+1)p ^{1}S-(n+2)s ^{1}P	0.3166	0.3219				(n+1)p ^{4}S-(n+2)s ^{4}P	0.2984	0.3139
(n+1)p ^{1}D-(n+2)s ^{1}P	0.3072	0.3131				(n+1)p ^{4}D-(n+2)s ^{4}P	0.2776	0 2724
np ^{3}P-n'd ^{3}(P,D)	0.1340	0.2752	np($^2A_2''$)-n'd($^2E''$, $^2A_1'$)	0.1093	0.2884	np ^{2}P-n'd ^{2}(P,^{2}D)	0.0415	0.1448

8. Concluding remarks

The Quantum Defect Orbital method both in its non-relativistic molecule-adapted (QDO) and atomic relativistic (RQDO) formulations have been able to reproduce the expected similarities in the intensities of analogous Rydberg transitions in the isovalent molecules methyl and silyl radicals, as well as in those of both their respective isolated central atoms and united atom limits. The same type of similarities have been reproduced for the homologous atoms C and Si, and F and Cl, respectively, whenever the levels involved in the transitions comply with the same spin-orbit coupling scheme. We take these features as an assessment of the reliability of our theoretical procedures.

Some practical consequences, such as the possibility of inter- or extrapolating data for other homologous atomic and molecular species, may be derived.

It is hoped that some of the present data, and those of future calculations, may aid in spectroscopic measurements.

9. Acknowledgments

This work has been supported by the D.G.E.S. of the Spanish Ministry of Education within Project No. PB97-0399-C03-01. A.M.V. wishes to acknowledge the award of a post-doctoral research fellowship by the Spanish M.E.C..

References

[1] M.E. Jacox, J. Phys. Chem. Ref. Data, Monograph 3, 1994.
[2] M. Bogey, M. Cordonnier, C. Demuynk, J.L. Destombes and A. Walters, in Newsletter on Analysis of Astronomical Spectra No. 22,(Ed. C. S. Jeffery, Daresbury Laboratory, Scottland, October 1995).
[3] I. Martín, C. Lavín and J. Karwowski, Chem. Phys. Lett. **255**, 89 (1996).
[4] M.E. Jacox, J. Phys. Chem. Ref. Data **17**, 269 (1988); *ibid* **19**, 1387 (1990).
[5] E. Hirota, Pure and Appl. Chem. **70**, 1145 (1998)
[6] T. Goto, Pure and Appl. Chem. **68**, 1059 (1996).
[7] J.M. Jasinski, B.S. Meyerson and B.A. Scott, Ann. Rev. Phys. Chem. **38**,

109 (1987).
[8] D.M. Goldhaber and A.L. Betz, Astrophys. J. **279**, L55 (1984).
[9] G. Olbrich, Chem. Phys. **101**, 381 (1986).
[10] R.D. Johnson III and J.W. Hudgens, Chem. Phys. Lett. **141**, 163 (1987).
[11] R.D. Johnson III, B.P. Tsai and J.W. Hudgens, J. Chem. Phys. **91**, 3340 (1989).
[12] R.D. Johnson III and J.W. Hudgens, J. Chem. Phys. **94**, 5331 (1991).
[13] W.C. Price, J. Chem. Phys. **3**, 256 (1935)
[14] S.R. La Paglia, J. Mol. Spectrosc. **10**, 240 (1963).
[15] I. Martín, C. Lavín, A.M. Velasco, M.O. Martín, J. Karwowski and G.H.F. Diercksen, Chem. Phys. **202**, 307 (1996).
[16] A.M. Velasco, C. Lavín and I. Martín, J. Quant. Spectrosc. Radiat. Transfer **57**, 509 (1997).
[17] C Lavín, A.M. Velasco and I. Martín, Astron. Astrophys. **328**, 426 (1997).
[18] G. Herzberg, Ann. Rev. Phys. Chem. **38**, 27 (1987).
[19] I. Martín, E. Charro and C. Lavín, in "Progress in Theoretical Chemistry and Physics", (Ed. J. Maruani, Kluwer Academic Publishers: Dordrecth, 2000).
[20] W.C. Martin and W.L. Wiese, in "Atomic, Molecular, and Optical Physics Handbook", (Ed. G.W.F. Drake, American Institute of Physics: Woodbury: New York 1996).
[21] I. Martín, Y. Pérez-Delgado and C. Lavín, Chem. Phys. Lett. **305**, 178 (1999).
[22] G. Herzberg, Proc. Roy. Soc. London Ser. A **262**, 291 (1961).
[23] G. Herzberg, "Molecular Spectra and Molecular Structure. III. Electronic Spectra and Electronic Structure of Polyatomic Molecules", Reprint Edition, Krieger: Florida (1991).
[24] J.W. Hudgens, T.G. DiGiuseppe and M.C. Lin, J. Chem. Phys. **79**, 571 (1983).
[25] F.A. Houle and J.L. Beauchamp, J. Am. Chem. Soc. **101**, 4067 (1979).
[26] J.M. Dyke, N. Johnathan, A. Morris, A. Ridha and J.M. Winter, Chem. Phys. **81**, 481 (1983).
[27] C.E. Moore, "Atomic Energy Levels", Nat. Bur. Stand. Ref. Ser. 35, Nat. Bur. Stand. : Washington D.C. (1971).
[28] I. Martín and J. Karwowski, J. Phys. B: Atom. Mol. Opt. Phys. **24**, 1539 (1991).
[29] J. Karwowski and I. Martín, Phys. Rev. A **43**, 4832 (1991).

Theoretical study of charge transfer mechanism in N^{4+} + H_e collisions at *keV* energies

Y. S. Tergiman and M. C. Bacchus-Montabonnel
Laboratoire de Spectrométrie Ionique et Moléculaire(UMR 5579)
CNRS and Université Lyon I
43 Bd du 11 Novembre 1918 – 69622 Villeurbanne Cedex, France

Abstract

Ab – initio potential energy curves and coupling matrix elements of the $^2\Sigma^+$molecular states involved in the collision of N^{4+} multicharged ion on helium have been determined by means of configuration interaction methods. The total and partial electron capture cross sections have been determined using a semi-classical approach in the 1 – 50 *keV* laboratory energy range. The comparision with experiment shows the importance of the double capture channels.

List of contents:

- Potential energy curves of the N^{4+}+*He* system
- Radial coupling matrix elements
- Total and partial cross sections of single and double electron capture

ADVANCES IN QUANTUM CHEMISTRY, VOLUME 39

0065-3276/01 $35.00

I. INTRODUCTION

Electron capture by multiply charged ionic species on atomic and molecular targets have been shown to be important processes in astrophysics and controlled thermonuclear fusion research, in particular the study of reactions involving carbon, nitrogen and, more recently, boron has been stimulated by the need of precise data for diagnostics of fusion plasmas. Translational energy spectroscopy experiments have been carried out by McLaughlin et al. [1] on the state selective electron capture of N^{4+} ions in collision with helium in the 4 – 28 *keV* impact energy range. They show evidence of a $N^{3+}(2p^2)^1S$ dominant product channel, with contribution of other $N^{3+}(2l2l')$ channels at higher energies which could not be interpreted by their MCLZ calculations [1]. This system has also been investigated experimentally by Okuno et al. [2], Hoekstra et al. [3] and Iwai et al. [4] who provided total cross sections for single and double electron capture but not accurate theoretical approach has been still performed.

We have thus undertaken an *ab – initio* theoretical treatment of the $N^{4+}(2s) + He(1s^2)$ charge transfer process at *keV* impact energies, taking into account both single and double electron capture channels. From a theoretical point of view, this is an extremely complex collisional system as we have to take into account, beyond the entry channel $^2\Sigma^+\{ N^{4+}(2s) + He(1s^2)\}$, all the $^2\Sigma^+$ and $^2\Pi$ states correlated to the single $N^{3+}(2l,2l') + He(1s)\}$ and $\{N^{3+}(2l3l') + He(1s)\}$ levels, as well as those correlated to the $\{N^{2+}(2s^22p) + He^{2+}\}$ and $\{N^{2+}(2s2p^2) + He^{2+}\}$ double electron capture channels. It seems thus reasonable in a first approach, to neglect the rotational coupling $\langle\psi_K|\ i\ L_y|\ \psi_L\rangle$ between Σ and Π states and consider only the transitions occurring by means of non-adiabatic radial couplings. The collision dynamics has been performed by means of semi-classical methods using EIKONXS algorithm.

II- MOLECULAR CALCULATIONS

The one-electron capture process has been shown experimentally [1] to be dominant on the $\{N^{3+}(2p^2)^1S + He^+(1s)\}$capture channel contributions of $N^{3+}(n=2)$ levels. From atomic data [5], this corresponds to very short range curve crossing interactions, far shorter than possible curve crossings between the entry channel and the $N^{3+}(2l3l') + He^+$ electron capture levels (Table 1). It seems thus reasonable for this problem to neglect the capture on the $N^{3+}(n=3)$ levels and calculate accurately the potential energy curves in the inner region mainly, then extrapolate the potentials for larger inter-nuclear distances taking into account the Coulomb repulsion term.

The potential energy curves and the non-adiabatic radial coupling matrix elements have been calculated using the quantum-chemistry code MOLPRO [6].

The potential energy curves have thus been determined accurately for a large number of inter-atomic distances in the 1.2-5 *a.u.* range by means of a state-

average *CASSCF/MRCI* calculation using a direct algorithm [7,8] with configuration interaction. The calculation has been extended at the same level of theory until $R = 15.0$ *a.u.* for the $N^{3+}(2l2l')$ and $N^{3+}(2s^22p)$ and $N^{3+}(2s2p^2)$ levels. The basis of atomic functions used in to represent N and He is the (16*s*, 10*p*, 5*d*, 4*f*/6*s*, 2*p*, 1*d*) correlation-consistent polarized cc-pV6Z basis set of Dunning [9]. In order to obtain maximum flexibility, we have not applied any contraction of the Gaussian primitives.

Table 1. Asymptotic experimental energies [5] and crossing points for one-electron collision capture channels in the $N^{4+}(2s)^2S + He$ reaction

channel	energy (a.u.)	R_c(a u.)
$N^{4+}(2s)^2S + He$	1.9428	
$N^{3+}(2s3d)^3D + He^+$	1.9135	102.4
$N^{3+}(2s3p)^3P + He^+$	1.8495	32.1
$N^{3+}(2s3p)^1P + He^+$	1.8431	30.1
$N^{3+}(2s3s)^1S + He^+$	1.7718	17.5
$N^{3+}(2s3s)^3S + He^+$	1.7187	13.4
$N^{3+}(2p^2)^3P + He^+$	1.0724	3.4
$N^{3+}(2p^2)^1D + He^+$	0.8606	2.8
$N^{3+}(2p^2)^3P + He^+$	0.8001	2.6
$N^{3+}(2s2p)^1P + He^+$	0.5955	2.2
$N^{3+}(2s3p)^3P + He^+$	0.3065	1.8
$N^{3+}(2s^2)^1S + He^+$	0.0	1.5

The asymptotic energy values extrapolated according to the Coulomb repulsion term are presented in Table 2 and are shown to be in relatively satisfactory agreement with the experimental data [5]. The agreement is somewhat lower for $N^{2+}(2s^22p)^2P + He^{2+}$ and $N^{2+}(2s^2)^1S + He^+$ levels, the difference energies between the N^{2+} levels being for their part correctly reproduced. The radial coupling matrix elements have been calculated by an analytic gradient program of the MOLPRO package. Provided that a common set of molecular orbitals is defined in a state-

Table 2. Comparision with experimental data [5] of the $^2\Sigma$ states of $(NHe)^4$

channel	experiment (a.u.)	calculation (a.u.)
$N^{4+}(2s)^2S + He$	1.9428	1.9621
$N^{3+}(2p^2)^1S + He^+$	1.0724	1.1006
$N^{3+}(2p^2)^1D + He^+$	0.8606	0.8659
$N^{3+}(2s2p^2)^1S + He^{2+}$	1.0724	0.8855
$N^{2+}(2s2p^2)^2D + He^{2+}$	0.7172	0.7341
$N^{3+}(2s2p)^1P + He^+$	0.5955	0.6040
$N^{3+}(2s2p)^3P + He^+$	0.3065	0.3040
$N^{2+}(2s^22p)^2P + He^{2+}$	0.2574	0.2695
$N^{3+}(2s^2)^1S + He^+$	0.0	0.0

average calculation for all the states involved, the required derivatives can be obtained by solving a set of coupled perturbed state-averaged CASSCF equations [10], the efficiency of the procedure arising from the use of analytic derivative methods [11]. The calculation has been performed with the parameter $\Delta = 0.0012$ *a.u.* as previously tested [12] and with the origin of the electronic coordinates at the center of mass of the nuclei. We have not corrected the dependence with origin of electronic coordinates of the radial coupling matrix elements by introducing electron translation factors, but we have imposed all couplings to be zero at $R = 10$ *a.u.* in order to avoid spurious couplings at long range.

The $^2\Sigma^+$ potential energy curves and the radial coupling matrix elements are displayed respectively in figure 1 and figure 2. They show evidence of a very sharp avoided crossing around $R = 3.7$ *a.u.* between the entry channel and the $\{N^{3+}(2p^2)^1S + He^+\}$ capture level corresponding to the dominant product channel evidenced experimentally [1]. Broader avoided crossings are exhibited between the one-electron capture levels $\{N^{3+}(2s^2)^1S + He^+\}$ and $\{N^{3+}(2s2p)^3P + He^+\}$ and between the double capture channel $\{N^{2+}(2s^22p)^1S + He^{2+}\}$ and the single charge exchange level $\{N^{3+}(2s2p)^1P + He^+\}$ around respectively 2.4 and 3.2 *a.u.*.

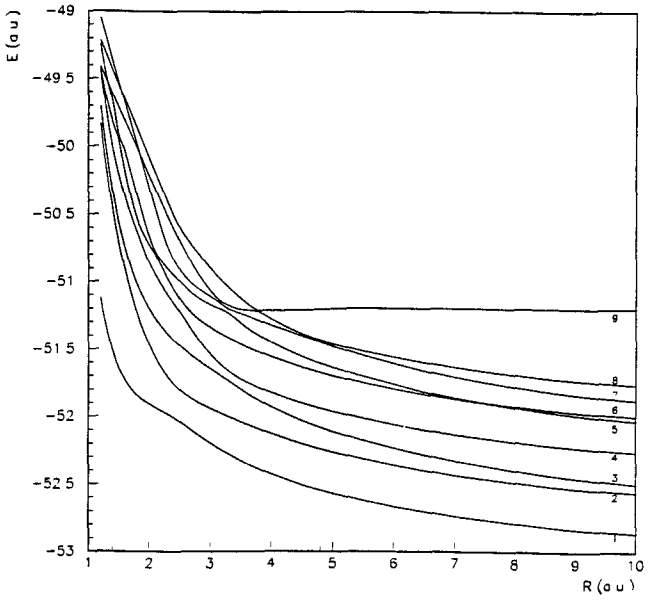

Figure 1: Adıabatic potential energy curves for the $^2\Sigma$ states of NHe^{4+}. Σ states dissociatıng to: 1-$\{N^{3+}(2^{-2})^1S+He^+(1s)^2S\}$; 2-$\{N^{3+}(2s2p)^3P+He^+(1s)^2S\}$, 3-$\{N^{2+}(2s^22p)^2P+He^{2+}\}$; 4-$\{N^{3+}(2s2p)^1P+He^+(1s)^2S\}$; 5-$\{N^{2+}(2s2p^2)^2D+He^{2+}\}$; 6- $\{N^{3+}(2p^2)^1D+He^+(1s)^2S\}$; 7-$\{N^{2+}(2s2p^2)^2S+He^{2+}\}$; 8-$\{N^{3+}(2s^2)^1S+He^+(1s)^2S\}$; 9-$\{N^{4+}(2s^2)^2S+He(1s^2)$

Furthermore, our calculation exhibits an intricate interaction region observable

for 3.44-3.6 *a.u.* inter-atomic distances corresponding to avoided crossings between the $\{N^{3+}(2p^2)^1S + He^+\}$, $\{N^{2+}(2s2p^2)^2S + He^{2+}\}$ and $\{N^{2+}(2s2p^2)^2D + He^{2+}\}$ levels as well as the $\{N^{3+}(2p^2)^1D + He^+\}$channel by means of the long range crossing between $\{N^{2+}(2s2p^2)^2D + He^{2+}\}$ and $\{N^{3+}(2p^2)^1D + He^+\}$ which has been considered as quasi-adiabatic since it occurs at a relatively long range inter-nuclear distance.

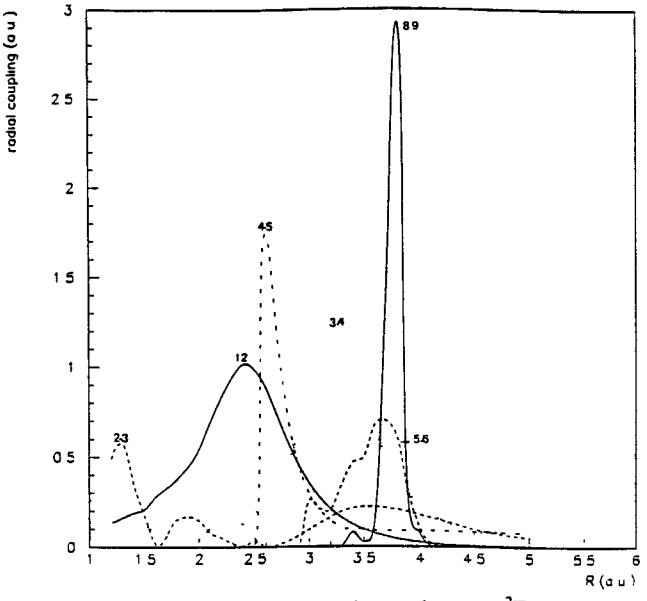

Figure 2: Non-adiabatic radial coupling matrix element between $^2\Sigma$ states of NHe^{4+} (same labels as in figure 1)

Such potential energy curves show evidence of a very complex charge exchange mechanism, including both single and double capture channels, which might be described by an extensive collision treatment. Such a complete treatment appears difficult to handle, thus we have considered here only the main capture channels in order to be compared to the experimental results.

III- COLLISION DYNAMICS

The collision dynamics has been treated by a semi-classical method using the *EIKONXS* program [13] based on an efficient propagation method in the 1-50 *keV* laboratory energy range, in order to be compared to the experimental data, in particular the state selective translation energy spectroscopy experiment of McLaughlin *et a.l.* [1]. The total and partial cross sections are presented in figure 3. As far as the single electron capture process is concerned, our calculated values are in satisfactory agreement with the experimental results of Iwai *et a.l.* [4], and to some extent, with those of Hoeksra *et a.l.* [3] which are somewhat lower for all

collision energies. As the results of McLaughlin *et a.l.* [1]are calibrated on the total single capture cross sections of Hoekstra [3], their partial cross sections should then be shifted to lower values. It is clear from our calculation, in accordance with the observation of McLaughlin *et a.l.* [1], that the single electron capture process is dominant on the $\{N^{3+}(2p^2)^1S + He^+\}$ product channel. Our calculations show also in creasing partial cross sections on $\{N^{3+}(2p^2)^1D + He^+\}$and $\{N^{3+}(2s^22p)^1P + He^+\}$channels with increasing collision energy. Nevertheless, our values are markedly lower than those of McLaughlin *et* a.l.[1] and could hardly account for the peaks B and C at 28 *keV.*

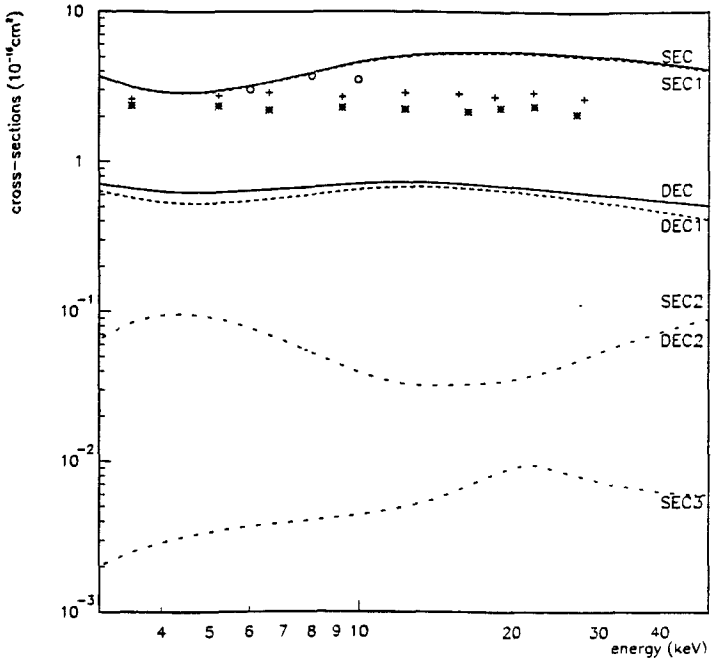

Figure 3: Total and partial cross-sections of single and double electron capture with respect to laboratory energies. — SEC : total cross section of single electron capture; — DEC: total cross section of double electron capture; - - - SEC1: total cross section on $N^{3+}(^1S)+ He^+$; SEC2 . partial cross section on $N^{3+}(^1S)+ He^-$, -- SEC3: partial cross section on $N^{3+}(^1P)+ He^+$; - - - DEC1: partial cross section on $N^{2+}(^2S)+ He^{2+}$;-- DEC2: partial cross section on $N^{2+}(^2D)+ He^{2+}$; o: total SEC (Iwai *et al.* [4]); +: total SEC (Hoekstra *et al.* [3]) ; *: total DEC (Hoekstra *et al.* [3])

The present figure exhibits also the importance of double electron capture levels, in particular the $\{N^{3+}(2s^22p)^2S + He^{2+}\}$channel which could not be neglected in the consideration of the $N^{4-} + He$ charge transfer process. Our total double electron capture cross sections are necessarily significantly lower than the measured values of Hoekstra *et al.*[3] because, in this study, only the $N^{2+}(2s^22p)$ and $N^{2+}(2s2p^2)$ double capture levels have been considered since we were

essentially interested in the single electron capture process in relation with the experiment of McLaughlin *et al.*[1]. The $N^{2+}(2p^3)$ and even the $N^{2+}(2s^2 3l)$ or $N^{2+}(2l2l'3l'')$ levels should be taken into account in a complete approach of the charge transfer reaction. Such a calculation might be considered as a first approach of this very complex collision system which provides however a first insight into the N^{4+} + *He* charge transfer mechanism and improves markedly the MLZ approach. A complete calculation has to take account of an even greater number of levels, in particular double capture channels which have been shown to be in tight interaction with the single capture channels and are necessary to have an accurate interpretation of both single and double electron capture mechanism, as well as excited *He* levels intervening in the single capture process with target excitation $N^{4+} + He \rightarrow N^{3+} + He^{+}(2l)$ [3]. Further calculations are in progress.

REFERENCES

[1] T. K. McLaughlin, H. Tanuma, J. Hodgkinson, R. W. McCullough and H. B. Gilbody, J. Phys. B 26, 3871 (1993)

[2] K. Okuno, K. Soejima and Y. Kaneko, Nucl. Instr. Meth. Phys. Res. B 53, 387 (1991)

[3] R. Hoekstra, F. J. De Heer and H. Winter, Nucl. Instr. Meth. Phys. Res. B 23, 104 (1987)

[4] T. Iwai, Y. Kaneko, M. Kimura, K. Kobayashi, S. Ohtani, K. Okuno, S. Takagi, H. Tawara and S. Tsurubushi, Phys. Rev. A 26, 105 (1992)

[5] C. Moore in " Atomic Energy Levels" (Washington, DC:US Govt Printing Office 1952)

[6] MOLPRO (version 98.1) is a package of *ab initio* programs written by H. J. Werner and P. Knowles with contribution from J. Almlöf, R. D. Amos, A. Berning, D. L. Cooper, M. J. O. Deegan, A. J. Dobbyn, F. Eckert, S. T. Elbert, C. Hampel, R. Lindh, A. W. Lloyd, W. Meyer, A. Nicklass, K. Peterson, R. Pitzer, A. J. Stone, P. R. Taylor, M. E. Mura, P. Pulay, M. Schütz, H. Stoll and T. Thorsteinsson

[7] H. J. Werner and P. J. Knowles, J. Chem. Phys. 82, 5053 (1985)

[8] P. J. Knowles and H. J. Werner, Chem. Phys. Lett. 115, 259 (1985)

[9] A. K. Wilson, T. V. Mourik and T. H. Dunning Jr., THEOCHEM 388, 339 (1997)

[10] B. H. Lengsfield, P. Saxxe and D. Y. Yarkony, J. Chem Phys. 81, 4549 (1994)

[11] M. Page, P. Saxe, G. F. Adams and B. H. lengsfield, J. Chem. Phys. 81, 434 (1984)

[12] M. C. Bacchus-Montabonnel, Phys. Rev. A 46, 217 (1992)

[13] R. J. Allan, C. Courbin, P. Salas and P. Wahnon, J. Phys. B 26, L461 (1990)

Intermediate Hamiltonian Fock-space coupled-cluster method

Arie LANDAU, Ephraim ELIAV, and Uzi KALDOR
School of Chemistry, Tel Aviv University, 69978 Tel Aviv, Israel

Abstract

An intermediate Hamiltonian Fock-space coupled cluster method is introduced, based on the formalism developed by Malrieu and coworkers in the context of perturbation theory. The method is designed to make possible the use of large P spaces while avoiding convergence problems traceable to intruder states, which often beset multi-reference coupled cluster approaches. The essence of the method is the partitioning of P into a main P_m and an intermediate P_i serving as buffer, with concomitant definition of two types of wave and excitation operators While Malrieu's formulation eliminated $P_m \rightarrow P_i$ transitions up to third order only, the requirement introduced here that $P_m \rightarrow Q$ amplitudes of the two excitation operators be equal makes possible an all-order method without these dangerous transitions. This requirement is shown to be satisfied for sufficiently large P_i. Application to atomic barium and radium yields converged results for a large number of states not accessible by traditional Fock-space coupled cluster. Moreover, states calculated by both methods exhibit better accuracy (by a factor of 2–5) in the intermediate Hamiltonian approach. Excellent agreement with experiment (better than 0.01 eV) is obtained for the electron affinities of alkali atoms, and excitation energies of Xe and Rn, not accessible by the traditional coupled-cluster Fock-space method, are calculated showing high accuracy.

ADVANCES IN QUANTUM CHEMISTRY VOLUME 39

0065-3276/01 $35 00

1 Introduction

The coupled-cluster (CC) method is one of the most powerful tools for atomic and molecular calculations [1]. The basic idea of the method [2] involves an exponential wave operator Ω, which takes the zero-order wave function Ψ_0 into the exact wave function Ψ,

$$\Omega|\Psi_0\rangle = |\Psi\rangle, \qquad \Omega = \exp S, \tag{1}$$

where S is the excitation operator. Intermediate normalization is usually assumed,

$$\langle\Psi_0|\Psi\rangle = 1. \tag{2}$$

This formulation is adequate for single reference systems, which may be described approximately by one determinant. In other cases, such as most excited states or near curve crossings, a multireference method is required [3]. Multireference schemes involve partitioning the eigenfunctions of the zero-order Hamiltonian H_0 are into a model space P and its complementary Q,

$$P = \sum_{\alpha\in P} |\alpha\rangle\langle\alpha|, \qquad Q = 1 - P. \tag{3}$$

The goal is to construct an effective Hamiltonian in P, the matrix elements of which include the approximate contribution of Q. The eigenvalues of the effective Hamiltonian give the energies of states with major components in P.

The most successful multireference coupled cluster method has been the Fock-space (FSCC) approach [3], which provides highly accurate transition energies and other atomic and molecular properties [4, 5]. The Fock-space scheme starts from a reference determinant, usually closed-shell, and reaches the states of interest by adding and/or removing electrons to that determinant The method is valence universal, meaning that one S operator is used for a manifold of states with different numbers of valence electrons. Starting from the reference determinant, S is written as a sum of sector excitation operators $S^{(n,m)}$, describing states with n valence holes (electrons removed from the reference) and m valence particles (electrons added),

$$S = \sum_n \sum_m S^{(n,m)}. \tag{4}$$

Haque and Mukherjee [6] showed that the partitioning allows for partial decoupling of the Fock-space CC equations. The equations for $S^{(n,m)}$ involve only $S^{(k,l)}$ elements with $k \leq n$ and $l \leq m$, so that the very large system of

nonlinear coupled equations separates into smaller subsystems, solved consecutively. The equations for $S^{(0,0)}$ are iterated to convergence, $S^{(1,0)}$ and $S^{(0,1)}$ are then solved using the known $S^{(0,0)}$, and so on.

After the equations are solved in a particular sector, the effective Hamiltonian in that sector (assuming intermediate normalization) is constructed by

$$H_{\text{eff}} = P\Omega HP \tag{5}$$

The eigenvalues of H_{eff} give the correlated energies of states in that sector relative to the correlated energy of the reference determinant

The coupled cluster equations in each sector are solved iteratively Convergence of the iterations is enhanced by having a large energy gap (and weak interaction) between the P and Q subspaces. A partitioning satisfying these conditions cannot always be affected, in particular if the simpler and more satisfactory complete model space method is employed, with P comprising all possible distributions of the valence electrons in a selected set of valence orbitals. This situation often leads to intruder states [7–11], Q-space states which couple strongly with P states and cause large excitation amplitudes and difficult or no convergence. The problem may sometimes be overcome by introducing an incomplete model space [8, 9, 12–15], which includes only the most strongly interacting state functions and leaves out potential intruders This is not always possible; in addition, an incomplete space makes the method more complicated and is not always compatible with connectivity in the intermediate normalization formalism [13, 16–18].

Malrieu et al [11], working in the framework of low-order degenerate perturbation theory, realized that convergence difficulties and intruder states result from the strict requirements imposed on the effective Hamiltonian, namely that *all* its roots must approximate eigenvalues of the real Hamiltonian H, and its eigenvectors must be the projections on P of the corresponding eigenvectors of H. This observation led them to propose a method for the construction of an intermediate Hamiltonian, where only some eigenvalues are required to approximate those of the real H. Instead of the traditional partitioning of the determinant space into P and Q subspaces, Malrieu introduced three subspaces: the main space P_m, the intermediate P_i, and the complementary Q The corresponding operators satisfy

$$P_m + P_i = P \ , \qquad P + Q = 1 \ . \tag{6}$$

The equations for the wave operator are now solved in two steps. At first, only $P_m \to Q$ excitations are included, which (for adequate P_i) should be relatively easy, since P_i serves as a buffer between P_m and Q, assuring a comfortable energy separation and avoiding the occurrence of intruder states. Next, another

set of equations is solved, involving another (pseudo)wave operator describing all $P \rightarrow Q$ excitations. This is not an exact wave operator because it is required to generate exact energies and P projections only for P_m states. The relevant equations include an arbitrary energy constant, which may be chosen so as to expedite convergence. This separation has been achieved by Malrieu et al. [11] up to third order only; $P_m \rightarrow P_i$ excitations appear in fourth and higher orders of the perturbation.

The intermediate Hamiltonian method is extended here to the Fock-space coupled cluster scheme. While Malrieu et al. [11] assumed exact degeneracy of the model space, we allow more general spaces; and, more important, instead of the perturbation theory framework, the method presented here is an all-order intermediate Hamiltonian Fock-space coupled-cluster (IHFSCC) scheme. While the coupled cluster method may be regarded as an infinite-order summation of perturbation terms, an intermediate Hamiltonian coupled cluster scheme cannot be obtained as a straightforward extension of Malrieu's method, since the $P_m \rightarrow P_i$ excitations appearing in fourth and higher orders would create divergences. The formalism derived below avoids these dangerous excitations altogether. As will be shown in the next section, the crucial step in avoiding these excitations involves the equality of the two wave operators discussed above for $P_m \rightarrow Q$ excitations. Other intermediate Hamiltonian schemes have been described in the framework of coupled-cluster [19,20] and configuration interaction [21] approaches. A similar scheme has been proposed by Heully et al. [22] in the framework of quasidegenerate perturbation theory. The self-consistent quasidegenerate coupled-cluster method of Hoffmann and Khait [23] uses similar partitioning of the function space.

The aim of the IHFSCC method is to avoid intruder states, which slow or even prevent convergence, while employing large *complete* model spaces. Completeness of the model space allows the use of the simple and convenient intermediate normalization, with finite expansion of the cluster equation and straightforward connectivity and energy extensivity The large model space improves the description of the wave function and is expected to yield more accurate energies and other properties; higher excitation energies, not accessible by traditional CC methods, may be obtained.

The basic coupled-cluster equations, following Lindgren's approach, have the form [24]

$$Q[S, H_0]P = Q\left(V\Omega - \chi PV\Omega\right)_{\text{conn}} P \,, \tag{7}$$

where the Hamiltonian is partitioned in the usual way,

$$H = H_0 + V, \tag{8}$$

$$\Omega = 1 + \chi = \{\exp S\} \tag{9}$$

is the wave operator, S is the excitation or cluster operator, and the curly brackets indicate normal order with respect to the reference determinant. The left-hand-side of (7) gives rise to denominators of the type $QH_0 - PH_0$, which may be small if the P and Q spaces are not well separated, leading to convergence problems. The crux of the intermediate Hamiltonian method is the definition of the intermediate space P_i, which serves as a buffer between P_m and Q, eliminating small denominators. Correlation is treated in two stages dynamic correlation, due to Q-space determinants, is included by the wave operator; non-dynamic correlation, contributed by the P space, comes in by diagonalizing the intermediate Hamiltonian in the whole model space P, which includes both the main P_m and intermediate P_i. The cluster operators and the intermediate Hamiltonian (which plays the role of the effective Hamiltonian in FSCC) are connected if P_m and P are complete model spaces, so that calculated energies are size-extensive [18].

The IHFSCC method has been described briefly in a recent publication [25], together with a pilot application to excited states of Sc^+. A full presentation is given in the next section, followed by applications to a variety of atomic systems, with comparisons to experimental and FSCC values.

2 Method

2.1 Wave operators and Bloch-type equations

The complete model space P is partitioned into a main space P_m of dimension N_m and an intermediate space P_i of dimension N_i. The orthogonal space is $Q = 1 - P$, with dimension N_q. The goal is to obtain an intermediate Hamiltonian H_I in P with N_m exact solutions of the real Hamiltonian [11],

$$H_I P|\Psi_m\rangle = E_m P|\Psi_m\rangle \,, \tag{10}$$

where Ψ_m are the eigenstates of the exact Hamiltonian with the largest components in P_m,

$$H|\Psi_m\rangle = E_m|\Psi_m\rangle \,. \tag{11}$$

It should be noted that $P|\Psi_i\rangle$ and the corresponding E_i are not required to be the exact eigenfunctions and eigenvalues of H_I; they are approximations, which may be more or less accurate. The requirements on H_I are thus less stringent than those of the FSCC effective Hamiltonian, which is expected to yield maximal information on all the states of P. This flexibility contributes

to an easier convergence of the CC iterations. The diagonalization of H_I in the whole P is designed to include non-dynamic correlation coming from P_m as well as P_i states.

Two wave-like operators are defined [11] and expanded in coupled-cluster normal-order exponential anzätze [24]. $\Omega = 1 + \chi$ is a standard wave operator in P_m,

$$\Omega P_m|\Psi_m\rangle = \{\exp S\}P_m|\Psi_m\rangle = |\Psi_m\rangle \ , \tag{12}$$

satisfying the wave equation

$$(Q + P_i)\Omega H\Omega P_m = (Q + P_i)H\Omega P_m. \tag{13}$$

Equation (13) actually represents $(N_i+N_q)\times N_m$ equations for the $(Q+P_i)\Omega P_m$ amplitudes It should be noted that the effective Hamiltonian corresponding to Ω, $P_m H\Omega P_m$, yields the eigenvalues for Ψ_m states only. The wave equation (13) leads upon projection by Q to the coupled cluster equation

$$Q[S, H_0]P_m = Q(\overline{V\Omega} - \overline{\chi P_m V\Omega})P_m, \tag{14}$$

where the bar indicates summation over connected terms only.

Another operator, $R = 1+\Delta$, is defined in the whole P. The corresponding coupled-cluster ansatz is

$$RP|\Psi_m\rangle = \{\exp T\}P|\Psi_m\rangle = |\Psi_m\rangle. \tag{15}$$

It should be emphasized that the last equation, and therefore all equations below derived from it, apply when operating on $|\Psi_m\rangle$ but not necessarily on $|\Psi_i\rangle$. This feature distinguishes R from a bona fide wave operator. Using intermediate normalization we get

$$\Omega = \Omega P_m = P_m + (Q + P_i)\chi P_m, \qquad \Omega^2 = \Omega, \tag{16}$$

and

$$R = RP = P + Q\Delta P, \qquad R^2 = R. \tag{17}$$

The intermediate Hamiltonian has the form

$$H_I = PHRP \ . \tag{18}$$

Using (11) and (15), it is easily seen that H_I of (18) satisfies (10):

$$H_I P|\Psi_m\rangle = PHRP|\Psi_m\rangle = PH|\Psi_m\rangle = E_m P|\Psi_m\rangle \ . \tag{19}$$

To find the energies one has to determine the amplitudes of the cluster operator QTP.

Operator relations between Δ and χ can be derived using equations (12,15)

$$RP|\Psi_m\rangle = R\Omega P_m|\Psi_m\rangle = |\Psi_m\rangle = \Omega P_m|\Psi_m\rangle, \tag{20}$$

which leads to

$$R\Omega P_m = \Omega P_m. \tag{21}$$

Using (16,17) and left-projecting unto Q, we get

$$Q\Delta P_i\chi P_m = Q(\chi - \Delta)P_m. \tag{22}$$

The system (22) includes $N_m \times N_q$ equations The quantities to be determined are $Q\Delta P_i$ and $Q\Delta P_m$, with a total number of $N_q \times (N_m + N_i)$. This leaves $N_i \times N_q$ degrees of freedom, which may be used, for example, to choose $Q\Delta P_i$ at will, after which $Q\Delta P_m$ may be found from (22). This freedom is used in a different way below.

Starting from the intermediate Hamiltonian equation (10) multiplied on the left by Ω and using (11,12,15), one gets

$$\Omega H_I P|\Psi_m\rangle = \Omega E_m P|\Psi_m\rangle = E_m\Omega P_m|\Psi_m\rangle = E_m|\Psi_m\rangle = H|\Psi_m\rangle = HRP|\Psi_m\rangle,$$

which together with (18) yields the wave equation

$$Q\Omega HRP|\Psi_m\rangle = QHRP|\Psi_m\rangle. \tag{23}$$

Equation (23) is a system of dimension $N_m \times N_q$. The $N_i \times N_q$ degrees of freedom discussed above are now used to ensure that a similar equation is satisfied for $|\Psi_i\rangle$ states too,

$$Q\Omega HRP|\Psi_i\rangle = QHRP|\Psi_i\rangle. \tag{24}$$

It is now possible to combine (23) and (24) in an operator relation [11]

$$Q\Omega HRP = QHRP. \tag{25}$$

This is a wave-like equation. A real wave equation would have R rather than Ω in (25).

2.2 Coupled cluster equations

Using arguments similar to those of Lindgren [26], it is shown in appendix A that equation (25) may be written in connected form

$$Q\overline{HR}P = Q\overline{\chi HR}P. \tag{26}$$

The last equation may be generalized by introducing an arbitrary energy parameter E,

$$Q\overline{(E-H)R}P = Q\overline{\chi(E-H)R}P. \tag{27}$$

The solution R of (27) satisfies the basic equation (22). The partitioning (8) and the expressions (16) and (17) lead to

$$Q\overline{((E-H_0)R)}P - Q\overline{(VR)}P = Q\overline{\chi P_m(E-H_0-V)(P+Q\Delta P)}.$$

Assuming that H_0 is a one-body operator, and using the relation

$$Q(\overline{\chi P_m(E-H_0)(P+Q\Delta P)}) = QS(E-H_0)P_m,$$

the first cluster equation for the (n) sector of the Fock space is obtained,

$$(E-H_0)QT^{(n)}P = Q(S(E-H_0)P_m + \overline{(VR)} - \overline{(\chi P_m VR)})^{(n)}P. \tag{28}$$

Equation (26) yields

$$Q\overline{HR}P_m = Q\overline{\chi HR}P_m,$$

which may be rewritten as

$$QSH_0P_m - QH_0TP_m = Q(\overline{VR} - \overline{\chi P_m VR})P_m. \tag{29}$$

Starting again from (26), one gets

$$Q\overline{HRP_i\chi}P_m = Q\overline{\chi HRP_i\chi}P_m,$$

which gives

$$-QH_0\sigma P_m = Q(\overline{VRP_i\chi} - \overline{\chi P_m VRP_i\chi})P_m, \tag{30}$$

where σ is defined by

$$Q\sigma P_m \equiv Q\overline{\Delta P_i\chi}P_m. \tag{31}$$

Table 1: Dependence of $Q\sigma P_m$ on size of P_i. Test on Mg atom, with a $18s13p8d4f$ basis. Mg^{2+} is the reference state, $2s2p$ electrons are correlated, P_m includes all Mg determinants with $3s$, $4s$, $3p$, $4p$, and $3d$ electrons.

P_i orbitals	$Q\sigma P_m$ amplitudes
5–6s, 5p, 4d	$< 10^{-3}$
5–7s, 5–6p, 4–5d, 4f	$< 10^{-4}$
5–8s, 5–7p, 4–6d, 4–5f	$< 7 \cdot 10^{-6}$

It is shown in appendix B that this definition, together with (22), gives

$$Q\sigma P_m = Q(S - T)P_m. \tag{32}$$

The two equations (29) and (30) together give Eq. (14), confirming the consistency of using the available degrees of freedom to derive equation (25).

Relation (30) may be rewritten as the commutator relation

$$Q[\sigma, H_0]P_m = Q(\sigma H_0 + \overline{VRP_i\chi} - \overline{\chi P_m VRP_i\chi})P_m \tag{33}$$

The last equation shows that σ gets smaller as the intermediate space P_i becomes larger. The denominators coming from the left-hand side of the equation become large, because they involve energy differences between well-separated P_m and Q states, the interaction terms on the right-hand side are at least second-order in V, and always include products of $P_m \to P_i$ and $P_i \to Q$ interactions For a large P_i separating P_m and Q, both interactions cannot be large at the same time. P_i may therefore be chosen so that σ virtually vanishes, as we indeed found in test calculations (see Table 1). For $\sigma \to 0$, (32) gives

$$QSP_m \simeq QTP_m. \tag{34}$$

QTP_m in equation (29) may therefore be replaced by QSP_m, yielding the cluster equation for S, which in the (n) sector of the Fock space has the form

$$Q[S^{(n)}, H_0]P_m = Q(\overline{VQ_i\Omega} - \overline{\chi P_m VQ_i\Omega})^{(n)}P_m, \tag{35}$$

where $Q_i = 1 - P_i = Q + P_m$. It should be noted that Ω in (35) was obtained from R in (29) when QTP_m was replaced by QSP_m. No P_iSP_m elements will therefore appear in (35)

Equations (28) and (35) are the working equations of the intermediate Hamiltonian Fock-space coupled cluster method. Eq. (35) has the same form (and, consequently, the same diagrammatic expansion) as the conventional

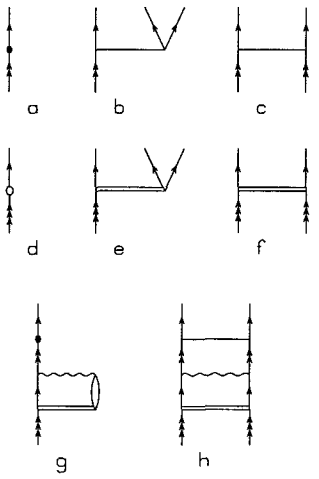

Figure 1: Examples of diagrams encountered in the IHFSCC formalism. Lines with single arrows are summed over hole or particle lines, lines with double arrows — over valence orbitals belonging to P_m, lines with triple arrows — over valence orbitals in P (P_m *and* P_i). Diagrams a–c come from Eq. (35) and involve S amplitudes only, with $P_m \rightarrow Q$ excitations (one-body S is denoted by a full circle, two-body S by a horizontal line) The other diagrams come from Eq. (28), with d–f involving T amplitudes only (denoted by an open circle and a double line for one-body and two-body amplitudes, respectively), while diagrams g and h mix S and T amplitudes. A wavy line represents the V interaction.

FSCC equation (7); the difference is that only QSP_m amplitudes, corresponding to $P_m \rightarrow Q$ excitations, are included in (35) (see Fig. 1(a,b,c)). Note that P_iSP_m terms, which appear in the initial equation (14) for Ω, have been eliminated. P_i serves as a buffer between P_m and Q, so that no intruder states can occur After (35) is converged, Eq. (28) is solved to find QTP (Fig 1(d,e,f)). Its diagrammatic structure is similar to that of (7) and (35), with some new diagrams coming from the QSP_m term. Notice that the last term of Eq. (28) involves the three spaces P_m, P, and Q, and care must be taken when evaluating the different terms (see examples in Fig. 1(g,h)).

The arbitrary energy E has to be chosen. It is conveniently expressed as

$$E = \sum_{i}^{\text{occ}} \epsilon_i + C \,, \tag{36}$$

where ϵ_i are orbital energies, and the summation is carried over all occupied orbitals C may be selected so that no small denominators appear in the

expansion In principle, the results do not depend on the constant C; in truncated coupled-cluster calculations this dependence does occur Previous calculations [25] show very weak dependence of converged energies on C over a broad range of values. changing C by several hundred hartree modified transition energies by a few wave numbers only. The major criterion for selecting C (or E) involves the convergence of the IHFSCC iterations The denominators in (28) are $(E - H_0)Q$; E should therefore fall outside the range of Q-space zero-order energies.

As mentioned above, the relations (28) and (35) are the working equations of the intermediate Hamiltonian coupled-cluster method. Since (28) includes S on the right-hand side, (35) is solved first for S, followed by solving (28) for T There is an apparent redundancy at this stage, since the $P_m \rightarrow Q$ excitations have already been evaluated at the first stage via QSP_m amplitudes, and are represented here again by the QTP_m amplitudes. Equation (34) shows that these two sets of amplitudes should be equal for the method to be valid, and the calculations provide an a posteriori check on this premise (see Table 1). Moreover, σ may be estimated from equation (31) by some low-order approach such as second-order perturbation theory, providing an a priori measure of the adequacy of the intermediate space P_i. It is worthwhile to note that an equation similar to (28) may be derived for the wave operator S in the usual CC method,

$$(E - H_0)QS^{(n)}P = Q(S(E - H_0)P_m + \overline{(V\Omega)} - \overline{(\chi P_m V\Omega)})^{(n)}P. \qquad (37)$$

Some tests have shown that the value of this equation for promoting convergence is limited, since the $E - H_0$ factor on the left-hand side which forms the denominators also multiplies S on the right-hand side.

After (28) has been solved, the intermediate Hamiltonian (18) is diagonalized in P to obtain the energies. It should be noted that the diagonalization yields energies for all P levels, however, levels with major components in P_m are expected to be calculated more accurately than levels heavily concentrated in P_i.

In common with many multireference methods, IHFSCC treats correlation in two stages: dynamic correlation is described by virtual excitation to Q-space determinants via the wave or cluster operator, while non-dynamic correlation comes in by diagonalizing the effective Hamiltonian. The distinction between the two kinds of correlation is, of course, somewhat arbitrary. The major advantage of the intermediate Hamiltonian scheme is making possible the use of much larger P spaces than other high-order many-body methods, accounting thereby for a larger part of correlation, and at the same time allowing convergence and avoiding intruders.

3 Applications

All applications described here were carried out in the framework of the relativistic four-component Dirac-Coulomb-Breit Hamiltonian. The self-consistent-field Dirac-Fock-Breit orbitals are first calculated [27], and correlation is then included by relativistic Fock-space coupled cluster with single and double excitations [5], either in the traditional or in the intermediate Hamiltonian form. The first pilot application of the IHFSCC method has been described in a recent publication [25]. The average error of the ionization potential and first twelve excitation energies of Sc^+ calculated by the traditional FSCC was 80 meV; IHFSCC gave an average error of 18 meV, four times smaller. Many states not obtainable by FSCC because of convergence difficulties, were readily available by the intermediate Hamiltonian method, with highly satisfactory results. The average error of the 32 energies of excitation to P_m states was 20 meV, with the largest error being 64 meV P_i states, which are not required by theory to be highly accurate, turned out rather well, with an average error of 69 meV and maximum error of 111 meV for 21 P_i states.

More recently, ionization potentials and a large number of excitation energies for the barium and radium atoms were calculated [28] and compared with previous FSCC work [29]. While convergence was difficult in the FSCC approach, requiring incomplete model spaces and yielding only a limited number of states, the intermediate Hamiltonian scheme gave many more states (including some low-lying radium states which have not been observed experimentally) and better accuracy, with an average error of 0.69% or 17 meV for 27 Ba excitation energies compared to 3.11% or 92 meV for FSCC, and a maximum error of 35 meV vs. 475 meV for FSCC. Similar levels of accuracy were obtained for radium [28]. In addition, many states which could not be calculated by the traditional FSCC method were obtained, including both P_m and P_i states. As expected, P_i energies were somewhat less accurate than P_m values; thus, the 21 Ra P_m states had an average error of 0.74% or 24 meV, whereas the average error for the seven P_i states for which experimental results [30,31] are available was 1.34% or 52 meV. The predictions for low-lying states which have not yet been observed are expected to have similar accuracy.

Another recent application involved an high-accuracy calculation of the electron affinities of the alkali atoms [32]. A large basis of $37s32p23d18f10g7h6i$ even-tempered Gaussian-type orbitals [33] was used, and the positive M^+ ion served as reference. Traditional FSCC calculations for the M^- anion converged only when ns was the sole valence orbital and the P space included just the ns^2 determinant. IHFSCC calculations were carried out with P_m comprising all determinants with two electron added to M^+ in the lowest four unoccupied s, three p, three d orbitals, or one f orbitals; P_i included, in addition,

Table 2 Electron affinities of alkali atoms (meV)

Atom	Expt.	FSCC	IHFSCC
K	501	525	510
Rb	486	519	494
Cs	472	516	480
Fr	(492±2%)	542	495

occupations in three more s, three p, three d and three f orbitals

The calculated electron affinities are compared with experiment [34] in Table 2 No experimental value is available for Fr, and we quote the recent semiempirical result of Bahrim and Thumm [35]. Excellent agreement with experiment (better than 0.01 eV) is obtained by IHFSCC, which is again 3–5 times more accurate than traditional FSCC.

All the applications reported above are in the two-particle sector, involving the addition of two electrons to the closed-shell reference state. Other applications have been carried out in the one-hole one-particle sector, where an electron is excited from an occupied to a virtual orbital. Many excitation energies have thus been obtained for the xenon and radon atoms. The average error for 18 $5p \to 6s$, $5p \to 6p$, and $5p \to 5d$ excitation in Xe was 0 90% or 90 meV, with similar accuracy obtained for Rn. These results are remarkable, since the traditional FSCC does not converge for *any* choice of valence holes and particles, so that no excitation energies can be obtained.

4 Summary and conclusion

An intermediate Hamiltonian Fock-space coupled-cluster method has been developed. The crucial step in going from Malrieu's formulation, which had $P_m \to P_i$ transitions in fourth and higher orders, to an all-order method eliminating these dangerous small-denominator transitions altogether, is equation (34), requiring that $P_m \to Q$ amplitudes of the two excitation operators S and T be equal. This requirement is satisfied for sufficiently large P_i. The partitioning of the function space into a main space P_m, an intermediate P_i and a complementary Q allows convergence of the CC iterations for much larger model spaces than before. This makes possible calculations for states which were not accessible by CC methods, and improves the accuracy for states which were accessible. While FSCC calculations for the Ba and Ra atoms could be converged for a limited number of states only, and even that required resorting

to incomplete model spaces, IHFSCC yielded a very large number of states, including some low-lying levels which have not yet been observed experimentally. The accuracy for levels obtainable by FSCC was improved by a factor of 2–5. Electron affinities of alkali atoms were reproduced to within 0.01 eV, and very good results were obtained for excitation energies of Xe and Rn, which are not accessible at all by the traditional FSCC approach. The intermediate Hamiltonian method shows promise of providing more and better results where other coupled cluster schemes are less successful.

Acknowledgments

Most of the results reported were calculated with the collaboration of Professor Yasuyuki Ishikawa. The authors are indebted to Dr. Leszek Meissner for helpful correspondence. The research reported above was supported by the Israel Science Foundation and the U.S.-Israel Binational Science Foundation.

Appendix A

Equation (25) may be written (ignoring projections) as

$$HR = \Omega HR. \tag{A.1}$$

Using Wick's theorem, the left-hand side of this equation may be written as [26]

$$HR = \{\overline{HR} \times R\}, \tag{A.2}$$

and the right-hand side is

$$\begin{aligned} \Omega HR &= \{\Omega HR\} + \{\overline{\chi \overline{H} R}\} + \{\Omega \overline{\overline{H} \Delta}\} + \{\overline{\chi \overline{H} \Delta}\} \\ &= \{H \times \Omega R\} + \{\overline{\chi H} \times \Omega R\} + \{\overline{H\Delta} \times \Omega R\} + \{\overline{\chi H \Delta} \times \Omega R\} \\ &= \{\overline{\Omega HR} \times \Omega R\}, \end{aligned} \tag{A.3}$$

where the notation in the first line describes contraction. The equations above yield

$$\{\overline{HR} \times R\} = \{\overline{\Omega HR} \times \Omega R\}. \tag{A.4}$$

The different terms resulting from the multiplications in (A 4) are linearly independent, and the connected parts may therefore be compared, giving

$$\overline{HR} = \overline{\Omega HR}, \tag{A.5}$$

confirming Eq. (26)

Appendix B

Equation (22) gives

$$Q\Delta P_m + Q\Delta P_i\chi P_m = Q\chi P_m \tag{B.1}$$

Applying Wick's theorem and the exponential ansatz for the operators gives [26]

$$Q\Delta P_i\chi P_m = \{Q\Delta P_i\chi P_m\} + \{\overbrace{Q\Delta P_i\chi P_m}\} \tag{B.2}$$

$$\{\overbrace{Q\Delta P_i\chi P_m}\} = \sum_{m,n=1} \frac{1}{m!n!}\{\overbrace{QT^m P_i S^n P_m}\} \tag{B.3}$$

The contracted part may be separated into terms composed of products of one, two, ... , connected clusters, all multiplied by the same disconnected operator The term with one connected cluster is

$$\left\{\sum_{m,n=1}\frac{1}{m!n!}\sum_{r,s=1}\binom{m}{r}\binom{n}{s}Q\overbrace{\{T^r\}P_i\{S^s\}}P_m Q\{T^{m-r}\}P_i\{S^{n-s}\}P_m\right\} =$$

$$\left\{\sum_{r,s=1}\frac{1}{r!s!}Q\overbrace{\{T^r\}P_i\{S^s\}}P_m\sum_{m,n=1}\frac{1}{(m-r)!(n-s)!}Q\{T^{m-r}\}P_i\{S^{n-s}\}P_m\right\} =$$

$$\{Q\sigma P_m(1+Q\Delta P_i\chi P_m)\},$$

where the definition (31) is used. The terms with two connected clusters sum up in a similar way to $\{\frac{1}{2}(Q\sigma P_m)^2(1+Q\Delta P_i\chi P_m)\}$, and all clusters finally give

$$\{\overbrace{Q\Delta P_i\chi P_m}\} = \exp(Q\sigma P_m - 1)(1 + Q\Delta P_i\chi P_m)$$

Together with (B.1) and (B.2), we get

$$Q\Delta P_m + \{Q\Delta P_i\chi P_m\} + \{\exp(Q\sigma P_m - 1) + \exp(Q\sigma P_m)(Q\Delta P_i\chi P_m)\} = Q\chi P_m \tag{B.4}$$

As in the derivation leading to (A.5), the connected terms of (B.4) must be equal, giving $Q\sigma P_m = Q(S-T)P_m$, which is equation (32).

References

[1] For a recent review see R. J. Bartlett, in *Modern Electronic Structure Theory* edited by D. R Yarkony, (World Scientific, Singapore, 1995) Vol 2, p. 1047.

[2] J. Hubbard, *Proc. R. Soc. London Ser. A* **240**, 539 (1957); *ibid.* **243**, 336 (1958); F. Coester, *Nucl. Phys.* **7**, 421 (1958); F. Coester and H. Kümmel, *Nucl. Phys.* **17**, 477 (1960); H. Kümmel, K. H. Lührmann, and J. G. Zabolitzky, *Phys. Rev.* **36**, 1 (1978); J. Čížek, *J. Chem. Phys.* **45**, 4256 (1966); *Adv. Chem. Phys.* **14**, 35 (1969); J. Paldus, J. Čížek, and I. Shavitt, *Phys. Rev. A* **5**, 50 (1972); J. Paldus, *J. Chem. Phys.* **67**, 303 (1977); B. G. Adams and J Paldus, *Phys. Rev. A* **20**, 1 (1979); I. Lindgren, *Int. J Quantum Chem. Symp.* **12**, 33 (1978); H. Kümmel, *Theor. Chim. Acta* **80**, 81 (1991); J. Čížek, *Theor. Chim. Acta* **80**, 91 (1991).

[3] For a review of multi-reference CC methods see D. Mukherjee and S. Pal, *Advan Quantum Chem* **20**, 292 (1989).

[4] For a review of nonrelativistic FSCC applications see U. Kaldor, *Theor. Chim. Acta* **80**, 427 (1991).

[5] For reviews of relativistic FSCC see U. Kaldor, in *Recent Progress in Many-Body Theories*, Vol. 4, E. Schachinger, H. Mitter, and M. Sormann, eds. (Plenum, New York, 1995), p. 135; U. Kaldor, *Few-Body Systems Suppl.* **8**, 68 (1995); Y. Ishikawa and U. Kaldor, in *Computational Chemistry: Review of Current Trends*, edited by J. Leszczynski (World Scientific, Singapore, 1996), Vol. 1, p. 1; U. Kaldor, in *Recent Advances in Coupled-Cluster Methods*, edited by R. J. Bartlett (World Scientific, Singapore, 1997) p. 125; U. Kaldor and E Eliav, *Advan. Quantum Chem.* **31**, 313 (1998).

[6] A Haque, Ph.D. Thesis, Calcutta University (1983); A. Haque and D. Mukherjee, *J. Chem. Phys.* **80**, 5058 (1984).

[7] T H. Schucan and H.A. Weidenmüller, *Ann. Phys.* **73**, 108 (1972); *Ann. Phys.* **76**, 483 (1972).

[8] G. Hose and U. Kaldor, *J. Phys. B* **12**, 3827 (1979); G. Hose and U Kaldor, *Phys. Scripta* **21**, 357 (1980).

[9] U. Kaldor, *Phys. Rev. A* **38**, 6013 (1988).

[10] D. Hegarty and M.A. Robb, *Mol. Phys.* **37**, 1455 (1979); H. Baker, M.A. Robb, and Z Slattery, *Mol. Phys.* **44**, 1035 (1981).

[11] J.-P. Malrieu, Ph Durand, and J.-P. Daudey, *J. Phys. A* **18**, 809 (1985)

[12] B. Jeziorski and H.J. Monkhorst, *Phys. Rev. A* **24**, 1668 (1981).

[13] I. Lindgren, *Phys. Scripta* **32**, 291, 611 (1985)

[14] L Meissner, S. A. Kucharski and R. J Bartlett, *J. Chem. Phys* **91**, 6187 (1989)

[15] L. Meissner and R J. Bartlett, *J. Chem Phys.* **92**, 561 (1990).

[16] B.H. Brandow, in: C.E. Dykstra (Ed.), *Advanced Theories and Computational Approaches to the Electronic Structure of Molecules*, Reidel, Dortrecht, 1984.

[17] D Mukherjee, *Chem. Phys. Lett.* **125**, 207 (1986).

[18] I Lindgren and D. Mukherjee, *Phys. Rep.* **151**, 93 (1987)

[19] D Mukhopadhyay, B Datta, and D. Mukherjee, *Chem. Phys Lett* **197**, 236 (1992)

[20] L. Meissner, *J. Chem. Phys.* **108**, 9227 (1998).

[21] J.-P. Daudey, J.-L. Heully, and J.-P. Malrieu, *J. Chem Phys* **99**, 1240 (1993).

[22] J.-L Heully, S Evangelesti, and Ph. Durand, *J. Phys. II* **5**, 63 (1995).

[23] M R. Hoffmann and Y. G. Khait, *Chem. Phys. Lett.* **311**, 372 (1999)

[24] I. Lindgren and J. Morrison, *Atomic Many-Body Theory*, 2nd edition, Springer-verlag, Berlin, 1986.

[25] A Landau, E. Eliav, and U. Kaldor, *Chem. Phys. Lett.* **313**, 399 (1999)

[26] I Lindgren, *J. Phys. B* **24**, 1143 (1991), appendix.

[27] Y. Ishikawa, R.C. Binning, Jr., and K.M Sando, *Chem. Phys. Lett.* **101**, 111 (1983), Y. Ishikawa, R. Barrety, and R. C. Binning, Jr., *Chem. Phys Lett.* **121**, 130 (1985), Y. Ishikawa, *Phys. Rev. A* **42**, 1142 (1990); Y Ishikawa and H. M. Quiney, *Phys. Rev. A* **47**, 1732 (1993).

[28] A. Landau, E. Eliav, Y. Ishikawa, and U. Kaldor, *J. Chem. Phys.* **113**, 9905 (2000).

[29] E. Eliav, U. Kaldor, and Y. Ishikawa, *Phys. Rev. A* **53**, 3050 (1996)

[30] C.E. Moore, *Atomic Energy Levels*, Natl. Bur Stand. (U S.) Circ No. 467, U S. GPO, Washington, DC, Vol I, 1948.

[31] C.E. Moore, *Ionization Potentials and Ionization Limits*, Natl. Bur. Stand. (U.S.) NSRDS-NBS 34, U.S. GPO, Washington, DC, 1970

[32] A. Landau, E. Eliav, Y. Ishikawa, and U. Kaldor, to be published.

[33] G. L Malli, A.B.F. Da Silva, and Y. Ishikawa, *Phys. Rev. A* **47**, 143 (1993)

[34] H. Hotop and W. C. Lineberger, *J. Phys. Chem. Ref Data* **4**, 539 (1975); *ibid.* **14**, 731 (1985).

[35] C. Bahrim and U. Thumm, *Phys. Rev A* **61**, 022722 (2000).

FULL CI SOLUTION OF PERTURBATIVE EQUATIONS

Gian Luigi Bendazzoli † and Stefano Evangelisti †◇

† Dipartimento di Chimica Fisica ed Inorganica, Università di Bologna, Italy
◇ Laboratoire de Physique Quantique, Université Paul Sabatier, Toulouse, France

Table of contents

ADVANCES IN QUANTUM CHEMISTRY, VOLUME 39

0065-3276/01 $35.00

1 Introduction

The problem we address in this paper is the computation of second and third order properties, static and dynamic by solving, at the Full CI level, inhomogeneous equations of perturbation theory like the following:

$$(\hat{H} - E_0 \pm \hbar\omega)\psi_{\pm} = \left(< \psi_0|\hat{V}|\psi_0 > -\hat{V}\right)\psi_0 \tag{1}$$

where ψ_0 is an eigenstate of the molecular hamiltonian $\hat{H}$ with energy E_0 and $\hat{V}$ is a perturbation operator.

Equation (1) arises e.g. from a perturbation theory treatment of a molecule in an external alternating electric field of frequency ω. The latter gives rise to a time dependent harmonic perturbation of the type:

$$\hat{V}(t) = -\frac{1}{2}\mathbf{r}\cdot\mathcal{E}\left[e^{-\imath\omega t} + e^{\imath\omega t}\right] \tag{2}$$

where the vectors $\mathbf{r}$ and $\mathcal{E}$ are the dipole operator of the molecule and the electric field, respectively. Eq. (2) also describes the interaction of the molecule with radiation in the dipole approximation [1], i.e. at optical frequencies, when the molecular dimensions are small compared to the wavelenght of the radiation. In this case the relevant molecular properties are the dynamic polarizabilities and hyperpolarizabilities and other non linear optical properties [2], [3].

The solution of eq. (1) can be approximated by expanding both ψ_0 and $\psi_{\pm}$ in a linear space $\mathcal{L}$. In case of ψ_0 this procedure leads to the familiar eigenvalue problem for the matrix $\mathbf{H}$ of the hamiltonian in the chosen basis of the space, while eq. (1) becomes a system of linear equations (bold capital letters denote matrices, bold lowercase denote vectors)·

$$\mathbf{H}\mathbf{v}_0 = E_0\mathbf{v}_0 \tag{3}$$

$$(\mathbf{H} - E_0 + \hbar\omega)\mathbf{v}_1 = E_1\mathbf{v}_0 - \mathbf{w}_0 \tag{4}$$

where $\mathbf{v}_0$, $\mathbf{v}_1$ and $\mathbf{w}_0$, are, respectively, the vectors of the components of the eigenvector ψ_0, of the first order function ψ_+, and of the function $\hat{V}\psi_0$.

Here we choose $\mathcal{L}$ to be the full CI space; this choice gives the best approximation for a given atomic basis and therefore the quantities computed can be considered as benchmarks. However, as it is well known, the dimensions

of full CI space grow factorially with the number of electrons and atomic orbitals, so our problem is how to deal with large dimensions. In the case of eigenvalue equation (3) a number of efficient algorithms have been implemented [4] [5] [6]. They combine the idea of iterative methods of Krylov type [7], like Lanczos [8] or Davidson [9], where the eigenvector is expressed as a polynomial in $\mathbf{H}$ applied to a guess $\mathbf{x}_0$, with the direct CI technique introduced by Roos [10]. In this context, the main operation one has to implement efficiently is the following: given a vector $\mathbf{x}$ in full CI space, compute the vector $\mathbf{y} = \mathbf{H}\mathbf{x}$, resulting from the multiplication of the hamiltonian matrix $\mathbf{H}$ by vector $\mathbf{x}$. In the direct CI technique, the hamiltonian matrix $\mathbf{H}$ is never computed, but $\mathbf{y}$ is obtained directly from the one and two electron integrals. These methods allow for the computation of very large full CI expansions (our largest amounts to nine billions symmetry adapted Slater determinants [11]).

Systems of linear equations can be solved using similar methods. there exists a family of iterative methods for large sparse linear systems [12] exploiting the fundamental operation $\mathbf{y} = \mathbf{H}\mathbf{x}$; in quantum chemistry they have been used by several authors [13] [14] [15].

Compared to finite field calculations, the main advantages of the direct solution of perturbative equations are i)full exploitation of the symmetry of the molecule, avoiding computations with non totally symmetric hamiltonians including external fields ii) access to frequency dependent properties. The purpose of this work is to provide benchmark computations useful to study the effectiveness of approximate methods. For a recent review of the latter see [16].

In the following we describe our implementation of the Full CI solution of the perturbative equation (4) and present some calculations on the dipole polarizability and hyperpolarizability of lithium hydride.

2 Methods of solution

The right hand side $\mathbf{b} = E_1\mathbf{v}_0 - \mathbf{w}_0$ of the system of linear equation eq. (4) is easily computed from the eigenvector $\mathbf{v}_0$ of a previous full CI computation. The perturbation operator $\hat{V}$ of eq. (1) is usually a one-electron operator expressed in second quantized form as:

$$\hat{V} = \Sigma_{ij} V_{ij} a_i^\dagger a_j \tag{5}$$

so its application to $\mathbf{v}_0$ using the methods described in ref. [6] is a simple matter. The only feature to be pointed out is the following. $\hat{V}$ is in general non totally symmetrical, and $\hat{V}\psi_0$ and ψ_{+1} may belong to a symmetry class different from that of ψ_0. This requires only minor modifications of the program. A similar application of $\hat{V}$ to a first order perturbed function is needed to compute third order properties (see eq.s 29,30).

We rewrite eq. (4) in the simplified form:

$$\mathbf{A}(\eta)\mathbf{x} = \mathbf{b} \tag{6}$$

where $\mathbf{A}(\eta) = \mathbf{H} - (E_0 + \eta)\mathbf{I}$ and $\eta = \hbar\omega$. We notice that the matrix $\mathbf{A}(0)$ is real symmetrical and has eigenvalues $E_k - E_0$ corresponding to the excitation energies from state $\mathbf{v}_0$. It also has a null eigenvector $\mathbf{v}_0$; we will assume it is non degenerate.

Equation (6) has solutions only if:
i) either $det\mathbf{A}(\eta) \neq 0$ or
ii) $\mathbf{b}$ is orthogonal to the null space of $\mathbf{A}(\eta)$
Condition i) is fulfilled when η is different from an excitation energy $E_k - E_0$ and from zero. For real η, we restrict its range to $\pm$the distance of the closest eigenvalue from E_0; this limit is the same imposed by perturbation theory. In this case the solution is unique. Since the right hand side $\mathbf{b}$ of e.q. (6) is orthogonal to $\mathbf{v}_0$ by construction, so is the solution $\mathbf{x}$.

When $\eta = 0$, we fall under case ii), and eq. (6) has a linear manifold of solutions. In this manifold we will choose the solution of minimal norm, i.e. the one orthogonal to $\mathbf{v}_0$; this ensures continuity for $\eta \to 0$.

A compact notation for the solutions and other quantities is obtained by using the reduced resolvent [17] of the molecular hamiltonian defined according to:

$$\mathbf{R}(\eta) = (\mathbf{H} - E_0 - \eta)^{-1}\mathbf{P}_0 \tag{7}$$

$$\mathbf{x} = \mathbf{R}(\eta)\mathbf{b} \tag{8}$$

where $\mathbf{P}_0$ is the projection on the eigenvector $\mathbf{v}_0$.

A unified presentation of the numerical methods to solve eq. (6) can be given in terms of variational principles. The solution of eq. (6) corresponds to a stationary point of the quadratic forms:

1. $Q_1(\mathbf{x}) = \frac{1}{2}\mathbf{x}^T\mathbf{A}(\eta)\mathbf{x} - \mathbf{b}^T\mathbf{x}$ (this is nothing but Hylleraas variational principle in the linear space $\mathcal{L}$);
2. $Q_2(\mathbf{x}) = \| \mathbf{b} - \mathbf{A}(\eta)\mathbf{x} \|^2$;

The vector $\mathbf{r} = \mathbf{b} - \mathbf{A}(\eta)\mathbf{x}$ is known as the residual vector associated to $\mathbf{x}$; when its norm is zero (or small enough), $\mathbf{x}$ is a solution; $-\mathbf{r}$ is also the gradient of Q_1.

The stationary point is always a minimum in case of form Q_2; in the other case it is a minimum only when the matrix $\mathbf{A}(\eta)$ is real and positive definite

The methods of solution can be sketched as follows:

- at iteration i-1 we are in point $\mathbf{x}_{i-1}$ and the form has value Q_{i-1};
- move to another point $\mathbf{x}_i = \mathbf{x}_{i-1} + \alpha_i\mathbf{p}_i$, such that $Q_i < Q_{i-1}$;
- a good direction $\mathbf{p_i}$ is the residual vector $\mathbf{r}_{i-1}$ of previous iteration (steepest descent); a better one is the 'preconditioned' residual $\mathbf{M}^{-1}\mathbf{r}_{i-1}$.
- choose α_i to minimize Q in the direction of $\mathbf{p_i}$.
- stop when norm of residual is small enough; otherwise iterate.

The preconditioner $\mathbf{M}$ is an easily invertable matrix which corrects the direction of steepest descent and (hopefully) speeds up convergence. In principle, $\mathbf{M}^{-1}$ should be an approximation to $\mathbf{A}^{-1}$, as preconditioner we always use $\mathbf{M} = Diag[\mathbf{A}(\eta)]$.

The time consuming operation is the 'multiplication' $\mathbf{A}(\eta)\mathbf{x}_i$ which is needed at each iteration to determine the optimal α_i and the residual vector $\mathbf{r}$. When the form involved is Q_1, we get the conjugate gradient method which is well documented in the literature [12]. This method requires the matrix $\mathbf{A}(\eta)$ to be positive definite; this condition is fulfilled when $-E_0 - \hbar\omega$ is greater than the minimum eigenvalue of $\mathbf{H}$ in the symmetry subspace of the product $\hat{V}\psi_0$ (which can be different from that of the eigenvector). The

method is stable and has good convergence properties. The minimum of the form Q_1 is equal to

$$-\frac{1}{2}\mathbf{b}^\dagger\mathbf{A}^{-1}\mathbf{b}$$

i.e. half the value of a second order property with a change of sign.

In other cases when $A(\eta)$ is not positive definite, which is common when dealing with excited states, we use methods based on the minimisation of the residual norm Q_2. The convergence is usually slower and the disk space requirements are greater. The computational cost per iteration is essentially the same for both methods for real matrices $\mathbf{A}$. In Appendix 1 we describe in detail our implementation of the method using form Q_2.

For $\omega = 0$ the computed solution is not in general orthogonal to the eigenvector $\mathbf{v}_0$; this is due to the preconditioner which introduces components along the direction of $\mathbf{v}_0$. In this case we add a Schmidt ortogonalization step.

3 Applications to LiH

In this section we present the results of some test calculations of dipole polarizabilities α and hyperpolarizabilities β tensors of lithium hydride. These quantities are the first and second derivatives, respectively, of the dipole moment with respect to the field strength; see eq. (15) in Appendix 1.

We considered three AO basis sets. Our smallest basis B66 derives from one proposed by Sadlej [18] by uncontracting all the gaussians and amounts to 66 AO's. This basis was used to study α and β as a function of the internuclear separation, and originates Full CI spaces of the order of about one million Slater determinants in C_{2v} symmetry. Our second basis B109 contains 109 contracted gaussians, (11s6p3d/11s6p1d) on hydrogen and (14s9p4d3f/14s9p1d1f) on Lithium, both derived from the (11s6p) and (13s9p) sets of van Duijneveldt [19] by adding diffuse functions (see Appendix). The dimensions of the Full CI space is about nine millions in this case. The last basis B83 is the Roos-Sadley basis of 83 contracted gaussians [20]; the Full CI space has dimension about three millions.

In Table 1 we report a comparison of our results of static dipole polarizability for the ground state with some of the most recent calculations at equilibrium geometry. The method used was the preconditioned conjugated

gradient; convergence to $\| \mathbf{r} \| < 10^{-6}$ is achieved in 15 iterations for the ground state equation in the nine billion case. The dipole polarizability of the ground state is a sum of positive contributions, as can be seen from eq. (28) using the spectral resolution of the reduced resolvent $R(0)$. Therefore larger values of polarizability are considered to mean better quality of the computation, even if, strictly speaking, the comparison should be performed between computations using the same unperturbed eigenvector $\mathbf{v}_0$ (compare Hylleraas' variational principle [21]). The Full CI values are indeed greater, as expected, than values computed with other methods using AO bases of comparable quality. Coupled cluster results closely approximate the Full CI value, as can be seen from the data computed by Lee et al. [22] and by us using the same AO basis (B83). From the values of α_{zz} reported in Table 1 and according to this criterion our largest basis B109 seems to be poorer than expected in the A_1 symmetry.

In Table 2 we report similar results for the excited states $A^1\Sigma^+$ and $B^1\Pi$, but at the equilibrium internuclear separation of the ground state, i.e. R_e=3.015 bohr. The values are larger than those of the ground state, as expected. In this case the conjugated gradient cannot be used, and one has to resort to method based on the minimization of the residual norm. The convergence is slower and for large size vectors restarts (see Appendix 1) are needed. This affects the convergence rate, which also depends upon the maximum dimension allowed for the iterative subspace. In general it is better to set this limit on the dimension at the maximum value compatible with available disk space.

Sometimes we found helpful to start from a guess generated in the following way. Prepare a modified system with a right hand side $\mathbf{b}$ orthogonalized not only to the eigenvector $\mathbf{v}_0$, but also to the lower lying eigenvectors of the appropriate symmetry. Iterating on this system with the preconditioned conjugated gradient shows an oscillating behaviour of the residual norm, which goes through some minima and maxima before reaching a value less than threshold. However this does not mean real convergence, because in preconditioned conjugate gradient the residual norm is computed in the metric of the preconditioner, which is now not positive definite. We stop the procedure at the first minimum, take the solution, complete it with the contribution of the lower lying eigenvectors and use it as guess in the original system with method Q_2. In this way, for the excited state $A^1\Sigma^+$ we got convergence to $\| \mathbf{r} \| < 5.10^{-6}$ in 10 iterations (restart after 6 iterations), starting from a

guess converged to 10^{-3} in a dozen of conjugate gradient iterations.

In Table 3 we display some results of frequency dependent polarizability of the ground state. The dynamic polarizability gives also the energy shift due to the quadratic Stark effect [23]; in this case $\hbar\omega = 0.1$ hartree corresponds to a wavelenght of $\approx$ 4557 Å. The values at imaginary frequency are computed with the variant of method Q_2 for complex systems and vectors.

In Table 4 we collect our computed values of hyperpolarizabilities and compare them with data in the literature. The values are computed from the first order functions according to eq.s (29-30). The hyperpolarizability appears to be very much dependent from the method used; again coupled cluster provides values closer to Full CI, even if the agreement is poorer compared to polarizabilities. Excited state values are very large and most likely extremely sensitive to a number of factors (quality of AO basis, accuracy of the solution and so on).

Table 1. Comparison of static dipole moments and polarizabilities for LiH $X^1\Sigma^+$ at equilibrium R_e=3.015 bohr. z is the internuclear axis; all quantities are in a.u.

Authors	μ	α_{zz}	α_{xx}	method	AO basis
Tunega et al.	2.362	21.88	25.41	SCF	14s8p6d5f/11s8p6d5f
[24]	2.236	23.49	27.07	MP2	12s8p6d5f/9s8p6d5f
	2.296	25.78	29.60	CCSD	198 orb.s
	2.294	25.88	29.63	CCSD(T)	
Papadopoulos	2.365	21.66	25.21	SCF	13s7p3d1f/10s7p5d
et al.	2.335	23.11	26.95	MP2	112 orb.s
[25]	2.315	24.33	28.58	MP4	
Lee et al.$^+$	2.363	21.92	25.28	SCF	13s8p6d2f/8s5p3d1f
[22]	2.332	23.90	27.06	MP2	12s8p5d/8s5p3d
	2.301	25.73	29.52	CCD/BO	83 orb.s
this work$^+$	2.298	26.64	29.70	FCI	83 orb.s $\approx$ 3 10^6 C_{2v} det.
this work	2.299	26.58	29.48	FCI	10s6p3d/6s4p
					66 orb.s $\approx$ 10^6 C_{2v} det.
this work	2.294	26.15	29.70	FCI	14s9p4d3f/14s9p1d1f
					11s6p3d/11s6p1d
					109 orb.s$\approx$ 10^7 C_{2v} det.
expt.	2.314				

$^+$: R_e=3.0158 bohr.

Table 2. Comparison of static dipole moments and polarizabilities for excited states of LiH at R_e=3.015 bohr. z is the internuclear axis; all quantities are in a.u.

State	μ	α_{zz}	α_{xx}	method	AO/CI basis
$A^1\Sigma^+$	-2.011	74.94	213.59	FCI	14s9p4d3f/14s9p1d1f 11s6p3d/11s6p1d 109 orb.s$\approx$ 10^7 C_{2v} det.
$A^1\Sigma^+$	-2.011	75.37	211.40	FCI	10s6p3d/6s4p 66 orb.s $\approx$ 10^6 C_{2v} det.
$B^1\Pi$	-0.182	155.75	209.29	FCI	10s6p3d/6s4p 66 orb.s $\approx$ 10^6 C_{2v} det.

Table 3. Selected values of matrix elements and dynamic Full CI polarizabilities of LiH ground state $X^1\Sigma^+$ at real and imaginary frequency. R_e=3.015 bohr, AO basis set 10s6p3d/6s4p (66 orb.s). z is the internuclear axis; all quantities are in a.u.

$\hbar\omega$ (†)	-0.1	0.1	0.1i
$\Re< (\hat{x}-E_{1x})\psi_0\|R(\bar{\omega})\|(\hat{x}-E_{1x})\psi_0 >$	9.847	32.10	11.60
$\Im< (\hat{x}-E_{1x})\psi_0\|R(\bar{\omega})\|(\hat{x}-E_{1x})\psi_0 >$	0.000	0.00	5.782
$\alpha_{xx}(\omega)$		41.95	23.21
$\Re< (\hat{z}-E_{1z})\psi_0\|R(\bar{\omega})\|(\hat{z}-E_{1z})\psi_0 >$	8.785	38.33	10 13
$\Im< (\hat{z}-E_{1z})\psi_0\|R(\bar{\omega})\|(\hat{z}-E_{1z})\psi_0 >$	0.000	0.00	5.148
$\alpha_{zz}(\omega)$		47.11	20.26

(†) the wavelenght corresponding to 0.1 hartree is 4557 Å.

Table 4. Comparison of static hyperpolarizabilities for LiH at R_e=3.015 bohr. z is the internuclear axis; all quantities are in a.u.

Authors	State	βzzz	βxxz	method	AO basis
Tunega et al. [24]	$X^1\Sigma^+$	-426.	-158.	SCF	14s8p6d5f/11s8p6d5f
		-471.	-175.	MP2	12s8p6d5f/9s8p6d5f
		-514.	-232.	CCSD	198 orb.s
		-639.	-237.	CCSD(T)	
Papadopoulos et al. [25]	$X^1\Sigma^+$	-1055.	-358.	MP4	13s7p3d1f/10s7p5d 112 orb.s
Lee et al.$^+$ [22]	$X^1\Sigma^+$	-308.	-188.	SCF	13s8p6d2f/8s5p3d1f
		-742.	-364.	MP2	12s8p5d/8s5p3d
		-635.	-593.	CCD/BO	83 orb.s
this work$^+$	$X^1\Sigma^+$	-655.	-345.	FCI	83 orb.s $\approx$3 10^6 C_{2v} det.
this work	$X^1\Sigma^+$	-661.	-350.	FCI	14s9p4d3f/14s9p1d1f 11s6p3d/11s6p1d 109 orb.s$\approx$ 10^7 C_{2v} det.
this work	$A^1\Sigma^+$	-1885.	6417.	FCI	14s9p4d3f/14s9p1d1f 11s6p3d/11s6p1d 109 orb.s$\approx$ 10^7 C_{2v} det.

$^+$: R_e=3.0158 bohr.

We have performed computations with basis B66 for a number of internuclear separations, from near equilibrium (2.5 bohr) to a region of avoided crossings (10.0 bohr), in order to assess the sensitivity of the property values and of the computational procedure to the changes of molecular geometry.

In Table 5 we report the values of some properties of the Full CI wavefunctions of the ground and first excited state of $^1\Sigma^+$ symmetry; these data show the change of the nature of the wavefunction with the internuclear separation. In particular from the values of the occupation numbers of 2σ and 3σ natural orbitals we seee that the ground state is essentially one-determinant in the equilibrium region and up to $\approx$ 6.5 bohr, while the first excited state starts at

small R as two-determinant. In the avoided crossing region (6.5 to 10. bohr) the two states undergo a strong mixing.

Modifications of the nature of the molecular wavefunction are reflected and amplified on the values of first, second and third order properties, in order of increasing sensitivity. This can be seeen from the values of polarizability and hyperpolarizability reported in Table 6, which show very large oscillations. We did not perform a detailed numerical analysis of the computation, so we do not really know the relative accuracy of the values reported.

As previously mentioned, the rate of convergence is satisfactory at equilibrium geometries, when the structure of the wavefunction is relatively simple. The convergence rate slows down at large R, and it worse for the excited state. At $R = 9.5$ bohr, 80 iterations of the Q_2 method were needed to achieve a convergence of 5 10^{-5} (restart after 6 iterations)

Table 5. Properties of the LiH $X^1\Sigma^+$ and $A^1\Sigma^+$ wavefunctions as a function of the internuclear separation R (bohr): $n_{2\sigma}$ and $n_{3\sigma}$ are the occupation numbers of the frontier natural orbitals of σ symmetry, μ denotes dipole moment of the state, and μ_T is the transition dipole between the two states. AO basis set 10s6p3d/6s4p (66 orb.s). z is the internuclear axis; all quantities are in a.u.

	$X^1\Sigma^+$				$A^1\Sigma^+$		
R	$n_{2\sigma}$	$n_{3\sigma}$	μ	$\lvert\mu_T\rvert$	μ	$n_{2\sigma}$	$n_{3\sigma}$
2.5	.972328	.0127560	2 096	0.765	-2.055	.638506	.358590
3.015	.970089	.0149270	2.299	0.951	-2.011	.649199	.347872
3.5	.965900	.0195430	2.508	1.143	-1.893	.664566	.332412
4.0	.959030	.0272734	2.718	1.371	-1.697	.685742	.311083
4 494	948985	0384244	2 888	1.638	-1.422	.711928	284630
4.913	.937090	.0514009	2.976	1.904	-1.110	.738035	.258135
5.0	.934133	.0545988	2.985	1.964	-1.034	.743864	.252203
5.5	.912931	.0773011	2.950	2.332	-0.511	.779474	.215811
6.5	.839997	.153823	2.314	3.010	1.068	.850359	.142535
7.5	.730333	.266761	1.216	3.090	2.937	.889646	.101295
8.5	.634929	.363836	-.4846	2.722	4.070	.889204	.101812
9.5			-.1787		4.118		
10.0	.556711	.442819	-.1082	2.371	3.721	.831467	.162424

Table 6. FCI polarizabilities and hyperpolarizabilities for LiH as a function of the internuclear separation R. AO basis set 10s6p3d/6s4p (66 orb.s). z is the internuclear axis; all quantities are in a.u.

	Ground state $X^1\Sigma^+$				Excited state $A^1\Sigma^+$			
R	α_{zz}	α_{xx}	βzzz	βxxz	α_{zz}	α_{xx}	βzzz	βxxz
2.500	18.98	25.70	-309	-232	70.14	210.66	-2360	6486
3.015	26.58	29.48	-694	-355	75.37	211.40	-1720	6156
3.500	37.42	34.38	-1439	-553	77.51	206.25	-681	5644
4.000	54.53	40.79	-2995	-894	76.57	198.29	1193	5242
4.494	81.37	48.78	-6067	-1453	70.47	188.87	4572	5081
4.913	116.72	57.22	-10721	-2194	58.05	179.67	9394	5193
5.000	126.02	59.20	-11990	-2386	54.27	177.59	10671	5251
5.500	195.90	72.34	-21039	-3779	22.16	164.40	19392	5838
6.500	395.84	107.35	-18775	-6945	-61.67	132.13	11620	7199
7.500	435.04	141.09	45077	-5731	102.22	105.79	-74612	3851
8.500	312.52	158.28	45218	-2456	593.47	101.31	-121488	-2056
9.500	229.96	164.37	22538	-862	1294.46	112.24	-34777	-6130
10.000	208.08	165.66	14968	-512	1650.83	119.91	223860	-6649

4 Conclusions

The Full CI expansion technique can be applied to the perturbation theory equations as easily as to eigenvalue problem for the wavefunction. It has also a similar purpose, i.e. providing benchmark calculations to calibrate approximate methods of wider applicability.

5 Appendix

5.1 Description of the algorithm

Given the system of linear equations:

$$\mathbf{Ax} = \mathbf{b} \tag{9}$$

where the matrix $\mathbf{A} = \mathbf{A}^\dagger$, we look for a (pseudo)solution fulfilling

$$\| \mathbf{b} - \mathbf{Ax} \| < \epsilon^2 \tag{10}$$

and expressed at iteration n, as a linear combination of n vectors $\mathbf{h}_k$:

$$\mathbf{x}_n = \alpha_1 \mathbf{h}_1 + \alpha_2 \mathbf{h}_2 + \ldots + \alpha_n \mathbf{h}_n \tag{11}$$

where the coefficients α_k are chosen in such a way to minimize the quadratic form (10). At each iteration a new $\mathbf{h}_n$ is generated according to the prescription: $\mathbf{h}_n = Diag(\mathbf{A})^{-1}\mathbf{r}_{n-1}$.

The vectors $\mathbf{h}_k$ generate a subspace $\mathcal{I}_\backslash$ called the 'iterative subspace', growing at each iteration. This vector $\mathbf{x}_n$ is such that $\mathbf{Ax}_n$ has the minimal distance from $\mathbf{b}$, i.e. it is the projection of $\mathbf{b}$ in the subspace $\mathbf{A}\mathcal{I}_\backslash$ spanned by

$\mathbf{Ah}_1, \mathbf{Ah}_2, \ldots, \mathbf{Ah}_n$

It is desirable to have an orthogonal base of $\mathbf{A}\mathcal{I}f$, since this simplifies the formalism. Indeed, if $\mathbf{Ap}_k$ is such a base, the projection of $\mathbf{b}$ in $\mathbf{A}\mathcal{I}f$ is given by:

$$\mathbf{Ax}_n = \sum_{k=0}^{n} \frac{\mathbf{Ap}_k^\dagger \mathbf{b}}{\mathbf{Ap}_k^\dagger \mathbf{Ap}_k} \mathbf{Ap}_k = \beta_k \mathbf{Ap}_k \tag{12}$$

In this way the expansion coefficients β_k are independent from n, i e. once computed,they keep their values in the following iterations. This feature also simplifies the computation of the residual vector:

$$\mathbf{r}_n = \mathbf{b} - \mathbf{Ax}_n \tag{13}$$

$$\mathbf{r}_n - \mathbf{r}_{n-1} = \mathbf{A}(\mathbf{x}_n - \mathbf{x}_{n-1}) = \beta_n \mathbf{Ap}_n \tag{14}$$

The residual is simply updated at each iteration according to eq.(14).

In other words, we need a basis of the 'iterative subspace' $\mathcal{I}_\setminus$ orthogonal in the metric $\mathbf{A}^\dagger\mathbf{A}$, while the prescription to enlarge the iterative subspace generates a vector not having this property. This requires the introduction of an orthogonalization step in the algorithm, which, in its final form, looks like that:

1. choose a guess $\mathbf{x}_0$, compute $\mathbf{r}_0 = \mathbf{b} - \mathbf{A}\mathbf{x}_0$; a null guess is a possible choice; set $k = 0$
2. set $k = k + 1$
3. compute $\mathbf{h}_k = Diag(\mathbf{A})^{-1}\mathbf{r}_{k-1}$. and write it to disk;
4. compute $\mathbf{A}\mathbf{h}_k$
5. compute all scalar products $\gamma_{jk} = \mathbf{p}_j\mathbf{A}^\dagger\mathbf{A}\mathbf{h}_k$ and Schmidt-orthogonalize $\mathbf{A}\mathbf{h}_k$ to all previous $\mathbf{A}\mathbf{p}_j$ for $j = 1, 2, \ldots, k-1$;
6. the Schmidt orthogonalized vector is $\mathbf{A}\mathbf{p}_k$; write it on disk;
7. compute the square norm of $\mathbf{A}\mathbf{p}_k$ and the coefficient β_k according to eq. (12);
8. update residual according to e.q. (14);
9. check convergence; if not converged, go to (2);
10. compute the expansion coefficients of the solution in the basis $\mathbf{h}_k$ by inverting the triangular matrix γ_{jk};
11. compute solution by linear combination with coefficients β_k, of the vectors $\mathbf{h}_k$ previously saved on disk;
12. Schmidt orthogonalize to eigenvector $\mathbf{v}_0$ if needed and exit

The disk requirements are two vectors for each iteration step. For this reason one puts a limit on the dimension of the iterative subspace and restarts the procedure from the beginning using as a guess the non converged solution obtained.

In case of a complex matrix $\mathbf{A}$, the scheme is essentially the same from the mathematical point of view. However the computer implementation is slightly

different, because now all the vectors (but **b**) are complex and require twice as much disk space. In our implementation we organized the code by separating real and imaginary parts of vectors. The computational cost per iteration is also doubled.

5.2 Formulae for second and third order properties

The time dependent perturbation theory is a well known subject since long time; here we quote only two references [2], [3]. For the reader's convenience we report here the explicit formulae, taken from [3], of the dynamic polarizabilities and hyperpolarizabilities used in this work.

Under the action of the alternating field, eq. (2), the molecule acquires an induced dipole moment given by:

$$\mu(t) = \mu_0 + \alpha\mathcal{E}\cos(\omega t) + \frac{1}{2}\beta_0\mathcal{E}\mathcal{E} + \frac{1}{2}\beta_2\mathcal{E}\mathcal{E}\cos(2\omega t) + \ldots \tag{15}$$

where α and β are 2nd and 3rd rank tensors known as polarizability and hyperpolarizabilities, respectively. These quantities can be computed by solving the perturbation theory equations. Due to the vectorial nature of the perturbation, first order quantities are vectors, second order quantities are 2-tensors and so on. If we denote the cartesian components of the perturbation operator as $\hat{x}$, $\hat{y}$, $\hat{z}$, and label cartesian components of tensors with indexes x, y, z, the equations to be solved are:

$$\left[\vec{H} - E_0\right]\psi_0 = 0 \tag{16}$$

$$\left[\vec{H} - E_0 \pm \omega\right]\psi_{\pm x} = (E_{1x} - \hat{x})\,\psi_0 \tag{17}$$

$$\left[\vec{H} - E_0 \pm 2\omega\right]\psi_{\pm 2xy} = E_{2xy}\psi_0 + (E_{1x} - \hat{x})\,\psi_{\pm y} \tag{18}$$

$$\left[\vec{H} - E_0\right]\psi_{02xy} = E_{2xy}\psi_0 + (E_{1x} - \hat{x})\,\frac{1}{2}(\psi_{+y} + \psi_{-y}) \tag{19}$$

$$E_{1x} = <\psi_0|\hat{x}|\psi_0> \tag{20}$$

$$E_{2xy} = \frac{1}{2} <\psi_0|\hat{x}|(\psi_{+y} + \psi_{-y})> \tag{21}$$

$<|>$ being the usual scalar product in the space-spin coordinates. Notice that the $E_{..}$'s are defined in such a way to ensure the ortogonality of the right

hand side of the equations to ψ_0. This guarantees the existence of solutions for $\omega = 0$. In this case we choose the solution orthogonal to ψ_0; in this way we have continuity for $\omega \to 0$:

$$\lim_{\omega\to 0} \psi_{+x} = \lim_{\omega\to 0} \psi_{-x} \tag{22}$$

$$\lim_{\omega\to 0} \psi_{+2xy} = \lim_{\omega\to 0} \psi_{-2xy} = \frac{1}{2} \lim_{\omega\to 0} \psi_{02xy} \tag{23}$$

Using the reduced resolvent notation:

$$\psi_{\pm x} = -R(\pm\hbar\omega)(\hat{x} - E_{1x})\psi_0 \tag{24}$$

$$\psi_{\pm 2xy} = -R(\pm 2\hbar\omega)(\hat{x} - E_{1x})R(\pm\hbar\omega)(\hat{y} - E_{1y})\psi_0 \tag{25}$$

$$\psi_{\pm 0xy} = -R(0)(\hat{x} - E_{1x})R(\hbar\omega)(\hat{y} - E_{1y})\psi_0 \tag{26}$$

The expression of the polarizability tensor in terms of the solutions of the previous equations is:

$$\alpha_{x,y}(\omega) = < \psi_0(\hat{x} - E_{1x})|\psi_{+y} > + < \psi_{-y}(\hat{y} - E_{1y})|\psi_0 > \tag{27}$$

$$\alpha_{x,y}(0) = 2 < \psi_0(\hat{x} - E_{1x})|R(0)|(\hat{y} - E_{1y})\psi_0 > \quad \text{static limit} \tag{28}$$

For the hyperpolarizability one may fulfill eq. (15) by writing:

$$\begin{aligned} \beta_{0xyz}(\omega) &= \frac{1}{2}[< \psi_0|(\hat{x} - E_{1x})\psi_{02yz} > + < \psi_{02xy}|(\hat{z} - E_{1z})\psi_0 > + \\ &+ < \psi_{+1x}|(\hat{y} - E_{1y})\psi_{+z} > + < \psi_{-1x}|(\hat{y} - E_{1y})\psi_{-z} >] \end{aligned} \tag{29}$$

$$\begin{aligned} \beta_{2xyz}(\omega) &= < \psi_0|(\hat{x} - E_{1x})\psi_{+2yz} > + < \psi_{-2xy}|(\hat{z} - E_{1z})\psi_0 > + \\ &+ < \psi_{-1x}|(\hat{y} - E_{1y})\psi_{+z} > \end{aligned} \tag{30}$$

but, from the physical point of view it is desirable to require the tensor β to be symmetrical in all its indexes [2]. Therefore we replace the previous definitions with their symmetrized forms:

$$\beta_{zzz} \leftarrow \beta_{zzz} \tag{31}$$

$$\beta_{xzz} \leftarrow \frac{1}{3}(\beta_{xzx} + \beta_{xzx} + \beta_{xxz}) \tag{32}$$

$$\beta_{xyz} \leftarrow \frac{1}{6}(\beta_{xyz} + \beta_{xzy} + \beta_{yxz} + \beta_{yzx} + \beta_{zxy} + \beta_{zyx}) \tag{33}$$

Since in the static limit $\beta_{0xyz}(0) = \beta_{2xyz}(0)$, and given the symmetry of the molecule LiH, the reported values of the static hyperpolarizability were computed according to·

$$\beta_{zzz} = 6 < \psi_0(\hat{z} - E_{1z})R(0)(\hat{z} - E_{1z})R(0)(\hat{z} - E_{1z})\psi_0 > \quad (34)$$

$$\beta_{xxz} = 4 < \psi_0(\hat{x} - E_{1x})R(0)(\hat{x} - E_{1x})R(0)(\hat{z} - E_{1z})\psi_0 > + \\ + 2 < \psi_0(\hat{x} - E_{1x})R(0)(\hat{z} - E_{1z})R(0)(\hat{x} - E_{1x})\psi_0 > \quad (35)$$

5.3 Specification of B109 AO basis

Each contracted gaussian is specified in the form: $(\alpha_1, c_1 \parallel \alpha_2, c_2 \parallel \ldots)$ where α_k is an exponent and c_k its contraction coefficient.

- Hydrogen s functions:
  (188.614450 , 1.0), (28.276596 , 1.0), (6.424830 , 1.0),
  (1.815041 , 1.0), (.591063 , 1.0), (.212149 , 1.0), (.079891 , 1 0),
  (.027962 , 1.0), (.009787 , 1.0), (.003425 , 1.0), (.001199 , 1.0)

- Hydrogen p functions:
  (2.305000 , 1.0), (.806750 , 1.0), (.282362 , 1.0), (.098827 , 1.0),
  (.054590 , 1.0), (.012107 , 1.0)

- Hydrogen d functions:
  (1.819000, .270513 || .727600, .551013 || .291040, .331087)

- Lithium s functions:
  (9497.934400, 1.0), (1416.811200, 1.0), (321.459940, 1.0),
  (91.124163, 1.0), (29.999891, 1.0), (11 017631, 1.0),
  (4.372801, 1.0), (1.831256, 1.0), (.802261, 1.0),
  (.362648, 1.0), (.113995, 1.0), (.051237, 1.0),
  (.022468, 1.0), (.007860, 1.0)

- Lithium p functions:
  (13.119504, 1.0), (3.077424, 1.0), (1.098800, 1.0),
  (.435778, 1.0), (.180243, 1.0), (.076133, 1.0),
  (.032546, 1.0), (.014018, 1.0), (.004906, 1.0)

- Lithium d functions:
  (.450000, .176679 || .157500, .994472 || .055125, −1.552621 || .019294, .878690)
- Lithium f functions:
  (.240000, .387778 || .096000, .401610 || 038400, .446150)

References

[1] see e.g. Louisell, W.H. *Quantum Statistical Properties of Radiation* , **1973**, John Wiley & Sons, New York.

[2] Buckingham, A.D. *Adv. Chem. Phys.*, **1967**, *12*, 107.

[3] Langhoff, P.W., Epstein S.T., and Karplus, M. *Rev. Mod. Phys.*,**1972**, *44*, 602.

[4] Olsen, J., Roos, B.O., Jorgensen, P. and Jensen, J.Å. *J.Chem.Phys.*, **1988**,*89*, 2185. J.Olsen, P. Jorgensen and J. Simons, *Chem. Phys. Lett.*, **1990**,*169*, 463.

[5] Zarrabian, S. Sarma, C.R. and Paldus, J. *Chem. Phys. Lett.*, **1989**,*155*, 463; Harrison R.J. and Zarrabian, S. *Chem. Phys. Lett.*, **1989**,*158*, 393.

[6] Bendazzoli, G.L. and Evangelisti, S. *J.Chem.Phys.*, **1992**,*98*, 3141.

[7] Golub, G.H., van Loan, C.F. *Matrix Computations*, **1983**, North Oxford Academic, Oxford.

[8] Lanczos, C.*J.Res. Nat. Bur. Stand.*, **1950**, *45*, 255.

[9] Davidson, E.R. *J.Comp.Phys.*, **1975**, *17*, 87.

[10] Roos, B.O. *Chem. Phys. Lett.*, **1972**, *15*, 153.

[11] Rossi, E. Bendazzoli, G.L., Evangelisti, S., and Maynau, D. *Chem Phys. Lett.*, **1999**, *310*, 530.

[12] see e.g. Barrett, R. *et al.* ,
Templates for the Solution of Linear Systems: Building Blocks for Iterative Methods , www.netlib.org/linalg/html_templates/node1.html

[13] Pople, J.A., Krishnan, R., Schlegel, H.B., and Binkley, J.S., *Int.J. Quantum. Chem. Symp.*, **1979**, *13*, 225.

[14] Spelsberg, D. , Lorenz, T. and Meyer, W. ,*J. Chem. Phys.*, **1993**, *99*, 7845.

[15] Bendazzoli, G.L., Evangelisti, S., Palmieri, P. *Int.J. Quantum Chem.*, **1987**, *XXXI*, 673.

[16] Shelton, D.P. and Rice, J E. *Chem. Rev.*,**1994**, *94*, 3.

[17] see e.g. Löwdin, P.O., *Internat.J. Quantum Chem.* , **1968**, *II*, 867.

[18] Sadlej, A.J., *Coll. Czech. Chem. Commun.* ,**1988**, *53*, 1995. Sadlej, A.J. and Urban, M. *J. Mol. Struct. (THEOCHEM)*, **1991**, *234*, 147.

[19] van Duijneveldt, F.B., *IBM Research RJ 945*,**1971**, san José, California.

[20] Roos, B.O. and Sadlej, A.J. *Chem. Phys.*,**1985**, *94*, 43.

[21] Hirschfelder, J.O., Byers Brown, W. and Epstein, S.T. *Adv. Quantum Chem.*, **1964**, *1s*, 255.

[22] Lee, B.K., Stout, J.M. and Dykstra, C.E. *J. Mol. Struct. (THEOCHEM)*, **1997**, *400*, 57.

[23] Bonch-Bruevich A.M. and Khodovoi, V.A. *Usp Fiz. Nauk* **1967** , *93*, 71.

[24] Tunega, D. and Noga, J. *Theor. Chem. Acc.*, **1998**, *100*, 78.

[25] Papadopoulos, M.G., Willetts, A., Handy, N.C. and Underhill, A.E. *Mol. Phys.*, **1996**, *88*, 1063.

On the generalized Brillouin-Wigner perturbation theory and the many-body problem

I. Hubač[†‡] and S. Wilson[¶]

[†]*Department of Chemical Physics, Faculty of Mathematics and Physics, Comenius University, 842 15 Bratislava, Slovakia*
[‡]*Insitute of Physics, Silesian University, 74601 Opava, Czech Republic*
[¶] *Rutherford Appleton Laboratory, Chilton, Oxfordshire OX11 0QX, England*

Abstract

The generalized Brillouin-Wigner perturbation theory introduced by Löwdin is re-examined and its use in describing many-body systems is investigated. The Bloch equation and the Lippmann-Schwinger equation for the generalized Brillouin-Wigner perturbation theory are presented. Corrections to the finite-order theory which restore linear scaling with the number of electrons are presented. A generalized Brillouin-Wigner coupled cluster theory is also given.

ADVANCES IN QUANTUM CHEMISTRY, VOLUME 39

0065-3276/01 $35 00

Contents

1. Introduction

There is renewed interest [1] - [12] in the use of Brillouin-Wigner perturbation theory in the study of the many-body molecular electronic structure problem. This interest is fuelled by the need to develop robust techniques for describing dynamic electron correlation effects based on multireference functions. Such techniques are an essential ingredient of the theoretical description of many molecular processes and especially those involving dissociation. Wenzel and Steiner [5] have emphasized that "the reference energy in Brillouin-Wigner perturbation theory is the fully dressed energy" and that further "[this] feature guarantees the existence of a natural gap and thereby rapid convergence of the perturbation series." However, it is well known that the perturbation series originally developed by Lennard-Jones [13] Brillouin [14] and Wigner [15] is not a many-body theory [16] - [19] in that the energy components do not scale linearly with the number of electrons [20] - [25].

Recently, we have critically re-examined [12] the single root Brillouin-Wigner perturbation theory and its application to many-body systems. In this work, we consider the application of

generalized Brillouin-Wigner perturbation theory to the many-body problem. This theory was introduced by Löwdin in Part XII of a series of papers[26]-[38] devoted to perturbation theory. We again concentrate on the single reference formalism for simplicity. Like the familiar Brillouin-Wigner perturbation theory, the generalized theory does not scale linearly with the number of electrons in the system and it cannot be regarded as a "many-body" theory. Two solutions to this problem can be identified: *(i)* "many-body" corrections can be derived; *(ii)* the theory can be applied to an ansatz which is intrinsically suited to "many-body" systems. In this paper, we explore both of these avenues. In section 2, we re-examined the generalized Brillouin-Wigner perturbation theory deriving both the Bloch equation and the corresponding Lippmann-Schwinger equation. The "many-body" corrections for finite-order genralized Brillouin-Wigner perturbation theory are deduced and discussed in section 3. In section 4, the application of the generalized Brillouin-Wigner perturbation theory to the coupled cluster expansion is considered and the generalized Brillouin-Wigner coupled cluster theory obtained. Section 5 contains a summary and a brief discussion of future prospects.

2. Generalized Brillouin-Wigner perturbation theory

For quantum problems defined by the time-independent Schrödinger equation

$$\mathcal{H}\Psi = (\mathcal{H}_0 + \lambda\mathcal{H}_1)\,\Psi = \mathcal{E}\Psi, \quad \mathcal{H} = \mathcal{H}_0 + \lambda\mathcal{H}_1 \tag{1}$$

perturbation theory may be developed from the effective eigenequation

$$H_{eff}\Phi_0 = \mathcal{E}\Phi_0 \tag{2}$$

with

$$H_{eff} = \left[P\mathcal{H}P + P\mathcal{H}Q\left(\mathcal{E} - Q\mathcal{H}Q\right)^{-1}Q\mathcal{H}P\right] \tag{3}$$

where P is the projector onto the model function, Φ_0, which is an eigenfunction of $\mathcal{H}_0$,

$$P = |\Phi_0\rangle \langle\Phi_0| \tag{4}$$

and Q is its orthogonal complement

$$\begin{aligned} Q &= I - P \\ &= \sum_{k\neq 0} |\Phi_k\rangle \langle\Phi_k| . \end{aligned} \tag{5}$$

The exact energy, $\mathcal{E}$, is given by

$$\mathcal{E} = \langle\Phi_0 |H_{eff}| \Phi_0\rangle \tag{6}$$

with

$$\langle\Phi_0 \mid \Phi_0\rangle = 1. \tag{7}$$

Various types of perturbation expansion can be obtained by expanding the inverse operator in (3). Using the operator identity

$$\begin{aligned} (X-Y)^{-1} &= \sum_{n=0}^{\infty} X^{-1}\left(YX^{-1}\right)^n \\ &= X^{-1} + X^{-1}YX^{-1} + X^{-1}YX^{-1}YX^{-1} + ... \end{aligned} \tag{8}$$

or

$$(X-Y)^{-1} = X^{-1} + X^{-1}Y(X-Y)^{-1} \tag{9}$$

the widely used Rayleigh-Schrodinger perturbation theory is developed by putting

$$X \equiv E_0 - Q\mathcal{H}_0Q \quad \text{and} \quad Y \equiv Q\mathcal{H}_1Q - (\mathcal{E} - E_0), \tag{10}$$

whereas the usual Brillouin-Wigner perturbation theory is obtained by taking

$$X \equiv \mathcal{E} - Q\mathcal{H}_0Q \quad \text{and} \quad Y \equiv Q\mathcal{H}_1Q. \tag{11}$$

In this paper, we consider an alternative choice for the operators X and Y; namely,

$$X \equiv \mathcal{E} \quad \text{and} \quad Y \equiv Q\mathcal{H}Q. \tag{12}$$

This leads to what Löwdin [36] has called generalized Brillouin-Wigner perturbation theory.

We can write

$$\mathcal{G} = \frac{1}{\mathcal{E}}Q = \frac{1}{\mathcal{E}}\sum_{k\neq 0}^{\infty} |\Phi_k\rangle \langle\Phi_k| \tag{13}$$

Using (3) and (6), (8) and (12) together with (13) gives the following expansion for the energy

$$\mathcal{E} = \langle\Phi_0|\mathcal{H}|\Phi_0\rangle + \langle\Phi_0|\mathcal{H}\mathcal{G}\mathcal{H}|\Phi_0\rangle + \langle\Phi_0|\mathcal{H}\mathcal{G}\mathcal{H}\mathcal{G}\mathcal{H}|\Phi_0\rangle + \ldots \tag{14}$$

We can then introduce the reaction operator

$$\mathcal{V} = \mathcal{H}\mathcal{G}\mathcal{H} + \mathcal{H}\mathcal{G}\mathcal{H}\mathcal{G}\mathcal{H} + \ldots \tag{15}$$

so that the energy may be written

$$\mathcal{E} = \langle\Phi_0|\mathcal{H}|\Phi_0\rangle + \langle\Phi_0|\mathcal{V}|\Phi_0\rangle \tag{16}$$

Equation (15) may be written

$$\mathcal{V} = \mathcal{H}\mathcal{G}\mathcal{H} + \mathcal{H}\mathcal{G}\mathcal{V} \tag{17}$$

Equation (17) is the Lippmann-Schwinger equation [39]

Defining the wave operator[40]-[42] by

$$|\Psi\rangle = \Omega|\Phi\rangle \tag{18}$$

we write

$$\mathcal{E} = \langle\Phi_0|\mathcal{H}|\Psi\rangle \tag{19}$$

with

$$\langle\Phi_0 \mid \Phi_0\rangle = 1 \tag{20}$$

and

$$\langle \Phi_0 \mid \Psi \rangle = 1 \tag{21}$$

in the form

$$\mathcal{E} = \langle \Phi_0 | \mathcal{H}\Omega | \Phi_0 \rangle \tag{22}$$

Comparing (16)and (22) gives

$$\mathcal{V} = \mathcal{H}\Omega - \mathcal{H}$$

which upon substituting in (17) and rearranging yields

$$\Omega = I + \mathcal{G}\mathcal{H}\Omega \tag{23}$$

(23) is the Bloch equation[43]. Together with (22) it provides the fundamental equation of the generalized Brillouin-Wigner perturbation theory.

Iteration of the equation (23) and substitution in (22) generates the *generalized* Brillouin-Wigner perturbation expansion for the energy

$$\mathcal{E} = \varepsilon_1 + \varepsilon_2 + \varepsilon_3 + \varepsilon_4 + \ldots \tag{24}$$

where the energy coefficients, ε_k, have the general form

$$\varepsilon_k = \left(\frac{1}{\mathcal{E}}\right)^{k-1} \left\langle \Phi_0 \left| \mathcal{H} \left(Q\mathcal{H}\right)^{k-1} \right| \Phi_0 \right\rangle \tag{25}$$

The denominator is simply the exact energy raised to the power $k-1$ in order k.

The energy through second order, for example, is

$$\mathcal{E} = \langle \Phi_0 | \mathcal{H} | \Phi_0 \rangle + \frac{1}{\mathcal{E}} \sum_{k \neq 0}^{\infty} \langle \Phi_0 | \mathcal{H} | \Phi_k \rangle \ \langle \Phi_k | \mathcal{H} | \Phi_0 \rangle \tag{26}$$

which, if we define

$$\mathcal{W}_1 = \langle \Phi_0 | \mathcal{H} | \Phi_0 \rangle \tag{27}$$

$$\mathcal{W}_2 = \sum_{k \neq 0}^{\infty} \langle \Phi_0 | \mathcal{H} | \Phi_k \rangle \ \langle \Phi_k | \mathcal{H} | \Phi_0 \rangle \,, \tag{28}$$

can be written

$$\mathcal{E} = \mathcal{W}_1 + \frac{1}{\mathcal{E}}\mathcal{W}_2 \tag{29}$$

or

$$\mathcal{E}^2 - \mathcal{E}\mathcal{W}_1 - \mathcal{W}_2 = 0 \tag{30}$$

so that

$$\mathcal{E}_\pm = \frac{1}{2}\left[\mathcal{W}_1 \pm \sqrt{(\mathcal{W}_1)^2 + 4\mathcal{W}_2}\right] \tag{31}$$

Through third order we have

$$\mathcal{E} = \mathcal{W}_1 + \frac{1}{\mathcal{E}}\mathcal{W}_2 + \frac{1}{\mathcal{E}^2}\mathcal{W}_3 \tag{32}$$

where

$$\mathcal{W}_3 = \sum_{k\neq 0,\ell\neq 0}^{\infty} \langle\Phi_0|\,\mathcal{H}\,|\Phi_k\rangle\ \langle\Phi_k|\,\mathcal{H}\,|\Phi_\ell\rangle\ \langle\Phi_\ell|\,\mathcal{H}\,|\Phi_0\rangle\,, \tag{33}$$

so that

$$\mathcal{E}^3 - \mathcal{E}^2\mathcal{W}_1 - \mathcal{E}\mathcal{W}_2 - \mathcal{W}_3 = 0 \tag{34}$$

In general, the energy through order k may be written

$$\mathcal{E} = \sum_{p=1}^{k} \frac{1}{\mathcal{E}^{p-1}}\mathcal{W}_p \tag{35}$$

where

$$\mathcal{W}_p = \sum_{k_1\neq 0}^{\infty}\sum_{k_2\neq 0}^{\infty}\cdots\sum_{k_{p-1}\neq 0}^{\infty} \langle\Phi_0|\,\mathcal{H}\,|\Phi_{k_1}\rangle\ \langle\Phi_{k_1}|\,\mathcal{H}\,|\Phi_{k_2}\rangle\ \cdots\ \left\langle\Phi_{k_{p-1}}\right|\mathcal{H}\,|\Phi_0\rangle \tag{36}$$

The evaluation of the $\mathcal{W}_p$ is non-iterative The determination of the generalized Brillouin-Wigner perturbation theory energy in order k requires the determination of the lowest root of the k order polynomial

$$\mathcal{E}^k - \sum_{p=1}^{k} \mathcal{E}^{k-p}\mathcal{W}_p = 0. \tag{37}$$

3. Many-body corrections to finite-order generalized Brillouin-Wigner perturbation theory

Although the generalized Brillouin-Wigner perturbation theory has a very simple form it does not scale linearly with the number of electrons in the system and therefore does not provide a true "many-body" theory. However, we can introduce corrections.

The exact energy may be written

$$\mathcal{E} = E_0 + \Delta E \tag{38}$$

where E_0 is the ground state eigenvalue of $\mathcal{H}_0$ and ΔE is the level shift. We can then expand the generalized Brillouin-Wigner perturbation theory denominator in (26) as

$$\mathcal{E}^{-1} = {E_0}^{-1} + {E_0}^{-1}(-\Delta E)\,\mathcal{E}^{-1} \tag{39}$$

or

$$\mathcal{E}^{-1} + {E_0}^{-1}(\Delta E)\,\mathcal{E}^{-1} = {E_0}^{-1} \tag{40}$$

$$\begin{aligned}\mathcal{E} &= \langle\Phi|\mathcal{H}|\Phi\rangle + \frac{1}{\mathcal{E}}\sum_{k\neq 0}^{\infty}\langle\Phi|\mathcal{H}_1|\Phi_k\rangle\ \langle\Phi_k|\mathcal{V}|\Phi\rangle \\ &\quad\left\{+\frac{1}{\mathcal{E}}\frac{\Delta E}{E_0}\sum_{k\neq 0}^{\infty}\langle\Phi|\mathcal{H}_1|\Phi_k\rangle\ \langle\Phi_k|\mathcal{V}|\Phi\rangle\right\}\end{aligned} \tag{41}$$

and

$$\begin{aligned}\langle\Phi_k|\mathcal{V}|\Phi\rangle &= \langle\Phi_k|\mathcal{H}|\Phi\rangle + \frac{1}{\mathcal{E}}\sum_{p\neq 0}^{\infty}\langle\Phi_k|\mathcal{H}_1|\Phi_p\rangle\ \langle\Phi_p|\mathcal{V}|\Phi\rangle \\ &\quad\left\{+\frac{1}{\mathcal{E}}\frac{\Delta E}{E_0}\sum_{p\neq 0}^{\infty}\langle\Phi_k|\mathcal{H}_1|\Phi_p\rangle\ \langle\Phi_p|\mathcal{V}|\Phi\rangle\right\}, \quad \forall k\end{aligned} \tag{42}$$

4. Generalized Brillouin-Wigner coupled cluster theory

The Brillouin-Wigner perturbation theory can be applied to an ansatz which is intrinsically suited to the description of "many-body" systems and a valid many-body theory thus obtained. Consider, as an example, the application of generalized Brillouin-Wigner perturbation theory to the coupled cluster expansion [44], [45], [46].

In the cluster ansatz the wave operator is written

$$\Omega = e^S \tag{43}$$

so that equation (22) for the energy becomes

$$\begin{aligned} \mathcal{E} &= \langle \Phi_0 | \mathcal{H}\Omega | \Phi_0 \rangle \\ &= \left\langle \Phi_0 \middle| \mathcal{H}e^S \middle| \Phi_0 \right\rangle . \end{aligned} \tag{44}$$

The wave operator satisfies equation (23) which now becomes

$$e^S = I + \mathcal{G}\mathcal{H}e^S. \tag{45}$$

In general, for an N-electron system, the cluster operator, S, is a sum of one-body (S_1), two-body (S_2), . , N-body (S_N) cluster components defined with respect to a single reference function. In the simplest case we make the approximation

$$S \approx S_2 \tag{46}$$

Using equation (44) together with (1)

$$\begin{aligned} \mathcal{E} &= \langle \Phi_0 | \mathcal{H} [1 + S_2] | \Phi_0 \rangle \\ &= \langle \Phi_0 | \mathcal{H} | \Phi_0 \rangle + \langle \Phi_0 | \mathcal{H}_1 S_2 | \Phi_0 \rangle \end{aligned} \tag{47}$$

We take the $N[...]$ product form of the hamiltonian

$$\begin{aligned} \mathcal{H} &= \langle \Phi_0 | \mathcal{H} | \Phi_0 \rangle + \frac{1}{2} \sum_{A,B} \langle A | v | B \rangle \, N[X_A^+ X_B] + \\ &\quad \sum_{A,B,C,D} \langle AB | f | CD \rangle \, N[X_A^+ X_B^+ X_D X_C] \end{aligned} \tag{48}$$

The correlation energy is then

$$\Delta\mathcal{E} = \langle \Phi_0 | \mathcal{H}_1 S_2 | \Phi_0 \rangle \tag{49}$$

Using equation (45) the amplitudes are given by

$$\mathcal{E} \left\langle \Phi_{ij}^{ab} | S_2 | \Phi_0 \right\rangle = \left\langle \Phi_{ij}^{ab} \middle| \mathcal{H} \left[1 + S_2 + \frac{1}{2} S_2^2 \right] \middle| \Phi_0 \right\rangle . \tag{50}$$

Defining

$$S_{ij}^{ab} = \left\langle \Phi_{ij}^{ab} | S_2 | \Phi_0 \right\rangle \tag{51}$$

this becomes

$$\mathcal{E} S_{ij}^{ab} = \left\langle \Phi_{ij}^{ab} \middle| \mathcal{H} e^{S_2} \middle| \Phi_0 \right\rangle_{connected} + \frac{1}{2} \left\langle \Phi_{ij}^{ab} \middle| \mathcal{H} S_2^2 \middle| \Phi_0 \right\rangle_{disconnected} \tag{52}$$

where the subscripts denote whether the terms are *connected* or *disconnected*.

$$\frac{1}{2} \left\langle \Phi_{ij}^{ab} \middle| \mathcal{H} S_2^2 \middle| \Phi_0 \right\rangle_{disconnected} = \Delta\mathcal{E} S_{ij}^{ab} \tag{53}$$

Substituting (53) into (52)

$$\mathcal{E} S_{ij}^{ab} = \left\langle \Phi_{ij}^{ab} \middle| \mathcal{H} e^{S_2} \middle| \Phi_0 \right\rangle_{connected} + \Delta\mathcal{E} S_{ij}^{ab} \tag{54}$$

$$\mathcal{E} = E_0 + \Delta\mathcal{E} \tag{55}$$

and therefore

$$(E_0 + \Delta\mathcal{E}) S_{ij}^{ab} = \left\langle \Phi_{ij}^{ab} \middle| \mathcal{H} e^{S_2} \middle| \Phi_0 \right\rangle_{connected} + \Delta\mathcal{E} S_{ij}^{ab} \tag{56}$$

which is

$$E_0 S_{ij}^{ab} = \left\langle \Phi_{ij}^{ab} \middle| \mathcal{H} e^{S_2} \middle| \Phi_0 \right\rangle_{connected} \tag{57}$$

giving a manifestly connected scheme.

5. Summary and prospects

In this work, we have consider the application of generalized Brillouin-Wigner perturbation theory to the many-body problem. We have concentrated on the single reference formalism because of its simplicity. In section 2, we re-examined the generalized Brillouin-Wigner perturbation theory deriving both the Bloch equation and the corresponding Lippmann-Schwinger equation. Like the familiar Brillouin-Wigner perturbation theory, the generalized theory does not scale linearly with the number of electrons in the system and it cannot be regarded as a "many-body" theory. Two solutions to this problem were identified: *(i)* "many-body" corrections to the finite order generalized Brillouin-Wigner perturbation theory were derived in section 3, *(ii)* the theory can be applied to an ansatz which is intrinsically suited to "many-body" systems and, in section 4, the application of the generalized Brillouin-Wigner perturbation theory to the coupled cluster expansion was considered and the generalized Brillouin-Wigner coupled cluster theory obtained.

ACKNOWLEDGMENTS

This work was carried out under the auspices of the EU COST D9/0001/97 programme. IH acknowledges support under 1/4197/97 VEGA and 202/98/1028 GACR. SW acknowledges the support of EPSRC under Research Grant GR/M74627.

References

[1] Hubač, I., and Neogrady, P., Phys. Rev. A 50, 4558 (1994)

[2] Hubač, I., in *New Methods in Quantum Theory*, NATO ASI Series, ed. C.A. Tsipis, V.S. Popov, D.R Herschbach and J.S. Avery, pp. 183, Kluwer, Dordrecht (1996)

[3] Mášik, J., and Hubač, I., Coll. Czech. Chem. Commun. 62, 829 (1997)

[4] Mášik, J., and Hubač, I., in *Quantum Systems in Chemistry and Physics: Trends in Methods and Applications*, ed. R. McWeeny, J. Maruani, Y.G. Smeyers and S. Wilson, pp. 283, Kluwer Academic Publishers, Dordrecht (1997)

[5] Wenzel, W., and Steiner, M.M, J. Chem. Phys. 108, 4714 (1998)

[6] Mášik, J., and Hubač, I., Adv. Quantum Chem. **31**, 75 (1998)

[7] Mášik, J., Mach P. and Hubač, I., J. Chem. Phys. **108**, 6571 (1998)

[8] Mach, P., Mášik, J., Urban, J., and Hubač, I., Molec. Phys. **94**, 173 (1998)

[9] Mášik, J., Mach, P., Urban, J., Polasek, M., Babinec, P., and Hubač, I., Collect. Czech. Chem. Comm. **63**, 1213 (1998)

[10] Čársky, P., Hrouda, V., Sychrovsky, V., Hubač, I., Babinec, P., Mach, P., Urban, J , and Mášik, J , Collect Czech. Chem. Comm. **60**, 1419 (1995)

[11] Pittner, J., Nechtigall, P., Čársky, P., Mášik, J. and Hubač, I., J. Chem. Phys. **110**, 10275 (1999)

[12] Hubač, I., and Wilson, S., J. Phys B: At Mol. Opt. Phys **33**, 365 (2000)

[13] Lennard-Jones, J.E., Proc. Roy Soc. Lond. A129, 598 (1930)

[14] Brillouin, L., J. Physique 7, 373 (1932)

[15] Wigner, E.P., Math. naturw. Anz. ungar. Akad. Wiss. 53, 475 (1935)

[16] March, N.H., Young, W.H., and Sampanthar, S., *The many-body problem in quantum mechanics*, Cambridge University Press (1967)

[17] Lindgren, I., and Morrison, J., *Atomic Many-Body Theory,* Springer-Verlag, Berlin (1982)

[18] Wilson, S., *Electron correlation in molecules*, Clarendon Press, Oxford (1984)

[19] Harris, F.E., Monkhorst, H.J., and Freeman, D.L , *Algebraic and Diagrammatic Methods in Many-Fermion Theory*, Oxford University Press (1992)

[20] Brueckner, K.A., Phys Rev. **100**, 36 (1955)

[21] Goldstone, J., Proc. Roy. Soc. (London) A**239**, 267 (1957)

[22] Hubbard, J., Proc. Roy. Soc. (London) A**240**, 539 (1957)

[23] Hugenholtz, N., Physica **23**, 481 (1957)

[24] Brandow, B., Rev. Mod. Phys. **39**, 771 (1967)

[25] Wilson, S., in *Chemical Modelling: Applications and Theory*, Specialist Periodical Reports, Senior Reporter A. Hinchliffe, The Royal Society of Chemistry, London (in press); see also S. Wilson, in *Theoretical Chemistry*, **4**, Senior Reporter C. Thomson, The Royal Society of Chemistry, London (1981)

[26] Löwdin, P.-O., J. Chem. Phys. **19**, 1396 (1951)

[27] Löwdin, P.-O., J. Molec. Spectros. **10**, 12 (1963)

[28] Löwdin, P.-O., J. Molec. Spectros. **13**, 326 (1964)

[29] Löwdin, P.-O., J. Math. Phys. **3**, 969 (1962)

[30] Löwdin, P.-O., J. Math. Phys. **3**, 1171 (1962)

[31] Löwdin, P.-O., J. Molec. Spectros. **14**, 112 (1964)

[32] Löwdin, P.-O., J. Molec. Spectros. **14**, 119 (1964)

[33] Löwdin, P.-O., J. Molec. Spectros. **14**, 131 (1964)

[34] Löwdin, P.-O., J. Math. Phys. **6**, 1341 (1965)

[35] Löwdin, P.-O., Phys. Rev. A **139**, 357 (1965)

[36] Löwdin, P.-O., in *Perturbation Theory and its Application to Quantum Mechanics*, ed. C.H. Wilcox, John Wiley and Sons, New York (1966)

[37] Löwdin, P.-O., Intern. J. Quantum Chem. **2**, 867 (1968)

[38] Löwdin, P.-O., and O GOSCINSKI, Intern. J. Quantum Chem. **5**, 685 (1971)

[39] Lippmann, B.P., and Schwinger, J., Phys. Rev. **79**, 469 (1950)

[40] Eden, R.J., and Francis, N.C., Phys. Rev. **97**, 1366 (1955)

[41] Lindgren, I., J. Phys. B: At. Mol Phys. **7**, 2441 (1974)

[42] Lindgren, I., Intern J. Quantum Chem. Symp. **12**, 33 (1978)

[43] Bloch, C., Nucl. Phys. **6**, 329 (1958)

[44] Paldus, J., in *Methods in Computational Molecular Physics*, NATO ASI Series, edited by S. Wilson and G.H.F. Diercksen, p. 99*ff*, Plenum Press, New York (1992)

[45] Paldus, J., in Relativistic and Correlation Effects in Molecules and Solids, NATO ASI Series, edited by G.L. Malli, p. 207, Plenum Press, New York (1994)

[46] *Recent Advances in Coupled Cluster Methods*, Recent Advances in Computational Chemistry, Vol. 3, edited by R.J. Bartlett, World Scientific, Singapore (1997)

Multireference Brillouin-Wigner methods for many-body systems

I. Hubač[†‡], P. Mach [†] and S. Wilson[¶]

[†] *Department of Chemical Physics, Faculty of Mathematics and Physics, Comenius University, 842 15 Bratislava, Slovakia*

[‡] *Institute of Physics, Silesian University, 74601 Opava, Czech Republic*

[¶] *Rutherford Appleton Laboratory, Chilton, Oxfordshire OX11 0QX, England*

Abstract

Brillouin-Wigner perturbation theory has a number of advantages over the much more widely used Rayleigh-Schrödinger perturbation theory in studies of the electron correlation problem in atoms and molecules. This article briefly reviews some historical background, the perceived advantages and disadvantages of the Brillouin-Wigner perturbation theory. The convergence difficulties of the Rayleigh-Schrödinger perturbation theory when applied to problems demanding the use of multireference formalism is described. The problems created by the appearance of intruder states, of both the "physical" and the "backdoor" variety, in the multireference Rayleigh-Schrödinger formalism are outlined. Recent progress in the formulation and application of Brillouin-Wigner methods to the atomic and molecular many-body problem is then described. The use of Brillouin-Wigner theory in solving the equations associated with many-body theories, such as coupled cluster theory, is described as well as in the development of *a posteriori* corrections to theories which contain terms which scale non-linearly with particle number, such as limited configuration interaction or finite-order Brillouin-Wigner perturbation theory. Particular attention is given to multireference Brillouin-Wigner methods.

ADVANCES IN QUANTUM CHEMISTRY VOLUME 39

0065-3276/01 $35 00

Contents

1 Introduction

For almost thirty years Rayleigh-Schrödinger perturbation theory in its "many-body" form has been regarded as the method of choice in describing electron correlation effects in atoms and molecules. The linear proportionality of the calculated energy or other expectation values with respect to the number of electrons in a given system - also known as "size-consistency" or "size-extensivity" - is seen as one the principal advantages of the many-body perturbation theory approach; a property that is rendered most transparent in its diagrammatic formulation.

The method which is most usually designated "MP2" (second order many-body perturbation theory developed with respect to a Moeller-Plesset reference hamiltonian) is nowadays the most intensively used *ab initio* molecular electronic structure technique for describing electron correlation effects in molecular systems [1]. It is regarded as one of the most important components of the arsenal of electronic structure methods available to the contemporary quantum chemist combining computational efficiency with ease of interpretability. Its computational efficiency, especially in so-called 'direct' algorithms [2], facilitates application both to large molecules and in calculations of high accuracy for small molecular systems using extended basis sets. It is well suited to parallel computation enabling the effective exploitation of modern computing machines.

The "MP2" method is robust for systems for which a single reference function is appropriate, such as the ground state of the neon atom or the water molecule at its equilibrium geometry. However, for systems where such a simple reference function is unsuitable the method becomes fragile as applications which are best regarded as cases of "deliberate stupidity" have demonstrated. For example, the unreliability of the "MP2" method for the ground state of the water molecule with symmetrically stretched bonds is well documented in

the literature. Even when multireference functions are employed the Rayleigh-Schrödinger perturbation theory can exhibit convergence difficulties. These difficulties are associated with the so-called "intruder state problem".

Interest in Brillouin-Wigner perturbation theory has been rekindled over the past few years since it does possess some features which suggest that it may provide a robust and efficient approach for the theoretical description of correlation effects in systems demanding the use of multireference function formalism. Brillouin-Wigner perturbation theory has not been widely used in quantum chemistry over recent decades principally because it is not seen as a valid many-body theory. We, therefore, present some historical background to Brillouin-Wigner methods in section 2. In particular, we compare the basic structure of the Brillouin-Wigner perturbation theory with the Rayleigh-Schrödinger expansion. We list the known advantages of the Brillouin-Wigner approach as well as its disadvantages. In section 3, we briefly describe the convergence difficulties assoicated with intruder states which can arise in the Rayleigh-Schrödinger perturbation theory in applications to problems demanding the use of multireference formalisms. In section 4, we give an overview of recent work on the application of Brillouin-Wigner methods to many-body systems and solving the problems described in section 3. Section 5 contains a summary and indicates the prospects for this approach.

2 Some historical background

The theory which is today called "Brillouin-Wigner perturbation theory" was introduced in three seminal papers published in the 1930s. The first of these was published in 1930 by Lennard-Jones [3]. [Some authors [4], [5] refer to the method as "Lennard-Jones-Brillouin-Wigner perturbation theory".] Subsequently, Brillouin published his contribution in 1932 [6] and Wigner's paper appear two year later [7].

Brillouin-Wigner perturbation theory has a number of advantages over the Rayleigh-Schrödinger perturbation theory. It also has significant disadvantages. Before describing these let us recall the basic structure of these two theories.

We seek to develop approximate solutions of the time-independent Schrödinger equation

$$\mathcal{H}\Psi_\mu = \mathcal{E}_\mu \Psi_\mu, \quad \mu = 0, 1, 2, ... \tag{1}$$

starting from some reference or model defined by the equation

$$\mathcal{H}_0 \Phi_k = E_k \Phi_k, \quad k = 0, 1, 2, ... \tag{2}$$

for which the solutions are known. We write the total hamiltonian in the form

$$\mathcal{H} = \mathcal{H}_0 + \lambda \mathcal{H}_1 \tag{3}$$

where the parameter λ is used to interpolate between the unperturbed problem ($\lambda = 0$) and the perturbed problem ($\lambda = 1$). Perturbation theories are developed by making expansions for the exact eigenvalue, $\mathcal{E}$, and the corresponding eigenfunction, Ψ.

In Brillouin-Wigner perturbation theory, we obtain the following expansion for the ground state energy of the perturbed systems

$$\mathcal{E}_0 = E_0 + \varepsilon_1 + \varepsilon_2 + \varepsilon_3 + ... \tag{4}$$

where the energy coefficients are given by

$$\varepsilon_p = \langle \Phi_0 | \, \mathcal{H}_1 \, (\mathcal{G}_{BW} \mathcal{H}_1)^{p-1} \, | \Phi_0 \rangle \tag{5}$$

and $\mathcal{G}_{BW}$ is the Brillouin-Wigner resolvent

$$\mathcal{G}_{BW} = \sum_{r \neq 0} \frac{|\Phi_r\rangle \, \langle \Phi_r|}{\mathcal{E} - E_r} \tag{6}$$

In Rayleigh-Schrödinger perturbation theory, the expansion for the ground state energy of the perturbed system can be written

$$\mathcal{E}_0 = E_0 + E_0^{(1)} + E_0^{(2)} + E_0^{(3)} + ... \tag{7}$$

where the energy coefficients have a more complicated structure and the first few terms take the form

$$E_0 = \langle \Phi_0 | \, \mathcal{H}_0 \, | \Phi_0 \rangle \tag{8}$$

$$E_0^{(1)} = \langle \Phi_0 | \, \mathcal{H}_1 \, | \Phi_0 \rangle \tag{9}$$

$$E_0^{(2)} = \langle \Phi_0 | \, \mathcal{H}_1 \mathcal{G}_{RS} \mathcal{H}_1 \, | \Phi_0 \rangle \tag{10}$$

$$E_0^{(3)} = \langle \Phi_0 | \, \mathcal{H}_1 \mathcal{G}_{RS} \mathcal{H}_1 \mathcal{G}_{RS} \mathcal{H}_1 \, | \Phi_0 \rangle - E_0^{(1)} \langle \Phi_0 | \, \mathcal{H}_1 (\mathcal{G}_{RS})^2 \mathcal{H}_1 \, | \Phi_0 \rangle \tag{11}$$

$$\begin{aligned} E_0^{(4)} \;=\; & \langle \Phi_0 | \, \mathcal{H}_1 \mathcal{G}_{RS} \mathcal{H}_1 \mathcal{G}_{RS} \mathcal{H}_1 \mathcal{G}_{RS} \mathcal{H}_1 \, | \Phi_0 \rangle \\ & - E_0^{(1)} \langle \Phi_0 | \, \mathcal{H}_1 (\mathcal{G}_{RS})^2 \mathcal{H}_1 \mathcal{G}_{RS} \mathcal{H}_1 \, | \Phi_0 \rangle \\ & - E_0^{(1)} \langle \Phi_0 | \, \mathcal{H}_1 \mathcal{G}_{RS} \mathcal{H}_1 (\mathcal{G}_{RS})^2 \mathcal{H}_1 \, | \Phi_0 \rangle \\ & + \left(E_0^{(1)} \right)^2 \langle \Phi_0 | \, \mathcal{H}_1 (\mathcal{G}_{RS})^3 \mathcal{H}_1 \, | \Phi_0 \rangle \\ & - E_0^{(2)} \langle \Phi_0 | \, \mathcal{H}_1 (\mathcal{G}_{RS})^2 \mathcal{H}_1 \, | \Phi_0 \rangle \end{aligned} \tag{12}$$

In these expressions, $\mathcal{G}_{RS}$ is the Rayleigh-Schrödinger resolvent

$$\mathcal{G}_{RS} = \sum_{r \neq 0} \frac{|\Phi_r\rangle \langle \Phi_r|}{E_0 - E_r} \tag{13}$$

Let us now turn to the advantages of the Brillouin-Wigner perturbation theory. Brillouin-Wigner perturbation theory has five main advantages over the Rayleigh-Schrödinger perturbation theory. These are:-

(i) Rayleigh-Schrödinger theory can be regarded as a approximation to Brillouin-Wigner theory [3], [4]. Consider, for example, the second order energy, ε_2, in the Brillouin-Wigner expansion. This may be written in sum-over-states form as

$$\varepsilon_2 = \sum_{r \neq 0} \frac{\langle \Phi_0 | \mathcal{H}_1 | \Phi_r \rangle \langle \Phi_r | \mathcal{H}_1 | \Phi_0 \rangle}{\mathcal{E} - E_r} \tag{14}$$

If we make the approximation

$$\mathcal{E} \sim E_0 \tag{15}$$

then we are led immediately to the Rayleigh-Schrödinger second order energy component

$$E_0^{(2)} = \sum_{r \neq 0} \frac{\langle \Phi_0 | \mathcal{H}_1 | \Phi_r \rangle \langle \Phi_r | \mathcal{H}_1 | \Phi_0 \rangle}{E_0 - E_r} \tag{16}$$

If we write

$$\mathcal{E} = E_0 + \Delta E_0 \tag{17}$$

then the denominator in (14) becomes

$$\begin{aligned} \frac{1}{\mathcal{E} - E_r} &= \frac{1}{E_0 - E_r + \Delta E_0} \\ &= \frac{1}{E_0 - E_r} + \left[\frac{1}{E_0 - E_r} (-\Delta E_0) \frac{1}{E_0 - E_r + \Delta E_0} \right] \end{aligned} \tag{18}$$

and

$$\frac{1}{\mathcal{E} - E_r} \sim \frac{1}{E_0 - E_r} \tag{19}$$

if ΔE_0 is small and the second term on the right hand side of (18) is negligible.

(ii) Brillouin-Wigner theory is formally much simpler than the Rayleigh-Schrödinger theory [4],[7]. This is evident from a comparison of equations (4), (5) and (6) defining Brillouin-Wigner perturbation theory with (7), (12) and (13) for the Rayleigh-Schrödinger theory. In fact, equations (4), (5) and (6) provide a complete definition of Brillouin-Wigner perturbation theory through all orders. The Brillouin-Wigner perturbation series is a simple geometric

series whereas in every order beyond second order in the energy the Rayleigh-Schrödinger perturbation theory gives rise to a very much more complicated structure. In every order there is a principle term of the form

$$\varepsilon_p^{RS} = \langle \Phi_0 | \mathcal{H}_1 (\mathcal{G}_{RS} \mathcal{H}_1)^{p-1} | \Phi_0 \rangle , \quad p = 1, 2, ... \tag{20}$$

which is analogous to the Brillouin-Wigner term ε_p defined in (5) together with other terms in third and higher orders which are often called 'renormalization' terms for reasons that will be elaborated below. There is only one 'renormalization' term in third order, four in fourth order, thirteen in fifth order, rising to, for example, 4,861 in tenth order of perturbation [8].

(iii) Convergence of the Brillouin-Wigner perturbation theory is often more rapid than that of the Rayleigh-Schrödinger theory for a given problem [3], [4], [6], [9]. For example, it is well known that energy eigenvalue for a two-state problem is given exactly by second order Brillouin-Wigner perturbation theory. However, the Rayleigh-Schrödinger perturbation expansion, in general, has to be taken to infinite order to solve this simple problem. Specifically, taking a zero order matrix

$$\mathbf{H_0} = \begin{bmatrix} 0 & 0 \\ 0 & \alpha \end{bmatrix}, \tag{21}$$

and a perturbation

$$\mathbf{H_1} = \begin{bmatrix} 0 & \beta \\ \beta & 0 \end{bmatrix}, \tag{22}$$

and then solving the secular problem

$$\begin{vmatrix} -\varepsilon & \beta \\ \beta & \alpha - \varepsilon \end{vmatrix} = 0 \tag{23}$$

or

$$\varepsilon^2 - \alpha\varepsilon - \beta^2 = 0 \tag{24}$$

gives an exact solution

$$\varepsilon = \frac{1}{2} \left[\alpha \pm \sqrt{\alpha^2 + 4\beta^2} \right] . \tag{25}$$

The Brillouin-Wigner perturbation expansion through second order for this problem is

$$\varepsilon = \frac{\beta^2}{\varepsilon - \alpha} \tag{26}$$

which is seen to be equivalent to equation (24) and thus the exact solution, equation(25). For the two-state problem defined above second order

Brillouin-Wigner perturbation theory provides an exact result. The Rayleigh-Schrödinger perturbation series for this problem can be obtained by writing (25) in the form

$$\varepsilon = \frac{\alpha}{2}\left[1 \pm \sqrt{1+x}\right], \quad x = \frac{4\beta^2}{\alpha^2} \tag{27}$$

and using the identity

$$\sqrt{1+x} = 1 + \frac{1}{2}x - \frac{1}{8}x^2 + \frac{1}{16}x^3 - \frac{5}{128}x^4 + \frac{7}{256}x^5 - \frac{21}{1026}x^6 \ldots \tag{28}$$

The Rayleigh-Schrödinger expansion therefore has the form

$$\varepsilon = -\frac{\beta^2}{\alpha} + \frac{\beta^4}{\alpha^3} - 2\frac{\beta^6}{\alpha^5} + \ldots \tag{29}$$

and summation to all orders is required to obtained the exact energy eigenvalue.

(iv) Brillouin-Wigner perturbation theory may converge for problems for which the Rayleigh-Schrödinger theory does not [4], [7]. An example is again provided by the two-state problem defined by (21) and (22). The Brillouin-Wigner perturbation expansion leads to an exact solution by second order irrespective of the particular values of the parameters defining the zero-order problem and the perturbation, i.e. α and β. For this problem the Brillouin-Wigner perturbation expansion has an infinite radius of convergence. Let us explicitly introduce the perturbation parameter, λ, and determine the radius of convergence of the Rayleigh-Schrödinger perturbation expansion. We write the hamiltonian matrix for the perturbed problem as

$$\mathbf{H_0} + \lambda \mathbf{H_1} = \begin{bmatrix} 0 & 0 \\ 0 & \alpha \end{bmatrix} + \lambda \begin{bmatrix} 0 & \beta \\ \beta & 0 \end{bmatrix} \tag{30}$$

which has exact solutions

$$\varepsilon = \frac{1}{2}\left[\alpha \pm \sqrt{(\alpha^2 + 4\beta^2\lambda^2)}\right] \tag{31}$$

The Rayleigh-Schrödinger perturbation expansion now takes the form

$$\varepsilon = -\frac{\beta^2}{\alpha}\lambda^2 + \frac{\beta^4}{\alpha^3}\lambda^4 - 2\frac{\beta^6}{\alpha^5}\lambda^6 + \ldots \tag{32}$$

The radius of convergence may be obtained directly by setting the discriminant in (31) to zero, i.e. $\alpha^2 + 4\beta^2\lambda^2 = 0$. We are thus led to the result that the Rayleigh-Schrödinger perturbation expansion for the two-state model converges for values of λ satisfying

$$|\lambda| > \frac{1}{2}\left|\frac{\alpha}{\beta}\right| \tag{33}$$

For values of λ which do not satisfy (33) the expansion (32) will diverge.

However, it is important to note that it is usually possible to obtain valuable estimates of the energy eigenvalue by employing Padé approximants in cases where the Rayleigh-Schrödinger perturbation theory diverges because such approximants are able to handle a wider class of functions than the power series usually assumed in perturbation theory.

(v) Brillouin-Wigner perturbation theory is often more convenient to use for degenerate problems. This is one of the properties of the method which were emphasized by Wigner [7] in his orginal paper. Indeed the Brillouin-Wigner perturbation theory can be formally applied to degenerate problems without modification.

For example, setting $\alpha = 0$ in the two-state problem defined by (21) and (22) above so as to generate a degenerate problem leads immediately from (23) and (24) to the exact solution $\varepsilon^2 = \beta^2$. The Brillouin-Wigner second order energy (26) becomes $\varepsilon = \beta^2/\varepsilon$ which clearly agrees with the exact solution. On the other hand, the non-degenerateRayleigh-Schrödinger perturbation theory breaks down because the radius of convergence (33) is now zero.

However, in spite of the five advantages listed above, the Brillouin-Wigner perturbation theory also has some disadvantages. Specifically, Brillouin-Wigner perturbation theory has two disadvantages in comparison with the Rayleigh-Schrödinger perturbation theory. These are:-

(i) Brillouin-Wigner perturbation theory is iterative, since the exact energy is contained in the denominators arising in the expressions for the energy components.

Consider, for example, the Brillouin-Wigner perturbation through second order:-

$$\mathcal{E} = \langle\Phi_0|\,\mathcal{H}_0\,|\Phi_0\rangle + \langle\Phi_0|\,\mathcal{H}_1\,|\Phi_0\rangle + \sum_{r\neq 0} \frac{\langle\Phi_0|\,\mathcal{H}_1\,|\Phi_r\rangle\ \langle\Phi_r|\,\mathcal{H}_1\,|\Phi_0\rangle}{\mathcal{E} - E_r} \tag{34}$$

Equation (34) is solved iteratively. The right-hand-side of this equation may be written $f^{(2)}(\mathcal{E})$ and equation(34) itself can then be put in the form

$$\mathcal{E}^{(2)}_{i+1} = f^{(2)}(\mathcal{E}^{(2)}_i) \tag{35}$$

Taking an initial value $\mathcal{E}^{(2)}_0$ successive application of (35) defines a sequence of approximations $\mathcal{E}^{(2)}_i, i = 0, 1, 2, \ldots$ which, if they are convergent, converge to the second order Brillouin-Wigner energy, which we denote $\mathcal{E}^{(2)}$. In general, of course, $\mathcal{E}^{(2)}$ is not necessarily equal to the exact energy, $\mathcal{E}$.

In third order Brillouin-Wigner perturbation theory, we have

$$\mathcal{E} = \langle\Phi_0|\,\mathcal{H}_0\,|\Phi_0\rangle + \langle\Phi_0|\,\mathcal{H}_1\,|\Phi_0\rangle + \sum_{r\neq 0} \frac{\langle\Phi_0|\,\mathcal{H}_1\,|\Phi_r\rangle\ \langle\Phi_r|\,\mathcal{H}_1\,|\Phi_0\rangle}{\mathcal{E} - E_r} \tag{36}$$

$$\sum_{r\neq 0}\sum_{s\neq 0}\frac{\langle\Phi_0|\,\mathcal{H}_1\,|\Phi_r\rangle\;\langle\Phi_r|\,\mathcal{H}_1\,|\Phi_s\rangle\;\langle\Phi_s|\,\mathcal{H}_1\,|\Phi_0\rangle}{(\mathcal{E}-E_r)\;(\mathcal{E}-E_s)} \tag{37}$$

The right-hand-side of this equation may be written $f^{(3)}(\mathcal{E})$ and equation(37) itself can then be put in the form

$$\mathcal{E}^{(3)}_{i+1} = f^{(3)}(\mathcal{E}^{(3)}_i) \tag{38}$$

As for the second order energy we take an initial value $\mathcal{E}^{(3)}_0$ and generate successive application of (38) defines a sequence of approximations $\mathcal{E}^{(3)}_i, i = 0, 1, 2, ...$ which, if they are convergent, converge to the third order Brillouin-Wigner energy, which we denote $\mathcal{E}^{(3)}$. Again, in general, $\mathcal{E}^{(3)}$ is not necessarily equal to the exact energy, $\mathcal{E}$.

In contrast to the Brillouin-Wigner approach, the Rayleigh-Schrödinger perturbation theory is manifestly non-iterative.

(ii) Brillouin-Wigner perturbation theory is not explicitly a many-body theory in that the energy expressions in each order do not scale linearly with particle number. This property of the Brillouin-Wigner expansion which was first pointed out by Brueckner in the mid-1950s is the main reason for the paucity of applications to the atomic and molecular electronic structure problem until recent years. In their treatise on the many-body problem in quantum mechanics, March, Young and Sampanthar write that *"the Brillouin-Wigner form of the [many-body] theory is completely inappropriate"*. They explicitly show that

> *"... the first term N and that all succeeding terms [are] individually negligible compared to the first term, whatever the strength of the perturbation. However, it would be wrong to conclude that the above argument proves that the Brillouin-Wigner series is convergent and that only the first term need by considered. Among other reasons, we know that [the first order term] does not include dynamical correlations between particles and these must be important (on physical grounds) for a strongly interacting system. The situation therefore must be that many (N) of the small terms beyond the first are of roughly comparable size, and add up to change the energy/particle by a finite amount. Thus it will be completely misleading to apply many-body perturbation theory in the Brillouin-Wigner form, short of considering an infinite number of terms in the limit of large N."*

In contract to the Brillouin-Wigner perturbation theory, it is well known that Rayleigh-Schrödinger perturbation theory in its "many-body" form does afford a theoretical basis for the description of many-body systems. Again March, Young and Sampanthar [10] write

> *"the Rayleigh-Schrödinger perturbation theory ... if carefully and systematically used, can yield and energy/particle proportional to N as required, in spite of the appearance of spurious terms proportional to N^2, etc., in any given order. In fact, Brueckner showed that the non-physical terms cancel up to fourth order, and the generalization to all orders was effected by Goldstone."*

They continue

> *"To third order (and to any higher order) one can in fact verify that the terms of the Rayleigh-Schrödinger perturbation expansion either vanish or increase as N in the limit N, the non-physical terms proportional to N^2, N^3, etc., all neatly cancelling each other."*

and then conclude

> *"... the Rayleigh-Schrödinger series is more useful than the Brillouin-Wigner form in that it yields an expansion leading to the energy per particle as independent of the size of the system for large N."*

It is for these reasons coupled with the efficiency of the corresponding computer algorithms in low-order that Rayleigh-Schrödinger perturbation theory has been regarded as the method of choice in describing electron correlation effects in atoms and molecules for almost thirty years.

3 Rayleigh-Schrödinger perturbation theory and the intruder state problem

The convergence difficulties of the Rayleigh-Schrödinger theory when applied to problems demanding the use of multireference formalisms has rekindled interest in the Brillouin-Wigner theory. The appearance of intruder states in the Rayleigh-Schrödinger theory can render it useless in, for example, applications to molecular dissociative problems which required the use of a multireference function. The renewed interest in Brillouin-Wigner theory is fuelled by the need to develop a robust and efficient apparatus for the theoretical description of such systems.

The development of a multireference perturbation theory requires the selection of a reference space or model space with respect to which a perturbation expansion is made. This selection is based on the physics of the problem in hand and most often involves the identification of those functions required to accurately describe molecular dissociation. The definition of the reference

space usually begins with the partition of the single particle states or orbitals into three subsets as follows:-

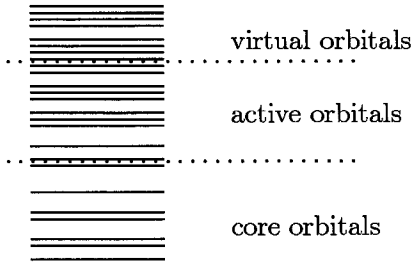

The core subset is fully occupied in all reference functions. The active subset of state functions is occupied in some of the reference functions. The virtual subset is unoccupied in all reference functions.

For the unperturbed problem the energies associated with the reference functions should lie below the energies associated with other functions. The situation can be represented pictorially as follows:-

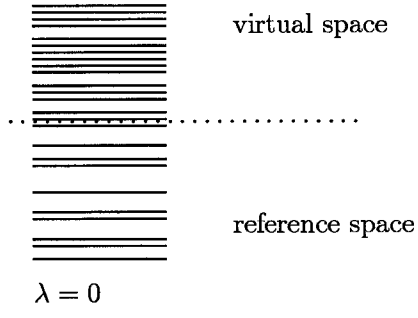

Now for some values of the perturbation parameter, λ, in the range of values of interest, *i.e.* $0 \leq |\lambda| \leq 1$, the energies associated with some functions which are not in the reference space may lie below the energies of functions in the reference space. These states are termed *intruder states.* Their presence can impair or even completely destroy the convergence of multireference perturbation expansions. Intruder states can be divided into two types:- *(i)* those satisfying

$$0 < \lambda \leq +1 \tag{39}$$

and which might be termed *physical* intruder states since their occurrence usually has some physical origin, which, once recognized, can be used to eliminate

them; *(ii)* those satisfying

$$0 > \lambda \geq -1 \tag{40}$$

which are unphysical and are termed *backdoor* intruder states. Such states are both more difficult to identify and more difficult to eliminate.

Most formulations of many-body multireference theories require the use of a complete active space. The reference space must consist of functions generated by considering all possible occupancies of the active orbitals. Failure the satisfy this requirement often destroys the linear scaling properties of the theory with particle number. On the other hand, the imposition of this requirement can easily lead to a situation in which functions which are not in the reference space have an energy significantly below the energies associated with the highest state included in the model space. Over the years a number of solutions to this intruder state problem have been advanced but none of these are wholly satisfactory failing to provide a robust and general framework for handling problems which demand a multireference formulation.

4 Recent progress in Brillouin-Wigner methods for the many-body problem

Recent years have witnessed [11]-[22] a revival of interest in Brillouin-Wigner perturbation theory principally because it is seen as a possible remedy to the intruder state problem. Wenzel and Steiner [15] write (p. 4714)

> *"... the reference energy in Brillouin-Wigner perturbation theory is the fully dressed energy ... This feature guarantees the existence of a natural gap and thereby rapid convergence of the perturbation series."*

We consider the application of multireference Brillouin-Wigner methods to many-body systems. Two distinct approaches can be taken:-

(i) the Brillouin-Wigner perturbation theory can be employed to solve the equations associated with an explicitly many-body method. For example, the full configuration interaction problem can be solved in this way as can the coupled cluster equations [23]-[25].

Hubač and his coworkers [11] have explored the use of Brillouin-Wigner perturbation theory in solving the equations of coupled cluster theory. By adopting an exponential expansion for the wave operator they obtain the Brillouin-Wigner coupled cluster theory [11]- [14] which is entirely equivalent to other many-body formulations for the case of a single reference function

since the perturbation expansion is summed through all orders. The application of the Brillouin-Wigner coupled cluster approach to the multi-reference function problem has given some useful insights [26]-[27].

Multireference generalized Brillouin-Wigner coupled cluster theory, in particular, has been shown to have considerable potential [29, 30].

(ii) a posteriori corrections can be obtained to the Brillouin-Wigner perturbation theory itself and to methods such as limited configuration interaction. These *a posteriori* corrections are based on a very simple idea. We compare the Brillouin-Wigner resolvent (6) with the Rayleigh-Schrödinger resolvent (13). We see that they differ in denominators. Using identity relation [28]

$$(\mathcal{E} - E_k)^{-1} = (E_0 - E_k)^{-1} + (E_0 - E_k)^{-1} (-\Delta E) (\mathcal{E} - E_k)^{-1} \tag{41}$$

where the exact energy is written as

$$\mathcal{E} = E_0 + \Delta E \tag{42}$$

and where E_0 is the ground state eigenvalue of $\mathcal{H}_0$ and ΔE is the level shift, we can find a posteriori size extensivity corrections to Brillouin-Wigner series. If we adopt the fact that Rayleigh-Schrödinger perturbation theory series employing the linked cluster theorem use the $(E_0 - E_k)^{-1}$ as denominator (the theory is fully size extensive) the second term on right-hand-side of eq.(41) can be viewed as extensivity correction term for Brillouin-Wigner series. This simple idea was used to find *a posteriori* correction for limited configuration interaction method [31] as well as for state specific multireference Brillouin-Wigner coupled cluster theory [26],[27].

5 Summary and prospects

In this article we discussed some advantages of Brillouin-Wigner perturbation theory over standardly in quantum chemistry used Rayleigh-Schrödinger perturbation theory. Beside the fact that Brillouin-Wigner perturbation theory is not often used in quantum chemistry we believe that it has perspective to be a many-body method. We studied the use of Brillouin-Wigner perturbation theory for limited configuration interaction calculations as well as for coupled cluster theory (both single reference and multireference versions). We were able to develop a posteriori corrections to both limited configuration interaction method and MRBWCC theory by comparing Brillouin-Wigner perturbation theory and Rayleigh-Schrödinger perturbation theory series. We demonstrated that these a posteriori corrections works well. This gives perspective to MRBWCC theory because as we demonstrated this theory is simple and its extension to more than 2 state problem makes this theory very interesting.

By comparing both Rayleigh-Schrödinger perturbation theory and Brillouin-Wigner perturbation theory series and their advantages and disadvantages we believe that the method which will employ the advantages of both methods(something in between) can be developed which will be suitable for studying "difficult molecules" which are generally of multireference character.

ACKNOWLEDGMENTS

This work was carried out under the auspices of the EU COST D9/0001/97 programme. IH also acknowledges support under 1/4197/97 VEGA and 202/98/1028 GACR. SW acknowledges the support of EPSRC under Research Grant GR/M74627.

References

[1] S. Wilson, in *Chemical Modelling: Applications and Theory*, Senior Reporter: A. Hinchliffe, Specialist Periodical Reports **1**, 364-452 (The Royal Scoiety of Chemistry, London, 2000)

[2] J. Almlof, K. Faegri and K. Korsell, J. Comput. Chem. **3**, 385 (1982); M. Head-Gordon, J.A. Pople and M.J. Frisch, Chem. Phys. Lett. **153**, 503 (1988); S. Saebo and J. Almlof, Chem. Phys. Lett. **154**, 83 (1989); S. Wilson in *Electron correlation in atoms and molecules*, ed. S. Wilson, Meth. Comput. Chem. **1** *p.* 301*ff* (New York: Plenum, 1987)

[3] J.E. Lennard-Jones, Proc. Roy. Soc. (London) **A129**, 598 (1930)

[4] A. Dalgarno, in *Quantum Theory. I. Elements*, edited by D.R. Bates, Vol. 1, Chap. 5 (Academic Press, New York, 1961)

[5] S. Wilson, *Electron correlation in molecules*, (Clarendon Press, Oxford, 1984)

[6] L. Brillouin, J. Phys. Radium **7**, 373 (1932)

[7] E.P. Wigner, Math. Naturwiss. Anz. Ungar. Akad. Wiss **53**, 475 (1935)

[8] S. Wilson, in *Methods in Computational Molecular Physics*, NATO ASI Series B, Vol. 293, p. 203, (Plenum Press, New York, 1992)

[9] P.M. Morse and H. Feshbach, *Methods of Theoretical Physics*, Chap. 9.1 (McGraw-Hill, New York, 1953)

[10] N.H. March, W.H. Young and S. Sampanthar, *The many-body problem in quantum mechanics*, (Cambridge University Press, 1967)

[11] I. Hubač and P. Neogrady, Phys. Rev. **A50**, 4558 (1994)

[12] I. Hubač, in *New Methods in Quantum Theory*, NATO ASI Series, ed. C.A. Tsipis, V.S. Popov, D.R. Herschback and J.S. Avery, pp. 183, Kluwer, Dordrecht (1996)

[13] J. Mášik and I. Hubač, Coll. Czech. Chem. Commun. **62**, 829 (1997)

[14] J. Mášik and I. Hubač, in *Quantum Systems in Chemistry and Physics: Trends in Methods and Applications*, ed. R. McWeeny, J. Maruani, Y.G. Smeyers and S. Wilson, pp. 283, Kluwer Academic Publishers, Dordrecht (1997)

[15] W. Wenzel and M.M Steiner, J. Chem. Phys. **108**, 4714 (1998)

[16] W. Wenzel, Intern. J. Quantum Chem. **70**, 613 (1998)

[17] J. Mášik and I. Hubač, Adv. Quantum Chem. **31**, 75 (1998)

[18] J. Mášik, P. Mach and I. Hubač, J. Chem. Phys. **108**, 6571 (1998)

[19] P. Mach, J. Mášik, J. Urban and I. Hubač, Molec. Phys. **94**, 173 (1998)

[20] J. Mášik, P. Mach, J. Urban, M. Polasek, P. Babinec and I. Hubač, Collect. Czech. Chem. Comm. **63**, 1213 (1998)

[21] P. Čársky, V. Hrouda, V. Sychrovsky, I. Hubač, P. Babinec, P. Mach, J. Urban and J. Mášik, Collect. Czech. Chem. Comm. **60**, 1419 (1995)

[22] J. Pittner, P. Nechtigall, P. Čársky, J. Mášik and I. Hubač, J. Chem. Phys. **110**, 10275 (1999)

[23] J. Paldus, in *Methods in Computational Molecular Physics*, NATO ASI Series, edited by S. Wilson and G.H.F. Diercksen, p. 99*ff*, Plenum Press, New York (1992)

[24] J. Paldus, in Relativistic and Correlation Effects in Molecules and Solids, NATO ASI Series, edited by G.L. Malli, p. 207, Plenum Press, New York (1994)

[25] *Recent Advances in Coupled Cluster Methods*, Recent Advances in Computational Chemistry, Vol. 3, edited by R.J. Bartlett, World Scientific, Singapore (1997)

[26] I. Hubač, J. Pittner, and P. Čársky, J. Chem. Phys. **112**, 8779 (2000)

[27] J. Sancho-García, J. Pittner, P. Čársky, and I. Hubač, J. Chem. Phys. **112**, 8785 (2000)

[28] I. Hubač and S. Wilson, J. Phys. B: At. Mol. Opt. Phys. **33**, 365 (2000)

[29] I. Hubač, and S. Wilson, Adv. Quantum Chem. *this volume*

[30] I. Hubač, and S. Wilson, *to be submitted for publication*

[31] I. Hubač, P. Mach and S. Wilson, J. Phys. B: At. Mol. Opt. Phys. **33**, 4735 (2000)

The Dirac Equation in the algebraic approximation. VII. A comparison of molecular finite difference and finite basis set calculations using distributed Gaussian basis sets

by

H.M. Quiney[†], V.N. Glushkov[‡] & S. Wilson[§] ,

[†] *School of Chemistry, University of Melbourne, Parkville, Victoria 3052, Australia*

[‡] *Physics Department, State University, 320625, per. Nauchniy 13, Dniepropetrovsk, Ukraine*

[§] *Rutherford Appleton Laboratory, Chilton, Oxfordshire OX11 0QX, England*

Abstract

A comparison is made of the accuracy achieved in finite difference and finite basis set approximations to the Dirac equation for the ground state of the hydrogen molecular ion. The finite basis set calculations are carried out using a distributed basis set of Gaussian functions the exponents and positions of which were determined by invoking the variational principle for the corresponding non-relativistic problem. Using only 27 s-type functions for the large component and a small component basis set constructed according to the kinetic balance prescription a sub-μHartree level of accuracy is achieved in the finite basis set solutions when compared with the finite difference study reported by Sundholm et al. Some advantages of the distributed basis set approach in relativistic electronic structure studies are discussed.

ADVANCES IN QUANTUM CHEMISTRY, VOLUME 39

0065-3276/01 $35 00

Contents

1 Introduction

During the 1980s, it was conclusively demonstrated that the solutions of the Dirac equation and the Dirac-Hartree-Fock equations could be successfully approximated within the algebraic approximation or finite basis set expansion technique [1]-[14]. This approximation has been routinely employed in non-relativistic molecular electronic structure studies since the work of Hall [15]and of Roothaan [16], [17] in the early 1950s. Attempts[18], [19] to use this approximation in relativistic problem during the 1960s exposed certain difficulties which were termed "the finite basis set disease". It was not until the early 1980s that the "disease" was cured [1]-[6]. Today, in studies of the relativistic atomic and molecular electronic structure problem, it is recognized that the algebraic approximation affords a representation of not only the positive energy branch but also the negative energy branch of the relativistic spectrum[9]. It is, therefore, a powerful tool since it facilitates the study of not only a relativistic many-body perturbation theory but also the covering theory, quantum electrodynamics[12].

Systematic implementation of the algebraic approximation has allowed, for example, the Dirac-Hartree-Fock energies of atoms to be determined to an accuracy which matches that achieved in finite difference calculations; typically $10^{-8} - 10^{-9}$ Hartree [13], [14]. A systematic approach to basis set construction can be developed in relativistic many-body perturbation theory. Recent work by Moncrieff and Wilson[20] on the non-relativistic neon ground state has made a detailed comparison of many-body perturbation theory calculations using finite basis set and finite element approximations.

The situation is far less satisfactory for molecular systems than for atoms [10]. Even in non-relativistic molecular structure calculations, the basis set truncation error is often seen as the largest source of error[21]. The magnitude of this error in molecular Dirac-Hartree-Fock calculations can be illustrated by comparing the recently reported finite element study of the ground state of the HCl molecule by Kullie et al [23] with the previously reported finite basis set results of Laaksonen et al [10] and of Parpia and Mohanty [24]. For a nuclear separation of 2.400 bohr, Kullie et al [23] used a grid of 6561 points and $5th$ order polynomials to obtain a relativistic ground state energy of -461.569181 Hartree. This energy is compared with values obtained from finite basis set studies in Table 1. In this Table, ε denotes the difference between the energy supported by a given basis set and the reference energy which for the Dirac-Hartree-Fock calculations is the finite element result of Kullie et al [23]. For the non-relativistic calculation reported in Table 1 the reference is the finite difference Hartree-Fock energy reported by Laaksonen et al [10]. The matrix Hartree-Fock and matrix Dirac-Hartree-Fock calculations of Laaksonen et al employed what could today be described as "rather modest" basis sets. Specifically, they used a basis set due to Roos and Siegbahn [25] centred on the Cl atom containing functions of s and p symmetry only and an even-tempered set centred on the H atom. It can be seen from Table 1 that an error of about 50 *milli*Hartree is associated with this basis set. However, the difference between the Hartree-Fock and Dirac-Hartree-Fock calculations carried out with this modest basis set is 1.465 Hartree which should be compared with the difference of 1.456 Hartree between the finite element Dirac-Hartree-Fock and the finite difference Hartree-Fock energies. The difference between these two relativistic corrections is only 8.7 *milli*Hartree, which is almost an order of magnitude smaller than the basis set truncation errors associated with the corresponding total energies. The molecular basis set employed by Parpia and Mohanty [24] could be described as a one composed of large, atom-centred even-tempered subsets. The error associated with this basis set is of the order of 2 *milli*Hartree.

Table 1
Some Hartree-Fock and Dirac-Hartree-Fock calculations for the ground state of the HCl molecule with a nuclear separation of 2.400 bohr..

Energy	$E/Hartree$	$\varepsilon/mHartree$	Reference
E_{mHF}	−460.06054	52.51	Laaksonen et al (1988) [10]
E_{fdHF}	−460.11305		Laaksonen et al (1988) [10]
E_{mDHF}	−461.52538	43.80	Laaksonen et al (1988) [10]
E_{mDHF}	−461.5670806	2.100	Parpia and Mohanty (1995) [24]
E_{feDHF}	−461.569181		Kullie et al (1999) [23]

If high precision is to be supported, molecular basis sets constructed from atom-centred subsets necessitate the use of functions of higher angular quantum number, ℓ, particularly in electron correlation studies. This has prompted a recent renewal of interest in the use of off-atom functions of lower symmetry. Atom-centred basis sets have been most widely used in molecular calculations but, in calculations designed to match the accuracy achieved in numerical Hartree-Fock studies of diatomic molecules, it has recently been shown that they can be usefully supplemented by off-centre sets [26]−[29]. Indeed, by including bond centred functions in a systematically constructed basis set for the ground state of the nitrogen molecule it has been possible to obtain an energy that is within a few μHartree of the numerical result. The success of these calculations suggests investigation of the construction of basis sets including off-atom basis functions in more general terms.

The distributed basis set [30] [31] is a development which shows some promise. In such basis sets the exponents and the distribution of the Gaussian functions are generated according to empirical prescriptions. Gaussian functions are particularly well suited for such a procedure since, unlike exponential basis functions, they do not introduce a cusp. This approach is distinct from the use Gaussian lobe functions[32] and the Floating Spherical Gaussian Orbital (F.S.G.O.) model[33]-[35] in that there is no attempt to mimic higher harmonics directly and non-linear optimization is avoided. This allows the use of large basis sets resulting in high precision. However, a central problem in the distributed basis set approach is in deciding where the basis functions centres should be placed. In previous work, both the position and the exponents for the functions comprising the distributed basis set have been determined by empirical prescriptions. The Gaussian cell model [36], a distributed basis set in which s-type basis functions are arranged on a regular cubic lattice, has been

reexamined [37] and shown to support an accuracy approaching the 1 μHartree level for the total energy of one-electron diatomic [38] and triatomic systems [39]. The distribution of s-type basis functions based on a Laplace transform relating elliptical functions and Gaussian functions has been shown [40] to lead to systematic convergence for the hydrogen molecular ion. More recently, a stochastic variational approach has been applied to the nitrogen molecule [41]. In very recent work published in this volume, Glushkov and Wilson [42] have investigated the optimal distribution and exponents for a sequence of Gaussian basis sets for the ground state of the hydrogen molecular ion at its equlibrium geometry by invoking the variation principle. The sequence of distributions and exponents thus obtained will be used to devised empirical schemes for constructing distributed Gaussian basis sets for larger systems for which the optimization of non-linear parameters would be computationally intractable.

The purpose of the present work is to explore the use of a distributed Gaussian basis set in an application to the Dirac equation for the ground state of the H_2^+ molecular ion. At the equilibrium nuclear separation of 2 bohr the non-relativistic energy is known to an accuracy of 10^{-13} Hartree from the work of Madsen and Peek [43] whilst Sundholm et el [44] record the relativistic energy to an accuracy of 10^{-10} Hartree. Specificially, we used the $27s$ basis set of distributed s-type Gaussian basis functions obtained by Glushkov and Wilson [42] which supports a non-relativistic ground state energy of sub-μHartree accuracy to approximation the solution of the Dirac equation for the ground state of the hydrogen molecular ion.

2 The molecular Dirac equation in the algebraic approximation for distributed Gaussian basis sets of s-type functions

For a system involving a time-independent scalar potential the Dirac equation may be written

$$h_D\psi_k = \varepsilon_k\psi_k \tag{1}$$

where $\psi_k(\mathbf{x})$ is a four-component function of position

$$\psi_k(\mathbf{x}) = \begin{pmatrix} \psi_k^1(\mathbf{x}) \\ \psi_k^2(\mathbf{x}) \\ \psi_k^3(\mathbf{x}) \\ \psi_k^4(\mathbf{x}) \end{pmatrix} = \begin{pmatrix} \psi_k^L(\mathbf{x}) \\ \psi_k^S(\mathbf{x}) \end{pmatrix} \tag{2}$$

and ε_k is the corresponding eigenvalue. The Dirac hamiltonian takes the form

$$h_D = c\alpha\cdot\mathbf{p} + V(\mathbf{r}) + \beta mc^2 \tag{3}$$

where c is the speed of light, α and β are the 4×4 Dirac matrices

$$\alpha = \begin{pmatrix} \alpha_x & \alpha_y & \alpha_z \end{pmatrix}, \quad \alpha_\mu = \begin{pmatrix} \mathbf{0} & \sigma_\mu \\ \sigma_\mu & \mathbf{0} \end{pmatrix} \tag{4}$$

$$\beta = \begin{pmatrix} \mathbf{I} & 0 \\ 0 & -\mathbf{I} \end{pmatrix} \tag{5}$$

The σ_μ are the Pauli matrices

$$\sigma_x = \begin{pmatrix} 0 & 1 \\ 1 & 0 \end{pmatrix} \quad \sigma_y = \begin{pmatrix} 0 & -\imath \\ \imath & 0 \end{pmatrix} \quad \sigma_z = \begin{pmatrix} 1 & 0 \\ 0 & -1 \end{pmatrix} \tag{6}$$

and $\mathbf{I}$ is the 2×2 unit matrix. $\mathbf{p}$ is the momentum vector

$$\mathbf{p}_\mu = -\imath \nabla_\mu \tag{7}$$

and m is the mass.

For the hydrogenic molecular ions the potential $V(\mathbf{r})$ takes the form

$$V(\mathbf{r}) = V_A(\mathbf{r}) + V_B(\mathbf{r}) \tag{8}$$

where

$$V_A(\mathbf{r}) = -\frac{Z_A}{r_A}; \quad V_B(\mathbf{r}) = -\frac{Z_B}{r_B} \tag{9}$$

in which Z_P is the charge associated with nucleus P and r_P is the distance between the electron and nucleus P; $P = A, B$.

Now to recover the non-relativistic limit of the Dirac equation (1) we must have

$$(\sigma.\mathbf{p})\,(\sigma.\mathbf{p}) = p^2\mathbf{I} \tag{10}$$

The operator $\sigma \cdot \mathbf{p}$ has the explicit form in cartesian co-ordinates

$$\begin{aligned} \sigma \cdot \mathbf{p} &= \begin{pmatrix} p_z & p_x - \imath p_y \\ p_x + \imath p_y & -p_z \end{pmatrix} \\ &= \begin{pmatrix} \imath \frac{\partial}{\partial z} & \imath \left(\frac{\partial}{\partial x} - \imath \frac{\partial}{\partial y} \right) \\ \imath \left(\frac{\partial}{\partial x} + \imath \frac{\partial}{\partial y} \right) & -\imath \frac{\partial}{\partial z} \end{pmatrix} \end{aligned} \tag{11}$$

When the problem is formulated in the algebraic approximation by expanding the components of $\psi_k(\mathbf{x})$ in a finite basis set, the requirement (10) leads to what is now known as the 'kinetic balance condition'. The matrix representation of (10) necessitates that the basis sets employed in the parametrization of the large and small components of the relativistic eigenfunctions are matched.

Failure to recognize this restriction was the underlying cause of the 'finite basis set diease' which undermined early attempts to solve the Dirac equation and the Dirac-Hartree-Fock equations in the algebraic approximation. One of the most damaging symptoms of this 'disease' was the appearance of intruder states destroying the clean separation of the positive and negative energy branches of the spectrum which must be seen as an essential prerequisite of a sound treatment of many-body effects in a relativistic formalism.

Given a basis set of scalar functions $\chi_k, k = 1, 2, ..., N$ the large component, $\psi_k^L(\mathbf{x})$, is expanded in the basis set

$$\chi_k^L = \chi_k \begin{pmatrix} 1 \\ 0 \end{pmatrix} + \chi_k \begin{pmatrix} 0 \\ 1 \end{pmatrix} \tag{12}$$

The kinetic balance condition requires that the small component basis set be generated from (12) according to the prescription

$$\left\{\chi_k^S\right\} = \left\{N_k^S \sigma.\mathbf{p}\chi_k^L\right\} \tag{13}$$

where N_k^S is a normalization constant. The relation (13) implies that if χ_k^L contains an angular dependence ℓ then χ_k^S will be a fixed linear combination of two functions; one with angular dependence $\ell - 1$ and the other $\ell + 1$. So a large component function of d-symmetry will lead to a matched small component function which is a fixed linear combination of functions of p- and f-symmetry. (Some workers employ a small component basis set which contains these functions with angular dependence $\ell - 1$ and $\ell + 1$ as distinct entities rather than as fixed linear combinations. This has been term extended kinetic balance. The calculation reported in this work employ *strict* kinetic balance to construct the small component basis set.)

In the present approach, the large component basis set is a distributed set of s-type Gaussian functions

$$\chi_k(\zeta_k, x_k, y_k, z_k) = \exp\left\{-\zeta_k\left[(x - x_k)^2 + (y - y_k)^2 + (z - z_k)^2\right]\right\} \tag{14}$$

which are centred on the point (x_k, y_k, z_k) with exponent ζ_k. The small component basis set is defined by the kinetic balance condition (13) and is constructed from the primitive p-type Gaussians

$$\begin{aligned}
&(x - x_k)\exp\left\{-\zeta_k\left[(x - x_k)^2 + (y - y_k)^2 + (z - z_k)^2\right]\right\} \\
&(y - y_k)\exp\left\{-\zeta_k\left[(x - x_k)^2 + (y - y_k)^2 + (z - z_k)^2\right]\right\} \\
&(z - z_k)\exp\left\{-\zeta_k\left[(x - x_k)^2 + (y - y_k)^2 + (z - z_k)^2\right]\right\}
\end{aligned} \tag{15}$$

centred on the same point as the corresponding large component basis function and with the same exponent. When the large component basis set is a

distributed set of s-type Gaussian functions then kinetic balance prescription for the small component set assumes a particular simple form.

3 Distributed s-type Gaussian basis sets for H_2^+ ground state

3.1 The non-relativistic total electronic energy

The exact non-relativistic ground state electronic energy of the H_2^+ molecular ion at its equilibrium nuclear separation of 2 *bohr* is known to be [43]

$$-1.102\,634\,214\,494\,9\ \textit{Hartree}.$$

In previous work [42], we have carefully optimized a sequence of distributed basis sets of Gaussian s-type functions for this one-electron system. The basis sets, which are labelled $2n+1$, contain an odd number of functions. All basis functions are centred on points lying on the line passing through the nuclei (the z-axis) and one function centred on the bond mid-point ($z = 0$) and the remaining functions are distributed symmetrically. N denotes the total number of basis functions in a given basis set. δ is the difference between a given entry and the exact energy, again in μHartree. It was found that only 9 functions are required to support sub-milliHartree accuracy, 13 functions can support an accuracy of 100 μHartree and 19 functions yield an energy which an accuracy below the 10 μHartree level. A basis set of 25 functions was found to be capable of supporting an accuracy at the sub-μ Hartree level.

Some of the energies reported in Table 2 are those reported by Wilson and Moncrieff [30] using an *ad hoc* distribution based on electric field variant basis sets associated with each of the nuclei, a subset located on the bond centre and another subset at off-centre positions beyond the nuclei. A near saturated set of s functions centred on each nucleus is designated $30s$. Replacing these atom-centred sets by electric field variant sets gives a basis set which is labelled $30s(efv)$, whilst adding bond centre functions gives $-0.602\,577\,5$ Hartree. The addition of off-centre subsets gives the lowest energy recorded in the study of Wilson and Moncrieff using a basis set designated $30s(efv)$: $30s$ *bc*; $30s$ *oc*, which lies some 0.014 μHartree above the lowest energy reported in Table 1. However, the distributed sets investigated by Wilson and Moncrieff[30] were constructed from even-tempered subsets. No exponent optimization was undertaken. This *ad hoc* distributed basis set considered of a total of 150 basis functions (30 associated with each nucleus, 30 located at the bond centre and 30 at each of the off-centre positions beyond the nuclei.)

Table 2
Total non-relativistic energies for the ground state of the H_2^+ molecular ion at R=2.0 bohr supported by various distributed Gaussian basis sets of s-type functions.

Basis set	N	E	δ	Reference
$2 \times 13 + 1$	27	−1.102 633 875	0.339	(a)
$30s$	60	−1.090 950 5	11683.7	(b)
$30s(efv)$	60	−1.102 274 4	359.8	(b)
$30s(efv); 30s\ bc$	90	−1.102 577 5	56.7	(b)
	150	−1.102 633 861	0.353	(b)
$5 \times 5 \times 7$	1588	−1.102 631	3.2	(c)
Laplace transform	312	−1.102 631	3	(d)
Exact		−1.102 634 214 494 9		(e)

(a) Glushkov and Wilson [42]
(b) Wilson and Moncrieff [30]
(c) Wilson [38]
(d) Wilson[39]
(e) Madsen and Peek [43]

3.2 The optimized distributed Gaussian basis set

The optimized distributed Gaussian basis set of s-type functions employed in the present work was obtained in a previous non-relativistic study[42] of the H_2^+ ground state. The basis functions were taken to have the form (14) and both the exponents, ζ_k, and the positions (x_k, y_k, z_k) are determined by invoking the variation principle. The total electronic energy is determined subject to the conditions

$$\frac{\partial E}{\partial \zeta_k} = 0, \quad \frac{\partial E}{\partial \mu_k} = 0, \quad \mu = x, y, z, \quad \forall k \tag{16}$$

Details of the optimization procedures followed are given in [45] and [46].

3.2.1 Optimal exponents

The optimal values of the exponents for a basis set of 27 s-type Gaussian functions distributed along the line passing through both nuclei are collected in Table 3. The exponents, ζ_p, are arranged in *increasing order of magnitude*. The index p defines this order.

The optimal exponents of the s-type Gaussian functions in the $(2 \times 13 + 1)$ basis set plotted as a function of the basis function index, p, in Figure 1 on a logarithmic scale. We recall that for an even-tempered basis set the exponents form a geometric series and the plot of the logarithms of the exponents against the index, p, is linear.

Table 3
Exponents for a variationally optimized distributed Gaussian basis set of 27 s-type functions for the ground state of the H_2^+ molecular ion with a nuclear separation of 2.000 bohr.

p	ζ_p
1	$0.825\,657\,9 \times 10^{-1}$
2	0.178 753 2
3	0.345 619 0
4	0.446 132 9
5	0.761 678 0
6	$0.100\,487\,6 \times 10^{+1}$
7	$0.211\,070\,6 \times 10^{+1}$
8	$0.243\,218\,1 \times 10^{+1}$
9	$0.614\,265\,8 \times 10^{+1}$
10	$0.170\,160\,4 \times 10^{+2}$
11	$0.522\,443\,2 \times 10^{+2}$
12	$0.184\,642\,3 \times 10^{+3}$
13	$0.811\,832\,6 \times 10^{+3}$
14	$0.542\,254\,8 \times 10^{+4}$

3.2.2 Optimal distribution

The optimal positions of the 27 s-type Gaussian functions centred on points along the internuclear axis are given in Table 4. The first function is located at the mid-point between the nuclei and the remaining functions are arranged in pairs on either side of the first. In Table 4, the values of z_q are ordered *according to their distance from the mid-point of the bond.* It should be noted that the order of the optimal positions given in Table 4 does *not* correspond to that of the optimal exponents given in Table 3. We have employed different orderings of the exponents and positions so as to display the dependence on

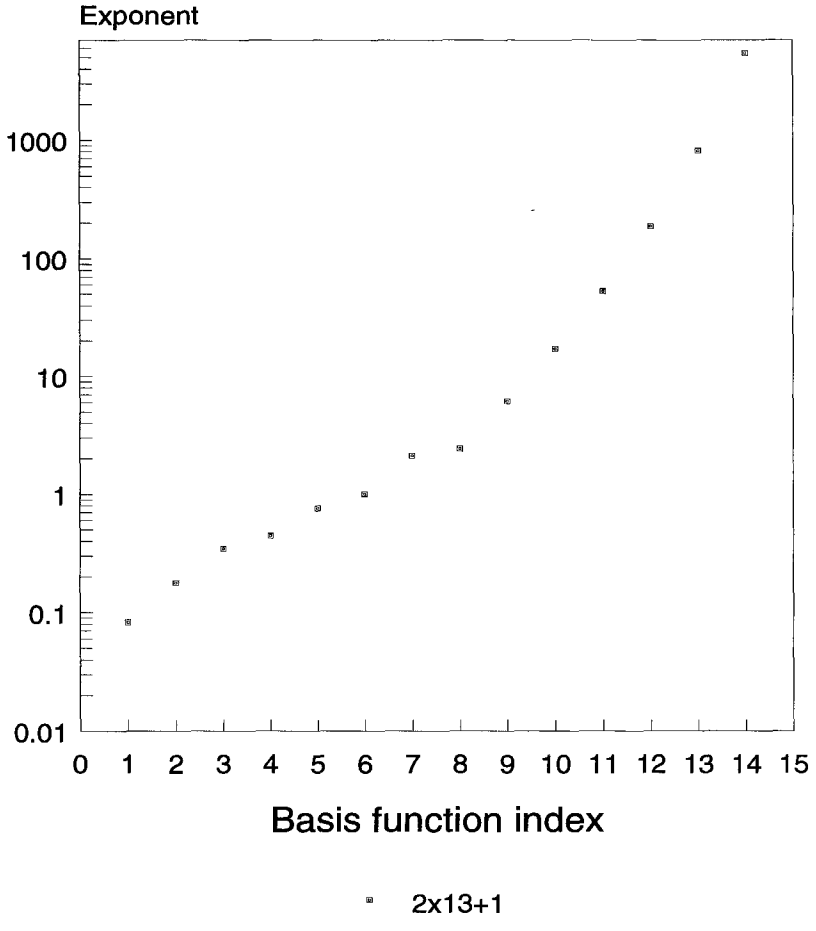

Figure 1: Optimal positions of the s-type Gaussian functions in the $(2\times 13+1)$ basis set plotted as a function of the basis function index, p.

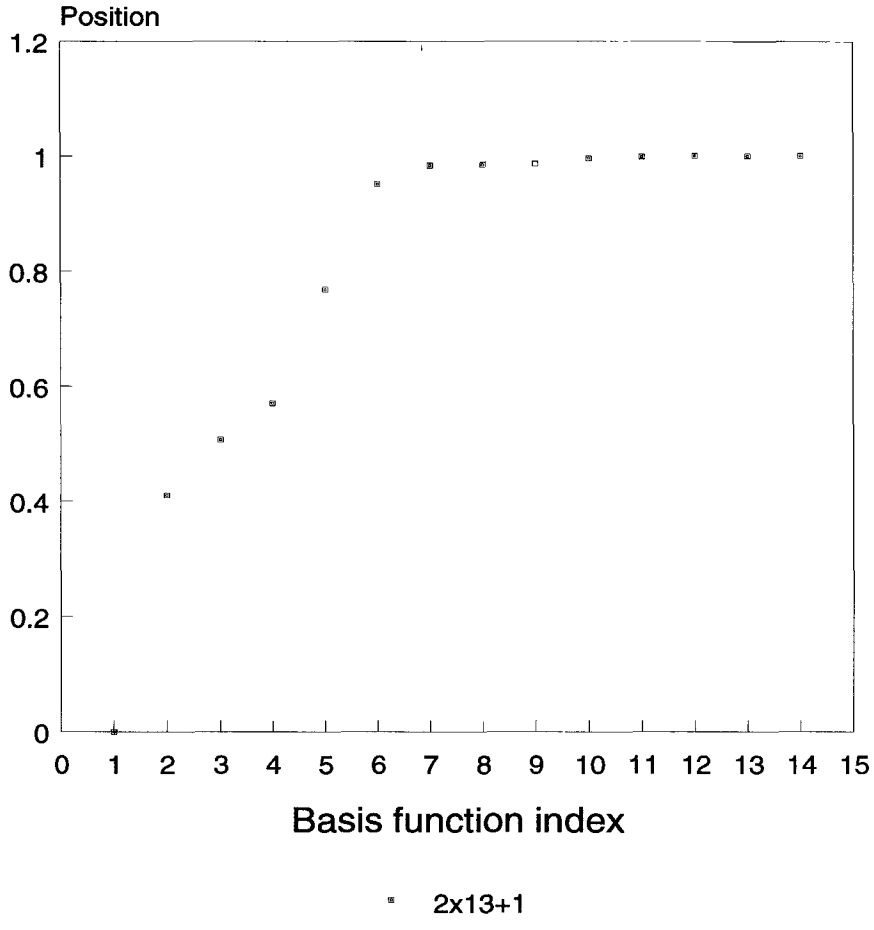

Figure 2: Optimal positions of the s-type Gaussian functions in the $(2\times 13+1)$ basis set plotted as a function of the basis function index, q.

Table 4
Positions for a variationally optimized distributed Gaussian basis set of 27 s-type functions for the ground state of the H_2^+ molecular ion with a nuclear separation of 2.000 bohr

q	z_q
1	0
2	±0.410 673 9
3	±0.506 980 7
4	±0.570 306 8
5	±0.768 222 3
6	±0.950 979 9
7	±0.983 634 6
8	±0.984 937 1
9	±0.986 431 9
10	±0.995 979 9
11	±0.998 319 0
12	±0.999 672 2
13	±0.999 879 9
14	±0.999 991 4

4 Matrix Dirac energy for the H_2^+ molecular ion

Using the distributed Gaussian basis set defined in Tables 3 and 4 approximate solutions of the matrix Dirac equation for the H_2^+ molecular ion were obtained. The calculations were carried out using subroutines extracted from the *BERTHA* computer program of Quiney et al [47]. The approximate eigenvalue of the matrix Dirac equation, which is designated E_{mDE}, was found to be −1.102 641 239 0 Hartree.

In Table 5, a comparison of finite basis set and finite difference electronic structure calculations for the ground state of the H_2^+ molecular ion for a nuclear separation of 2.0 bohr is made. In this Table, E_{mSE} denotes the energy resulting from the solution of the matrix Schrödinger equation reported by Glushkov and Wilson [42], E_{fdSE} is the energy obtained by the finite difference solution of the Schrödinger equation reported by Sundholm et al [44], E_{mDE} denotes the energy obtained by solving the matrix Dirac equation ac-

cording to the procedure defined in the present work, and E_{fdDE} is the finite difference solution of the Dirac equation reported by Sundholm et al[44].

The energy difference

$$\Delta E^{fb}_{rel.} = E_{mSE} - E_{mDE}$$

is based on the present work and that of Glushkov and Wilson[42], whilst the difference

$$\Delta E^{fd}_{rel.} = E_{fdSE} - E_{fdDE}$$

is determined from the work of Sundholm et al[44].

In Table 5, ε denotes the basis set truncation error in energies resulting from calculations with finite basis sets in μHartree. It can be seen that the error in E_{mSE} is identical to that in E_{mDE} to an accuracy of $0.1\,n$Hartree. Furthermore, the energy difference $\Delta E^{fb}_{rel.}$ agrees with $\Delta E^{fd}_{rel.}$ to this level of accuracy.

Table 5
A comparison of finite basis set and finite difference electronic structure calculations for the ground state of the H_2^+ molecular ion for a nuclear separation of 2.0 bohr.

Energy	*E/Hartree*	$\varepsilon/\mu Hartree$	Reference
E_{mSE}	−1.102 633 873 6	0.340 9	(a)
E_{fdSE}	−1.102 634 214 5		(b)
E_{mDE}	−1.102 641 239 0	0.340 9	(c)
E_{fdDE}	−1.102 641 579 9		(b)
ΔE^{fb}_{rel}	$-7.365\,5 \times 10^{-6}$	0.000 0	(c)
$\Delta E^{fd}_{rel.}$	$-7.365\,5 \times 10^{-6}$		(b)

(a) Glushkov and Wilson [42]
(b) Sundholm et al (1987) [44]
(c) Present work

5 Discussion and conclusions

We have demonstrated that the total relativistic energy of the ground state of the H_2^+ molecular ion at its equilibrium nuclear separation of 2.0 bohr can be

determined to a sub-μHartree level of accuracy by using a basis set developed according to the (*strict*) kinetic balance prescription from a distributed set of s-type Gaussian functions optimized for the corresponding non-relativistic problem.

According to the kinetic balance prescription, a large component basis set containing only s-type functions distributed along the axis passing through the nuclei gives rise to a small component basis set consisting of p-type Gaussian functions also distributed along this axis. Relativistic electronic structure calculations using distributed Gaussian basis sets can therefore avoid the need to include higher harmonics which are essentially if high precision is to be achieved using the more widely used atom-centred expansions.

The calculation reported in this paper has cleary demonstrated that the techniques developed in recent years for designing molecular basis sets which are capable of supporting the approach to the Hartree-Fock limit at the sub-μHartree level [26]-[29] can also be exploited in the approximate solution of the corresponding relativistic molecular electronic structure problem. Formally, this approach can be applied to arbitrary many-electron molecules, including polyatomic systems and to calculations which take account of electron correlation effects. Progress in this direction will be reported in due course.

Acknowledgments

HMQ wishes to acknowledge the hospitality of the School of Chemistry at the University of Melbourne and the facilities made available by Prof. F.P. Larkins. SW acknowledges the support of the UK Engineering and Physical Sciences Research Council under Grant GR/M74627.

References

[1] Y. Ishikawa, R.C. Binning and K.M. Sando, Chem. Phys. Lett. **101**, 111 (1983)

[2] K.G. Dyall, I.P. Grant and S. Wilson, J. Phys. B: At. Mol. Opt. Phys. **17**, 493 (1984)

[3] K.G. Dyall, I.P. Grant and S. Wilson, J. Phys. B: At. Mol. Opt. Phys. **17**, L45 (1984)

[4] K.G. Dyall, I.P. Grant and S. Wilson, J. Phys. B: At. Mol. Opt. Phys. **17**, 1201 (1984)

[5] R. Stanton and S. Havriliak, J. Chem. Phys. **81**, 1910 (1984)

[6] P. Aerts and W.C. Nieuwpoort, Chem. Phys. Lett. **113**, 165 (1985)

[7] H.M. Quiney, I.P. Grant and S. Wilson, J. Phys. B: At. Mol. Opt. Phys. **18**, 2805 (1985)

[8] H.M. Quiney, I.P. Grant and S. Wilson, J. Phys. B: At. Mol. Opt. Phys. **20**, 1413 (1987)

[9] H.M. Quiney, I.P. Grant and S. Wilson, Physica Scripta **36**, 460 (1987)

[10] L. Laaksonen, I.P. Grant and S. Wilson, J. Phys. B: At. Mol. Opt. Phys. **21**, 1969 (1988)

[11] H.M. Quiney, I.P. Grant and S. Wilson, 1989, J. Phys. B: At. Mol. Opt. Phys. **22**, L15 (1989)

[12] H.M. Quiney, I.P. Grant and S. Wilson, in Many-Body Methods in Quantum Chemistry, Lecture Notes in Chemistry 52, 307, edited by U. Kaldor, Springer-Verlag, Berlin (1989)

[13] H.M. Quiney, I.P. Grant and S. Wilson, J. Phys. B: At. Mol. Opt. Phys **23**, L271 (1990)

[14] S. Wilson, in The Effects of Relativity in Atoms, Molecules and the Solid State, edited by S. Wilson, I.P. Grant and B.L. Gyorffy, Plenum Press, New York (1991)

[15] G.G. Hall, Proc. Roy. Soc. (London) **A205**, 541 (1951)

[16] C.C.J. Roothaan, J. Chem. Phys. **59**, 5956 (1951)

[17] C.C.J. Roothaan, Rev. Mod. Phys. 23, 69 (1961)

[18] M. Synek, Phys. Rev. **136**, 1556 (1964)

[19] Y.-K. Kim, Phys. Rev. **154**, 17 (1967); **159**, 190 (1968)

[20] D. Moncrieff and S. Wilson, J. Phys. B: At. Mol. Opt. Phys. **32**, 5379 (1999)

[21] S. Wilson, in Methods in Computational Molecular Physics, ed. G.H.F. Diercksen and S. Wilson, Reidel, Dordrecht (1983)

[22] S. Wilson, Adv. Chem. Phys. **67**, 439 (1987)

[23] O. Kullie, C. Düsterhöft and D. Kolb, Chem. Phys. Lett. **314**, 307 (1999)

[24] F.A. Parpia and A.K. Mohanty, Phys. Rev. **A52**, 2 (1995)

[25] B.O. Roos and P.E.M. Siegbahn, Theor. chim. Acta **17**, 209 (1970)

[26] D. Moncrieff and S. Wilson, J. Phys. B: At. Mol. Opt. Phys. 26, 1605 (1993)

[27] D. Moncrieff and S. Wilson, Chem. Phys. Lett. 209, 423 (1993)

[28] J. Kobus, D. Moncrieff and S. Wilson, J. Phys. B: At. Mol. Opt. Phys. 27, 2867 (1994)

[29] J. Kobus, D. Moncrieff and S. Wilson, J. Phys. B: At. Mol. Opt. Phys. 27, 5139 (1994)

[30] S. Wilson and D. Moncrieff, Molec. Phys. **80**, 461 (1993)

[31] D. Moncrieff and S. Wilson, Molec. Phys. **82**, 523 (1994)

[32] H. Preuss, Z. Naturforsch. **11a**, 823 (1956); H. Preuss, Z. Naturforsch. **19a**, 1335 (1964); ibid. **20a**, 17, 21 (1965); J.L. Whitten, J. Chem. Phys. **39**, 349 (1963); F. Driessler and R. Ahlrichs, Chem. Phys. Lett. **23**, 571 (1973); V.R. Saunders, in Methods in Computational Molecular Physics, edited by G.H.F. Diercksen and S. Wilson, Reidel, Dordrecht

[33] A.A. Frost, J. Chem. Phys. **47**, 3707 (1967)

[34] A.A. Frost, J. Chem. Phys. **47**, 3714 (1967)

[35] B. Ford, G.G. Hall and J.C. Packer, Intern. J. Quantum Chem. **4**, 533 (1970)

[36] L.M. Haines, J.N. Murrell, B.J. Raltson and D.J. Woodnutt, J. Chem. Soc., Faraday Trans. 2, **70**, 1794 (1974)

[37] B.J. Ralston and S. Wilson, J. Mol. Struct. (Theochem) **341**, 115 (1995)

[38] S. Wilson, J. Mol. Struct. (Theochem) **357**, 37 (1995)

[39] S. Wilson, Intern. J. Quantum Chem. **60**, 47 (1996)

[40] S. Wilson, J. Phys. B: At. Mol. Opt. Phys. **28**, L495 (1995)

[41] S. Wilson, Intern. J. Quantum Chem. **74**, 547 (1999)

[42] V.N. Glushkov and S. Wilson, Adv. Quantum Chem. *(this volume)*

[43] M.M.Madsen and J.M. Peek, At. Data **2**, 171 (1971)

[44] D. Sundholm, P. Pyykkö and L. Laaksonen, Physica Scripta, **36**, 400 (1987)

[45] V.I. Karliichuk, V.N. Glushkov, A.I. Aprasyukhin, A.Y. Tsaune, J Structural Chem. 24, 914 (1983)

[46] A.Y. Tsaune, V.N. Glushkov and A.I. Aprasyukhin, Teoreticheskaya i Eksperimentalnaya Khimiya 24, 215 (1988)

[47] H.M. Quiney, H. Skaane and I.P. Grant, in *Quantum Systems in Chemistry and Physics. II*, ed. S. Wilson et al, Adv. Quantum Chem. **32**, 1 (1998)

Relativistic multireference Møller-Plesset perturbation theory calculations for the term energies and transition probabilities of ions in the nitrogen isoelectronic sequence

by

Marius Jonas Vilkas, Yasuyuki Ishikawa,

Department of Chemistry, University of Puerto Rico, P.O. Box 23346, San Juan, PR 00931-3346, USA

Abstract

Highly accurate relativistic multireference Møller-Plesset perturbation calculations are performed on the energy levels, transition probabilities, and lifetimes of ions in the nitrogen isoelectronic sequence

Contents

ADVANCES IN QUANTUM CHEMISTRY VOLUME 39

0065-3276/01 $35 00

1 INTRODUCTION

There has been considerable interest in the excited state energies and transition rates of openshell ions [1, 2, 3, 4]. Accurate estimates of radiative transition probabilities among multiplet states are important for diagnosing astrophysical and laboratory plasmas as they provide a major source for successful experimental identifications of the spectra. Of particular interest are the electric dipole-allowed and -forbidden transition probabilities, which are important in interpreting decay curves of the observed spectral lines. However, accurate calculations of transition energies, fine structure (FS) splittings, and transition probabilities of nitrogen and nitrogenlike ions are particularly difficult for three reasons. First, the ions possess significant nondynamical correlation due to near-degeneracy of the multiplet states that arise from the five open shell electrons in $2s^l_{1/2}2p^m_{1/2}2p^n_{3/2}$ $(l+m+n{=}5)$ configurations, mandating a multiconfigurational treatment. Second, relativistic effects, which are small for low Z (Z - nuclear charge) and may be treated by perturbation theory [5], become large enough to cause a breakdown of LS coupling with increasing Z, and the accuracy achieved in low-Z ions by use of the Breit-Pauli Hamiltonian quickly deteriorates for intermediate and large Z. Last, both relativity and electron correlation must simultaneously be accurately accounted for to obtain the relative positions of the multiplet states.

In the present study, we employ recently developed relativistic multireference Møller-Plesset (MR-MP) perturbation theory [6, 7, 8] to calculate accurately the energies of seven odd-parity and eight even-parity states, FS splittings, $2s^22p^3\ {}^2D^o_{3/2,5/2}$ - $2s^22p^3\ {}^4S^o_{3/2}$ magnetic dipole (M1), $2s^22p^3\ {}^2D^o_{3/2,5/2}$ - $2s^22p^3\ {}^4S^o_{3/2}$ electric quadrupole (E2) and the sixteen strongest electric dipole (E1) transition probabilities of nitrogen and nitrogenlike ions. This is a successful implementation and application of relativistic MR many-body perturbation theory to multiple openshell systems that exhibit the near degeneracy characteristic of a manifold of strongly interacting configurations. Relativistic MR-MP perturbation theory accounts for relativistic, nondynamical and dynamical Dirac-Coulomb (DC) and Breit correlation corrections in addition to Lamb shifts, providing accurate term energies and FS splittings. The DC and Breit correlation corrections include the relativistic many-body shift, the nonadditive interplay of relativity and electron correlation [9, 10]. Contributions to the term energy separations and FS splittings from relativity, DC and Breit correlation corrections and the Lamb shift are analyzed. The forbidden (M1 and E2) transitions, which appear at longer wavelengths, provide a useful diagnostic tool for high-Z ions [1] because the M1 and E2 decay rates scale at higher powers of Z than do E1 decay rates. The implementation of the relativistic MR-MP procedure, using G spinors, and the procedure for calculating

transition probabilities with relativistic MR-MP wavefunctions are outlined in the next section. In section 4, relativistic MR-MP calculations of term energy separations and transition probabilities are presented.

2 THEORY

2.1 The relativistic no-pair Dirac-Coulomb-Breit Hamiltonian

The effective N-electron Hamiltonian (in atomic units) for the development of our MR-MP algorithm is taken to be the relativistic "no-pair" Dirac-Coulomb (DC) Hamiltonian [11, 12],

$$H_{DC}^{+} = \sum_{i}^{N} h_D(i) + \mathcal{L}_+ \left(\sum_{i>j}^{N} \frac{1}{r_{ij}} \right) \mathcal{L}_+. \tag{1}$$

$\mathcal{L}_+ = L_+(1)L_+(2)\ldots L_+(N)$, where $L_+(i)$ is the projection operator onto the space $D^{(+)}$ spanned by the positive-energy eigenfunctions of the matrix DF SCF equation [12]. $\mathcal{L}_+$ is the projection operator onto the positive-energy space $\mathfrak{D}^{(+)}$ spanned by the N-electron configuration-state functions (CSFs) constructed from the positive-energy eigenfunctions ($\in D^{(+)}$) of the matrix DF SCF. It takes into account the field-theoretic condition that the negative-energy states are filled and causes the projected DC Hamiltonian to have normalizable bound-state solutions. This approach is called the no-pair approximation [11] because virtual electron-positron pairs are not permitted in the intermediate states. The eigenfunctions of the matrix DF SCF equation clearly separate into two discrete manifolds, $D^{(+)}$ and $D^{(-)}$, respectively, of positive-energy and negative-energy states. As a result, the positive-energy projection operators can be accommodated easily in many-body calculations. The formal conditions on the projection are automatically satisfied when only the positive-energy spinors ($\in D^{(+)}$) are employed. h_D is the Dirac one-electron Hamiltonian (in a.u.)

$$h_D(i) = c(\boldsymbol{\alpha}_i \cdot \mathbf{p}_i) + (\beta_i - 1)c^2 + V_{nuc}(r_i). \tag{2}$$

Here $\boldsymbol{\alpha}$ and β are the 4×4 Dirac vector and scalar matrices, respectively. $V_{nuc}(r)$ is the nuclear potential, which for each nucleus takes the form

$$Vnuc(r) = \begin{cases} -\frac{Z}{r}, r > R, \\ -\frac{Z}{2R}(3 - \frac{r^2}{R^2}), r \leq R \end{cases}. \tag{3}$$

The nuclei are modeled as spheres of uniform proton-charge distribution; Z is the nuclear charge. R (Bohr) is the radius of that nucleus and is related to the atomic mass, A (amu), by R= $2.2677 \cdot 10^{-5} A^{1/3}$. Adding the frequency-independent Breit interaction,

$$B_{12} = -\frac{1}{2}[\boldsymbol{\alpha}_1 \cdot \boldsymbol{\alpha}_2 + (\boldsymbol{\alpha}_1 \cdot \mathbf{r}_{12})(\alpha_2 \cdot \mathbf{r}_{12})/r_{12}^2]/r_{12}, \tag{4}$$

to the electron-electron Coulomb interaction, in Coulomb gauge, results in the Coulomb-Breit potential which is correct to order α^2 (α being the fine structure constant) [11]. Addition of the Breit term yields the no-pair Dirac-Coulomb-Breit (DCB) Hamiltonian [11, 12]

$$H_{DCB}^{+} = \sum_{i}^{N} h_D(i) + \mathcal{L}_+ \left(\sum_{i>j}^{N} \frac{1}{r_{ij}} + B_{ij} \right) \mathcal{L}_+, \tag{5}$$

which is covariant to first order and increases the accuracy of calculated fine-structure splittings and inner-electron binding energies. Higher-order QED effects appear first in order α^3.

2.2 The matrix multiconfiguration Dirac-Fock SCF method

N-electron eigenfunctions of the no-pair DC Hamiltonian are approximated by a linear combination of M configuration-state functions, $\{\Phi_I^{(+)}(\gamma_I \mathcal{J}\pi); I = 1, 2, \ldots, M\}$, constructed from positive-energy eigenfunctions of the matrix DF SCF equation. The M configuration-state functions form a subspace $\mathfrak{P}^{(+)}$ of the positive-energy space $\mathfrak{D}^{(+)}$.

$$\psi_K(\gamma_K \mathcal{J}\pi) = \sum_{I}^{M} C_{IK} \Phi_I^{(+)}(\gamma_I \mathcal{J}\pi). \tag{6}$$

Here the MC DF SCF wave function $\psi_K(\gamma_K \mathcal{J}\pi)$ is an eigenfunction of the angular momentum and parity operators with total angular momentum $\mathcal{J}$ and parity π. γ denotes a set of quantum numbers other than $\mathcal{J}$ and π necessary to specify the state uniquely. The total DC energy of the general MC DF state $|\psi_K(\gamma_K \mathcal{J}\pi) >$ can be expressed as

$$E^{MC}(\gamma_K \mathcal{J}\pi) = < \psi_K(\gamma_K \mathcal{J}\pi) | H_{DC}^{+} | \psi_K(\gamma_K \mathcal{J}\pi) > =$$

$$= \sum_{I,J=1}^{\mathfrak{P}(+)} C_{IK} C_{JK} < \Phi_I^{(+)}(\gamma_I \mathcal{J}\pi) | H_{DC}^{+} | \Phi_J^{(+)}(\gamma_J \mathcal{J}\pi) > . \tag{7}$$

Here it is assumed that $\psi_K(\gamma_K \mathcal{J}\pi)$ and $\Phi_I^{(+)}(\gamma_I \mathcal{J}\pi)$ are normalized.

Given a trial orthonormal set of one-particle radial spinors $\{\phi^{(0)}_{n_p\kappa_p}(r)\}(\in D^{(+)} \cup D^{(-)})$, the optimum occupied electronic radial spinors $\{\phi^{(+)}_{n_e\kappa_e}(r)\}(\in D^{(+)})$ can be found by a unitary transformation $\mathbf{U} = 1 + \mathbf{T}$ via

$$\phi^{(+)}_{n_e\kappa_e}(r) = \frac{1}{r}\begin{pmatrix} P_{n_e\kappa_e}(r) \\ Q_{n_e\kappa_e}(r) \end{pmatrix} = \sum_{p\in D^{(+)}\cup D^{(-)}}^{2N_\kappa} \phi^{(0)}_{n_p\kappa_p}(r) U_{pe} =$$

$$= \sum_{p}^{2N_\kappa} \phi^{(0)}_{n_p\kappa_p}(r)(T_{pe} + \delta_{pe}). \tag{8}$$

Here, the summation extends over both N_κ negative and N_κ positive energy spinors. $P_{n\kappa}(r)$ and $Q_{n\kappa}(r)$ are the large and small radial components and are expanded in N_κ G spinors, $\{\chi^L_{\kappa i}\}$ and $\{\chi^L_{\kappa i}\}$, that satisfy the boundary conditions associated with the finite nucleus [13],

$$P_{n\kappa}(r) = \sum_{i}^{N_\kappa} \chi^L_{\kappa i}\xi^L_{n\kappa i} \text{ and } Q_{n\kappa}(r) = \sum_{i}^{N_\kappa} \chi^S_{\kappa i}\xi^S_{n\kappa i}. \tag{9}$$

Here $\{\xi^L_{n\kappa i}\}$ and $\{\xi^S_{n\kappa i}\}$ are linear variation coefficients. Second-order variation of the MC DF energy (Eq. 7) with respect to the parameters $\{T_{pe}\}$ and configuration mixing coefficients $\{C_{IK}\}$ leads to the Newton-Raphson (NR) equations for second-order MC DF SCF,

$$\begin{pmatrix} g^o_{pe} \\ g^c_\gamma \end{pmatrix} + \sum_{qf\gamma''} \begin{pmatrix} h^{oo}_{pe,qf} & h^{oc}_{pe,\gamma''} \\ h^{co}_{\gamma',qf} & h^{cc}_{\gamma',\gamma''} \end{pmatrix} \begin{pmatrix} T_{qf} \\ B_{\gamma''} \end{pmatrix} = \begin{pmatrix} 0 \\ 0 \end{pmatrix}. \tag{10}$$

Here g^o_{pe}, g^c_γ, $h^{oo}_{pe,qf}$, etc. are those defined in previous work [14]. Intermediate coupling is built in through the MC DF SCF process. For the ground electronic state, the Hessian matrix possesses N_κ positive and N_κ negative eigenvalues corresponding to a minimum and a maximum, respectively, in the space of large and small component parameters. Therefore, the energy functional is minimized with respect to spinor rotations between the occupied electronic spinors and the positive energy virtual spinors. The functional is maximized with respect to spinor rotations between the occupied electronic spinors and the negative energy spinors. By maximazing the vacuum charge-current density polarization contribution, the MC DF mean-field potential defines its dressed vacuum [15]. Quiney recently gave a comprehensive account on the participation of the negative-energy states from the point of view of

quantum electrodynamics to illustrate how they enter into relativistic mean-field theory [16]. The quadratically convergent NR algorithm for relativistic MC DF SCF calculations has been discussed in detail in previous work [14] and is not discussed further. To remove the arbitrariness of the MC SCF spinors and density weighting, the canonical SCF spinors are transformed into natural spinors $\{\omega^{(+)}_{n_p\kappa_p}\}$ for subsequent perturbation calculations [17]. The key to successful implementation of the subsequent MR-MP perturbation theory calculations is rapid convergence of our quadratically convergent matrix MC DF SCF method [14] for a general class of MC DF wave functions for open-shell quasidegenerate systems.

2.3 Relativistic multireference many-body perturbation theory

The no-pair DC Hamiltonian H^+_{DC} is partitioned into an unperturbed Hamiltonian and a perturbation term following Møller and Plesset [18],

$$H^+_{DC} = H_0 + V, \tag{11}$$

where the unperturbed model Hamiltonian H_0 is a sum of "average" DF operators F_{av} ,

$$H_0 = \sum_i^N F_{av}(i) \text{ and } V = H^+_{DC} - \sum_i^N F_{av}(i). \tag{12}$$

Here, the one-body operator F_{av} diagonal in $\{\omega^{(+)}_{n_p\kappa_p}\}$ may be defined by,

$$F_{av} = \sum_{p\in D(+)} |\omega^{(+)}_{n_p\kappa_p} >< \omega^{(+)}_{n_p\kappa_p}|f_{av}|\omega^{(+)}_{n_p\kappa_p} >< \omega^{(+)}_{n_p\kappa_p}| =$$

$$= \sum_{p\in D(+)} |\omega^{(+)}_{n_p\kappa_p} > \varepsilon^+_p < \omega^{(+)}_{n_p\kappa_p}|, \tag{13}$$

where

$$\varepsilon^+_p =< \omega^{(+)}_{n_p\kappa_p}|f_{av}|\omega^{(+)}_{n_p\kappa_p} > \text{ and } f_{av} = h_D + \sum_p^{occ} \widetilde{n}_p \left(J_p - K_p\right). \tag{14}$$

The generalized fractional occupation $\widetilde{n}_p$ is related to diagonal matrix elements of the first-order reduced density matrix constructed in natural spinors by,

$$\widetilde{n}_p = D_{pp} = \sum_r^{\mathfrak{P}(+)} C_{IK} C_{IK} n_{n_p\kappa_p}[I], \tag{15}$$

where $n_{n_p\kappa_p}[I]$ is the occupation number of the κ-symmetry shell in the CSF $\Phi_I(\gamma_I \mathcal{J}\pi)$. J_p and K_p are the usual Coulomb and exchange operators constructed in natural spinors.

The unperturbed Hamiltonian H_0 may be given in second quantized form,

$$H_0 = \sum_{p \in D(+)} \left\{a_p^+ a_p\right\} \varepsilon_p^+, \tag{16}$$

where $\left\{a_p^+ a_p\right\}$ is a normal product of creation and annihilation operators, a_p^+ and a_p, respectively. The zero-order Hamiltonian, H_0, is arbitrary but should be chosen as close to the full Hamiltonian H_{DC}^+ as possible so that the perturbation series converges rapidly in low order. The zero-order Hamiltonian is usually chosen to be a sum of effective one-electron operators (Møller-Plesset partitioning [18]). For closed-shell systems, the best results have been obtained with Møller-Plesset partitioning, i.e. with the sum of closed-shell Fock operators as H_0. An effective one-body operator for general MC DF SCF closely related to the closed-shell Fock operator is the "average" DF operator F_{av} , a relativistic generalization of a nonrelativistic average Fock operator [17, 19]. The theory provides a hierarchy of well-defined algorithms that allow one to calculate relativistic correlation corrections in non-iterative steps and, in low order, yields a large fraction of the dynamical correlation. In this form of partitioning, perturbation corrections describe relativistic electron correlation, including cross contributions between relativistic and correlation effects.

Many-electron wave functions correct to α^2 may be expanded in a set of CSFs that spans the entire N-electron positive-energy space $\mathfrak{D}^{(+)}$, $\{\Phi_I^{(+)}(\gamma_I \mathcal{J}\pi)\}$, constructed in terms of Dirac one-electron spinors. Individual CSFs are eigenfunctions of the total angular momentum and parity operators and are linear combinations of antisymmetrized products of positive-energy spinors ($\in D^{(+)}$). The one-electron spinors are mutually orthogonal so the CSFs $\{\Phi_I^{(+)}(\gamma_I \mathcal{J}\pi)\}$ are mutually orthogonal. The unperturbed Hamiltonian is diagonal in this space;

$$H_0 = \sum_I^{\mathfrak{D}(+)} |\Phi_I^{(+)}(\gamma_I \mathcal{J}\pi) > E_I^{CSF} < \Phi_I^{(+)}(\gamma_I \mathcal{J}\pi)|, \tag{17}$$

so that

$$H_0 |\Phi_I^{(+)}(\gamma_I \mathcal{J}\pi) >= E_I^{CSF} |\Phi_I^{(+)}(\gamma_I \mathcal{J}\pi) > (I = 1, 2, \ldots). \tag{18}$$

Since the zero-order Hamiltonian is defined as a sum of one-electron operators F_{av} (Eq. 12), E_I^{CSF} is a sum of the products of one-electron energies defined

by ε_q^+ and an occupation number $n_{n_q\kappa_q}[I]$ of the κ_q-symmetry shell in the CSF $\Phi_I^{(+)}(\gamma_I\mathcal{J}\pi)$;

$$E_I^{CSF} = \sum_q^{D(+)} \varepsilon_q^+ n_{n_q\kappa_q}[I]. \tag{19}$$

The subset, $\{\Phi_I^{(+)}(\gamma_I\mathcal{J}\pi); I = 1, 2, \ldots, M\}$, with which we expand the MC DF SCF function $\psi_K(\gamma_K\mathcal{J}\pi)$ (Eq. 6) also defines an active subspace $\mathfrak{P}^{(+)}$ spanned by $\psi_K(\gamma_K\mathcal{J}\pi)$ and its M-1 orthogonal complements, $\{\psi_K(\gamma_K\mathcal{J}\pi); K = 1, 2, \ldots, M\}$. The matrix of H_{DC}^+ in this subspace is diagonal

$$< \psi_K(\gamma_K\mathcal{J}\pi)|H_{DC}^+|\psi_L(\gamma_L\mathcal{J}\pi) >= \delta_{KL}\left(E_K^{(0)} + E_K^{(1)}\right) =$$

$$= \delta_{KL}E^{MC}(\gamma_K\mathcal{J}\pi), \tag{20}$$

where

$$E_K^{(0)} =< \psi_K(\gamma_K\mathcal{J}\pi)|H_0|\psi_K(\gamma_K\mathcal{J}\pi) >= \sum_I^M C_{IK}C_{IK}E_I^{CSF} = \sum_p^{occ} \varepsilon_p^+ \widetilde{n}_p$$

and

$$E_K^{(1)} =< \psi_K(\gamma_K\mathcal{J}\pi)|V|\psi_K(\gamma_K\mathcal{J}\pi) > .$$

The residual space in the positive-energy subspace is $\mathfrak{Q}^{(+)} = \mathfrak{D}^{(+)} - \mathfrak{P}^{(+)}$, which is spanned by CSFs $\{\Phi_I^{(+)}(\gamma_I\mathcal{J}\pi); I = M+1, M+2, \ldots\}$. Application of Rayleigh-Schrödinger perturbation theory provides order-by-order expressions of the perturbation series for the state approximated by the wavefunction $|\psi_K(\gamma_K\mathcal{J}\pi) >$,

$$E_K(\gamma_K\mathcal{J}\pi) = E^{MC}(\gamma_K\mathcal{J}\pi) + E_K^{(2)} + E_K^{(3)} + \ldots, \tag{21}$$

where

$$E_K^{(2)} =< \psi_K(\gamma_K\mathcal{J}\pi)|V\mathcal{R}V|\psi_K(\gamma_K\mathcal{J}\pi) > \tag{22}$$

and

$$E_K^{(3)} =< \psi_K(\gamma_K\mathcal{J}\pi)|V\mathcal{R}(H_0 - E_K^{(1)})\mathcal{R}V|\psi_K(\gamma_K\mathcal{J}\pi) > . \tag{23}$$

Here, $\mathcal{R}$ is the resolvent operator,

$$\mathcal{R} = \frac{\mathcal{Q}^{(+)}}{E_K^{(0)} - H_0} \text{ with } \mathcal{Q}^{(+)} = \sum_I^{\Omega(+)} |\Phi_I^{(+)}(\gamma_I \mathcal{J}\pi) >< \Phi_I^{(+)}(\gamma_I \mathcal{J}\pi)|. \quad (24)$$

The projection operator $\mathcal{Q}^{(+)}$ projects onto the subspace $\Omega^{(+)}$ spanned by CSFs $\{\Phi_I^{(+)}(\gamma_I \mathcal{J}\pi); I = M+1, M+2, \dots\}$. Using the spectral resolution of the resolvent operator acting on $V|\Phi_I^{(+)}(\gamma_I \mathcal{J}\pi) >$, the second-order correction may be expressed as,

$$E_K^{(2)} = \sum_{IJ} C_{IK} C_{JK} < \Phi_I^{(+)}(\gamma_I \mathcal{J}\pi)|V\mathcal{R}V|\Phi_J^{(+)}(\gamma_J \mathcal{J}\pi) >=$$

$$= \sum_{L=M+1}^{\Omega(+)} \sum_{I,J=1}^{\mathfrak{P}(+)} C_{IK} C_{JK} \frac{< \Phi_I^{(+)}(\gamma_I \mathcal{J}\pi)|V|\Phi_L^{(+)}(\gamma_L \mathcal{J}\pi) >}{E_J^{CSF} - E_L^{CSF}} \cdot$$

$$\cdot < \Phi_L^{(+)}(\gamma_L \mathcal{J}\pi)|V|\Phi_J^{(+)}(\gamma_J \mathcal{J}\pi) > . \quad (25)$$

In this form, all perturbation corrections beyond first order describe relativistic electron correlation for the state approximated by the MC DF SCF wavefunction $|\psi_K(\gamma_K \mathcal{J}\pi) >$. When the effective electron-electron interaction is approximated by the instantaneous Coulomb interaction $\frac{1}{r_{ij}}$, relativistic electron correlation is termed Dirac-Coulomb (DC) correlation [20]. Inclusion of the frequency-independent Breit interaction in the effective electron-electron interaction yields the no-pair DCB Hamiltonian (Eq. 5), and relativistic electron correlation arising from the DCB Hamiltonian is the DCB correlation [20].

Summations over the CSFs in Eqs. 17 through 25 are restricted to CSFs ($\in \mathfrak{D}^{(+)}$) constructed from the positive-energy branch ($D^{(+)}$) of the spinors, effectively incorporating into the computational scheme the "no-pair" projection operator $\mathcal{L}_+$ contained in the DC and DCB Hamiltonians. Further, the CSFs $\Phi_L^{(+)}(\gamma_L \mathcal{J}\pi)$ ($\in \Omega^{(+)}$) generated by excitations higher than double, relative to the reference CSFs $\Phi_I^{(+)}(\gamma_I \mathcal{J}\pi)$ ($\in \mathfrak{P}^{(+)}$), do not contribute to the second- and third-order because for them $< \Phi_I^{(+)}(\gamma_I \mathcal{J}\pi)|\ V\ |\Phi_L^{(+)}(\gamma_L \mathcal{J}\pi) >= 0$ and $< \Phi_I^{(+)}(\gamma_I \mathcal{J}\pi)|\ H_{DC}^+\ |\Phi_L^{(+)}(\gamma_L \mathcal{J}\pi) >= 0$.

Neglecting interactions with the filled negative-energy sea, i.e. neglecting virtual electron-positron pairs in summing the MBPT diagrams, we have a straightforward extension of nonrelativistic MBPT. Negative energy states ($\in D^{(+)}$), as part of the complete set of states, do play a role in higher-order

QED corrections. Studies have appeared which go beyond the "no-pair" approximation where negative-energy states are needed to evaluate the higher-order QED effects [21, 22, 23, 24, 25]. Contributions from the negative energy states due to creation of virtual electron-positron pairs are of the order α^3, and estimations of the radiative corrections are necessary in order to achieve spectroscopic accuracy for higher Z. In the present study, the lowest-order radiative corrections were estimated for each state to achieve better accuracy.

2.4 Transition probabilities

The interaction of a single electron with the electromagnetic field is described by the interaction Hamiltonian h_{int} as

$$h_{int}(\mathbf{r}, w) = e(-c\boldsymbol{\alpha} \cdot \mathbf{A}(\mathbf{r}, w) + \phi(\mathbf{r}, w)). \tag{26}$$

Here the four-component potential is expressed in terms of the vector potential $\mathbf{A}(\mathbf{r}, w)$ and scalar potential $\phi(\mathbf{r}, w)$, and e is the electron charge. It is assumed that the interaction Hamiltonian has incoming photon field time dependence e^{-iwt}. Using a multipole expansion of the vector potential $\mathbf{A}(\mathbf{r}, w)$ and scalar potential $\phi(\mathbf{r}, w)$ [26], the multipole interaction Hamiltonian $(h_{int}(\mathbf{r}, w))_{JM}$ can be expressed in terms of multipole transition operators $t^{\vartheta}_{JM}(\mathbf{r}, w)$ for the magnetic multipoles ($\vartheta = M$) and electric multipoles ($\vartheta = E$) as follows

$$(h_{int}(\mathbf{r}, w))_{JM} = -iec\sqrt{\frac{(2J+1)(J+1)}{4\pi J}} \quad t^{\vartheta}_{JM}(\mathbf{r}, w). \tag{27}$$

The one-electron reduced matrix elements $< t^{\vartheta}_J >_{ij}$ for transition between the single-particle states i and j are given (see [27, 28] for details) in the length form as

$$< t^M_J >_{ij} = < -\kappa_i || C^{(J)} || \kappa_j > \int \frac{\kappa_i + \kappa_j}{J+1} j_J(kr)(P_i(r)Q_j(r) + P_j(r)Q_i(r))dr \tag{28}$$

$$< t^E_J >_{ij} = < \kappa_i || C^{(J)} || \kappa_j > \int \{ j_J(kr)(P_i(r)P_j(r) + Q_i(r)Q_j(r)) + j_{J+1}(kr) \times$$

$$\times [\frac{\kappa_i - \kappa_j}{J+1}(P_i(r)Q_j(r) + P_j(r)Q_i(r)) + (P_i(r)Q_j(r) - P_j(r)Q_i(r))] \} dr \tag{29}$$

and in velocity form as

$$< t_J^M >_{ij}=< -\kappa_i||C^{(J)}||\kappa_j > \int \frac{\kappa_i + \kappa_j}{J+1} j_J(kr)(P_i(r)Q_j(r) + P_j(r)Q_i(r))dr \tag{30}$$

$$< t_J^E >_{ij}=< \kappa_i||C^{(J)}||\kappa_j > \int \{\frac{\kappa_j - \kappa_i}{J+1}[j'_J(kr) + \frac{j_J(kr)}{kr}](P_i(r)Q_j(r) +$$

$$P_j(r)Q_i(r)) + +J\frac{j_J(kr)}{kr}](P_i(r)Q_j(r) - P_j(r)Q_i(r))\}dr \tag{31}$$

where $j_J(kr)$ is a spherical Bessel function, $\mathbf{k}$ is photon wave vector and k $=\mid \mathbf{k} \mid$. $C^{(J)}$ is an irreducible tensor of rank J with components related to the spherical harmonics as $C_q^{(J)} = \sqrt{\frac{4\pi}{2J+1}} Y_q^{(J)}$. The electromagnetic interaction H_{int} of a many-electron system is the sum of the interactions of all electrons

$$H_{int} = \sum_{ij} < h_{int} >_{ij} a_i^+ a_j. \tag{32}$$

as well as multipole transition operator T_{JM}^{ϑ}

$$T_{JM}^{\vartheta} = \sum_{ij} < t_{JM}^{\vartheta} >_{ij} a_i^+ a_j. \tag{33}$$

The absorption probability $< B >_{K \to K'}$ per unit time of transition between states $|\psi_K(\gamma_K \mathcal{J}\pi) >$ and $|\psi_{K'}(\gamma_{K'} \mathcal{J}'\pi') >$ with transition energy $\Delta E = hw = E_{K'} - E_K$ is equal to the spontaneous emission probability $< A >_{K' \to K}$ and is expressed as

$$< B^{\vartheta J} >_{K \to K'}= 2\alpha w \frac{(2J+1)(J+1)}{(2\mathcal{J}+1)J}[< T_J^{\vartheta} >_{K'K}]^2 =< A^{\vartheta J} >_{K' \to K} . \tag{34}$$

In the lowest-order of Rayleigh-Schrödinger perturbation theory, the multipole transition amplitude between states K and K' is

$$< T_J^{\vartheta} >_{KK'}^{(0)} =< \psi_K(\gamma_K \mathcal{J}\pi)|T_{JM}^{\vartheta}|\psi_{K'}(\gamma_{K'} \mathcal{J}'\pi') >=$$

$$= \sum_{IL} C_{IK} C'_{LK} < \Phi_I^{(+)}(\gamma_I \mathcal{J}\pi)|T_{JM}^{\vartheta}|\Phi_L^{\prime(+)}(\gamma_L \mathcal{J}'\pi') > . \tag{35}$$

and using the order-by-order expressions of the perturbation series for the state approximated by MCDF SCF wavefunction $\psi_K(\gamma_K \mathcal{J}\pi)$ of Eq. 6, the next-order transition amplitude is

$$< T_J^{\vartheta} >_{KK'}^{(1)} = < \psi_K^{(1)}(\gamma_K \mathcal{J}\pi)|T_{JM}^{\vartheta}|\psi_{K'}(\gamma_{K'}\mathcal{J}'\pi') > +$$

$$+ < \psi_K(\gamma_K \mathcal{J}\pi)|T_{JM}^{\vartheta}|\psi_{K'}^{(1)}(\gamma_{K'}\mathcal{J}'\pi') > + \ldots \tag{36}$$

where the first-order wavefunction is defined as

$$|\psi_K^{(1)}(\gamma_K \mathcal{J}\pi) >= \mathcal{R}V|\psi_K(\gamma_K \mathcal{J}\pi) > . \tag{37}$$

As with the second-order energy (Eqs. 22 and 25), the first-order transition amplitude can be expressed in terms of CSFs in the following way

$$< T_J^{\vartheta} >_{KK'}^{(1)} = \sum_{L=M+1}^{\Omega(+)} \sum_{I,I'=1}^{\mathfrak{P}(+)} C_{IK} C_{I'K'} [\frac{< \Phi_I^{(+)}|V|\Phi_L^{(+)} >< \Phi_L^{(+)}|T_{JM}^{\vartheta}|\Phi_{I'}^{(+)} >}{E_I^{CSF} - E_L^{CSF}} +$$

$$+ \frac{< \Phi_I^{(+)}|T_{JM}^{\vartheta}|\Phi_L^{(+)} >< \Phi_L^{(+)}|V|\Phi_{I'}^{(+)} >}{E_{I'}^{CSF} - E_L^{CSF}}]. \tag{38}$$

One-electron reduced matrix elements $< t_J^{\vartheta} >_{ij}$ given in Eqs. 28 - 31 are frequency-dependent through the spherical Bessel functions $j_J(kr)$. The corrections arising from approximate photon frequency may be eliminated semi-empirically using experimental transition energies. In the present study, transition energies (and photon frequencies $\omega^{(0+1+2)}$) calculated by MR-MP second-order perturbation theory are close to the experimental values, and the terms arising from corrections to the photon frequency $\delta\omega = \omega^{exp} - \omega^{(0+1+2)}$ in both zero- and first-order transition amplitudes are significantly smaller and may be neglected. When the first-order corrections to transition probabilities (Eq. 38) are calculated using second-order MR-MP transition energies, however, the zero-order transition amplitude (Eq. 35) must also be recalculated using the frequency $\omega^{(0+1+2)}$.

3 COMPUTATIONAL

The large radial component is expanded in a set of Gaussian-type functions (GTF) [29]

$$\chi^L_{\kappa i}(r) = A^L_{\kappa i} r^{n[\kappa]} \exp(-\zeta_{\kappa i} r^2) \tag{39}$$

with $n[\kappa] = -\kappa$ for $\kappa < 0$, and $n[\kappa] = \kappa + 1$ for $\kappa > 0$. $A^L_{\kappa i}$ is the normalization constant. The small component basis set, $\{\chi^S_{\kappa i}(r)\}$ is constructed to satisfy the boundary condition associated with the finite nucleus with a uniform proton charge distribution [29]. With the finite nucleus, GTFs of integer power of r are especially appropriate basis functions because the finite nuclear boundary results in a solution which is Gaussian at the origin [29]. Basis functions which satisfy the nuclear boundary conditions are also automatically kinetically balanced. Imposition of the boundary conditions results in particularly simple forms with spherical G spinors [29].

For all the nitrogen-like systems studied, even-tempered basis sets [30] of 24s22p Gaussian-type were used for MC DF SCF. In basis sets of even-tempered Gaussians [30], the exponents, $\{\zeta_{\kappa i}\}$ are given in terms of the parameters, α and β, according to the geometric series;

$$\zeta_{\kappa i} = \alpha\beta^{i-1}; i = 1, 2, \ldots, N_\kappa. \tag{40}$$

In MC DF SCF calculations on nitrogen-like species, the parameters α and β are optimized until a minimum in the DF total energy is found. The optimal α and β values thus determined for, e.g., nitrogen-like neon (Z=10) are, respectively, 0.148055 and 2.11. The radial functions that possess a different κ quantum number but the same quantum number ℓ are expanded in the same set of basis functions (e.g., the radial functions of $p_{1/2}$ and $p_{3/2}$ symmetries are expanded in the same set of p-type radial Gaussian-type functions). The nuclei were again modeled as spheres of uniform proton charge in every calculation. The nuclear model has been discussed in detail in Ref. [29].

Virtual spinors used in the MR-MP perturbation calculations were generated in the field of the nucleus and all electrons (V^N potential) by employing the "average" DF operator F_{av} (Eq. 13). The order of the partial-wave expansion, L_{max}, the highest angular momentum of the spinors included in the virtual space, is $L_{max} = 7$ (a 24s22p20d18f16g16h14i14j G spinor basis set) throughout this study. All-electron MR-MP perturbation calculations including the frequency-independent Breit interaction in the first and second orders of perturbation theory are based on the no-pair Dirac-Coulomb-Breit Hamiltonian, H^+_{DCB}. The speed of light was taken to be 137.0359895 a.u. Radiative corrections, or Lamb shifts, were estimated for each state by evaluating the electron self-energy and vacuum polarization following an approximation

scheme discussed by Indelicato, Gorceix, and Desclaux [25]. The code described in Refs. [25] and [31] was adapted to our basis set expansion calculations for this purpose. In this scheme [31], the screening of the self energy is estimated by employing the charge density of a spinor integrated to a short distance from the origin, typically 0.3 Compton wavelength. The ratio of the integral computed with an MC DF SCF spinor and that obtained by using the corresponding hydrogenic spinor is used to scale the self-energy correction for a bare nuclear charge computed by Mohr [22]. The effect on the term energy splittings of mass polarization and reduced mass are non-negligible. In the present study, however, we neglect these effects.

4 RESULTS AND DISCUSSION

4.1 Energy levels

Like carbon- and oxygen-like ions [7, 15], ground and low-lying excited states of ions of the nitrogen isoelectronic sequence exhibit the near degeneracy characteristic of a manifold of strongly interacting configurations. The strongly interacting configurations arise from different occupations of the $2s_{1/2}$, $2p_{1/2}$ and $2p_{3/2}$ spinors by five valence electrons. MC DF SCF and MR-MP calculations were carried out on the ground $^4S^o_{3/2}$ state and six odd-parity and eight even-parity low-lying excited states of nitrogen and nitrogen-like ions with Z=8, 9, 10, 11, 12, 13, 14, 16, 20, 26, 30, 40, 50 and 60. Critically evaluated experimental data are available for these ions up to Z=42 [32, 33]. In Table I, we illustrate our calculations on three representative ions with Z= 10, 20, 30. The Table displays the MC DF SCF energies, E_{SCF}, MR-MP second-order Dirac-Coulomb correlation energies, $E^{(2)}_{DC}$, first- and second-order Breit interaction energies, $B^{(1)}$ and $B^{(2)}$, radiative corrections, and total energies of the 15 lowest states. The radiative corrections, or the electron self-energy and vacuum polarization, estimated by the method described in Refs. [25] and [31], are given in the sixth column of the Table under the heading "LS" (LS for "Lamb shift"). These low-lying excited states consist of two J=1/2 ($^2P^o_{1/2}$, $^2P^o_{1/2}$), three J=3/2 ($^2P^o_{3/2}$, $^2P^o_{3/2}$, $^2D^o_{3/2}$) and one J=5/2 ($^2D^o_{5/2}$) odd-parity states arising from $2s^22p^3$ and $2p^5$ configurations, three J=1/2 ($^4P_{1/2}$, $^2S_{1/2}$, $^2P_{1/2}$), three J=3/2 ($^4P_{3/2}$, $^2D_{3/2}$, $^2P_{3/2}$) and one J=5/2 ($^4P_{3/2}$) even-parity state arising from $2s^12p^4$.

MC DF SCF calculations were performed to obtain a single set of spinors for each of the $^2P^o_J$, $^2D^o_J$ odd-parity and ^4P_J, ^2D_J, ^2P_J, even-parity fine-structure states by optimizing the J-averaged MC energies: $E^{MC}_{J-ave}(\gamma_K\pi) = \sum_J(2J+1)E^{MC}(\gamma_K J\pi)/\sum_{J'}(2J'+1)$ instead of performing state-specific MC

Table I: MC DF SCF, second-order MR-MP energies, and Lamb shifts (LS) (a u.) of seven odd parity ($2s^22p^3$ and $2p^5$) and eight even parity ($2s2p^4$) states of representative nitrogenlike ions.

State		E_{SCF}	$E^{(2)}_{DC}$	$B^{(1)}$	$B^{(2)}$	LS	E_{total}
		Z=10					
$2s^22p^3$	$^4S^o_{3/2}$	-124 250850	-0 200036	0 015840	-0 001787	0 010797	-124 426036
	$^2D^o_{5/2}$	-124 045416	-0 217412	0 015580	-0 001810	0 010800	-124 238064
	$^2D^o_{3/2}$	-124 045589	-0 217396	0.015948	-0 001818	0 010799	-124 238251
	$^2P^o_{3/2}$	-123 965144	-0 202023	0 015866	-0 001829	0.010787	-124 142342
	$^2P^o_{1/2}$	-123 965227	-0.202087	0 015941	-0 001826	0 010787	-124 142412
$2p^5$	$^2P^o_{3/2}$	-121 911713	-0 338522	0 015987	-0 001864	0 010080	-122 226031
	$^2P^o_{1/2}$	-121 906972	-0.338949	0.015594	-0 001876	0 010090	-122 222112
$2s2p^4$	$^4P_{5/2}$	-123 409725	-0.206314	0 015778	-0 001763	0 010436	-123 591588
	$^4P_{3/2}$	-123 406962	-0 206277	0.015803	-0 001779	0 010442	-123 588774
	$^4P_{1/2}$	-123 405331	-0 206206	0 015650	-0 001772	0 010445	-123 587214
	$^2D_{3/2}$	-123 035229	-0 261696	0 015828	-0.001844	0 010440	-123 272616
	$^2D_{5/2}$	-123 035199	-0 261791	0 015681	-0 001847	0 010440	-123 272599
	$^2S_{1/2}$	-122.832376	-0 254007	0 016127	-0.001975	0.010439	-123.061792
	$^2P_{3/2}$	-122.696345	-0 297088	0.015921	-0.001892	0.010437	-122 968967
	$^2P_{1/2}$	-122 693001	-0 297026	0.015777	-0.001893	0.010444	-122.965699
		Z=20					
$2s^22p^3$	$^4S^o_{3/2}$	-570 740260	-0 218894	0 153741	-0 008183	0 125914	-570 687682
	$^2D^o_{5/2}$	-570 199886	-0 236815	0 149116	-0 008305	0 125987	-570 169902
	$^2D^o_{3/2}$	-570.244388	-0.234134	0 157095	-0 008417	0 125809	-570.204035
	$^2P^o_{3/2}$	-569.899965	-0 220731	0.150382	-0.008446	0 126032	-569.852728
	$^2P^o_{1/2}$	-569 956081	-0.218111	0 154942	-0.008524	0.125807	-569.901968
$2p^5$	$^2P^o_{3/2}$	-564 471782	-0 343394	0 159746	-0 008790	0 114371	-564 549849
	$^2P^o_{1/2}$	-564.319965	-0.344269	0 154125	-0 008770	0 114683	-564 404195
$2s2p^4$	$^4P_{5/2}$	-568 388448	-0.216788	0.154746	-0 008170	0 120005	-568 338655
	$^4P_{3/2}$	-568 297417	-0 216569	0 154760	-0 008261	0 120204	-568 247283
	$^4P_{1/2}$	-568 253799	-0 216750	0 153388	-0 008222	0.120276	-568 205106
	$^2D_{3/2}$	-567 443650	-0 273242	0 155187	-0 008523	0 120118	-567 450110
	$^2D_{5/2}$	-567 433588	-0 272790	0 152317	-0.008474	0 120163	-567 442372
	$^2S_{1/2}$	-566 931009	-0 267492	0 160092	-0.009072	0 120094	-566 927387
	$^2P_{3/2}$	-566 729078	-0.315405	0 155196	-0 008553	0.120097	-566 777743
	$^2P_{1/2}$	-566 606325	-0 311665	0 152571	-0 008611	0.120381	-566.653650
		Z=30					
$2s^22p^3$	$^4S^o_{3/2}$	-1352.246070	-0 226324	0 571030	-0 019826	0 503145	-1351.418044
	$^2D^o_{5/2}$	-1351 040898	-0.243477	0 539155	-0 019787	0 504722	-1350 260286
	$^2D^o_{3/2}$	-1351 375735	-0 237139	0 566043	-0.019946	0.504223	-1350 562554
	$^2P^o_{3/2}$	-1349 930990	-0 229665	0 536403	-0 019958	0 506040	-1349.138170
	$^2P^o_{1/2}$	-1350 614351	-0 224200	0.563335	-0 020487	0 504192	-1349 791511
$2p^5$	$^2P^o_{3/2}$	-1340.920892	-0 346418	0.586098	-0.021083	0 453105	-1340 249190
	$^2P^o_{1/2}$	-1339 966294	-0 346866	0 562752	-0 020828	0.454884	-1339.316352
$2s2p^4$	$^4P_{5/2}$	-1347 863102	-0 224305	0 568715	-0 019611	0 477794	-1347 060510
	$^4P_{3/2}$	-1347 277210	-0 225229	0 566364	-0 019811	0 478920	-1346 476966
	$^4P_{1/2}$	-1347 161882	-0 227447	0 571236	-0 020016	0.478782	-1346 359327
	$^2D_{3/2}$	-1346 115010	-0 279277	0 569953	-0 020336	0.478551	-1345 366119
	$^2D_{5/2}$	-1345 901891	-0 274328	0 549004	-0.020036	0.479241	-1345 168012
	$^2S_{1/2}$	-1345 263284	-0 280177	0 577702	-0 020970	0.478904	-1344 507826
	$^2P_{3/2}$	-1344 924916	-0.315970	0 557788	-0.020079	0 479062	-1344 224114
	$^2P_{1/2}$	-1344 075028	-0 303246	0.548871	-0 020457	0 480809	-1343 369052

Table II: Configuration mixing coefficients for the ground and low-lying excited J=3/2 odd-parity states of Ne^{3+}, Ca^{13+} and Zn^{23+}.

	$C_{2s^22p^2_{1/2}2p^1_{3/2}}$	$C_{2s^22p^1_{1/2}2p^2_{3/2}}$	$C_{2s^22p^3_{3/2}}$	$C_{2p^2_{1/2}2p^3_{3/2}}$
		Ne^{+3}		
$^4S^o_{3/2}$	0.479659	0.745164	-0.463308	0.001687
$^2D^o_{3/2}$	-0.558529	0.666516	0 493709	-0.007319
$^2P^o_{3/2}$	0.666320	0.022494	0.727088	0.163874
		Ca^{+13}		
$^4S^o_{3/2}$	0.578699	0.718121	-0.386165	0.016920
$^2D^o_{3/2}$	-0.702937	0.679026	0.206297	-0.047377
$^2P^o_{3/2}$	0.400486	0.153737	0.893706	0.131407
		Zn^{+23}		
$^4S^o_{3/2}$	0.871039	0.437875	-0.217042	0.049501
$^2D^o_{3/2}$	-0.457237	0.886337	-0.059580	-0.042334
$^2P^o_{3/2}$	0.158500	0.152173	0.969656	0.107182

DF SCF calculations on each fine-structure state. For low-Z ions with small fine-structure splittings (near degeneracy among $2p_{1/2}$ and $2p_{3/2}$ spinors), this approach is more effective in computing the fine structure splittings with the subsequent state-by-state MR-MP procedure. The numbers of reference CSFs for the J-averaged MC DF SCF and state-specific MR-MP calculations were, respectively, 2, 4, and 1 for the J=1/2, 3/2, and 5/2 odd-parity states. For the even-parity states, they were, respectively, 3, 3, and 2; these account for all the CSFs arising from the n=2 complex. All electrons were correlated in the state-specific MR-MP calculations. J-averaged MC DF SCF calculations, including the frequency-independent Breit interaction in the configuration-mixing step of the MC SCF algorithm, have also been performed to study the effect of the Breit interaction on fine-structure term energies. Energy shifts due to the first-order Breit interactions $B^{(1)}$ thus obtained are given in the fourth column of Table I. The relativistic many-body shifts $B^{(2)}$ [20, 34, 35] that arise from including the Breit interaction in the effective electron-electron interaction in the second-order MR-MP perturbation calculations are also displayed in the fifth column of the Table. $B^{(2)}$ is computed as the difference between the second-order correlation correction evaluated with B_{12} (Eq. 4) in the effective electron-electron interaction and the second-order DC correlation correction, $E^{(2)}_{DC}$.

The configuration mixing coefficients displayed in Table II for the ground and lowest two excited odd-parity $J = 3/2$ states of Ne^{3+} (Z=10), Ca^{13+} (Z=20) and Zn^{23+} (Z=30) are representative of those obtained in the MC DF calculations. The magnitude of the configuration mixing coefficients is a measure of configuration interaction. The electronic configurations, $2s^22p^2_{1/2}2p^1_{3/2}$,

$2s^22p^1_{1/2}2p^2_{3/2}$, $2s^22p^3_{3/2}$, and $2p^2_{1/2}2p^3_{3/2}$, give rise to four $J = 3/2$ odd-parity states, and they do interact strongly. The $2p_{1/2}$ and $2p_{3/2}$ spinors are nearly degenerate in low-Z Ne^{3+} ion because relativistic effects are small (i.e., weak spin-orbit coupling), and consequently the CSFs arising from the $2s^22p^2_{1/2}2p^1_{3/2}$, $2s^22p^1_{1/2}2p^2_{3/2}$,and $2s^22p^3_{3/2}$ configurations are nearly degenerate, and there is a strong configuration interaction among them (See Table II). Four-configuration MC DF SCF calculations yield the configuration mixing coefficients, 0.479659, 0.745164, -0.463308 and 0.001687, for the lowest $J = 3/2$ ($^4S_{3/2}$) state of Ne^{3+}, coefficients nearly equal in magnitude for the three CSFs arising from the $2s^22p^2_{1/2}2p^1_{3/2}$, $2s^22p^1_{1/2}2p^2_{3/2}$,and $2s^22p^3_{3/2}$. As Z increases, relativity gradually lifts the near degeneracy and weakens the configuration interaction among the three CSFs because it induces a large separation between the $2p_{1/2}$ and $2p_{3/2}$ spinor energies and simultaneously a smaller separation between the $2s_{1/2}$ and $2p_{1/2}$ spinor energies (the $2s_{1/2}$ and $2p_{1/2}$ spinor energies become asymptotically degenerate in the hydrogenic limit). Table II displays such a trend as the nuclear charge increases. Four-configuration MC DF SCF on the ground J=3/2 state of Zn^{23+} yields mixing coefficients of 0.871039, 0.437875 and -0.217042 for the three CSFs. The configuration interaction among the three CSFs for Zn^{23+} (Z=30) is reduced by relativity, with the $2s^22p^2_{1/2}2p^1_{3/2}$ CSF possessing the largest configuration-mixing coefficient. Yet the ground state is far from the jj coupling regime where only one CSF dominates; it still displays intermediate coupling, mandating MC DF SCF and MR-MP treatment.

In Table III, a detailed comparison of theoretical and experimental data is made on the term energies (cm^{-1}) of the low-lying even- and odd-parity states of nitrogen and nitrogen-like ions with Z=10, 20 and 30 relative to the ground $2s^22p^3\ ^4S^o_{3/2}$ state. Theoretical term energy separations of the low-lying excited states evaluated by MC DF (third column of the Table) and by MR-MP (fourth column) were computed by subtracting the total MCDF SCF and MR-MP energies of the ground $2s^22p^3\ ^4S^o_{3/2}$ state from those of the excited levels. Experimental term energy separations[32, 33] are reproduced in the second column for comparison. The values in parentheses are the percentage deviations from experiment. The last column (denoted NR-MBPT) contains the term energy separations obtained in previous nonrelativistic correlated calculations for comparison. In the NR-MBPT calculations [5, 36], multireference second-order perturbation theory was employed to account for electron correlation for the ions with $10 \leq Z \leq 30$. Relativistic corrections were included in the Breit-Pauli approximation. The percentage deviations from experiment of the NR-MBPT term energy separations range from 0.2 % to 2.0 %, consistently larger than those ($\leq$0.39 %) obtained by our relativistic MR-MP. In Zn^{23+} ion relativistic corrections included in the Breit-Pauli approximation fail to provide sufficient accuracy. Although dynamical correlation is not accounted for, the

Table III: Comparison, with experiment and previous work, of the energy levels (cm^{-1}) relative to the ground $2s^2 2p^3\ {}^4S^o_{3/2}$ state obtained by MCDF and MR-MP calculations Percentage deviations of the theoretical results from experimental data are given in parentheses

Level		Experiment[a]	MCDF	MR-MP	NR-MBPT[b]
		Ne^{+3}			
$2s^2 2p^3$	$^2D^o_{5/2}$	41235	45030(9 20)	41212(0 06)	40406(2.01)
	$^2D^o_{3/2}$	41280	45073(9 19)	41256(0 06)	40451(2 01)
	$^2P^o_{1/2}$	62435	62712(0 44)	62256(0.29)	61465(1.55)
	$^2P^o_{3/2}$	62441	62714(0 44)	62244(0 32)	61467(1 56)
$2s2p^4$	$^4P_{5/2}$	183860	184592(0.40)	183140(0 39)	180633(1 76)
	$^4P_{3/2}$	184477	185203(0.39)	183757(0 39)	181238(1 76)
	$^4P_{1/2}$	184799	185528(0 39)	184100(0 38)	181557(1.75)
	$^2D_{5/2}$	254081	266795(5.00)	253150(0 37)	249532(1 79)
	$^2D_{3/2}$	254102	266769(4 99)	253146(0 38)	249557(1.79)
	$^2S_{1/2}$	299628	311382(3.92)	299416(0 07)	295404(1.41)
	$^2P_{3/2}$	320030	341192(6.61)	319789(0 08)	317793(0.70)
	$^2P_{1/2}$	320741	341894(6.60)	320506(0 07)	318481(0.70)
$2p^5$	$^2P^o_{3/2}$	484904	513273(5.85)	489161(0 88)	475910(1 85)
	$^2P^o_{1/2}$	485867	514228(5.84)	490131(0 88)	476842(1.86)
		Ca^{+13}			
$2s^2 2p^3$	$^2D^o_{3/2}$	105870	109567(3 49)	106101(0 22)	106086(0.20)
	$^2D^o_{5/2}$	113520	117583(3.58)	113640(0 11)	113537(0 01)
	$^2P^o_{1/2}$	172400	172374(0 02)	172528(0 07)	171900(0 29)
	$^2P^o_{3/2}$	183360	183689(0 18)	183562(0.11)	182590(0 42)
$2s2p^4$	$^4P_{5/2}$	515800	516383(0.11)	515551(0 05)	514483(0 26)
	$^4P_{3/2}$	535870	536365(0 09)	535605(0.05)	534245(0.30)
	$^4P_{1/2}$	545090	545637(0 10)	544862(0.04)	543331(0 32)
	$^2D_{3/2}$	710710	723839(1 85)	710564(0.02)	708466(0 32)
	$^2D_{5/2}$	712500	725418(1.81)	712263(0.03)	710126(0 33)
	$^2S_{1/2}$	825050	837427(1.50)	825289(0 03)	821828(0.39)
	$^2P_{3/2}$	858240	880672(2 61)	858132(0 01)	855066(0 37)
	$^2P_{1/2}$	885610	907037(2.42)	885367(0 03)	881912(0.42)
$2p^5$	$^2P^o_{3/2}$	1347870	1376725(2 14)	1349510(0.12)	1342557(0 39)
	$^2P^o_{1/2}$	1380110	1408818(2 08)	1381765(0 12)	1374158(0 43)
		Zn^{+23}			
$2s^2 2p^3$	$^2D^o_{3/2}$	188130	189921(0 95)	187731(0.21)	186054(1 10)
	$^2D^o_{5/2}$	254110	257508(1.34)	254100(0 00)	251711(0.94)
	$^2P^o_{1/2}$	357130	356431(0 20)	357059(0 02)	352584(1 27)
	$^2P^o_{3/2}$	501140	500501(0 13)	500780(0.07)	491017(2 02)
$2s2p^4$	$^4P_{5/2}$	956600	961442(0 51)	956368(0 02)	949938(0 70)
	$^4P_{3/2}$	1084810	1089514(0.43)	1084441(0 03)	1074345(0 96)
	$^4P_{1/2}$	1110540	1115895(0 48)	1110260(0 03)	1100110(0 94)
	$^2D_{3/2}$	1328550	1345375(1 27)	1328244(0.02)	1317523(0 83)
	$^2D_{5/2}$	1371750	1387552(1 15)	1371723(0.00)	1359434(0.90)
	$^2S_{1/2}$	1516340	1534008(1 17)	1516617(0 02)	1500825(1 02)
	$^2P_{3/2}$	1578630	1603901(1 60)	1578885(0 02)	1562012(1 05)
	$^2P_{1/2}$	1767650	1788473(1.18)	1766549(0 06)	1743983(1 34)
$2p^5$	$^2P^o_{3/2}$	2451700	2488405(1.50)	2452620(0.04)	2431016(0 84)
	$^2P^o_{1/2}$	2657600	2692812(1 32)	2657717(0 00)	2629555(1.06)

[a] Reference [33]
[b] Reference [5, 36]

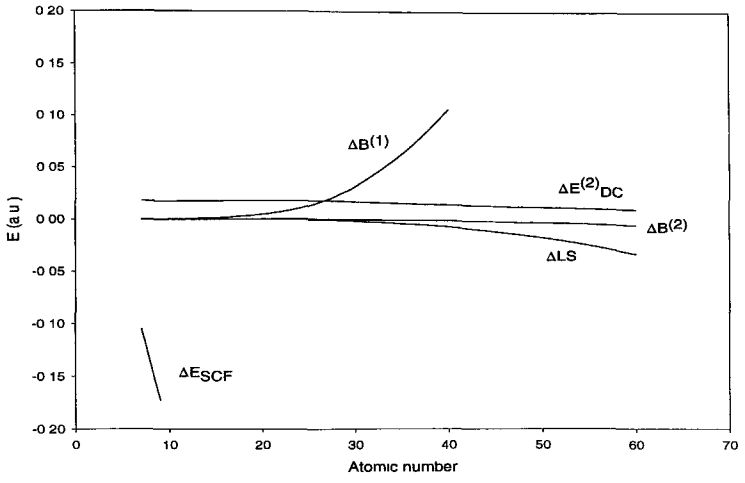

Figure 1: Contributions from each order of perturbation theory to the term energy separation $2s^22p^3$ ($^4S^o_{3/2}$ - $^2D^o_{5/2}$) (in a.u.) as functions of nuclear charge Z.

n=2 complex MC DF SCF calculations yield accuracy comparable in percentage deviation with the correlated NR-MBPT calculations, clearly indicating the importance of accounting for relativity with a fully relativistic treatment. Accounting for dynamical correlation with state-specific MR-MP theory based on MC DF wave functions as reference functions dramatically improves the accuracy in term energy separations, reducing percentage deviations between theory and experiment to within 0.1 %.

Figure 1 displays the contribution from each order of perturbation theory to energy separations (a.u.) of excited $2s^22p^3\ ^2D^o_{5/2}$ states relative to the ground $2s^22p^3\ ^4S^o_{3/2}$ states plotted against nuclear charge Z. These contributions were computed by subtracting the energy of the ground $2s^22p^3\ ^4S^o_{3/2}$ odd-parity state from that of the excited state in each order of perturbation theory. The MC DF SCF and MR-MP calculations, which include the Breit interaction in the effective electron-electron interaction, as well as the Lamb shifts, result in significant corrections and yield close agreement between the calculated and experimental term energy separations. The first-order correction $\Delta B^{(1)}$ becomes much larger than $\Delta E^{(2)}_{DC}$ for Z $\gtrsim$ 30. The Lamb shift correction, ΔLS, is comparable at the low-Z end, but increases rapidly as Z increases and becomes much larger in magnitude for Z $\gtrsim$ 30 than the relativistic many-body shift $\Delta B^{(2)}$. The Figure shows the importance of ΔLS in accurately predicting

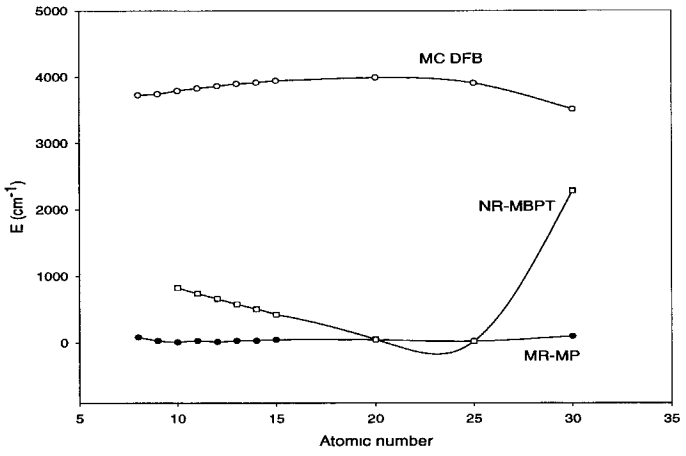

Figure 2: Deviations from experiment of the computed $2s^22p^3$ ($^4S^o_{3/2}$ - $^2D^o_{5/2}$) (cm^{-1}) term energy separations as a function of nuclear charge Z.

term energy separations. The difference, ΔLS, becomes large in large-Z ions and results in significant corrections to term energy separations, as does $\Delta B^{(1)}$.

Figure 2 illustrates the differences $E^{exp}(^2D^o_{5/2}$ - $^4S^o_{3/2})$ - $E^{theor}(^2D^o_{5/2}$ - $^4S^o_{3/2})$ between theoretical and experimental term energy separations (in cm^{-1}), $2s^22p^3\ ^2D^o_{5/2}$ - $2s^22p^3\ ^4S^o_{3/2}$, as functions of the atomic number Z. The deviations from experiment of the term energy separations computed by NR-MBPT [5, 36] are also given to illustrate the sharp increases as Z increases. NR-MBPT starts to show significant deviation from experiment for Z $<$ 20 and Z $>$25. Again the failure to reproduce experimental term energy separations may be attributed to the absence of fully relativistic treatment including QED corrections. The term energy separations computed by MC DF SCF plus first-order Breit interaction correction (denoted MC DFB in Fig. 2) deviate significantly over the range of Z numbers, necessitating dynamic correlation and radiative corrections. Figure 2 illustrates that relativistic MR-MP calculations (the curve labeled MR-MP in the Figure), which include the Breit interaction in the effective electron-electron interaction, as well as the Lamb shifts, result in significant corrections and yield close agreement between the calculated and experimental term energy separations throughout the 7$\leq$ Z$\leq$ 30 series.

Table IV compares with experiment the $2s^22p^3$ ($^2D^o_{5/2}$ - $^2D^o_{3/2}$), $2s^22p^3$ ($^2P^o_{3/2}$ - $^2P^o_{1/2}$), $2s^12p^4$ ($^4P_{5/2}$ - $^4P_{3/2}$), and $2p^5$ ($^2P^o_{3/2}$ - $^2P^o_{1/2}$) fine-structure

Table IV: Comparison of fine-structure splittings computed by MCDF and MR-MP with experiment and with previous work.

Z	Experiment[a]	MCDF	MR-MP	NR-MBPT[b]
	$2s^22p^3$ ($^2D^o_{5/2}$ - $^2D^o_{3/2}$)			
30	65980	67587	66369	65136
26	37510	38401	37510	
20	7650	8016	7539	7373
16	1153	1281	1116	
12	-17	0	-20	2
10	-45	-42	-44	-39
	$2s^22p^3$ ($^2P^o_{3/2}$ - $^2P^o_{1/2}$)			
30	144010	144070	143721	143874
26	63070	63716	63235	
20	10960	11315	11034	11394
16	1829	1929	1838	
12	108	111	91	179
10	7	2	-12	65
	$2s2p^4$ ($^4P_{3/2}$ - $^4P_{5/2}$)			
30	128210	128072	128073	128177
26	68090	67698	67902	
20	20070	19982	20054	20013
16	6904	6877	6899	
12	1636	1628	1638	1653
10	617	611	617	642
	$2p^5$ ($^2P^o_{1/2}$ - $^2P^o_{3/2}$)			
30	205900	204407	205097	204580
26	107680	107322	107737	
20	32240	32093	32255	32119
16	11123	11057	11131	
12	2606	2579	2607	2564
10	963	955	970	935

[a] Reference [33].

[b] Reference [5, 36].

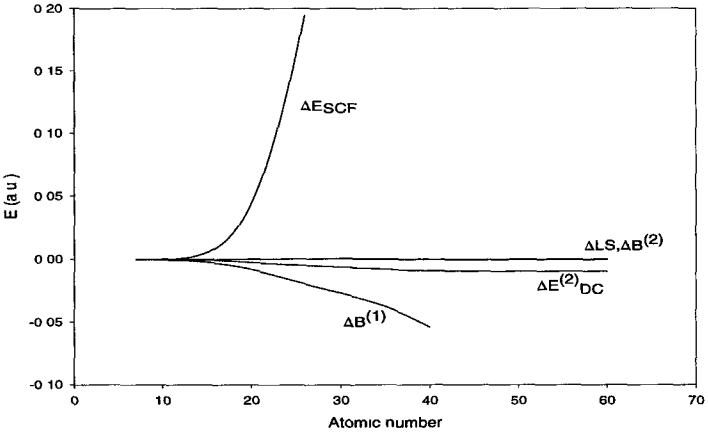

Figure 3: Contributions from each order of perturbation theory for the fine-structure splitting $2s^22p^3$ ($^2D^o_{5/2}$ - $^2D^o_{3/2}$) (in a.u.) as functions of nuclear charge Z.

separations computed with MC DF SCF and MR-MP for several nitrogen-like ions with $10 \leq Z \leq 30$. The MR-MP fine-structure separations are in excellent agreement with experiment, the deviation being well within 1 % in most instances. Figure 3 displays the contribution from each order of perturbation theory to the $2s^22p^3\ ^2D^o_{5/2}-2s^22p^3\ ^2D^o_{3/2}$ fine-structure splitting of nitrogen-like ions as functions of nuclear charge Z. The MC DF SCF and MR-MP calculations, which include the Breit interaction in the effective electron-electron interaction result in significant corrections and yield close agreement between the calculated and experimental fine-structure separations. The first-order correction $\Delta B^{(1)}$ becomes much larger than $\Delta E^{(2)}_{DC}$ for $Z \gtrsim 15$. The Figure shows the importance of $\Delta B^{(1)}$ and $\Delta E^{(2)}_{DC}$ in accurately predicting the fine-structure separation, while the Lamb shift correction, ΔLS, and relativistic many-body shift $\Delta B^{(2)}$ have negligible contributions throughout the Z range.

In Tables V and VI, a detailed comparison of theoretical and experimental data is made on the term energies of the low-lying even- and odd-parity states of nitrogen and nitrogen-like ions with Z=8-60, given relative to the ground $2s^22p^3\ ^4S^o_{3/2}$ state. Theoretical term energy separations, E^{theor}, of the low-lying excited states were computed by subtracting the total energy of the ground $2s^22p^3\ ^4S^o_{3/2}$ state from those of the excited levels. Experimental term energy separations E^{exp} [32, 33] are reproduced in an adjacent column for comparison.

Table V: Energies (cm^{-1}) of low-lying even-parity states of nitrogen and nitrogenlike ions relative to the ground $2s^2 2p^3\ ^4S^o_{3/2}$ state.

Z	$2s2p^4\ ^4P_{5/2}$		$2s2p^4\ ^4P_{3/2}$		$2s2p^4\ ^4P_{1/2}$		$2s2p^4\ ^2D_{3/2}$	
	E^{theor}	E^{exp}	E^{theor}	E^{exp}	E^{theor}	E^{exp}	E^{theor}	E^{exp}
60	6278056		6919231		6931725		10690088	
50	3398969		3894487		3906822		5374014	
40	1797437		2136607		2138650		2593996	
30	956368	956600	1084441	1084810	1110260	1110540	1328244	1328550
26	752506	752730	820408	820820	842316	842740	1042466	1042570
20	515551	515800	535605	535870	544862	545090	710564	710710
16	378115	378458	385014	385362	388574	388883	520334	520723
14	312231	312670	315810	316250	317715	318140	429811	430390
13	279721	280200	282188	282670	283516	283970	385263	385910
12	247414	247948	249052	249584	249940	250450	341056	341793
11	215242	215860	216278	216896	216846	217440	297061	297916
10	183140	183860	183757	184477	184100	184799	253146	254102
9	151015	151900	151355	152237	151545	152411	209135	210256
8	118676	119837	118840	120000	118935	120083	164688	165997
7	86368	88107	86429	88151	86463	88171	119958	

Z	$2s2p^4\ ^2D_{5/2}$		$2s2p^4\ ^2S_{1/2}$		$2s2p^4\ ^2P_{3/2}$		$2s2p^4\ ^2P_{1/2}$	
	E^{theor}	E^{exp}	E^{theor}	E^{exp}	E^{theor}	E^{exp}	E^{theor}	E^{exp}
60	10978394		11337441		11421993		15710499	
50	5615280		5872831		5966716		7833060	
40	2759642		2936689		3030830		3799562	
30	1371723	1371750	1516617	1516340	1578885	1578630	1766549	1767650
26	1058172	1058360	1195579	1195260	1242491	1242430	1339907	1340040
20	712263	712500	825289	825050	858132	858240	885367	885610
16	520426	520864	608805	608784	636549	636898	645272	645660
14	429829	430360	504500	504630	530006	530430	534370	532800
13	385291	385860	452944	453060	477283	477690	480244	480660
12	341080	341751	401662	401822	424765	425190	426702	427135
11	297074	297880	350532	350747	372317	372731	373529	373932
10	253150	254081	299416	299628	319789	320030	320506	320741
9	209132	210256	248110	248261	266965	266562	267358	266945
8	164679	165989	196112	195711	213418	212594	213610	212762
7	119949	121201	144061		158879		158956	

Table VI: Energies (cm^{-1}) of low-lying odd-parity states of nitrogen and nitrogenlike ions relative to the ground $2s^22p^3\ ^4S^o_{3/2}$ state.

Z	$2s^22p^3\ ^2D^o_{5/2}$		$2s^22p^3\ ^2D^o_{3/2}$		$2s^22p^3\ ^2P^o_{3/2}$	
	E^{theor}	E^{exp}	E^{theor}	E^{exp}	E^{theor}	E^{exp}
60	4409853		4236940		8956637	
50	1969066		1817303		4017967	
40	751390		631405		1540370	
30	254098	254110	187731	188130	500374	501140
26	176135	176130	138625	138620	323610	323340
20	113640	113520	106101	105870	183562	183360
16	83656	83595	82540	82442	128861	128804
14	69461	69421	69226	69168	105866	105890
13	62422	62369	62362	62313	94824	94869
12	55378	55358	55398	55373	83934	84028
11	48315	48330	48361	48366	73098	73255
10	41212	41235	41256	41280	62244	62441
9	34030	34087	34062	34123	51286	51561
8	26698	26811	26718	26831	40077	40468
7	19022	19224	19029	19233	28286	28839
	$2s^22p^3\ ^2P^o_{1/2}$		$2p^5\ ^2P^o_{3/2}$		$2p^5\ ^2P^o_{1/2}$	
	E^{theor}	E^{exp}	E^{theor}	E^{exp}	E^{theor}	E^{exp}
60	4709093		13676612		18103636	
50	2191910		7718186		9688193	
40	908778		4329265		5064831	
30	357059	357130	2452620	2451700	2657717	2657600
26	260375	260270	1955729	1954520	2063466	2062200
20	172528	172400	1349510	1347870	1381765	1380110
16	127023	126975	993204	991249	1004335	1002372
14	105333	105348	822527	820200	828278	825930
13	94581	94603	738391	735750	742340	739700
12	83843	83920	654871	651867	657478	654473
11	73081	73218	571829	568348	573469	569977
10	62256	62435	489161	484904	490131	485867
9	51281	51560	406804	401206	407334	401724
8	40087	40470	324706		324965	
	28294	28839	242740		242848	

Table VII: Comparison of the M1 transition probabilities for Z=7-30 nitrogen-like ions.

Z	Relativistic transition operator This work DC MCDF	DC MR-MP	DCB MCDF	DCB MR-MP	SPST[a]	Nonrelativistic operator NR-MBPT[b]	MCHF[c]
$2s^22p^3$ ($^2D^o_{3/2}$ - $^4S^o_{3/2}$)							
7	1.924(-6)	3.141(-5)	2.187(-5)	1.246(-5)	1.90(-5)		1.484(-5)
8	3.864(-5)	1.603(-4)	1.867(-4)	1.226(-4)	1.59(-4)		1.314(-4)
9	4.497(-5)	2.613(-4)	1.204(-3)	8.673(-4)	9.36(-4)		8.563(-4)
10	3.688(-3)	2.451(-3)	6.638(-3)	5.020(-3)	5.28(-3)	4.73(-3)	4.744(-3)
11	2.318(-2)	1.695(-2)	3.227(-2)	2.534(-2)	2.62(-2)	2.37(-2)	2.343(-2)
12	1.182(-1)	9.166(-2)	1.398(-1)	1.130(-1)	1.16(-1)	1.06(-1)	1.030(-1)
14	1.898(+0)	1.595(+0)	1.900(+0)	1.597(+0)	1.62(+0)	1.51(+0)	1.462(+0)
21	1.143(+3)	1.032(+3)	1.048(+3)	9.465(+2)	9.42(+2)	9.35(+2)	8.910(+2)
26	1.739(+4)	1.622(+4)	1.625(+4)	1.517(+4)	1.36(+4)	1.50(+4)	1.100(+4)
30	1.027(+5)	9.860(+4)	9.917(+4)	9.519(+4)		9.08(+4)	9.944(+4)
$2s^22p^3$ ($^2D^o_{5/2}$ - $^4S^o_{3/2}$)							
7	4.431(-8)	5.634(-7)	5.528(-7)	2.270(-7)	2.45(-7)		9.122(-7)
8	8.574(-8)	1.774(-6)	3.810(-6)	1.920(-6)	1.98(-6)		6.994(-6)
9	8.030(-8)	1.203(-8)	2.105(-5)	1.244(-5)	1.30(-5)		3.766(-5)
10	9.315(-6)	4.252(-6)	1.055(-4)	6.926(-5)	7.76(-5)	1.69(-4)	1.545(-4)
11	1.241(-4)	8.044(-5)	4.877(-4)	3.478(-4)	4.05(-4)	7.16(-4)	7.164(-4)
12	9.231(-4)	6.765(-4)	2.081(-3)	1.575(-3)	1.86(-3)	2.79(-3)	2.745(-3)
14	2.185(-2)	1.916(-2)	2.918(-2)	2.375(-2)	2.78(-2)	3.41(-2)	3.312(-2)
21	3.476(+1)	3.109(+1)	3.235(+1)	2.906(+1)	3.12(+1)	3.16(+1)	3.036(+1)
26	1.374(+3)	1.279(+3)	1.266(+3)	1.178(+3)	1.29(+3)	1.18(+3)	9.558(+2)
30	1.448(+4)	1.382(+4)	1.368(+4)	1.305(+4)		1.25(+4)	1.361(+4)

[a] Zeippen [42, 43, 44].
[b] Merkelis *et al.* [5, 36].
[c] Godefroid and Froese Fischer [37].

Experimental data are not available for ions with Z=40, 50, 60.

4.2 Spin-forbidden $2s^22p^3$ transitions

Probabilities of forbidden transitions are of importance in the diagnostics of astrophysical and fusion plasmas, but experimental determination of these quantities is difficult and accurate theoretical estimates provide valuable information. A number of theoretical calculations on spin-forbidden transitions has been performed by various approximations in past years, and it has become evident that accurate intermediate-coupled wavefunctions must be used to evaluate forbidden transition probabilities accurately. Among the nonrelativistic methods, the most accurate are MCHF and MBPT methods.

Table VII summarizes the $^2D^o_{3/2}$ - $^4S^o_{3/2}$ and $^2D^o_{5/2}$ - $^4S^o_{3/2}$ M1 transition

probabilities of nitrogen and nitrogen-like ions with Z=8-30 computed at MC DF SCF and MR-MP levels of theory. The M1 transition probabilities computed without and with the Breit interaction in the MC DF and MR-MP are given, respectively, under the headings, DC and DCB. As Z increases, the M1 transition probabilities increase dramatically, by nine to ten orders of magnitude. Significant differences in the transition probabilities computed in the DC and DCB schemes clearly indicate that the Breit interaction significantly affects the transition probabilities, especially in low-Z ions.

Godefroid and Froese Fischer [37] performed nonrelativistic multiconfigurational Hartree-Fock (MC HF) calculations, including relativistic corrections in the Breit-Pauli approximation, on the E2 and M1 transitions that arise within the ground $2s^2 2p^3$ configuration along the nitrogen isoelectronic sequence. The Breit-Pauli interaction matrix was built on a set of 67 configuration states ($11\ ^4S + 26\ ^2D + 30\ ^2P$), omitting the orbit-orbit contribution. The transition probabilities were calculated with wavelengths derived from Ref. [38] and employing the non-relativistic M1 transition operator, $\mathbf{O}_{M1} = \mu_B \sum_i \mathbf{O}_{M1}(i) = \mu_B \sum_i (\mathbf{l}_i + 2\mathbf{s}_i)$. Their results are given in the last row of the Table. NR-MBPT was applied to nitrogen-like ions by Merkelis *et al.* [5, 36] to estimate the E1, M1 and E2 transitions of ions from Ne^{3+} to Zn^{+23}. Relativistic corrections were included in the Breit-Pauli approximation, analogous to MC HF calculations, and one-body spin-orbit interaction was accounted for at the second-order of perturbation theory. Their results are given in the seventh column. The $^2D^o_{3/2} - {}^4S^o_{3/2}$ transition probabilities computed by both MC HF and NR-MBPT agree reasonably well with our MR-MP (DCB) results. However, the $^2D^o_{5/2} - {}^4S^o_{3/2}$ transition probabilities computed by the nonrelativistic methods grossly overestimate our MR-MP values.

Eissner and Zeippen performed limited CI calculations on the forbidden transitions in O^{1+} [39] using the computer program SUPERSTRUCTURE (hereafter denoted SPST) [40]. The Breit-Pauli approximation accounted for relativistic effects. Semi-empirical term-energy corrections to shift the calculated energy levels to their observed values were applied. In contrast to the case with the MC HF calculations, the Breit-Pauli interaction matrix did not include two-body corrections. The M1 transition probabilities were calculated using the relativistic operator introduced by Drake, [41] $\mathbf{O}_{M1} = \mu_B \sum_i \mathbf{O}_{M1}(i) + \mu_B \sum_{ij} \mathbf{O}_{M1}(ij)$, which includes all the radiative correction terms of order α^2. Zeippen extended those calculations to all members of the isoelectronic sequence from N^0 to Fe^{19+}. Later SPST calculations on N^0 by Butler and Zeippen [43] and on O^{1+} by Zeippen [44] included a larger configurational space than in the MC HF calculations [37]. In these studies, the importance of higher-order relativistic corrections in the M1 transition operator for spin-forbidden transitions was emphasized. The results of the SPST

Table VIII: Comparison of the $2s^22p^3$ ($^2D_{5/2}$ - $^2P_{1/2}$) E2 transition probabilities for nitrogenlike ions.

Z	Relativistic transition operator This work				Nonrelativistic operator	
	DC		DCB		MCHF[a]	NR-MBPT[b]
	MCDF	MR-MP	MCDF	MR-MP		
7	9.019(-3)	3.048(-2)	9.019(-3)	3.049(-2)	2.914(-2)	
8	1.907(-2)	5.055(-2)	1.907(-2)	5.057(-2)	5.382(-2)	
9	3.232(-2)	7.926(-2)	3.232(-2)	7.930(-2)	7.860(-2)	
10	4.808(-2)	1.019(-1)	4.808(-2)	1.020(-1)	1.039(-1)	1.04(-1)
11	6.591(-2)	1.322(-1)	6.590(-2)	1.323(-2)	1.295(-1)	1.29(-1)
12	8.555(-2)	1.567(-1)	8.555(-2)	1.568(-1)	1.563(-1)	1.55(-1)
14	1.299(-1)	2.160(-1)	1.299(-1)	2.161(-1)	2.122(-1)	
21	3.480(-1)	4.665(-1)	3.480(-1)	4.670(-1)	4.570(-1)	4.49(-1)
26	5.969(-1)	7.447(-1)	5.969(-1)	7.458(-1)	7.191(-1)	6.96(-1)
30	8.866(-1)	1.061(+0)	8.864(-1)	1.063(+0)	9.381(-1)	9.67(-1)

[a] Merkelis et al. [5, 36].

[b] Godefroid and Froese Fischer [37].

calculations are displayed in the sixth column of the Table. Our MR-MP results agree reasonably well with the SPST throughout $7 \leq Z \leq 30$. There is several-fold disagreement between our MR-MP calculations and highly correlated MC HF and NR-MBPT methods in some instances.

Godefroid and Froese Fischer pointed out [37] that the E2 processes without change of the spin multiplicity are allowed in the LS coupling scheme, and that the correlation corrections are more important than relativistic for low-Z ions. The $\Delta S \neq 0$ spin-forbidden M1 and E2 transitions occur due to the small admixing in the Breit-Pauli approximation. In the case of $2s^22p^3$ ($^2D^o_{5/2}$– $^4S^o_{3/2}$), with the non-relativistic magnetic dipole operator and Breit-Pauli wavefunction, the reduced transition matrix element is given only by admixture of $^4S_{3/2}$ with $^2D_{3/2}$. Since the one-body spin-orbit interaction vanishes, the resulting mixing coefficients in the Breit-Pauli approximation are small and inaccurate. When those admixtures arise not from spin-orbit interaction, but from two-electron magnetic effects, the use of the nonrelativistic transition operator yields inaccurate results. Thus, consistent use of relativistic correlated wavefunctions and the relativistic transition operator is required to achieve accuracy. The spin-forbidden transitions in the nitrogen isoelectronic sequence involving the half-filled $2p$ shell is just such a case.

Table VIII displays the E2 transition probabilities for the $2s^22p^3$ ($^2D_{5/2}$ - $^2P_{1/2}$) transition computed by MC DF and MR-MP theories. The Breit interaction has little or no effect on the calculated E2 transition probabilities, and DC and DCB results are nearly identical at both the MC DF and MR-MP levels of theory. On the other hand correlation corrections significantly alter

Table IX: Comparison of the E2 and M1 transition probabilities and high-density limit ratio $r(\infty)$ of O^{1+}.

Type	This work		MCHF[a]	SPST[b]	SPST[c]	Experiment
	MCDF	MR-MP				
		$2s^22p^3\ ^2D^o_{3/2}$ - $^4S^o_{3/2}$				
E2	6.586(-5)	3.486(-5)	2.888(-5)	3.39(-5)	3.39(-5)	
M1	1.868(-4)	1.226(-4)	1.314(-4)	1.46(-4)	1.59(-4)	
		$2s^22p^3\ ^2D^o_{5/2}$ - $^4S^o_{3/2}$				
E2	4.264(-5)	2.269(-5)	1.879(-5)	2.20(-5)	2.20(-5)	
M1	3.810(-6)	1.920(-6)	6.994(-6)	7.58(-6)	1.98(-6)	
$r(\infty)$	0.455	0.379	0.358	0.370	0.297	0.36±0.02

[a] Godefroid and Froese Fischer [37]
[b] SUPERSTRUCTURE calculations of Zeipen without relativistic corrections to M1 operator [44].
[c] SUPERSTRUCTURE calculations of Zeipen with relativistic corrections to M1 operator [44].

the calculated transition probabilities. The E2 transition probabilities depend on the excitation energies to the fifth power and inaccuracy in the calculated transition energies is thus the major source of error. The first-order transition probabilities (Eq. 38) increase over the lowest-order by about 70% for N^0 and 16% for Zn^{+23}. The bulk of the improvement is due to more accurate transition energies.

In the last two columns of the Table the E2 transition probabilities computed by MC HF and NR-MBPT are displayed. Because the correlation corrections to the E2 line strength in the light Si^{7+} ion are similar in both relativistic (MR-MP) and non-relativistic theories, there is good agreement in the calculated E2 transition probabilities among the three methods. Both MR-MP and NR-MBPT provide accurate transition energies in the second-order of perturbation theories for low- to middle-Z ions and there are only slight differences in the calculated line strengths. For high-Z ions the relativistic effects are more pronounced, mandating fully relativistic methods.

In Table IX, we present the high electron density limit ratio $r(\infty) = \frac{3}{2}A(^2D_{5/2} - {}^4S_{3/2})/A(^2D_{3/2} - {}^4S_{3/2})$ which is of particular importance in nebulae studies (for a detailed discussion see [44]). Here both the E2 and M1 transitions are important. In the $^2D_{5/2} - {}^4S_{3/2}$ case, the E2 transition is dominant, and in the $^2D_{3/2} - {}^4S_{3/2}$ case the M1 transition dominates. A number of studies have been devoted to obtaining accurate $r(\infty)$. Most noncorrelated methods overestimate the ratio by as much as 50%, and only correlated methods such as MCHF and CI with a large CSF expansion have provided reliable values. In the present study MC DF SCF wavefunctions provide excellent

reference functions, and we obtain reliable results with second-order MR-MP. While MC DF SCF fails to predict an accurate ratio (0.455 compare to experimental value of 0.36±0.02), MR-MP gives 0.379, in good agreement with the experimental estimate. The results of Zeipen (denoted SPST[b]) are somewhat inconsistent in that the ratio is significantly lower, by 20%, than the value obtained by nonrelativistic SPST[a] although the M1 transition operator includes relativistic corrections and Breit-Pauli wavefunctions were employed.

While the MC HF method grossly overestimates the $^2D_{5/2}-\ ^4S_{3/2}$ M1 transition probability obtained by the MR-MP method, it yields a high electron density limit ratio of 0.358, in good agreement with MR-MP and experimental estimates, largely because the $^2D_{5/2}-\ ^4S_{3/2}$ E2 transition probability, which all three methods yield accurately, is one order of magnitude larger than the overestimated M1 value.

4.3 E1 transition probabilities and lifetimes

Allowed E1 transitions have been extensively treated by several methods. One of the most accurate is the non-closed shell many-electron theory (NCMET) [45]. It accounts for electron correlation by configuration interaction and includes some contributions to all orders of perturbation theory. However, NCMET employs the LS coupling scheme and high-Z results provide only crude estimates. In the intermediate coupling case, such as in the Si^{+7}ion, relativistic multireference many-body perturbation theory accounts for relativity and electron correlation accurately, and provides accurate transition energies in the second order of perturbation theory. Because MC HF and MC DF methods do not account for dynamical correlation, these methods fail to calculate transition energies within 1% accuracy.

Table X summarizes the E1 transition probabilities of Si^{7+} computed in length gauge with MC DF and MR-MP. In the last column, the values computed by NR-MBPT are displayed for comparison. The Breit-Pauli approximation is valid for the light ion, and the agreement between the fully relativistic MR-MP and quasirelativistic NR-MBPT, is very good. MCDF overestimates transition probabilities because dynamic correlation, missing in MC DF, is important in the light system.

In Table XI we compare the calculated lifetimes of the even-parity excited $^4P_{1/2,3/2,5/2}$,$^2D_{3/2,5/2}$ and $^2P_{1/2,3/2}$ states of nitrogen-like silicon with experiment. The E1 transition probabilities and lifetimes were computed with our MR-MP method because this is one of the very few systems to which experimental lifetimes of the excited ^4P_J, ^2D_J and ^2P_J states have been measured, and theoretical lifetimes have been estimated by several methods. Experimental estimates in the second column are taken from Ref. [47]. The theoretical

Table X: Comparison of the 16 strongest $2s2p^4$ - $2s^22p^3$ E1 transition probabilities for nitrogen-like silicon Si^{7+}.

	This work				NR-MBPT[a]
	DC		DCB		
	MCDF	MR-MP	MCDF	MR-MP	
$^2P_{3/2}$ - $^2P^o_{3/2}$	8.480(+9)	6.658(+9)	8.583(+9)	6.742(+9)	6.812(+9)
$^2P_{3/2}$ - $^2P^o_{1/2}$	2.226(+9)	1.736(+9)	2.214(+9)	1.728(+9)	1.716(+9)
$^2P_{3/2}$ - $^2D^o_{5/2}$	3.874(+10)	3.023(+10)	3.870(+10)	3.022(+10)	3.021(+10)
$^2P_{3/2}$ - $^2D^o_{3/2}$	5.957(+9)	4.687(+9)	5.876(+9)	4.627(+9)	4.441(+9)
$^2P_{1/2}$ - $^2P^o_{3/2}$	1.073(+10)	8.220(+9)	1.032(+10)	7.913(+9)	8.048(+9)
$^2P_{1/2}$ - $^2P^o_{1/2}$	6.957(+9)	5.503(+9)	7.038(+9)	5.567(+9)	5.195(+9)
$^2P_{1/2}$ - $^2D^o_{3/2}$	3.761(+10)	2.928(+10)	3.803(+10)	2.963(+10)	2.987(+10)
$^2D_{3/2}$ - $^2P^o_{1/2}$	1.444(+9)	1.059(+9)	1.448(+9)	1.061(+9)	1.025(+9)
$^2D_{3/2}$ - $^2D^o_{5/2}$	9.667(+8)	7.358(+8)	9.825(+8)	7.486(+8)	7.148(+8)
$^2D_{3/2}$ - $^2D^o_{3/2}$	1.125(+10)	8.569(+9)	1.122(+10)	8.547(+9)	8.404(+9)
$^2D_{5/2}$ - $^2P^o_{3/2}$	2.045(+9)	1.498(+9)	2.031(+9)	1.489(+9)	1.434(+9)
$^2D_{5/2}$ - $^2D^o_{3/2}$	4.243(+8)	3.229(+8)	4.417(+8)	3.366(+8)	3.567(+8)
$^2D_{5/2}$ - $^2D^o_{5/2}$	1.095(+10)	8.366(+9)	1.095(+10)	8.371(+9)	8.212(+9)
$^4P_{1/2}$ - $^4S^o_{3/2}$	5.027(+9)	3.973(+9)	5.026(+9)	3.974(+9)	3.870(+9)
$^4P_{3/2}$ - $^4S^o_{3/2}$	4.925(+9)	3.891(+9)	4.925(+9)	3.893(+9)	3.792(+9)
$^4P_{5/2}$ - $^4S^o_{3/2}$	4.748(+9)	3.750(+9)	4.749(+9)	3.753(+9)	3.675(+9)

[a] Merkelis et al. [5, 36].

Table XI: Comparison of the lifetimes (in ps) of even-parity excited states of nitrogen-like silicon, Si^{7+}.

State	Experiment[a]	This work		NR-MBPT[b]	NCMET[c]
		MCDF	MR-MP		
$^4P_{1/2}$		199.0	251.6	258.4	
$^4P_{3/2}$		203.0	256.9	263.7	
$^4P_{5/2}$		210.6	266.5	272.1	
mean	280±30				266
$^2D_{3/2}$		73.0	96.6	98.6	
$^2D_{5/2}$		74.5	98.1	100.0	
mean	90±15				100
$^2P_{3/2}$		18.1	23.1	23.2	
$^2P_{1/2}$		18.1	23.2	23.2	
mean	23±3				23

[a] Träbert *et al.* [47].

[b] Merkelis *et al.* [5, 36].

[c] Nicolaides and Beck [46]

lifetimes computed by NR-MBPT and NCMET [46] are also displayed in the last two columns for comparison. All calculated lifetimes, excepting those computed by MC DF, are within the error bounds of the experimental estimates. The mean lifetimes estimated by NCMET tend to be slightly higher than those of each fine structure state computed by MR-MP. Lacking dynamical correlation, MC DF grossly underestimates the lifetimes.

References

[1] Träbert, E. Physica Scripta **1999**, 59, 443..

[2] Safronova, M. S.; Derevianko, A.; Johnson, W. R. Phys. Rev. A **1998**, 58, 1016.

[3] Biemont, E.; Zeippen C. J. Physica Scripta **1996**, T65, 192.

[4] Ynnerman, A.; Froese-Fischer, C. Phys. Rev. A **1995**, 51, 2020.

[5] Merkelis, G.; Vilkas, M. J.; Kisielius, R.; Gaigalas, G.; Martinson, I. Physica Scripta **1997**, 56, 41.

[6] Vilkas, M. J.; Koc, K.; Ishikawa, Y. Chem. Phys. Letters **1998**, 296, 68.

[7] Vilkas, M. J.; Ishikawa, Y.; Koc, K. Phys. Rev. A **1999**, 60, 2808.

[8] Ishikawa, Y.; Vilkas, M. J.; Koc, K. Int. J. Quantum Chem. **2000**, 77, 433.

[9] Ishikawa, Y.; Koc, K. Phys. Rev. A **1996**, 53, 3966.

[10] Ishikawa, Y.; Koc, K. Phys. Rev. A **1997**, 56, 1295.

[11] Sucher, J. Phys. Rev. A **1980**, 22, 348.

[12] Mittleman, M. H. Phys. Rev. A **1981**, 24, 1167.

[13] Weiss, A. W.; Kim, Y.-K. Phys. Rev. A **1995**, 51, 4487.

[14] Vilkas, M. J.; Ishikawa, Y.; Koc, K. Phys. Rev. E **1998**, 58, 5096.

[15] Vilkas, M. J.; Koc, K.; Ishikawa, Y. In "Progress in Theoretical Chemistry and Physics"; Kluwer: Dordrecht, 2000.

[16] Quiney, H. M. In "Progress in Theoretical Chemistry and Physics"; Kluwer: Dordrecht, 2000.

[17] Hirao, K. Chem. Phys. Letters **1992**, 190, 374.

[18] Møller, C.; Plesset, M. S. Phys. Rev. **1934**, 46, 618.

[19] Hirao, K. Chem. Phys. Letters **1993**, 201, 59.

[20] Ishikawa, Y. Phys. Rev. A **1990**, 42, 1142.

[21] Quiney, H. M.; Grant, I. P. J. Phys. B **1994**, 27, L299.

[22] Mohr, P. J. Phys. Rev. A **1992**, 46, 4421.

[23] Blundell, S. A.; Mohr, P. J.; Johnson, W. R.; Sapirstein, J. Phys. Rev. A **1993**, 48, 2615.

[24] Labzowsky, L.; Karasiev, V.; Lindgren, I.; Persson, H.; Salomonson, S. Physica Scripta **1993**, T46, 150.

[25] Indelicato, P.; Gorceix, O.; Desclaux, J. P. J. Phys. B **1987**, 20, 651.

[26] Akhiezer, A. I.; Berestetskii, V. B. "Quantum Electrodynamics"; Wiley Interscience: New York, 1965.

[27] Grant, I. P. J. Phys. B **1974**, 7, 1458.

[28] Johnson, W. R.; Plante, D. R.; Sapirstein, J. In "Advances in atomic, molecular and optical physics", *1995;* Vol. 35, 255.

[29] Ishikawa, Y.; Quiney, H. M.; Malli, G. L. Phys. Rev. A **1991**, 43, 3270.

[30] Schmidt, M. W.; Ruedenberg, K. J. Chem. Phys. **1979**, 71, 3951.

[31] Kim, Y.-K. In "Atomic Processes in Plasmas", AIP Conf. Proc. 1990; No. 206, 19.

[32] Edlén, B. Physica Scripta **1984**, 30, 135.

[33] Fuhr, J. R.; Martin, W. C.; Musgrove, A.; Sugar, J.; Wiese, W. L. NIST Atomic Spectroscopic Database, available at http://physics.nist.gov/PhysRefData/contents.html (December 1997).

[34] Johnson, W. R.; Sapirstein, J. Phys. Rev. Lett. **1986**, 57, 1126.

[35] Blundell, S. A.; Johnson, W. R.; Sapirstein, J. Phys. Rev. Lett. **1991**, 65, 1411.

[36] Merkelis, G.; Martinson, I.; Kisielius, R.; and Vilkas, M. J. Physica Scripta 1999, **59**, 122 (1999).

[37] Godefroid, M.; Froese Fischer, C. J. Phys. B **1984**, 17, 681.

[38] Fawcett, B. C.; At. Data Nucl. Data Tables **1975**, 16, 135.

[39] Eissner, W.; Zeippen, C. J. J. Phys. B **1981**, 14, 2125.

[40] Eissner, W.; Jones, M.; Nussbaumer, H. Comput. Phys. Commun. **1974**, 8, 270.

[41] Drake, G. W. F.; Phys. Rev. A **1971**, 3, 908.

[42] Zeippen, C. J. Mon. Not. R. astr. Soc. **1982**, 198, 111.

[43] Butler, K.; Zeippen, C. J. Astron. Astrophys. **1984**, 141, 274.

[44] Zeippen, C. J. Astron. Astrophys. **1987**, 173, 410.

[45] Sinanoglu, O. Nucl. Instr. and Meth.**1973**, 110, 193.

[46] Nicolaides, C. A.; Beck, D. R. J. Phys. B **1973**, 6, 535.

[47] Träbert, E.; Heckman, P. H.; Schlagheck, W.; Buttlar, H. V. Physica Scripta **1980**, 21, 27.

[48] Cheng, K. T.; Kim, Y.-K.; Desclaux, J. P. At. Data Nucl. Data Tables **1979**, 24, 111.

[49] Pyper, N. C. J. Phys. B **1983**, 16, L211.

[50] Layzer, D.; Bahcall, J. Ann. Phys. (New York) **1962**, 17, 177.

[51] Cheng, K. T.; Froese Fischer, C.; Kim, Y-.K. J. Phys. B **1982**, 15, 181.

[52] Vilkas, M. J.; Ishikawa, Y.; Hirao, K. Chem. Phys. Letters **2000** (in press).

[53] Desclaux, J. P. Computer Phys Comm **1975**, 9, 31.

Reduced density-matrix treatment of spin-spin interaction terms in many-electron systems

R. L. PAVLOV*,#, A. I. KULEFF*,#, P. Tz. YOTOV* and J. MARUANI#

* *Institute of Nuclear Research and Nuclear Energy, BAS, 72 Tzarigradsko Chaussee, 1784 Sofia, Bulgaria*

Laboratoire de Chimie Physique, CNRS and UPMC, 11 rue Pierre et Marie Curie, 75005 Paris, France

Abstract

In the formalism of the reduced density matrices and functions, using the irreducible tensor-operator technique and the space-spin separation scheme, the matrix elements of some of the spin-relativistic corrections of the Breit-Pauli Hamiltonian, namely the spin-spin interactions, are expressed in a form suitable for numerical implementation. A comparison with other methods is made and the advantages of such an approach are discussed.

1. Introduction

In the formalism of the reduced density matrices and functions (RDM & RDF) [1-3], the matrix elements and expectation values of the different types of spin-involving operators take the form of a product of space and spin factors [1, 4]. The spin part is determined by the spin symmetry and reduces to 3j-symbols, while the spatial part is determined by the action of space operators on the spin distribution or spin-spin cor-

ADVANCES IN QUANTUM CHEMISTRY VOLUME 39

0065-3276/01 $35 00

relation matrices or functions [1, 4, 5]. The spin distribution and correlation functions are built from the spatial parts of the RDMs of first and second order, respectively. In this approach, the space-spin separation results from the possibility of separating the space and spin variables in RDMs [6-9] and from the use of the split RDMs to represent the matrix elements of the perturbation terms in the Hamiltonian [10].

In terms of the RDMs and RDFs and in the scheme of the space-spin separation, there are presented in Refs [1, 4] the matrix elements and expectation values of the various spin-involving operators, which are relativistic corrections in the Breit-Pauli Hamiltonian. The matrix elements and expectation values of the operators corresponding to the different types of spin interactions are reduced to products of a multiplier determined by the spin symmetry, which characterize a spin state or a transition between two states in a given spin multiplet, and a space part that depends neither on the spin state nor on a transition between two states. This space part is expressed by the action of the considered space operator on the space part of the relevant spin distribution or spin-spin correlation matrix or function.

In Ref. [11] we took a further step in the treatment of the matrix elements of one of the main relativistic corrections, the spin-orbit interaction terms, in a form convenient for numerical implementation. In the present work we shall consider the matrix elements of another type of spin-involving relativistic corrections, the spin-spin interactions, which should also be amenable to direct numerical implementation.

Using the technique of the irreducible tensor operators and applying the Wigner-Eckart theorem, the matrix elements of the dipolar spin-spin interactions are expressed as products, or sums of products, of three parts: the first one is a multiplier determined by the spin symmetry; the second one is a multiplier characterizing the orbital symmetry, and the third one is a spatial part determined by the action of the symmetrized space tensor operators on the normalized spin distribution or correlation matrices or functions. The action of these space tensor operators, which are the same for a given spin multiplet and are independent of the investigated (splitting or transition) effect, is reduced to a standard procedure. The expectation values of the spin-spin interaction operators, which give the amount of splitting of the energy levels, are expressed in an analytical form suitable for numerical implementation. We also consider the transition matrix elements of these operators, which give the contribution of the spin-spin interactions to the corresponding induced spin transitions.

2. Spin distribution and correlation densities

2.1. Spin distribution densities

In a spin eigenstate - with the eigenvalues $S(S+1)$ and M of the operators $\mathbf{S}^2$ and $\mathbf{S}_z$, respectively - the spin distribution matrix has the following form [1, 2, 4, 5]:

$$q(\vec{r}_1;\vec{r}_1') = \tfrac{1}{2}[\rho^{\alpha,\alpha}(\vec{r}_1;\vec{r}_1') - \rho^{\beta,\beta}(\vec{r}_1;\vec{r}_1')], \tag{1}$$

where the $\rho^{\gamma,\gamma}(\vec{r}_1;\vec{r}_1')$ are the two diagonal space components of the first-order RDM (RDM1) $\rho(\tau_1;\tau_1')$, $\tau_1 = (\vec{r}_1,\sigma_1)$ representing the (space, spin) components of an electron and $\gamma(\sigma) = \alpha(\sigma)$, $\beta(\sigma)$ being the electron spin functions. These space components also define the charge distribution matrix:

$$\rho(\vec{r}_1;\vec{r}_1') = \rho^{\alpha,\alpha}(\vec{r}_1;\vec{r}_1') + \rho^{\beta,\beta}(\vec{r}_1;\vec{r}_1'). \tag{2}$$

The spin distribution matrices $q^{(M)}(\vec{r}_1;\vec{r}_1')$ for the different spin eigenstates (with $M = S, S-1, \ldots, -S$) can be expressed by using the normalized spin distribution matrices $D(\vec{r}_1;\vec{r}_1')$, which are independent of M [12]:

$$q^{(M)}(\vec{r}_1;\vec{r}_1') \equiv q(KK \mid \vec{r}_1;\vec{r}_1') = \frac{M}{S} q(\underline{K}\underline{K} \mid \vec{r}_1;\vec{r}_1') = M\, D(\vec{r}_1;\vec{r}_1'), \tag{3}$$

with:

$$D(\vec{r}_1;\vec{r}_1') = \frac{1}{S} q(\underline{K}\underline{K} \mid \vec{r}_1;\vec{r}_1'), \tag{4}$$

where K is the index of the spin state corresponding to $\langle Sz \rangle = M$ and $\underline{K}$ is the index corresponding to the maximal value $M = S$. Similar formulas can be written for the spin distribution functions when $\vec{r}_1 = \vec{r}_1'$.

2.2. Spin-spin correlation densities

In a spin eigenstate, the spin-spin correlation density matrix is [1, 2, 4, 5]:

$$\begin{aligned} q_{SS}(\vec{r}_1,\vec{r}_2;\vec{r}_1',\vec{r}_2') = \frac{1}{2}[&\rho^{\alpha\alpha,\alpha\alpha}(\vec{r}_1,\vec{r}_2;\vec{r}_1',\vec{r}_2') + \rho^{\alpha\beta,\alpha\beta}(\vec{r}_1,\vec{r}_2;\vec{r}_1',\vec{r}_2') - \\ &- \rho^{\alpha\beta,\beta\alpha}(\vec{r}_1,\vec{r}_2;\vec{r}_1',\vec{r}_2') + \rho^{\beta\alpha,\alpha\beta}(\vec{r}_1,\vec{r}_2;\vec{r}_1',\vec{r}_2') - \\ &- \rho^{\beta\alpha,\beta\alpha}(\vec{r}_1,\vec{r}_2;\vec{r}_1',\vec{r}_2') - \rho^{\beta\beta,\beta\beta}(\vec{r}_1,\vec{r}_2;\vec{r}_1',\vec{r}_2')]. \end{aligned} \tag{5}$$

where the $\rho^{\gamma\delta,\gamma'\delta'}(\vec{r}_1,\vec{r}_2;\vec{r}_1',\vec{r}_2')$ are the six (on sixteen) independent space components of the second-order RDM (RDM2) $\rho(\tau_1,\tau_2;\tau_1',\tau_2')$ with $\tau_i = (\vec{r}_i,\sigma_i)$, $i = 1, 2$.

The normalized spin-spin correlation density matrix, defined for the state $\underline{K}$ with maximal value $M = S$, takes the form [4, 6, 13]:

$$D_{SS}(\vec{r}_1,\vec{r}_2;\vec{r}_1',\vec{r}_2') = \frac{1}{S(2S-1)} q_{SS}(\underline{KK}\,|\,\vec{r}_1,\vec{r}_2;\vec{r}_1',\vec{r}_2'). \tag{6}$$

In an arbitrary eigenstate, the matrices $q_{SS}^{(M)}$ can be written:

$$q_{SS}(KK\,|\,\vec{r}_1,\vec{r}_2;\vec{r}_1',\vec{r}_2') = \frac{3M^2 S(S+1)}{S(2S-1)} q_{SS}(\underline{KK}\,|\,\vec{r}_1,\vec{r}_2;\vec{r}_1',\vec{r}_2'), \tag{7}$$

where K takes on all values corresponding to $M = S$, S - 1, ..., - S. Similar formulas can be written for the spin-spin correlation functions when $\vec{r}_1 = \vec{r}_1'$ and $\vec{r}_2 = \vec{r}_2'$.

The coefficients in Eqs (3), (4), (6) and (7) are determined by the spin symmetry of the system. For spin-degenerate states, one can take as values for these coefficients in Eqs (3) and (7) those defined by the irreducible representations of the group SO(3) corresponding to the considered spin multiplet. Within a given spin multiplet the normalized spin distribution and correlation matrices and functions do not depend on M.

3. Spin-spin interactions

3.1. Electron-electron dipolar interaction

For an N-electron system, the operator of dipole coupling between electron spin magnetic moments in the effective Breit-Pauli Hamiltonian takes the form [1, 4, 5]:

$$\mathbf{g}_{SS}(i,j) = g_0^2 \alpha^2 \mathbf{S}(i) \cdot \frac{\mathbf{d}(\mathbf{u}_{ij})}{r_{ij}^3} \cdot \mathbf{S}(j), \tag{8}$$

where $\alpha = 1/2c$ is half the fine-structure constant (in atomic units), g_0 is the g-factor for the free electron, and:

$$\mathbf{d}(\mathbf{u}_{ij}) = \frac{\mathbf{u}}{r_{ij}^3} - 3\frac{\mathbf{r}_{ij} \otimes \mathbf{r}_{ij}}{r_{ij}^5}, \tag{9}$$

where $\mathbf{u}$ is the unit tensor. One can easy transform $\mathbf{g}_{SS}(i,j)$ to the form:

$$\mathbf{g}_{SS}(i,j) = g_0^2\alpha^2\left\{r_{ij}^2\mathbf{S}(i).\mathbf{S}(j) - 3[\mathbf{S}(i).\mathbf{r}_{ij}][\mathbf{S}(j).\mathbf{r}_{ij}]\right\}r_{ij}^{-5}. \tag{10}$$

Applying the irreducible tensor-operator technique, one obtains:

$$\mathbf{g}_{SS}(i,j) = g_0^2\alpha^2\left[\mathbf{D}^{(2)}.\mathbf{S}^{(2)}\right]r_{ij}^{-5}, \tag{11}$$

where $\mathbf{D}^{(2)}$ is the second-rank, symmetric, traceless tensor with components:

$$D_{kl} = \delta_{kl}(r_{ij})_k(r_{ij})_l - 3(r_{ij})_k(r_{ij})_l, \tag{12}$$

and $\mathbf{S}^{(2)}$, given by:

$$\mathbf{S}^{(2)}(i,j) = [\mathbf{S}^1(i)\otimes\mathbf{S}^1(j)]^{(2)}, \tag{13}$$

is a second-rank tensor that can be constructed from the components of $\mathbf{S}^1(i)$ and $\mathbf{S}^1(j)$:

$$S_\sigma^2 = \sum_{\mu,\lambda} C_{\mu\lambda\sigma}^{112} S_\mu^1(i) S_\lambda^1(j), \tag{14}$$

where the $C_{m_1m_2m_3}^{j_1j_2j_3}$ are the 3j-symbols. From the symmetric tensor $\mathbf{D}^{(2)}$ one can build an irreducible tensor proportional to the second-rank tensor $[(\mathbf{r}_{ij})^1\otimes(\mathbf{r}_{ij})^1]^{(2)}$ with components:

$$[(\mathbf{r}_{ij})^1\otimes(\mathbf{r}_{ij})^1]_\sigma^{(2)} = \sum_{\mu,\lambda} C_{\mu\lambda\sigma}^{112}(r_{ij})_\mu^1(r_{ij})_\lambda^1. \tag{15}$$

Substituting these expressions into Eq. (11) one obtains:

$$\begin{aligned}\mathbf{g}_{SS}(i,j) &= C g_0^2\alpha^2 r_{ij}^{-5}\sum_m (-1)^m D_{-m}^2 S_m^2 = \\ &= C g_0^2\alpha^2 r_{ij}^{-5}\sum_m (-1)^m \sum_{\mu,\lambda} C_{\mu,\lambda,-m}^{112}(r_{ij})_\mu^1(r_{ij})_\lambda^1 \sum_{p,q} C_{pqm}^{112} S_p^1(i) S_q^1(j).\end{aligned} \tag{16}$$

After determining the constant C in Eq. (16) by comparing the coefficients of $(r_{ij})_0^1(r_{ij})_0^1$ and $S_0^1(i)S_0^1(j)$ in this equation with those calculated in Ref. [9], one gets:

$$\mathbf{g}_{SS}(i,j) = -\frac{4}{3} g_0^2\alpha^2 r_{ij}^{-5}\sum_m (-1)^m \sum_{\mu,\lambda} C_{\mu,\lambda,-m}^{112}(r_{ij})_\mu^1(r_{ij})_\lambda^1 S_m^{(2)}(i,j). \tag{17}$$

Then, using Eq. (17) for the matrix elements of $\mathbf{g}_{SS}(i,j)$ in the transition between spin states $K(SM_S)$ and $K'(SM'_S)$, one obtains (dropping from now on arrows on $\vec{r}_i$):

$$\begin{aligned}
&\left\langle KSM_S\left|\frac{1}{2}\sum_{i,j}\mathbf{g}_{SS}(i,j)\right|K'SM'_S\right\rangle = \\
&=-\frac{2}{3}g_0^2\alpha^2\sum_m(-1)^m\sum_{\mu,\lambda}C^{112}_{\mu,\lambda,-m}\int\limits_{\substack{r'_1=r_1\\ r'_2=r_2}} r_{12}^{-5}(r_{12})^1_\mu(r_{12})^1_\lambda S^{(2)}_m(1,2)\rho(KK'|\tau_1,\tau_2;\tau'_1,\tau'_2)d\tau_1 d\tau_2 = \\
&=-\frac{2}{3}g_0^2\alpha^2\sum_m(-1)^m\sum_{\mu,\lambda}C^{112}_{\mu,\lambda,-m}\frac{\left\langle SM_S\left|S^2_{-m}(1,2)\right|SM'_S\right\rangle}{S(2S-1)}\times \\
&\qquad\times\int\limits_{\substack{r'_1=r_1\\ r'_2=r_2}} r_{12}^{-5}(r_{12})^1_\mu(r_{12})^1_\lambda q_{SS}(\underline{KK'}|r_1,r_2;r'_1,r'_2)^2_m dr_1 dr_2,
\end{aligned}$$

where $\rho(KK'|\tau_1,\tau_2;\tau'_1,\tau'_2)$ is the RDM2 for the transition $K\to K'$. Here we use the standard definition of the spin-spin correlation density matrix for the transition $K\to K'$ [1, 4, 5]. We consider transition matrix elements between two states within the same spin multiplet because transitions between different multiplets are forbidden by symmetry (it is impossible to express elements of a given irreducible representation of SO(3) with elements of a different irreducible representation of the same group).

Following the Wigner-Eckart theorem, we express $\left\langle SM_S\left|S^2_{-m}(1,2)\right|SM'_S\right\rangle$ by the corresponding reduced matrix element, and we obtain:

$$\begin{aligned}
&\left\langle KSM_S\left|\frac{1}{2}\sum_{i,j}\mathbf{g}_{SS}(i,j)\right|K'SM'_S\right\rangle = \\
&=-\sqrt{\frac{5}{3}}g_0^2\alpha^2\sum_m(-1)^m C^{S2S}_{M_S m M'_S}\sum_{\mu,\lambda}C^{112}_{\mu,\lambda,-m}\int\limits_{\substack{r'_1=r_1\\ r'_2=r_2}} r_{12}^{-5}(r_{12})^1_\mu(r_{12})^1_\lambda D_{SS}(r_1,r_2;r'_1,r'_2)dr_1 dr_2,
\end{aligned}\tag{18}$$

where $D_{SS}(r_1,r_2;r'_1,r'_2)=q_{SS}(\underline{KK}|r_1,r_2;r'_1,r'_2)^2_0/[S(2S-1)]$ is, according to Eq. (6), the normalized spin-spin correlation matrix, the same for the whole spin multiplet.

For $M=M'$, Eq. (18) takes a simple form that gives the width of the spectral line splitting due to the electron-electron spin-spin interactions:

$$\begin{aligned}
&\left\langle KSM_S\left|\frac{1}{2}\sum_{i,j}\mathbf{g}_{SS}(i,j)\right|KSM_S\right\rangle = \\
&=-\frac{2}{3}g_0^2\alpha^2\left[3M^2-S(S+1)\right]\sum_q C^{112}_{q,-q,0}\int\limits_{\substack{r'_1=r_1\\ r'_2=r_2}} r_{12}^{-5}(r_{12})^1_q(r_{12})^1_{-q}D_{SS}(r_1,r_2;r'_1,r'_2)dr_1 dr_2.
\end{aligned}\tag{19}$$

3.2. Electron-nuclei dipolar interactions

For a N-electron system in the field of M nuclei, the operator of dipole coupling between one electron spin magnetic moment and the nuclei takes the form [1, 4, 5]:

$$\begin{aligned}\mathbf{h}_S(i) &= g_0\,\alpha \sum_{\lambda} g_\lambda\,\alpha_p\,\mathbf{S}(i)\cdot\left[3\frac{\mathbf{r}_{\lambda i}\otimes\mathbf{r}_{\lambda i}}{r_{\lambda i}^5}-\frac{\mathbf{u}}{r_{\lambda i}^3}\right]\cdot\mathbf{I}(\lambda) = \\ &= g_0\alpha\sum_{\lambda} g_\lambda\alpha_p\left\{3\left[\mathbf{S}(i)\cdot\mathbf{r}_{\lambda i}\right]\left[\mathbf{I}(\lambda)\cdot\mathbf{r}_{\lambda i}\right]-r_{\lambda i}^2\,\mathbf{S}(i)\cdot\mathbf{I}(\lambda)\right\}r_{\lambda i}^{-5},\end{aligned} \tag{20}$$

where the proton constant $\alpha_p = \alpha\,(m_e/m_p)$, g_λ is the g-factor for nucleus λ, and $\mathbf{I}(\lambda)$ is its spin momentum vector. For any one nucleus λ, the many-electron operator can be written as:

$$\sum_i \mathbf{h}_S(i) = g_0\alpha g_\lambda\alpha_p\sum_i r_{\lambda i}^{-3}\mathbf{K}(i)\cdot\mathbf{I}(\lambda), \tag{21}$$

where

$$\mathbf{K}(i) = 3[\mathbf{S}(i)\cdot\mathbf{n}_i]\mathbf{n}_i - \mathbf{S}(i), \quad \mathbf{n}_i = \mathbf{r}_{\lambda i}/r_{\lambda i}. \tag{22}$$

The components of the axial vector $\mathbf{K}(i)$ can be written in the form:

$$K_k(i) = \sum_l D_{kl}S_l(i), \tag{23}$$

where

$$D_{kl} = 3n_k(i)n_l(i) - \delta_{kl}\,n_k(i)n_l(i) \tag{24}$$

is a seconk-rank, symmetric, traceless tensor which is proportional to the normalized spherical functions $\mathbf{C}^2(\theta_i,\varphi_i)$.

Then, the components of the symmetrized vector $\mathbf{K}^1(i)$ are:

$$(K)_q^1 = C[D^2\otimes S^1]_q^1 = C\sum_{m,m'} C_{mm'q}^{211}\mathbf{C}_m^2(\theta_i,\varphi_i)S_{m'}^1(i), \tag{25}$$

where $[D^2\otimes S^1]^1$ is an irreducible first-rank tensor built from the tensor product of D^2 and S^1. The constant C can be derived from atomic spectroscopy theory [15] and its value is $10^{1/2}$.

Using the above relations, Eq. (21) takes the form:

$$\sum_i \mathbf{h}_S(i) = g_0 \alpha g_\lambda \alpha_p \sum_i r_i^{-3} \sum_q (-1)^q (K)^1_q(i) \cdot I^1_{-q}(\lambda) = \\ = \sqrt{10} g_0 \alpha g_\lambda \alpha_p \sum_q (-1)^q \sum_{m,m'} C^{211}_{mm'q} \sum_i r_i^{-3} \mathbf{C}^2_m(\theta_i, \varphi_i) S^1_{m'}(i) I^1_{-q}(\lambda). \tag{26}$$

If now one separates the electron and nuclear parts of the wavefunction one obtains, for the matrix elements of $\sum_i \mathbf{h}_S(i)$:

$$\langle KSM_S l | \sum_i \mathbf{h}_S(i) | K'SM'_S l' \rangle = \\ = \sqrt{10} g_0 \alpha g_\lambda \alpha_p \sum_q (-1)^q \sum_{m,m'} C^{211}_{mm'q} \langle KSM_S | \sum_i r_i^{-3} \mathbf{C}^2_m(\theta_i, \varphi_i) S^1_{m'}(i) | K'SM'_S \rangle \langle l | I^1_{-q}(\lambda) | l' \rangle. \tag{27}$$

Using the same scheme as in previous paragraphs we can express the matrix elements of the electron part in the form:

$$\langle KSM_S | \sum_i r_i^{-3} \mathbf{C}^2_m(\theta_i, \varphi_i) S^1_{m'}(i) | K'SM'_S \rangle = \\ = \int_{r'_1 = r_1} r_1^{-3} \mathbf{C}^2_m(1) q_S(KK' | r_1; r'_1)^1_m \, dr'_1 = \sqrt{\frac{3}{2}} C^{S1S}_{M_S m' M'_S} \int_{(r_1)} r_1^{-3} \mathbf{C}^2_m(1) D_S(r_1) dr_1, \tag{28}$$

where, as in Eq. (4), $D_S(r_1) = q_S(\underline{KK} | r_1; r_1)^1_0 / S$ is the normalized spin density, the same within the whole spin multiplet.

Finally, for the matrix elements of $\sum_i \mathbf{h}_S(i)$ we obtain:

$$\langle KSM_S l | \sum_i \mathbf{h}_S(i) | K'SM'_S l' \rangle = \\ = \sqrt{15} g_0 \alpha g_\lambda \alpha_p \sum_q (-1)^q \sum_{m,m'} C^{211}_{mm'q} C^{S1S}_{M_S m' M'_S} \int r_1^{-3} \mathbf{C}^2_m(1) D_S(r_1) dr_1 \langle l | I^1_{-q}(\lambda) | l' \rangle. \tag{29}$$

For a given term, this matrix element takes the form:

$$\langle KSM_S | \sum_i \mathbf{h}_S(i) | KSM_S \rangle = \\ = \sqrt{15} g_0 \alpha g_\lambda \alpha_p \sum_q (-1)^q \sum_m C^{211}_{m0q} M_S \int r_1^{-3} \mathbf{C}^2_m(1) D_S(r_1) dr_1. \tag{30}$$

The expectation value (30) gives the width of the spectral line splitting due to the electron-nucleus spin-spin interaction.

4. Discussion

The results presented here allow not only to include spin-spin electron-electron and electron-nuclei interactions in the variational approach of density matrix theory but also to perform calculations in terms of vector-model and valence-bond schemes.

These results give the possibility to include spin-spin interactions in a rigorous density functional for spin-polarized systems. The same holds for density functionals built in terms of density matrices. We could use the local-density form of the derived density matrices and functionals in Kohn-Sham theory to include the spin-spin interactions. The effect of electron-nuclei spin-spin interactions in the splitting of energy levels can be taken into account by using Eq. (29) or (30) in the Kohn-Sham scheme, while the contribution of the electron-electron spin-spin interactions can be accounted for by expressing Eq. (18) or (19) in the local-density approximation [16] for the spin-spin correlation density matrix (5). The spin (and other) correlations neglected in this approximation are compensated in the corresponding effective potential of the Kohn-Sham self-consistent procedure.

In the Barth-Hedin construction [17-19], the most widely used in the Kohn-Sham type calculations for spin-polarized systems, the energy functional is defined in terms of the first-order density matrix. This does not permit the description of relativistic corrections (including spin-spin interactions), which require a two-particle density matrix. There it is only possible to determine the influence of an external magnetic field and only for the ground state.

The formalism presented here can be used for the determination of all relativistic corrections from the Breit-Pauli Hamiltonian as well as for the calculation of the effect of an external magnetic field, not only for the ground state but for any arbitrary state of the spin multiplet. In practice, the problem is reduced to the construction of the reduced spin distribution and spin-spin correlation matrices and functions within a suitable quantum mechanical approach, and the performance of elementary mathematical operations analogous to those described in this work.

The use of a suitable minimization procedure, e.g. the local-scaling transformation scheme [20-22], or more precisely its formulation for spin-polarized systems [23, 24] - which automatically preserves space and spin symmetry, would allow direct minimization of the energy density-matrix functional, including relativistic terms. This is the aim of our future investigations.

Acknowledgments

This work was partly supported by a twinning convention between the Universities Pierre et Marie Curie (Paris) and Saint Kliment Ohridski (Sofia) and by the European COST-D9/010 contract. One of us (AIK) would like to thank the French Government for a PhD scholarship in Paris. Professor Matey Mateev is gratefully acknowledged for helpful discussions.

References

1. R. McWeeny, *Methods of Molecular Quantum Mechanics*, Academic Press, New York, 1989.
2. M.M. Mestetchkin, *Methods of Reduced Density Matrices in Quantum Molecular Theory,* Naukova Dumka, Kiev, 1977 (in Russian).
3. K. Husimi, Proc. Phys. Math. Soc. Japan **22** (1940) 264.
4. R. McWeeny, J. Chem. Phys. **42** (1965) 1717.
5. J. Maruani, in P. Becker (ed.), *Electron and Magnetization Densities in Molecules and Crystals*, Plenum Press, New York, 1980, p. 633.
6. V. A. Fock, J.E.T.P. **10** (1940) 961.
7. R. McWeeny and Y. Mizuno, Proc. Roy. Soc. **A259** (1961) 554.
8. R. McWeeny, Mol. Eng. **7** (1997) 7.
9. R. McWeeny, Adv. Quant. Chem. **31** (1999) 15.
10. A. P. Yutsis, I. B. Levinson and V. V. Vanagas, *Mathematical Formalism of Angular Momentum Theory*, Gospolizdat, Vilnius, 1968 (in Russian).
11. R. L. Pavlov, A. I. Kuleff, J. Maruani, P. Tz. Yotov and Ya. I. Delchev, Progr. Theor. Chem. & Phys. **B6** (2001) 63.
12. H. M. McConnell, J. Chem. Phys. **28** (1958) 1188.
13. W. H. Moores and R. McWeeny, Proc. Roy. Soc. (London) **A322** (1973) 365.
14. L. C. Biedenharn and J. D. Louck, *Angular Momentum in Quantum Physics*, Addison Wesley, Massachusetts, 1981.
15. I. I. Sobelman, *Introduction to Atomic Spectra Theory*, Nauka, Moscow, 1977 (in Russian).
16. O. Gunnarsson and B. I. Lunqvist, Phys. Rev. **B13** (1976) 4274.
17. U. Barth and L. von Hedin, J. Phys. **C5** (1972) 1629.
18. M. M. Pant and A. K. Rajagopal, Solid State Comm. **10** (1972) 1157.
19. A. Rajagopal and J. Gallaway, Phys. Rev. **B7** (1973) 1912.
20. I. Zh. Petkov and M. V. Stoitsov, T.M.F. **55** (1983) 407; Yad. Fisica **37** (1983) 1167 (in Russian).

21. I. Zh. Petkov, M. V. Stoitsov and E. S. Kryachko, Int. J. Quant. Chem. **29** (1986) 140.
22. I. Zh. Petkov and M. V. Stoitsov, *Nuclear Density Functional Theory*, Oxford University Press, Oxford, 1991.
23. R. L. Pavlov, J. Maruani, Ya. I. Delchev and R. McWeeny, Int. J. Quant. Chem. **65** (1997) 241; erratum in ibid. **68** (1998) 75.
24. R. L. Pavlov, F. E. Zakhariev, Ya. I. Delchev and J. Maruani, Int. J. Quant. Chem. **65** (1997) 257; erratum in ibid. **68** (1998) 77.

A method of combined treatment for the evaluation of core excitation energies in molecules involving heavy atoms: application to CrF_6, MoF_6, and WF_6

J. MARUANI, A. KHOUDIR, A. KULEFF *,
M. TRONC, G. GIORGI and C. BONNELLE

Laboratoire de Chimie Physique - Matière et Rayonnement,
UMR 7614, CNRS and UPMC,
11 rue Pierre et Marie Curie, 75005 Paris, France
Fax: (+ 33 1) 44 27 62 26 - e-mail: maruani@ccr.jussieu.fr

** On leave from INRNE, Bulgarian Academy of Sciences,*
72 Tzarigradsko Chaussee, 1784 Sofia, Bulgaria

Abstract

Core excitation energies (CEs) are known to depend on the chemical environment mostly through the charge transfered from or to the would-be excited atom in the ground-state molecule. We have made use of this peculiarity to set up a combined method for evaluating the CEs of molecules involving heavy atoms, where cumulated handicaps make direct calculations very difficult. We have evaluated the CEs of *np* levels in chromium, molybdenum and tungsten hexafluorides and compared the contributions of relaxation and relativity. In a first step, various approximate methods were used to evaluate the amount of charge transfered in the three hexafluorides, using the experimental geometries and testing different definitions of the charge. Results show the following trends: i) the calculated charge transfer increases as $CrF_6 << MoF_6 < WF_6$; ii) Mulliken (balanced) charges vary in the order REX >> RHF > CISD > DFT, and Weinhold (natural) charges tend to be slightly larger; iii) our best (CISD) calculations give a natural percentage of electron transfer from the metal atom to the bonded fluorines of about 45% for CrF_6, 56% for MoF_6, and 59% for WF_6. In a second step, numerical *ab-initio*, relativistic, ΔDF calculations of the total and orbital energies were performed on the ground-state and core-excited metal ions involving 1 to 5 valence ionizations. Core excitation energies were deduced and the relative importance of relaxation and relativity effects was discussed. In a last step, the core excitation energies for the molecules were evaluated by interpolating between values previously obtained for the free ions, using the net atomic charges derived for the ground-state molecules in our

ADVANCES IN QUANTUM CHEMISTRY, VOLUME 39

0065-3276/01 $35 00

best previous approximation. The results are particularly striking for WF_6: 1) for core excitations from the $2p_{1/2}$, $2p_{3/2}$ and $3p_{1/2}$, $3p_{3/2}$ levels, experimental energies are reproduced within 0.4-1.2 eV; 2) there is a relaxation alteration of the charge transfer stronger for the *3p* than for the *2p* levels; 3) relativistic corrections are much larger than and opposite to relaxation corrections.

1. Introduction

The investigation of the chemical bond (ionic, covalent with $d\pi$-$p\pi$ retro-bond, sandwich-compound bond) and of the spectroscopic properties of transition-metal complexes, in particular those of Group-VI elements (Cr, Mo, W) with simple ligands (C_5H_5, CN, CO, halogens, ...), has been extensively developed in recent years because some of them play a role in biological or industrial homogeneous catalysis, particularly due to the diversity of redox reactions to which they may lead in liquid solution [1]. The simplest complexes are also used as models for the metal-ligand interactions in condensed phases [2].

X-ray photoelectron and absorption spectroscopies (XPS, XAS, ...) are well adapted to the study of deep-core or non-occupied levels, particularly the first empty state (LUMO), whose role is primordial in chemical reactivity. The evolution of physicochemical properties and spectroscopic quantities of series of molecules involving atoms from successive rows or columns of the periodic table [3] has been related to the effective charge transfer from the atom to the ligands as well as to the variation of ligand-field multiplet effects and spin-orbit coupling [4].

The present investigation is concerned with the evaluation of core ionization and excitation energies for molecules involving heavy atoms (such as CrF_6, MoF_6 and WF_6), where cumulated handicaps make direct calculations very difficult. A method of combined exact-atomic (EA) / approximate-molecular (AM) treatment of those properties in such molecules, assuming charge transferability between the EA and AM atoms, is proposed. Effects of correlation, relaxation and relativity are assessed, and theoretical results derived using this combined method are compared

with NEXAFS experimental data. A detailed account of the interpretation of experimental results is reported elsewhere [5].

2. Methodology and Calculations

It is established that such atom-centered properties as nuclear electron-capture, isomeric transition or beta-decay rates [e.g. 6], Mössbauer isomer shifts [e.g. 7], nuclear magnetic resonance (NMR) isotropic chemical shifts (ICS) [e.g. 8, 9], or X-ray photoelectron spectroscopy (XPS) core ionization energies (CIE) [e.g. 10, 11] depend on the chemical environment of the perturbed atom mostly through the net (negative or positive) charge transfered to (or from) the bonded ligands. The same holds true for the Coulomb repulsion and exchange integrals [12] involved in the core-hole energies. We have recently performed a thorough investigation of the quasi-linear dependence of XPS CIEs in various fluorine compounds upon the electronegativity of the central atom as well as on the resulting amount of negative charge transfered to the bonded fluorines [13]. For sulfur compounds we have previously shown [14] that the degree of valence ionization of the molecule affects quasi-linearly the sulfur core ionization energies. On the other hand, it has been proposed [15] to use a linear relationship between NMR ICSs and charge increments in ^{13}C-containing compounds for the retrieval and ranking of organic structures. The dependence of both NMR ICSs and XPS CIEs on the net atomic charge is so close to linear, for a given atom in a given series, that it entails a similar dependence between the two properties [13], even though they belong to frequency ranges differing by twelve orders of magnitude.

We have made use of this peculiarity to set up a strategy for evaluating XPS or XAS CIEs of complex molecules involving heavy atoms, where cumulated handicaps make direct calculations very difficult. This strategy has been applied to the 2p and 3p levels of chromium, molybdenum and tungsten hexafluorides, and has helped us to compare the relative contributions of correlation, relaxation and relativity effects in these compounds.

2.1. The approximate molecular (AM) step

Various calculations were performed in order to estimate the amount of charge transfer in the three hexafluorides, using experimental geometries and testing different definitions of the charge. Due to the importance of relativistic effects on the bonding of such compounds, involving heavy atoms [16], all the techniques we used involved to some extent these effects. Relativistic Extended Hückel (REX) calculations - including charge-parameter self-consistent interations - were done using Pyykkö's program [17]. For SCF calculations we used the *Gaussian* package [18] with Hay-Wadt pseudo-potentials and LANL1DZ basis sets [19], both at

the RHF and CISD levels. DFT calculations were done using the *Dmol* package [20] with the BLYP gradient-corrected exchange-correlation density functional [21] and a double numeric polarized (DNP) basis set. The results obtained (Table 1) show the following trends:

Table 1. Atomic charges calculated, under various approximations and using different models, for chromium, molybdenum and tungsten in their hexafluoride compounds. The second column gives the experimental metal-fluorine (M-F) distances and the molecular symmetry group (MSG). Charges in the two right cells are Mulliken charges. In the middle cells are given Mulliken (left) and Weinhold (right) charges.

Settings Molecule	d(M-F) / Å * MSG	RHF / HW LANL2DZ	CISD / HW LANL2DZ	DFT-BLYP DNP	REX level 3
CrF_6	1.716 * O_h	2.416 2.883	2.268 2.710	2.013	3.643
MoF_6	1.820 * O_h	3.054 3.616	2.860 3.387	2.563	3.840
WF_6	1.831 * O_h	3.259 3.796	3.066 3.579	2.734	3.723

- i) the calculated charge transfer increases as $CrF_6 << MoF_6 < WF_6$, which recalls the outstanding character of Cr relative to Mo and W;

- ii) Mulliken (balanced) charges vary in the order REX >> RHF > CISD > DFT, because electron correlation is neglected in RHF but overestimated in DFT, and Weinhold (natural) charges tend, as often, to be greater;

- iii) our 'best' (CISD) calculations give a natural percentage of electrons transfered from the central metal atom to the six bonded fluorines of about 45.2 % for CrF_6, 56.4 % for MoF_6 and 59.6 % for WF_6. Surprisingly, the heavier the central atom, the closer the Weinhold CISD charges to the much less sophisticated, Mulliken REX charges.

2.2. The exact atomic (EA) step

Making use of Bruneau's numerical *ab-initio* fully relativistic MCDF (BRAN) program [22], we then performed calculations on atoms of the investigated metals, including appropriate core excitations and from 1 to 5 additional valence ionizations. Core excitation energies for the corresponding molecules were evaluated by interpolating between values obtained for the central atoms, using charges derived from the previous, approximate calculations on the ground-state molecules.

The BRAN program is based on a rigorous numerical resolution of the Breit-Dirac equation for multielectronic systems in a central nuclear field, corrected for qed effects such as vacuum polarization. The program can perform computations

in an MCDF scheme as well as on a DF basis if one considers a single reference configuration. It is fully vectorized and a large choice of options, either physical (e.g., inclusion of nuclear size) or technical (e.g., iteration procedures) is available. The program yields, on request, the various eigenstate multiplicities, energies and vectors, the relevant atomic integrals and such properties as the effective Z^*, <1/r> or λ (spin-orbit coupling parameter) for the different orbitals. Non-relativistic, HF or MCHF calculations can also be made by setting the speed of light (c # 137.036 in the default option) to a very large value.

BRAN calculations were performed on the following systems:

- i) for chromium, the ground-state neutral-atom configuration:

$$Cr^{0+}gs \equiv (1s^2 2s^2 2p^6 3s^2 3p^6 3d^5 4s^1),$$

and the systems $Cr^{n+}gs$, $Cr^{(n-1)+}2p^*$ (n = 1,3,5), these notations designating the configurations that correspond, respectively, to the ionization of *n valence* electrons from the highest occupied atomic orbitals (HOAO) in the atomic ground state (*gs*) followed by the *excitation* of a (*2p*) core electron to the lowest unoccupied atomic orbital (LUAO), i.e.:

- $Cr^{1+}gs \equiv (1s^2 2s^2 2p^6 3s^2 3p^6 3d^5)$, $Cr^{0+}2p^* \equiv (1s^2 2s^2 2p^5 3s^2 3p^6 3d^5 4s^1)$;
- $Cr^{3+}gs \equiv (1s^2 2s^2 2p^6 3s^2 3p^6 3d^3)$, $Cr^{2+}2p^* \equiv (1s^2 2s^2 2p^5 3s^2 3p^6 3d^4)$;
- $Cr^{5+}gs \equiv (1s^2 2s^2 2p^6 3s^2 3p^6 3d^1)$, $Cr^{4+}2p^* \equiv (1s^2 2s^2 2p^5 3s^2 3p^6 3d^2)$.

Configuration pairs such as $Cr^{1+}gs^{\neq} \equiv (1s^2 2s^2 2p^6 3s^2 3p^6 3d^5, 1s^2 2s^2 2p^6 3s^2 3p^6 3d^4 4s^1)$ or $Cr^{0+}2p^{\neq} \equiv (1s^2 2s^2 2p^5 3s^2 3p^6 3d^5 4s^1, 1s^2 2s^2 2p^5 3s^2 3p^6 3d^4 4s^2)$ were also considered, in order to assess electron correlation effects.

- ii) for molybdenum, the ground-state neutral-atom configuration:

$$Mo^{0+}gs \equiv (1s^2 2s^2 2p^6 3s^2 3p^6 3d^{10} 4s^2 4p^6 4d^5 5s^1),$$

and the systems $Mo^{n+}gs$, $Mo^{(n-1)+}2p^*$ (n = 1,3,5), these notations designating configurations similar to those described above but with $3d^5$, $4s^1$ replaced by $4d^5$, $5s^1$. Here again a few configuration pairs were checked to assess electron correlation effects.

- iii) for tungsten, the ground-state neutral-atom configuration:

$$W^{0+}gs \equiv (1s^2 2s^2 2p^6 3s^2 3p^6 3d^{10} 4s^2 4p^6 4d^{10} 4f^{14} 5s^2 5p^6 5d^4 6s^2),$$

and the systems $W^{n+}gs$, $W^{(n-1)+}2p^*$ and $W^{(n-1)+}3p^*$ (n = 1,3,5), these notations designating configurations similar to those given above but with $4d^5$, $5s^1$ replaced by $5d^4$, $6s^2$ and $3p^*$ added to $2p^*$. Configuration pairs here checked were of a slightly different type, e.g.: $W^{1+}gs^{\neq} \equiv (K2s^2 2p^6 MN5s^2 5p^6 5d^4 6s^1, K2s^2 2p^6 MN5s^2 5p^6 5d^3 6s^2)$ or $W^{0+}2p^{\neq} \equiv (K2s^2 2p^5 MN5s^2 5p^6 5d^4 6s^2, K2s^2 2p^5 MN5s^2 5p^6 5d^5 6s^1)$.

The relaxed, near-edge core excitation energies were derived by using the ΔDF (or ΔMCDF) protocol: $E^M{}_{mp^*} = M^{(n-1)+}mp^* - M^{n+}gs$ (M = Cr, Mo, W; m = 2 for all M and also 3 for W; n = 1,3,5). The non-relaxed, near-edge core excitation energies were obtained by applying Koopman's theorem to the relevant *mp* core orbi-

tals and *nd* LUAOs. For the sake of comparison, in addition to these relativistic calculations we also made non-relativistic ones, both with and without electron correlation and / or relaxation.

2.3. The combined treatment

Core excitation energies for the molecules were evaluated by interpolating between values obtained for the atomic ions, assuming transferability from the atom to the molecule and from the ground to the excited state and using charges derived from the previous, approximate calculations on the ground-state molecules. As the charge distribution may be very sensitive to electron correlation [23], we used our best correlated (CISD) results, standing between the under- (RHF) and over- (DFT) correlated values. Although the definition of the charge transfer is not so critical here, since this quantity is used mainly as a scaling factor and since Mulliken and Weinhold charges vary nearly in the same ratio along our series, we have selected the more consistent, Weinhold values.

A more critical point is that the charge transfer calculated for the ground-state molecule may not be very relevant for the molecule in an excited state. However, as we are dealing with core excitations, we may assume that electron relaxation does not drastically affect the charge distribution around the central atom, and that the excitation energy is determined mainly by the ground-state charges. This point will be discussed further below.

The dependence of core-hole energies on the net atomic charges is privileged only for deep-core ionizations, for details of the charge distribution in the molecule become more important when one approaches the Fermi level, i.e., for shallow-core or valence ionizations as well as for deep-core excitations, where the ejected electron settles on an unoccupied orbital (much more sensitive to the multipolar terms of the charge distribution). However, the contribution of this outer orbital to the total excitation energy is much smaller than that of the inner orbital, and therefore one may neglect the details of its dependence upon the multipolar expansion of the charge distribution.

A related problem is that, in the excited atom, the ejected electron settles on an unoccupied *nd* atomic orbital ($n = 4$ for Mo and 5 for W), whereas in the excited molecule it settles on an unoccupied $3t_{2g}$ or $5e_g$ (for MoF_6) or $4t_{2g}$ or $6e_g$ (for WF_6) molecular orbital. The $5e_g$ orbital is about 0.16 a.u. higher than the $3t_{2g}$ LUMO in MoF_6 and the $6e_g$ orbital about 0.20 a.u. higher than the $4t_{2g}$ LUMO in WF_6. However, the central metal *nd* orbitals contribute much more to both t_{2g} and e_g molecular orbitals than the bonded fluorine *2s* and *2p* orbitals. Therefore, we shall use as experimental data the weighted averages of the measured excitation energies to these molecular levels.

Our test calculations have shown that electron correlation contributions to the excitation energies are, in all cases, at least one order of magnitude smaller than

both relaxation and relativity effects, and about of the same order as contributions neglected in the above approximations. Therefore, we have not performed a systematic investigation of these effects, which will be the subject of another study.

3. Results and Discussion

In some applications [e.g. 5] it may be useful to know atomic integrals involved in the calculation of eigenstate energies and vectors. In the transition-metal series we are dealing with, the integrals relevant to our measurements are (F_0), F_2, G_1, G_3 [e.g. 12] between *2p* and *3d* orbitals for Cr, *2p* and *4d* orbitals for Mo, and both *2p* and *5d* and *3p* and *5d* orbitals for W. Following the above discussion the Coulomb repulsion and exchange integrals were calculated for the isolated Cr, Mo and W atoms depleted of 1, 3 or 5 electrons in the ground and core-excited states, using the program BRAN. The searched integrals are weighted averages of the non-zero relevant integrals ($mp_{i/2}\ mp_{j/2}\ /\ nd_{k/2}\ nd_{l/2}$), with $m = 2$ for Cr and Mo and also $m = 3$ for W, and $n = 3$ for Cr, 4 for Mo and 5 for W. The momentum indices are $i = j = 1$ or 3 and $k = l = 3$ or 5 for F_0, $i = j = 3$ and $k = l = 3$ or 5 for F_2, $j = l = 3$ or 5 when $i = k = 3$ for both G_1 and G_3 whereas $j = l = 3$ for G_1 and $j = l = 5$ for G_3 when $i = k = 1$. The results are displayed in Table 2. We also give for comparison non-relativistic integrals for the core-excited states of the W ions. In addition to the integrals of the above ions we also give those fitted for fractional charges in Table 1 and for charges derived from experimental data further below.

Table 2. Coulomb repulsion and exchange integrals (/ eV) computed for chromium, molybdenum and tungsten ions in their ground state and in an *mp* core-hole state (for every integral, **gs** stands for "ground state" and **ch** for "core-hole state"). For W we also give, for comparison, the non-relativistic values for core-hole states of the ions (**nr-ch**) and values interpolated for the 'experimental' metal charges in the molecular excited state.

Atom / charge in ground state	Cr^{1+}	Cr^{3+}	Cr^{5+}	Cr q_{the} ($q_{the} = 2.71$)
F_0 (2p 3d) **gs**	26.912	31.299	34.908	30.711
" **ch**	29.475	33.481	36.826	32.941
F_2 (2p 3d) **gs**	4.317	5.724	7.129	5.520
" **ch**	5.232	6.621	8.000	6.420
G_1 (2p 3d) **gs**	2.917	4.038	5.272	3.868
" **ch**	3.822	5.009	6.287	4.831
G_3 (2p 3d) **gs**	1.644	2.282	2.989	2.185
" **ch**	2.136	2.808	3.537	2.707

Atom / charge in ground state	Mo $^{1+}$	Mo $^{3+}$	Mo $^{5+}$	Mo q_{the} (q_{the} = 3.39)
F_0 (2p 4d) **gs**	19.319	21.873	24.054	22.328
" **ch**	20.969	23.363	25.413	23.790
F_2 (2p 4d) **gs**	1.214	1.585	1.968	1.659
" **ch**	1.445	1.819	2.195	1.892
G_1 (2p 4d) **gs**	0.967	1.279	1.606	1.342
" **ch**	1.171	1.490	1.819	1.553
G_3 (2p 4d) **gs**	0.555	0.734	0.925	0.770
" **ch**	0.672	0.858	1.048	0.895

Atom / charge in ground state	W $^{1+}$	W $^{3+}$	W $^{5+}$	W $q_{the\,/\,exp}$ (3.58 / *3.36*)
F0 (2p 5d) **gs**	17.539	19.759	21.597	20.331 /
" **ch**	18.743	20.787	22.514	21.320 /
nr-ch	19.084	21.032	22.677	
F0 (3p 5d) **gs**	17.125	19.212	20.915	19.745 /
" **ch**	18.186	20.091	21.680	20.584 /
nr-ch	18.509	20.319	21.830	
F2 (2p 5d) **gs**	0.531	0.696	0.863	0.744 /
" **ch**	0.619	0.780	0.945	0.827 / 0.841
nr-ch	0.642	0.801	0.960	
F2 (3p 5d) **gs**	1.080	1.390	1.694	1.479 /
" **ch**	1.242	1.543	1.839	1.629 / 1.539
nr-ch	1.316	1.614	1.907	
G1 (2p 5d) **gs**	0.440	0.579	0.721	0.620 /
" **ch**	0.514	0.651	0.791	0.691 / 0.703
nr-ch	0.547	0.685	0.826	
G1 (3p 5d) **gs**	0.194	0.255	0.318	0.273 /
" **ch**	0.230	0.291	0.355	0.309 / 0.290
nr-ch	0.249	0.311	0.375	
G3 (2p 5d) **gs**	0.253	0.334	0.417	0.358 /
" **ch**	0.295	0.375	0.458	0.399 / 0.406
nr-ch	0.326	0.409	0.493	
G3 (3p 5d **gs**	0.200	0.265	0.331	0.284 /
" **ch**	0.235	0.299	0.365	0.318 / 0.298
nr-ch	0.256	0.321	0.387	

As expected, the integrals for core-hole ions are larger than those for ground-state ions. The relativistic integrals are smaller than the non-relativistic ones, due

to the induced contraction of the core orbitals and corresponding expansion of the valence orbitals [16]. The values used for q_{exp} in W are taken from Table 4: 3.75 for *2p-5d* excitations and 2.97 for *3p-5d* excitations.

Another property of interest computed by the program BRAN from first principles is the effective spin-orbit coupling parameter λ. This parameter is important for interpreting spectroscopic data (splittings or intensities) [e.g. 5], but we used it to identify the other relativistic effects in our computed energies. In order to help estimate these other relativistic effects, the spin-orbit splitting has been added to the non-relativistic values, using for the $np_{1/2}$ and $np_{3/2}$ energies the formulae:

$$(q\text{-}rx, n\text{-}rt)_{1/2} = (q\text{-}rx, n\text{-}rt) + \lambda, (q\text{-}rx, n\text{-}rt)_{3/2} = (q\text{-}rx, n\text{-}rt) - \lambda/2 \ (q = n \text{ or } y).$$

The parameter λ is known to increase roughly as Z^4 and, for a given Z, to decrease with *n* and *l* increasing while moving away from the nucleus. As it can be seen on Table 3, it also slightly increases with the degree of valence ionization, the remaining electrons becoming less screened from the central nucleus.

Table 3. Effective spin-orbit coupling parameters (/ a.u.) computed the *np* core orbitals in core-excited, valence-ionized Cr, Mo and W atoms in the y-rx and n-rx cases (numbers in parentheses give the range of the next decimals for the 1^+ to 5^+ ions). The λ values for the *md* valence orbitals are quasi independent of relaxation and range from 0.004 to 0.015.

M-ch	**Cr-*2p*** (y-rx)	**Cr-*2p*** (n-rx)	**Mo-*2p*** (y-rx)	**Mo-*2p*** (n-rx)
λ	0.22 (36-92)	0.21 (61-79)	2.56 (78-79)	2.62 (74-77)
M-ch	**W-*2p*** (y-rx)	**W-*2p*** (n-rx)	**W-*3p*** (y-rx)	**W-*3p*** (n-rx)
λ	32.7578	33.2091	7.17 (30-35)	7.29 (23-28)

In Tables 4a-4c there are given the core excitation energies yielded by the program BRAN for the Cr, Mo and W (1^+ to 5^+) ions, and those interpolated for the ground-state molecules using the CISD Weinhold charges from Table 1. For the sake of comparison, we also give the values obtained when neglecting relaxation and / or relativity effects, together with experimental values. The results corresponding to the atomic ions are also displayed in Figs 1-3. One can make the following observations on these results.

- i) For all ions and all levels, relaxation effects tend to decrease the core excitation energies while relativity effects tend to increase them.

- ii) For Cr ions, relaxation effects tend to decrease when the positive charge increases while for W ions, the trend is opposite, the balance point occurring just beyond the Mo ions. There is no such, clearcut variation for relativity effects.

Table 4-a,b. Some *2p* excitation energy values (/ a.u.) obtained for valence ions of chromium (Z = 24) and molybdenum (Z = 42): y and n stand for including or not-including, and rx and rt for relaxation and relativity effects, respectively. In order to help estimate other relativity effects, the spin-orbit splitting has been added to the non-relativistic values. The non-relaxed values are Koopman's excitation energies, whereas relaxed values are ΔDF excitation energies from *2p* to *3d* (Cr) or to *4d* (Mo) levels. For Mo, the experimental values are averages between values measured for the excitation energies from the '*2p*' to $3t_{2g}$ and $5e_g$ molecular orbitals.

Atom / charge (ground state)	Cr^{1+}	Cr^{3+}	Cr^{5+}	Cr q_{the} (q_{the} = 2.71)	Cr 'q_{exp}' ('q_{exp}' = ?)
L (n-rx, n-rt)	21.870	21.943	22.163		
L (y-rx, n-rt)	*21.183*	*21.343*	*21.605*		
LII ($2p_{1/2}$)					
(n-rx, n-rt)$_{1/2}$	22.087	22.160	22. 381		
(n-rx, y-rt)	22.154	22.226	22.445		
(y-rx, n-rt)$_{1/2}$	*21.407*	*21.568*	*21.834*		
(y-rx, y-rt)	***21.452***	***21.610***	***21.882***	***21.580***	
LIII ($2p_{3/2}$)					
(n-rx, n-rt)$_{3/2}$	21.762	21.835	22.054		
(n-rx, y-rt)	21.830	21.901	22.118		
(y-rx, n-rt)$_{3/2}$	*21.071*	*21.231*	*21.491*		
(y-rx, y-rt)	***21.116***	***21.247***	***21.538***	***21.218***	
Atom / charge (ground state)	Mo^{1+}	Mo^{3+}	Mo^{5+}	Mo q_{the} (q_{the} = 3.39)	Mo 'q_{exp}' ('q_{exp}' = 4.27)
L (n-rx, n-rt)	94.166	94.263	94.458		
L (y-rx, n-rt)	*92.950*	*93.082*	*93.307*		{4.269}
LII ($2p_{1/2}$)					
(n-rx, n-rt)$_{1/2}$	96.794	96.890	97.086		
(n-rx, y-rt)	97.973	98.067	98.261		
(y-rx, n-rt)$_{1/2}$	*95.518*	*95.648*	*95.874*		(4.226)
(y-rx, y-rt)	***96.523***	***96.652***	***96.875***	***96.688***	**96.763**
LIII ($2p_{3/2}$)					
(n-rx, n-rt)$_{3/2}$	92.853	92.949	93.144		
(n-rx, y-rt)	94.031	94.125	94.319		
(y-rx, n-rt)$_{3/2}$	*91.666*	*91.799*	*92.023*		(4.312)
(y-rx, y-rt)	***92.671***	***92.803***	***93.023***	***92.839***	**92.924**

- iii) From Cr through Mo to W, relaxation effects increase six-fold, from about 0.6 through 1.2 to 3.5 a.u., whereas relativity effects increase 280-fold, from about 0.07 through 1.18 to 18.47 a.u.

Table 4-c. Some *np* (n = 2, 3) excitation energy values (/ a.u.) obtained for valence ions of tungsten (Z = 74): y and n stand for including or not-including, and rx and rt for relaxation and relativity effects, respectively. In order to help estimate other relativity effects, the spin-orbit splitting has been added to the non-relativistic values. The non-relaxed values are Koopman's excitation energies, whereas relaxed values are ΔDF excitation energies from *np* to *5d* (W) levels. Experimental values are averages between values measured for the excitation energies from the '*np*' to $4t_{2g}$ and $6e_g$ molecular orbitals.

Atom / charge (ground state)	W^{1+}	W^{3+}	W^{5+}	W q_{the} (q_{the} = 3.58)	W 'q_{exp}' ('q_{exp}' = 3.36)
L (n-rx, n-rt)	376.698	377.621	378.765		
L (y-rx, n-rt)	*374.163*	*374.276*	*374.451*		{3.748}
LII ($2p_{1/2}$)					
(n-rx, n-rt)$_{1/2}$	409.907	410.830	411.975		
(n-rx, y-rt)	428.399	429.298	430.428		
(y-rx, n-rt)$_{1/2}$	*406.920*	*407.034*	*407.208*		(3.550)
(y-rx, y-rt)	***424.135***	***424.245***	***424.416***	***424.288***	**424.282**
LIII ($2p_{3/2}$)					
(n-rx, n-rt)$_{3/2}$	360.094	361.016	362.161		
(n-rx, y-rt)	378.586	379.484	380.614		
(y-rx, n-rt)$_{3/2}$	*357.784*	*357.897*	*358.072*		(3.947)
(y-rx, y-rt)	***374.998***	***375.108***	***375.280***	***375.152***	**375.175**
M (n-rx, n-rt)	84.190	85.110	86.245		
M (y-rx, n-rt)	*82.538*	*82.649*	*82.814*		{2.974}
MII ($3p_{1/2}$)					
(n-rx, n-rt)$_{1/2}$	91.483	92.402	93.538		
(n-rx, y-rt)	96.678	97.574	98.694		
(y-rx, n-rt)$_{1/2}$	*89.711*	*89.822*	*89.987*		(2.964)
(y-rx, y-rt)	***94.661***	***94.768***	***94.931***	***94.809***	**94.765**
MIII ($3p_{3/2}$)					
(n-rx, n-rt)$_{3/2}$	80.544	81.464	82.599		
(n-rx, y-rt)	85.740	86.635	87.755		
(y-rx, n-rt)$_{3/2}$	*78.952*	*79.062*	*79.227*		(2.984)
(y-rx, y-rt)	***83.901***	***84.008***	***84.170***	***84.049***	**84.007**

- iv) As a result, while for the Cr ions relaxation effects are about 9 times larger than relativity effects, for W ions relativity overcomes relaxation by a factor of over 5, the balance point occurring again just beyond the Mo ions, where relaxation is still stronger than relativity by about 0.2 a.u.

Fig. 1. Core excitation energies for the $2p_{1/2}$ and $2p_{3/2}$ levels of Cr and Mo ions in the yes / no relaxation (rx) and relativity (rt) options (spin-orbit splitting has been added to the non-relativistic values) For the Mo ions, relativity corrections nearly compensate relaxation corrections.

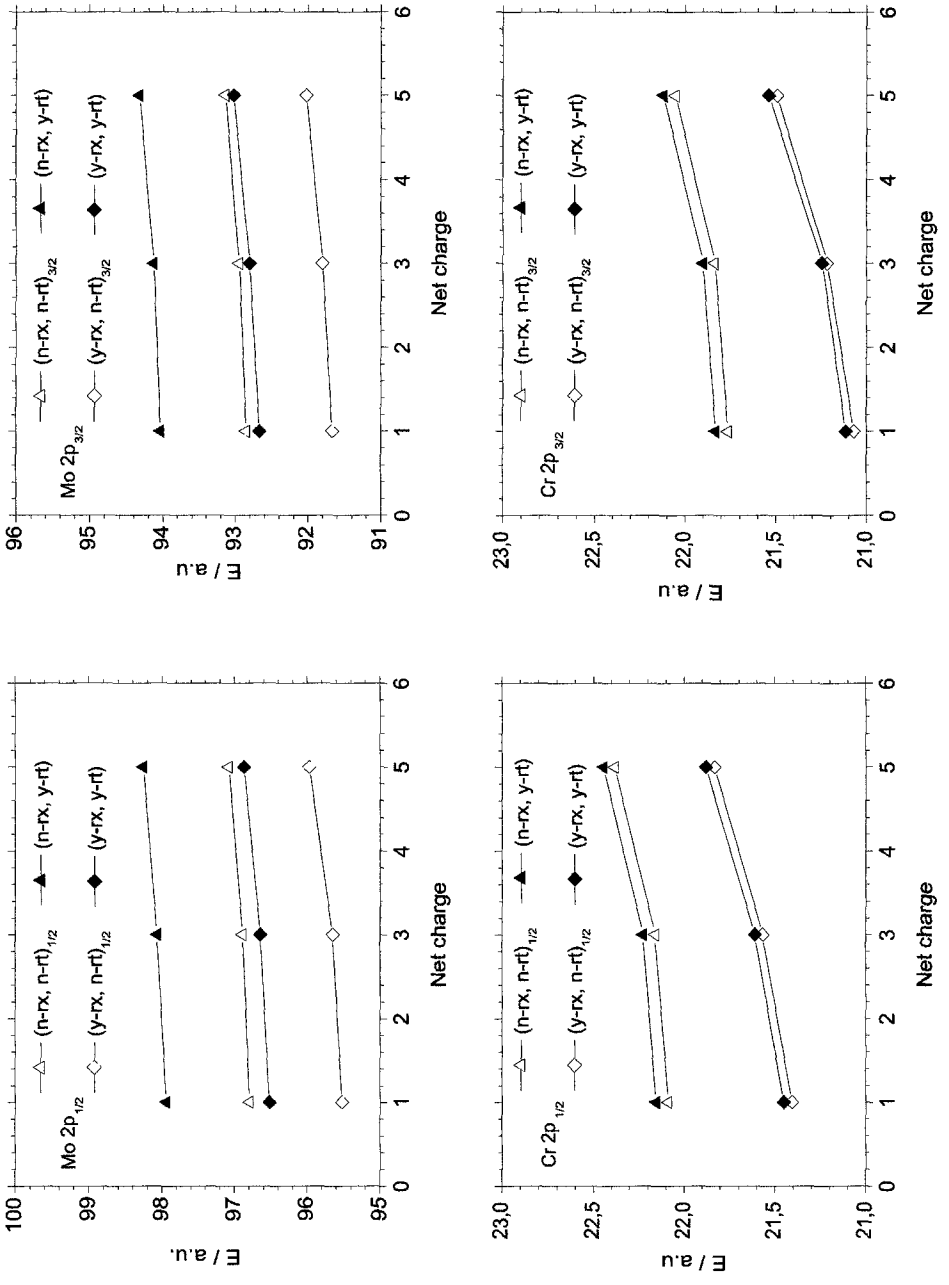

Fig. 2. Core excitation energies for the $2p_{1/2}$ and $2p_{3/2}$ levels of W ions in the yes / no relaxation (rx) and relativity (rt) options (spin-orbit splitting has been added to the non-relativistic values). One can see that relativity corrections largely overcome relaxation corrections.

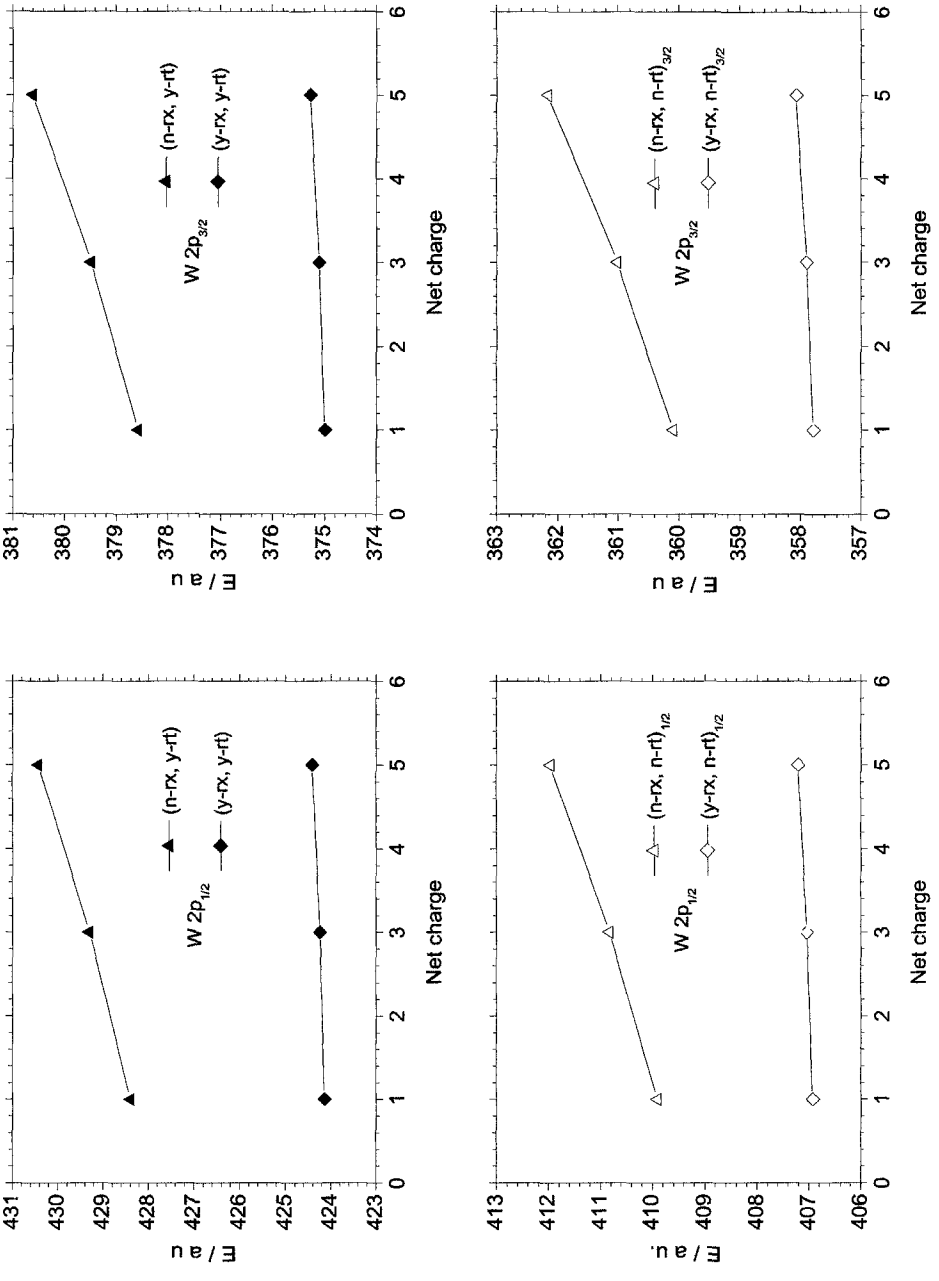

Fig. 3. Core excitation energies for the $3p_{1/2}$ and $3p_{3/2}$ levels of W ions in the yes / no relaxation (rx) and relativity (rt) options (spin-orbit splitting has been added to the non-relativistic values) One can see that relativity corrections largely overcome relaxation corrections.

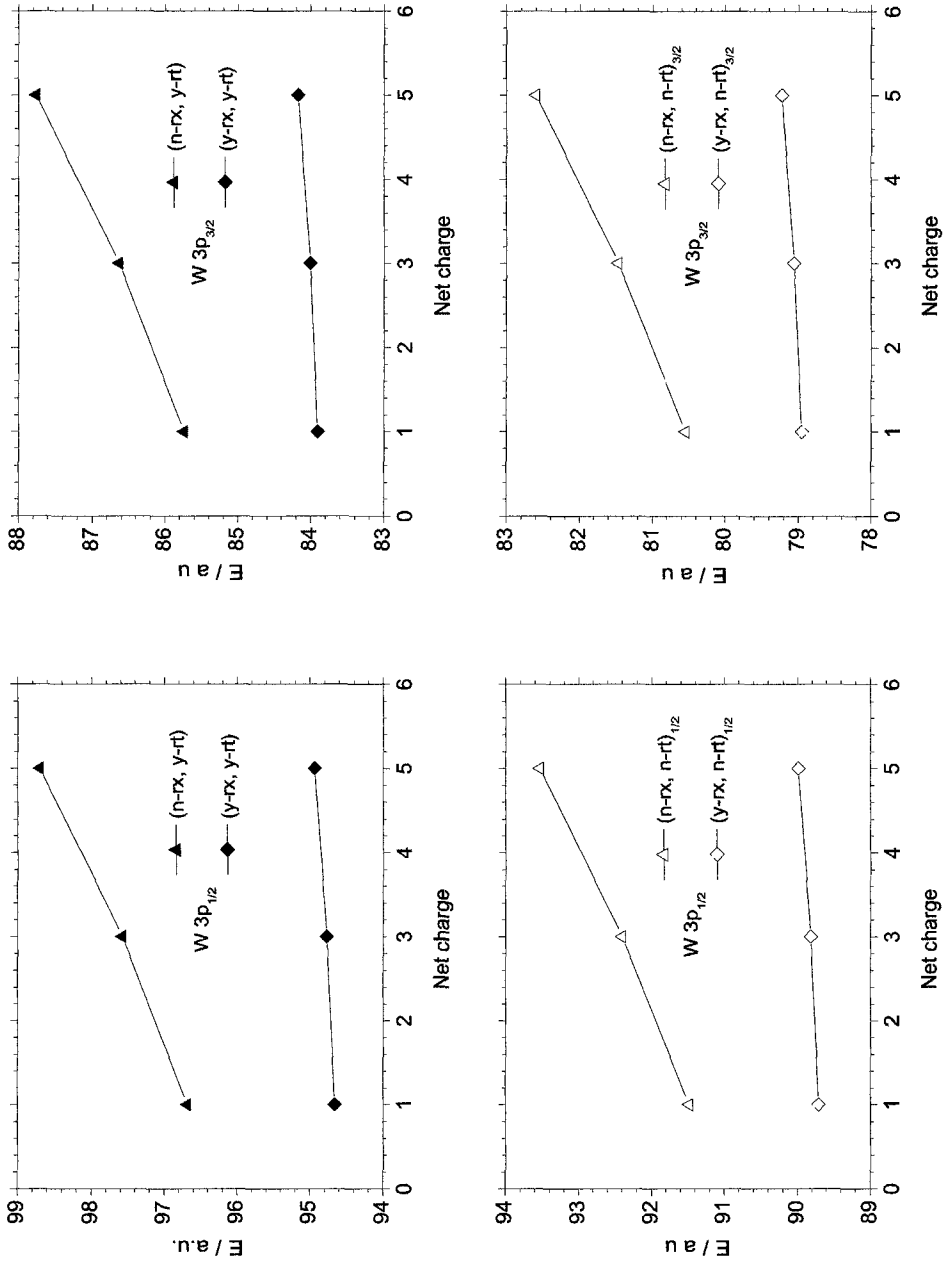

As those found with other compounds [13, 14], the variations displayed in Figs 1-3 are not so linear as expected. Therefore, we searched for quadratic fits of the variations of the core-level excitation energies with the valence charge (Tables 4a-4c). This will allow a Lagrange interpolation using the molecular charges. The coefficients of these fits are gathered in Table 5.

Table 5. Quadratic-fit coefficients for the charge dependence of excitation energies in Cr, Mo and W (Table 4-a,b,c).

	Cr $2p_{n\text{-}rt}$	**Cr $2p_{1/2}$**	**Cr $2p_{3/2}$**	**Mo $2p_{n\text{-}rt}$**	**Mo $2p_{1/2}$**	**Mo $2p_{3/2}$**
C	21.88865	21.41575	21.1105	94.15425	96.49375	92.6380
B(q)	-0.0370	0.0220	-0.0145	-0.0005	0.0175	0.0220
$A(q^2)$	0.01835	0.01425	0.0200	0.01225	0.01175	0.0110
	W $2p_{n\text{-}rt}$	**W $2p_{1/2}$**	**W $2p_{3/2}$**	**W $3p_{n\text{-}rt}$**	**W $3p_{1/2}$**	**W $3p_{3/2}$**
C	376.31935	424.10285	374.96625	83.81065	94.6285	83.8681
B(q)	0.3510	0.0245	0.0240	0.3525	0.0255	0.0260
$A(q^2)$	0.02765	0.0076	0.00775	0.0269	0.0070	0.0069

The core excitation energies interpolated for the hexafluorides of molybdenum and tungsten compare rather well with the experimental values. For the Mo $2p_{1/2}$ and $2p_{3/2}$ levels these latter are larger by only 0.08 a.u. (about 2 eV) than the interpolated values. For the W $3p_{1/2}$ and $3p_{3/2}$ (upper excited) levels the experimental values are now smaller by about 0.04 a.u. (1 eV) than the interpolated ones. When one proceeds deeper in the core, for the W $2p_{1/2}$ and $2p_{3/2}$ levels, the interpolated values become practically equal to the experimental ones, within 0.01-0.02 a.u. $\approx$ 0.4 eV, not far from experimental errors.

As it was conjectured in the previous section the correspondence between computed and measured values is the better when one deals with deeper core levels. In other words, our method of combined treatment, which involves approximate molecular charges and exact atomic energies in the evaluation of molecular energies, should be more appropriate for deep-core excitations.

On the other hand, if one reverses the interpolation procedure and calculates molecular charges from the measured energies (Tables 4a-4c), it seems to be that in WF_6 there is a relaxation-induced reduction of charge transfer for the shallower, $3p$ levels. This can be understood by tungsten becoming less electropositive when it looses a core electron closer to the valence levels. However, there is an opposite effect for molybdenum, which is yet to be understood.

4. Conclusion

In a previous paper [13] we made a systematic investigation of the well-recognized dependence of XPS and related chemical shifts on the net charge transfered to (or from) the core-ionized atom from (or to) its bonded neighbours. It was shown that, even though the use of this dependence to make a theoretical evaluation of a chemical shift of an atom in a molecule presents less interest since more direct and accurate methods have become available [24], a precise knowledge of this dependence can be very useful for it may help derive charge transfers, electronegativities and other properties of chemical interest from the measured chemical shifts. In addition, there seems presently to be no economical procedure for computing precisely core ionization energies for compounds involving heavy atoms, where relativistic effects (including charge-dependent spin-orbit coupling) are too large to allow other methods to be applied without major modifications.

As an example, we have used the method of atomic core-hole valence-ion calculations to evaluate the relative importance of relativity, relaxation and charge transfer effects in the hexafluorides of chromium, molybdenum and tungsten, and proposed a method of combined EA / AM treatment to evaluate inner-core excitation or ionization energies in these compounds. Test calculations have shown that for such properties electron correlation effects are much smaller than both relaxation and relativity effects. In chromium relativity corrections, though already quite important, remain smaller than relaxation effects, whereas in tungsten relativity corrections largely overcome relaxation effects, the balance point occurring just beyond molybdenum. Core excitation energies calculated for the corresponding molecules by interpolation from the results obtained for the atomic ions, assuming transferability from the atom to the molecule and from the ground to the excited state, reproduce rather well experimental results, slight discrepancies pointing to a level-dependent, relaxation-induced charge-transfer variation in the molecular excited state.

Further work is in progress on other heavy-element compounds – particularly organometallics of the (Fe, Co, Ni) series – in order to assess the reliability of this method of combined treatment for specific extended systems.

Acknowledgments

This work was done in the framework of COST-D9/010 European project and benefited from CNRS and UPMC financial help and from IDRIS computer time. We wish to thank Pr Hans Agren and Christophe Bureau for their interest in this work, and M.A.C. Nascimento and G. Berthier for a critical reading of previous versions of the manuscript.

References

1. (a) M. Ardon and A. Pernick, J. Less Common Met. **54**, 233 (1977). (b) S. P. Cramer, K. O. Hodgson, E. I. Stiefeld and W. E. Newton, J. Amer. Chem. Soc. **100**, 2748 (1978).

2. E. W. Plummer, W. R. Salamek and J. J. Miller, Phys. Rev. B **18**, 1673 (1978).

3. (a) R. G. Pearson, J. Amer. Chem. Soc. **85**, 3533 (1963). (b) Y. Sakai and E. Miyoshi, J. Chem. Phys. **87**, 2885 (1987).

4. (a) F. M. F. de Groot, Z. W. Hu, M. F. Lopez, G. Kaindl, F. Guillot and M. Tronc, J. Chem. Phys. **101**, 6570 (1994). (b) F. Guillot, C. Dezarnaud, M. Tronc, A. Lisini, P. Decleva and G. Fronzoni, Chem. Phys. **191**, 289 (1995).

5. F. Bournel, F. Guillot, C. Dezarnaud-Dandine and M. Tronc, Chem. Phys. Lett. **286**, 317 (1998).

6. (a) R. Daudel, J. Phys. Rad. **13**, 557 (1952). (b) J. I. Vargas, Chemical Applications of Angular Correlations and Half-Life Measurements, in M.T.P. Int. Rev. Sci. Ser. I **8** (1971) 45-70, and references therein.

7. G. K. Wertheim, *Mössbauer Effect: Principles and Applications,* Academic Press, New York, 1964, chap. 5.

8. (a) H. Spiesecke and W. G. Schneider, J. Chem. Phys. **35**, 722, 730 (1961). (b) T. Tokuhiro and G. Fraenkel, J. Am. Chem. Soc. **91**, 5005 (1969).

9. S. Fliszàr, *Charge Distributions and Chemical Effects*, Springer Verlag, New York (1983), chap. 4.

10. K. Siegbahn, C. Nordling, G. Johansson, *et al., ESCA Applied to Free Molecules*, North-Holland, Amsterdam, 1971.

11. W. L. Jolly, K. D. Bomben and C. J. Eyermann, Atomic Data & Nuclear Data Tables **31** (1984) 433-493.

12. E. U. Condon and G. H. Shortley, *The Theory of Atomic Spectra,* University Press, Cambridge, 1963, chap. 6.

13. A. Khoudir, J. Maruani and M. Tronc, Progr. Theor. Chem. Phys. B **2**, 57 (2000).

14. J. Maruani, M. Tronc and C. Dezarnaud, C. R. Acad. Sci. (Paris) II **318**, 1191 (1994); J. Molec. Struct. (Theochem) **330**, 145 (1995).

15. I. P. Bangov, Anal. Chim. Acta **209**, 29 (1988).

16. P. Pyykkö, Chem. Rev. **88**, 563 (1988).

17. (a) L. L. Lohr, Jr., M. Hotokka and P. Pyykkö, Int. J. Quantum Chem. **18**, 347 (1980). (b) S. Larsson and P. Pyykkö, Chem. Phys. **101**, 355 (1986). (c) P. Pyykkö in S. Wilson (ed.), *Methods in Computational Chemistry* **2**, Plenum Press, London (1989).

18. 'Gaussian' is a software package devised by Pople, Foresman, Frisch *et al.* and updated by *Gaussian Inc.*, 4415 Fifth Avenue, Pittsburgh, PA 15213, USA.

19. P. J. Hay and W. R. Wadt, J. Chem. Phys. **82**, 270, 284, 299 (1985).

20. 'Dmol' stems from the implementation of Delley's DFT molecular program by *Biosym Technologies*, 9685 Scranton Road, San Diego, CA 92121, USA.

21. (a) A. D. Becke, Phys. Rev. A **38**, 3098 (1988). (b) C. Lee, W. Yang and R. G. Parr, Phys. Rev. B **37**, 785 (1988).

22. (a) J. Bruneau, J. Phys. B **16**, 4135 (1983); CEA / CEL MCDF Technical Report (1995). (b) C. Bonnelle, P. Jonnard, C. Barré, G. Giorgi and J. Bruneau, Phys. Rev. A **55**, 3422 (1997).

23. K. B. Wiberg, C. M. Hadad, T. J. LePage, C. M. Breneman and M. J. Frisch, J. Phys. Chem. **96**, 671 (1992). K. Raghavachari and J. B. Anderson, J. Phys. Chem. **100**, 12960 (1996).

24. D. P. Chong, Chem. Phys. Lett. **232**, 486 (1995); J. Chem. Phys. **103**, 1842 (1995); Can. J. Chem. **74**, 1005 (1996); D. P. Chong, C. H. Hu and P. Duffy, Chem. Phys. Lett. **249**, 491 (1996); C. Bureau and D. P. Chong, ibid. **264**, 186 (1997).

Spectroscopic constants of Pb and Eka-lead compounds: comparison of different approaches

by

Wenjian Liu*

Lehrstuhl für Theoretische Chemie,
Ruhr-Universität Bochum,
D-44780 Bochum, Germany

Christoph van Wüllen

Technische Universität Berlin, Sekr. C3
Straße des 17. Juni 135
D-10623 Berlin, Germany

Young Kyu Han, Yoon Jeong Choi, Yoon Sup Lee

Department of Chemistry and School of Molecular Science (BK21), Korea Advanced Institute of Science and Technology, Taejon 305-701, Korea

* Author to whom all correspondance should be addressed.
Electronic mail: wenjian.liu@ruhr-uni-bochum.de

Abstract

Three *independent* relativistic approaches, four-component density functional theory (4c-DFT), two-component DFT-ZORA(MP) (Zeroth order regular approximation with model potentials) and two-component ECP-CCSD(T) (Effective core potentials, coupled-cluster theory with singles, doubles and perturbative triples), have been employed by three

ADVANCES IN QUANTUM CHEMISTRY, VOLUME 39

0065-3276/01 $35 00

independent groups to calculate the bond lengths, binding energies and vibrational frequencies for the eka-lead (E114) compounds E114X (X = H, F, Cl, Br, I, O, O_2) and the E114 dimer. For calibration, we also report results for homologous lead compounds. The dipole moments and dipole moment derivatives for the diatomic molecules are presented as well. The bonds in E114 compounds are considerably weaker than those of lead due to much larger relativistic (spin-orbit) effects It is predicted that $E114O_2$ is thermodynamically unstable with respect to the decomposition into E114 + O_2, in contrast to $PbO_2 \rightarrow Pb + O_2$. Both $2PbO_2 \rightarrow 2PbO + O_2$ and $2E114O_2 \rightarrow 2E114O + O_2$ are thermodynamically unstable. The agreement between the two-component (ZORA) and the four-component (BDF) density functional results is quite good even for the E114 compounds. However, this requires a careful construction of the Gaussian basis sets used in the ZORA calculations

Contents

1 Introduction

The discovery of several new superheavy elements with nuclear charge 100, 111, 112, 114, 116, and 118 [1, 2, 3, 4, 5, 6] is one of the most significant scientific achievements in the end of last century. However, chemical experiments on most of these elements are difficult to perform due to either too short half-lives or too low production rates. Eka-lead (E114) is the heaviest element discovered up to date that can last as long as 30 seconds before flickering out [4]. This in some sense supports previous predictions based on shell closure effects that E114 is the peak of the island of nuclear stability [7]. Possibly an atom-at-a-time radiochemical experiment (for the recent review, see ref. [8]) can be carried out for E114 in the near future, if the production rate is sufficient. However, standard spectroscopic studies (electronic, vibrational, rotational, NMR, etc) on molecules containing superheavy atoms are still rather difficult even if both the half-lives and production rates are sufficient. Quantum chemical calculations are thus so far the only way to investigate the physical and chemical properties of these superheavy elements (for recent comprehensive reviews, see refs. [9, 10]). It is known that periodic trends of lighter congeners of a certain group can not be simply extended down to superheavy elements due to enormous relativistic (and correlation) effects [10, 11]. The low reactivity of E114 was predicted by several authors [12, 13, 14] based on simple models. The main interest there was to investigate the stability of di- and tetra-valent oxidation states of E114 [15]. Most of the previous investigations dealt with closed-shell molecules. For open-shell molecules, spin-orbit (SO) coupling takes effect already to first-order and therefore requires SO calculations even at lowest order of approximation. For closed-shell systems, SO coupling is of higher order and has to be included from the very beginning of the calculation to account for spin-orbital relaxation effects. In this work, three independent relativistic approaches, four-component density functional theory (4c-DFT, hereafter denoted as BDF) [16], two-component ZORA(MP) (Zeroth order regular approximation using model potentials) in the framework of DFT [17, 18], and two-component ECP-CCSD(T) (Effective core potentials, coupled-cluster theory with singles, doubles and perturbative triples) [19, 20], have been employed to calculate the bond lengths, binding energies and vibrational frequencies for E114X (X = H, F, Cl, Br, I, O, O_2) and the E114 dimer. For comparison, the corresponding lead compounds are also investigated. The dipole moments for most of these diatomic molecules are still not known experimentally, and are thus calculated by the DFT approaches. Since four-component relativistic all-electron *highly correlated* calculations could not be performed to serve as benchmark due to the enormous demand of computational power, and since quite different Hamiltonians and basis sets have been

used here, it is necessary to critically discuss the consistency (agreement) of the chosen approaches. For this purpose, atomic calculations for Pb and E114 are first carried out. We mention that E114H was recently calculated by Nash et al. [11] and Han et al. [21] using relativistic ECP approaches. The results will be compared with the present work latter.

The paper is organized as follows: In Sec. II, the computational methods are briefly described. In Sec. III, results of atomic calculations of lead and E114 atoms are given. We also discuss the basis set dependence and the effect of different contraction schemes on the ZORA results since this turned out to be a critical issue. Sec. IV devotes to discussion of molecular calculations. The paper ends with the conclusions in Sec. V.

2 Computational details

2.1 BDF

The Beijing four-component density functional program (BDF) has been presented in detail elsewhere [16]. Briefly, the Dirac-Kohn-Sham equations were solved by using highly accurate numerical quadrature under the double point group symmetry Frozen-core approximations were used: $[1s^2 - 4f^{14}]$ for lead, $[1s^2 - 5f^{14}]$ for E114, $[1s^2]$ for oxygen and fluorine, $[1s^2 - 2p^6]$ for chlorine, $[1s^2 - 3d^{10}]$ for bromine, and $[1s^2 - 4d^{10}]$ for iodine. Four-component numerical atomic spinors generated from finite-difference atomic calculations were used for the cores, whereas the basis sets for the valence spinors were a combination of the numerical atomic spinors and kinetically balanced double-zeta Slater-type functions. Polarization functions of $2d2f$ for Pb and E114, and $2d1f$ for ligands were added. A diffuse s function was added for hydrogen, and a set of diffuse p functions were added for oxygen and halogens In the case of $E114_2$, one set of diffuse p functions were further added, leading to quadruple-zeta basis set for the $7p$. The Perdew-Wang formula [22] for the local density approximation (LDA) and Becke-exchange [23] and Perdew-correlation [24] gradient-corrected functionals were used as they stand to describe exchange-correlation interactions, since relativistic corrections to these functionals have no significant effects either on atomic valence-electron excitations [25, 26] or on molecular spectroscopic constants [27] (see also below). This gradient-corrected functional is denoted as BP. A self-correlation correction due to Stoll et al. [28] (denoted as BPSCC) was considered occasionaly. The moment polarization scheme [25, 29], which has one-to-one correspondence to the non-relativistic spin polarization, was used for open-shell systems. The effect of self-consistency of GGA (generalized gradient approximation) turned out to be very small for all systems studied here.

2.2 ZORA(MP)

The ZORA(MP) method has been described in ref. [17]. A two-component (2c) variant of this method has been implemented soon thereafter [18]. In open shell cases, we use a Kramers' *unrestricted* approach, and the exchange-correlation energy was calculated from a nonrelativistic spin-density functional (BP in this case, as described above). The spin density $s(\vec{r})$ used in such a method should be invariant with respect to rotation in spin space, therefore we define the spin density as the length of the magnetization vector $\vec{m}$,

$$s = \sqrt{\vec{m}^2} \tag{1}$$

$$\vec{m} = \sum_{i}^{occ} < \phi_i | \vec{\sigma} | \phi_i > \tag{2}$$

where $\{\phi_i\}$ are the occupied two-component molecular orbitals (spinors) and $\vec{\sigma} = (\sigma_x, \sigma_y, \sigma_z)$ is the vector of the Pauli spin matrices. Note that for *open-shell* systems, this approach leads to an exchange-correlation potential which is a full 2×2 matrix. This definition of the spin density is the symmetry-adapted [30] version of the traditional approach, which uses the projection of $\vec{m}$ to a fixed axis. In the present implementation of ZORA, as indicated by the above formulae, the change of picture for the position variable is ignored when constructing the density.

Triple-zeta type basis sets from ref. [31] were used for the atoms H, O, F, and Cl, but with new relativistic contraction coefficients derived from atomic ZORA calculations. Two sets of d-polarization functions were added. For Br, a $20s14p9d$ basis set from ref. [32] was contracted to $14s10p6d$, and then a d function was further added, using the next exponent from the well-tempered series. A $21s17p12d$ iodine basis set from the same compilation was contracted to $15s13p8d$, and $2d1f$ functions were added. These (l-adapted) segmentedly contracted basis sets were used in both the one- and two-component ZORA calculations. For Pb (E114), we optimized a $24s20p15d10f$ ($27s24p18d12f$) uncontracted basis set. This optimization has been performed at the nonrelativistic density functional level using a new atomic DFT program written for that purpose [33]. This basis set has been used in the scalar-relativistic ZORA calculations after contracting to $18s16p12d8f$ ($21s20p15d10f$) and adding a flat f-function with $\eta_f = 0.4$ ($\eta_f = 0.3$). For example, the steepest five p-type Gaussians have been contracted to form a single basis function. We will denote such a contraction scheme l-adapted. For the two-component calculations, we again start from the uncontracted basis set but first add two p-functions with exponents η_p which are 5 and 25 times larger than the exponent of the steepest p-function in the original basis set. This is necessary to improve the description of the $p_{1/2}$ orbitals, as has already been noted before [34]. This augmented

basis set was then contracted to $19s20p15d10f$ ($21s23p17d12f$). More specifically, for Pb, the steepest 6 s-functions have been contracted to a single basis function, while the steepest 4 p-type Gaussians give rise to two basis functions, with contraction coefficients taken from the $2p_{1/2}$ and $2p_{3/2}$ spinors of an atomic two-component calculation. We call this a j-adapted contraction scheme since these two basis functions serve to describe either the $p_{1/2}$ or $p_{3/2}$ spinors of the atomic calculation. For Pb, the d- and f-functions remain uncontracted. The E114 basis set is contracted as $7s \rightarrow 1s$, $5p \rightarrow 2p$, and $3d \rightarrow 2d$ in a similar way. Finally, a flat f-function was added as in the scalar relativistic basis set. A point charge was used to represent the nucleus in both the ZORA and BDF calculations, but finite nuclear size effects were investigated for the first four atomic ionization potentials and selected molecules (see below).

2.3 ECP-CCSD(T)

A two-component Kramers' *restricted* Hartree-Fock (KRHF) approach [19] was employed to treat spin-orbit interaction at the HF level of theory using relativistic effective core potentials (RECPs) and produce molecular spinors obeying double group symmetry. Electron correlation was then treated at the coupled-cluster singles and doubles with perturbative triple contributions (CCSD(T)) level of theory [20]. In this work, the following *shape-consistent* ECPs were used: VE22 (22-valence electrons) ECPs for Pb [11] and E114 [35], VE6 ECP for oxygen and VE7 ECPs for halogens [36, 37, 38]. To achieve good correlation treatments, the following extended basis sets (denoted as basis set A) were used in the spin-averaged one-component RECP (AREP, or 1c-ECP) calculations: $9p7sd3pf$ for Pb and E114, aug-cc-pVTZ basis sets for H, O, F, and Cl [39], and the $(7s7p3d2f)/[4s4p3d2f]$ valence basis sets for Br and I [40]. However, in the 2c-ECP calculations smaller basis sets (denoted as basis set B) had to be adopted: $6p6sd1pf$ for Pb [11] and E114 [35], $3s3p$ for oxygen and halogens [36, 37, 38], and the aug-cc-pVDZ basis set for hydrogen [39]. For oxygen and halogens, a set of diffuse s and p functions and a set of d-type polarization functions were added. If not otherwise stated, SO effects were derived as the difference between the 1c-ECP and 2c-ECP results calculated with the same basis set B at a given level of theory. The use of smaller basis sets for the evaluation of SO effects is in many cases justified [21]. However, the E114 oxides turned out to be examples of the exceptions, since there the interplay between SO coupling and correlation is sizable. For most of the molecules studied here, we noticed that the KRHF SO effects are rather close to the CCSD(T) values, although KRHF yielded repulsive energy curves for E114X other than E114F and E114Cl. The 1c-ECP calculations were carried out with the GAUSSIAN94 [41] and MOLPRO98 [42, 43, 44] programs and

the 2c-ECP calculations with two-component packages [19, 20] on the CRAY C90 at KORDIC.

2.4 Evaluation of the spectroscopic constants

The bond lengths, vibrational frequencies, and force constants were obtained from suitable polynomials (DFT) or Dunham (ECP) analysis. The mass of E114 was taken to be 280. The binding energies were evaluated using results of separate calculations for atoms.

A point should be made for the binding energies reported here. The ground state of E114 is close to a single $7s^2 7p_{1/2}^2$ configuration (99.2%) due to large spin-orbit splitting of the $7p$ shell, whereas the ground state of Pb is composed of 92.5% of $6s^2 6p_{1/2}^2$ and 7.5% of $6s^2 6p_{3/2}^2$ (MC-DFC results obtained with the GRASP program [45]). Nevertheless, a single Slater determinant for Pb was taken as reference in both the DFT and ECP calculations, although an intermediate coupling scheme would slightly lower the binding energies of the Pb compounds (by 0.22 eV [46]). Due to self-interaction problems inherent in the present (approximate) functionals, there is a certain degree of arbitrariness in the treatment of open-shell systems. In the present DFT calculations, the lowest-energy determinants for F and O were taken as references, which are lower than the spin (moment) polarized spherical atoms by 0.31 and 0.38 eV for F and O, respectively. This effect is very small for F and O at the LDA level and also small for the heavier halogen homologues at both the LDA and GGA levels [47]. By careful analysis we learned that the difference between jj- and LS-coupling for the ligands is quite small (e.g., < 0.03 eV).

3 Atomic calculations

In this section, the BPSCC functional was used in the DFT calculations. The necessity to account for self-interaction corrections when the number of electrons is changed was discussed in ref. [26]. The calculated first four ionization energies (IPi) and the $np_{1/2}$ to $np_{3/2}$ excitation energies (EE) for Pb ($n = 6$) and E114 ($n = 7$) are presented in Table 1. Since so far we can not exploit double point group symmetry in our ZORA calculations, the excitation energies by ZORA were not performed. The available experimental data for Pb [48] was included for comparison.

It is seen that the ZORA results for Pb agree with the BDF ones within numerical accuracy. The agreement of DFT with ECP-CCSD(T) and experimental data [48] is also quite good. The BDF results for E114 are in good agreement with the four-component Dirac-Fock-Coulomb (DFC)-CCSD(T) values

Table 1: Excitation and ionization energies (eV) of Pb and E114. BDF: four-component density functional theory. ZORA: two-component zeroth order regular approximation. BPSCC: Becke-Perdew86 and self-correlation correction. ECP: two-component effective core potential. DFC: Dirac-Fock-Coulomb CCSD(T): coupled-cluster with singles, doubles and perturbative triples.

		BDF BPSCC	ZORA BPSCC	ECP CCSD(T)	expt.[a]
Pb	$6s^2 6p^2_{1/2} \rightarrow 6s^2 6p^1_{1/2}$	7.02	7.01	7.01	7.42
	$6s^2 6p^1_{1/2} \rightarrow 6s^2 6p^1_{3/2}$	1.83		1.58	1.75
	$6s^2 6p^1_{1/2} \rightarrow 6s^2 6p^0_{1/2}$	14.82	14.84	14 61	15.03
	$6s^2 6p^0_{1/2} \rightarrow 6s^1 6p^0_{1/2}$	31.99	32.00	31.56	31.93
	$6s^1 6p^0_{1/2} \rightarrow 6s^0 6p^0_{1/2}$	42 74	42.66	41.95	42.31
E114	$7s^2 7p^2_{1/2} \rightarrow 7s^2 7p^1_{1/2}$	8.26	8 23	8.45	8.36[b]
	$7s^2 7p^1_{1/2} \rightarrow 7s^2 7p^1_{3/2}$	4.91		4.91	4.77[b]
	$7s^2 7p^1_{1/2} \rightarrow 7s^2 7p^0_{1/2}$	16.62	16.63	16.74	16.55[b]
	$7s^2 7p^0_{1/2} \rightarrow 7s^1 7p^0_{1/2}$	35.43	35.35	36.40	35.52[b]
	$7s^1 7p^0_{1/2} \rightarrow 7s^0 7p^0_{1/2}$	46.41	46.20	46 97	

[a]Ref. [48]. [b]DFC-CCSD(T) results from ref. [15].

of Seth [15], indicating that relativity is properly described in the BDF calculations. The IP_1, IP_2, and EE for E114 from the present ECP-CCSD(T) calculations are also in line. However, ECP-CCSD(T) overestimated the IP_3 and IP_4 of E114 by about 1.0 and 0.5 eV, respectively, compared to BDF and DFC-CCSD(T). Probably this illustrates the deficiency of the s set of the ECPs [35]. It can be expected that this set of ECPs would yield too weak bonds if the $7s$ orbital is indeed involved in the bonding. Nash et al. [11] reported 8.56 eV and 5.43 eV for, respectively, IP_1 and EE of E114 by using the same ECP as applied here but at the RCISD (relativistic configuration interaction with singles and doubles) correlation level. In both the ZORA and BDF calculations, the $7s$ orbital lies below the $6d_{5/2}$ spinors for E114 and $E114^{+1}$, but becomes higher for $E114^{+2}$ and $E114^{+3}$. Thus, the third and fourth ionizations indeed remove the $7s$ electrons. Actually, the $6d^5_{5/2}7s^27p^0_{1/2}$ ($6d^5_{5/2}7s^17p^0_{1/2}$) configuration lies above $6d^6_{5/2}7s^17p^0_{1/2}$ ($6d^6_{5/2}7s^07p^0_{1/2}$) by 1.94 (1.56) eV according to the BDF calculations.

There is good agreement between the four-component BDF and the two-component ZORA results. The largest error occurs for IP_4, and is about 0.2 eV (or 0.5% !). It is difficult to describe the s-type atomic spinors in the nuclear region if one uses Gaussian-type basis sets, and the differences between ZORA and BDF in IP_3 and IP_4 reflect this. To further investigate the basis set dependence of the two-component ZORA results, we calculated the ionization potentials of Pb and E114 using different basis sets (see Table 2). The fourth column (EXT) presents results from a very large 'reference basis set'. This brings the ZORA results in *complete* agreement with BDF. The first three columns document the performance of different basis sets. In the first column (UNC), we see the results from our 'original' basis set optimized at nonrelativistic DFT level. This basis set performs well for Pb if used uncontracted but shows sizable deviations for IP_1 and IP_2 of E114. This is due to an improper description of the $2p_{1/2}$ orbital which requires steep p functions The orthogonality of the atomic $p_{1/2}$ spinors transfers this error to the valence $7p_{1/2}$ spinor, whose orbital energy is too high, resulting in too low ionization potentials In the third column (j-AC) one sees that adding two steep p functions (see above for details) results in much improved values for the first two ionization potentials, bringing, e.g., IP_1 from 8.11 eV to 8.23 eV (the 'reference basis set' result is 8.24 eV). These results are the same whether one contracts the basis set (using j-adapted contraction !) or not. This is not true for the segmented (l-adapted) contraction scheme, as can be seen from the second column (l-AC). For Pb, the differences between the first two columns are small, but for E114, the l-adapted contraction scheme is clearly problematic, e.g., it reduces IP_1 and IP_2 by 0.25 and 0.38 eV, respectively. We note that IP_3 and IP_4 are fairly constant for the first three columns of Table 2. This is clear, as

the question of j-adapted vs. l-adapted contraction is not an issue for s-type orbitals. It is an open question whether it is meaningful to include ultra-steep s-type basis functions to reach the basis set limit. These functions serve to describe the singularity of the s-type atomic spinors caused by the point nucleus. In reality, nuclei are extended so we also investigated the finite nuclear size effects (last column of Table 2). As expected, IP_1 and IP_2 are not affected, since p electrons do not penetrate the nuclear region, but IP_3 and IP_4 of E114 are reduced substantially (by 0.36 and 0.42 eV). The same amount is found in the BDF calculations, where $IP_{3,4}$ are reduced to 35.08 and 45.99 eV if an extended (uniform finite) nucleus is used in the calculation. Different extended nuclear models thus do not matter too much for (valence) energy differences. We note in passing that the nuclear size effects on molecular spectroscopic constants are small, mainly because the E114 $7s$ orbital contributes little to the bonding, especially in the diatomic molecules (see below).

With both ZORA and BDF, we performed calculations on spherical and unpolarized neutral Pb and E114 atoms with the $np^1_{1/2}np^1_{3/2}$ configurations. The results are given in Table 3. For E114, we can also compare with results from numerical atomic calculations performed by van Lenthe [49], which probably mark the basis set limit. The 'excitation energy' is the energy difference between this (unphysical) configuration and the atomic closed-shell ground state ($np_{1/2}$ doubly occupied). There is perfect agreement between BDF and numerical Dirac, as can be expected. For these valence orbital energies, there is little difference between ZORA and the four-component calculations, in particular, when the 'reference basis set' is used. The atomic results obtained so far are thus very encouraging, as far as the applicability of two-component methods to *valence* properties of superheavy elements is concerned.

4 Molecular calculations

After having extensively discussed the atomic calculations, we now come to the molecular results. The atomic data would help our understanding on the difference between the E114 and Pb compounds. According to group theory, to form a full σ-bond a linear combination of $\frac{1}{3}p_{1/2} + \frac{2}{3}p_{3/2}$ must be taken [12]. The larger SO splitting of E114 $7p$ than that of Pb $6p$ thus results in weaker bonding (i.e, "inert" $7p_{1/2}$ pair) The large separation between $7p_{1/2}$ and $7s$ orbitals in E114 (difference in $7s/7p_{1/2}$ orbital energies: 10.4 eV; cf. 7.9 eV for Pb; results obtained by the GRASP program [45]) would reduce possible sp-hybridization.

Table 2· Basis set and finite nuclear size effects in the first four ionization potentials (IP_i) of Pb and E114 obtained with 2c-ZORA (BPSCC functional)

basis set		UNC[a]	l-AC[b]	j-AC[c]	EXT[d]	EXT[e]
Pb	IP_1	7.00	6.96	7.01	7.01	7 01
	IP_2	14.82	14.76	14.84	14.82	14.83
	IP_3	32.00	32.01	32.00	31.98	31.97
	IP_4	42.66	42.67	42.66	42.73	42.71
E114	IP_1	8.11	7.86	8.23	8.24	8.25
	IP_2	16.45	16.07	16.63	16.61	16.60
	IP_3	35 36	35 37	35.35	35.40	35.04
	IP_4	46.21	46.22	46.20	46.38	45.96

[a]'original' basis set, uncontracted. [b]l-adapted contraction. Basis set used in the one-component molecular calculations (see text). [c]j-adapted contraction. Basis set used in the two-component molecular calculations (see text) [d]uncontracted $50s45p40d30f$ reference basis set. [e]uncontracted $50s45p40d30f$ reference basis set and finite nuclear model (Gaussian charge distribution with exponent 0.13808566×10^9 for Pb and 0.11516791×10^9 for E114 [59]).

Table 3: Valence orbital energies (a.u.) of the neutral E114 atom with the spherical and unpolarized $np_{1/2}np_{3/2}$ configurations ($n = 6$ for Pb and $n = 7$ for E114). EE: excitation energy (eV) with respect to the ground state The $X\alpha$ functional ($\alpha = 0.7$) was used.

	Pb		E114			
orbital	BDF	ZORA	BDF	ZORA[a]	Dirac[b]	ZORA[c]
$np_{3/2}$	-0.0914	-0.0904	-0.0669	-0.0644	-0.0668	-0.0669
$np_{1/2}$	-0.1443	-0.1432	-0.2109	-0.2069	-0.2108	-0.2103
$ns_{1/2}$	-0.4150	-0.4133	-0.5333	-0.5280	-0.5331	-0.5323
$(n-1)d_{5/2}$	-0.7059	-0.7060	-0.5127	-0.5118	-0.5129	-0.5136
$(n-1)d_{3/2}$	-0.8020	-0.8020	-0.6726	-0.6717	-0.6725	-0.6732
EE	1.40	1.40	3.68	3.66	3.68	3.68

[a]basis '$j-$AC' in table 2 was used. The results match ZORA[c] if the 'reference basis set' is used. [b]numerical Dirac-Slater result [49]. [c]numerical ZORA (using electrostatic approximation) result [49]

4.1 Pb diatomics

The ZORA results for the Pb diatomics (cf. Table 4) are in excellent agreement with the BDF data. The ECP-CCSD(T) results are quite close to availabe experimental values [50, 51]. The DFT results deviate somewhat larger from experiment, but more systematic than the ECP-CCSD(T) ones. The binding energies of PbO and PbF are overestimated by the BP functional by 0.52 and 0.57 eV, respectively, while those of PbH, PbCl, PbBr and PbI are within 0.2 eV agreement with experiment. Note that an intermediate coupling scheme for Pb would reduce our DFT binding energies by 0.22 eV [46]. Thus the overestimations of 0.30 eV for PbO and 0.35 eV for PbF mainly come from the oxygen and fluorine atoms, e.g , the BDF(BP) binding energy for O_2 is 5.95 eV, 0.74 eV higher than the experimental value of 5 21 eV [50]. We note in passing that inclusion of ~20% 'exact exchange' in the density functional reduces the binding energy of O_2 by ~1 eV. It is believed that the hybrid functional would improve the DFT binding energies for the Pb compounds as well. The BP functional tends to yield slightly too long (by 0.02 to 0.04 $\AA$) bond lengths for the Pb compounds. Referring to the ECP-CCSD(T) as well as empirically corrected BP (subtracting 0.04 $\AA$) bond lengths, we predict the yet unknown bond lengths of PbCl, PbBr, and PbI are about 2.47, 2.61, and 2.81 $\AA$, respectively.

4.2 E114 diatomics

Similar to the Pb diatomic molecules, the BDF binding energies for the E114 diatomics (cf. Table 5) are in good agreement with the 2c-ECP-CCSD(T) values. Subtracting 0.3 eV for both E114O and E114F from the BDF values (see the above discussion), the agreement is within 0.15 eV. It is reasonable to assume that similar overestimations in the bond lengths (+0.04 $\AA$) by the BP functional should occur in E114X as well. Except E114H, such corrected BDF bond lengths are also in reasonable agreement with the ECP-CCSD(T) ones. Nash et al.'s [11] ECP-RCISD results for E114H (R_e, 1.954 $\AA$; D_e, 0.59 eV; ω_e, 1222 cm^{-1}) deviate somewhat from the present ECP-CCSD(T) values (1.972 $\AA$; 0.43 eV; 971 cm^{-1}).

There is fairly good agreement between the BDF and the two-component ZORA results. The differences in bond length are ~ 0.01$\AA$ (a little larger for E114H and E114I), binding energies agree within 0.05 eV and force constants within $5N/m$.

Table 4: Bond lengths (R_e, $\AA$), binding energies (D_e, eV, referring to the lowest configurations for ligands and a single-determinant for Pb[a]), vibrational frequencies (ω_e, cm^{-1}) and force constants (k_e, N/m) for PbX.

molecule		BDF(BP)	ZORA(MP)(BP)		ECP-CCSD(T)		expt.[d]
		4c	1c	2c	1c	2c	
PbH	R_e	1.868	1.870	1.868	1.820	1.822	1.839
	D_e	1.92	2.61	1.95	2.57	1.85	1.69
	ω_e	1493	1543	1491	1637	1592	1564
	k_e	132	141	131	158	150	
PbF	R_e	2.097	2.077	2.092	2.055	2.070	2.058
	D_e	4.24	4.88	4.17	4.64	3.91	3.67
	ω_e	476	504	484	518	503	503
	k_e	232	260	240	275	259	
PbCl	R_e	2.509	2.490	2.509	2.455	2.475	
	D_e	3.24	3 88	3.21	3.76	3.02	3.12
	ω_e	285	300	285	318	306	304
	k_e	145	161	145	178	165	
PbBr	R_e	2.650	2.630	2.650	2.598	2.618	
	D_e	2.73	3.55	2.74	3.43	2.61	2.51
	ω_e	194	202	191	218	209	208
	k_e	126	139	124	160	147	
PbI	R_e	2.850	2.823	2.846	2.792	2.815	
	D_e	2.17	3.08	2.18	2.95	2.01	2.01
	ω_e	150	161	149	170	163	161
	k_e	104	120	103	134	123	

Table 4: (Continued)

molecule		BDF(BP)	ZORA(MP)(BP)		ECP-CCSD(T)		expt.[d]
		4c	1c	2c	1c	2c	
PbO	R_e	1.939	1.939	1.937	1.926	1.924	1.922
		1.942[b]					
		1.943[c]					
	D_e	4.39	5.47	4.34	5.11	3.93	3.87
		4.37[b]					
		4.39[c]					
	ω_e	716	726	717	728	749	721
		711[b]					
		711[c]					
	k_e	448	462	450	464	491	
		442[b]					
		442[c]					

[a]An intermediate coupling scheme for Pb would reduce the DFT binding energies by 0.22 eV [46]. [b]Uniform finite nuclear model. [c]Uniform finite nuclear model and relativistically corrected functional (RLDA-exchange). [d]Ref. [50]. A value of 711 cm^{-1} for the vibrational frequency of PbO was documented in ref. [51].

Table 5: Bond lengths (R_e, $\AA$), binding energies (D_e, eV, referring to the lowest configurations for ligands), vibrational frequencies (ω_e, cm^{-1}) and force constants (k_e, N/m) for E114X. The mass of E114 is 280.

molecule		BDF(BP)	ZORA(MP)(BP)		ECP-CCSD(T)	
		4c	1c	2c	1c	2c
E114H	R_e	2.098	1.990	2.078	1.904	1.972
	D_e	0.40	2 47	0.45	2.61	0.43
	ω_e	839	1424	891	1550	971
	k_e	42	120	47	142	56
E114F	R_e	2.301	2.211	2.288	2.179	2.239
	D_e	2.29	4 71	2.25	4.49	1.95
	ω_e	364	461	371	483	431
	k_e	139	223	144	245	195
E114Cl	R_e	2.723	2.616	2.714	2.564	2.646
	D_e	1.56	3.85	1.56	3.78	1.41
	ω_e	211	281	216	304	256
	k_e	83	146	86	169	120
E114Br	R_e	2.874	2.749	2.865	2.708	2.802
	D_e	1.18	3.54	1.22	3.51	1.14
	ω_e	134	186	138	201	167
	k_e	66	127	70	167	101
E114I	R_e	3.100	2.937	3.084	2.891	3.062
	D_e	0.79	3.10	0 82	3.10	0.81
	ω_e	97	146	99	157	104
	k_e	48	109	50	127	56

Table 5: (Continued)

molecule		BDF(BP)	ZORA(MP)(BP)		ECP-CCSD(T)	
		4c	1c	2c	1c	2c
E114O	R_e	2.079	2.070	2.070	2.040	2.079[c]
		2.076[a]				
		2.077[b]				
	D_e	1.58	4.90	1.57	4.63	1.26[c]
		1.57[a]				
		1.62[b]				
	ω_e	562	651	571	652	523[c]
		562[a]				
		564[b]				
	k_e	281	378	291	379	244[c]
		282[a]				
		284[b]				

[a]Uniform finite nuclear model. [b]Uniform finite nuclear model and relativistically corrected functional (RLDA-exchange) [c]Basis set A.

4.3 PbO_2 and $E114O_2$

PbO_2 ($D_{\infty h}$) was recently observed in laser ablation experiment [51]. Both PbO_2 and $E114O_2$ were assumed to be of $D_{\infty h}$ symmetry in the present calculations. The results are presented in Table 6. Here we are mainly concerned with the energetic data. The BDF (2c-ZORA) atomization energy of PbO_2 is higher than that of ECP-CCSD(T) by about 1.04 eV, almost exactly twice that of PbO (~0.46 eV). This roughly holds at the scalar relativistic levels as well. Based on our ECP-CCSD(T) as well as empirically corrected DFT (-0.22 eV for Pb and -0.30 eV per oxygen) results we can predict the yet unkown atomization energy of PbO_2 to be 5.8±0.2 eV. For $E114O_2$ the difference between the BDF and 2c-ECP-CCSD(T) dissociation energy is 1.1 eV, larger than the expected difference ~0.6 eV, i.e., twice that of E114O. This indicates that the 2c-ECP-CCSD(T) atomization energy might be somewhat too low. Partially this is due to use of smaller basis sets (B) in the 2c-ECP-CCSD(T) calculations. For E114O, we have checked the basis set effect: 2.099 $\AA$, 1.41 eV, 511 cm^{-1} by basis set B and 2.079 $\AA$, 1.26 eV, 523 cm^{-1} by basis set A. Note that the basis effect turned out to be rather small for PbO. Similar calculations for $E114O_2$ could not be performed due to the limitation of computational power. Another reason is probably that the 7*s* orbital is involved in the bonding (see also below), while ECP-CCSD(T) substantially overestimated the ionization potentials of the 7*s* electrons (cf. Table 1) To confirm this point, we did a single point (R = 1.998 $\AA$) calculation by BDF for $E114O_2$ with the 7*s* orbital frozen, and found that the atomization energy was reduced by 0.99 eV. This effect is much smaller for E114O (0.27 eV) Now assuming that the difference between BDF and 2c-ECP-CCSD(T) for the atomization energy of $E114O_2$ is just twice that for E114O, which holds for PbO_2, then the *accurate* ECP-CCSD(T) atomization energy should be close to 2.1 eV for $E114O_2$. The resulting reaction energy (*RE*2, -3.5 eV) is then in better agreement with the BDF value (cf. Table 6). Here the reaction energy had to be evaluated by referring to the *accurate* binding energy for O_2 (5.21 eV [50]). The support of this analysis is that the SO reduction in the atomization energy of $E114O_2$ (PbO_2) is just similar to that of E114O (PbO).

Here we should mention that both the finite nuclear size effects and relativistic corrections to the functionals have little influence on the spectrocopic constants (see Tables 4, 5 and 6).

The decomposition of PbO_2 into Pb and O_2 turns out to be endothermic, while all the decompostion reactions of $2PbO_2 \rightarrow 2PbO + O_2$, $E114O_2 \rightarrow E114 + O_2$, and $2E114O_2 \rightarrow 2E114O + O_2$ are exothermic. The reactions of $E114X_4 \rightarrow E114X_2 + X_2$ (X = H, F, Cl) are also exothermic [15]. Therefore, the tetra-valent oxidation state of E114 is unlikely possible. The present results

Table 6: M-O bond lengths (R_e, $\mathring{A}$), atomization energies (D_e, eV)[a], symmetric stretching vibrational frequencies (ω_e, cm^{-1}) and force constants (k_e, N/m) for MO_2 (M=Pb, E114, $D_{\infty h}$). RE_1: reaction energy for $MO_2 \rightarrow M + O_2$; RE_2: reaction energy for $2MO_2 \rightarrow 2MO + O_2$.

molecule		BDF(BP)	ZORA(MP)(BP)		ECP-CCSD(T)		expt.[d]
		4c	1c	2c	1c	2c	
PbO_2[b]	R_e	1.902	1.902	1.898	1.895	1.893	
	D_e	6.64	7.73	6.54	6.78	5.60	
	RE_1	0.69	1.74	0.55	1.83	0.65	
	RE_2	-1.45	-1.47	-1.59	-1.61	-1.61	
	ω_e	680	683	687	665	674	659
	k_e	871	880	890	833	856	
$E114O_2$[c]	R_e	1.998	2.020	1 994	2.002	1.978	
	D_e	2.76	6.61	2.76	5.70	1.64	
	RE_1	-3.20	0.62	-3.23	0.75	-3.30	
	RE_2	-3.60	-2.57	-3.61	-2.82	-4.19	
	ω_e	599	586	604	535	584	
	k_e	676	648	687	539	643	

[a]An intermediate coupling scheme for Pb would reduce the DFT atomization energy for PbO_2 by 0.22 eV [46]. [b]By using uniform finite nuclear model the BDF results for PbO_2 are 1.900 $\mathring{A}$, 6.64 eV, 684 cm^{-1}, and 882 N/m. Further use of relativistically corrected functional (RLDA-exchange) yielded 1.901 $\mathring{A}$, 6.67 eV, 684 cm^{-1}, and 882 N/m. [c]By using uniform finite nuclear model the BDF results for $E114O_2$ are 1.995 $\mathring{A}$, 2.80 eV, 602 cm^{-1}, and 683 N/m. Further use of RLDA-exchange yielded 1.997 $\mathring{A}$, 2.86 eV, 602 cm^{-1}, and 682 N/m. [d]Ref. [51].

for PbO_2 are in line with the fact that $Pb^* + O_2 \rightarrow PbO_2$ is the main route to yield linear OPbO [51].

4.4 Pb_2 and $E114_2$

The most suitable candidate to demonstrate the inertness of the E114 $7p_{1/2}$ pair is the E114 dimer. The results for the Pb and E114 dimers are given in Table 7. The one-component results refer to $^3\Sigma_g$ states, while four- and two-component results to closed-shell molecules. Basis set superposition errors (BSSE) were corrected in all the calculations for $E114_2$. The agreement between ZORA and BDF is quite good for both Pb_2 and $E114_2$. Compared to other E114 diatomics, the SO effects are particularly large for $E114_2$. This is because the bonding in $E114_2$ is too weak. The (single-reference) ECP-CCSD(T) bond length for Pb_2 seems to be too long due to the multi-configuration nature of the (strong covalent) bonding [52]. Obviously, the GGA (*exchange*) functionals cover certain nondynamical (left-right) correlation even in terms of a single determinant. The situation is much better for $E114_2$, since the mixing-in of other configurations is prohibited due to large SO splitting. However, very large basis sets are needed to well describe such weak bonding. Although a basis set of $6p6sd3pf$ was used in the 2c-ECP-CCSD(T) calculations, the BSSE corrections estimated by the counterpoise method are still substantial (+0.46 $\mathring{A}$, -0.14 eV, -32 cm^{-1}).

The success of the available GGA functionals for describing very weak bonding is rather limited. However, we have recently found that the PBE [53] together with the SCC [28] functionals give the best results for the group 12 dimers (Zn_2, Cd_2, Hg_2, and $E112_2$) [54]. The PBESCC functional was thus applied for $E114_2$. It can be expected that the agreement between BDF(PBESCC) and ECP-CCSD(T) should be better if the basis set is improved in the latter. Anyway, it can be concluded that the bonding of $E114_2$ is much stronger than typical van der Waals interactions (say, 0.05 eV) and about twice the binding energy of $E112_2$ (0.075 eV) [54]. This is in line with the fact that the static dipole polarizability of E114 (33.5 a.u.) is larger than that of E112 (29.8 a.u.) (BDF PBESCC results).

From the above calculations, the molecular stabilites are summarized as PbO > PbF > PbCl > PbBr > PbI > PbH > Pb_2, and E114F > E114O $\approx$ E114Cl > E114Br > E114I > E114H > $E114_2$. Whereas PbO_2 is a stable molecule, $E114O_2$ is predicted to be thermodynamically unstable by all the three approaches.

Table 7: Bond lengths (R_e, $\mathring{A}$), binding energies (D_e, eV), vibrational frequencies (ω_e, cm^{-1}) and force constants (k_e, N/m) for Pb_2 and $E114_2$. The results by the PBE and PBESCC functionals are in brackets and parentheses, respectively. The 1c results refer to $^3\Sigma_g$ states.[a]

molecule		BDF(BP)	ZORA(MP)(BP)		ECP-CCSD(T)		expt
		4c	1c	2c	1c	2c	
Pb_2	R_e	2.982 [2.980]	2.926	2 974	2.962	3.057	2.93[b]
	D_e	1 14 [1.17]	2.38	1.16	1.69	0.64	0.82[c]
	ω_e	107 [108]	127	106	128	97	111[c]
	k_e	70 [71]	98	68	100	58	
$E114_2$	R_e	3.486 [3.448] (3.603)	3.122	3.463	3.070	3.732	
	D_e	0.12 [0.20] (0.15)	2.16	0.12	1.60	0.07	
	ω_e	50 [43] (35)	102	40	104	26	
	k_e	20 [15] (10)	86	14	89	6	

[a]An intermediate coupling scheme for Pb would reduce the DFT binding energy for Pb_2 by 0.44 eV [46]. For $E114_2$, the PBESCC functional gives the best DFT results [54]. In the 2c-ECP-CCSD(T) calculations, the Pb $5s5p$ (E114 $6s6p$) were frozen and virtual spinors higher than 20 a.u. were excluded. [b]Ref. [60]. [c]Ref. [50].

4.5 Spin-orbit effects

To facilitate the comparison, SO effects on the spectroscopic constants are given in Table 8 for the Pb and Table 9 for the E114 compounds. Except the oxides, the SO effects derived from ZORA and ECP-CCSD(T) are in fairly good agreement. Besides the basis set truncation error, the multi-configuration nature of the oxides seems to be responsible for these discrepancies.

The SO effects for the E114 systems are substantial, $\sim$ 0.1 Å for bond lengths, which is an order of magnitude larger than for the corresponding Pb compounds; 2 to 4 eV for binding energies, three times larger than for the Pb systems.

4.6 Mulliken population analysis and dipole moments

The Mulliken population analysis (MPA) of the charge distributions based on the AOIM (atomic orbitals in molecule) approach [55] is presented in Table 10. The merits of this approach are on one hand to improve the stability of MPA with respect to basis sets, and on the other hand provide pictorial interpretation of the electronic structure (i.e., "genuine" atomic orbitals rather than basis functions). The resulting Mulliken charges converge if the Fock matrix elements converge [55]. However, balanced basis sets still have to be used.

The ionicities of the E114 compounds are very much like that of the Pb compounds. However, the E114 $7p_{1/2}$ spinors are more inert than the Pb $6p_{1/2}$ spinors (e.g., occupied with more electrons), while the E114 $7p_{3/2}$ spinors are much less involved in the bonding than the Pb $6p_{3/2}$ spinors. As a consequence, the *sp* hybridization is less facile for E114 than that for Pb. $E114O_2$ is characteristic of *dsp*-hybridization, whereas PbO_2 mainly of *sp*-hybridization. This analysis is in line with the fact that relativistic (SO) effects in the E114 compounds are larger. The bonding of Pb_2 ($E114_2$) can be largely interpreted as charge transfer from $6p_{1/2}$ ($7p_{1/2}$) to $6p_{3/2}$ ($7p_{3/2}$). In the case of $E114_2$, the overlapping density accounts for the major part of the bonding, which indicates the reliability of the DFT results.

The dipole moments for the diatomics of both Pb and E114 are given in Table 11. The greement between ZORA(MP) and BDF is quite good. The dipole moments are not sensitive to steep functions, since the deep core density is spherical and makes no contribution to the dipole moment. The presently calculated dipole moment for PbO compares favorably with previous theoretical [56, 57, 58] and experimental values [50]. SO effects on the dipole moments are moderate. At a given geometry, the GGA correction to the LDA dipole moment is rather small (see also ref. [56]). Therefore, the GGA dipole

Table 8: Spin-orbit effects on the spectroscopic constants of PbX: R_e (Å), D_e (eV), ω_e (cm^{-1}), and k_e (N/m).

molecule		ZORA	CCSD(T)
PbH	R_e	-0.002	0.002
	D_e	-0.66	-0.72
	ω_e	-52	-45
	k_e	-10	-8
PbF	R_e	0.015	0.015
	D_e	-0.71	-0.73
	ω_e	-20	-15
	k_e	-20	-16
PbCl	R_e	0.019	0.020
	D_e	-0.67	-0.74
	ω_e	-15	-12
	k_e	-16	-13
PbBr	R_e	0.020	0.020
	D_e	-0.81	-0.82
	ω_e	-11	-9
	k_e	-15	-13
PbI	R_e	0.023	0.023
	D_e	-0.90	-0.94
	ω_e	-12	-7
	k_e	-17	-11
PbO	R_e	-0.002	-0.002
	D_e	-1.13	-1.18
	ω_e	-9	20
	k_e	-12	27
PbO2	R_e	-0.004	-0.002
	D_e	-1.19	-1.18
	ω_e	4	9
	k_e	10	23
Pb_2	R_e	0.048	0.095
	D_e	-1.22	-1.05
	ω_e	-21	-31
	k_e	-30	-42

Table 9. Spin-orbit effects on the spectroscopic constants of E114X. R_e (Å), D_e (eV), ω_e (cm^{-1}), and k_e (N/m).

molecule		ZORA	CCSD(T)
E114H	R_e	0 088	0.068
	D_e	-2.02	-2.18
	ω_e	-533	-579
	k_e	-73	-86
E114F	R_e	0.077	0.060
	D_e	-2.46	-2.54
	ω_e	-90	-52
	k_e	-79	-50
E114Cl	R_e	0.098	0.082
	D_e	-2.29	-2.37
	ω_e	-65	-48
	k_e	-60	-49
E114Br	R_e	0.116	0.094
	D_e	-2.32	-2.37
	ω_e	-48	-34
	k_e	-57	-66
E114I	R_e	0.147	0.171
	D_e	-2.28	-2.29
	ω_e	-47	-53
	k_e	-59	-71
E114O	R_e	0.000	0.039
	D_e	-3.33	-3.37
	ω_e	-80	-129
	k_e	-87	-135
$E114O_2$	R_e	-0.026	-0.024
	D_e	-3.85	-4.06
	ω_e	18	49
	k_e	39	104
$E114_2$	R_e	0.341	0.662
	D_e	-2.04	-1.53
	ω_e	-62	-78
	k_e	-72	-83

Table 10: Mulliken population analysis by the AOIM approach [55] for PbX and E114X (BDF results). Q: positive net charge on the metal.

	PbX							
	H	F	Cl	Br	I	O	O_2	Pb
$5d_{3/2}$	4.00	4.00	4.00	4.00	4.00	3.99	3.97	4.00
$5d_{5/2}$	5.99	5.99	5.99	6.00	6.00	5.98	5.92	6.00
$6s_{1/2}$	1.92	1.96	1.96	1.96	1.97	1.90	1.42	1.99
$6p_{1/2}$	1.17	0.98	1.03	1.06	1.11	0.65	0.48	1.57
$6p_{3/2}$	0.72	0.39	0.47	0.50	0.54	0.62	0.63	0.41
$ns_{1/2}$	1.12	1.96	1.96	1.97	1.98	1.92	1.92	
$np_{1/2}$	0.01	1.91	1.85	1.85	1.86	1.67	1.58	
$np_{3/2}$	0.02	3.69	3.61	3.54	3.44	3.03	3.04	
Q	0.19	0.58	0 45	0.41	0.33	0.68	1 23	0.00

	E114X							
	H	F	Cl	Br	I	O	O_2	E114
$6d_{3/2}$	4.00	4.00	4.00	4.00	4.00	3.98	3.95	4.00
$6d_{5/2}$	5.99	5.99	5.99	5.99	5.99	5.97	5.81	6.00
$7s_{1/2}$	1.98	1.99	1.98	1.99	1.99	1.95	1.77	1.99
$7p_{1/2}$	1.65	1.28	1.38	1.44	1.54	1.09	0.77	1.92
$7p_{3/2}$	0.24	0.14	0.19	0.18	0.17	0.28	0.30	0.07
$ns_{1/2}$	1.12	1.98	1.98	1.99	1.99	1.96	1.96	
$np_{1/2}$	0.01	1.94	1.90	1.91	1.92	1.84	1.57	
$np_{3/2}$	0.02	3.63	3.51	3.43	3.34	2.80	3.00	
Q	0 16	0.57	0.41	0.36	0.28	0.66	1.23	0.00

Table 11. Dipole moments (μ, Debye) and dipole moment derivatives ($d\mu/dR$, Debye/$\AA$) at the BP equilibrium distances from Tables 4 and 5. Positive values reflect polarity M^+X^-.

		PbH[a]	PbF	PbCl	PbBr	PbI	PbO[b]
μ	1c-ZORA	1.14	3.55	3.57	3.30	2 96	4.34
	2c-ZORA	1.04	3.68	3.81	3.55	3.14	4.17
	BDF	0.90	3.76	3.60	3.32	2.97	4.29
$d\mu/dR$	1c-ZORA	3.39	5.77	5.77	5.51	5.04	4.56
	2c-ZORA	3.41	5.77	5.80	5.53	4.96	4.37
	BDF	3.21	6.04	5.62	5.12	4.72	4.67
		E114H	E114F	E114Cl	E114Br	E114I	E114O
μ	1c-ZORA	2.21	4.82	5.01	4.80	4 52	5.25
	2c-ZORA	1.49	4.65	4.82	4.51	4.01	4.37
	BDF	1.40	4.73	4.51	4.12	3.68	4.39
$d\mu/dR$	1c-ZORA	3.50	5.48	5.55	5.43	4.97	4.67
	2c-ZORA	1.77	4.12	3.84	3.36	2.55	3.44
	BDF	1.13	4.29	3.32	2.64	1.91	3.75

[a] $\mu = 0.67$ Debye (ref. [61]). [b] $\mu = 4.35$ Debye (ref. [56]; 3.52-4.70 Debye (ref. [57]; 4.46 Debye ([58]; 4.64 Debye (expt. [50]).

moments can be obtained by interpolation from LDA values if GGA is treated perturbatively. The dipole moments of the E114 compounds are larger than those of the Pb compounds due to longer bond lengths and similar ionicities. However, the variation of the dipole moments of the E114 compounds are much smaller.

4.7 A general statement

Finaly we want to judge our work qualitatively from a methodological point of view. On the DFT side, we could get rid of other numerical noises than the differences in the Hamiltonians. For the valence properties considered in this work, the two-component ZORA results are very close to the BDF ones. As for the computational efforts, the BDF calculations were actually very cheap (even cheaper than the present implementation of ZORA, although the comparison was somewhat indirect), since very compact and yet sufficient basis sets and double point group symmetries ($C_{\infty v}$, $D_{\infty h}$) were used. Furthermore, the task for basis set optimization is very little since numerical bases always serve as the backbone of the basis set. Especially, the difficult optimization of steep functions to describe the cores of heavy elements is completely avoided! Actually, it took us a quite hard and long time to bring the ZORA results in agreement with the BDF ones. This had not been possible before the new basis set optimizer[33] was available. On the *ab initio* (wave-function based approach) side, however, such calibration appears infeasable so far On the other hand, we can not claim that our ECP-CCSD(T) results have converged with respect to basis sets, since higher angular momentum functions have not been considered and smaller basis sets often have to be used in the two-component calculations. However, since the results for the Pb compounds appear good when compared to experiment, our ECP-CCSD(T) results for the E114 compounds should be mostly reasonable.

5 Conclusions

Spin-orbit effects play dominant roles in the bonding of E114 compounds. At the scalar relativistic level, the binding energies of the E114 compounds are very similar to those of the Pb homologues. Spin-orbit effects strongly weaken the strengths of the E114 compounds. The formally tetra-valent oxidation states of E114 is likely unfavored. However, E114 can not be simply regarded as a *noble* atom, e.g., the bonding of E114 dimer is much stronger than typical van der Waals interactions. The application of transformed relativistic Hamiltonians to valence properties of very heavy elements appears to

be justified, since E114 (like E113) turns out to be a particularly difficult case (weak singularity for $2p_{1/2}$). Such problems are much less severe for $p_{3/2}$ and d spinors. For example, in our calculations on eka-gold (E111) compounds[26], we found good agreement between BDF and ZORA, although l-adapted segmentedly contracted basis functions were directly used in the two-component calculations. The reason is that the valence $6d_{5/2}$ spinors of E111 form the bonding. The performance of ZORA for eka-thallium (E113, $7p^1_{1/2}$) and eka-bismuth (E115, $7p^2_{1/2}7p^1_{3/2}$) systems is being investigated in our laboratory. The remaining task is thus to investigate the performance of such Hamiltonians for core properties. So far calibration of such approaches can be carried out readily only at the DFT level. Spin-orbit effects estimated by ZORA and ECP-CCSD(T) are generally in good agreement with each other. The discrepancies for the oxides are probably due to the multi-configuration nature and/or insufficiency of basis sets. For better description of high oxidation states (e g., $E114O_2$), the s set of the ECPs for E114 needs to be improved and progress is being made.

6 Acknowledgments

The first two authors Dr. E. van Lenthe for critical comments. Y.-K. H. thanks the Japan Society for the Promotion of Science for financial support. The research at KAIST is in part supported by KISTEP/MOST and KOSEF (1999-2-121-005-3)

References

[1] Hofmann, S.; Ninov, V.; Heßberger, F. P.; Armbruster, P.; Folger, H.; Münzenberger, G.; Schött, H. J.; Popeko, A. G., Yeremin, A. V.; Andreyev, A. N.; Saro, S.; Janik, R.; Leino, M. *Z. Phys. A* **1995**, *350*, 277.

[2] Hofmann, S.; Ninov, V.; Heßberger, F P.; Armbruster, P.; Folger, H.; Münzenberger, G.; Schött, H. J.; Popeko, A. G.; Yeremin, A. V.; Andreyev, A. N.; Saro, S.; Janik, R.; Leino, M. *Z. Phys. A* **1995**, *350*, 281.

[3] Hofmann, S.; Ninov, V.; Heßberger, F. P.; Armbruster, P.; Folger, H.; Münzenberg, G.; Schött, H. J.; Popeko, A. G.; Yeremin, A. V.; Saro, S.; Janik, R.; Leino, M. *Z. Phys. A* **1996**, *354*, 229.

[4] Oganessian, Yu. Ts.; Yeremin, A. V.; Popeko, A. G.; Bogomolov, S. L.; Buklanov, G. V.; Chelnokov, M. L.; Chepigin, V. I.; Gikal, B. N.; Gorshkov, V. A.; Gulbekian, G. G.; Itkis, M. G.; Kabachenko, A. P.; Lavrentev, A. Yu.; Malyshev, O. N.; Rohac, J.; Sagaidak, R. N.; Hofmann, S.; Saro, S.; Giardina, G.; Morita, K. *Nature* (London) **1999**, *400*, 242.

[5] Oganessian, Yu. Ts.; Utyonkov, V. K.; Lobanov, Yu. V.; Abdullin, F. Sh.; Polykov, A. N.; Shirokovsky, I. V.; Tsyganov, Yu. S.; Gulbekian, G. G.; Bogomolov, S. L.; Gikal, B. N.; Mezentsev, A. N.; Iliev, S.; Subbotin, V. G.; Sukhov, A. M.; Buklanov, G. V.; Subotic, K.;Itkis, M. G. *Phys. Rev. Lett.* **1999**, *83*, 3154.

[6] Ninov, V ; Gregorich, K. E.;Loveland, W., Ghiorso, A., Hoffman, D. C.; Lee, D. M.; Nitsche, H.; Swiatecki, W. J.; Kirbach, U. W.; Laue, C. A.; Adams, J. L.; Patin, J B.; Shaughnessy, D. A.; Strellis, D. A.; Wilk, P. A. *Phys. Rev. Lett.* **1999**, *83*, 1104.

[7] Goepper-Mayer, M. *Phys. Rev.* **1948**, *74*, 235; Meldner, H. *Ark. Fysik* **1967**, *36*, 593; Herrmann, G. *Angew. Chem. Int Ed.* **1995**, *34*, 1713; Möller, P.; Nix, J. R.; Kratz, J. V. *At. Data Nucl. Data Tables* **1997**, *66*, 131.

[8] Hoffmann, D. C. *Chem. Eng. News* **1994**, *72*, 24; Hoffman, D. C. *Radiochim. Acta* **1996**, *72*, 1.

[9] Pershina, V. *Chem Rev.* **1996**, *96*, 1977.

[10] Schwerdtfeger P.; Seth, M. In "The Encylopedia of Computational Chemistry", von R. Schleyer, P.; Allinger, N. L ; Clark, T.; Gasteiger, J.; Kollman, P.; Schaefer III, H. F.; Schreiner, P., Eds.; Wiley· New York, 1998; Vol. 4, 2480.

[11] Nash, C. S.; Bursten, B. E. *J. Phys. Chem (A)* **1999**, *103*, 402.

[12] Pitzer, K. S. *J. Chem. Phys.* **1975**, *63*, 1032; Pitzer, K. S. *Int. J. Quant. Chem.* **1984**, *25*, 131.

[13] Grant, I. P.; Pyper, N. C *Nature* **1977**, *265*, 715.

[14] Pyykko, P.; Desclaux, J. P. *Nature* **1977**, *266*, 336.

[15] Seth, M.; Faegri, K.; Schwerdtfeger, P. *Angew. Chem. Int. Ed.* **1998**, *37*, 2493.

[16] Liu, W.; Hong, G.; Dai, D.; Li, L.; Dolg M. *Theor. Chem. Acc* **1997**, *96*, 75.

[17] van Wüllen, C. *J. Chem. Phys.* **1998**, *109*, 392.

[18] van Wüllen, C.; Boese, A. D. (unpublished)

[19] Lee, S. Y.; Lee, Y. S. *J. Comput. Chem.* **1992**, *13*, 595.

[20] Lee, H. S.; Han, Y. K.; Kim, M. C.; Bae, C.; Lee, Y S. *Chem. Phys. Lett.* **1998**, *293* 97.

[21] Han, Y. K., Bae, C., Son, S. K.; Lee, Y. S. *J. Chem Phys.* **2000**, *112*, 2684.

[22] Perdew, J. P.; Wang, Y. *Phys. Rev. B* **1992**, *45*, 13244

[23] Becke, A. D. *Phys. Rev. A* **1988**, *38*, 3098.

[24] Perdew, J. P *Phys. Rev. B* **1986**, *33*, 8822; ibid, **1986**, *34*, 7406(E)

[25] Liu, W.; Küchle, W.; Dolg, M. *Phys. Rev. A* **1998**, *58*, 1103.

[26] Liu, W.; van Wüllen, C. *J. Chem. Phys.* **1999**, *110*, 3730.

[27] Mayer, M.; Häberlen, O. D.; Rösch, N. *Phys. Rev. A* **1996**, *54*, 4775.

[28] Stoll, H.; Pavlidou, C. M. E., Preuss, H. *Theor. Chim. Acta* **1978**, *49*, 143; Stoll, H.; Golka, E.; Preuss, H. *Theor. Chim. Acta* **1980**, *55*, 29.

[29] Liu, W.; Dolg, M. *Phys. Rev. A* **1998**, *57*, 1721.

[30] Görling, A *Phys. Rev. A* **1993**, *47*, 2783.

[31] Schäfer, A.; Ahlrichs, R. *J. Chem. Phys.* **1992**, *97*, 2751.

[32] Huzinaga, S.; Klobukowski, M. *J Mol. Struct. (Theochem)* **1988**, *167*, 1.

[33] van Wüllen, C.; Schaeffer, R. (unpublished).

[34] Dyall, K. G.; Faegri, K. *Theor. Chim. Acta* **1996**, *94*, 39.

[35] Nash, C. S., Bursten, B. E.; Ermler, W. C. *J. Chem. Phys* **1997**, *106*, 5133.

[36] Pacios, L F.; Christiansen, P. A. *J. Chem. Phys.* **1985**, *82*, 2664.

[37] Hurley, M. M.; Pacios, L. F.; Christiansen, P. A ; Ross, R. B.; Ermler, W. C *J. Chem. Phys.* **1986**, *84*, 6840.

[38] Lajohn, L. A.; Christiansen, P. A ; Ross, R. B.; Atashroo, T.; Ermler, W. C. *J. Chem. Phys.* **1987**, *87*, 2812.

[39] Dunning, Jr., T. H.; *J. Chem. Phys.* **1989**, *90*, 1007.

[40] Lee, H. S. (unpublished).

[41] Gaussian 94, Revision B.2, Frisch, M. J ; Trucks, G. W.; Schlegel, H. B.; Gill, P M. W.; Johnson, B. G.; Robb, M. A.; Cheeseman, J. R.; Keith, T.; Petersson, G. A.; Montgomery, J. A.; Raghavachari, K.; Al-Laham, M. A.; Zakrzewski, V. G.; Ortiz, J. V.; Foresman, J. B.; Cioslowski, J.; Stefanov, B. B.; Nanayakkara, A.; Challacombe, M.; Peng, C. Y.; Ayala, P. Y.; Chen, W.; Wong, M. W.; Andres, J. L.; Replogle, E. S.; Gomperts, R.; Martin, R. L.; Fox, D. J.; Binkley, J. S.; Defrees, D. J.; Baker, J.; Stewart, J. P.; Head-Gordon, M.; Gonzalez, C.; Pople, J. A. (Gaussian, Inc., Pittsburgh PA, 1995).

[42] MOLPRO is a package of *ab initio* programs written by Werner, H.-J.; and Knowles, P. J. with contributions from Almlöf, J.; Amos, R. D.; Berning, A ; Cooper, D. L.; Deegan, M J. O.; Dobbyn, A. J.; Eckert, F.; Elbert, S. T.; Hampel, C.; Lindh, R.; Lloyd, A. W.; Meyer, W.; Nicklass, A.; Peterson, K.; Pitzer, R.; Stone, A. J.; Taylor, P. R.; Mura, M. E.; Pulay, P.; Schütz, M., Stoll, H.; Thorsteinsson, T..

[43] Hampel, C.; Peterson, K.; Werner, H.-J. *Chem. Phys. Lett.* **1992**, *190*, 1.

[44] Knowles, P. J., Hampel, C.; Werner, H.-J. *J Chem. Phys.* **1993**, *99*, 5219.

[45] Dyall, K. G.; Grant, I. P.; Johnson, C. T.; Parpia, F. A.; Plummer, E. P. *Comput. Phys Commun.* **1989**, *55*, 425.

[46] Mayer, M. (private communication).

[47] Metz, B.; Schweizer, M.; Stoll, H.; Dolg, M.; Liu, W. *Theor. Chem. Acc.* **2000**, *104*, 22.

[48] Moore, C. E. "Atomic Energy Levels", National Bureau of Standards Circular 467, U.S. Goverment Printing Office, Washington, DC, 1958; Vol. 3.

[49] van Lenthe, E. (private communication).

[50] Huber, K. P.; Herzberg, G. "Molecular spectra and molecular structure", IV. Constants of diatomic molecules, van Nostrand, New York, 1979.

[51] Chertihin, G. V.; Andrews, L. *J. Chem. Phys.* **1996**, *105*, 2561.

[52] Han, Y. K.; Hirao, K. *J. Chem. Phys.* **2000**, *112*, 9353.

[53] Perdew, J. P.; Burke, K.; Ernzerhof, M. *Phys. Rev. Lett.* **1996**, *77*, 3865.

[54] Liu, W.; Dolg, M.; Schwerdtfeger, P. (unpublished).

[55] Liu, W ; Li, L. *Theor Chim Acta* **1997**, *95*, 81.

[56] van Lenthe, E.; Snijders, J. G.; Baerends, E. J. *J. Chem. Phys.* **1996**, *105*, 6505.

[57] Dolg, M.; Nicklass, A.; Stoll, H. *J. Chem. Phys.* **1993**, *99*, 3614.

[58] Kellö, V.; Sadlej, A. J.; Faegri, K. *J. Chem. Phys.* **1998**, *108*, 2056.

[59] Visscher, L.; Dyall, K. G. *Atom. Data Nucl. Data* **1997**, *67*, 207.

[60] Sontag H.; Weber, R. *J. Mol. Spectrosc* **1983**, *100*, 75.

[61] Chapman, D. A.; Li, J.; Balasubramanian, K.; Lin, S. H. *J. Chem. Phys* **1988**, *88*, 3826.

FLOQUET STATES AND OPERATOR ALGEBRA[†]

V. M. León[1], M. Martín[2], L. Sandoval[2] and A. Palma[1,3(*)]

[1] *Universidad Autónoma de Puebla, Instituto de Física, Apartado Postal J-48 Puebla, Pue. 72570 (MEXICO)*

[2] *Universidad Autónoma de Puebla, Facultad de Ciencias de la Computación, Apartado Postal 589, Puebla, Pue. 72001 (MEXICO)*

[3] *Instituto Nacional de Astrofísica, Optica y Electrónica (INAOE), Apdo. Postal 51 y 216, Puebla, Pue. 72000 (MEXICO)*

ABSTRACT

The algebraic properties of boson operators are used to obtain the Floquet quasienergies and eigenfunctions for a particle in the harmonic oscillator potential, when the particle is simultaneously subjected to a monochromatic electric field. First, the differential equation for the evolution operator is solved then an appropriate initial wavefunction is used to obtain the quasienergies and eigenfunctions. For the parabolic barrier, a new pair of operators is defined and although none is the adjoint of the other they have the same commutator as the boson operators, thus allowing a very similar treatment for this potential.

LIST OF CONTENTS

[†]Dedicated to the memory of Per-Olov Löwdin

*Corresponding author, email palma@sirio ifuap buap mx

ADVANCES IN QUANTUM CHEMISTRY, VOLUME 39

0065-3276/01 $35 00

1. INTRODUCTION

The importance of the harmonic oscillator and the parabolic barrier interacting with a monochromatic electric field has long been recognized. In this connection, the Floquet quasienergies and eigenfunctions have been obtained with different analytical methods [1,2,3,4].

On the other hand, the algebraic approach by using boson operators has been applied to problems involving harmonic oscillator eigenfunctions, such as the Franck-Condon overlap, squeezed states and matrix elements calculations, [5,6,7].

In section II it is shown an alternative way to obtain the Floquet quasienergies and eigenfunctions for the harmonic oscillator and by using the algebraic properties of boson operators it is obtained and solved a differential equation for the evolution operator In section III we treat the parabolic barrier where we introduce a new pair of operators, which, although none is the adjoint of the other, they satisfy the same commutation relation. This procedure allows for a treatment very similar to that for a harmonic oscillator.

2. HARMONIC OSCILLATOR

Let us consider the time-dependent Schrödinger equation:

$$\imath \frac{\partial \Psi}{\partial t} = H\Psi \tag{1}$$

where the hamiltonian (in reduced units) is :

$$H = -\frac{\partial^2}{\partial x^2} + \omega_0^2 x^2 + \lambda x \cos \omega t \quad , \tag{2}$$

and where the last term represents the (semi-classical) monochromatic electric field.

From the Floquet theory of differential equations, we know that for Eq. (1) there exist solutions of the form:

$$\Psi_F^\nu(x,t) = exp[-iE_F^\nu t]\Phi_F^\nu(x,t) \quad , \tag{3}$$

E_F^ν is called a quasi-energy and $\Phi_F^\nu(x,t)$ is a periodic function of time, that is, with the property:

$$\Phi_F^\nu(x,t+T) = \Phi_F^\nu(x,t) \quad , \qquad T = \frac{2\pi}{\omega}. \tag{4}$$

In order to find such solutions let us introduce the boson operators (a, $a^\dagger$):

$$x = \frac{1}{\sqrt{2\omega_0}}(a + a^\dagger) \quad , \quad \frac{\partial}{\partial x} = \sqrt{\frac{\omega_0}{2}}(a - a^\dagger) \tag{5}$$

The hamiltonian (2) becomes:

$$H = \omega_0(2a^\dagger a + 1) + \frac{\lambda}{\sqrt{2\omega_0}}(a + a^\dagger)\cos \omega t \tag{6}$$

Now let $U(t)$ be the evolution operator.

$$\Psi(x,t) = U(t)\Psi(x,0) \tag{7}$$

It's easy to see that $U(t)$ satisfies

$$\imath\frac{\partial U}{\partial t} = \left\{\omega_0(2a^\dagger a + 1) + \frac{\lambda}{\sqrt{2\omega_0}}(a + a^\dagger)\cos\omega t\right\} U \tag{8}$$

with the initial condition $U(0) = 1$.

By using Louisell's technique[8], which introduces the concept of normal order, equation (8) becomes a differential equation involving only complex numbers for the function $U^{(n)}(\alpha,\alpha^*,t)$, where α is a complex number and $U^{(n)}(\alpha,\alpha^*,t)$ is obtained from the normal order form of $U(a,a^\dagger,t)$ through substitution of a by $\alpha + \partial/\partial\alpha^*$ and $a^\dagger$ by α^*. The differential equation is:

$$\imath\frac{\partial}{\partial t}U^{(n)} = \left\{\omega_0\left(2\alpha^*\alpha + 2\alpha^*\frac{\partial}{\partial\alpha^*} + 1\right) + \frac{\lambda}{\sqrt{2\omega_0}}\left(\alpha + \frac{\partial}{\partial\alpha^*} + \alpha^*\right)\cos\omega t\right\} U^{(n)}. \tag{9}$$

We note that once we have solved (9) for $U^{(n)}(\alpha,\alpha^*,t)$, we recover $U(a,a^\dagger,t)$ by using the normal order operator '$\aleph$', which by definition changes α by a and α^* by $a^\dagger$, puting all $a^\dagger$'s to the left of the a's in the series expansion for $U^{(n)}(\alpha,\alpha^*,t)$:

$$\aleph\left\{U^{(n)}(\alpha,\alpha^*,t)\right\} = U(a,a^\dagger,t) \quad . \tag{10}$$

Going back to equation (9), we propose as solution:

$$U^{(n)}(\alpha,\alpha^*,t) = exp\{G(\alpha,\alpha^*,t)\} \quad , \tag{11}$$

where $G(\alpha,\alpha^*,t)$ is of form:

$$G(\alpha,\alpha^*,t) = A(t) + B(t)\alpha + C(t)\alpha^* + D(t)\alpha^*\alpha \quad , \tag{12}$$

and the initial condition requres $A(0) = B(0) = C(0) = D(0) = 0$.

Substitution into equation (9) gives a set of four coupled linear differential equations:

$$\imath\frac{dA}{dt} = \omega_0 + \frac{\lambda C}{\sqrt{2\omega_0}}\cos\omega t$$

$$\imath\frac{dB}{dt} = \frac{\lambda}{\sqrt{2\omega_0}}(1 + D)\cos\omega t$$

$$\imath\frac{dC}{dt} = 2\omega_0\, C + \frac{\lambda}{\sqrt{2\omega_0}}\cos\omega t \tag{13}$$
$$\imath\frac{dD}{dt} = 2\omega_0\,(1+D)$$

whose solutions can be obtained through standard procedures, giving the next expression for the evolution operator:

$$U(a,a^\dagger,t) = e^{A(t)}e^{-B^*(t)exp(-2\imath\omega_0 t)\,a^\dagger}e^{-(2\imath\omega_0 t)\,a^\dagger a}e^{B(t)a} \tag{14}$$

By using this operator, one can in principle know the time development of an arbitrary initial wavefunction. However, we are rather interested in obtaining the Floquet quasienergies and eigenfunctions for our hamiltonian, that is, we are looking for functions $\Psi(x,t)$ that satisfy equation (3). Bearing this in mind, we propose the following initial function:

$$\Psi(x,0) = \chi_\nu(x-x_0) \qquad , \tag{15}$$

where $\chi_\nu(x)$ is the harmonic oscillator solution corresponding to the energy eigenvalue $E_\nu = \omega_0(2\nu+1)$, and x_0 is still an indeterminate constant. $\Psi(x,0)$ can be rewritten as:

$$\Psi(x,0) = e^{-S^2/2}e^{Sa^\dagger}e^{-Sa}\chi_\nu(x) \qquad , \qquad S = x_0\sqrt{\frac{\omega_0}{2}} \tag{16}$$

where we have used the displacement operator:

$$f(x-y) = e^{-y\frac{d}{dx}}f(x). \tag{17}$$

We substitute now $\Psi(x,0)$ into equation (7) together with $U(t)$, as given in equation (14), and we straightfordwardly apply the commutation properties of boson operators, until the factor $e^{-(2\imath\omega_0 t)a^\dagger a}$ appears to the left of $\chi_\nu(x)$, so that we can apply:

$$e^{-(2\imath\omega_0 t)a^\dagger a}\chi_\nu(x) = e^{-2\imath\omega_0 t\nu}\chi_\nu(x) \qquad . \tag{18}$$

It turns out, after some algebra, that in order for $\Psi_F^\nu(x,t)$ to be in the desired form, we must choose the indeterminate constant x_0 as $2\lambda/(\omega^2-4\omega_0^2)$. This choice of x_0 is not a strict consequence of the method proposed in this paper, in fact, it is a consequence of the periodicity of the wavefunction. Thus the Floquet quasienergies (labeled by the index ν) are given by:

$$E_F^\nu = \omega_0(2\nu+1) + \frac{\lambda^2}{2(\omega^2-4\omega_0^2)} \tag{19}$$

and the respective functions $\Phi_F^\nu(x,t)$ are:

$$\Phi_F^\nu(x,t) = e^{\beta(t)} e^{\gamma(t)a^\dagger} e^{-\gamma^*(t)a} \chi_\nu(x) \tag{20}$$

where

$$\beta(t) = \frac{-\imath\lambda \sin\omega t}{2\omega\sqrt{2\omega_0}}\,\gamma(t) - \frac{\omega_0}{4}\left\{\frac{2\lambda}{\omega^2 - 4\omega_0^2}\right\}^2 \tag{21}$$

$$\gamma(t) = \frac{\lambda}{\sqrt{2\omega_0}(\omega^2 - 4\omega_0^2)}\Big\{2\omega_0 \cos\omega t - \imath\omega \sin\omega t\Big\}.$$

We note that $\beta(t)$ and $\gamma(t)$ have a period $T = 2\pi/\omega$, so that $\Phi_F^\nu(x,t)$ in effect satisfies equation (4).

3. PARABOLIC BARRIER

The parabolic barrier seems to be very similar to the harmonic oscillator potential since, geometrically, the difference between them is a rotation by π or an inversion of coordinates. Regardless of the similarities that may exist, the hamiltonian of the parabolic barrier leads to complex eigenvalues for its resonances, and unnormalized eigenfunctions[2]. In order to solve such a problem one can use the complex rotation method[4]. Another way is via the mapping of the eigenket of the parabolic barrier to the Hilbert space corresponding to the harmonic oscillator.

If we start with the hamiltonian:

$$H = -\frac{\partial^2}{\partial x^2} - \omega_0^2 x^2 + \lambda x \cos\omega t \qquad , \tag{22}$$

we see from (2) that the only difference with the harmonic oscillator potential is just a sign. The use of boson operators as given in equation (5), leads to a hamiltonian involving quadratic terms in α and α^*, in such a way that the form of $G(\alpha,\alpha^*,t)$ given in equation (12) is not useful. We could then define a new functional form, including quadratic terms, though the resulting equations are not easy to handle. Instead we propose to introduce two new operators, which we call b_1 and b_2:

$$x = \frac{1}{\sqrt{2i\omega_0}}(b_1 + b_2) \quad , \quad \frac{\partial}{\partial x} = \sqrt{\frac{\imath\omega_0}{2}}(b_1 - b_2) \qquad , \tag{23}$$

whose definition is motivated by the fact that the harmonic oscillator potential can be obtained from the parabolic one by replacing ω_0 by $\imath\omega_0$ We note that b_1 and b_2 have the same commutator as a and $a^\dagger$, although none is the adjoint of the other, where instead we have $b_1^\dagger = \imath b_1$ and $b_2^\dagger = \imath b_2$.

At this point the only thing that really matters is that all the algebraic properties

of boson operators, including those which refer to normal ordering stem from their commutation relation and are independent of the fact that they are adjoint to each other. Thus, because b_1 and b_2 have the same commutator as a and $a^\dagger$, all identities used for a and $a^\dagger$ can be used immediately, just replacing a by b_1 and $a^\dagger$ by b_2. With these new operators the evolution operator becomes:

$$U(b_1, b_2, t) = e^{A(t)} e^{C(t)\, b_2} e^{(2\omega_0 t)\, b_2 b_1} e^{B(t) b_1}. \tag{24}$$

This operator enables us—as for the harmonic oscillator—to obtain the time development of any initial wavefunction, though in this case it is unknown how operators b_1 and b_2 act on wavefunctions. U, however, can be expressed in terms of the more common operators a and $a^\dagger$ through the following identities:

$$b_1 = \frac{\sqrt{\imath}}{2}\left[(a + a^\dagger) - \imath(a - a^\dagger)\right]$$

$$b_2 = \frac{\sqrt{\imath}}{2}\left[(a + a^\dagger) + \imath(a - a^\dagger)\right] \tag{25}$$

Since we are also interested in obtaining Floquet quasienergies, we will refrain ourselves of expressing U as a function of a and $a^\dagger$ until the last step. Thus, we now specify an initial function $\Psi(x, 0)$:

$$\Psi(x, 0) = \chi_\nu\big(\beta\{x - x_0\}\big) \quad . \tag{26}$$

By using the displacement operator (17) and the scaling operator:

$$f(\beta x) = exp\Big\{(ln\beta) x \frac{d}{dx}\Big\} f(x) \quad , \tag{27}$$

$\Psi(x, 0)$ can be rewritten as:

$$\Psi(x, 0) = exp\left\{-x_0\sqrt{\frac{\imath\omega_0}{2}}\big(b_1 - b_2\big)\right\} exp\left\{\frac{1}{2}\, ln\beta\, \big(b_1^2 - b_2^2 - 1\big)\right\}\chi_\nu(x) \tag{28}$$

because $x\ d/dx = \frac{1}{2}\big(b_1^2 - b_2^2 - 1\big)$.

If we proceeded as in the harmonic potential, we should commute the factor $e^{2\omega_0 t b_2 b_1}$ until it appears to the left of $\chi_\nu(x)$. However, there are two additional considerations: First, there is a new factor $exp\left\{\frac{1}{2}\ ln\,\beta\,(b_1^2 - b_2^2 - 1)\right\}$, and second, even if we put $e^{2\omega_0 t b_2 b_1}$ to the left of $\chi_\nu(x)$, one would have

$$e^{2\,\omega_0 t\, b_2 b_1}\chi_\nu(x) \neq e^{2\omega_0 t\nu}\chi_\nu(x) \tag{29}$$

because $b_2 b_1$ is not the number operator $N = a^\dagger a$. In fact it can be shown that,

$$b_2 b_1 = -\frac{1}{2} + \frac{\imath}{2}\big(a^2 + a^{\dagger 2}\big). \tag{30}$$

In order to proceed we commute $e^{2\omega_0 t b_2 b_1}$ until it appears to the left of the factor $exp\{\frac{1}{2} ln\beta\,(b_1^2 - b_2^2 - 1)\}$ and obtain:

$$\Psi_F^\nu(x,t) = e^{-\imath E' t} e^{\beta'(t)} e^{\gamma'(t) b_2} e^{\delta'(t) b_1} e^{2\omega_0 t b_2 b_1} e^{\frac{1}{2} ln\beta (b_1^2 - b_2^2 - 1)} \chi_\nu(x)\ , \qquad (31)$$

where $\beta'(t)$, $\gamma'(t)$ and $\delta'(t)$ are periodic if and only if $x_0 = 2\lambda/(\omega^2 + 4\omega_0^2)$, which results in

$$E' = \imath\omega_0 + \frac{\lambda^2}{2(\omega^2 + 4\omega_0^2)}. \qquad (32)$$

We see that, except for the factor $e^{2\omega_0 t b_2 b_1}$, we could identify a Floquet quasienergy (E'), and a periodic function $\Phi_F^\nu(x,t)$. The use of the BCH theorem and some identities like $a^2 - a^{\dagger 2} = b_1^2 - b_2^2$ allows us to obtain:

$$\begin{aligned}\Psi_F^\nu(x,t) = exp\left\{-\imath\left[\frac{\lambda^2}{2(\omega^2 + 4\omega_0^2)}\right] t\right\} exp\left\{\frac{\imath\lambda^2}{4\omega}\frac{\omega^2 - 4\omega_0^2}{(\omega^2 + 4\omega_0^2)^2}\sin 2\omega t\right\} \\ \times\ exp\left\{\frac{-\imath\lambda\omega}{\omega^2 + 4\omega_o^2}\frac{1}{\sqrt{2\omega_0}}\left(a + a^\dagger\right)\sin\omega t\right\} \\ exp\left\{\frac{-2\lambda}{\omega^2 + 4\omega_0^2}\sqrt{\frac{\omega_0}{2}}\left(a - a^\dagger\right)\cos\omega t\right\} \\ \times\ exp\left\{\imath\omega_0 t\left(a^2 + a^{\dagger 2}\right)\right\} exp\left\{\frac{1}{2} ln\beta\left(a^2 - a^{\dagger 2} - 1\right)\right\}\chi_\nu(x). \qquad (33)\end{aligned}$$

Finally, we want to commute the last two factors, which have quadratic terms in a and $a^\dagger$. To this end we could use some of the normal order theorems, however, precisely because of the quadratic terms, the resulting expressions are somewhat cumbersome. Instead, we use a technique described in reference [9], which consists of carrying out a Lie algebraic similarity transformation. First we need a set of operators $X_1, X_2, \cdots, X_n$ which form what it is called a 'Lie algebra'. We propose to use the following operators

$$X_1 = a^2 + a^{\dagger 2} \quad , \quad X_2 = a^2 - a^{\dagger 2} \quad , \quad X_3 = 2a^\dagger a + 1. \qquad (34)$$

These operators form the SU(1,1) algebra:

$$[X_1, X_2] = -4X_3 \quad , \quad [X_2, X_3] = 4X_1 \quad , \quad [X_1, X_3] = 4X_2 \qquad (35)$$

Then, by using the above mentioned technique it can be shown that if and only if $\beta = e^{-\imath\pi/4}$ (see appendix):

$$exp\left\{\imath\omega_0 t\,(a^2 + a^{\dagger 2})\right\} exp\left\{\frac{1}{2}\ ln\,\beta\,(a^2 - a^{\dagger 2})\right\} = e^{-\omega_0 t(2a^\dagger a + 1)}. \qquad (36)$$

By using this last result one can finally write equation (33) as:

$$\Psi_F^\nu(x,t) = e^{-\imath E_F^\nu t}\Phi_F^\nu(x,t) \tag{37}$$

where the Floquet quasienergy is:

$$E_F^\nu = -i(2\nu+1)\omega_0 + \frac{\lambda^2}{2(\omega^2+4\omega_0^2)} \tag{38}$$

and the periodic function $\Phi_F^\nu(x,t)$ is:

$$\Phi_F^\nu(x,t) = exp\left\{\frac{\imath\lambda^2}{4\omega}\frac{\omega^2-4\omega_0^2}{(\omega^2+4\omega_0^2)^2}\sin 2\omega t\right\} exp\left\{\frac{-\imath\lambda\omega}{\omega^2+4\omega_o^2}\frac{1}{\sqrt{2\omega_0}}\left(a+a^\dagger\right)\sin\omega t\right\}$$

$$\times\ exp\left\{\frac{-2\lambda}{\omega^2+4\omega_0^2}\sqrt{\frac{\omega_0}{2}}\left(a-a^\dagger\right)\cos\omega t\right\} exp\left\{-\frac{\imath\pi}{8}\left(a^2-a^{\dagger 2}-1\right)\right\}\chi_\nu(x). \tag{39}$$

4. CONCLUSIONS

It has long been known that the use of boson operators allows for an alternative and efficient way for solving quantum problems. In this paper we have shown another application for this approach and we have been able to obtain the Floquet quasienergies and eigenfunctions for the harmonic oscillator and the parabolic barrier interacting with an external field. This adds to previous derivations, where use was made of other classical concepts such as the Lagrangian [10].
In the case of the parabolic barrier we introduced two new operators which can be considered the analogous of boson operators for this potential. They have been very useful to obtain quantum mechanically the exact Floquet states.

5. ACKNOWLEDGMENTS

A.P. is grateful to Professor R.Lefebvre for stimulating discussions and hospitality in his group at Orsay, France. One of us (V. L.) acknowledges ANUIES-SEP for provision of a fellowship. This work has benefited from the ANUIES-ECOS program.

6. APPENDIX

In order to find a Lie algebra between boson operators, let us consider:

$$X_1 = a^2 + a^{\dagger 2} \quad , \quad X_2 = a^2 - a^{\dagger 2} \quad , \quad X_3 = 2a^\dagger a + 1\ . \tag{A.1}$$

We can trivially show that:

$$[X_1, X_2] = -4X_3 \quad , \quad [X_2, X_3] = 4X_1 \quad , \quad [X_1, X_3] = 4X_2 \tag{A.2}$$

Let us define

$$Z = \gamma X_1 + \delta X_2 + \rho X_3 \quad , \quad G = gX_1 + dX_2 + rX_3 \ . \tag{A.3}$$

and the similarity transformation

$$G_l(x) = e^{xZ} G e^{-xZ} \tag{A.4}$$

To find $G_l(x)$ we first note that it must also be a linear combination of X_1, X_2 and X_3 [9]:

$$G_l(x) = g_l(x)X_1 + d_l(x)X_2 + r_l(x)X_3 \tag{A.5}$$

and it must also satisfy the boundary condition $G_l(0) = G$. From (A.4) we have:

$$G_l'(x) = [Z, G_l(x)] \tag{A.6}$$

By using (A.2) and (A.5) in (A.6) one has

$$G_l'(x) = 4[\delta r_l(x) - \rho d_l(x)]X_1 + 4[\gamma r_l(x) - \rho g_l(x)]X_2 + 4[\delta g_l(x) - \gamma d_l(x)]X_3 \tag{A.7}$$

From (A.5) we also have

$$G_l'(x) = g_l'(x)X_1 + d_l'(x)X_2 + r_l'(x)X_3 \tag{A.8}$$

Now, because X_1, X_2 and X_3 are independent, we equate coefficients in (A.7) and (A.8) and obtain a set of coupled differential equations:

$$g_l'(x) = 4[\delta r_l(x) - \rho d_l(x)] \ ; \tag{A.9a}$$

$$d_l'(x) = 4[\gamma r_l(x) - \rho g_l(x)] \ ; \tag{A.9b}$$

$$r_l'(x) = 4[\delta g_l(x) - \gamma d_l(x)] \ ; \tag{A 9c}$$

subject to the boundary conditions $g_l(0) = g$, $d_l(0) = d$, and $r_l(0) = r$. In particular, we are interested in the following conditions: $\gamma = \rho = 0$, $\delta = 1$ ($Z = X_2 = a^2 - a^{\dagger 2}$); $d = r = 0$, $g = 1$ ($G = a^2 + a^{\dagger 2}$). Equations (A 9) thus become

$$g_l'(x) = 4r_l(x) \ ; \tag{A.10a}$$

$$d_l'(x) = 0 \ ; \tag{A.10b}$$

$$r_l'(x) = 4g_l(x) \ ; \tag{A.10c}$$

with the boundary conditions $g_l(0) = 1$, $d_l(0) = 0$, and $r_l(0) = 0$.
The solutions to these equations are:

$$g_l(x) = \cosh 4x, \qquad d_l(x) = 0, \qquad r_l(x) = \sinh 4x \tag{A.11}$$

Thus we have

$$e^{x(a^2-a^{\dagger 2})}\{a^2+a^{\dagger 2}\}e^{-x(a^2-a^{\dagger 2})} = \left(a^2+a^{\dagger 2}\right)\cosh 4x + \left(2a^{\dagger}a+1\right)\sinh 4x \tag{A.12}$$

and by linear superposition if follows that:

$$e^{x(a^2-a^{\dagger 2})}e^{y(a^2+a^{\dagger 2})}e^{-x(a^2-a^{\dagger 2})}$$

$$= exp\Big\{y\big[(a^2+a^{\dagger 2})\cosh 4x + (2a^{\dagger}a+1)\sinh 4x\big]\Big\} \tag{A.13}$$

According to the last two factors in equation (33) we choose $x = \frac{\imath\pi}{8}$ and $y = \imath\omega_0 t$, then

$$e^{\imath\omega_0 t(a^2+a^{\dagger 2})}e^{-\frac{\imath\pi}{8}(a^2-a^{\dagger 2})} = e^{-\frac{\imath\pi}{8}(a^2-a^{\dagger 2})}$$

$$\times exp\Big\{\imath\omega_0 t\big[(a^2+a^{\dagger 2})\cosh\frac{i\pi}{2} + (2a^{\dagger}a+1)\sinh\frac{i\pi}{2}\big]\Big\}. \tag{A.14}$$

Finally, we use $\cosh\frac{\imath\pi}{2} = 0$ and $\sinh\frac{\imath\pi}{2} = \imath$ to obtain:

$$e^{\imath\omega_0 t(a^2+a^{\dagger 2})}e^{-\frac{\imath\pi}{8}(a^2-a^{\dagger 2})} = e^{-\omega_0 t(2a^{\dagger}a+1)} \tag{A.15}$$

7. REFERENCES

[1] E.H. Kerner *Can.J.Phys., 36,371 (1958).*

[2] O.Atabek, R.Lefebvre, M.García-Sucre, J.Gomez-Llorente and H.Taylor *Int.J.Quantum Chem. 40,211-224 (1991).*

[3] R.Lefebvre and A.Palma *J. Mol.Structure (THEOCHEM) 390,23-32 (1997).*

[4] R.Lefebvre and A.Palma *Int.J.Quantum Chem. 65,487-497 (1997).*

[5] L.Sandoval, M.Martin, J.F.Rivas-Silva and A.Palma, *Phys. Rev. A. 46,6095 (1992).*

[6] A.Palma, L.Sandoval and M.Martín *Int.J.Quantum Chem. S28,261-264 (1994).*

[7] A.Palma, *Int.J.Quantum Chem. 63,229-232 (1997).*

[8] W.H. Louisell, *Quantum Statistical Properties of Radiation*, John Wiley & Sons, USA (1990).

[9] R.M. Wilcox, *J.Math.Phys. 8(4),962 (1967).*

[10] H.P.Breuer, M.Holthaus, *Z.Phys. D 11,1 (1989).*

Index

Boldface numerals indicate volume number

C

D

E

F

G

H

I

K

L

M

N

O

P

Q

R

U

V

W

Y

Z